

**UNIVERSITÀ DEGLI STUDI DI TORINO**

**DIPARTIMENTO DI NEUROSCIENZE “RITA LEVI MONTALCINI”**

**DOTTORATO DI RICERCA IN MEDICINA E TERAPIA SPERIMENTALE**

**DOCTOR OF PHILOSOPHY IN EXPERIMENTAL MEDICINE AND THERAPY**



**ASSESSMENT OF VASCULAR REACTIVITY TO  
INVESTIGATE CEREBRAL AND MUSCULAR CONTROL OF  
BLOOD FLOW IN HUMANS**

PhD Candidate: Dr. Anas Rashid

PhD Tutor: Prof. Silvestro Roatta  
PhD Coordinator: Prof. Pasquale Pagliaro

Cycle: XXXV

Academic Years: 2019 – 23

Scientific Discipline: BIO/09 – Physiology



## TABLE OF CONTENTS

ACKNOWLEDGMENT .....	1
ORIGINAL ARTICLES .....	4
ORAL AND POSTER PRESENTATIONS .....	7
ABBREVIATIONS USED IN ORIGINAL ARTICLES .....	9
ABSTRACT .....	11
INTRODUCTION .....	14
A. Blood Flow and Poiseuille's Law .....	14
B. Mechanisms Involved in the Control of Blood Flow .....	15
I. Myogenic Control of Blood Flow .....	15
II. Metabolic Control of Blood Flow .....	16
III. Endothelium-Derived Factors .....	18
IV. Humoral Control of Blood Flow .....	19
V. Neural-Astrocyte Control of Blood Flow .....	20
VI. Mechanical-Induced Vasodilation .....	22
VII. Carbon Dioxide-Mediated Vasodilation .....	22
VIII. Oxygen-Mediated Vasodilation .....	23
IX. Segmental Vascular Resistance .....	24
C. Vascular Reactivity and Its Assessment .....	24
I. Transcranial Doppler Ultrasound .....	25
II. Near-Infrared Spectroscopy .....	28
D. Hypnotizability and Its Assessment .....	30
E. Masticatory and Limb Muscles .....	31
F. Muscle Activity and Its Assessment .....	32
AIMS OF THE THESIS .....	34
A. Assessment of Cerebrovascular Reactivity in Hypnotizable vs. Non-Hypnotizable Subjects .....	34
B. Assessment of Vascular Reactivity to Stress in Masticatory and Limb Muscles .....	35
C. Additional Research .....	36
RESULTS .....	37
Paper I ( <i>Brain Sciences</i> ) .....	38
Paper II ( <i>Physiology and Behavior</i> ) .....	52
Paper III ( <i>Brain Research</i> ) .....	57
Paper IV ( <i>Archives of Oral Biology</i> ) .....	62
Paper V ( <i>Physiological Measurement</i> ) .....	72
Paper VI ( <i>European Journal of Applied Physiology</i> ) .....	82

DISCUSSION .....	96
A. Cerebrovascular Reactivity in Hypnotizable vs. Non-Hypnotizable Subjects .....	96
B. Vascular Reactivity to Stress in Masticatory and Limb Muscles .....	98
C. Additional Research .....	100
PERSPECTIVE AND CONCLUDING REMARKS .....	103
REFERENCES .....	104
APPENDIX .....	120
Paper VII ( <i>Experimental Physiology</i> ) .....	121
Paper VIII ( <i>Diagnostics</i> ) .....	129
Paper IX ( <i>Chromatographia</i> ) .....	143
Paper X ( <i>Journal of Separation Science</i> ) .....	159
Paper XI ( <i>Journal of Pharmaceutical Sciences</i> ) .....	183
Paper XII ( <i>Acta Chimica Slovenica</i> ) .....	195
Paper XIII ( <i>Journal of Separation Science</i> ) .....	219
Paper XIV ( <i>Exploration of Medicine</i> ) .....	246

# ACKNOWLEDGMENT

I would like to thank Almighty ALLAH (the Most Gracious, the Most Merciful) for enabling me to pursue this research opportunity and contribute to the benefit of mankind.

I would like to express my sincere gratitude to research tutor Silvestro Roatta for his guidance throughout this doctoral journey.

I could not complete this research endeavor without the consistent support of my beloved mother and siblings. Their love, encouragement, and continuous prayers have pushed me to achieve the last milestone of this doctoral journey earlier than expected. Further, the vivid figment of my playful childhood memories and cheerful relationship with my father (late) inspired me to pursue this research journey.

I would like to extend my deep-hearted thanks to the following scientific research collaborators across Europe, South, and North America.

- 1) Enrica Laura Santarcangelo (University of Pisa, Italy)
- 2) Aiman Rashid (University of Cagliari, Italy)
- 3) Marian Simka (University of Opole, Poland)
- 4) Jörn Rittweger (German Aerospace Center, Germany)
- 5) Syed Atif Iqrar (Aston University, United Kingdom)
- 6) María Segunda Aurora Prado (University of São Paulo, Brazil)
- 7) Bruno Moreira Silva (Federal University of São Paulo, Brazil)
- 8) Danilo Roman Campos (Federal University of São Paulo, Brazil)
- 9) Marco Rolando Aronés Jara (National University of San Cristóbal of Huamanga, Peru)
- 10) Ewart Mark Haacke (Wayne State University, United States of America)

I am thankful to the following clinicians for providing hospital training.

- 1) Urologist Kwanjin Park (Seoul National University Hospital, Republic of Korea)
- 2) Cardiologist Nazzareno Galiè (Polyclinic of Sant'Orsola – University of Bologna, Italy)
- 3) Cardiologist Massimiliano Palazzini (Polyclinic of Sant'Orsola – University of Bologna, Italy)
- 4) Pulmonologist Eloara Vieira Machado Ferreira Alvares da Silva Campos (Hospital São Paulo – Federal University of São Paulo, Brazil)
- 5) Thoracic Surgeon Paulo Francisco Guerreiro Cardoso (Heart Institute – University of São Paulo, Brazil)

This doctoral thesis becomes a reality with the valuable suggestions received from all reviewers including Antonio Colantuoni (University of Naples Federico II, Italy) and Diego Manzoni (University of Pisa, Italy) who timely reviewed the accompanying original research publications.

Besides, I am grateful to Raffaele Pertusio (University of Torino, Italy) for his technical assistance and Maria Paula Curado (AC Camargo Cancer Center, Brazil) for her fruitful discussion and enjoyable hospitality.

Moreover, I never forget Marina Maggiora (University of Torino, Italy) for superb organizational support during the documentation process, Pasquale Pagliaro (University of Torino, Italy) for accompanying and thoughtful discussion during the cardiology workshop in Erice (Italy), and Claudia Penna (University of Torino, Italy) for providing research recommendation.

Last, but not least, I would like to express my gratitude to Ministry of Foreign Affairs and International Cooperation, Italy (Ministero degli Affari Esteri e della Cooperazione Internazionale, Italia) for generous funding under Partnership for Knowledge (PFK) program of

Italian Agency for Development Cooperation (Agenzia Italiana per la Cooperazione allo Sviluppo), with the arrangement of four national meetings in various geographical locations of Italy (Milan, Como, Aosta Valley and Naples) to enrich my experiential learning with Italian culture and cuisine.

Finally, constructive criticisms and valuable suggestions are always welcome for continuous improvement. I hope the research presented in this doctoral thesis will be beneficial and influential for upcoming researchers, and pave the path for contribution and enhancement of scientific knowledge.

## ORIGINAL ARTICLES

This thesis is based on the original articles (I – VI) listed below. In the following text, these articles will be referred to by their Roman numerals:

- I. **Anas Rashid**, Enrica Laura Santarcangelo, Silvestro Roatta, Cerebral Blood Flow in Healthy Subjects with Different Hypnotizability Score, *Brain Sciences* 2022, Vol. 12, Issue 5, No. 558, pp. 1-13. DOI: 10.3390/brainsci12050558.
- II. **Anas Rashid**, Enrica Laura Santarcangelo, Silvestro Roatta, Does Hypnotizability Affect Neurovascular Coupling During Cognitive Tasks?, *Physiology and Behavior* 2022, Vol. 257, Issue 1, No. 113915, pp. 1-5. DOI: 10.1016/j.physbeh.2022.113915.
- III. **Anas Rashid**, Enrica Laura Santarcangelo, Silvestro Roatta, Cerebrovascular Reactivity During Visual Stimulation: Does Hypnotizability Matter?, *Brain Research* 2022, Vol. 1794, No. 148059, pp. 1-4. DOI: 10.1016/j.brainres.2022.148059.
- IV. **Anas Rashid**, Silvestro Roatta, Differential Control of Blood Flow in Masseter and Biceps Brachii Muscles During Stress, *Archives of Oral Biology* 2022, Vol. 141, No. 105490, pp. 1-10. DOI: 10.1016/j.archoralbio.2022.105490.
- V. **Anas Rashid**, Silvestro Roatta, Hemodynamic Monitoring in the Human Temporalis Muscle Using Near-Infrared Spectroscopy, *Physiological Measurement* 2023, Vol. 44, No. 6, pp. 1-10. DOI: 10.1088/1361-6579/acd6d5.
- VI. **Anas Rashid**, Silvestro Roatta, Hemodynamic Changes in the Temporalis and Masseter Muscles During Stress in Healthy Humans, *European Journal of*



*Applied Physiology* 2023, Under Review.

- VII.** Diogo Machado de Oliveira, Thiago Ribeiro Lopes, Felipe Silva Gomes, **Anas Rashid**, Bruno Moreira Silva, Ventilatory Response to Peripheral Chemoreflex and Muscle Metaboreflex During Static Handgrip in Healthy Humans: Evidence of Hyperadditive Integration, *Experimental Physiology* 2023, Vol. 108, Issue 4, pp.1-8. DOI: 10.1113/EP091094.
- VIII.** **Anas Rashid**, Syed Atif Iqar, Aiman Rashid, Marian Simka, Results of Numerical Modeling of Blood Flow in the Internal Jugular Vein Exhibiting Different Types of Strictures, *Diagnostics* 2022, Vol. 12, Issue 11, No. 2862, pp. 1-14. DOI: 10.3390/diagnostics12112862.
- IX.** Antonio Marcos Callejo de Souza, Frank Alonso Gavilano Fajardo, **Anas Rashid**, Marina Franco Maggi Tavares, María Segunda Aurora Prado, Capillary Electrophoresis Method for Simultaneous Quantification of Hypocholesterolemic Drugs in Binary Mixture Formulation: Fast, Green, and Cost-Effective Alternative to HPLC, *Chromatographia* 2023, Vol. 86, Issue 4, pp. 1-15. DOI: 10.1007/s10337-023-04243-6.
- X.** Claudia Vilela de Oliveira, Adriano Peron, **Anas Rashid**, Frank Alonso Gavilano Fajardo, Felipe Rebello Lourenço, Marina Franco Maggi Tavares, María Segunda Aurora Prado, Validation, Measurement Uncertainty Estimation and Green Evaluation of UHPLC for Simultaneous Determination of Antihypertensive Drugs in Binary Tablet, *Journal of Separation Science* 2023, Revision Submitted.

- XI.** Frank Alonso Gavilano Fajardo, Marina Franco Maggi Tavares, **Anas Rashid**, María Segunda Aurora Prado, Novel Eco-Friendly Stability Indicating Capillary Zone Electrophoresis Method for Determination of Aripiprazole in Tablet Dosage Form: DoE Directed Optimization, Development and Method Validation, *Journal of Pharmaceutical Sciences* 2022, Vol. 111, Issue 12, pp. 3340-3351. DOI: 10.1016/j.xphs.2022.08.025.
- XII.** Victor Barnabe de Pontes, **Anas Rashid**, María Segunda Aurora Prado, Development and Validation of an Analytical Method for the Determination of Risperidone in Tablet Formulation, *Acta Chimica Slovenica* 2023, Under Review.
- XIII.** Marco Rolando Aronés Jara, Edgar Cárdenas Landeo, Kirianova Godoy Bautista, Eylon Almendra Ortiz Pérez, Juan Clímaco Paniagua Segovia, Hugo Roberto Luna Molero, Stephanny Barbarán Vilcatoma, Mónica Gómez, Quispe, Jesús Javier Paniagua Segovia, **Anas Rashid**, María Segunda Aurora Prado, *Brachyotum naudinii* Triana Flower Chemical Screening by UHPLC-MS/MS, Preliminary Toxicity and *In Vitro* Antioxidant Potential, *Journal of Separation Science* 2023, Revision Submitted.
- XIV.** Rosy Yesela Mancilla Santa Cruz, Sharon Velásquez Arévalo, **Anas Rashid**, Marco Rolando Aronés Jara, María Segunda Aurora Prado, Antioxidant and Photoprotective Potential of *Polypodium leucotomos*, *Exploration of Medicine* 2022, Vol. 3, pp. 607-616. DOI: 10.37349/emed.2022.00117.

## ORAL AND POSTER PRESENTATIONS

- I. **Anas Rashid**, Syed Atif Iqrar, Aiman Rashid, Marian Simka, Results of Numerical Simulations of Blood Flow in the Models of Popliteal Vein with Elastic Valves and with the Leaflets of an Increased Stiffness, *23<sup>rd</sup> European Venous Forum, Germany*.
- II. **Anas Rashid**, Numerical Modeling of Blood Flow in Internal Jugular Vein, *Doctoral School of Experimental Medicine and Therapy of the University of Torino Annual Welcome Day, Italy*.
- III. **Anas Rashid**, Silvestro Roatta, Hemodynamic Monitoring of Human Temporal Muscle Using Near-Infrared Spectroscopy, *Swiss Physiology Meeting, Switzerland*.
- IV. **Anas Rashid**, Syed Atif Iqrar, Aiman Rashid, Marian Simka, Stenosis at the Beginning of the Internal Jugular Vein Compromises Outflow through this Blood Vessel and Can Alter the Geometry of the Jugular Valve Located Downstream: Results of Numerical Modeling of Blood Flow, *XV Congress of the Polish Society of Angiology, Poland*.
- V. Marian Simka, Syed Atif Iqrar, **Anas Rashid**, Aiman Rashid, Marta Nowak, Abnormal Jugular Valves are not the Sole Explanation of an Impaired Outflow from the Cranial Cavity through the Internal Jugular Veins: Results of *In Silico* Studies, *10<sup>th</sup> International Society for Neurovascular Disease Annual Meeting, United States of America (Veins and Lymphatics 2022)* Vol. 11 (No. 1). DOI: 10.4081/vl.2022.10957.

- VI.** Claudia Vilela de Oliveira, **Anas Rashid**, Marina Franco Maggi Tavares, María Segunda Aurora Prado, Simultaneous Determination of Anti-Hypertensive Drugs Using Analytical Method, *6<sup>th</sup> Italian Society of Cardiovascular Research Forum, Italy.*
- VII.** **Anas Rashid**, Summarizing Doctoral Research and Italian Cultural Experience, *3<sup>rd</sup> National Meeting of Partnership of Knowledge, Italy.*
- VIII.** **Anas Rashid**, Advances in Cardio-Oncology, *22<sup>nd</sup> Workshop of the International School of Cardiology, Italy.*
- IX.** **Anas Rashid**, Control of Skeletal Muscle Blood Flow, *Physiology and Pulmonology Meeting, Brazil.*
- X.** Diogo Machado de Oliveira, Thiago Ribeiro Lopes, Felipe Silva Gomes, **Anas Rashid**, Bruno Moreira Silva, Hyperadditive Ventilatory Responses to Simultaneous Peripheral Chemoreflex and Muscle Metaboreflex Activation in Humans, *VII Academic Congress of the Federal University of São Paulo, Brazil.*
- XI.** **Anas Rashid**, Silvestro Roatta, Dilatory Response of Masseter Muscle to Stress, *Medical and Clinical Conference of the University of Pécs, Hungary.*
- XII.** **Anas Rashid**, Silvestro Roatta, Differential Control of Blood Flow in Facial and Limb Muscles During Stress, *Annual Meeting of the American Physiological Society, United States of America (The FASEB Journal 2021) Vol. 35 (Issue S1). DOI: 10.1096/fasebj.2021.35.S1.02925.*

## **ABBREVIATIONS USED IN ORIGINAL ARTICLES**

ABP	Arterial Blood Pressure
CBF	Cerebral Blood Flow
CO	Cardiac Output
CPT	Cold Pressor Test
CVCi	Cerebrovascular Conductance Index
CVR	Cerebrovascular Reactivity
EMG	Electromyography
FMD	Flow-Mediated Dilatation
HHb	Deoxyhemoglobin + Deoxymyoglobin
HR	Heart Rate
HVT	Hyperventilation
MAT	Mental Arithmetic Task
MC	Mental Computation
MCAv	Middle Cerebral Artery Flow Velocity
MVC	Maximum Voluntary Contraction
NIRS	Near-Infrared Spectroscopy

NO	Nitric Oxide
NOS	Nitric Oxide Synthase
O <sub>2</sub> Hb	Oxyhemoglobin + Oxymyoglobin
PCAv	Posterior Cerebral Artery Flow Velocity
P <sub>ET</sub> CO <sub>2</sub>	Partial Pressure of End-Tidal Carbon Dioxide
RBT	Rebreathing
SHSS	Stanford Hypnotic Susceptibility Scale
TCD	Transcranial Doppler
THI	Tissue Hemoglobin Index
TMT	Trail Making Task
TOI	Tissue Oxygenation Index
VS	Visual Stimulation
WM	Working Memory

## **ABSTRACT**

The control of blood flow is a sophisticated physiological function accomplished through the integration of several concurrent mechanisms and pathways (e.g., myogenic, metabolic, humoral, and neuronal). These mechanisms are differentially expressed in different tissues and organs (e.g., brain and muscle) and may have developed to better serve the specific need to meet the enhanced oxygen demand. One part of the thesis concerns cerebral circulation, known to absorb ~15% of cardiac output and ~20% of the available oxygen. Another part concerns muscle circulation, whose peculiarity is its capacity to change over an extremely broad range, e.g., from an average of 20 up to 80-fold during exercise, compared to the resting state.

The control of blood flow can be investigated by assessing the hemodynamic response to specific stimuli and by devising appropriate vascular reactivity tests. In this thesis, vascular responses in the brain and skeletal muscles were investigated using two noninvasive imaging techniques: transcranial Doppler ultrasound and near-infrared spectroscopy. The vascular reactivity was used as a tool to understand and address two physiological issues: 1) the control of cerebral blood flow in relation to hypnotizability; and 2) the control of blood flow in the head compared to limb muscles, during stress conditions.

Before proceeding to address the first physiological question, it is worth mentioning that hypnotizability is a psychophysiological and dispositional feature characterized by different attentional abilities, information processing, and cardiovascular control, that can be measured by a validated scale. Previous studies evidenced hypnotizability-related differences in the control of peripheral circulation. Based on this, possible differences in cerebral circulation were hypothesized between low- and highly-

hypnotizable individuals. Three investigations were carried out to assess vascular reactivity during different stimuli (chemical, mechanical, cognitive, and sensory). The results showed different correlations among hemodynamic variables in med-low and med-high hypnotizable individuals and revealed that hypnotizability affects the control of cerebral circulation independently from suggestion and induction of the hypnotic state.

The second issue addresses a different physiological question: whether the sympathetic nervous system exerts a different control over blood flow in head muscles (masseter and temporalis) compared to limb muscles (biceps brachii). In fact, the sympathetic nervous system is known to play a general constrictory role, but with possible differences between body areas (e.g., upper and lower limbs). Even opposite (dilatory) responses were reported in the literature for the masseter muscle although simultaneous monitoring of head and limb muscles was never performed.

To this aim, first a methodological study was necessary to validate the near-infrared spectroscopy monitoring in the temporalis muscle. In particular, the expected response patterns were observed during isometric muscle contractions (teeth clenching), while no effect was produced by hyperventilation (provoking cerebral vasoconstriction), which proved that this technique is adequate to investigate muscle hemodynamics with no interference from cerebral circulation. Two investigations were then carried out to investigate the vascular response to different sympathetic activation tests in biceps brachii, masseter, and temporalis muscles using near-infrared spectroscopy. The results showed that the masseter and temporalis appear more prone to dilatation than the biceps, exhibiting opposite changes (oxygenation increase in head muscles and decrease in the biceps) in response to painful stimuli such as the cold pressor test and the post-handgrip muscle ischemia. This allowed us to infer differential control of



muscle blood flow in the head and upper limbs. Several mechanisms may mediate this effect, including a reduced sympathetic outflow to the extracranial vasculature of the head, generally exposed to lower hydrostatic loads than the rest of the body.

# INTRODUCTION

The contents of this thesis are organized as follows. First, general principles and mechanisms (intrinsic/extrinsic) involved in the control of blood flow are thoroughly summarized. Second, the concept of vascular reactivity is presented, and two noninvasive hemodynamic techniques for the assessment of vascular reactivity, that have been mainly employed in this thesis, will be discussed and mentioned in a broader context. Third, hypnotizability is introduced and a reliable measurement of hypnotic susceptibility is presented. Fourth, masticatory and limb muscles are introduced and compared to address the notion that control of blood flow to these muscles remains to be investigated which may contribute to the etiology of pain in orofacial and head regions. Finally, the muscle activity assessment technique is concisely summarized.

## A. Blood Flow and Poiseuille's Law

Blood flow is described with the help of French Physiologist Jean Louis Marie Poiseuille, as directly proportional to the magnitude of arteriovenous pressure gradient across the vascular bundle and inversely proportional to the overall resistance of the vascular network [1]. This is mathematically expressed as:

$$Q = \frac{\pi \Delta P r^4}{8 \eta \lambda}$$

- Q = blood flow rate (mL/min)
- $\pi$  (Greek letter pi) = ratio of a circle's circumference to its diameter
- $\Delta P$  = pressure difference (mmHg)
- $r^4$  = vessel radius to the fourth power (cm)

- $\eta$  (Greek letter eta) = blood viscosity (Pa.s)
- $\lambda$  (Greek letter lambda) = vessel length (cm)

Blood flows from higher-pressure regions to lower-pressure regions in the same direction, and very little pressure remains by the time blood leaves the capillaries and enters the venules. Blood flow velocity varies inversely with the total cross-sectional area of the blood vessels. In blood vessels, most of the resistance is due to the vessel radius. As vessel radius increases, the resistance decreases and blood flow increases (vasodilation). Therefore, this relationship serves to understand how physiological (e.g., vascular tone) and pathological (vascular stenosis) changes in vessel radius significantly affect flow and pressure [2].

## **B. Mechanisms Involved in the Control of Blood Flow**

Blood flow is the movement of blood through a vessel, tissue, or organ from the arteries to the capillaries and then into the veins. Control of blood flow is different for the different tissues and may be altered in pathologies and may change with adaptation (e.g., altitude, temperature). Understanding the physiological mechanisms of blood flow control within the skeletal muscles and cerebral vasculature is obviously captivating due to the extremely tight coupling between hemodynamics and tissue oxygenation [3].

### **I. Myogenic Control of Blood Flow**

The myogenic response is an intrinsic property of the blood vessel or more specifically vascular smooth muscle to respond to changes in intravascular pressure and mechanical stretch [4]. The smooth muscle of both large arteries and small arterioles dilates in response to decreased pressure and constricts in response to increased pressure [5]. The myogenic behavior, prevalent in resistance arteries and arterioles

involves myogenic tone, a state of partial constriction at constant pressure, and myogenic reactivity, the adjustment of tone in response to a change in pressure [6].

This response to increased transmural pressure occurs via the activation of ion channels, depolarization of the smooth muscle cell membrane, and calcium influx through the opening of voltage-operated calcium channels. The myosin light chain phosphorylation increases with the increased intracellular calcium concentration and results in vasoconstriction [7]. The increase in wall tension, rather than elongation, has been proposed as a stimulus for the myogenic response development since it has been shown to correlate with changes in intracellular calcium and phosphorylation of myosin light chain, a relationship not seen with vessel diameter [8]. Stretch-activated ion channels, including transient receptor potential channels, are thought to serve as mechanosensors, although voltage-operated calcium channels may also be directly activated by transmural pressure changes [9]. In addition, chloride channels may also participate in pressure-induced depolarization of smooth muscle because their activation increases an inward current, causing depolarization [10]. In addition to ionic mechanisms, there is evidence for other factors involved in mechanotransduction during myogenic tone initiation, including actin cytoskeletal dynamics and cell surface integrins. Both transient receptor potential channels and integrins are associated with the actin cytoskeleton, which provides a mean to transduce stretch or pressure into a depolarization and contractile response [11].

## **II. Metabolic Control of Blood Flow**

The metabolic control of blood flow relates to the physiological necessity to maintain a balance between metabolic demand (hemodynamics) and metabolic supply (tissue oxygenation). Functional or active hyperemia is referred to increase blood flow in response to the elevated metabolic activity of the tissue. Remarkably, the interstitial

concentrations of metabolic products yield vasodilation that reflects the integrated activity of several processes including metabolic production rate, dilator metabolite washout by diffusion from interstitium into the bloodstream and removal by the flowing blood, and vasodilator reuptake by tissue cells. For instance, hydrogen peroxide, released at increased rates due to enhanced electron flux via respiratory chain and coupled to myocyte oxygen consumption, may act as a metabolic vasodilator and contribute to the hyperemia induced by skeletal muscle contraction [12].

The metabolite-sensitive small arterioles initiate a vasomotor response quite early (e.g., with contraction, as soon as metabolites are released) along the interconnected endothelial and arteriolar smooth muscle cells giving rise to *conducted vasodilation*, which does not depend on vessel wall shear rate [13]. This dilatation may result from acetylcholine local binding to muscarinic receptors on the endothelial plasma membrane, which in turn activates the inositol 1,4,5-triphosphate receptor on endoplasmic reticulum to release calcium, subsequently triggering intermediate- and small-conductance calcium-activated potassium channels, ultimately resulting in hyperpolarization, *per se* sufficient to cause vasodilation [3].

The myogenic and metabolic mechanisms are also involved in reactive hyperemia. When the arterial inflow to skeletal muscle is suddenly occluded, the decreased blood flow reduces the washout of metabolic vasodilators and decreases arteriolar wall tension. Removal of occlusion increases blood flow and vascular resistance progressively returns to normal levels [2].

For instance, skeletal muscles contain the largest single pool or reservoir of potassium [14]. During activation, the depolarized skeletal muscle cells immediately release potassium into the interstitial space surrounding the arterioles attaining values around 8 mmol/L, which subsequently stimulates the sodium-potassium pump in vascular

smooth muscle cells (hyperpolarization) leading to the vasodilation underlying functional hyperemia [15,16]. Potassium also increases the noradrenaline uptake into the sympathetic nerve terminals yielding a vasodilatory response [16]. Upon relaxation, muscles regain lost potassium by sodium-potassium pumps within minutes leading to the normalization of potassium levels which may be preceded by temporary potassium undershoot and transient hypokalemia ( $< 3.5$  mmol/L) [14]. Epoxyeicosatrienoic acids also produce vasodilation directly through calcium-activated potassium channels or transient receptor potential channels [17].

The metabolic control of blood flow is also a powerful mechanism in cerebral circulation which partly relies on astrocytes, providing a coupling between neurons and blood vessels (mentioned below).

### **III. Endothelium-Derived Factors**

Various vasodilators (i.e., nitric oxide, endothelium-derived hyperpolarizing factors, and prostacyclin) and vasoconstrictors (thromboxane A<sub>2</sub>, endothelin, and superoxide) are released from endothelium to influence vascular smooth muscle in a paracrine way [18]. For instance, hydrogen peroxide induces endothelium-dependent relaxation e.g., via cyclooxygenase-1-mediated release of prostaglandin E<sub>2</sub> [19].

Flow-induced vasodilation occurs, independently of humoral and neural mechanisms, in larger arterioles, resistance arteries, and conduit vessels [12]. This involves the production and/or release of nitric oxide from endothelial cells to relax vascular smooth muscle. In the vasculature, shear stress is defined as the tangential force of blood flow that acts on the endothelium. The increased shear stress activates endothelial nitric oxide synthase through raised endothelial calcium concentrations [20].

Endothelium-derived hyperpolarizing factors are non-prostanoid and non-nitric oxide, including potassium ions, hydrogen peroxide, cannabinoids, and epoxyeicosatrienoic acid, which also participate in flow-mediated dilatation of blood vessels [20]. In response to physical forces (such as vessel wall shear and circumferential stress) and neurohormonal mediators, potassium ions are also released by endothelial cells that contribute to endothelium-dependent vasodilation [15]. A similar mechanism of vasodilation is observed during brain tissue activation [21].

Other endothelium-derived factors exist that mediate vasoconstriction, such as Endothelin-1, which is constitutively produced by the endothelial cells and its receptors are expressed on vascular smooth muscle cells and endothelium [22]. Like angiotensin II-dependent superoxide formation, endothelin-1 can indirectly influence muscle blood flow by quenching nitric oxide and/or inducing endothelial nitric oxide synthase uncoupling, therefore limiting flow-dependent vasodilation [12].

It is worth mentioning that endothelium-mediated vasodilatory response may vary with skeletal muscle fiber type. For instance, the blockade of endothelial nitric oxide synthase decreases blood flow to oxidative fibers compared to fast glycolytic fibers [23]. Also, the sensitivity of arterioles to adenosine differs with fiber type, most probably due to endothelium phenotype variations [24]. To summarize, flow-mediated dilatation acts in concert with endothelium-dependent mediators to facilitate the vasodilation of blood vessels.

#### **IV. Humoral Control of Blood Flow**

Humoral mechanism is also important for the control of blood flow. For instance, noradrenaline released from the adrenal medulla produces vasoconstriction via alpha-1 receptor activation. At the same time, the release of adrenaline promotes vasodilation through beta-2 receptors as well as constriction through alpha-1 receptors. The overall effect may depend on relative receptor

density (which is tissue-dependent) and on the actual adrenaline concentration. Vasopressin may cause constriction of skeletal muscle arteries and arterioles as well as contraction of vascular smooth muscles and becomes significantly relevant in the conditions of liquid loss [12]. Angiotensin II also produces vasoconstriction and stimulates the production of superoxide via nicotinamide adenine dinucleotide phosphate oxidase.

## **V. Neural-Astrocyte Control of Blood Flow**

The central control mechanisms play a crucial role to adjust vascular resistance and cardiac output to regulate arterial blood pressure [25]. For instance, skeletal muscle vessels are highly innervated by the sympathetic nervous system. The withdrawal of sympathetic tone to skeletal muscle vasculature and/or local interference with neurotransmitter release from sympathetic nerve terminals produces vasodilation. Sympathetically-induced changes in the vasculature are mediated by adrenergic receptors expressed on endothelium and vascular smooth muscle cells that respond to catecholamines, noradrenaline, and adrenaline [26].

Catecholamines are released from the adrenal medulla and transported to skeletal muscles through the bloodstream, exerting their effects with the help of alpha- and beta-adrenergic receptors interaction. Vascular smooth muscle cells express alpha-1 and alpha-2 adrenergic receptors to evoke vasoconstriction. In addition, endothelium expresses alpha-2 adrenergic receptors which can lead to vasodilation through a release of endothelium-derived nitric oxide [27]. Skeletal muscle vasodilation may also occur due to the activation of beta-2 adrenergic receptors located on vascular smooth muscle cells, upon exposure to adrenaline [28,29].

Perivascular release of noradrenaline activates alpha receptors to induce vasoconstriction. Importantly, adventitial fibroblast also expresses alpha-1 adrenergic



receptors similar to vascular smooth muscle cells. Both cell types respond to noradrenaline by inducing protein synthesis and proliferation, which may contribute to the vascular modeling that occurs with long-term catecholamine exposure. Concomitantly, sympathetic nerve stimulation activates angiotensin II via renin-angiotensin system in the kidneys. This evokes vasoconstriction thus amplifying the effect of the noradrenaline released from sympathetic nerve terminals to induce arterial vascular smooth muscle contraction in skeletal muscles [12].

The sympathetic innervation in the brain specifically concentrates on the basal and pial arteries, before they enter the parenchyma, in addition, the parasympathetic nervous system is also believed to innervate brain vessels, as well as fibers from sensory afferents. Notably, the efficient blood-brain barrier prevents the entry of circulating catecholamines into the brain tissue.

A relevant role in the control of cerebral blood flow (the so-called *neurovascular coupling*) is played by astrocytes, which have an intimate relationship with cerebral vasculature [30]. Release of neurotransmitters (e.g., serotonin, noradrenaline, and acetylcholine) from active neurons evokes calcium-dependent release of vasoactive metabolites of arachidonic acid from astrocyte endfeet to modulate cerebral blood flow [31]. Synthesis and release of epoxyeicosatrienoic acid and prostaglandin E2 results in vasodilation, whereas tonic release of 20-hydroxyepoxyeicosatrienoic acid and adenosine triphosphate produces vasoconstriction of vascular smooth muscle cells [32]. Moreover, the release of potassium ions from astrocyte endfeet may also play a significant contribution to dilate cerebral arterioles [33]. Oxygen modulates astrocyte regulation of blood flow. Under normoxia, astrocytic calcium signaling results in vasodilation, while under hyperoxia, vasoconstriction is favored. Further, astrocytes also contribute to the generation of vascular tone [31].

## **VI. Mechanical-Induced Vasodilation**

While muscle contraction impedes the arterial inflow due to the increased intramuscular pressure, which occludes intramuscular vessels [34], different mechanisms have been suggested through which mechanical activity of muscle contraction and relaxation may contribute/cause muscle hyperemia [35]. Muscle contraction, which “squeezes” intramuscular vessels would be expected to facilitate blood flow from arteries into those veins where pressure and volume have been decreased. Pressure gradient increases during muscle relaxation due to venous negative luminal pressure, which may increase muscle perfusion without requiring changes in the diameter of the vessel (the so-called *muscle pump*) [36,37]. Further, vascular smooth muscle cells mechanical deformation may disrupt the attachment of actin-myosin, therefore increasing muscle perfusion [34]. Lastly, blood flow transiently impeded by muscle contraction also creates higher pressure in arterioles and, upon muscle relaxation, this increased pressure gradient drives the transient venous flow though this response remains for a short time due to less arterial compliance [38]. A mechanically-induced, rapid dilatation has also been observed to occur in different experimental conditions and to anticipate slower metabolic dilatation [39–41].

## **VII. Carbon Dioxide-Mediated Vasodilation**

Carbon dioxide causes dilatation of blood vessels; e.g., arterioles in skeletal muscle have been shown to vasodilate in response to hypercapnia [42]. Whether this vasodilatory response is shared among the different segments of arterial microvasculature in skeletal muscles is not clear [43], but an increased concentration of carbon dioxide in tissues is known to affect perfusion and hemoglobin capacity to release oxygen [44].

Cerebral blood flow and its distribution are highly sensitive to changes in the partial pressure of arterial carbon dioxide [45] to the extent that 5% and 7% of CO<sub>2</sub> in the inhaled air causes an increase in cerebral blood flow by 50% and 100%, respectively [46]. Hence, hypocapnia causes marked constriction of cerebral arteries and arterioles and a decrease in blood flow, while hypercapnia causes dilation and an increase in blood flow [46,47]. Several mechanisms governing hypercapnic vasodilation have been reported. The major proposed mechanism appears to be related to a direct effect of extracellular hydrogen ions on vascular smooth muscle [48]. This is supported by the observation that neither change in partial pressure of carbon dioxide nor bicarbonate ion alone affect the diameter of cerebral arteries. Other proposed mechanisms include vasodilator nitric oxide and prostanoid, however, the involvement of these mediators appears to be species-specific [10].

### **VIII. Oxygen-Mediated Vasodilation**

Brain has a very high oxygen requirement and is one of the most sensitive organs to hypoxia. Acute hypoxia produces marked cerebral blood flow increase via direct effects on vascular cells of cerebral arteries and arterioles [49]. Hypoxia-induced drop in adenosine triphosphate levels opens potassium channels on smooth muscle and causes hyperpolarization and vasodilation [50]. In addition, hypoxia rapidly increases the local production of nitric oxide and adenosine which facilitate vasodilation. Chronic hypoxia increases cerebral circulation by affecting capillary density [51,52]. Interestingly, cerebral blood flow increase does not affect metabolism, but arterial hemoglobin oxygen saturation decreases from ~100% at a tissue partial pressure of oxygen greater than 70 mmHg to ~50% at a tissue partial pressure of oxygen less than 50 mmHg [53].

In the skeletal muscle, during contraction, tissue partial pressure of oxygen decreases and may contribute to vasodilation leading to functional hyperemia which, in turn, will increase diffusion gradient and oxygen delivery [12].

### **IX. Segmental Vascular Resistance**

Both small arterioles and large arteries in the brain play a significant role in vascular resistance. In fact, direct pressure gradient measurement across different segments of the cerebral vasculature reveals that intracranial pial vessels and large extracranial vessels such as vertebral and internal carotid contribute ~50% of cerebral vascular resistance [54]. Interestingly, large cerebral arterial resistance is likely important to provide constant blood flow under physiological conditions e.g., metabolism that changes blood flow locally. The dilation of large arteries is important for the determination of microvascular perfusion and pressure, and to avoid the phenomena of *vascular steal*. Under control conditions, the blood perfusion to two different regions of the cerebrum is the same with a microvascular pressure of ~50 mmHg. Due to increased metabolism, regional cerebral blood flow increases, and in case of fixed resistance of upstream arteries, a decrease in microvascular pressure would take place thus causing decreased perfusion in the neighboring region (vascular steal). However, if large arteries dilate during these conditions, then microvascular pressure will be maintained thus preventing perfusion deficits [10]. The constriction of large cerebral arteries is also considered to be a protective mechanism from hypertensive states.

### **C. Vascular Reactivity and Its Assessment**

The response of the vasculature to a specific stimulus including stress (e.g., cognitive tasks), metabolic (e.g., functional or active and reactive hyperemia), chemical (e.g., partial pressure of end-tidal carbon dioxide and pH), and mechanical (e.g., changes in

transmural pressure) is termed as vascular reactivity and it can be used to characterize the functionality of the vascular network. Whereas, vasodilation and vasoconstriction are the most common physiological responses to external stimuli due to the fundamental role of the vasculature to distribute and regulate blood flow via functional and structural mechanisms. The balance between vasoconstrictor and vasodilator factors ultimately defines wall tension, resistance, tone, and blood flow; which is of utmost importance when assessing vascular reactivity in any experimental setting. A common example of vasodilatory response occurs during exercise as the oxygen consumption by skeletal muscles rapidly increases and therefore, it is necessary to increase the oxygen supply [55].

The vascular response can be measured in different ways (blood flow velocity, tissue oxygenation) using imaging techniques such as Doppler ultrasound, near-infrared spectroscopy, functional magnetic resonance, and positron emission tomography in healthy (physiological) and diseased (pathological) conditions [56]. Here, I will describe the two noninvasive techniques that I employed in my research.

### **I. Transcranial Doppler Ultrasound**

Transcranial Doppler is a noninvasive technique that enables us to monitor and, consequently, understand the changes in cerebral circulation under physiological and pathological conditions. It involves the use of a low-frequency ( $\leq 2$  MHz) transducer either handheld or fixed in a headset to insonate the basal cerebral arteries through relatively thin bone windows. Therefore, it allows dynamic monitoring of cerebral blood flow velocity and pulsatility over extended periods of time [57].

In physical terms, the ultrasound wave emitted from the transducer crosses the skull and propagates through, and is reflected by brain tissue and blood vessels. The reflected wave from erythrocytes undergoes a change in frequency (Doppler shift)

directly proportional to the erythrocytes' velocity [58]. This is mathematically expressed as:

$$v = \frac{c f_d}{2 f_0 \cos \theta}$$

- $v$  = blood flow velocity (cm/s)
- $c$  = incident wave speed ( $1.54 \times 10^5$  cm/s) [59]
- $f_d$  = Doppler shift (Hz)
- $f_0$  = incident wave pulse frequency (Hz)
- $\theta$  (Greek letter theta) = angle of the reflective wave relative to the direction of the vessel (blood flow)

A cerebral artery can be insonated and recognized by appropriate selection of the acoustic window (either foramina or thin bone), depth of the sample volume, probe angle, flow direction, blood velocity, and vascular resistance (as inferred from the pulsatility of the signal) [58].

Four acoustic windows allow the sonographer to investigate cerebral hemodynamics in both the anterior and posterior circulation. The transtemporal window (the primary window of the anterior circulation) allows for insonation of the middle cerebral artery, the anterior cerebral artery, the posterior cerebral artery, and the intracranial portion of the internal carotid artery. The transorbital window allows for the evaluation of the ophthalmic vessels and the carotid siphon. The submandibular window allows for the evaluation of the extracranial portion of the internal carotid artery. Lastly, the suboccipital/transforaminal window is used to assess the vertebrobasilar system of the posterior circulation [60].

Mean flow velocity is the central parameter, derived from the spectral envelope of the Doppler signal [61] as indicated by the following formula (or obtained by low-pass filtering the spectral outline):

$$\text{Mean Flow Velocity} = \frac{(\text{Peak Systolic Velocity cm/s} + [\text{End Diastolic Velocity cm/s} \times 2])}{3}$$

Cerebral blood flow velocity is inversely proportional to viscosity and hematocrit [62,63]. The device also reveals Pourcelot's resistivity index and Gosling's pulsatility index to estimate downstream resistance in cerebral circulation [61], while Lindegaard ratio allows differentiation between hyperdynamic flow and vasospasm [58]. The equations are expressed as:

$$\text{Pourcelot's Resistivity Index} = \frac{\text{Peak Systolic Velocity (cm/s)} - \text{End Diastolic Velocity (cm/s)}}{\text{Peak Systolic Velocity (cm/s)}}$$

$$\text{Gosling's Pulsatility Index} = \frac{\text{Peak Systolic Velocity (cm/s)} - \text{End Diastolic Velocity (cm/s)}}{\text{Mean Flow Velocity (cm/s)}}$$

$$\text{Lindegaard Ratio} = \frac{\text{Middle Cerebral Artery Mean Flow Velocity (cm/s)}}{\text{Extracranial Internal Carotid Artery Mean Flow Velocity (cm/s)}}$$

Further, cerebrovascular reactivity (to a dilatory stimulus such as carbon dioxide), conductance [64] and resistance indices [65,66] can also be calculated based on the following formula:

$$\text{Cerebrovascular Reactivity} = \frac{\Delta \text{ Cerebral Blood Flow Velocity (cm/s)}}{\Delta \text{ Partial Pressure of End - Tidal Carbon Dioxide (mmHg)}}$$

$$\text{Cerebrovascular Conductance Index} = \frac{\text{Cerebral Blood Flow Velocity (cm/s)}}{\text{Mean Arterial Blood Pressure (mmHg)}}$$

$$\text{Cerebrovascular Resistance} = \frac{\text{Mean Arterial Blood Pressure (mmHg)} - \text{Mean Intracranial Pressure (mmHg)}}{\text{Cerebral Blood Flow Velocity (cm/s)}}$$

$$\text{Cerebrovascular Resistance Index} = \frac{\text{Mean Arterial Blood Pressure (mmHg)}}{\text{Cerebral Blood Flow Velocity (cm/s)}}$$

To conclude, the noninvasiveness, repeatability, portability and high temporal resolution of transcranial Doppler ultrasound have promoted its use, especially in continuous bedside monitoring of cerebral hemodynamics.

## II. Near-Infrared Spectroscopy

Near-infrared spectroscopy is a noninvasive optical imaging technique that allows the penetration of near-infrared light (wavelength range from 700 to 900 nm) for the continuous real-time assessment of tissue blood volume and oxygenation [67,68]. In fact, three important chromophores for this technique are cytochrome *c* oxidase (C*c*O), deoxyhemoglobin (HHb), and oxyhemoglobin (O<sub>2</sub>Hb), while the concentration of these varies with oxygenation and metabolic status of tissue under investigation [69]. Each chromophore has a unique absorption spectrum, where the specific extinction coefficient is expressed as a function of wavelength [68]. Although C*c*O is a mitochondrial enzyme that changes with intracellular oxygenation status, its concentration is not entirely the result of changes in oxygen availability and its signal is ten times smaller than hemoglobin [70]. Therefore, HHb and O<sub>2</sub>Hb are taken into consideration during measurement as they are responsible for the transport, delivery, and removal of carbon dioxide and oxygen [71]. This technique is based on the modified Beer-Lambert law [72] and mathematically expressed as:

$$A = \log\left(\frac{I}{I_0}\right) = \epsilon \times [C] \times d \times DPF + G$$

- A = light attenuation
- I = emerged light
- I<sub>0</sub> = incident light
- $\epsilon$  = specific extinction coefficient



- C = chromophore concentration
- d = inter-optode distance
- DPF = differential path-length factor
- G = loss fraction of light due to scattering

So far, three main categories of near-infrared spectroscopy i.e., frequency domain, time domain, and continuous wave have been developed, each with various levels of complexity and distinct types of information they can retrieve [72,73]. Here, I will focus on spatially resolved spectroscopy that is categorized under continuous wave spectroscopy and provides tissue oxygenation and blood volume by the tissue oxygenation index, expressed in %, and the tissue hemoglobin index, expressed in arbitrary units (a.u.), respectively. Whereas Beer-Lambert parameters indicate changes in the concentration of oxyhemoglobin + oxymyoglobin ( $O_2Hb$ ), deoxyhemoglobin + deoxymyoglobin (HHb), and total hemoglobin ( $tHb = O_2Hb + HHb$ ), expressed in  $\mu\text{mol/L}$ .

A particular feature of spatially resolved spectroscopy is its capacity to focus the measurement in depth thus excluding the hemodynamic contribution from superficial tissue, namely the skin and subcutaneous tissues [69]. This is relevant for both muscle and cerebral studies as changes in cutaneous circulation may take place during exercise for thermoregulatory reasons [74] as well as on the scalp due to sympathetic activation e.g., during cognitive tasks, emotional stimulation, or vegetative tests [75–77].

It is well known that near-infrared spectroscopy does not provide a direct measurement of blood flow. However, if a condition of constant metabolism can be hypothesized (e.g., in completely relaxed muscles), changes in blood flow would be associated with

concordant changes in tissue oxygenation and, consequently, changes in oxygenation may be used as a surrogate of blood flow [78]. To conclude, this hemodynamic technique has several advantages including a high degree of sensitivity and selectivity to extracranial and intracranial changes [79] and allows measurements with a high time resolution and a good signal-to-noise ratio [80].

#### **D. Hypnotizability and Its Assessment**

Susceptibility to hypnosis or hypnotizability are usually associated with the proneness to modify perception, memory, and behavior according to mental images [81]. In particular, the individuals scoring high on hypnotizability scales can reduce their perception of acute, procedural, and chronic pain through their own cognitive strategies [82]. Hypnotizability, however, is a very pervasive psychophysiological and dispositional trait characterized by different attentional abilities, sensory-cognitive information processing, and cardiovascular control [83] as well as by structural and functional brain variants [84–86]. It can be measured by various scales focused on behavior and/or experience [87].

The scale used in the reported studies is the Italian version of the Stanford Hypnotic Susceptibility Scale [88]. It includes motor and cognitive items indicating motor inhibition, hallucination, and dissociation abilities and its administration requires ~20 min [88]. It classifies subjects through 12 items that can be passed or not passed (score: min 0 and max 12) and can be divided into three groups [89]. Namely,

- Lows (score: 0 – 4 out of 12)
- Mediums (score: 5 – 7 out of 12)
- Highs (score: 8 – 12 out of 12)

Alternatively, if the subjects are less than they can be divided into two groups and in this case, subject with a score of 6 will be excluded [88,90,91]:

- Low-to-Medium (Med-Lows range: 0 – 5)
- Medium-to-High (Med-Highs range: 7 – 12)

Though, some researchers and clinicians use alternative scales, such as Hypnotic Induction Profile and Harvard Group Scale of Hypnotic Susceptibility, perhaps Stanford Hypnotic Susceptibility Scale remains the *gold standard* for the reliable measurement of hypnotic susceptibility [92].

### **E. Masticatory and Limb Muscles**

Human masticatory muscles are skeletal muscles, categorized into elevator (masseter, temporalis, and medial pterygoid) and depressor (lateral pterygoid, digastric, mylohyoid, and geniohyoid) muscles [93].

The masseter muscle is a composite masticatory multipennate jaw-closing muscle with superficial, intermediate, and deep portions with three heads that originate from the zygomatic arch [93]. The contraction force of the superficial portion of this muscle results in elevation, contralateral movements, and mandibular protrusion. The intermediate and deep portions of this muscle allow retrusive mandibular movements together with the action of the pterygoid muscles, which also favors contralateral and ipsilateral movements during mandibular elevation [94].

Compared to limb and trunk muscles, the masticatory muscles: a) possess a higher percentage of hybrid fibers, and express more type I, type II, and fetal myosin heavy chain isoforms; b) present a smaller volume of single fibers [95]; and c) present a higher capillary density [96]. More specifically, type I fibers are more abundant in percentage and associated with higher expression of myosin light chain in the masseter

than limb and trunk muscles [97]. The numerous type I fibers with a small cross-sectional area in the masticatory muscles could facilitate greater nutrient and oxygen exchange with the extracellular environment, and increase fiber resistance to fatigue [95]. These muscles resist fatigue better than upper limbs due to the rich capillary supply and comparatively high oxidative enzyme activity in the type II fibers. Hence, in masticatory muscles, a finer gradation of force and contraction speeds is possible than in limb and trunk muscles. The presence of localized motor unit territories and task-specific motor unit activity facilitates differential control of separate muscle portions [98]. The differences during complex functional tasks (such as mastication, postural control, and facial expression), reflect a relatively higher need and demand for blood supply in the masticatory and orofacial muscles [96].

## **F. Muscle Activity and Its Assessment**

The electrical activity of the muscles is generated by the firing of motor neurons and causes skeletal muscle fibers to contract. This muscle activity can be detected using electromyography to provide information on the recruitment and firing patterns of motor units within the muscle. There are two main types of electromyography: a) surface electromyography (which involves placing surface electrodes on the skin above the muscle); and b) intramuscular electromyography (which involves placing fine-wire or needle electrodes directly in the muscle) [99].

In humans, surface electromyography can be measured using either single differential or multi-differential electrodes noninvasively. Single differential electrodes consist of two small metal plates that are placed on the skin surface directly over the muscle of interest. Multi-differential electrodes consist of an array of electrodes that are placed at multiple locations on the muscle surface, providing more detailed information on the propagation and distribution of action potentials over the muscle's surface [100].

Surface electromyographic activity can be quantified in terms of amplitude (root mean square) and frequency (median/mean/peak) of the power spectrum: the former depends on the recruitment and firing rate of motor units and may be used as an index of contraction intensity; the latter may be an index of fatigue development, as the power spectrum tends to shift towards lower frequencies with increasing muscle fatigue. However, surface electromyography is also affected by skin impedance, electrode placement, and crosstalk from adjacent muscles, which can affect the accuracy and reliability of the recordings. Additionally, it can only provide information on the muscle's electrical activity and does not provide direct information on muscle force or contractile properties [101].

Overall, surface electromyography is a valuable tool to study the relationship between muscle activity and other physiological measures such as heart rate variability and blood pressure [78]. Its non-invasive nature, ease of use, and ability to provide detailed information on individual muscle activation patterns and the effects of various interventions on muscle activity make it a popular choice in research and clinical settings.

## AIMS OF THE THESIS

In this thesis the multifaceted control of blood flow is investigated to address specific physiological issues of cerebral and muscle circulation.

### **A. Assessment of Cerebrovascular Reactivity in Hypnotizable vs. Non-Hypnotizable Subjects**

Previous studies evidenced hypnotizability-related differences in the control of peripheral circulation. Particularly, the research was motivated by the observation that brachial artery post-occlusion flow-mediated dilatation is differently affected in low- and high-hypnotizable groups of individuals. In the latter, flow-mediated dilatation was neither influenced by mental stress nor nociceptive stimulation, as compared to lows with decreased flow-mediated dilatation [102,103]. Based on functional magnetic resonance imaging, *Hoefl et al.* reported greater resting state brain sub-region functional connectivity between the left dorsolateral prefrontal cortex and the dorsal anterior cingulate cortex among highs compared to lows [104]. Also evidenced by the multiple reports of highs' higher absorption in cognitive tasks as compared to lows [86,105,106], measured by the Tellegen Absorption Scale [107]. Moreover, topological analysis using electroencephalography revealed that purely sensory stimulation may be processed differentially by med-highs and med-lows, as suggested for the sensorimotor actual and imagined information [108]. Whereas, there was no information on possible hypnotizability-related influence on cerebral circulation. Therefore, different types of cerebrovascular reactivity to cognitive (mental computation and trail making tasks), chemical (hyperventilation and rebreathing), and sensory (visual) stimuli are investigated with transcranial Doppler ultrasound and near-infrared spectroscopy techniques. Hence, I addressed the following questions in **Papers I to III** related to cerebral circulation in healthy humans.

a) Whether middle cerebral artery flow velocity is influenced by hypnotizability during hyperventilation, rebreathing, mental computation, and trail making tasks (**Paper I**).

b) Whether changes in partial pressure of end-tidal carbon dioxide, heart rate, and arterial blood pressure are associated with changes in middle cerebral artery flow velocity in med-low and med-high hypnotizable subjects (**Paper I**).

c) Whether neurovascular coupling is differentially associated with med-low and med-high hypnotizable subjects during cognitive (mental computation and trail making) tasks (**Paper II**).

d) Whether posterior cerebral artery flow velocity is influenced by hypnotizability during visual stimulation (**Paper III**).

## **B. Assessment of Vascular Reactivity to Stress in Masticatory and Limb Muscles**

The research was motivated by the fact that different patterns of sympathetic activation may be elicited by different stressors (stressor-specificity) [109,110], with differential activation to the various organs and tissues [111]. There is evidence that sympathetic outflow also varies depending on the body area, e.g., in arms and legs [112,113]. In some cases, dilatory responses to stress were reported in the masseter muscle [114]. Whether a differentiated hemodynamic response to stress also concerns the skeletal muscles of the head is unclear. To our knowledge, no comparative studies based on the simultaneous recording from head and limb muscles were ever reported. I focused on two human masticatory muscles (masseter and temporalis). Among head muscles, temporalis muscle hemodynamics is rarely investigated and previous research lacks evidence regarding the possible interference from brain hemodynamics. To address this issue, I establish a technique based on near-

infrared spectroscopy for reliable monitoring of muscle hemodynamics. Further, this technique helps me to monitor two masticatory muscles (masseter and temporalis) simultaneously in response to stress. To achieve the above aims, I addressed the following specific aims in **Papers IV to VI** related to skeletal muscle hemodynamics in healthy humans.

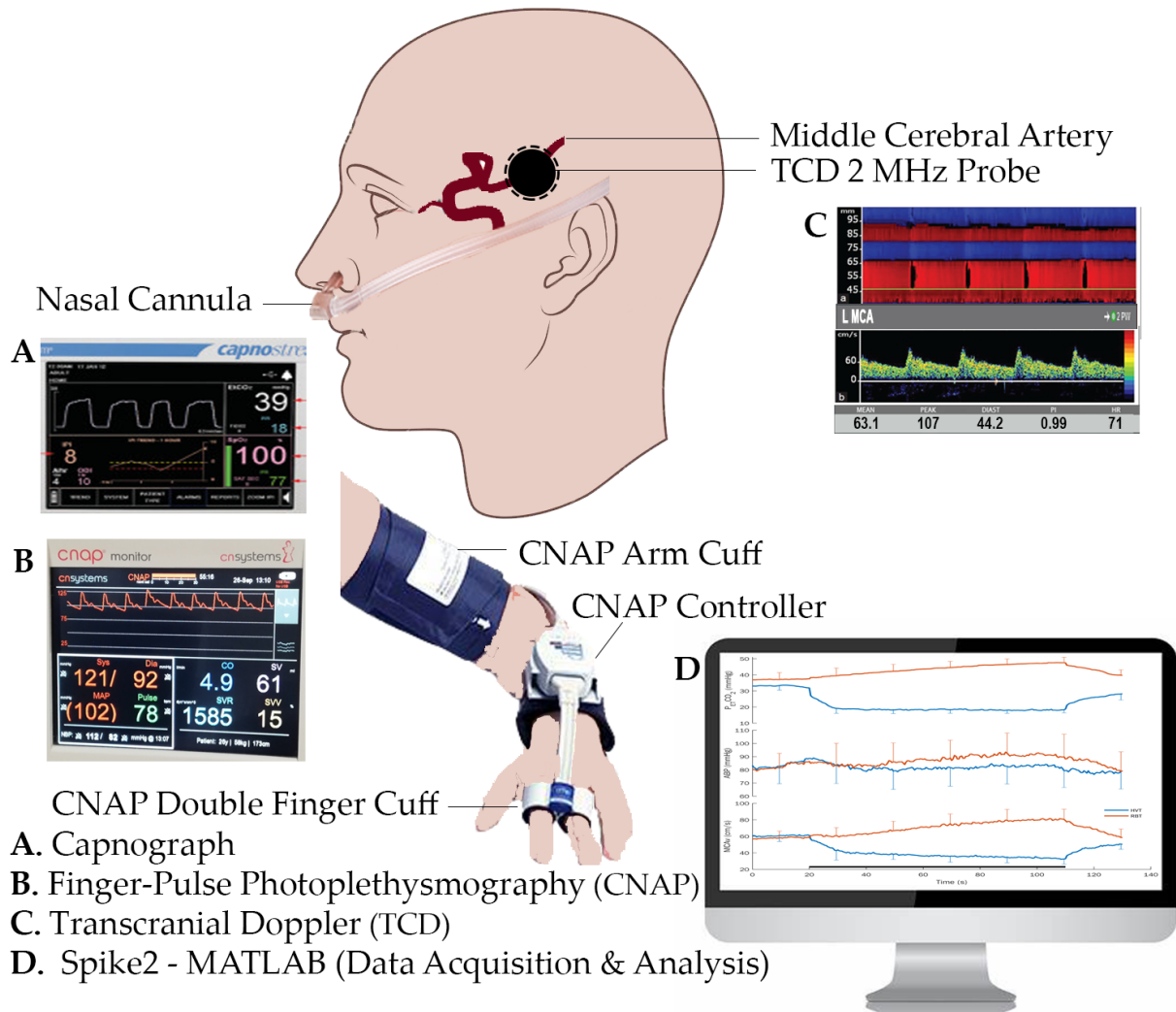
- a) To investigate whether the masseter and biceps brachii muscles' blood flow is differentially controlled in a stressor-dependent way (**Paper IV**).
- b) To address the reliability of near-infrared spectroscopy monitoring in detecting hemodynamic changes in the temporalis muscle to rule out the possible inference from cerebral hemodynamics (**Paper V**).
- c) To investigate and compare the sympathetic hemodynamic effects in masseter and temporalis muscles in a stressor-dependent way (**Paper VI**).
- d) To test whether the absence of stress-induced vasoconstriction was peculiar to masseter muscle or rather a common feature of head muscles (**Paper VI**).

### **C. Additional Research**

In addition, I had got a couple of collaborative opportunities (in this limited doctoral time period, while managing allied administrative matters simultaneously) to participate in research activities that are only partially related to the above-stated aims. The outcomes of the published research (from **Paper VII to XIV**) are, therefore, not included in the main results but are provided in the appendix (at the end of this doctoral thesis).



# RESULTS



- A. Capnograph
- B. Finger-Pulse Photoplethysmography (CNAP)
- C. Transcranial Doppler (TCD)
- D. Spike2 - MATLAB (Data Acquisition & Analysis)

## GRAPHICAL ABSTRACT

# Cerebral Blood Flow in Healthy Subjects with Different Hypnotizability Scores

Anas Rashid <sup>1</sup>, Enrica Laura Santarcangelo <sup>2,\*</sup> and Silvestro Roatta <sup>1</sup>

<sup>1</sup> Lab of Integrative Physiology, Department of Neuroscience “Rita Levi Montalcini”, University of Torino, Torino 10125, Italy; anas.rashid@unito.it (A.R.); silvestro.roatta@unito.it (S.R.)

<sup>2</sup> Lab of Cognitive and Behavioral Neuroscience, Department of Translational Research and New Technologies in Medicine and Surgery, University of Pisa, Pisa 56127, Italy

\* Correspondence: enrica.santarcangelo@unipi.it; Tel.: +39 050 2213465

**Abstract:** Hypnotizability is a cognitive trait associated with differences in the brachial artery flow-mediated dilatation of individuals with high hypnotizability (highs) and low hypnotizability scores (lows). The study investigated possible hypnotizability-related cerebrovascular differences. Among 24 healthy volunteers, the Stanford Hypnotic Susceptibility Scale Form A identified 13 medium-to-lows (med-lows), 11 medium-to-highs (med-highs), and 1 medium hypnotizable. Hypnotizability did not influence the significant changes produced by the trail making task (TMT), mental arithmetic task (MAT), hyperventilation (HVT), and rebreathing (RBT) on heart rate (HR), arterial blood pressure (ABP), and partial pressure of end-tidal CO<sub>2</sub> (P<sub>ET</sub>CO<sub>2</sub>), but moderated the correlations between the changes occurring during tasks with respect to basal conditions ( $\Delta$ ) in ABP and P<sub>ET</sub>CO<sub>2</sub> with middle cerebral artery flow velocity (MCAv). In HVT, med-lows exhibited a significant correlation between  $\Delta$ MCAv and  $\Delta$ P<sub>ET</sub>CO<sub>2</sub>, and med-highs showed a significant correlation between  $\Delta$ ABP and  $\Delta$ MCAv. Cerebrovascular reactivity (CVR) and conductance ( $\Delta$ CVCi) were significantly correlated with  $\Delta$ MCAv only in med-lows during HVT and RBT. For the first time, cerebrovascular reactivity related to hypnotizability was investigated, evidencing different correlations among hemodynamic variables in med-highs and med-lows.

**Citation:** Rashid, A.; Santarcangelo, E.L.; Roatta, S. Cerebral Blood Flow in Healthy Subjects with Different Hypnotizability Scores. *Brain Sci.* **2022**, *12*, 558. <https://doi.org/10.3390/brainsci12050558>

Academic Editor: Luigi De Gennaro

Received: 23 February 2022

Accepted: 26 April 2022

Published: 26 April 2022

**Publisher’s Note:** MDPI stays neutral with regard to jurisdictional claims in published maps and institutional affiliations.



**Copyright:** © 2022 by the author. Licensee MDPI, Basel, Switzerland. This article is an open access article distributed under the terms and conditions of the Creative Commons Attribution (CC BY) license (<https://creativecommons.org/licenses/by/4.0/>).

**Keywords:** TCD; NIRS; hyperventilation; rebreathing; cognitive tasks; hypnotic susceptibility

## 1. Introduction

Hypnotizability—the proneness to modify perception, memory, and behavior according to specific suggestions and to enter a hypnotic state [1]—is a psychophysiological trait [2] measured by scales whose scores are stable during adulthood [3]. Individuals with high- (highs) and low-hypnotizability scores (lows) display different morpho-functional brain characteristics mainly concerning the salience and executive networks [4] and the cerebellum [5]. They also exhibit differences in the cognitive, sensorimotor, and cardiovascular domains observable in the absence of hypnotic induction and suggestions, thus being relevant to everyday life [2]. For instance, with respect to lows and medium-hypnotizable individuals (mediums), highs show a greater ability in respect of attention and dissociation [6–8], stronger functional equivalence between imagery and perception [9,10], low interoceptive accuracy [11], greater interoceptive sensitivity [12], and less close postural and visuomotor control [2].

In the vascular system, the brachial artery post occlusion flow-mediated dilatation (FMD) is similar in highs and lows in basal conditions, whereas FMD is less impaired in highs than in lows during nociceptive stimulation [13] and is not impaired at all in highs during mental stress, at variance with lows and the general population [14,15]. This can be accounted for by different control of the release of nitric oxide (NO) by endothelial cells [16] in highs and lows/general population during cognitive and physical stimulation.

Hypnotizability-related differences in the cerebral artery blood flow are possibly due to different NO availability, which has not been studied. They could be relevant to the observed negative correlation between hypnotizability and brain total grey matter volume [4,5,8]. NO is required, in fact, for the development and maturation of the nervous tissue, but its excessive amount can be toxic, mainly for regions particularly rich in NO such as the cerebellum and hippocampus [17].

### *1.1. Changes in the Cerebral Artery Diameter Induced by Hypercapnia/Hypocapnia and Arterial Pressure*

In the brain tissue, perfusion, or cerebral blood flow (CBF), is a measure of the rate of delivery of arterial blood to a capillary bed [18]. Hypocapnia is associated with reduced CBF [19], NO availability [20], and artery diameter [21], not depending on extracellular pH [22]. It seems unlikely that the formation of NO is the only mechanism involved in hypercapnia, because increases in CBF during very high levels of hypercapnia (>100 mmHg) are not altered by the inhibition of NO synthase (NOS). In contrast, vasodilation during moderate hypercapnia appears to be dependent on the production of NO due to increased activity of NOS [23]. Another possibility is that NO is not the direct mediator of vessel relaxation, but that normal basal levels of NO and/or cyclic guanosine monophosphate (cGMP) are required for the response to hypercapnia to occur [24].

The hypothesis that artery dilation may be mediated by a decreased pH in the extracellular fluid, as CO<sub>2</sub> freely diffuses across the cerebrovascular endothelium, is contradicted by experiments reporting the effects of blockade of the cerebrovascular action of CO<sub>2</sub> by brainstem lesions [25,26] or decerebration [27–29], cholinergic blockers [30–33], inhibitors of prostaglandin [34,35], and NO synthesis [36].

Cerebrovascular changes induced by increased or decreased CO<sub>2</sub> cannot be reliably studied without concomitant assessment of arterial blood pressure [37]. It has also been shown, however, that NO release is not obligatory for cerebrovascular reactivity to CO<sub>2</sub>, whereas transient increases in CBF induced by increases in blood pressure mostly rely on NO release [38]. Cerebral autoregulation, in fact, stabilizes blood flow by buffering the steady state increase in cerebral perfusion pressure, but cannot compensate for brief elevations in blood pressure and consequent increases in CBF [39,40].

### *1.2. Changes in the Cerebral Artery Diameter Induced by Brain Activity*

NO mediates the brain vessel dilation, which follows increased neuronal activity leading to the increased need for O<sub>2</sub> supply [41,42]. In this perspective, we may expect that hypnotizability-related differences in the cerebral artery diameters occur during cognitive tasks. The highs' greater proneness to focused attention and absorption [6,43], in fact, might enable them to activate task-related areas more than lows' and, thus, exhibit a larger increase in CBF. However, the highs' greater attentional abilities [43–45] may require less neural engagement, as observed, for instance, in motor imagery tasks performed by individuals with greater motor experience of those tasks [46]. In addition, the highs' and lows' modes of information processing—that is, their neural activities—is different. During sensory and cognitive tasks, the former display slight and diffuse changes in the general asset of brain activation, whereas the latter exhibit more localized task-related changes [9,47,48]. This may lead to negligible differences in the highs' brain metabolic changes during tasks with respect to basal conditions. Thus, we cannot reliably predict whether and how hypnotizability modulates cerebral hyperemia induced by cognitive tasks.

### *1.3. Aims of the Study*

The study aimed to assess a) whether the flow velocity in the middle cerebral artery (MCAv) is influenced by hypnotizability during cognitive tasks, hyperventilation, and

rebreathing; and b) how MCAv is associated with the partial pressure of end-tidal CO<sub>2</sub> and arterial blood pressure (ABP) in healthy subjects with different hypnotizability.

## 2. Materials and Methods

### 2.1. Subjects

A total of 24 healthy subjects (age:  $26.1 \pm 4.5$  years; 12 females and 12 males), 20 right-handed and 4 left-handed according to the Edinburgh Handedness Inventory [49], were enrolled in this study. They were all university students with no medical, neurological, and psychiatric disease; hypertension (resting blood pressure  $<120/80$  mmHg); sleep and attention disturbance; substance abuse throughout their life; or drug intake in the last 3 months, as self-reported while signing the informed consent.

### 2.2. Experimental Procedure

The hypnotic assessment was performed by the validated Italian version of the Stanford Hypnotic Susceptibility Scale (SHSS), Form A [50], which is a behavioral scale classifying highs (score: 8–12 items passed out of 12), mediums (score: 5–7 out of 12), and lows (score: 0–4 out of 12). It includes motor and cognitive items indicating motor inhibition, hallucination, and dissociation abilities and its administration requires approximately 20 min. It was administered to all participants by the same expert experimenter. Owing to the small number of participants, they were divided into two groups: medium-low (SHSS score: 0–5) and medium-high (SHSS score: 7–12) hypnotizable.

Experiments were conducted in a quiet, sound and light attenuated, temperature-controlled (21–23 °C) room between 9 and 11 AM, and 4 and 6 PM, at least 3 h after the latest food and caffeine/alcohol intake. Before starting the recordings, the partial pressure of end-tidal CO<sub>2</sub> ( $P_{ET}CO_2$ ) was measured and the signal visual feedback was provided to the participants, who were invited to relax sitting in an armchair. After all signals reached a stable condition, i.e., at least for 5 min, they were recorded for a 10 min baseline period and during a sequence of four tasks separated from each other by a minimum of a 5 min rest (with additional time if required by the participant) and randomly presented within med-lows and med-highs.

Since hypnotizability is a dispositional trait that is substantially stable through life [3], the recordings performed 2 months earlier than hypnotic assessment could be reliably studied as a function of hypnotizability.

### 2.3. Tests

Before starting the test sequence, participants were briefly familiarized with the tasks and respiratory maneuvers, particularly with the visual feedback during hyperventilation (described below). Each test consisted of a basal and a task condition. The test sequence was randomized for the different subjects.

#### 2.3.1. Trail Making Task (TMT)

The participant was instructed to connect numbers (1 to 40) and 21 Italian letters (A to Z) by lines in ascending sequence, which was performed on paper over 3 min with alternating numbers and letters (1 – A – 2 – B – 3 – C and so on).

#### 2.3.2. Mental Arithmetic Task (MAT)

The participant was asked to progressively subtract odd numbers (1, 3, 5, and so on) from 1000 for 3 min, writing each result on a paper. One operator standing behind the subject monitored the outcome, promptly asking the subject to repeat the calculation in case of error.

After TMT and MAT, the participant was invited to rate the experienced cognitive fatigue using a numerical rating scale from 0 (min) to 10 (max).

### 2.3.3. Hyperventilation (HVT)

The participant was asked to hyperventilate to achieve and maintain for 90 s 50% of the normal  $P_{ET}CO_2$ . To this end, they were provided with visual feedback from the display of the capnograph, which was continuously monitoring  $P_{ET}CO_2$  from the expiratory flow collected by a nasal cannula and a horizontal cursor placed at 50%  $P_{ET}CO_2$  indicating the target  $P_{ET}CO_2$ .

### 2.3.4. Rebreathing (RBT)

The nose was closed with the help of a nose clip. The participant was asked to take a large breath of room air and then exhale into a previously empty plastic bag, closing the bag so that it stayed full. Once the bag was full of expired air, the participant resumed normal breathing in and out of the closed bag, hence maintaining a spontaneous breathing frequency, and when the participant began to rebreathe, we started a stopwatch. The participant continued to rebreathe for 90 s. The mouthpiece was also connected with a sampling line to the capnograph to allow continuous recording of  $P_{ET}CO_2$ .

## 2.4. Measurements

The heart rate (HR, bpm) and arterial blood pressure (ABP, mmHg) were measured by continuous finger-pulse photoplethysmography (CNAP Monitor 500, CNSystems Medizintechnik GmbH, Graz, Austria). Calibration of ABP was periodically performed using a regular pneumatic cuff at the right arm.

A capnograph (Capnostream™ 20p Bedside Patient Monitor with Microstream™ Technology, Oridion Medical, Jerusalem, Israel) was used to monitor the partial pressure of end-tidal carbon dioxide ( $P_{ET}CO_2$ ) in the respiratory gases.

Transcranial Doppler (TCD) ultrasound with a 2 MHz monitoring probe (Dolphin IQ and 4D, Viasonix, Netanya, Israel) was used to measure unilateral cerebral flow velocity from the middle cerebral artery (MCAv, cm/s) during all tasks. The probe was held in place by a 3D-printed custom-made helmet.

Cerebrovascular reactivity (CVR, cm/s/mmHg) was computed as a ratio between task-related changes in MCAv and  $P_{ET}CO_2$  ( $\Delta MCAv/\Delta P_{ET}CO_2$ ), and cerebrovascular conductance index (CVCi, cm/s/mmHg) was computed as a ratio between MCAv and ABP.  $\Delta CVCi$  was computed as  $([MCAv/ABP]_t - [MCAv/ABP]_b)$ , where t and b represent task and basal values, respectively.

All signals were continuously digitally sampled (CED Micro 1401, Cambridge Electronic Design Ltd., Cambridge, UK) at 100 Hz and stored on a computer. Spike2 software (Version 9.14, Cambridge Electronic Design Ltd., Cambridge, UK) was used for both data acquisition and analysis.

## 2.5. Statistical Analysis

Statistical analysis was performed using MATLAB® Version R2022a (The MathWorks, Natick, MA, USA). After normality assessment (Kolmogorov–Smirnov test), the entire sample HR, ABP,  $P_{ET}CO_2$ , and MCAv were submitted to repeated-measures ANOVA according to a 4 test (basal(b)-TMT, b-MAT, b-HVT, b-RBT) × 2 condition (b, task) experimental design. Post hoc analyses were performed through paired t-tests. Since sample size did not allow a reliable comparison between groups, ANOVA was repeated using SHSS scores as a covariate.

For the tasks showing changes in MCAv with respect to basal conditions, Spearman coefficients able to reveal nonlinear correlations were computed between the averaged basal values of MCAv, ABP, and  $P_{ET}CO_2$ . Assuming that ABP and  $P_{ET}CO_2$  were the systemic variables influencing MCAv, the changes in MCAv ( $\Delta MCAv$ ), ABP ( $\Delta ABP$ ), and  $P_{ET}CO_2$  ( $\Delta P_{ET}CO_2$ ) occurring during tasks with respect to basal conditions were computed for the entire sample. The correlations of  $\Delta MCAv$  with  $\Delta ABP$  and  $\Delta P_{ET}CO_2$ , and with the derived variables, i.e., CVR and  $\Delta CVCi$ , were computed. Partial correlations controlling

for hypnotizability were also performed, and successive within-group correlations were studied when the entire sample partial correlations revealed a moderation by hypnotizability. For all analyses, significance was set at  $p = 0.05$ .

### 3. Results

Hypnotic assessment identified 11 lows (SHSS mean score  $\pm$  standard deviation (SD);  $2 \pm 1.58$ ), 5 mediums ( $6 \pm 1$ ), and 8 highs ( $8.5 \pm 0.71$ ). Excluding the subject with SHSS score = 6, the sample included 13 medium-lows (med-lows; SHSS range: 0–5; mean score  $\pm$  SD:  $1.38 \pm 1.98$ ) and 10 medium-highs (med-highs; SHSS range: 7–12; mean score  $\pm$  SD:  $8.1 \pm 0.73$ ).

On a numerical rating scale ranging from 0 (minimum) to 10 (maximum), the experienced cognitive fatigue during TMT and MAT tasks considered together (Mean  $\pm$  SD) was  $6.5 \pm 0.63$  (med-lows:  $6.27 \pm 0.63$ ; med-highs:  $6.75 \pm 0.54$ ).

Systemic and Doppler variables exhibited different changes during the four tasks with respect to basal conditions, which were not influenced by hypnotizability (repeated-measures ANOVA). Correlational analysis, in contrast, revealed hypnotizability-related differences in the correlation of MCAv with ABP (which was significant only in med-highs) and with  $P_{ET}CO_2$  (which was significant only in med-lows); these were the main findings of the study, together with the observation that ABP and  $P_{ET}CO_2$  jointly control CVR and  $\Delta CVC_i$  only in med-lows. Table 1 reports mean values and standard deviations of HR, ABP,  $P_{ET}CO_2$ , and MCAv.

**Table 1.** Variable mean values and standard deviations.

Condition	Variable	Med-lows		Med-highs	
		Mean	SD	Mean	SD
<b>TMT</b>					
Basal	HR (bpm)	72.02	12.08	78.50	14.66
	ABP (mmHg)	82.29	17.23	80.71	14.66
	$P_{ET}CO_2$ (mmHg)	37.31	1.91	34.63	3.45
	MCAv (cm/s)	59.52	9.61	52.13	10.43
Task	HR* (bpm)	79.09	13.66	81.62	14.46
	ABP* (mmHg)	87.95	14.72	86.56	13.98
	$P_{ET}CO_2$ (mmHg)	37.13	1.40	34.46	3.43
	MCAv (cm/s)	59.02	10.10	50.18	9.87
<b>MAT</b>					
Basal	HR (bpm)	75.98	11.61	76.50	14.10
	ABP (mmHg)	78.19	14.59	83.71	15.15
	$P_{ET}CO_2$ (mmHg)	36.51	1.92	34.53	3.29
	MCAv (cm/s)	60.25	8.70	52.56	10.61
Task	HR* (bpm)	84.20	12.41	84.51	15.00
	ABP* (mmHg)	88.64	12.91	96.89	9.80
	$P_{ET}CO_2$ (mmHg)	36.96	2.61	34.91	3.68
	MCAv (cm/s)	61.60	10.27	55.66	11.87
<b>HVT</b>					
Basal	HR (bpm)	72.93	10.09	77.88	11.36
	ABP (mmHg)	85.65	12.47	83.03	14.77
	$P_{ET}CO_2$ (mmHg)	33.61	2.49	32.21	3.73
	MCAv (cm/s)	61.25	7.24	59.68	6.67
Task	HR* (bpm)	99.34	19.71	84.12	13.01
	ABP (mmHg)	83.58	12.93	82.53	10.65
	$P_{ET}CO_2^*$ (mmHg)	18.34	1.46	17.92	1.59
	MCAv* (cm/s)	34.19	7.07	33.35	5.17
<b>RBT</b>					
Basal	HR (bpm)	74.26	9.36	76.77	11.24
	ABP (mmHg)	78.35	12.82	85.23	11.25

	P <sub>ET</sub> CO <sub>2</sub> (mmHg)	38.15	4.47	35.96	4.05
	MCAv (cm/s)	58.38	6.51	56.53	9.58
Task	HR* (bpm)	87.52	11.91	87.57	13.70
	ABP* (mmHg)	88.47	11.57	95.33	17.84
	P <sub>ET</sub> CO <sub>2</sub> * (mmHg)	48.12	3.13	46.08	3.22
	MCAv* (cm/s)	82.71	13.50	75.59	11.53

Note: HR: heart rate; ABP: arterial blood pressure; P<sub>ET</sub>CO<sub>2</sub>: partial pressure of end-tidal CO<sub>2</sub>; and MCAv: middle cerebral artery flow velocity. (\*) statistically significant differences between basal and task conditions in the entire sample. No significant difference in any of the variables was observed between the two groups.

### 3.1. Differences between Med-Highs and Med-Lows

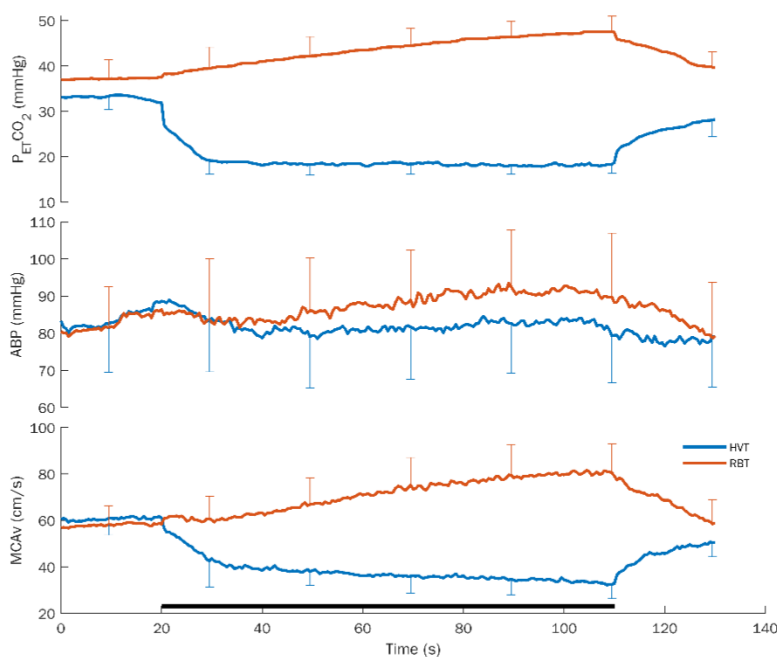
#### 3.1.1. Systemic Measures

Systemic variables did not exhibit significant difference between the two groups. In detail: HR exhibited a significant test x condition interaction ( $F(3,69) = 7.511, p = 0.002, \eta^2 = 0.246, \alpha = 0.982$ ) whose decomposition revealed significant increases during tasks for all tests (TMT,  $t = 4.561$ ; MAT,  $t = 4.895$ ; HVT,  $t = 5.048$  and RBT,  $t = 8.306$ ;  $p = 0.0001$ ). It survived after controlling for SHSS scores and was sustained by larger values during HVT than during MAT ( $t = 2.138, p = 0.043$ ) and TMT ( $t = 3.242, p = 0.004$ ).

For ABP, ANOVA revealed a significant test x condition interaction ( $F(3,69) = 218.26, p = 0.0001, \eta^2 = 0.905, \alpha = 1.00$ ), surviving after controlling for SHSS scores. Its decomposition showed significant differences between basal and task conditions for TMT ( $t(1,23) = 3.27, p = 0.003$ ), MAT ( $t = 6.47, p = 0.0001$ ), and RBT ( $t = 4.25, p = 0.0001$ ), but not for HVT.

P<sub>ET</sub>CO<sub>2</sub> exhibited a significant test x condition interaction ( $F(3,69) = 566.28, p = 0.0001, \eta^2 = 0.961, \alpha = 1.00$ ), which remained significant after controlling for SHSS scores. Decomposition revealed significant basal vs. task differences for HVT ( $t = 24.18, p = 0.0001$ ) and RBT ( $t = 18.73, p = 0.0001$ ) only.

Average response curves for hyperventilation (HVT) and rebreathing (RBT) with standard deviation for P<sub>ET</sub>CO<sub>2</sub>, ABP, and MCAv are shown in Figure 1.



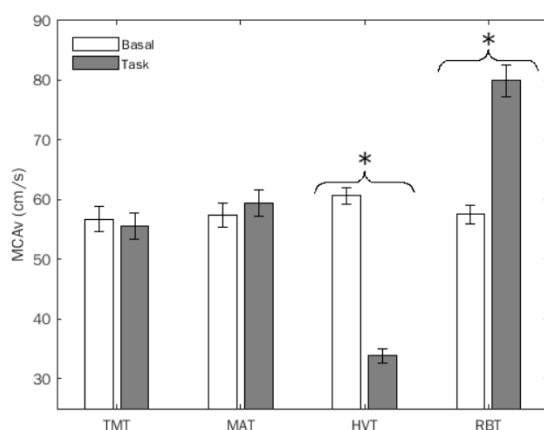
**Figure 1.** Average response curves for hyperventilation (HVT) and rebreathing (RBT) with standard deviation for the different variables. P<sub>ET</sub>CO<sub>2</sub>: partial pressure of end-tidal CO<sub>2</sub>; ABP: arterial blood pressure; and MCAv: middle cerebral artery flow velocity. The black bar at the bottom indicates the duration of the task. Note the opposite effects on each variable exhibited by the HVT and RBT.



### 3.1.2. Doppler Measures

Doppler variables did not exhibit significant differences between the two groups. In detail: MCAv exhibited a significant test  $\times$  condition interaction ( $F(3,69) = 217.48, p = 0.0001, \eta^2 = 0.904, \alpha = 1.00$ ), which remained significant considering SHSS as a covariate. As shown in Figure 2, its decomposition revealed a significant difference between basal and task conditions for HVT ( $t(1,23) = 24.91, p = 0.0001$ ) and RBT ( $t = 12.58, p = 0.0001$ ) only.

For the derived variable  $\Delta\text{CVC}_i$ , the significant test  $\times$  condition interaction ( $F(3,69) = 73.30, p = 0.0001, \eta^2 = 0.761, \alpha = 1.00$ ), which survived after controlling for hypnotizability, was sustained by a significant difference between basal and task conditions in all tests (TMT,  $t = 2.93, p = 0.008$ ; MAT,  $t = 3.51, p = 0.002$ ; HVT,  $t = 16.48, p = 0.0001$ ; and RBT,  $t = 6.98, p = 0.0001$ ).



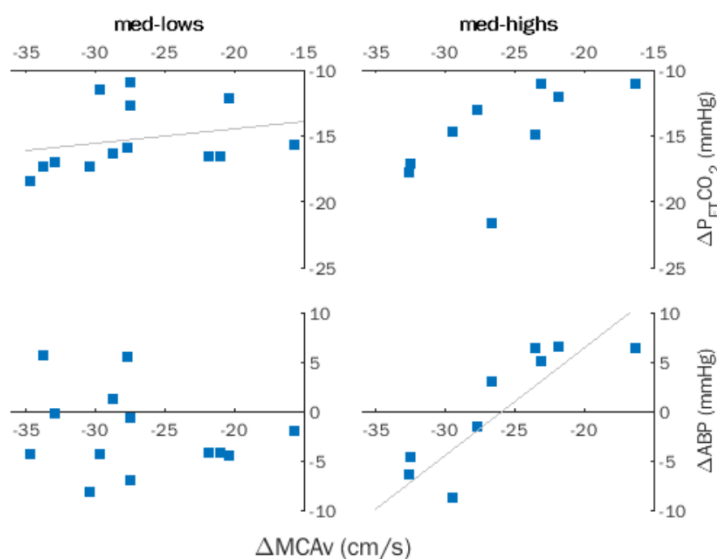
**Figure 2.** Middle cerebral artery flow velocity (MCAv) (mean, SEM) of the entire sample. TMT: trail making task; MAT: mental arithmetic task; HVT: hyperventilation; RBT: rebreathing. \*, statistically significant differences.

### 3.2. Associations between Systemic and Doppler Variables

Since MCAv did not exhibit significant differences between basal and experimental conditions in TMT and MAT, further analyses were conducted only on HVT and RBT.

#### 3.2.1. Hyperventilation (HVT)

Spearman coefficients computed for  $\Delta\text{MCA}_v$ ,  $\Delta\text{ABP}$ , and  $\Delta\text{P}_{\text{ETCO}_2}$  for the entire sample indicated a significant correlation between  $\Delta\text{MCA}_v$  and  $\Delta\text{P}_{\text{ETCO}_2}$  ( $\rho = 0.484, p = 0.017$ ), which became non-significant after removing the effects of hypnotizability by partial correlation. Successive within-group analyses revealed a significant correlation between  $\Delta\text{MCA}_v$  and  $\Delta\text{P}_{\text{ETCO}_2}$  ( $\rho = 0.606, p = 0.028$ ) and disclosed a significant correlation of  $\Delta\text{MCA}_v$  with  $\Delta\text{ABP}$  ( $\rho = 0.842, p = 0.002$ ) in med-highs (Figure 3).



**Figure 3.** Hyperventilation (HVT). Within-group correlations between changes in middle cerebral artery flow velocity (MCAv), partial pressure of end-tidal CO<sub>2</sub> (P<sub>ET</sub>CO<sub>2</sub>), and arterial blood pressure (ABP) in med-lows and med-highs. Trendlines indicate significant correlations.

In the entire sample, the significant correlations of  $\Delta$ MCAv and CVR ( $\rho = -0.533$ ,  $p = 0.007$ ) and  $\Delta$ CVCi ( $\rho = 0.598$ ,  $p = 0.002$ ) became non-significant after removing the effects of hypnotizability. Indeed, only med-lows exhibited significant correlations of  $\Delta$ MCAv with CVR ( $\rho = -0.602$ ,  $p = 0.020$ ) and  $\Delta$ CVCi ( $\rho = 0.861$ ,  $p = 0.0001$ ).

CVR and  $\Delta$ CVCi mean values and standard deviations are reported in Table 2.

**Table 2.** Derived Doppler variables.

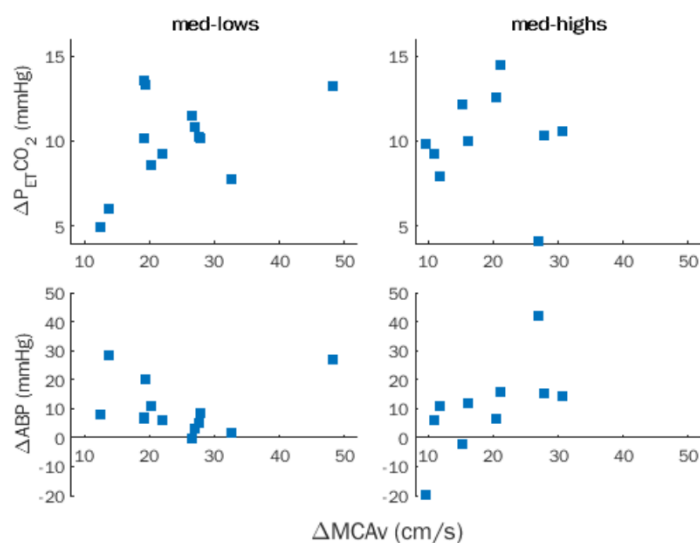
Task	Variable	Med-lows		Med-highs	
		Mean	SD	Mean	SD
HVT	$\Delta$ CVCi (cm/s/mmHg)	-0.32	0.12	-0.33	0.07
	CVR (cm/s/mmHg)	1.81	0.46	1.91	0.49
RBT	$\Delta$ CVCi (cm/s/mmHg)	0.18	0.12	0.16	0.13
	CVR (cm/s/mmHg)	2.49	0.76	2.17	1.66

Note: CVCi: cerebrovascular conductance index; CVR: cerebrovascular reactivity.

### 3.2.2. Rebreathing (RBT)

No significant correlation between  $\Delta$ MCAv with  $\Delta$ P<sub>ET</sub>CO<sub>2</sub> and  $\Delta$ ABP was observed in the entire sample and was disclosed after removing the effects of hypnotizability (Figure 4).

$\Delta$ MCAv was significantly correlated with CVR ( $\rho = 0.818$ ,  $p = 0.0001$ ), but not with  $\Delta$ CVCi, and the correlation survived after removing the effects of hypnotizability ( $\rho = 0.629$ ,  $p = 0.001$ ).



**Figure 4.** Rebreathing (RBT). Within-group correlations between changes in middle cerebral artery flow velocity (MCAv), partial pressure of end-tidal CO<sub>2</sub> (P<sub>ET</sub>CO<sub>2</sub>), and arterial blood pressure (ABP) in med-lows and med-highs.

#### 4. Discussion

Our study was motivated by the observation of different brachial artery post-occlusion FMD in lows and highs. In the latter, FMD was scarcely and not influenced by nociceptive stimulation and mental stress, respectively, in contrast to lows who behaved like the general population [13,14], displaying decreased FMD. We wondered whether hypnotizability-related differences may also occur in the cerebrovascular responses to physical and mental stimulation.

##### 4.1. Comparisons between Groups

The absence of significant changes in blood flow velocity during cognitive tasks in both groups contrasts with other authors' findings reporting increased blood flow with increasing cognitive load in the general population [51]. However, Csipo et al. employed a visual text inspection task with high time pressure (a new task every 2 s); the methodological differences could account for different results. In addition, the discrepancy may be due to the characteristics of the studied sample, which does not reflect the distribution of hypnotizability in the general population [52]. The absence of increases in the middle cerebral artery blood flow, despite significant increases in systemic blood pressure, can be accounted for by the pre-eminent local control of cerebral blood flow. The similar results of med-lows and med-highs could be due to their different cognitive abilities, as med-lows may have paid poor attention to the tasks, and med-highs may have experienced low cognitive effort [9,43,45]. Thus, scarce neural engagement and, consequently, scarce increase in metabolism may have taken place in both groups.

The present findings confirm that, in the entire sample, hyperventilation and rebreathing induced a decrease and increase in middle cerebral artery flow velocity [53]. These responses occurred in the presence of significant changes in ABP only during rebreathing and in P<sub>ET</sub>CO<sub>2</sub> during both rebreathing and hyperventilation and were not moderated by hypnotizability.

##### 4.2. Association between Systemic and Doppler Variables

Even in the absence of significant differences between med-lows and med-highs in the mean values of ABP, P<sub>ET</sub>CO<sub>2</sub>, and MCAv, however, the task-related changes in these variables were differentially associated between each other in the two groups. This suggests different control mechanisms of blood flow velocity in med-lows and med-highs.

During HVT, in fact, within-group correlational analyses revealed different relevance of the chemical ( $P_{ETCO_2}$ ) and mechanical stimulation (ABP) to the med-lows' and the med-highs' cerebral blood flow velocity.

The absence of significant ABP changes during HVT does not allow us to exclude that the observed non-significant ABP decreases may have influenced the med-highs' changes in cerebral blood flow  $\Delta MCA_V$ . An opposite behavior occurred in med-lows, who exhibited a significant association between  $\Delta MCA_V$  and  $\Delta P_{ETCO_2}$ , indicating a preferential control of  $MCA_V$  by chemical stimulation.

Theoretically, the decrease in  $MCA_V$  observed in med-highs during HVT, despite scarce changes in ABP, could be sustained by more sensitivity of their vessel muscle cells to blood pressure. The effect of NO on precapillary sphincters and pericytes [54] may have contributed to the observed changes in  $MCA_V$ .

The lack of significant correlation between  $\Delta MCA_V$  and  $\Delta P_{ETCO_2}$  occurring in both groups during RBT may be due to  $CO_2$  ceiling effects.

During both hyperventilation and rebreathing, an association of cerebrovascular reactivity (CVR, related to  $P_{ETCO_2}$ ) and cerebrovascular conductance index (CVCi, related to ABP) was found only in med-lows. We hypothesize that a different interaction between arterial blood pressure and  $CO_2$  [37] occurred in med-highs and med-lows, respectively, owing to the presence of different local metabolic conditions depending on different modes of information processing [9].

## 5. Limitations and Conclusions

This study has a few limitations. One is the small sample size, which did not allow a direct comparison between highs, lows (each representing 15% of the general population), and mediums, which represent its largest part (70%) [52]. In a few tasks, in fact, highs or lows can behave like mediums [12]. Another limitation is the absence of very highly hypnotizable persons in the studied sample (the maximum SHSS score was 9 out of 12). Thus, the present study should be repeated in a larger sample including lows, mediums, and highs. Moreover, hemogas analyses may reflect blood  $CO_2$  better than end-tidal measures. Finally, given the complexity of the cerebrovascular control, recent approaches based on the complexity of the arterial pressure and cerebral blood flow time series may allow better detection of relationships between these two variables [55].

The present findings do not allow us to exclude the possibility that med-highs may exhibit a different association between ABP,  $P_{ETCO_2}$ , and CBF with respect to med-lows also when ABP increases instead of decreasing as occurs during HVT. In this respect, it may be interesting that more frequent increases in systemic blood pressure are likely to occur in highs than in lows owing to their greater emotional intensity, empathy [56,57], and interoceptive sensitivity [12,56]. In addition, changes in synaptic glutamate due to tasks could induce increases in astrocyte calcium-mediated dilatory action independently from systemic blood pressure [58]. Since highs respond to cognitive tasks with larger glutamatergic cortical activity [59], they might be more prone than lows to undergo astrocyte-dependent NO release in everyday life. Thus, the hypothesis that the earlier-observed highs' reduced cerebral grey matter volume [4,5] may be due to the toxic effects of too much NO availability during environmental stimulation cannot be excluded.

In conclusion, this is the first assessment of hypnotizability-related differences in the mechanisms controlling cerebral blood flow, cerebrovascular reactivity, and conductance in response to hyperventilation and rebreathing, given the med-highs preferential response to arterial blood pressure, the med-lows apparently better response to  $CO_2$ , and the different interaction between cerebrovascular conductance and reactivity in the two groups. The findings support the view that hypnotizability is associated with physiological correlates influencing everyday life independently from suggestions and induction of the hypnotic state [2,60]. Finally, it is noticeable that at variance with highs and lows, med-highs and med-lows represent half of the general population each. Thus, in a general perspective, the cerebrovascular reactivity of half of the population is expected to be more

sensitive to changes in systemic blood pressure and the other half to the local increases in CO<sub>2</sub> following the changes in blood pressure. Whether the different vascular reactivity to ABP changes of med-highs and med-lows is related to the different involvement of NO in the regulation of the vascular response remains to be ascertained. It may be speculated that this difference could influence the capacity to adapt to cerebrovascular insults.

**Author Contributions:** Conceptualization, A.R., E.L.S., and S.R.; methodology, A.R., E.L.S., and S.R.; formal analysis, E.L.S.; investigation, A.R. and E.L.S.; resources, S.R.; data curation, A.R.; writing—original draft preparation, A.R. and E.L.S.; writing—review and editing, E.L.S. and S.R.; visualization, A.R. and E.L.S.; supervision, S.R.; funding acquisition, E.L.S., and S.R. All authors have read and agreed to the published version of the manuscript.

**Funding:** This study was supported by the Ministero dell’Istruzione, dell’Università e della Ricerca (MIUR) under the program “Dipartimenti di Eccellenza ex L.232/2016” of the Dipartimento di Neuroscienze “Rita Levi Montalcini”, Università degli Studi di Torino (UNITO) and under the program “Progetti Ricerca Ateneo 2018” of the Università di Pisa (UniPi). A.R. was supported by a Doctoral Fellowship funded by the Partnership for Knowledge (PfK) program of the Agenzia Italiana per la Cooperazione allo Sviluppo (AICS), Ministero degli Affari Esteri e della Cooperazione Internazionale (MAECI), Italy.

**Institutional Review Board Statement:** The study was carried out in accordance with the Declaration of Helsinki and was approved by the Institutional Ethical Committee of the University of Torino (# 219859, issued on April 8, 2021).

**Informed Consent Statement:** All subjects signed informed consent for hypnotic assessment and utilization of their recordings performed two months earlier (during a short period of availability of the entire instrumentation) for the present study. Written informed consent was obtained from all subjects to publish this paper.

**Data Availability Statement:** Data available upon request.

**Acknowledgments:** We are grateful to Raffaele Pertusio for his technical assistance.

**Conflicts of Interest:** The authors declare no conflicts of interest.

## References

- Elkins, G.R.; Barabasz, A.F.; Council, J.R.; Spiegel, D. Advancing Research and Practice: The Revised APA Division 30 Definition of Hypnosis. *Int. J. Clin. Exp. Hypn.* **2015**, *63*, 1–9. <https://doi.org/10.1080/00207144.2014.961870>.
- Santarcangelo, E.L.; Scattina, E. Complementing the Latest APA Definition of Hypnosis: Sensory-Motor and Vascular Peculiarities Involved in Hypnotizability. *Int. J. Clin. Exp. Hypn.* **2016**, *64*, 318–330. <https://doi.org/10.1080/00207144.2016.1171093>.
- Piccione, C.; Hilgard, E.R.; Zimbardo, P.G. On the Degree of Stability of Measured Hypnotizability Over a 25-Year Period. *J. Pers. Soc. Psychol.* **1989**, *56*, 289–295. <https://doi.org/10.1037//0022-3514.56.2.289>.
- Landry, M.; Lifshitz, M.; Raz, A. Brain Correlates of Hypnosis: A Systematic Review and Meta-Analytic Exploration. *Neurosci. Biobehav. Rev.* **2017**, *81*, 75–98. <https://doi.org/10.1016/j.neubiorev.2017.02.020>.
- Picerni, E.; Santarcangelo, E.L.; Laricchiuta, D.; Cutuli, D.; Petrosini, L.; Spalletta, G.; Piras, F. Cerebellar Structural Variations in Subjects with Different Hypnotizability. *Cerebellum* **2019**, *18*, 109–118. <https://doi.org/10.1007/s12311-018-0965-y>.
- Raz, A. Attention and Hypnosis: Neural Substrates and Genetic Associations of Two Converging Processes. *Int. J. Clin. Exp. Hypn.* **2005**, *53*, 237–258. <https://doi.org/10.1080/00207140590961295>.
- Cojan, Y.; Waber, L.; Schwartz, S.; Rossier, L.; Forster, A.; Vuilleumier, P. The Brain under Self-Control: Modulation of Inhibitory and Monitoring Cortical Networks during Hypnotic Paralysis. *Neuron* **2009**, *62*, 862–875. <https://doi.org/10.1016/j.neuron.2009.05.021>.
- McGeown, W.J.; Mazzoni, G.; Vannucci, M.; Venneri, A. Structural and Functional Correlates of Hypnotic Depth and Suggestibility. *Psychiatry Res. Neuroimaging* **2015**, *231*, 151–159. <https://doi.org/10.1016/j.psychres.2014.11.015>.
- Ibáñez-Marcelo, E.; Campioni, L.; Phinyomark, A.; Petri, G.; Santarcangelo, E.L. Topology Highlights Mesoscopic Functional Equivalence between Imagery and Perception: The Case of Hypnotizability. *Neuroimage* **2019**, *200*, 437–449. <https://doi.org/10.1016/j.neuroimage.2019.06.044>.
- Spina, V.; Chisari, C.; Santarcangelo, E.L. High Motor Cortex Excitability in Highly Hypnotizable Individuals: A Favourable Factor for Neuroplasticity? *Neuroscience* **2020**, *430*, 125–130. <https://doi.org/10.1016/j.neuroscience.2020.01.042>.
- Rosati, A.; Belcari, I.; Santarcangelo, E.L.; Sebastiani, L. Interoceptive Accuracy as a Function of Hypnotizability. *Int. J. Clin. Exp. Hypn.* **2021**, *69*, 1–12. <https://doi.org/10.1080/00207144.2021.1954859>.
- Diolaiuti, F.; Huber, A.; Ciaramella, A.; Santarcangelo, E.L.; Sebastiani, L. Hypnotisability-related Interoceptive Awareness and Inhibitory/Activating Emotional Traits. *Arch. Ital. Biol.* **2019**, *157*, 111–119. <https://doi.org/10.12871/00039829202042>.

13. Jambrik, Z.; Santarcangelo, E.L.; Rudisch, T.; Varga, A.; Forster, T.; Carli, G. Modulation of pain-induced endothelial dysfunction by hypnotizability. *Pain* **2005**, *116*, 181–186. <https://doi.org/10.1016/j.pain.2005.03.041>.
14. Jambrik, Z.; Santarcangelo, E.L.; Ghelarducci, B.; Picano, E.; Sebastiani, L. Does hypnotizability modulate the stress-related endothelial dysfunction? *Brain Res. Bull.* **2004**, *63*, 213–216. <https://doi.org/10.1016/j.brainresbull.2004.01.011>.
15. Jambrik, Z.; Chunzeng, L.; Santarcangelo, E.L.; Sebastiani, L.; Ghelarducci, B.; Picano, E. Traditional acupuncture does not modulate the endothelial dysfunction induced by mental stress. *Int. J. Cardiovasc. Imaging* **2004**, *20*, 357–362. <https://doi.org/10.1023/B:CAIM.0000041939.61963.b0>.
16. Hu, Y.; Chen, M.; Wang, M.; Li, X. Flow-Mediated Vasodilation through Mechanosensitive G Protein-Coupled Receptors in Endothelial Cells. *Trends Cardiovasc. Med.* **2021**, *32*, 61–70. <https://doi.org/10.1016/j.tcm.2020.12.010>.
17. Contestabile, A. Role of Nitric Oxide in Cerebellar Development and Function: Focus on Granule Neurons. *Cerebellum* **2012**, *11*, 50–61. <https://doi.org/10.1007/s12311-010-0234-1>.
18. Fantini, S.; Sassaroli, A.; Tgavalekos, K.T.; Kornbluth, J. Cerebral Blood Flow and Autoregulation: Current Measurement Techniques and Prospects for Noninvasive Optical Methods. *Neurophotonics* **2016**, *3*, 031411. <https://doi.org/10.1117/1.NPh.3.3.031411>.
19. Severinghaus, J.W.; Lassen, N. Step Hypocapnia to Separate Arterial from Tissue PCO<sub>2</sub> in the Regulation of Cerebral Blood Flow. *Circ. Res.* **1967**, *20*, 272–278. <https://doi.org/10.1161/01.res.20.2.272>.
20. Fathi, A.R.; Yang, C.; Bakhtian, K.D.; Qi, M.; Lonser, R.R.; Pluta, R.M. Carbon dioxide influence on nitric oxide production in endothelial cells and astrocytes: Cellular mechanisms. *Brain Res.* **2011**, *1386*, 50–57. <https://doi.org/10.1016/J.BRAINRES.2011.02.066>.
21. Hoiland, R.L.; Fisher, J.A.; Ainslie, P.N. Regulation of the Cerebral Circulation by Arterial Carbon Dioxide. *Compr. Physiol.* **2019**, *9*, 1101–1154. <https://doi.org/10.1002/cphy.c180021>.
22. Caldwell, H.G.; Howe, C.A.; Hoiland, R.L.; Carr, J.M.J.R.; Chalifoux, C.J.; Brown, C.V.; Patrician, A.; Tremblay, J.C.; Panerai, R.B.; Robinson, T.G.; et al. Alterations in Arterial CO<sub>2</sub> rather than pH affect the Kinetics of Neurovascular Coupling in Humans. *J. Physiol.* **2021**, *599*, 3663–3676. <https://doi.org/10.1113/JP281615>.
23. Faraci, F.M.; Brian, J.E. Nitric oxide and the cerebral circulation. *Stroke* **1994**, *25*, 692–703. <https://doi.org/10.1161/01.str.25.3.692>.
24. Leffler, C.W. Nitric Oxide in Control of the Cerebral Circulation. In *Nitric Oxide and the Regulation of the Peripheral Circulation*; Kadowitz, P.J., McNamara, D.B., Eds.; Birkhäuser Boston: Boston, MA, USA, 2000; pp. 113–127 ISBN 978-1-4612-1326-0.
25. Shalit, M.N.; Shimojo, S.; Reinmuth, O.M.; Shalit, M.N. Carbon dioxide and cerebral circulatory control. I. The extravascular effect. *Arch. Neurol.* **1967**, *17*, 298–303. <https://doi.org/10.1001/archneur.1967.00470270076009>.
26. Skinhoj, E.; Paulson, O.B. Carbon Dioxide and Cerebral Circulatory Control: Evidence of a Nonfocal Site of Action of Carbon Dioxide on Cerebral Circulation. *Arch. Neurol.* **1969**, *20*, 249–252. <https://doi.org/10.1001/archneur.1969.00480090037004>.
27. Seylaz, J. Contribution to the study of the mechanism of cerebral blood flow regulation. *Helv. Physiol. Pharmacol. Acta* **1968**, *26*, 33–61.
28. Seylaz, J.; Pinard, E.; Dittmar, A.; Birer, A. Measurement of Blood Flow, Tissue PO<sub>2</sub> and Tissue PCO<sub>2</sub> Continuously and Simultaneously in the Same Structure of the Brain. *Med. Biol. Eng. Comput.* **1979**, *17*, 19–24. <https://doi.org/10.1007/BF02440949>.
29. Scremin, O.U.; Scremin, A.M.; Somani, S.M.; Giacobini, E. Brain Regional Distribution of Physostigmine and Its Relation to Cerebral Blood Flow following Intravenous Administration in Rats. *J. Neurosci. Res.* **1990**, *26*, 188–195. <https://doi.org/10.1002/jnr.490260208>.
30. Rovere, A.A.; Scremin, O.U.; Beresi, M.R.; Raynald, A.C.; Giardini, A. Cholinergic Mechanism in the Cerebrovascular Action of Carbon Dioxide. *Stroke* **1973**, *4*, 969–972. <https://doi.org/10.1161/01.str.4.6.969>.
31. Kawamura, Y.; Meyer, J.S.; Hiromoto, H.; Aoyagi, M.; Tagashira, Y.; Ott, E.O. Neurogenic Control of Cerebral Blood Flow in the Baboon. *J. Neurosurg.* **1975**, *43*, 676–688. <https://doi.org/10.3171/jns.1975.43.6.0676>.
32. Busija, D.W.; Heistad, D.D. Effects of Cholinergic Nerves on Cerebral Blood Flow in Cats. *Circ. Res.* **1981**, *48*, 62–69. <https://doi.org/10.1161/01.res.48.1.62>.
33. Scremin, O.U.; Sonnenschein, R.R.; Rubinstein, E.H. Cholinergic Cerebral Vasodilatation in the Rabbit: Absence of Concomitant Metabolic Activation. *J. Cereb. Blood Flow Metab.* **1982**, *2*, 241–247. <https://doi.org/10.1038/jcbfm.1982.24>.
34. Shohami, E.; Sidi, A. Accumulation of Prostacyclin in Rat Brain During Haemorrhagic Hypotension-Possible Role of PGI<sub>2</sub> in Autoregulation. *J. Cereb. Blood Flow Metab.* **1984**, *4*, 107–109. <https://doi.org/10.1038/jcbfm.1984.14>.
35. Pickard, J.D. Role of Prostaglandins and Arachidonic Acid Derivatives in the Coupling of Cerebral Blood Flow to Cerebral Metabolism. *J. Cereb. Blood Flow Metab.* **2016**, *1*, 361–384. <https://doi.org/10.1038/jcbfm.1981.41>.
36. Iadecola, C. Does Nitric Oxide Mediate the Increases in Cerebral Blood Flow Elicited by Hypercapnia? *Proc. Natl. Acad. Sci. U. S. A.* **1992**, *89*, 3913–3916. <https://doi.org/10.1073/pnas.89.9.3913>.
37. Panerai, R.B.; Evans, D.H.; Naylor, A.R. Influence of arterial blood pressure on cerebrovascular reactivity. *Stroke* **1999**, *30*, 1293–1295.
38. Hoiland, R.L.; Caldwell, H.G.; Carr, J.M.J. R.; Howe, C.A.; Stacey, B.S.; Dawkins, T.; Wakeham, D.J.; Tremblay, J.C.; Tymko, M.M.; Patrician, A.; et al. Nitric oxide contributes to cerebrovascular shear-mediated dilatation but not steady-state cerebrovascular reactivity to carbon dioxide. *J. Physiol.* **2021**, *600*, 1385–1403. <https://doi.org/10.1113/JP282427>.
39. Lucas, S.J.E.; Tzeng, Y.C.; Galvin, S.D.; Thomas, K.N.; Ogoh, S.; Ainslie, P.N. Influence of changes in blood pressure on cerebral perfusion and oxygenation. *Hypertension* **2010**, *55*, 698–705. <https://doi.org/10.1161/HYPERTENSIONAHA.109.146290>.

40. Smirl, J.D.; Hoffman, K.; Tzeng, Y.C.; Hansen, A.; Ainslie, A.P.N. Methodological comparison of active- and passive-driven oscillations in blood pressure; implications for the assessment of cerebral pressure-flow relationships. *J. Appl. Physiol.* **2015**, *119*, 487–501. <https://doi.org/10.1152/jappphysiol.00264.2015>.
41. Nippert, A.R.; Biesecker, K.R.; Newman, E.A. Mechanisms Mediating Functional Hyperemia in the Brain. *Neuroscientist* **2018**, *24*, 73–83. <https://doi.org/10.1177/1073858417703033>.
42. Poplawsky, A.J.; Iordanova, B.; Vazquez, A.L.; Kim, S.-G.; Fukuda, M. Postsynaptic Activity of Inhibitory Neurons evokes Hemodynamic fMRI Responses. *Neuroimage* **2021**, *225*, 117457. <https://doi.org/10.1016/j.neuroimage.2020.117457>.
43. Tellegen, A.; Atkinson, G. Openness to Absorbing and Self-Altering Experiences (“Absorption”), A Trait related to Hypnotic Susceptibility. *J. Abnorm. Psychol.* **1974**, *83*, 268–277. <https://doi.org/10.1037/h0036681>.
44. Presciuttini, S.; Gialluisi, A.; Barbuti, S.; Curcio, M.; Scatena, F.; Carli, G.; Santarcangelo, E.L. Hypnotizability and Catechol-O-Methyltransferase (COMT) polymorphisms in Italians. *Front. Hum. Neurosci.* **2014**, *7*, 1–6. <https://doi.org/10.3389/fnhum.2013.00929>.
45. Rominger, C.; Weiss, E.M.; Nagl, S.; Niederstätter, H.; Parson, W.; Papousek, I. Carriers of the COMT Met/Met allele have higher degrees of hypnotizability, provided that they have good attentional control: A case of gene-trait interaction. *Int. J. Clin. Exp. Hypn.* **2014**, *62*, 455–482. <https://doi.org/10.1080/00207144.2014.931177>.
46. Guillot, A.; Collet, C.; Nguyen, V.A.; Malouin, F.; Richards, C.; Doyon, J. Functional Neuroanatomical Networks Associated with Expertise in Motor Imagery. *Neuroimage* **2008**, *41*, 1471–1483. <https://doi.org/10.1016/j.neuroimage.2008.03.042>.
47. Cavallaro, F.I.; Cacace, I.; Testa, M. Del; Andre, P.; Carli, G.; Pascalis, V. De; Rocchi, R.; Santarcangelo, E.L. Hypnotizability-related EEG Alpha and Theta Activities during Visual and Somesthetic Imageries. *Neurosci. Lett.* **2010**, *470*, 13–18. <https://doi.org/10.1016/j.neulet.2009.12.044>.
48. Ibáñez-Marcelo, E.; Campioni, L.; Manzoni, D.; Santarcangelo, E.L.; Petri, G. Spectral and Topological Analyses of the Cortical Representation of the Head Position: Does Hypnotizability Matter? *Brain Behav.* **2019**, *9*, e01277. <https://doi.org/10.1002/brb3.1277>.
49. Oldfield, R.C. The Assessment and Analysis of Handedness: The Edinburgh Inventory. *Neuropsychologia* **1971**, *9*, 97–113. [https://doi.org/10.1016/0028-3932\(71\)90067-4](https://doi.org/10.1016/0028-3932(71)90067-4).
50. Weitzenhoffer, A.M.; Hilgard, E.R. *Stanford Hypnotic Susceptibility Scale, Forms A and B*; Consulting Psychologists Press: Palo Alto, CA, USA, 1959.
51. Csipo, T.; Lipecz, A.; Mukli, P.; Bahadli, D.; Abdulhussein, O.; Owens, C.D.; Tarantini, S.; Hand, R.A.; Yabluchanska, V.; Mikhail Kellawan, J.; et al. Increased cognitive workload evokes greater neurovascular coupling responses in healthy young adults. *PLoS ONE* **2021**, *16*, 1–16. <https://doi.org/10.1371/journal.pone.0250043>.
52. Pascalis, V. De; Bellusci, A.; Russo, P.M. Italian Norms for the Stanford Hypnotic Susceptibility Scale, Form C. *Int. J. Clin. Exp. Hypn.* **2000**, *48*, 315–323. <https://doi.org/10.1080/00207140008415249>.
53. Rastogi, R.; Morgan, B.J.; Badr, M.S.; Chowdhuri, S. Hypercapnia-induced vasodilation in the cerebral circulation is reduced in older adults with sleep-disordered breathing. *J. Appl. Physiol.* **2022**, *132*, 14–23. <https://doi.org/10.1152/jappphysiol.00347.2021>.
54. Zambach, S.A.; Cai, C.; Helms, H.C.C.; Hald, B.O.; Dong, Y.; Fordsmann, J.C.; Nielsen, R.M.; Hu, J.; Lønstrup, M.; Brodin, B.; et al. Precapillary sphincters and pericytes at first-order capillaries as key regulators for brain capillary perfusion. *Proc. Natl. Acad. Sci. U. S. A.* **2021**, *118*, 1–10. <https://doi.org/10.1073/pnas.2023749118>.
55. Porta, A.; Gelpi, F.; Bari, V.; Cairo, B.; De Maria, B.; Panzetti, C.M.; Cornara, N.; Bertoldo, E.G.; Fiolo, V.; Callus, E.; et al. Monitoring the Evolution of Asynchrony between Mean Arterial Pressure and Mean Cerebral Blood Flow via Cross-Entropy Methods. *Entropy* **2022**, *24*, 80. <https://doi.org/10.3390/e24010080>.
56. Younger, J.W.; Rossetti, G.C.; Borckardt, J.J.; Smith, A.R.; Tasso, A.F.; Nash, M.R. Hypnotizability and somatic complaints: A gender-specific phenomenon. *Int. J. Clin. Exp. Hypn.* **2007**, *55*, 1–13. <https://doi.org/10.1080/00207140600995745>.
57. Facco, E.; Testoni, I.; Ronconi, L.; Casiglia, E.; Zanette, G.; Spiegel, D. Psychological Features of Hypnotizability: A First Step Towards Its Empirical Definition. *Int. J. Clin. Exp. Hypn.* **2017**, *65*, 98–119. <https://doi.org/10.1080/00207144.2017.1246881>.
58. Gordon, G.R.J.; Howarth, C.; MacVicar, B.A. Bidirectional Control of Blood Flow by Astrocytes: A Role for Tissue Oxygen and Other Metabolic Factors. *Adv. Exp. Med. Biol.* **2016**, *903*, 209–219. [https://doi.org/10.1007/978-1-4899-7678-9\\_15](https://doi.org/10.1007/978-1-4899-7678-9_15).
59. Acunzo, D.J.; Oakley, D.A.; Terhune, D.B. The neurochemistry of hypnotic suggestion. *Am. J. Clin. Hypn.* **2021**, *63*, 355–371. <https://doi.org/10.1080/00029157.2020.1865869>.
60. Santarcangelo, E.L.; Scattina, E. Responding to Sensorimotor Suggestions: From Endothelial Nitric Oxide to the Functional Equivalence Between Imagery and Perception. *Int. J. Clin. Exp. Hypn.* **2019**, *67*, 394–407. <https://doi.org/10.1080/00207144.2019.1649539>.



# Does hypnotizability affect neurovascular coupling during cognitive tasks?

Anas Rashid<sup>a</sup>, Enrica Laura Santarcangelo<sup>b,\*</sup>, Silvestro Roatta<sup>a</sup>

<sup>a</sup> Lab of Integrative Physiology, Department of Neuroscience "Rita Levi Montalcini", University of Torino, Torino, Italy

<sup>b</sup> Lab of Cognitive and Behavioral Neuroscience, Department of Translational Research and New Technologies in Medicine and Surgery, University of Pisa, Pisa, Italy

## ARTICLE INFO

### Keywords:

NIRS  
Hypnotizability  
Mental computation  
Trail making task  
Cognitive tasks

## ABSTRACT

Susceptibility to hypnosis is a very pervasive psychophysiological trait characterized by different attentional abilities, information processing, and cardiovascular control. Since near infrared spectroscopy is a good index of neurovascular coupling, we used it during mental computation (MC) and trail making task (TMT) in 13 healthy low-to-medium (med-lows) and 10 healthy medium-to-high (med-highs) hypnotizable participants classified according to the Stanford Hypnotic Susceptibility Scale, form A, and characterized for the level of proneness to be deeply absorbed in related experiences by the Tellegen Absorption Scale. The med-highs reported greater absorption than med-lows. The tissue hemoglobin index (THI) and the tissue oxygenation index (TOI) increased across the tasks only in med-highs who displayed also different time courses of THI and TOI during MC and TMT, which indicates different tasks processing despite the two groups' similar performance. The findings suggest that med-highs' tissue oxygenation is more finely adjusted to metabolic demands than med-lows'.

## 1. Introduction

Susceptibility to hypnosis, or hypnotizability, indicates the disposition to modify perception, memory, and behavior according to mental images, is stable through life [1] and is measured by standard scales [2]. High hypnotizability is associated with individual differences – most importantly, greater absorption [3] and stronger functional equivalence between imagery and perception/action [4] – and with physiological correlates in the sensorimotor and cardiovascular domains [5]. High hypnotizable persons (highs) do not reduce their brachial artery post-occlusion flow-mediated dilation during mental computation (MC), in contrast to low hypnotizable individuals (lows) and to the general population [6,7]. Moreover, the cerebrovascular reactivity during hyperventilation correlates with systemic blood pressure in participants with medium-to-high hypnotizability scores (med-highs) and with partial pressure of end-tidal CO<sub>2</sub> in those with low-to-medium (med-lows) hypnotizability [8]. Both findings can be accounted for by larger availability of endothelial nitric oxide in highs.

The present study was motivated by the multiple reports of highs' higher absorption in cognitive tasks with respect to lows [3,9–11]. The association between high hypnotizability and high Tellegen Absorption

Scale (TAS) scores, however, depends on specific tasks [12] and, in fact, recent findings did not support such association [13]. In addition, both Corsi and Digit Span tests failed to detect significant differences between highs, mediums and lows in working memory (WM), which is involved in many if not most high level cognitive tasks [14].

The near-infrared spectroscopy (NIRS) is a method suitable to detect hypnotizability-related brain activation during cognitive tasks. Compared to transcranial Doppler, it focuses the measurement on a much smaller sample volume, and it is sensitive to hemodynamic changes at the capillary level [15]. Thus, it can be more directly correlated to neuronal activity. Frontal NIRS reliably indicates cognitive activities, as activation of the frontal cortex has been associated with WM [16], which is responsible for temporary maintenance and manipulation of the information required by complex tasks [17]. During WM tests, NIRS has shown increased tissue oxygenation index (TOI) and/or decreased deoxygenated hemoglobin in healthy individuals [18–20]; whereas reduced WM-related frontal oxygenation has been observed in patients with attention deficit hyperactive disorder [21], mild cognitive impairment [22], schizophrenia [19] and major depression [23,24]. Moreover, increased levels of mental workload during WM tasks have been associated with increased frontal TOI [25].

*Abbreviations:* WM, Working memory; NIRS, Near-infrared spectroscopy; MC, Mental Computation; TMT, Trail Making Task; SHSS, Stanford Hypnotic Susceptibility Scale; TOI, Tissue Oxygenation Index; THI, Tissue Hemoglobin Index.

\* Corresponding author: Prof. Enrica Laura Santarcangelo, Lab of Cognitive and Behavioral Neuroscience, Department of Translational Research and New Technologies in Medicine and Surgery, University of Pisa, Via San Zeno 31, Pisa (PI) 56127, Italy.

E-mail address: [enrica.santarcangelo@unipi.it](mailto:enrica.santarcangelo@unipi.it) (E.L. Santarcangelo).

<https://doi.org/10.1016/j.physbeh.2022.113915>

Received 11 June 2022; Received in revised form 9 July 2022; Accepted 11 July 2022

Available online 14 July 2022

0031-9384/© 2022 Elsevier Inc. All rights reserved.



Since NIRS is an optimal indicator of neuronal activity, the aim of the present study was to measure frontal NIRS during MC and trail making task (TMT) in med-highs and med-lows. Greater absorption is expected to be associated with stronger neurovascular coupling that is the hyperemia induced by cerebral metabolic activity.

## 2. Materials and methods

### 2.1. Ethical approval

After approval from the Ethics Committee of the University of Torino (# 219859; April 8, 2021), the frontal NIRS signal was recorded in 23 subjects (age:  $26.1 \pm 4.6$  years; 12 females and 11 males) enrolled in earlier studies [8] after signing an informed consent.

Anamnesis was negative for medical, neurological and psychiatric disease. None of them reported taking drugs in the last three months, sleep or attention disturbance. All of them had obtained a master degree, thus their education level was homogeneous.

### 2.2. Experimental procedure

Hypnotic assessment was performed two months later than NIRS recording [8] using the validated Italian version of the Stanford Hypnotic Susceptibility Scale (SHSS), form A [26,27]. It classifies subjects through 12 items which can be passed or not passed (score: min 0, max 12). Thirteen participants exhibited hypnotizability scores from low-to-medium (med-lows range: 0-5; mean  $\pm$  SD:  $1.38 \pm 1.98$ ), while ten participants displayed medium-to-high hypnotizability (med-highs range: 7-9; mean  $\pm$  SD:  $8.10 \pm 0.74$ ); excluding one participant with SHSS score of 6. On the day of hypnotic assessment, participants completed TAS [3], which consists of 34 items and measures the disposition to be absorbed in mental events (score: min 0, max 34).

After hypnotic assessment, further participants could not be enrolled due to the limited availability of the instruments. The recordings had been performed in a quiet, sound and light attenuated, temperature ( $21-23^\circ\text{C}$ ) controlled room between 5 to 7 PM, at least 2 hours after the latest food and caffeine or alcohol intake, as self-reported during signing the informed consent form. The participants had been invited to relax on an armchair for 20 minutes. Then, that they had completed a random sequence of four tasks (hyperventilation, rebreathing, MC, TMT) separated from each other by 5 minutes rest (Baseline, B). An experimenter sitting nearby had provided start and stop instructions. The arterial blood pressure, partial pressure of end-tidal  $\text{CO}_2$ , heart rate and middle cerebral artery flow velocity had been monitored throughout the experiment. The hemodynamic response to hyperventilation, rebreathing, MC, TMT have been reported in an earlier paper [8]. During MC and TMT, hemodynamic responses at frontal level had also been monitored by NIRS.

### 2.3. Tasks

MC consisted of progressively subtracting the odd numbers (1, 3, 5, and so) from 1000 for 180-sec while writing the outcome on a sheet of paper. One operator standing behind the subject monitored the outcome and compared it to a table reporting the correct one, promptly asking the subject to repeat the calculation in case of mistake. The performance was evaluated as the number of subtractions performed in 180-s time.

In TMT [28], the participants had to connect with lines the numbers (1 to 21) and 21 Italian letters (A to Z) in ascending sequence on the paper over 180-sec with alternating numbers and letters (1 – A – 2 – B – 3 – C and so). The performance was evaluated as the number of lines drawn in 180-s time.

Both tasks included a minimal sensorimotor component (writing numbers for MC, drawing lines for TMT).

### 2.4. Variables

The continuous-wave NIRS (NIRO-200NX, Hamamatsu Photonics, Hamamatsu, Japan) was adopted to monitor cerebral hemodynamics from the frontal lobe. The spatially-resolved spectroscopy method [29] was preferred to the Beer-Lambert method [30] due to its capacity to detect the cerebral rather than the cutaneous tissues [31,32]. The following variables were considered: tissue hemoglobin index (THI), which represents the total hemoglobin content and is conventionally set to 1 at the beginning of the baseline condition, and TOI, which represents the percentage of oxygenated hemoglobin. The signals were digitally sampled (CED Micro 1401, Cambridge Electronic Design, Cambridge, UK) at 100 Hz and stored for further analysis (Spike2 ver. 9.14, Cambridge Electronic Design, Cambridge, UK).

### 2.5. Statistical analysis

We used MATLAB<sup>®</sup> ver. R2022a (The MathWorks, Natick, MA, USA) to analyze signals and the Statistical Package for Social Sciences (SPSS) ver. 28.0 (SPSS Inc., Chicago, IL, USA) for statistical analyses. The baseline (B) values of NIRS variables were taken over a 20-s interval preceding the beginning of the task (MC and TMT), while the task effect was assessed over three consecutive 60-sec sub-periods (T1, T2, T3) to study the NIRS variables time course.

One outlier was excluded from THI analysis. Owing to the nature of the variables (see Section 2.4), we used nonparametric statistics to compare med-highs' and med-lows' THI and TOI as well as TAS and the performance during MC and TMT (Kolmogorov-Smirnov test). Within subjects, THI and TOI time courses i.e., over T1, T2, and T3 were than studied in comparison to B and between each other; MC and TMT values of THI and TOI were compared (Wilcoxon test). The level of significance was set at  $p = 0.05$ . Results are reported as mean  $\pm$  standard deviation (SD), unless stated otherwise.

## 3. Results

### 3.1. Self-reports

TAS scores were significantly higher ( $Z = 1.774$ ,  $p = 0.004$ ) in med-highs ( $16.89 \pm 4.54$ ) than in med-lows ( $7.37 \pm 4.12$ ), while t-test confirmed a significant difference between two groups ( $p = 0.0001$ ).

The two groups exhibited the same level of performance for both MC (med-highs:  $10.80 \pm 3.16$ ; med-lows:  $11.92 \pm 3.82$ ) and TMT (med-highs:  $8.70 \pm 2.58$ ; med-lows:  $9.54 \pm 2.99$ ).

### 3.2. Near-infrared spectroscopy

No significant differences were observed between groups in THI and TOI values computed over B, T1, T2 and T3 for both TMT and MC. The variables time courses were different in the two groups (Table 1, Fig. 1).

#### 3.2.1. Trail making task

Med-lows did not exhibit any significant difference in THI between B and subperiods as well as between subperiods. Their TOI showed only a trend to increase between T1 and T2 ( $Z = 1.89$ ,  $p = 0.059$ ). In contrast, in med-highs THI decreased significantly in T1 with respect to B ( $Z = 2.05$ ,  $p = 0.040$ ), while TOI increased in T2 with respect to T1 ( $Z = 1.99$ ,  $p = 0.047$ ), and recovered its basal values in T3. Thus, only med-highs exhibited time related changes in THI and TOI.

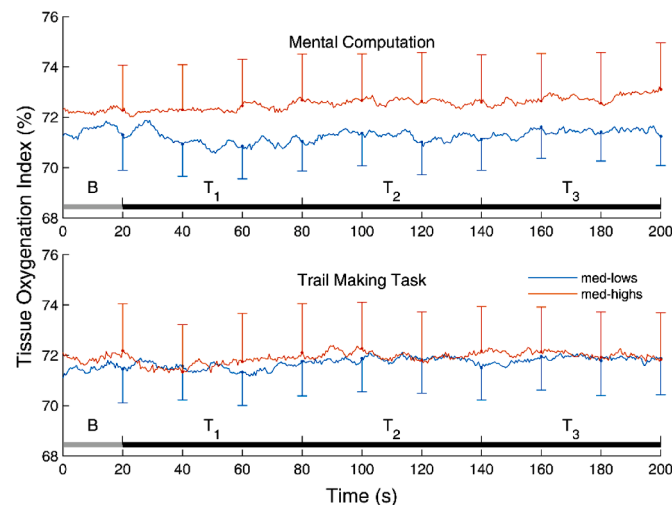
#### 3.2.2. Mental computation

Med-lows' THI did not show significant differences between B and tasks subperiods as well as between task subperiods, whereas med-highs showed an increase in T2 ( $Z = 2.32$ ,  $p = 0.020$ ) and T3 ( $Z = 1.930$ ,  $p = 0.054$ ) compared to B and in T3 compared to T2 ( $Z = 2.00$ ,  $p = 0.046$ ).

**Table 1**  
Tissue Oxygenation Index (TOI) and Tissue Hemoglobin Index (THI) time course (mean, SD).

Condition	Variable	med-lows		med-highs	
		Mean	SD	Mean	SD
<b>TMT</b>					
	TOI (%)	71.48	4.76	71.90	5.81
B					
T1		71.51	4.74	71.70	5.98
T2		71.83	4.75	72.00	5.93
T3		71.84	4.84	72.05	5.63
B	THI (a.u.)	1.02	0.11	0.99	0.05
T1		1.01	0.11	1.00	0.05
T2		1.02	0.11	1.00	0.05
T3		1.02	0.11	1.01	0.07
<b>MC</b>					
B	TOI (%)	71.50	5.48	72.25	5.73
T1		71.09	4.58	72.33	5.80
T2		71.24	4.47	72.61	5.93
T3		71.40	4.14	72.75	6.09
B	THI (a.u.)	1.03	0.12	1.02	0.16
T1		1.02	0.11	1.02	0.15
T2		1.02	0.10	1.03	0.15
T3		1.02	0.11	1.03	0.15

Note: B: baseline 0-20 s; T1: task 0-60 s; T2: task 60-120 s; T3: task 120-180 s

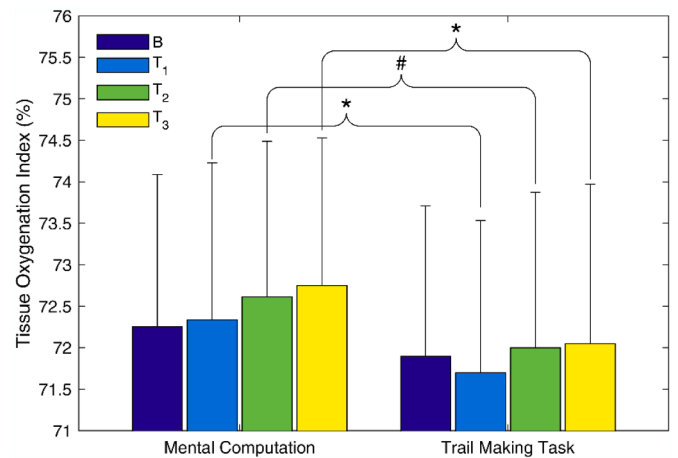


**Fig. 1.** Tissue Oxygenation Index time course during mental computation and trail making task (mean, standard error of the mean). The gray and black bar at the bottom indicate the baseline (B) and task subperiods (T1: 20-80 s, T2: 80-140 s and T3: 140-200 s), respectively.

Med-lows' TOI decreased in T1 with respect to B ( $Z = 1.96$ ,  $p = 0.050$ ), and increased in T3 with respect to T2 ( $Z = 2.13$ ,  $p = 0.033$ ) and did not differ between B and the other subperiods. In med-highs, Wilcoxon test failed to identify differences between B and task subperiods. Thus, during MC med-highs maintained their basal value of TOI throughout the task, whereas med-lows initially decreased their TOI, then recovered B.

**3.2.3. Comparison between TMT and MC**

No significant difference between TMT and MC was observed in med-lows in both THI and TOI. In contrast, med-highs did not show significant differences in THI but exhibited significantly higher TOI values (Fig. 2) in MC than TMT during T1 ( $Z = 2.29$ ,  $p = 0.022$ ) and T3 ( $Z = 2.191$ ,  $p = 0.028$ ) and as a trend to significant higher values during T2 ( $Z = 1.89$ ,  $p = 0.059$ ), with no difference in B.



**Fig. 2.** Tissue oxygenation index during mental computation and trail making task (mean, standard error of the mean) in med-highs. (\*) and (#) indicate statistically and quasi significant differences between TMT and MC, respectively.

**4. Discussion**

Med-highs reported greater absorption than med-lows and similar performance. During cognitive tasks only med-highs increased their mean cerebral blood supply (THI) and exhibited larger mean TOI during mental computation than trail making task.

The same behavioral performance observed in the two groups seems to accord with the absence of mean differences between med-highs and med-lows in NIRS variables. Nonetheless, the absence of significant differences in mean THI and mean TOI between groups may depend on the variables different time courses, which suggest different ways to perform the tasks.

During TMT an initial decrease in THI was observed only in highs, in agreement with the decrease observed during a motor task triggered by an external cue, like our tests are, whereas self-initiated actions are not associated with any initial decrease [33]. It could be due to the vascular reaction to the increase in systemic blood pressure [8] inducing a reactive vasoconstriction [34,35] successively overcome by functional hyperemia, whereby the local increase in perfusion exceeds the increase in metabolic activity [36]. The extent of such increase may be related to the extent of neuronal activation, possibly dependent on cognitive engagement and/or on the effectiveness of the neurovascular coupling. Med-highs functional hyperemia could be due to larger synaptic glutamate release, which increases the astrocytes' calcium mediated dilatory actions through large release of nitric oxide [36,37], in accordance with what was observed at peripheral level [6,7]. Highs, indeed, respond to cognitive tasks with larger glutamatergic cortical activity [11].

Since the increase in systemic blood pressure during both tasks was similar in the two groups [8], but only med-highs exhibited the initial reduction in THI, med-highs' vessels smooth cells display greater sensitivity than med-lows to blood pressure changes, as observed during hyperventilation [8]. Moreover, in med-highs the initial decrease in THI ( $T1 < B$ ) may be responsible for the absence of changes in TOI in T1 followed by later increase in TOI in T2 when THI recovers B.

In med-highs greater cognitive demand by MC with respect to TMT may have overcome the initial vasoconstriction observed during TMT. Internally directed cognition like MC is in fact characterized by greater cognitive load with respect to tasks requiring an external focus of attention like TMT [38]. Med-highs performed such highly demanding attentional tasks through progressive increase in THI and slight progressive increase in TOI, so that their TOI during the three subperiods of MC were higher than during TMT. Importantly, these differences occurred in the presence of similar increase in systemic blood pressure [8].

Med-highs' higher score of absorption accords with part of earlier literature [10,13] and seem to contrast with the similar performance of med-highs and med-lows. In this respect, more sophisticated hypnotic assessment, that is the evaluation of single items rather than the scales total score, could be more informative on the individual cognitive abilities [39] and better predict the performance during cognitive tasks. Moreover, we enrolled mediums scoring 7 together with highs in the med-highs group and mediums scoring 5 together with lows in the med-lows group and could not enroll very high hypnotizable participants (SHSS scores > 9 out of 12).

A limitation of the study is the availability of NIRS at the frontal lobes only. Nonetheless, it has been shown that both purely cognitive tasks and exercise can activate the orbitofrontal cortex [40]. Other limitations are that we cannot exclude the difference in the sensorimotor component of the two tasks which may influence this finding, and that the small sample size did not allow to study highs, lows and mediums, who represent the largest part of the population, separately [41], and to investigate gender differences, which are present in most cognitive tasks [42]. Finally, we are aware that the self-reports of cognitive load and more sophisticated signal analysis might improve the significance of results [43,44].

To conclude, cognitive tasks were processed by med-highs and med-lows differentially. Only med-highs exhibited evidence of functional hyperemia (increase in tissue oxygenation, possibly accompanied by increase in blood volume), and of differences between mental computation and trail making task. Thus, med-highs seem more responsive than med-lows to specific cognitive demands. An open question is whether their stronger vascular response is a correlate or the cause of their greater disposition to be absorbed in mental tasks.

#### CRediT author statement

**Anas Rashid:** Conceptualization, Methodology, Investigation, Data Curation, Writing - Original Draft Preparation, Visualization. **Enrica Laura Santarcangelo:** Conceptualization, Methodology, Formal Analysis, Investigation, Writing - Original Draft Preparation, Writing - Reviewing & Editing, Visualization, Funding Acquisition. **Silvestro Roatta:** Conceptualization, Methodology, Resources, Writing - Reviewing & Editing, Supervision, Funding Acquisition.

#### Declaration of Competing Interest

The authors declare no conflict of interest.

#### Acknowledgements

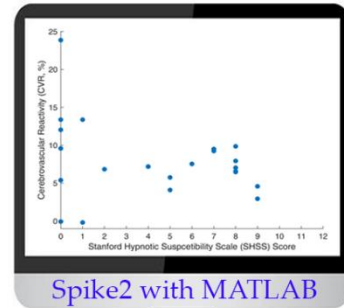
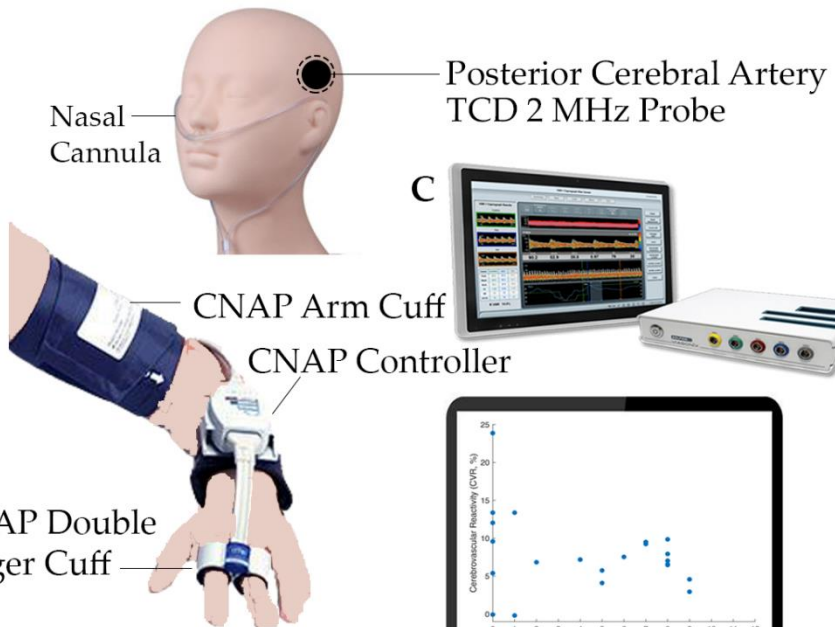
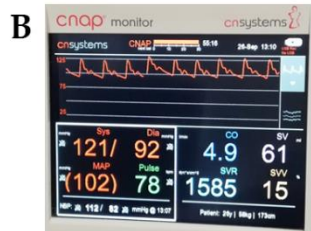
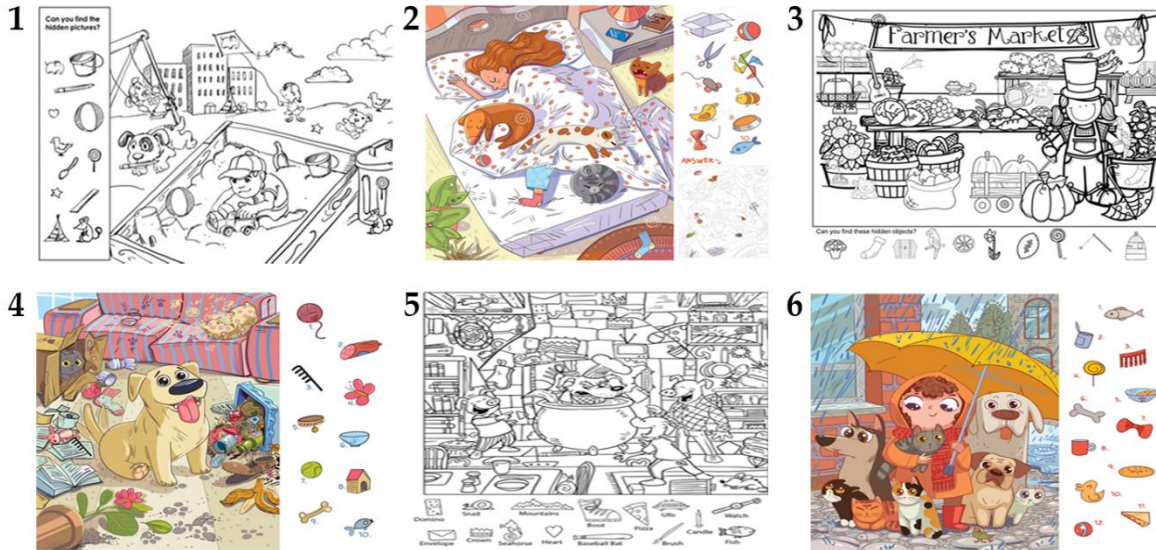
This study was supported by Ministero della Università e della Ricerca (MUR) under the program "Dipartimenti di Eccellenza ex L.232/2016" to the Dipartimento di Neuroscienze "Rita Levi Montalcini", Università degli Studi di Torino (UNITO) and under the program "Progetti di Ricerca di Ateneo 2018" to the Università di Pisa (UniPi). Dr. Anas Rashid was recipient of a Doctoral Fellowship funded by the Partnership for Knowledge (Pfk) program of the Agenzia Italiana per la Cooperazione allo Sviluppo (AICS), Ministero degli Affari Esteri e della Cooperazione Internazionale (MAECI), Italy.

#### References

- Piccione, E.R., Hilgard, P.G., Zimbardo, On the Degree of stability of measured hypnotizability over a 25-year period, *J. Pers. Soc. Psychol.* 56 (1989) 289–295, <https://doi.org/10.1037//0022-3514.56.2.289>.
- G.R. Elkins, A.F. Barabasz, J.R. Council, D. Spiegel, Advancing research and practice: the revised APA division 30 definition of hypnosis, *Int. J. Clin. Exp. Hypn.* 63 (2015) 1–9, <https://doi.org/10.1080/00207144.2014.961870>.
- A. Tellegen, G. Atkinson, Openness to absorbing and self-altering experiences ("Absorption"), a trait related to hypnotic susceptibility, *J. Abnorm. Psychol.* 83 (1974) 268–277, <https://doi.org/10.1037/h0036681>.
- E. Ibáñez-Marcelo, L. Campioni, A. Phinyomark, G. Petri, E.L. Santarcangelo, Topology highlights mesoscopic functional equivalence between imagery and perception: the case of hypnotizability, *Neuroimage* 200 (2019) 437–449, <https://doi.org/10.1016/j.neuroimage.2019.06.044>.
- E.L. Santarcangelo, E. Scattina, Responding to sensorimotor suggestions: from endothelial nitric oxide to the functional equivalence between imagery and perception, *Int. J. Clin. Exp. Hypn.* 67 (2019) 394–407, <https://doi.org/10.1080/00207144.2019.1649539>.
- Z. Jambrik, E.L. Santarcangelo, B. Ghelarducci, E. Picano, L. Sebastiani, Does hypnotizability modulate the stress-related endothelial dysfunction? *Brain Res. Bull.* 63 (2004) 213–216, <https://doi.org/10.1016/j.brainresbull.2004.01.011>.
- Z. Jambrik, L. Sebastiani, E. Picano, B. Ghelarducci, E.L. Santarcangelo, Hypnotic modulation of flow-mediated endothelial response to mental stress, *Int. J. Psychophysiol.* 55 (2005) 221–227, <https://doi.org/10.1016/j.ijpsycho.2004.07.007>.
- A. Rashid, Enrica L. Santarcangelo, S. Roatta, Cerebral Blood flow in healthy subjects with different hypnotizability scores, *Brain Sci.* 12 (2022) 558, <https://doi.org/10.3390/brainsci12050558>.
- A. Raz, Attention and hypnosis: neural substrates and genetic associations of two converging processes, *Int. J. Clin. Exp. Hypn.* 53 (2005) 237–258, <https://doi.org/10.1080/00207140590961295>.
- E. Facco, I. Testoni, L. Ronconi, E. Casiglia, G. Zanette, D. Spiegel, Psychological features of hypnotizability: a first step towards its empirical definition, *Int. J. Clin. Exp. Hypn.* 65 (2017) 98–119, <https://doi.org/10.1080/00207144.2017.1246881>.
- D.J. Acunzo, D.A. Oakley, D.B. Terhune, The neurochemistry of hypnotic suggestion, *Am. J. Clin. Hypn.* 63 (2021) 355–371, <https://doi.org/10.1080/00029157.2020.1865869>.
- A. Tellegen, Practicing the two disciplines for relaxation and enlightenment: comment on "Role of the feedback signal in electromyograph biofeedback: the relevance of attention" by Qualls and Sheehan - PubMed, *J. Exp. Psychol. Gen.* 110 (1981) 217–231.
- A. Vanhaudenhuyse, D. Ledoux, O. Gosseries, A. Demertzi, S. Laureys, M. E. Faymonville, Can subjective ratings of absorption, dissociation, and time perception during "Neutral Hypnosis" Predict Hypnotizability?: An exploratory study, *Int. J. Clin. Exp. Hypn.* 67 (2019) 28–38, <https://doi.org/10.1080/00207144.2019.1553765>.
- O. Incognito, E. Menardo, F. Di Gruttola, F. Tomaiuolo, L. Sebastiani, E. L. Santarcangelo, Visuospatial imagery in healthy individuals with different hypnotizability levels, *Neurosci. Lett.* 690 (2019) 158–161, <https://doi.org/10.1016/j.neulet.2018.10.039>.
- S. Kobayashi, Y. Iwama, H. Nishimaru, J. Matsumoto, T. Setogawa, T. Ono, H. Nishijo, Examination of the prefrontal cortex hemodynamic responses to the fist-edge-palm task in naive subjects using functional near-infrared spectroscopy, *Front. Hum. Neurosci.* 15 (2021) 617–626, <https://doi.org/10.3389/fnhum.2021.617626>.
- T. Takeda, Y. Kawakami, M. Konno, Y. Matsuda, M. Nishino, Y. Suzuki, Y. Kawano, K. Nakajima, T. Ozawa, Y. Kondo, K. Sakatani, PFC blood oxygenation changes in four different cognitive tasks, *Adv. Exp. Med. Biol.* 977 (2017) 199–204, [https://doi.org/10.1007/978-3-319-55231-6\\_27](https://doi.org/10.1007/978-3-319-55231-6_27).
- A.D. Baddeley, G. Hitch, Working memory, *Psychol. Learn. Motiv.* 8 (1974) 47–89, [https://doi.org/10.1016/S0079-7421\(08\)60452-1](https://doi.org/10.1016/S0079-7421(08)60452-1).
- Y. Hoshi, B.H. Tsou, V.A. Billock, M. Tanosaki, Y. Iguchi, M. Shimada, T. Shinba, Y. Yamada, I. Oda, Spatiotemporal characteristics of hemodynamic changes in the human lateral prefrontal cortex during working memory tasks, *Neuroimage* 20 (2003) 1493–1504, [https://doi.org/10.1016/S1053-8119\(03\)00412-9](https://doi.org/10.1016/S1053-8119(03)00412-9).
- S. Koike, R. Takizawa, Y. Nishimura, M. Kinou, S. Kawasaki, K. Kasai, Reduced but broader prefrontal activity in patients with schizophrenia during n-back working memory tasks: a multi-channel near-infrared spectroscopy study, *J. Psychiatr. Res.* 47 (2013) 1240–1246, <https://doi.org/10.1016/j.jpsychires.2013.05.009>.
- C. Herff, D. Heger, O. Fortmann, J. Hennrich, F. Putze, T. Schultz, Mental workload during n-back task-quantified in the prefrontal cortex using fNIRS, *Front. Hum. Neurosci.* 7 (2014) 1–9, <https://doi.org/10.3389/fnhum.2013.00935>.
- A.C. Ehlis, C.G. Bähne, C.P. Jacob, M.J. Herrmann, A.J. Fallgatter, Reduced lateral prefrontal activation in adult patients with attention-deficit/hyperactivity disorder (ADHD) during a working memory task: a functional near-infrared spectroscopy (fNIRS) study, *J. Psychiatr. Res.* 42 (2008) 1060–1067, <https://doi.org/10.1016/j.jpsychires.2007.11.011>.
- M.K. Yeung, S.L. Sze, J. Woo, T. Kwok, D.H.K. Shum, R. Yu, A.S. Chan, Reduced frontal activations at high working memory load in mild cognitive impairment: near-infrared spectroscopy, *Dement. Geriatr. Cogn. Disord.* 42 (2016) 278–296, <https://doi.org/10.1159/000450993>.
- S. Pu, T. Yamada, K. Yokoyama, H. Matsumura, H. Kobayashi, N. Sasaki, H. Mitani, A. Adachi, K. Kaneko, K. Nakagome, A multi-channel near-infrared spectroscopy study of prefrontal cortex activation during working memory task in major depressive disorder, *Neurosci. Res.* 70 (2011) 91–97, <https://doi.org/10.1016/j.neures.2011.01.001>.
- M.K. Yeung, T.L. Lee, W.K. Cheung, A.S. Chan, Frontal underactivation during working memory processing in adults with acute partial sleep deprivation: a near-infrared spectroscopy study, *Front. Psychol.* 9 (2018) 1–15, <https://doi.org/10.3389/fpsyg.2018.00742>.
- M.J. Saikia, W.G. Besio, K. Mankodiya, The validation of a portable functional NIRS system for assessing mental workload, *Sensors (Basel)* 21 (2021) 1–13, <https://doi.org/10.3390/s21113810>.
- A.M. Weitzenhoffer, E.R. Hilgard, Stanford Hypnotic Susceptibility Scale, *Forms A and B*, Consult, Psychol. Press, 1959.

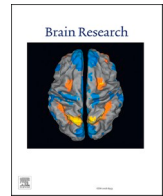
- [27] A.M. Weitzenhoffer, E.R. Hilgard, *Scala Stanford di Suscettibilità Ipnocica, Forme A e B, Organizzazioni Speciali, Firenze, 1959.*
- [28] C.R. Bowie, P.D. Harvey, Administration and interpretation of the trail making test, *Nat. Protoc.* 1 (2006) 2277–2281, <https://doi.org/10.1038/nprot.2006.390>.
- [29] S.J. Matcher, C.E. Elwell, C.E. Cooper, M. Cope, D.T. Delpy, Performance comparison of several published tissue near-infrared spectroscopy algorithms, *Anal. Biochem.* 227 (1995) 54–68, <https://doi.org/10.1006/abio.1995.1252>.
- [30] M. Ferrari, M. Muthalib, V. Quaresima, The use of near-infrared spectroscopy in understanding skeletal muscle physiology: recent developments, *Philos. Trans. R. Soc. A Math. Phys. Eng. Sci.* 369 (2011) 4577–4590, <https://doi.org/10.1098/rsta.2011.0230>.
- [31] D. Canova, S. Roatta, D. Bosone, G. Micieli, Inconsistent detection of changes in cerebral blood volume by near infrared spectroscopy in standard clinical tests, *J. Appl. Physiol.* 110 (2011) 1646–1655, <https://doi.org/10.1152/jappphysiol.00003.2011>.
- [32] A. Messere, S. Roatta, Influence of cutaneous and muscular circulation on spatially resolved versus standard Beer-Lambert near-infrared spectroscopy, *Physiol. Rep.* 1 (2013) 1–10, <https://doi.org/10.1002/phy2.179>.
- [33] K. Matsukawa, R. Asahara, M. Uzumaki, Y. Hashiguchi, K. Ishii, J. Wang, S. A. Smith, Central command-related increases in blood velocity of anterior cerebral artery and prefrontal oxygenation at the onset of voluntary tapping, *Am. J. Physiol. Hear. Circ. Physiol.* 321 (2021) H518–H531, <https://doi.org/10.1152/ajpheart.00062.2021>.
- [34] S.J.E. Lucas, Y.C. Tzeng, S.D. Galvin, K.N. Thomas, S. Ogoh, P.N. Ainslie, Influence of changes in blood pressure on cerebral perfusion and oxygenation, *Hypertension* 55 (2010) 698–705, <https://doi.org/10.1161/HYPERTENSIONAHA.109.146290>.
- [35] J.D. Smirl, K. Hoffman, Y.C. Tzeng, A. Hansen, A.P.N. Ainslie, Methodological comparison of active- and passive-driven oscillations in blood pressure; implications for the assessment of cerebral pressure-flow relationships, *J. Appl. Physiol.* 119 (2015) 487–501, <https://doi.org/10.1152/jappphysiol.00264.2015>.
- [36] A.R. Nippert, K.R. Biesecker, E.A. Newman, Mechanisms mediating functional hyperemia in the brain, *Neuroscientist* 24 (2018) 73–83, <https://doi.org/10.1177/1073858417703033>.
- [37] A.J. Poplawsky, B. Iordanova, A.L. Vazquez, S.-G. Kim, M. Fukuda, Postsynaptic activity of inhibitory neurons evokes hemodynamic fMRI responses, *Neuroimage* 225 (2021), 117457, <https://doi.org/10.1016/j.neuroimage.2020.117457>.
- [38] S.M. Ceh, S. Annerer-Walcher, K. Koschutnig, C. Körner, A. Fink, M. Benedek, Neurophysiological indicators of internal attention: An fMRI-eye-tracking coregistration study, *Cortex* 143 (2021) 29–46, <https://doi.org/10.1016/j.cortex.2021.07.005>.
- [39] D.B. Terhune, E. Cardena, Differential patterns of spontaneous experiential response to a hypnotic induction: a latent profile analysis, *Conscious. Cogn.* 19 (2010) 1140–1150, <https://doi.org/10.1016/j.concog.2010.03.006>.
- [40] S. Miyashiro, Y. Yamada, T. Muta, H. Ishikawa, T. Abe, M. Hori, K. Oka, F. Koshikawa, E. Ito, Activation of the orbitofrontal cortex by both meditation and exercise: a near-infrared spectroscopy study, *PLoS One* 16 (2021) 1–15, <https://doi.org/10.1371/journal.pone.0247685>.
- [41] V. De Pascalis, A. Bellusci, P.M. Russo, Italian norms for the stanford hypnotic susceptibility scale, form C, *Int. J. Clin. Exp. Hypn.* 48 (2000) 315–323, <https://doi.org/10.1080/00207140008415249>.
- [42] A. Gaillard, D.J. Fehring, S.L. Rossell, Sex differences in executive control: A systematic review of functional neuroimaging studies, *Eur. J. Neurosci.* 53 (2021) 2592–2611, <https://doi.org/10.1111/ejn.15107>.
- [43] X. Hou, Z. Zhang, C. Zhao, L. Duan, Y. Gong, Z. Li, C. Zhu, NIRS-KIT: A MATLAB toolbox for both resting-state and task fNIRS data analysis, *Neurophotonics* 8 (2021), <https://doi.org/10.1117/1.NPh.8.1.010802>, 010802-1–20.
- [44] S. Molina-Rodríguez, M. Mirete-Fructuoso, L.M. Martínez, J. Ibañez-Ballesteros, Frequency-domain analysis of fNIRS fluctuations induced by rhythmic mental arithmetic, *Psychophysiology* (2022) 1–25, <https://doi.org/10.1111/psyp.14063>.

## Visual Stimulation



- A. Capnograph
- B. Finger-Pulse Photoplethysmography (CNAP)
- C. Transcranial Doppler (TCD)

## GRAPHICAL ABSTRACT



# Cerebrovascular reactivity during visual stimulation: Does hypnotizability matter?

Anas Rashid<sup>a</sup>, Enrica Laura Santarcangelo<sup>b,\*</sup>, Silvestro Roatta<sup>a</sup>

<sup>a</sup> Lab of Integrative Physiology, Department of Neuroscience "Rita Levi Montalcini", University of Torino, Torino, Italy

<sup>b</sup> Lab of Cognitive and Behavioral Neuroscience, Department of Translational Research and New Technologies in Medicine and Surgery, University of Pisa, Pisa, Italy

## ARTICLE INFO

### Keywords:

Transcranial Doppler  
Hypnotizability  
Visual stimulation  
Posterior cerebral artery  
Cerebrovascular reactivity

## ABSTRACT

Hypnotizability is a trait associated with several physiological correlates including cardiovascular control. The present study aimed to investigate the posterior cerebral artery flow velocity (PCAv) in basal closed eyes (B) and during visual stimulation (VS) conditions in med-highs and med-lows. Twenty-four healthy volunteers were submitted to the hypnotic assessment through the Stanford Hypnotic Susceptibility Scale, form A which classified 13 low-to-medium (med-lows) and 10 high-to-medium (med-highs) hypnotizable participants. One subject scoring 6 out of 12 was excluded from the comparisons between groups. Arterial blood pressure, heart rate, and partial pressure of end-tidal CO<sub>2</sub> were monitored during both B and VS conditions. Simultaneously, PCAv was assessed by transcranial Doppler. Cerebrovascular Reactivity (CVR) was computed as a percentage of the PCAv change occurring during VS with respect to B ( $\Delta$ PCAv). During VS both groups increased their PCAv (mean  $\pm$  SD:  $7.9 \pm 5.2\%$ ) significantly with no significant group difference. However, among med-highs, CVR was negatively correlated with hypnotizability scores. Thus, higher hypnotizability may be associated with lower metabolic demand in response to VS only within med-highs hypnotizable participants.

## 1. Introduction

The cognitive trait of hypnotizability, as measured by standardized scales, is associated with several physiological correlates (Santarcangelo and Scattina, 2019). They include a more pronounced parasympathetic control of heart rate during long-lasting relaxation (Santarcangelo et al., 2012) and less reduced brachial artery post occlusion flow-mediated dilation in highly hypnotizable participants (highs) with respect to low hypnotizables (lows) during mental computation and nociceptive stimulation, which indicates larger availability of nitric oxide (NO) in highs (Jambrík et al., 2005; Jambrík et al., 2004). Recent research showed that during cognitive tasks only med-highs significantly modulate their neurovascular coupling in the presence of arterial blood pressure increase similar to med-lows (Rashid et al., 2022), whereas, there is no information on possible hypnotizability-related influence on blood flow velocity during a purely sensory stimulation.

Large variations in cerebral blood flow and other vascular responses between and within-subjects have been observed during visual

stimulation (VS). The variability in oxidative demand (Leontiev and Buxton, 2007) and vascular tone (Ito et al., 2008) may partly explain cerebral blood flow variability both at baseline and during VS (Ho et al., 2011; Leontiev and Buxton, 2007; Paulson et al., 2010). In both humans (Dorner et al., 2003) and cats (Kondo et al., 1997), systemic administration of non-selective nitric oxide synthase (NOS) inhibitors reduces visually-evoked increases in blood flow. In addition, the reduction of NOS activity in the cerebral cortex by topical administration of a neuronal NOS inhibitor results in the reduction of functional hyperemia (Lindauer et al., 1999), and the response is restored when NO levels are raised by the addition of an NO donor. However, functional hyperemia in the cortex is not diminished when neuronal NOS activity is reduced by genetic manipulation (Ma et al., 1996). These results suggest that NO is a modulator of neurovascular coupling although probably not an essential factor. Other vasodilatory agents including K<sup>+</sup>, arachidonic acid metabolites prostaglandin E<sub>2</sub> and epoxyeicosatrienoic acids are released from glial cells upon the action of several transmitters, acting on glial metabotropic receptors, during increased neuronal activity (Newman,

*Abbreviations:* NO, nitric oxide; VS, visual stimulation; NOS, nitric oxide synthase; PCAv, posterior cerebral artery flow velocity; B, baseline closed eyes; SHSS, Stanford Hypnotic Susceptibility Scale.

\* Corresponding author at: Enrica Laura Santarcangelo, Lab of Cognitive and Behavioral Neuroscience, Department of Translational Research and New Technologies in Medicine and Surgery, University of Pisa, Via San Zeno 31, Pisa (PI) 56127, Italy.

E-mail address: [enrica.santarcangelo@unipi.it](mailto:enrica.santarcangelo@unipi.it) (E.L. Santarcangelo).

<https://doi.org/10.1016/j.brainres.2022.148059>

Received 19 May 2022; Received in revised form 1 July 2022; Accepted 18 August 2022

Available online 22 August 2022

0006-8993/© 2022 Elsevier B.V. All rights reserved.

2013).

VS may be processed differentially by med-highs and med-lows, as suggested for sensorimotor actual and imagined information by topological analysis of the highs' and lows' electroencephalography (Ibáñez-Marcelo et al., 2019). In fact, that study reported hypnotizability-related differences suggesting a distributed processing of sensorimotor information in highs and a more localized processing in lows. Such different modes of information processing may be associated with different cerebrovascular response to sensory stimulation. Thus, the present study aimed to investigate whether this occurs during VS by analyzing the blood flow velocity in the Posterior Cerebral Artery (PCAv) in baseline closed eyes (B) and VS conditions in healthy med-highs and med-lows.

## 2. Materials and methods

### 2.1. Ethical approval

The investigation was approved by the Institutional Review Board (# 219859) and was conducted according to the Declaration of Helsinki. All subjects signed informed consent for hypnotic assessment and utilization of their physiological signals acquired two months earlier for the present and an earlier study (Rashid et al., 2022).

### 2.2. Subjects

Twenty-four healthy university students (12 males; age:  $26.1 \pm 4.5$  years) who had joined an earlier study of cerebrovascular reactivity (Rashid et al., 2022) were enrolled in this study. Participants did not report medical, neurological, and psychiatric disease, sleep and attention disturbance, substance abuse throughout their life, drugs intake in the last three months.

### 2.3. Experimental procedure

Experiments were conducted in a quiet, sound, and light attenuated, temperature-controlled ( $21\text{--}23^\circ\text{C}$ ) room between 5 and 7 PM, at least 3 h after the latest food and caffeine or alcohol intake. Participants were invited to relax by sitting in an armchair for 5 min. Then, they were recorded for a 10 mins baseline period and during a sequence of tests (Rashid et al., 2022a,b).

This test consisted of a baseline closed eyes (B) and a VS condition. For VS participants were invited to solve six different hidden object games, three black and white and three colored pictures, each picture presenting 10–15 hidden objects. They had to alternate a 30-s eyes-closed interval (baseline) to 30-s engagement in the game (VS), as signaled by an audio cue (total time six min). The subjects were not allowed to write/speak during the VS thus no assessment of accuracy or performance (e.g., number of objects spotted in each picture) was carried out. At the end of VS participants were asked to "rate the attention paid to the VS on a standardized numerical rating scale from 0 (minimum) to 10 (maximum)".

In a second session, the validated, Italian version of the behavioral Stanford Hypnotic Susceptibility Scale (SHSS), form A (Weitzenhoffer and Hilgard, 1959) was used for hypnotic assessment. It classifies highs (score: 8–12 items passed out of 12); mediums (score: 5–7 out of 12); and lows (score: 0–4 out of 12). For the present study, the participants were divided into med-lows ( $N = 13$ ; SHSS score: 0–5; mean  $\pm$  SD:  $1.38 \pm 1.98$ ) and med-highs ( $N = 10$ ; SHSS score: 7–9; mean  $\pm$  SD:  $8.1 \pm 0.78$ ), excluding one participant with SHSS of 6.

Analyses of part of the acquired signals – those related to the middle cerebral artery flow velocity recorded during cognitive tasks, hyperventilation as well as rebreathing – were published in different papers (Rashid et al., 2022a,b).

### 2.4. Measurements

The partial pressure of carbon dioxide ( $P_{\text{ETCO}_2}$ ) in the respiratory gases was monitored using a capnograph (Capnostream™ 20p Bedside Patient Monitor with Microstream™ Technology, Oridion Medical, Jerusalem, Israel).

The continuous finger-pulse photoplethysmography (CNAP Monitor 500, CNSystems Medizintechnik GmbH, Graz, Austria) was used to measure the arterial blood pressure (ABP, mmHg) and heart rate (HR, bpm). Using a regular pneumatic cuff on the left arm, the calibration of ABP was periodically performed.

The unilateral cerebral flow velocity from the P2 segment of the left posterior cerebral artery (PCAv, cm/s) was measured using Transcranial Doppler ultrasound (Dolphin IQ and 4D, Viasonix, Netanya, Israel) with a 2 MHz monitoring probe. A 3D-printed custom-made helmet was used to hold the probe in place.

The cerebrovascular reactivity (CVR, %) to VS was computed as  $[\text{CVR} = (\Delta\text{PCAv}/\text{PCAv}_B) \times 100]$ , in which  $\Delta\text{PCAv}$  is the change of blood flow velocity in the posterior cerebral artery during VS with respect to the B ( $\text{PCAv}_B$ ).

All signals were continuously digitally sampled (CED Micro 1401 acquisition board and Spike2 ver. 9.14 software, Cambridge Electronic Design, Cambridge, UK) at 100 Hz and stored on the computer.

For each subject and each variable, the six consecutive (B + VS) cycles were averaged in a single one. In this 60-s lasting average cycle, the first 30 s correspond to B and the last 30 s correspond to the VS. Time average values were collected over the following sub-intervals: 15–25 s (B) and 45–55 s (VS), to exclude from the analysis the transients associated with the change between conditions.

### 2.5. Statistical analysis

We used MATLAB® ver. R2022a (The MathWorks, Natick, MA, USA) to perform statistical analysis. After normality assessment (Kolmogorov-Smirnov test), separate univariate ANOVAs were conducted on self-reported attention and on systemic (ABP, HR,  $P_{\text{ETCO}_2}$ ) and Doppler (PCAv) variables according to 2 groups (med-lows, med-highs)  $\times$  2 conditions design (B, VS) with and without hypnotizability as a covariate. Then, the CVR of med-highs and med-lows was compared between groups through univariate analysis. The Greenhouse-Geisser correction was used for non-sphericity. Spearman correlations and partial correlations controlling for hypnotizability of PCAv with CVR and reported attention as well as ABP and  $P_{\text{ETCO}_2}$  were computed. The level of significance was set at  $p = 0.05$ . Sample size and power were reported for all analyses.

## 3. Results

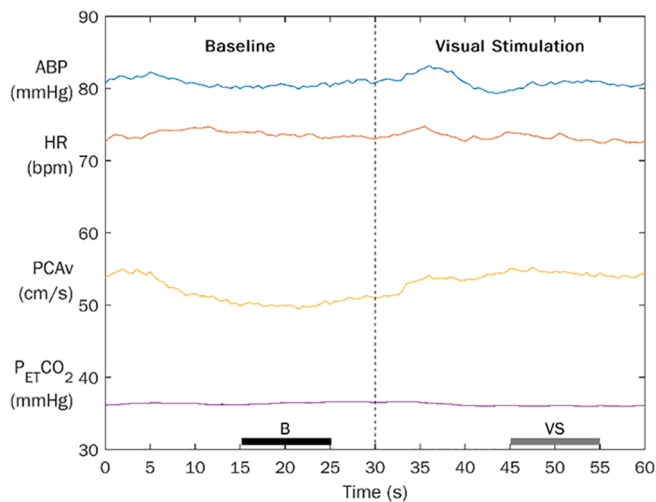
Two subjects (one med-low and one med-high) were outliers for PCAv and were excluded from analyses. Average traces during B and VS for the different variables are shown (Fig. 1).

Self-reported attention was not significantly different between med-lows (Mean  $\pm$  SD:  $8.71 \pm 0.58$ ) and med-highs ( $8.06 \pm 0.63$ ) although it was negatively correlated with hypnotizability ( $\rho = -0.597$ ,  $p = 0.003$ ).

PCAv increased significantly during VS with respect to B ( $F(1,21) = 67.45$ ;  $p = 0.0001$ ;  $\eta^2 = 0.970$ ;  $\alpha = 1.00$ ) independently from hypnotizability. The group effect, however, had low effect size ( $\eta^2 = 0.050$ ). On average, CVR was  $7.9 \pm 5.2\%$  (the two groups pooled together). Table 1 reports the mean values and standard deviations of all variables.

PCAv was not significantly correlated with ABP, HR, and  $P_{\text{ETCO}_2}$  in the baseline condition and its change during VS with respect to B ( $\Delta\text{PCAv}$ ) was not significantly correlated to  $\Delta\text{ABP}$ ,  $\Delta\text{HR}$ ,  $\Delta P_{\text{ETCO}_2}$  and reported attention. Partial correlation controlling for hypnotizability did not disclose any correlation.

No significant difference ( $\eta^2 = 0.014$ ,  $\alpha = 0.08$ ) was observed in CVR (Fig. 2) between med-lows (mean  $\pm$  SD:  $8.4 \pm 7.0\%$ ) and med-highs

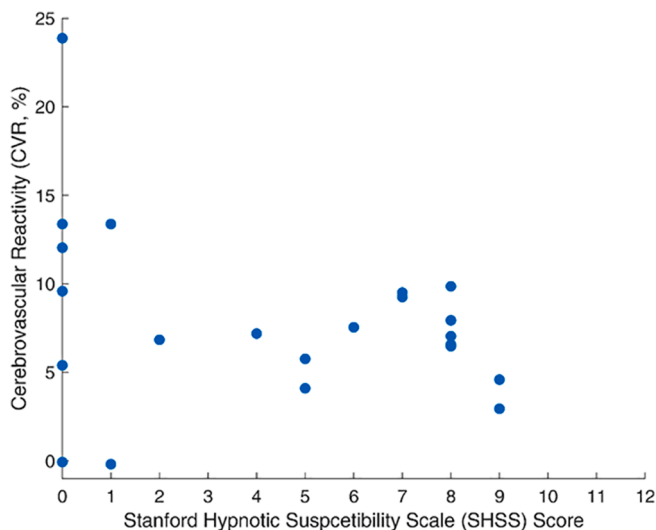


**Fig. 1.** Average traces during Baseline (B) and Visual Stimulation (VS) for the different variables (N = 21). ABP: arterial blood pressure; HR: Heart rate; PCAv: posterior cerebral artery flow velocity, and P<sub>ET</sub>CO<sub>2</sub>: partial pressure of end-tidal CO<sub>2</sub>. The black and gray bar at the bottom indicates the 10-s sub-interval taken from PCAv for both B and VS to compute cerebrovascular reactivity (CVR, %).

**Table 1**  
Variables mean values and standard deviation.

Condition	Variable	med-lows (N = 12)		med-highs (N = 9)	
		Mean	SD	Mean	SD
Basal	ABP (mmHg)	81.08	15.25	81.33	12.74
	HR (bpm)	71.07	11.38	78.12	12.97
	PCAv (cm/s)	50.58	9.57	50.65	9.92
	P <sub>ET</sub> CO <sub>2</sub> (mmHg)	37.08	2.23	34.66	3.32
VS	ABP (mmHg)	81.20	15.53	79.68	13.94
	HR (bpm)	71.52	11.05	77.19	13.01
	PCAv* (cm/s)	54.79	10.78	54.20	9.13
	P <sub>ET</sub> CO <sub>2</sub> (mmHg)	36.64	1.80	34.85	3.21

Note: (\*) indicates a significant difference between baseline (B) and visual stimulation (VS) conditions.



**Fig. 2.** Distribution of cerebrovascular reactivity (CVR) of 22 subjects as a function of hypnotizability score. The subject with SHSS score 6 intermediates between med-lows and med-highs is shown, although not included in the comparisons between two groups.

(7.0 ± 2.0 %), and effect size was very low ( $\eta^2 = 0.002$ ).

No significant correlation was observed between self-reported attention and CVR and was disclosed by partial correlation controlling for hypnotizability.

No significant correlation was observed between SHSS scores and CVR. Nonetheless, within groups correlation coefficients revealed a significant negative correlation between SHSS and CVR in med-highs ( $\rho = -0.814$ ,  $p = 0.008$ ) and no significant correlation in med-lows.

**4. Discussion**

Visual stimulation is one of the most effective means to induce pronounced blood flow increases in large cerebral arteries, considering that half of the brain cortex is dedicated to the processing of visual stimuli (Buerk and Riva, 2002; Donati et al., 1995). It has been effectively used to detect alterations in neurovascular coupling in several disease states such as Parkinson’s (Azevedo et al., 2010), cerebral amyloid angiopathy (Smith et al., 2008), familial amyloidotic polyneuropathy (Azevedo et al., 2011), severe carotid disease (Roje-Bedeković et al., 2010), hypertension as well as diabetes (Monteiro et al., 2021).

The VS increased blood flow velocity in the posterior cerebral artery in med-highs and med-lows, which agrees with earlier reports regarding the general population (Lisak et al., 2005; Samora et al., 2020; Spelsberg et al., 1998; Zaletel et al., 2002). The present findings do not reveal hypnotizability-related differences between med-lows’ and med-highs’ stimulation-related hyperemia. Low metabolic cost of tasks in highs was hypothesized owing to their mode of information processing which consists of poor local modulation of the electroencephalographic activity (Ibáñez-Marcelo et al., 2019). Moreover, the neurovascular coupling during cognitive tasks differs between med-lows and med-highs (Rashid et al., 2022). The unexpected absence of difference during VS can be due to the characteristics of the stimulus, although the low effect size of the comparisons between groups may have prevented the detection of significant hypnotizability-related differences.

However, the concomitant absence of changes in HR and ABP during VS allows us to exclude that possible hypnotizability-related differences in CVR were buffered by different systemic autonomic involvement. Moreover, the emotional content of the presented images may have buffered potential hypnotizability-related differences, as high hypnotizability is associated with high emotional intensity (Diolaiuti et al., 2019; Kirenskaya et al., 2011). Zaletel et al. (2002) suggested that the complexity of the task significantly elevated visually induced CVR as compared to the conventional types of VS such as silent reading (Balogh et al., 2022), white light (Leacy et al., 2018), flashing alternating (Frid et al., 2015) or flickering checkerboard (Monteiro et al., 2021), whereas repetitive VS measurements may result in attenuation of the CVR (Roje-Bedeković et al., 2010). The brightness does not appear to affect CVR (Zaletel et al., 2002). Based on these considerations, we adopted a more engaging VS requiring to detect hidden objects, expecting to observe a large CVR. However, the observed CVR was lower (mean ± SD: 7.9 ± 5.2 %) than what has been reported in response to conventional VS (mean ± SEM: 16.4 ± 1.5 %) (Aaslid, 1987). We can only speculate that the active engagement of the subject could have activated brain areas outside of PCA territory, which, conversely, might have been little affected by a static VS.

The expected lower metabolic cost of the VS in med-highs with respect to med-lows, however, was at least partially confirmed, as participant with med-highs hypnotizability showed a negative correlation between hypnotizability scores and CVR.

The absence of very high hypnotizable participants (SHSS score > 9 out of 12) in the sample may account for the unexpected negative correlation between hypnotizability and self-reported attention as highs usually display greater absorption than lows (Acunzo et al., 2021; Rominger et al., 2014; Tellegen and Atkinson, 1974).

A limitation of the study is that we did not investigate the blood flow



velocity in the main cortical branches of PCA separately. For example, one study found that the largest increase in blood flow velocity was observed in the calcarine artery after VS and it progressively declined in P2 PCA, the parieto-occipital artery, the occipital temporal artery, and the anterior temporal artery (Frid et al., 2015). Future studies could focus the measurement on smaller brain areas possibly characterized by higher reactivity.

To conclude, the present findings indicate that the cerebral hyperemia occurring during visual stimulation is independent from hypnotizability in participants with med-low hypnotizability scores, although it decreases with increasing hypnotizability scores at high hypnotizability levels. This finding concerning cerebrovascular reactivity fits with the view that the higher hypnotizability the lower the metabolic cost of the task, possibly owing to the highs' distributed rather than localized information processing (Ibáñez-Marcelo et al., 2019).

### Declaration of Competing Interest

The authors declare that they have no known competing financial interests or personal relationships that could have appeared to influence the work reported in this paper.

### Acknowledgments

This study was supported by the Ministero dell'Università e della Ricerca (MUR) under the program "Dipartimenti di Eccellenza ex L.232/2016" of the Dipartimento di Neuroscienze "Rita Levi Montalcini", Università degli Studi di Torino (UNITO) and under the program "Progetti di Ricerca di Ateneo 2018" of the Università di Pisa (UniPi). A.R. was supported by a Doctoral Fellowship funded by the Partnership for Knowledge (Pfk) program of the Agenzia Italiana per la Cooperazione allo Sviluppo (AICS), Ministero degli Affari Esteri e della Cooperazione Internazionale (MAECI), Italy. We are grateful to Dr. Raffaele Pertusio for his technical assistance.

### References

- Aaslid, R., 1987. Visually evoked dynamic blood flow response of the human cerebral circulation. *Stroke* 18, 771–775. <https://doi.org/10.1161/01.str.18.4.771>.
- Acunzo, D.J., Oakley, D.A., Terhune, D.B., 2021. The neurochemistry of hypnotic suggestion. *Am. J. Clin. Hypn.* 63, 355–371. <https://doi.org/10.1080/00029157.2020.1865869>.
- Azevedo, E., Santos, R., Freitas, J., Rosas, M.J., Gago, M., Garrett, C., Rosengarten, B., 2010. Deep brain stimulation does not change neurovascular coupling in non-motor visual cortex: an autonomic and visual evoked blood flow velocity response study. *Parkinsonism Relat. Disord.* 16, 600–603. <https://doi.org/10.1016/j.parkreidis.2010.08.016>.
- Azevedo, E., Castro, P., Santos, R., Coelho, T., Rosengarten, B., Panerai, R., 2011. Autonomic dysfunction affects cerebral neurovascular coupling. *Clin. Auton. Res.* 21, 395–403. <https://doi.org/10.1007/s10286-011-0129-3>.
- Balogh, E., Árokzallási, T., Körtefai, K., Nagy, V.É., Csiba, L., Oláh, L., 2022. Effects of acute alcohol consumption on neuronal activity and cerebral vasomotor response. *Neurol. Sci.* 43, 625–631. <https://doi.org/10.1007/s10072-021-05273-4>.
- Buerk, D.G., Riva, C.E., 2002. Adenosine enhances functional activation of blood flow in cat optic nerve head during photic stimulation independently from nitric oxide. *Microvasc. Res.* 64, 254–264. <https://doi.org/10.1006/mvre.2002.2432>.
- Diolaiuti, F., Huber, A., Ciaramella, A., Santarcangelo, E.L., Sebastiani, L., 2019. Hypnotizability-related Interoceptive Awareness and Inhibitory/Activating Emotional Traits. *Arch. Ital. Biol.* 157, 111–119. <https://doi.org/10.12871/00039829202042>.
- Donati, G., Pourmaras, C.J., Munoz, J.L., Poitry, S., Poitry-Yamate, C.L., Tsacopoulos, M., 1995. Nitric oxide controls arteriolar tone in the retina of the miniature pig. *Invest. Ophthalmol. Vis. Sci.* 36, 2228–2237.
- Dorner, G.T., Garhofer, G., Kiss, B., Polska, E., Polak, K., Riva, C.E., Schmetterer, L., 2003. Nitric oxide regulates retinal vascular tone in humans. *Am. J. Physiol. Hear. Circ. Physiol.* 285, H631–H636. <https://doi.org/10.1152/ajpheart.00111.2003>.
- Frid, P.E., Schreiber, S.J., Pade, O., Doepp, F., Valdeza, J., 2015. The Posterior Cerebral Artery and its Main Cortical Branches Identified with Noninvasive Transcranial Color-Coded Duplex Sonography. *Ultrasound Int. Open* 1, E53–E57. <https://doi.org/10.1055/s-0035-1565130>.
- Ho, Y.C.L., Petersen, E.T., Zimine, I., Golay, X., 2011. Similarities and differences in arterial responses to hypercapnia and visual stimulation. *J. Cereb. Blood Flow Metab.* 31, 560–571. <https://doi.org/10.1038/jcbfm.2010.126>.
- Ibáñez-Marcelo, E., Campioni, L., Phinyomark, A., Petri, G., Santarcangelo, E.L., 2019. Topology Highlights Mesoscopic Functional Equivalence between Imagery and Perception: The Case of Hypnotizability. *Neuroimage* 200, 437–449. <https://doi.org/10.1016/j.neuroimage.2019.06.044>.
- Ito, H., Kanno, I., Ibaraki, M., Suhara, T., Miura, S., 2008. Relationship between baseline cerebral blood flow and vascular responses to changes in PaCO<sub>2</sub> measured by positron emission tomography in humans: implication of inter-individual variations of cerebral vascular tone. *Acta Physiol.* 193, 325–330. <https://doi.org/10.1111/j.1748-1716.2008.01847.x>.
- Jambrik, Z., Santarcangelo, E.L., Ghelarducci, B., Picano, E., Sebastiani, L., 2004. Does hypnotizability modulate the stress-related endothelial dysfunction? *Brain Res. Bull.* 63, 213–216. <https://doi.org/10.1016/j.brainresbull.2004.01.011>.
- Jambrik, Z., Santarcangelo, E.L., Rudisch, T., Varga, A., Forster, T., Carli, G., 2005. Modulation of pain-induced endothelial dysfunction by hypnotizability. *Pain* 116, 181–186. <https://doi.org/10.1016/j.pain.2005.03.041>.
- Kirenskaya, A.V., Novototsky-Vlasov, V.Y., Chistyakov, A.N., Zvonikov, V.M., 2011. The relationship between hypnotizability, internal imagery, and efficiency of neurolinguistic programming. *Int. J. Clin. Exp. Hypn.* 59, 225–241. <https://doi.org/10.1080/00207144.2011.546223>.
- Kondo, M., Wang, L., Bill, A., 1997. The role of nitric oxide in hyperaemic response to flicker in the retina and optic nerve in cats. *Acta Ophthalmol. Scand.* 75, 232–235. <https://doi.org/10.1111/j.1600-0420.1997.tb00762.x>.
- Leacy, J.K., Zouboules, S.M., Mann, C.R., Peltonen, J.D.B., Saran, G., Nysten, C.E., Nysten, H.E., Brutsaert, T.D., O'Halloran, K.D., Sherpa, M.T., Day, T.A., 2018. Neurovascular Coupling Remains Intact During Incremental Ascent to High Altitude (4240 m) in Acclimatized Healthy Volunteers. *Front. Physiol.* 9 <https://doi.org/10.3389/fphys.2018.01691>.
- Leontiev, O., Buxton, R.B., 2007. Reproducibility of BOLD, perfusion, and CMRO<sub>2</sub> measurements with calibrated-BOLD fMRI. *Neuroimage* 35, 175–184. <https://doi.org/10.1016/j.neuroimage.2006.10.044>.
- Lindauer, U., Megow, D., Matsuda, H., Dirnagl, U., 1999. Nitric oxide: a modulator, but not a mediator, of neurovascular coupling in rat somatosensory cortex. *Am. J. Physiol.* 277, H799–H811. <https://doi.org/10.1152/ajpheart.1999.277.2.H799>.
- Lisak, M., Trkanjec, Z., Mikula, L., Demarin, V., 2005. Mean blood flow velocities in posterior cerebral arteries during visual stimulation. *Mt. Sinai J. Med.* 72, 346–350.
- Ma, J., Ayata, C., Huang, P.L., Fishman, M.C., Moskowitz, M.A., 1996. Regional cerebral blood flow response to vibrissal stimulation in mice lacking type I NOS gene expression. *Am. J. Physiol.* 270, H1085–H1090. <https://doi.org/10.1152/ajpheart.1996.270.3.H1085>.
- Monteiro, A., Castro, P., Pereira, G., Ferreira, C., Sorond, F., Milstead, A., Higgins, J.P., Polónia, J., Azevedo, E., 2021. Neurovascular Coupling Is Impaired in Hypertensive and Diabetic Subjects Without Symptomatic Cerebrovascular Disease. *Front. Aging Neurosci.* 13, 1–11. <https://doi.org/10.3389/fnagi.2021.728007>.
- Newman, E.A., 2013. Functional hyperemia and mechanisms of neurovascular coupling in the retinal vasculature. *J. Cereb. Blood Flow Metab.* 33, 1685–1695. <https://doi.org/10.1038/jcbfm.2013.145>.
- Paulson, O.B., Hasselbalch, S.G., Rostrup, E., Knudsen, G.M., Pelligrino, D., 2010. Cerebral blood flow response to functional activation. *J. Cereb. Blood Flow Metab.* 30 (1), 2–14.
- Rashid, A., Santarcangelo, E.L., Roatta, S., 2022a. Cerebral Blood Flow in Healthy Subjects with Different Hypnotizability Scores. *Brain Sci.* 12, 558. <https://doi.org/10.3390/brainsci12050558>.
- Rashid, A., Santarcangelo, E.L., Roatta, S., 2022b. Does Hypnotizability Affect Neurovascular Coupling During Cognitive Tasks? *Physiology & Behavior*, 113915. <https://doi.org/10.1016/j.physbeh.2022.113915>. In press.
- Roje-Bedeković, M., Bosnar-Puretić, M., Lovrenčić-Huzjan, A., Demarin, V., 2010. Cerebrovascular Evoked Response to Repetitive Visual Stimulation in Severe Carotid Disease – Functional Transcranial Doppler Study. *Acta Clin. Croat.* 49, 267–274.
- Rominger, C., Weiss, E.M., Nagl, S., Niederstätter, H., Parson, W., Papousek, I., 2014. Carriers of the COMT Met/Met allele have higher degrees of hypnotizability, provided that they have good attentional control: a case of gene-trait interaction. *Int. J. Clin. Exp. Hypn.* 62, 455–482. <https://doi.org/10.1080/00207144.2014.931177>.
- Samora, M., Vianna, L.C., Carmo, J.C., Macedo, V., Dawes, M., Phillips, A.A., Paton, J.F.R., Fisher, J.P., 2020. Neurovascular coupling is not influenced by lower body negative pressure in humans. *Am. J. Physiol. Hear. Circ. Physiol.* 319, H22–H31. <https://doi.org/10.1152/ajpheart.00076.2020>.
- Santarcangelo, E.L., Paoletti, G., Balocchi, R., Carli, G., Morizzo, C., Palombo, C., Varanini, M., 2012. Hypnotizability modulates the cardiovascular correlates of subjective relaxation. *Int. J. Clin. Exp. Hypn.* 60, 383–396. <https://doi.org/10.1080/00207144.2012.700609>.
- Santarcangelo, E.L., Scattina, E., 2019. Responding to Sensorimotor Suggestions: From Endothelial Nitric Oxide to the Functional Equivalence Between Imagery and Perception. *Int. J. Clin. Exp. Hypn.* 67, 394–407. <https://doi.org/10.1080/00207144.2019.1649539>.
- Smith, E.E., Vijayappa, M., Lima, F., Delgado, P., Wendell, L., Rosand, J., Greenberg, S.M., 2008. Impaired visual evoked flow velocity response in cerebral amyloid angiopathy. *Neurology* 71, 1424–1430. <https://doi.org/10.1212/01.wnl.0000327887.64299.a4>.
- Spelsberg, B., Böhning, A., Kömpf, D., Kessler, C., 1998. Visually induced reactivity in posterior cerebral artery blood flow. *J. Neuro-Ophthalmology* 18, 263–267.
- Tellegen, A., Atkinson, G., 1974. Openness to Absorbing and Self-Altering Experiences ("Absorption"), A Trait related to Hypnotic Susceptibility. *J. Abnorm. Psychol.* 83, 268–277. <https://doi.org/10.1037/h0036681>.
- Weitzenhoffer, A.M., Hilgard, E.R., 1959. *Stanford Hypnotic Susceptibility Scale*. Press, Forms A and B. Consult. Psychol.
- Zaletel, M., Ž, B., Š, M., Pogač, T., Kiauta, T., 2002. The influence of brightness, colour and complexity on visual evoked doppler flow responses. *Ultrasound Med. Biol.* 28 (7), 917–922.



# Differential control of blood flow in masseter and biceps brachii muscles during stress

Anas Rashid, Silvestro Roatta\*

Lab of Integrative Physiology, Department of Neuroscience "Rita Levi Montalcini", University of Torino, Torino, Italy

## ARTICLE INFO

### Keywords:

Blood flow  
Oxygenation  
Masseter  
Biceps  
Muscle  
Stress

## ABSTRACT

**Objective:** The present study aimed to compare sympathetic hemodynamic effects in masticatory and limb muscles in response to different stressors.

**Design:** Twelve healthy participants were subjected to a randomized series of stressors, including cold pressor test (CPT), mental arithmetic test, apnea, isometric handgrip (IHG) and post-handgrip muscle ischemia (PHGMI), while in the supine position. Spatially-resolved near-infrared spectroscopy was used to measure relative changes in blood volume and oxygenation (TOI) of the resting masseter and biceps muscles. Cardiac output, heart rate, and arterial blood pressure (ABP) were also monitored.

**Results:** Except apnea, all tests increased ABP. Different response patterns were observed in the 2 muscles: TOI significantly increased during contralateral IHG ( $1.24 \pm 1.17\%$ ) but markedly decreased during CPT ( $-4.84 \pm 4.09\%$ ) and PHGMI ( $-6.65 \pm 5.31\%$ ) in the biceps muscle, while exhibiting consistent increases in the masseter ( $1.88 \pm 1.85\%$ ;  $1.60 \pm 1.75\%$ ;  $1.06 \pm 3.29\%$ , respectively) ( $p < 0.05$ ).

**Conclusions:** The results allow us to infer differential control of blood flow in head and limb muscles. In general, the masseter appears more prone to dilatation than the biceps, exhibiting opposite changes in response to painful stimuli (CPT and PHGMI). Several mechanisms may mediate this effect, including reduced sympathetic outflow to the extracranial vasculature of the head, generally exposed to lower hydrostatic loads than the rest of the body.

## 1. Introduction

Sympathetic activation generally increases heart rate and contractility as well as the total peripheral resistance, which then results in increased arterial blood pressure. However, different patterns of sympathetic activation may be elicited by different stressors (stressor-specificity) (Pacák & Palkovits, 2001; Roatta et al., 2011), with differential activation to the various organs and tissues (Vissing, 1997). In addition, there is evidence that sympathetic outflow also varies depending on the body area, e.g., with upper and lower limbs. In some cases, opposite vascular effects have been reported, e.g., during unilateral handgrip, dilatation in the contralateral forearm and vasoconstriction in legs has been reported, and similar effects were observed during cognitive tasks (Eklund & Kaijser, 1976; Rusch et al., 1981). Along the same line, Carter et al. (2005) report a less marked dilatation in legs than in arms during mental stress. It was hypothesized that these differences in the vascular

control between arms and legs could be related to the different hydrostatic gradients that affect blood vessels in the two areas (Jacob et al., 2000).

In this respect, the head is a peculiar body area: because of its position above heart level (whenever the body is sitting or standing), its vascular networks are affected by low hydrostatic load and lower perfusion pressure, compared to other body regions. Interestingly, a different vascular control has been reported for cutaneous tissues of the head as compared to the limbs. In general, the studies evidenced dilatatory rather than constrictory responses in the facial districts, e.g., during verbal tasks, public speech and mental stress (Vassend & Knardahl, 2005). Whether a differentiated hemodynamic response to stress also concerns the skeletal muscles of the head is unclear. Only a few studies investigated vascular stress responses in head muscles, reporting an increase in tissue oxygenation in the masseter muscle during both mental stress (Hidaka et al., 2004b; Tanosoto et al., 2012) and cold

**Abbreviations:** ABP, arterial blood pressure; NIRS, near-infrared spectroscopy; EMG, electromyography; THI, tissue hemoglobin index; TOI, tissue oxygenation index; HR, heart rate; CO, cardiac output; MVC, maximum voluntary contraction; CPT, cold pressor test.

\* Correspondence to: Lab of Integrative Physiology, Department of Neuroscience, University of Torino, Corso Raffaello 30, Torino 10125, Italy.

E-mail address: [silvestro.roatta@unito.it](mailto:silvestro.roatta@unito.it) (S. Roatta).

<https://doi.org/10.1016/j.archoralbio.2022.105490>

Received 18 February 2022; Received in revised form 3 June 2022; Accepted 16 June 2022

Available online 18 June 2022

0003-9969/© 2022 Elsevier Ltd. All rights reserved.

pressor test (Maekawa et al., 1998a). However, standard near-infrared spectroscopy measurement could have been affected by the concomitant increase in skin blood flow, as has now been demonstrated in many different experimental conditions (Canova et al., 2011; Messere & Roatta, 2013; Tew et al., 2010). Moreover, sporadic contractions and increase in muscle tone, which are a specific component of the stress response (Hidaka et al., 2004a, 2004b; Sjøgaard et al., 2000) may affect hemodynamics in the relevant muscles.

To our knowledge, comparative studies based on the simultaneous recording from head and limb muscles have never been reported in humans and the few available animal studies do not clarify the issue, reporting no difference in the vascular response of masseter and quadriceps muscles to adrenaline continuous infusion (Terakawa & Ichinohe, 2012), but stronger vascular constriction in the quadriceps, in response to hypercapnia (Ichinohe et al., 2020).

The study aimed to test the hypothesis that blood flow of head and limb muscles is differentially controlled, in a stressor-dependent way. To this aim five different stress tests were implemented and several methodological arrangements were devised to control for confounding factors such as interference from involuntary electromyographic activity and hemodynamic changes in cutaneous circulation, as detailed in methods.

## 2. Methods

### 2.1. Subjects

Twelve (9 males, 3 females) healthy volunteers (age:  $26 \pm 3$  years; weight:  $68 \pm 11$  kg; height:  $175 \pm 9$  cm) were enrolled in this study. All of them were non-obese and normotensive (resting blood pressure  $<140/90$  mmHg).

### 2.2. Ethical approval

This study was carried out in accordance with the Declaration of Helsinki and was approved by the Institutional Ethical Committee of the University of Torino (prot. 60195). All subjects signed informed consent before participating in the study.

### 2.3. Measurements

A continuous-wave near-infrared spectroscopy (NIRS) (NIRO-200NX, Hamamatsu Photonics, Hamamatsu, Japan) was used to measure changes in tissue haemoglobin index (THI) and tissue oxygenation index (TOI). The device implements both the classical modified Beer-Lambert method and the spatially-resolved spectroscopy (Grassi & Quaresima, 2016). Based on our previous experience we focused our attention on spatially-resolved parameters which, being less affected by cutaneous circulation, (Canova et al., 2011) provide a more specific monitoring of muscle tissue hemodynamics (Messere & Roatta, 2013; Messere et al., 2018a). In particular, the TOI estimates the percentage ratio of oxygenated to total hemoglobin. However, since NIRS cannot discriminate between myoglobin and hemoglobin, all measurements refer to the whole (myoglobin + hemoglobin) concentration (Messere et al., 2018a). In addition, THI detects changes in (hemoglobin + myoglobin) concentration. Since no change in myoglobin concentration is expected to take place in the short term, it is employed to detect changes in blood volume (within the sample volume). Since this variable reveals relative changes with respect to a reference level it is generally normalized to the basal value (taken in resting conditions). The device has two probes: one was placed over the biceps brachii short head muscle of the left arm, and the other over the right superficial masseter muscle, electromyography (EMG) electrodes over the left masseter not leaving enough room for the NIRS probe over the same muscle (see below).

The continuous surface electromyography (Quattro, OT

Bioelectronics, Torino, Italy; gain:1200; bandwidth: 10 – 500 Hz) is used to detect any possible involuntary muscle contraction during the tests. Two differential recordings were collected from bipolar adhesive electrodes (inter-electrode distance 2.3 cm; FIAB Spa, Florence, Italy) from the left masseter and biceps brachii muscles. The electrodes were placed on the masseter symmetrically to the NIRS probe and on the biceps just aside of the NIRS probe, in both cases, the inter-electrode axis being parallel to orientation of muscle fibers. The ground electrode was placed over the wrist.

The heart rate (HR), arterial blood pressure (ABP) and cardiac output (CO) were measured by continuous finger-pulse photoplethysmography (CNAP Monitor 500, CNSystems Medizintechnik GmbH, Graz, Austria) in order to quantify the extent and pattern of sympathetic activation. Calibration of ABP was periodically performed using a regular pneumatic cuff at the right arm.

Handgrip force was measured by a custom-made device based on two flexiforce sensors (Tekscan, Inc. Massachusetts, USA), previously calibrated (Testa et al., 2016).

All signals were continuously digitally sampled (CED Micro 1401, Cambridge Electronic Design, Cambridge, UK) at 100 Hz, except EMG which was sampled at 2 kHz and stored on the computer. The Spike2 software (Version 9.14, Cambridge Electronic Design, Cambridge, UK), was used for both data acquisition and analysis.

### 2.4. Experimental procedures

The experiments were performed in a quiet room with a constant ambient temperature of about 21–23 °C. Before starting the recordings, the maximum voluntary contraction (MVC) has been measured and the visual feedback has been provided to the participant.

The participants were asked to relax while staying in a supine position. This position was chosen to eliminate the hydrostatic gradient between the masseter and the biceps muscles which would have complicated the comparison of hemodynamic responses. After all signals reached a stable condition, a 10 min baseline period was recorded, after which participants completed a sequence of 5 different tasks, described below.

Even short muscle contractions are known to evoke rapid and prominent hemodynamic changes which could overlap with and disturb the response to the stressor. Thus, the subjects were periodically reminded to maintain relaxed all muscles, particularly the jaw and left arm muscles. The tasks were separated by a minimum of 5-mins rest (with additional time if required) to ensure that all variables were stable before starting the next task and were performed in a randomized order, except post-handgrip muscle ischemia, which immediately followed isometric handgrip.

#### 2.4.1. Cold pressor test (CPT)

The subject was asked to immerse the right hand for 2 min into a bucket filled with cold water (8 °C, measured by a digital thermometer: Omega 450-ATH, OMEGA Engineering, Norwalk, CT, USA). After the task, participants were asked to report the peak pain level experienced by the visual analogue scale: 0 corresponding to 'no pain' and 10 corresponding to 'the worst pain imaginable'.

#### 2.4.2. Mental arithmetic test

The subject was asked to progressively subtract the odd numbers (1, 3, 5, etc.) from 1000 for 2 min, writing each result on a paper with the right hand. For this purpose, a clipboard was placed over a cushion, on the subject's chest. The clipboard was supported by an operator, who also monitored the outcome, promptly asking the subject to repeat the calculation in case of a mistake.

#### 2.4.3. Apnea

The subject was asked to hold their breath as long as possible. All subjects were able to sustain the apnea for at least 40 s

#### 2.4.4. Isometric handgrip

The subject was requested to grip the handgrip dynamometer at 50% of their MVC for 1 min, with the right hand. The visual feedback of the exerted force was provided on a computer screen, a horizontal cursor placed at 50% MVC indicating the target force level.

#### 2.4.5. Post-handgrip muscle ischemia

Ten seconds before the cessation of the isometric handgrip, a blood pressure cuff (Gima, Gessate, Italy) was wrapped around the right arm and inflated to a supra-systolic pressure of 250 mmHg and maintained at this level for 2 min to occlude blood flow to the forearm muscles. After the task, the subject was asked to report the peak pain intensity during the test according to a visual analogue scale.

#### 2.5. Data analysis and statistics

The average response to each stressor was computed for all relevant variables: ABP, HR, CO, THI and TOI and presented graphically. Stress-induced changes were evaluated by comparing the time average over the last 10 s of stress exposure with the baseline, computed over the 10 s before. Average effects for the NIRS variables were calculated as follows:  $\Delta\text{THI} = (\text{THI}_{\text{stress}} - \text{THI}_{\text{baseline}}) / \text{THI}_{\text{baseline}} * 100$ , expressed as % of baseline;  $\Delta\text{TOI} = \text{TOI}_{\text{stress}} - \text{TOI}_{\text{baseline}}$ , expressed as % of oxygenated hemoglobin. Normality of data distribution was first verified by the Kolmogorov-Smirnov test. Statistical significance (with familywise alpha level of 0.05) of stress-induced changes in all these variables was then assessed by Student-t and Hochberg's tests, with Dunn/Sidak alpha correction method for multiple comparisons. Differences between masseter and biceps muscles in terms of  $\Delta\text{THI}$  and  $\Delta\text{TOI}$  were tested

with the same procedure. The Student-t test was used to compare basal oxygenation levels in the biceps and masseter muscles. Statistical analysis was performed using MATLAB® Version R2020b (The MathWorks, Natick, MA, USA). Post-hoc power analysis (two-tails,  $\alpha = 0.05$ ) was conducted using G-Power ver. 3.1.9.6 (Heinrich-Heine-Universität Düsseldorf, Düsseldorf, Germany). Pearson's correlation coefficient was used to assess correlation between pain scores and ABP and TOI responses. Data in the Results section are presented using box plots.

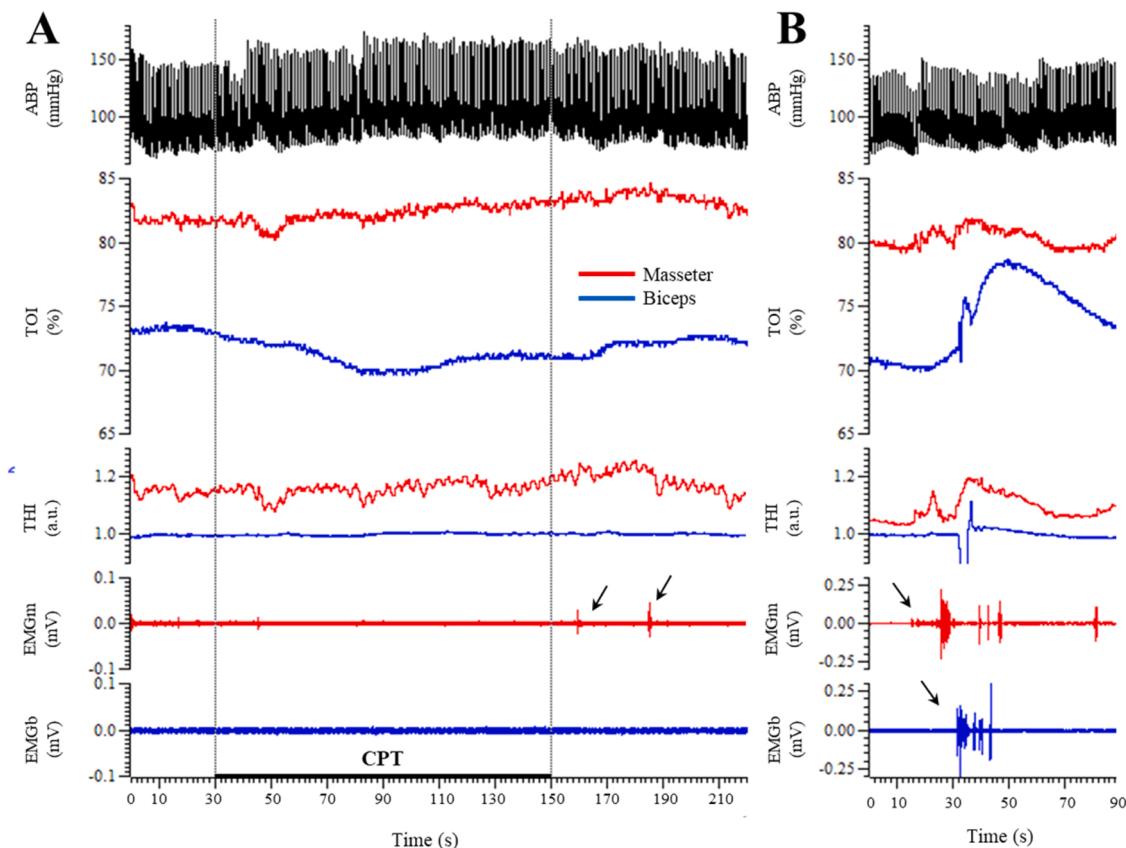
### 3. Results

During basal conditions, the TOI in the masseter muscle ( $80.0 \pm 2.6\%$ ) was higher than in the biceps in 9 out of 12 subjects, although not reaching overall statistical significance ( $76.7 \pm 4.7\%$ ,  $p = 0.058$ ).

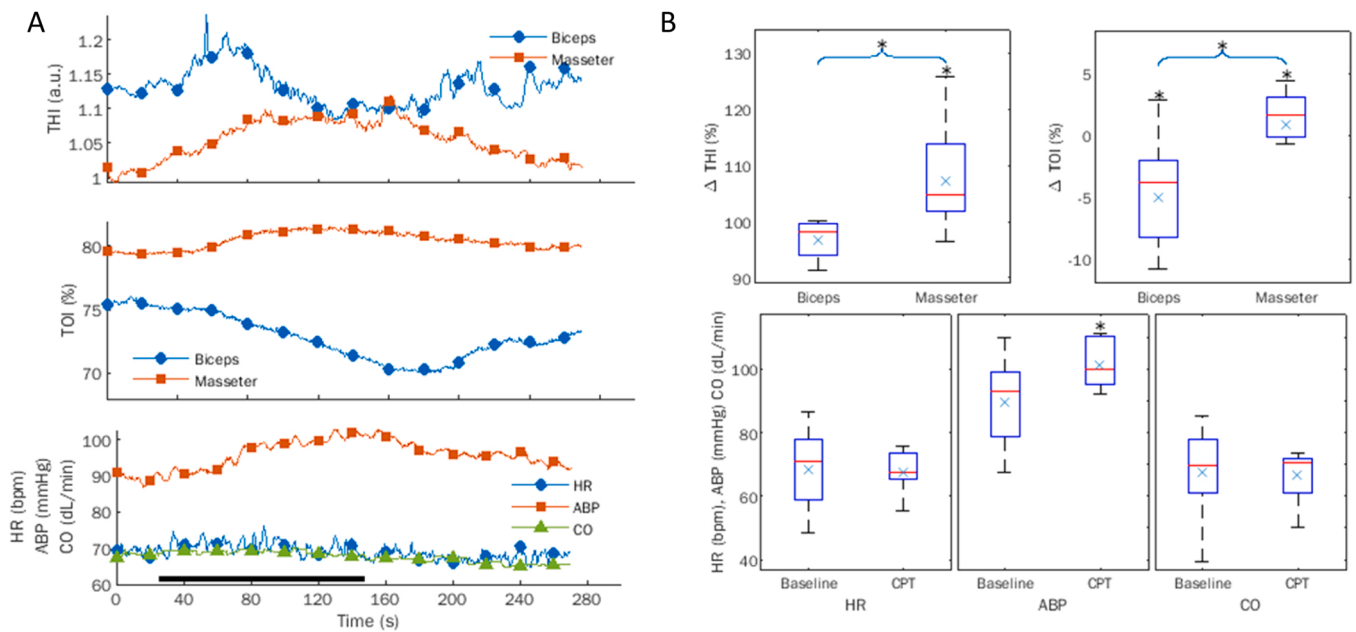
Absence of relevant signs of EMG activation during baseline intervals and during the different tasks was verified by visual inspection of the recordings. An example of original recordings from a representative subject during the CPT test is given in Fig. 1A. As a term of comparison, EMG activation and corresponding changes in NIRS variables evoked by short voluntary isometric contractions are shown in Fig. 1B.

#### 3.1. Cold pressor test

The response to CPT is described by the average curves of Fig. 2A, and distribution of the effects for the different variables are reported in Fig. 2B. The test significantly increased ABP (from  $90.1 \pm 14.0$ – $101.6 \pm 15.9$  mmHg,  $p < 0.05$ ) while producing a non-significant decrease in HR (from  $69.1 \pm 11.9$ – $68.2 \pm 9.8$  bpm,  $p < 0.05$ ) and CO (from  $68.2 \pm 13.7$ – $67.2 \pm 13.6$  dL/min,  $p < 0.05$ ).



**Fig. 1.** Original recordings from a representative subject during the cold pressor test (CPT) (A) and in response to voluntary isometric contractions of the masseter and the biceps muscles (B). Note that electromyography recordings, which are magnified in A compared to B, effectively reveal even the smallest involuntary contractions, e.g., after the end of the CPT in the masseter muscle (black arrows, A) and that stronger contractions (black arrows, B) may produce visible hemodynamic changes in near-infrared spectroscopy variables. Vertical dotted lines indicate start and end of CPT. ABP: arterial blood pressure, TOI: tissue oxygenation index, THI: tissue hemoglobin index (a.u.: arbitrary units), electromyograms from masseter and biceps muscles: EMGm and EMGb, respectively.



**Fig. 2.** Response to cold pressor test (CPT). Average response curves (A) and distribution of the effects for the different variables (B), as described by the median (red line), the interquartile range (blue box), minimum and maximum values (lower and upper whiskers, respectively), and mean (green x). THI: tissue hemoglobin index (a.u.: arbitrary units); TOI: tissue oxygenation index; HR: heart rate; ABP: arterial blood pressure; CO: cardiac output. The black bar at the bottom indicates the duration of the CPT. Note the opposite effects on TOI and THI exhibited by the masseter and the biceps muscles. \*)  $p < 0.05$ ;  $n = 12$ .

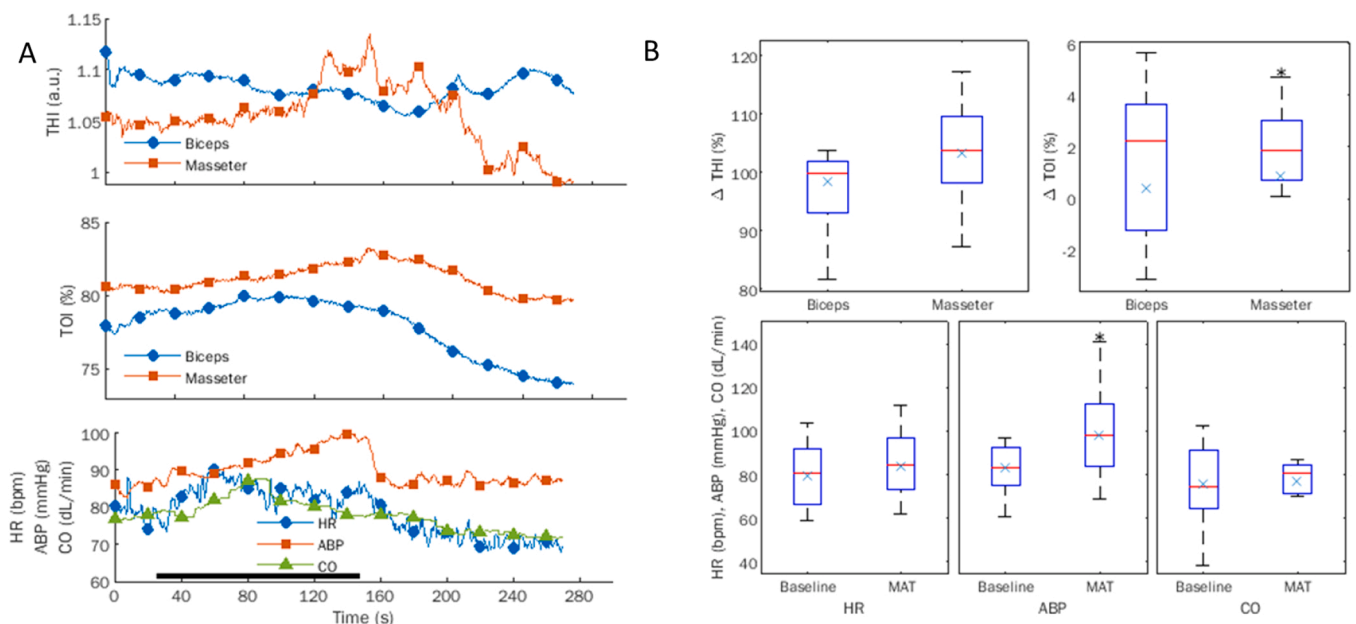
Notably, the CPT effects on NIRS variables were opposite in the two muscles, increasing in the masseter muscle ( $\Delta$ THI:  $9 \pm 9\%$ ,  $P < 0.05$ ; TOI: from  $79.5 \pm 2.9$ – $81.1 \pm 2.2\%$ ,  $p < 0.05$ ) and decreasing in the biceps muscle ( $\Delta$ THI:  $-2 \pm 7\%$ , n.s.; TOI: from  $75.6 \pm 4.2\%$  to  $70.7 \pm 4.8$ ,  $p < 0.05$ ).

On average the subjects reported a maximum pain score of  $7.0 \pm 2.1$ . Pain did not correlate with ABP nor with TOI, except for TOI vs. pain in the biceps muscle:  $r = -0.55$  ( $p < 0.01$ ).

### 3.2. Mental arithmetic test

The average response to mental arithmetic test (Fig. 3A and B) also exhibited a significant increase in ABP (from  $84.1 \pm 15.8$ – $98.7 \pm 20.6$  mmHg,  $p < 0.05$ ) while producing a non-significant increase in HR and CO.

The masseter muscle exhibited a significant increase in oxygenation (TOI: from  $80.5 \pm 3.1$ – $82.5 \pm 3.6\%$ ,  $p < 0.05$ ) and a non-significant increase in blood volume ( $\Delta$ THI:  $5 \pm 9\%$ ) while non-significant changes were observed in the biceps muscle.



**Fig. 3.** Response to mental arithmetic test (MAT). Average response curves (A) and distribution of the effects (B) for the different variables. Notations and abbreviations as in Fig. 2. The black bar at the bottom indicates the duration of the MAT. \*)  $p < 0.05$ ;  $n = 12$ .

### 3.3. Apnea

No significant changes were exhibited by the different variables during apnea (see Fig. 4A and B), although THI showed a tendency to increase in the masseter muscle ( $\Delta$ THI:  $14 \pm 21\%$ , n.s.) that was not exhibited by the biceps ( $-2 \pm 5\%$ ).

### 3.4. Isometric handgrip and post-handgrip muscle ischemia

The response to isometric handgrip and post-handgrip ischemia is described by the average curves of Fig. 5A, and distribution of the effects for the different variables are reported in Fig. 5B and C. With isometric handgrip, both HR (from  $72.4 \pm 12.8$ – $85.5 \pm 12.6$  bpm;  $p < 0.05$ ) and in ABP (from  $86.9 \pm 21.2$ – $106.5 \pm 22.1$  mmHg;  $p < 0.05$ ) were significantly increased. TOI similarly increased in both the masseter (from  $80.2 \pm 2.5$ – $82.1 \pm 3.4\%$ ,  $p < 0.05$ ) and the biceps muscle (from  $76.5 \pm 5.0\%$  to  $78.2 \pm 4.9\%$ ,  $p < 0.05$ ) while THI increased only in the masseter muscle ( $\Delta$ THI:  $7 \pm 7\%$ ,  $p < 0.05$ ) and significantly more than in the biceps muscle ( $p < 0.05$ ).

Compared to resting levels (before isometric handgrip), post-handgrip ischemia resulted in a marked increase in ABP (from  $86.9 \pm 21.2$ – $103.0 \pm 18.1$  mmHg;  $p < 0.05$ ), accompanied by a decreasing trend in HR (from  $72.4 \pm 12.8$ – $67.1 \pm 10.2$  bpm; n.s.) and a decrease in CO (from  $74.7 \pm 12.8$ – $66.7 \pm 14.0$  dL/min;  $p < 0.05$ ). As with CPT, NIRS response to post-handgrip ischemia produced significantly different responses in the two muscles, with significant increases in the masseter (TOI: from  $80.2 \pm 2.5\%$  to  $81.2 \pm 3.8\%$ ,  $p < 0.05$ ;  $\Delta$ THI:  $6 \pm 10\%$ ,  $p < 0.05$ ) and decreases in the biceps (TOI: from  $76.9 \pm 5.0\%$  to  $70.3 \pm 5.5\%$ ,  $p < 0.05$ ;  $\Delta$ THI:  $-3 \pm 7\%$ , n.s.).

On average the subjects reported a maximum pain score of  $7.1 \pm 1.6$ . Pain did not correlate with ABP nor with TOI.

Post-hoc power analysis confirmed that the sample size was adequate to support the major outcomes of the study, namely, the TOI increase in the masseter muscle (in all tests except apnea) and the opposite response patterns in masseter and biceps muscles (in CPT and post-handgrip ischemia).

## 4. Discussion

For the first time, to our knowledge, the study focused on the

differential control of blood flow in head and limb muscles during stress. We hypothesized that the autonomic vascular control could be differentiated to these body areas, also depending on the type of stress.

The results evidenced that: 1) all tests effectively activated the sympathetic nervous system as revealed by significant increases in arterial blood pressure and/or heart rate, except apnea. 2) in the masseter muscle tissue oxygenation index increased in all tests (although, non-significantly in apnea); 3) in the biceps muscle tissue oxygenation index exhibited both increases (in isometric handgrip) and marked decrease (in cold pressor test and post-handgrip muscle ischemia) depending on the stressor. 5) tissue hemoglobin index changes were always concordant with tissue oxygenation index's, although generally less significant. As will be discussed below, these observations support the hypothesis that sympathetic outflow to skeletal muscles of the head and limbs is differentially controlled in a stressor-dependent way.

### 4.1. Interpretation of near-infrared spectroscopy signals

It is well known that near-infrared spectroscopy does not provide a direct measurement of blood flow. However, if a condition of constant metabolism can be hypothesized (e.g., in completely relaxed muscles), changes in blood flow would be associated with concordant changes in tissue oxygenation and, consequently, changes in oxygenation may be used to detect changes in blood flow. This concept has been demonstrated in several studies in which a blood flow reduction induced by sympathetic vasoconstriction also resulted in decreased tissue oxygenation (Boushel & Piantadosi, 2000; Fadel et al., 2004; Ogata et al., 2012; Ogata et al., 2002). Conversely, the transient hyperemia produced by a short-lasting compressive stimulus, in relaxed muscles results in a consistent increase in tissue oxygenation (Messere et al., 2017; Messere et al., 2018b). Constriction/dilatation of blood vessels may also produce a slight reduction/increase in blood volume indices, (Ogata et al., 2002) unless this effect is hidden by a larger volume change of the venous compartment, e.g., due to vessel compression (Messere et al., 2017). Consistent with this concept, an increase in tissue oxygenation was never associated with a decrease in tissue hemoglobin index, in the present study. On this basis, considering that both masseter and biceps muscles remained relaxed throughout the tests, as verified by continuous electromyography monitoring, we can reasonably interpret

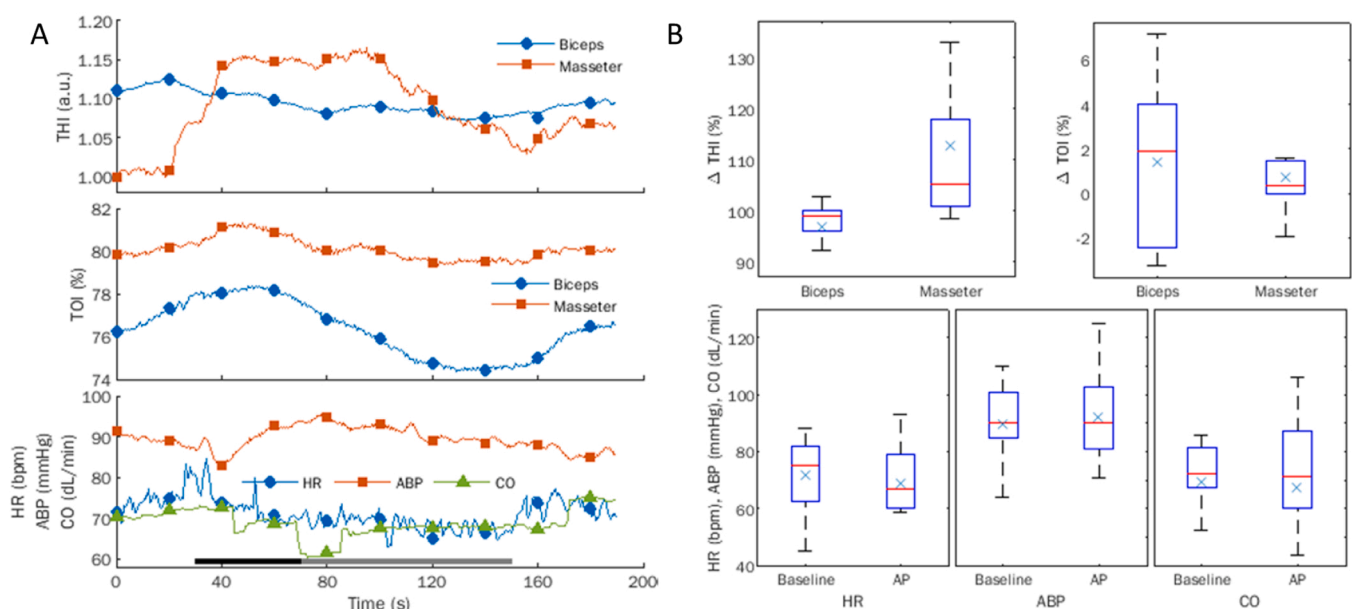
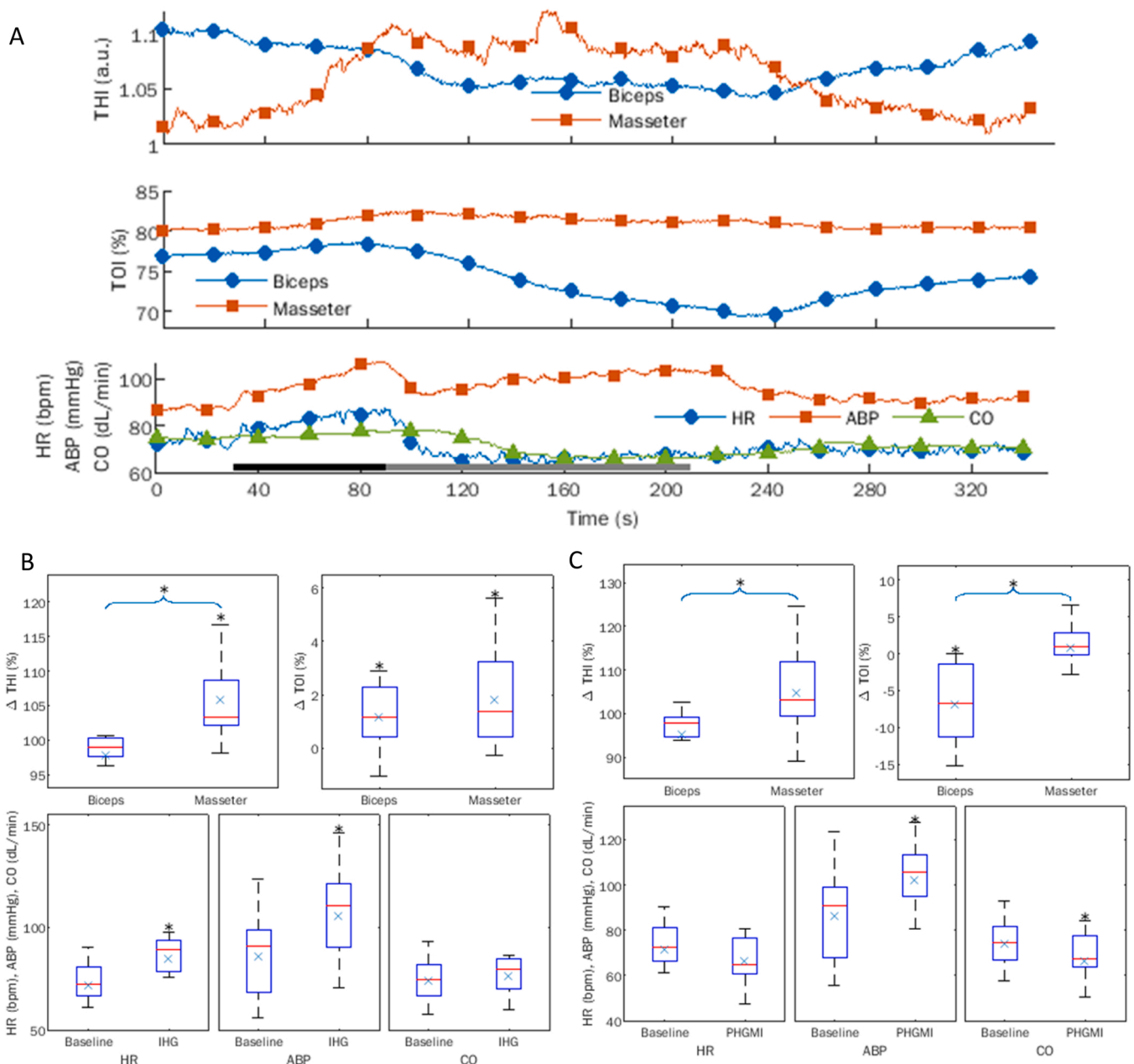


Fig. 4. Response to apnea (AP). Average response curves (A) and distribution of the effects (B) for the different variables. Notations and abbreviations as in Fig. 2. Duration of apnea lasted between 40 s (black bar) and 120 s (gray bar), in the different subjects; n = 12.



**Fig. 5.** Response to isometric handgrip (IHG) and post-handgrip muscle ischemia (PHGMI). Average response curves (A); distribution of the effects of IHG (B) and PHGMI (C) for the different variables. Notations and abbreviations as in Fig. 2. The black and grey bars at the bottom indicates the duration of IHG and PHGMI, respectively. Note that TOI exhibits opposite effects in masseter and biceps muscles during PHGMI but not during IHG. \* )  $p < 0.05$ ;  $n = 12$ .

changes in tissue oxygenation index as a consequence of corresponding changes in muscle blood flow. The responses to the different stressors will be here briefly individually discussed.

#### 4.2. Cold pressor test

The cold pressor test is an established sympathetic activation test (Seals, 1991). Somatosensory stimulation induced by the cold stimulus increases blood pressure; impulses from receptors in the skin relay via afferent pathways to C1 cells in the rostral ventrolateral reticular nucleus and are transmitted via efferent sympathetic neurons to peripheral blood vessels from thoracic spinal cord (Reis et al., 1989) evoking a general rise in total peripheral resistance with alpha-adrenergic vasoconstriction of upper and lower limbs, (Montoya et al., 1997; Wray et al., 2007) accompanied by decreased tissue oxygenation (Ogata et al.,

2012). Few reports described effects of opposite signs in head muscles, i. e., increase in blood volume and oxygen saturation during cold pressor test, suggesting increased blood flow in this area (Maekawa et al., 1998a). As anticipated in the introduction the standard near-infrared spectroscopy monitoring as used in these studies could have been affected by cutaneous circulatory changes. However, the present data are in agreement with this general picture: we confirm the occurrence of these opposite responses in head and limb muscles, consisting of increased perfusion of the masseter muscle and a strong decrease in the biceps muscle (Fig. 2).

#### 4.3. Mental arithmetic test

As compared to cold pressor test, the actively demanding situations such as information processing and problem-solving (mental arithmetic

test) are considered to be characterized by a beta-adrenergic dominance, i.e., they tend to elicit cardiovascular responses that are mediated by an increase in myocardial contractility and heart rate, increased adrenergic release, resulting in increased cardiac output, with minor changes in total peripheral resistance (Goldberg et al., 1996; Montoya et al., 1997; Tidgren & Hjemdahl, 1989). Within this frame, vasodilation in skeletal muscle has also been reported (Carter et al., 2005; Linde et al., 1989; Rusch et al., 1981), besides reduced blood flow to the kidneys (Tidgren & Hjemdahl, 1989) and the skin (Marriott et al., 1990). As for the head muscles two early reports from a single group are available, based on standard Beer-Lambert near-infrared spectroscopy, in which the effect of this test on masseter tissue oxygenation was investigated. Again, the issue of skin contribution to the near-infrared spectroscopy measurement is relevant, as skin blood flow is known to be affected by this test and cognitive tasks (Drummond, 1994; Vassend & Knardahl, 2005). In the first study, an early decrease in tissue oxygenation, assessed over a 10-s interval, was reported to occur in association with the beginning of sudomotor activity at the finger (Hidaka et al., 2004a). In the second study, a persistent increase in tissue oxygenation of the masseter muscle was observed in subjects exposed to a long-lasting (2 h) mental task, although, this stressful activity also increased basal electromyographic activity (significantly in the temporal muscle) (Hidaka et al., 2004b). More recently, using spatially-resolved near-infrared spectroscopy Tanosoto et al. (2012) also reported increased tissue oxygenation in the masseter muscle during a paced auditory mental task. The present results are compatible with the general response to mental arithmetic test described above and clarify that a significant tissue oxygenation increase takes place in the masseter muscle within a standard 2-min lasting test, in the absence of electromyographic activity, besides a non-significant increasing trend in the biceps (Fig. 3).

#### 4.4. Apnea

A complex circulatory response is generated by apnea, whereby the dilatory effects of hypoxia are counteracted by the constrictor sympathetic activation (Halliwill, 2003). In fact, an increased muscle sympathetic nerve activity as well as in circulating catecholamines has been reported (Leuenberger et al., 2001) along with decreased oxygenation in skeletal muscles of the limbs (Bouten et al., 2020), while no indication about the effects on head muscles was found in the literature. In our experiments, we did not evidence a decrease in tissue oxygenation in both masseter and biceps muscles, and weak and non-significant effects were reported also for the other variables. This is likely because the test was not pushed to maximal individual limits and that all responses were analysed at the shortest duration of 40 s, which certainly contributed to attenuate the effects. We only observe that a larger although not significant increase in tissue hemoglobin index takes place in the masseter, compared to the biceps. We speculate that this is a consequence of increased venous pressure due to the increased intra-thoracic pressure provoked by the passive holding of the deep breath (similarly to the Valsalva manoeuvre). Since venous pressure would similarly affect both muscles, a larger effect in the masseter muscle could reveal a lesser constrictor tone.

#### 4.5. Isometric handgrip

Handgrip exercise is an established test for sympathetic activation, producing marked increases in arterial blood pressure, heart rate, cardiac out, and muscle sympathetic nerve activity in general (Low, 2003). This results in a systematic increase in vascular resistance in muscles. However, a dilatory response is generally observed in the contralateral arm. Once attributed to sympathetic dilatory cholinergic fibers (Sanders et al., 1989) it appears now to be essentially a beta2 adrenergic mechanism that also implicates endothelium-released nitric oxide (Joyner & Dietz, 2003). The description of vascular effects in head muscles during handgrip appears to be missing in the literature.

The response we observed fits with the current picture described above, in particular, the dilatory response of the contralateral arm is confirmed by the significant increase in tissue oxygenation index. In addition, the same response is exhibited by the masseter muscles, which also manifests an increase in tissue hemoglobin index.

#### 4.6. Post-handgrip muscle ischemia

Post-handgrip muscle ischemia consistently results in a pressor response characterized by powerful peripheral vasoconstriction and decreased heart rate and cardiac output (Boulton et al., 2018; Rusch et al., 1981). While tissue oxygenation decreases in the concerned muscles prior to exercise and subsequent ischemia, (Boushel & Piantadosi, 2000) the present observation of a marked tissue oxygenation decrease in the contralateral biceps muscle (not concerned by the contraction and the ischemia) supports the occurrence of a general constrictor response during post-handgrip muscle ischemia, that was reported to concern both upper and lower limbs (Rusch et al., 1981). Surprisingly, this effect is not apparent in the masseter muscle, which exhibits instead a significant increase in oxygenation, again suggesting increased perfusion, during post-handgrip muscle ischemia. We further observe that the average pattern of response to post-handgrip muscle ischemia qualitatively mimics the response to cold pressor test. It is tempting to speculate that this represents the sympathetic response pattern to painful stimuli, even though the relevant somatosensory pathways are different for the two tests, originating mostly from cutaneous receptors for cold pressor test, and from group III and IV muscle afferents for post-handgrip muscle ischemia. This possibility is further supported by the observation that muscle sympathetic nerve activity is not differently affected by skin or muscle pain produced by injection of hypertonic saline (Burton et al., 2009).

#### 4.7. Peculiarity of the masseter muscle

Several studies investigated the histological characteristics of jaw and limb muscles evidencing a richer composition of different fiber types, higher compartmentalization, and smaller average fiber size in the jaw than in limb muscles, which was interpreted as functional to implement a higher variability of tasks (speaking, chewing, singing, yawning, etc.), better force gradation and better adaptations to environmental constraints (English, 1985; Korfage et al., 2005; Österlund et al., 2011). One study specifically addressed differences in anatomical vascularization: capillary density was significantly higher in the head (orofacial and masseter) than in limb muscles (Stål et al., 1996). In particular, the authors found in the masseter the highest capillary density ever reported of 686–813 capillaries/mm<sup>2</sup>, which in the biceps muscle only reached 440 capillaries/mm<sup>2</sup> (Stål et al., 1996). They interpreted this observation as due to a relatively higher demand of blood supply in orofacial and masticatory muscles, possibly related to 1) the high oxidative capacity of type II masseter fibers, and 2) a stronger control over facial blood flow, as may be necessary for the temperature regulation, of tissues more exposed to environmental challenges as compared to other body areas.

The presently observed weak or absent sympathetic constrictor action in the masseter muscle under a variety of stressful challenges fits with the idea that the head region is particularly protected against the risk of hypoperfusion and ischemia as indicated by histological reports.

One additional explanation could be that extracranial head districts are affected by a lower perfusion pressure, compared to other body areas situated at or below heart level, whenever the body is in an erect or sitting posture. The head is continuously exposed to this condition during the whole day, with basically the only exception of sleeping time. Increased vascularization and weakened constrictor action could be the results of an adaptation to this situation. Other data support this interpretation: 1) Increased vascularization is not limited to the jaw muscles but is shared by orofacial muscles in general, sharing the same



hemodynamic situation (Stål et al., 1996), 2) a similar difference, i.e., weaker sympathetic constrictor responses is reported in upper, compared to lower limbs, (Rusch et al., 1981) thereby indicating increased sympathetic tone to body areas affected by high hydrostatic pressure.

It should be considered that hemodynamic responses are likely to be affected by changes in transmural and perfusion pressure that would differently affect head and limb muscles in a vertical position of the trunk, compared to the supine. In fact, differences in the transmural pressure of blood vessels were shown to affect vascular responses to dilatory stimuli (Jasperse et al., 2015; Seddone et al., 2020). To what extent the stress-related hemodynamic responses could change in the different positions cannot be predicted from the present results, however, we point out that some of the previous studies in the masseter muscle were conducted in the sitting position e.g., (Maekawa et al., 1998b) and reported similar dilatory response to cold pressor test, which suggests that the presently highlighted differences between the two muscles would not be altered during erect trunk posture.

#### 4.8. Mechanisms underlying differential sympathetic control

Although the present study was not designed to identify the mechanisms underlying the differential sympathetic action to the two muscles, the different possibilities can be briefly discussed. While the general sympathetic action on vascular networks is known to be an alpha-adrenergic mediated vasoconstriction, a dilatory response has often been reported in skeletal muscles and is considered to be mediated by beta-2 adrenergic receptors. The alternative hypothesis of parasympathetic- (Ishii et al., 2011) or, more generally, Ach-mediated dilatation (Sanders et al., 1989) has been dismissed since vascular cholinergic fibers have never been observed in human skeletal muscles (Joyner & Dietz, 2003). As such, a beta-2 mediated-dilatation is likely to result from the action of circulating adrenaline (which has a higher affinity to beta2-adrenergic receptors than noradrenaline) as far as the alpha-1 mediated constriction does not prevail. Exposure to a small amount of adrenaline produced dilatation in both masseter and quadriceps rabbit muscles, while higher doses produced vasoconstriction (Terakawa & Ichinohe, 2012). Thus, the net “beta” or “alpha” effect (Montoya et al., 1997) observed on a given muscle, may depend on several factors such as the density of beta- and alpha-adrenergic receptors in the muscle under study as well as on the relative concentrations of adrenaline and noradrenaline, resulting from a stressor-dependent hormonal vs. neural sympathetic outflow (Goldstein & Kopin, 2008; Roatta et al., 2011). The hyperemic responses to stress observed in the present study could result from a higher density of beta2-adrenergic receptors in the masseter compared to the biceps muscle, but we could find no comparative study in the literature supporting this hypothesis. Alternatively, the increase in sympathetic outflow to head muscles could be generally lower than to limb muscles, but also in this case there is no direct support to the hypothesis, given that, to our knowledge, muscle sympathetic nerve activity has never been investigated in head muscles.

It should also be observed that increased muscle perfusion may also take place during vasoconstriction if a concomitant and proportionally stronger increase in arterial blood pressure also occurs. Irrespective of the underlying mechanisms the present results evidence a differential vascular effect in the two muscles pointing to a consistent dilatory or a weaker constrictory action in the masseter compared to the biceps muscle.

#### 4.9. Implications

The reason for investigating the effect of sympathetic activation on facial and masticatory muscles has often been the possible implication of the sympathetic nervous system in painful muscle syndromes (Hidaka et al., 2004a; Hidaka et al., 2004b; Maekawa et al., 1998a). In fact, the

masseter muscle, is a common site for myofascial pain, more often localized in the deep part of the muscle (Fricton et al., 1985).

Most investigations on the issue were carried out in the trunk and limbs, leading to several causative hypotheses (Jänig and Häbler, 2000; Sjøgaard et al., 2000). A major mechanism in the development/maintenance of the chronic syndrome is considered to be the ischemia or hypoperfusion leading to the increase in oxidative stress and inflammation and then to pain and tenderness to palpation (Simons & Mense, 1998). In this respect, the vasoconstrictory sympathetic action is considered to worsen the situation (Koltzenburg, 1997; Passatore & Roatta, 2006; Queme et al., 2017).

Although blood flow reduction is commonly observed in response to electrical sympathetic stimulation in animal models (Roatta et al., 2009) or physiological stressful stimuli, (Ichinohe et al., 2020; Roatta et al., 2011) we could not find any report of sympathetic vasoconstriction in orofacial muscles in humans. Human studies based on near-infrared spectroscopy investigations generally report increased blood volume and/or oxygenation in response to stress, suggestive of increased perfusion (Hidaka et al., 2004b; Maekawa et al., 1998a). It was suggested that the lack of such dilatory response could be related to the occurrence of myofascial pain (Maekawa et al., 2002). Conversely, excessive dilatation in extra-cranial territories was also considered as a possible cause of pain (see Shevel, 2011 for a review), while additional pathways not based on hemodynamic alterations have also been hypothesized (Inchiosa Jr, 2013). The present study confirms the general absence of vasoconstriction in the masseter muscle in response to a variety of different stressors but does not provide additional elements to clarify the mechanisms behind chronic muscle pain.

## 5. Conclusion

Simultaneous hemodynamic monitoring of head and limb muscles by spatially-resolved near-infrared spectroscopy evidenced differential patterns of response to different stressors: while the biceps muscle exhibited both constrictory and dilatory responses, no evidence of constriction was ever observed in the masseter, often exhibiting a significant increase in tissue oxygenation and blood volume. In particular, clear-cut opposite changes were exhibited by the two muscles in response to painful stimuli (cold pressor test and post-handgrip muscle ischemia). We speculate that this results from a general strategy aimed at preserving blood flow to the head region, which is generally perfused at a lower blood pressure because of the hydrostatic gradient associated with the erect posture.

## Funding

A.R. was supported by a Doctoral Fellowship funded by the Partnership for Knowledge (Pfk) program of the Agenzia Italiana per la Cooperazione allo Sviluppo (AICS), Ministero degli Affari Esteri e della Cooperazione Internazionale (MAECI), Italy.

## Declaration of Competing Interest

The authors declare no conflict of interest.

## Acknowledgments

We are grateful to Dr. Raffaele Pertusio for his technical assistance.

## References

- Boulton, D., Taylor, C. E., Green, S., & Macefield, V. G. (2018). The metaboreflex does not contribute to the increase in muscle sympathetic nerve activity to contracting muscle during static exercise in humans. *The Journal of Physiology*, 596(6), 1091–1102. <https://doi.org/10.1113/JP275526>

- Boushel, R., & Piantadosi, C. A. (2000). Near-infrared spectroscopy for monitoring muscle oxygenation. *Acta Physiologica Scandinavica*, 168(4), 615–622. <https://doi.org/10.1046/j.1365-201x.2000.00713.x>
- Bouten, J., Bourgois, J. G., & Boone, J. (2020). Hold your breath: peripheral and cerebral oxygenation during dry static apnea. *European Journal of Applied Physiology*, 120(10), 2213–2222. <https://doi.org/10.1007/s00421-020-04445-y>
- Burton, A. R., Birznieks, I., Spaak, J., Henderson, L. A., & MacEfield, V. G. (2009). Effects of deep and superficial experimentally induced acute pain on skin sympathetic nerve activity in human subjects. *Experimental Brain Research*, 195(2), 317–324. <https://doi.org/10.1007/s00221-009-1790-9>
- Canova, D., Roatta, S., Bosone, D., & Micieli, G. (2011). Inconsistent detection of changes in cerebral blood volume by near infrared spectroscopy in standard clinical tests. *Journal of Applied Physiology*, 110(6), 1646–1655. <https://doi.org/10.1152/jappphysiol.00003.2011>
- Carter, J. R., Cooke, W. H., & Ray, C. A. (2005). Forearm neurovascular responses during mental stress and vestibular activation. *American Journal of Physiology - Heart and Circulatory Physiology*, 288(2 57–2). <https://doi.org/10.1152/ajpheart.00569.2004>
- Drummond, P. D. (1994). The effect of anger and pleasure on facial blood flow. *Australian Journal of Psychology*, 46(2), 95–99. <https://doi.org/10.1080/00049539408259479>
- Eklund, B., & Kaijser, L. (1976). Effect of regional alpha- and beta-adrenergic blockade on blood flow in the resting forearm during contralateral isometric handgrip. *The Journal of Physiology*, 262(1), 39–50. <https://doi.org/10.1113/jphysiol.1976.sp011584>
- English, A. W. (1985). Limbs vs. jaws: Can they be compared? *Integrative and Comparative Biology*, 25(2), 351–364. <https://doi.org/10.1093/icb/25.2.351>
- Fadel, P. J., Keller, D. M., Watanabe, H., Raven, P. B., & Thomas, G. D. (2004). Noninvasive assessment of sympathetic vasoconstriction in human and rodent skeletal muscle using near-infrared spectroscopy and Doppler ultrasound. *Journal of Applied Physiology*, 96(4), 1323–1330. <https://doi.org/10.1152/jappphysiol.01041.2003>
- Fricton, J. R., Kroening, R., Haley, D., & Siegert, R. (1985). Myofascial pain syndrome of the head and neck: a review of clinical characteristics of 164 patients. *Oral Surgery, Oral Medicine, Oral Pathology*, 60(6), 615–623. [https://doi.org/10.1016/0030-4220\(85\)90364-0](https://doi.org/10.1016/0030-4220(85)90364-0)
- Goldberg, A. D., Becker, L. C., Bonsall, R., Cohen, J. D., Ketterer, M. W., Kaufman, P. G., & Sheps, D. S. (1996). Ischemic, hemodynamic, and neurohormonal responses to mental and exercise stress: Experience from the Psychophysiological Investigations of Myocardial Ischemia study (PIMI). *Circulation*, 94(10), 2402–2409. <https://doi.org/10.1161/01.cir.94.10.2402>
- Goldstein, D. S., & Kopin, I. J. (2008). Adrenomedullary, adrenocortical, and sympathoneural responses to stressors: a meta-analysis. *Endocrine Regulations*, 42(4), 111–119. (<https://pubmed.ncbi.nlm.nih.gov/1899898/>).
- Grassi, B., & Quaresima, V. (2016). Near-infrared spectroscopy and skeletal muscle oxidative function in vivo in health and disease: a review from an exercise physiology perspective, 0913131–20 *Journal of Biomedical Optics*, 21(9). <https://doi.org/10.1117/1.JBO.21.9.091313>
- Halliwill, J. R. (2003). Hypoxic regulation of blood flow in humans. *Skeletal Muscle Circulation and the role of epinephrine Advances in Experimental Medicine and Biology*, 543, 223–236. (<https://pubmed.ncbi.nlm.nih.gov/14713125/>).
- Hidaka, O., Yanagi, M., & Takada, K. (2004a). Changes in masseteric dynamics time-related to mental stress. *Journal of Dental Research*, 83(2), 185–190. <https://doi.org/10.1177/154405910408300220>
- Hidaka, O., Yanagi, M., & Takada, K. (2004b). Mental stress-induced physiological changes in the human masseter muscle. *Journal of Dental Research*, 83(3), 227–231. <https://doi.org/10.1177/154405910408300308>
- Ichinohe, T., Akiike, Y., Saito, N., Koike, M., Koshika, K., & Matsuura, N. (2020). Effects of Stellate Ganglion Blockade on Muscle Blood Flow During Hypercapnia. *Scientific Reports*, 67(3), 135–139. <https://doi.org/10.2344/anpr-67-01-04>
- Inchiosa, M. A., Jr. (2013). Phenoxylbenzamine in complex regional pain syndrome: Potential role and novel mechanisms. *Anesthesiology Research and Practice*, 2013, 1–7. <https://doi.org/10.1155/2013/978615>
- Ishii, H., Niioka, T., & Izumi, H. (2011). Parasympathetic reflex vasodilatation in the masseter muscle compensates for carotid hypoperfusion during the vagus-mediated depressor response. *Brain Research*, 1370, 145–153. <https://doi.org/10.1016/j.brainres.2010.11.046>
- Jacob, G., Costa, F., Shannon, J., Robertson, D., & Biaggioni, I. (2000). Dissociation Between Neural and Vascular Responses to Sympathetic Stimulation. *Hypertension*, 35(1), 76. <https://doi.org/10.1161/01.hyp.35.1.76>
- Jänig, W., & Häbler, H. J. (2000). Sympathetic nervous system: contribution to chronic pain. *Progress in Brain Research*, 129, 451–468. [https://doi.org/10.1016/S0079-6123\(00\)80003-5](https://doi.org/10.1016/S0079-6123(00)80003-5)
- Jaspere, J. L., Shoemaker, J. K., Gray, E. J., & Clifford, P. S. (2015). Positional differences in reactive hyperemia provide insight into initial phase of exercise hyperemia. *Journal of Applied Physiology*, 119(5), 569–575. <https://doi.org/10.1152/jappphysiol.01253.2013>
- Joyner, M. J., & Dietz, N. M. (2003). Sympathetic vasodilation in human muscle. *Acta Physiologica Scandinavica*, 177(3), 329–336. <https://doi.org/10.1046/j.1365-201X.2003.01090.x>
- Koltzenburg, M. (1997). The Sympathetic Nervous System and Pain. In D. A., & B. JM. (Eds.), *The Pharmacology of Pain (Handbook of Experimental Pharmacology)* (Volume 130, pp. 61–91). Springer Verlag. [https://doi.org/10.1007/978-3-642-60777-6\\_4](https://doi.org/10.1007/978-3-642-60777-6_4)
- Korfae, J. A. M., Koolstra, J. H., Langenbach, G. E. J., & Van Eijden, T. M. G. J. (2005). Fiber-type composition of the human jaw muscles - (Part 2) Role of hybrid fibers and factors responsible for inter-individual variation. *Journal of Dental Research*, 84(9), 784–793. <https://doi.org/10.1177/154405910508400902>
- Leuenberger, U. A., Hardy, J. C., Herr, M. D., Gray, K. S., & Sinoway, L. I. (2001). Hypoxia augments apnea-induced peripheral vasoconstriction in humans. *Journal of Applied Physiology*, 90(4), 1516–1522. <https://doi.org/10.1152/jappl.2001.90.4.1516>
- Linde, B., Hjemdahl, P., Freyschuss, U., & Juhlin-Dannfelt, A. (1989). Adipose tissue and skeletal muscle blood flow during mental stress. *The American Journal of Physiology*, 256(1 Pt 1), E12–E18. <https://doi.org/10.1152/ajpendo.1989.256.1.E12>
- Low, P. A. (2003). Testing the autonomic nervous system. *Seminars in Neurology*, 23(4), 407–421. <https://doi.org/10.1055/s-2004-817725>
- Maekawa, K., Clark, G. T., & Kuboki, T. (2002). Intramuscular hypoperfusion, adrenergic receptors, and chronic muscle pain. *The Journal of Pain*, 3(4), 251–260. <https://doi.org/10.1054/jpai.2002.125923>
- Maekawa, K., Kuboki, T., Clark, G. T., Shinoda, M., & Yamashita, A. (1998a). Cold pressor stimulus temperature and resting masseter muscle haemodynamics in normal humans. *Archives of Oral Biology*, 43(11), 849–859. [https://doi.org/10.1016/S0003-9969\(98\)00072-7](https://doi.org/10.1016/S0003-9969(98)00072-7)
- Maekawa, K., Kuboki, T., Clark, G. T., Shinoda, M., & Yamashita, A. (1998b). Cold pressor stimulus temperature and resting masseter muscle haemodynamics in normal humans. *Archives of Oral Biology*, 43(11), 849–859. [https://doi.org/10.1016/S0003-9969\(98\)00072-7](https://doi.org/10.1016/S0003-9969(98)00072-7)
- Marriott, I., Marshall, J. M., & Johns, E. J. (1990). Cutaneous vascular responses evoked in the hand by the cold pressor test and by mental arithmetic. *Clinical Science*, 79(1), 43–50. <https://doi.org/10.1042/cs0790043>
- Messere, A., Ceravolo, G., Franco, W., Maffiodo, D., Ferraresi, C., & Roatta, S. (2017). Increased tissue oxygenation explains the attenuation of hyperemia upon repetitive pneumatic compression of the lower leg. *Journal of Applied Physiology*, 123(6), 1451–1460. <https://doi.org/10.1152/jappphysiol.00511.2017>
- Messere, A., & Roatta, S. (2013). Influence of cutaneous and muscular circulation on spatially resolved versus standard Beer-Lambert near-infrared spectroscopy. *Physiological Reports*, 1(7), 1–10. <https://doi.org/10.1002/phy2.179>
- Messere, A., Tschakovsky, M., Seddone, S., Lulli, G., Franco, W., Maffiodo, D., & Roatta, S. (2018a). Hyper-Oxygenation Attenuates the Rapid Vasodilatory Response to Muscle Contraction and Compression. *Frontiers in Physiology*, 9(1078). <https://doi.org/10.3389/fphys.2018.01078>
- Messere, A., Tschakovsky, M., Seddone, S., Lulli, G., Franco, W., Maffiodo, D., & Roatta, S. (2018b). Hyper-Oxygenation Attenuates the Rapid Vasodilatory Response to Muscle Contraction and Compression. *Frontiers in Physiology*, 9, 1078. <https://doi.org/10.3389/fphys.2018.01078>
- Montoya, P., Brody, S., Beck, K., Veit, R., & Rau, H. (1997). Differential beta- and alpha-adrenergic activation during psychological stress. *European Journal of Applied Physiology and Occupational Physiology*, 75(3), 256–262. <https://doi.org/10.1007/s004210050157>
- Ogata, H., Hobara, H., Uematsu, A., & Ogata, T. (2012). Limb oxygenation during the cold pressor test in spinal cord-injured humans. *Clinical Autonomic Research*, 22(2), 71–78. <https://doi.org/10.1007/s10286-011-0143-5>
- Ogata, H., Yunoki, T., & Yano, T. (2002). Effect of arm cranking on the NIRS-determined blood volume and oxygenation of human inactive and exercising vastus lateralis muscle. *European Journal of Applied Physiology*, 86(3), 191–195. <https://doi.org/10.1007/s00421-001-0527-7>
- Österlund, C., Thornell, L. E., & Eriksson, P. O. (2011). Differences in fibre type composition between human masseter and biceps muscles in young and adults reveal unique masseter fibre type growth pattern. *Anatomical Record*, 294(7), 1158–1169. <https://doi.org/10.1002/ar.21272>
- Pacák, K., & Palkovits, M. (2001). Stressor specificity of central neuroendocrine responses: implications for stress-related disorders. *Endocrine Reviews*, 22(4), 502–548. <https://doi.org/10.1210/edrv.22.4.0436>
- Passatore, M., & Roatta, S. (2006). Influence of sympathetic nervous system on sensorimotor function: whiplash associated disorders (WAD) as a model. *European Journal of Applied Physiology*, 98(5), 423–449. <https://doi.org/10.1007/s00421-006-0312-8>
- Queme, L. F., Ross, J. L., & Jankowski, M. P. (2017). Peripheral mechanisms of ischemic Myalgia. *Frontiers in Cellular Neuroscience*, 11, 1–15. <https://doi.org/10.3389/fncel.2017.00419>
- Reis, D. J., Ruggiero, D. A., & Morrison, S. F. (1989). The C1 area of rostral ventrolateral medulla: A central site integrating autonomic responses to hemorrhage. *Resuscitation*, 18(2–3), 269–288. [https://doi.org/10.1016/0300-9572\(89\)90028-2](https://doi.org/10.1016/0300-9572(89)90028-2)
- Roatta, S., Mohammed, M., & Passatore, M. (2009). Acute stress reduces blood flow in the orofacial area, in conscious rabbits. *Archives of Oral Biology*, 54(4), 380–388. <https://doi.org/10.1016/j.archoralbio.2009.01.003>
- Roatta, S., Mohammed, M., & Passatore, M. (2011). Detecting activation of the sympatho-adrenal axis from haemodynamic recordings, in conscious rabbits exposed to acute stress. *Acta Physiologica (Oxford)*, 201(3), 323–337. <https://doi.org/10.1111/j.1748-1716.2010.02179.x>
- Rusch, N. J., Shepherd, J. T., Webb, R. C., & Vanhoutte, P. M. (1981). Different behavior of the resistance vessels of the human calf and forearm during contralateral isometric exercise, mental stress, and abnormal respiratory movements. *Circulation Research*, 48(6 Pt 2), 1118–1130. (<https://pubmed.ncbi.nlm.nih.gov/7226455/>).
- Sanders, J. S., Mark, A. L., & Ferguson, D. W. (1989). Evidence for cholinergically mediated vasodilation at the beginning of isometric exercise in humans. *Circulation*, 79(4), 815–824. <https://doi.org/10.1161/01.CIR.79.4.815>
- Seals, D. R. (1991). Sympathetic neural adjustments to stress in physically trained and untrained humans. *Hypertension*, 17(1), 36–43. <https://doi.org/10.1161/01.hyp.17.1.36>
- Seddone, S., Messere, A., & Roatta, S. (2020). Vascular reactivity of cutaneous circulation to brief compressive stimuli, in the human forearm. *European Journal of Applied Physiology*, 120(5), 1041–1050. <https://doi.org/10.1007/s00421-020-04343-3>

- Shevel, E. (2011). The extracranial vascular theory of migraine: A great story confirmed by the facts. *Headache*, 51(3), 409–417. <https://doi.org/10.1111/j.1526-4610.2011.01844.x>
- Simons, D. G., & Mense, S. (1998). Understanding and measurement of muscle tone as related to clinical muscle. *Pain Pain*, 75(1), 1–17. [https://doi.org/10.1016/S0304-3959\(97\)00102-4](https://doi.org/10.1016/S0304-3959(97)00102-4)
- Sjøogaard, G., Lundberg, U., & Kadefors, R. (2000). The role of muscle activity and mental load in the development of pain and degenerative processes at the muscle cell level during computer work. *European Journal of Applied Physiology*, 83(2–3), 99–105. <https://doi.org/10.1007/s004210000285>
- Stål, P., Eriksson, P. O., & Thornell, L. E. (1996). Differences in capillary supply between human oro-facial, masticatory and limb muscles. *Journal of Muscle Research and Cell Motility*, 17(2), 183–197. <https://doi.org/10.1007/BF00124241>
- Tanosoto, T., Taro Arima, A. T., Ohata, N., & Svensson, P. (2012). A Paced Auditory Serial Addition Task evokes stress and differential effects on masseter-muscle activity and haemodynamics. *European Journal of Oral Sciences*, 120(4), 363–367. <https://doi.org/10.1111/j.1600-0722.2012.00973.x>
- Terakawa, Y., & Ichinohe, T. (2012). Large-dose epinephrine reduces skeletal muscle blood flow under general anesthesia in rabbits. *Anesthesia Progress*, 59(3), 118–122. <https://doi.org/10.2344/12-00006.1>
- Testa, M., Marco, A., Di, Pertusio, R., Roy, P., Van, & Roatta, S. (2016). A validation study of a new instrument for low cost bite force measurement. *Journal of Electromyography and Kinesiology*, 30, 243–248. <https://doi.org/10.1016/j.jelekin.2016.08.005>
- Tew, G. A., Ruddock, A. D., & Saxton, J. M. (2010). Skin blood flow differentially affects near-infrared spectroscopy-derived measures of muscle oxygen saturation and blood volume at rest and during dynamic leg exercise. *European Journal of Applied Physiology*, 110(5), 1083–1089. <https://doi.org/10.1007/s00421-010-1596-2>
- Tidgren, B., & Hjemdahl, P. (1989). Renal responses to mental stress and epinephrine in humans. *American Journal of Physiology - Renal Fluid and Electrolyte Physiology*, 257(4 (26/4)). <https://doi.org/10.1152/ajprenal.1989.257.4.f682>
- Vassend, O., & Knardahl, S. (2005). Personality, affective response, and facial blood flow during brief cognitive tasks. *International Journal of Psychophysiology*, 55(3), 265–278. <https://doi.org/10.1016/j.ijpsycho.2004.08.005>
- Vissing, S. F. (1997). Differential activation of sympathetic discharge to skin and skeletal muscle in humans. *Acta Physiol Scand Suppl*, 639, 1–32. (<https://pubmed.ncbi.nlm.nih.gov/9421582/>).
- Wray, D. W., Donato, A. J., Nishiyama, S. K., & Richardson, R. S. (2007). Acute sympathetic vasoconstriction at rest and during dynamic exercise in cyclists and sedentary humans. *Journal of Applied Physiology*, 102(2), 704–712. <https://doi.org/10.1152/jappphysiol.00984.2006>



## PAPER

# Hemodynamic monitoring in the human temporalis muscle using near-infrared spectroscopy

RECEIVED  
10 March 2023REVISED  
3 May 2023ACCEPTED FOR PUBLICATION  
18 May 2023PUBLISHED  
13 June 2023

Anas Rashid and Silvestro Roatta\*

Lab of Integrative Physiology, Department of Neuroscience 'Rita Levi Montalcini', University of Torino, Torino, Italy

\* Author to whom any correspondence should be addressed.

E-mail: [anas.rashid@unito.it](mailto:anas.rashid@unito.it) and [silvestro.roatta@unito.it](mailto:silvestro.roatta@unito.it)

Keywords: hemodynamics, human temporal muscle, NIRS

## Abstract

**Objective.** Altered temporal muscle perfusion is implicated in several painful disorders afflicting orofacial and head regions, including temporomandibular joint dysfunctions, bruxism, and headache. Knowledge about the regulation of blood supply to the temporalis muscle is limited, due to methodological difficulties. The study aimed to test the feasibility of near-infrared spectroscopy (NIRS) monitoring of the human temporal muscle. **Approach.** Twenty-four healthy subjects were monitored with a 2-channel NIRS: a *muscle* probe placed over the temporal muscle and a *brain* probe placed on the forehead. A series of teeth clenching at 25, 50, and 75% of maximum voluntary contraction for 20 s and hyperventilation for 90 s at 20 mmHg of end-tidal CO<sub>2</sub> were performed, to elicit hemodynamic changes in muscle and brain, respectively. **Main results.** In twenty responsive subjects, NIRS signals from both probes were consistently different during both tasks. The absolute change in tissue oxygenation index ( $\Delta$ TOI) as detected by muscle and brain probes was  $-9.40 \pm 12.28$  and  $0.29 \pm 1.54\%$  during teeth clenching ( $p < 0.01$ ) at 50% maximum voluntary contraction, while  $-1.03 \pm 2.70$  and  $-5.11 \pm 3.81\%$  during hyperventilation ( $p < 0.01$ ), respectively. **Significance.** Distinct response patterns were observed from the temporal muscle and prefrontal cortex which proves that this technique is adequate to monitor tissue oxygenation and hemodynamic changes in human temporal muscle. Noninvasive and reliable monitoring of hemodynamics in this muscle will help to extend basic and clinical investigations about the peculiar control of blood flow in head muscles.

## Introduction

The human temporalis is a fan-shaped thin muscle that extends superficially from the temporal bone to the coronoid process of the mandible and serves as one of the essential masticatory muscles to perform elevation and retraction of the mandible (Yu *et al* 2021). The temporalis muscle is implicated in several painful disorders afflicting the orofacial and head regions, including temporomandibular joint dysfunctions, bruxism (Lavigne *et al* 2008, Yap and Chua 2016), and headache (Exposto *et al* 2021). Vascular dysfunctions in masticatory muscles have often been considered a possible cause of pain symptoms, related either to decreased muscle perfusion (Maekawa *et al* 2002, Shah *et al* 2019) or to excessive dilatory phenomena (Jensen 1993), although this latter issue is still debated (Jacobs and Dussor 2016, Mason and Russo 2018). It has also been suggested that blood flow is differently controlled in head muscles, compared to limb muscles but investigations in the head region are mostly limited to the masseter muscle (Nakamura *et al* 2005, Rashid and Roatta 2022). In fact, investigations about the regulation of blood flow in the temporalis muscle are scanty. The blood supply to the temporalis muscle is provided by the anterior and posterior deep temporal arteries, which are branches of the internal maxillary artery, and anastomose within the muscle with the middle temporal artery, which is a branch of the superficial temporal artery (Elazab and Abdel-Hameed 2006). For this reason, Doppler ultrasound of the

superficial temporal artery, which is taken downstream to the branching of the middle temporal artery (Arbeille *et al* 2011, Noumegni *et al* 2021) is not a viable investigative technique, for this purpose.

Temporalis muscle blood flow was measured in a few studies in healthy and headache-afflicted volunteers by the Xenon 133 ( $^{133}\text{Xe}$ ) clearance technique (Petersen and Christensen 1973, Jensen and Olesen 1985, Langemark *et al* 1990), which requires injection of tracer depots into the thickest part of the muscle and scintillation detectors over each depot to register the tracer washout. The technique has, obviously, the disadvantage of being invasive and exposing to gamma rays. More recently, magnetic resonance imaging has been employed for diagnostic imaging (Geers *et al* 2005, Veldhoen *et al* 2014). It is, however, quite expensive and can be affected by movement, e.g. by swallowing or coughing, making it unsuitable for continuous bedside monitoring.

A more convenient and noninvasive technique is near-infrared spectroscopy (NIRS), even though it does not measure blood flow: by detecting concentration changes in oxygenated and deoxygenated hemoglobin, NIRS reveals changes in tissue oxygenation and blood volume. This technique is widely adopted to investigate cerebral hemodynamics, with optical probes placed on the forehead as well as all over the skull, using dedicated helmets (Chen *et al* 2020). To our knowledge, only two early studies adapted NIRS to investigate hemodynamics of the temporalis muscle which, however, did not consider the possibility of interference from brain hemodynamics (Kim *et al* 1999, Tsukiyama *et al* 1999).

A constant issue with brain monitoring is that the cerebral NIRS measurement may be contaminated by blood flow changes occurring in the more superficial cutaneous and muscular extracranial tissues (Canova *et al* 2011, Schecklmann *et al* 2017). In the same way, the intended monitoring of superficial tissues could be contaminated by deeper ones. Reliable NIRS monitoring of temporalis muscle requires that contributions from more superficial (skin) and more deep tissues (brain) are both excluded from the measurement. While contributions of changes in cutaneous circulations have been successfully eliminated with different techniques, whether NIRS measurement can be focused on the temporalis muscle and unaffected by hemodynamic changes occurring at the cerebral level has not been investigated, but is a necessary condition for reliable measurements.

The issue is relevant considering many clinical conditions that have been related to vascular dysfunctions in this muscle and the lack of alternative monitoring methodologies. The study aimed to test the reliability of NIRS monitoring in detecting hemodynamic changes in the temporalis muscle with respect to possible interference from cerebral hemodynamics.

## Method

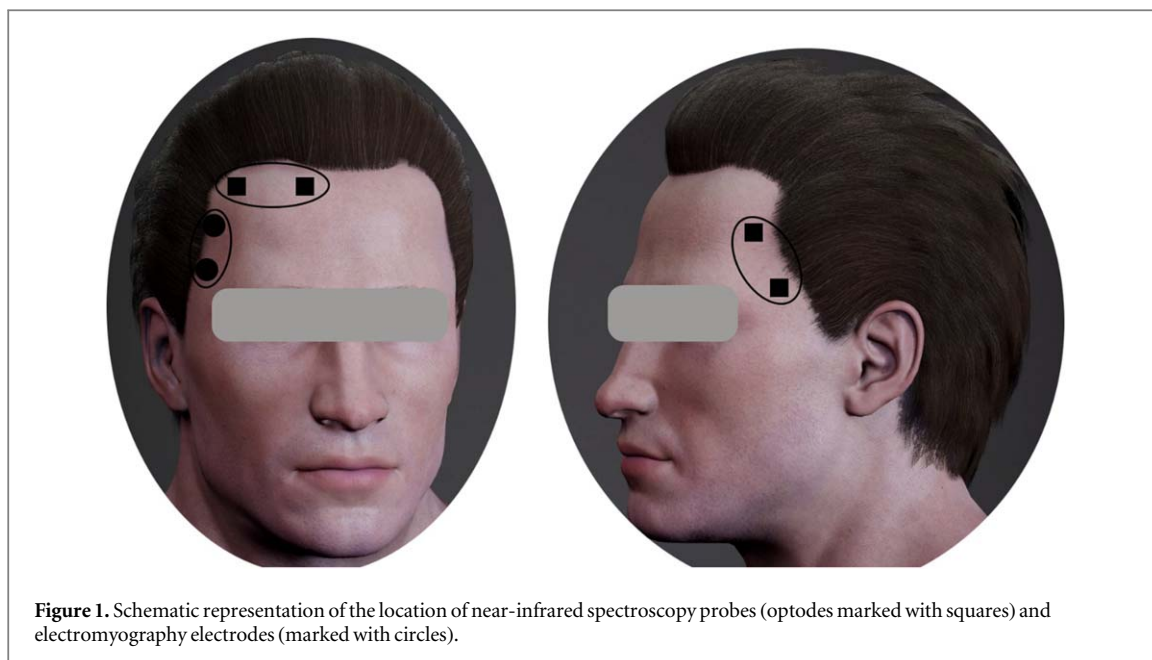
### Subjects and ethical approval

Twenty-four ( $22 \pm 2$  years; 13 males, 11 females) subjects with no history of bruxism, orofacial pain, craniomandibular or temporomandibular disorders were enrolled for this study, but four subjects (2 males and 2 females) were later excluded from the analysis due to unresponsiveness of NIRS variables (see Results). This study was carried out according to the Declaration of Helsinki and was approved by Comitato di Bioetica dell'Università degli Studi di Torino (Protocol # 60195). All subjects gave their written informed consent before participation.

### Monitoring equipment and measurements

The cerebral tissue oxygenation and blood volume were detected by near-infrared spectroscopy (NIRO-200NX, Hamamatsu Photonics, Hamamatsu, Japan), which simultaneously provided conventional Beer–Lambert (B–L) and spatially resolved spectroscopy (SRS) parameters, the latter methodology being less affected by changes in cutaneous circulation (Canova *et al* 2011, Messere and Roatta 2013). SRS measures of tissue oxygenation and blood volume are provided, respectively, by the tissue oxygenation index (TOI), expressed in %, and the tissue hemoglobin index (THI), expressed in arbitrary units (a.u.), whereas B–L parameters indicate changes in the concentration of oxyhemoglobin + oxymyoglobin ( $\text{O}_2\text{Hb}$ ), deoxyhemoglobin + deoxymyoglobin (HHb) and total hemoglobin ( $\text{tHb} = \text{O}_2\text{Hb} + \text{HHb}$ ), expressed in  $\mu\text{M}^*\text{cm}$ . The device has two probes: the *muscle* probe with an inter-optode distance of 3 cm was placed over the left anterior temporal muscle, while the *brain* probe with an inter-optode distance of 4 cm was placed more medially, over the right prefrontal cortex, as shown in figure 1. A larger inter-optode distance was chosen for the brain probe to increase the depth of the sample volume, approximately equal to half of the inter-optode distance.

The electromyography was recorded (Quattro, OT Bioelectronics, Torino, Italy; gain 1200; bandwidth 10–500 Hz) from the right anterior temporal muscle by means of 2 electrodes (FIAB Spa, Florence, Italy, inter-electrode distance 2.3 cm, inter-electrode axis parallel to the orientation of the muscle fibers, ground electrode stuck to the right ear) as shown in figure 1, aiming to monitor contraction levels during teeth clenching and possible involuntary contraction throughout the experiment.



The clenching force was bilaterally measured through an improved version of a custom-made device (Testa *et al* 2015, 2016) based on film sensors (FlexiForce A201 Tekscan, Boston, MA, USA) and visual feedback of the total clenching force (left + right) was provided to the subject to perform constant-force clenching tasks (Testa *et al* 2011).

The partial pressure of end-tidal carbon dioxide ( $P_{ET}CO_2$ ) was monitored using a capnograph (Capnostream™ 20p Bedside Patient Monitor with Microstream™ Technology, Oridion Medical, Jerusalem, Israel).

### Experimental procedures

The study was performed in a quiet room under constant environmental conditions, with the subject sitting in a comfortable chair, without any visual or auditory disturbances. After a 10 min resting period, necessary to reach stable hemodynamic levels, the subjects performed teeth clenching and hyperventilation, separated by a 10 min interval.

#### Teeth clenching

The subjects performed a series of teeth clenching at 25, 50, and 75% of maximum voluntary contraction for 20 s each. The visual feedback of the exerted clenching force was provided on a computer screen and a horizontal cursor was placed to indicate each targeting clenching force level.

#### Hyperventilation

The subjects were asked to hyperventilate to achieve and maintain for 90 s the  $P_{ET}CO_2$  of 20 mmHg. To this end, they were provided with visual feedback from the display of the capnograph, which was continuously monitoring  $P_{ET}CO_2$  from the expiratory flow collected by a nasal cannula, and a horizontal cursor was placed at 20 mmHg indicating the target  $P_{ET}CO_2$  (Rashid *et al* 2022).

Subjects were frequently reminded to maintain the jaw muscles relaxed, particularly during baseline recordings and during hyperventilation.

### Data acquisition, processing, and statistical analysis

All signals were continuously digitally sampled (CED Micro 1401 acquisition board and Spike2 ver. 9.15, Cambridge Electronic Design, Cambridge, UK) at 100 Hz and stored on the computer. MATLAB® ver. R2022b (The MathWorks, Natick, MA, USA) was used to analyze signals and construct the figures, while IBM® SPSS® Statistics ver. 29 (SPSS Inc., Chicago, IL, USA) was used to perform statistical analysis. The baseline values of all variables were taken as a time average calculated over the 20 s interval preceding the beginning of the task (teeth clenching and hyperventilation), while the task effect was assessed over the last 2 s of teeth clenching and over the last 20 s of hyperventilation. After normality assessment using Kolmogorov-Smirnov test, all variables ( $\Delta O_2Hb$ ,  $\Delta HHb$ ,  $\Delta TOI$ , and  $\Delta THI$ ) were analyzed. A repeated measures analysis of variance, with factors *probe* (muscle/brain) and *contraction level* (25, 50, and 75%) was used for teeth clenching analysis. Analysis of hyperventilation,

paired student *t*-test was used to test the difference between brain and muscle probes. Data in the results section are presented as mean  $\pm$  standard deviation and for all analyses, the significance level was set at  $p = 0.05$ .

## Results

In four subjects no contraction-related response in NIRS signals, i.e. a decrease in TOI and/or specular changes exhibited by O<sub>2</sub>Hb (decrease) and HHb (increase) was detected; they were therefore excluded from the analysis, which was then performed on twenty subjects. No relevant electromyography activation was observed during baseline intervals and during hyperventilation. The time course of hemodynamic responses to teeth clenching and hyperventilation are presented in figure 2 (left and right), respectively, by average curves of all NIRS variables, obtained from twenty subjects. Numerical values of observed changes are reported in table 1, while the statistical significance of differences between muscle and brain variables is reported in table 2.

### Teeth clenching

The responses to the three different contraction levels are superimposed for both probes with different colors (figure 2, left). Signals from the muscle probe exhibit the expected changes that take place during an isometric contraction, namely a decrease in oxygenation and O<sub>2</sub>Hb and an increase in HHb, accompanied by some decrease in blood volume (THI). The effects are generally increasing with the contraction level, although at 50 and 75% of maximum voluntary contraction, the curves are similar. Conversely signals from the brain probe are basically not responding to any level of teeth clenching. Notably, all variables exhibit a significant difference between muscle and brain. In particular, the absolute change in tissue oxygenation index ( $\Delta$ TOI) was  $-4.35 \pm 7.66$ ,  $-9.40 \pm 12.28$  and  $-11.36 \pm 13.66\%$  on the temporalis muscle while  $0.80 \pm 2.24$ ,  $0.29 \pm 1.54$  and  $0.45 \pm 1.88\%$  on the prefrontal cortex, during 25, 50, and 75% of maximum voluntary contraction, respectively.

The actual distribution of  $\Delta$ TOI values is shown by box plots (figure 3, left). In spite of the overall significant effects, seven subjects exhibited little or no change in tissue oxygenation ( $\Delta$ TOI  $< -3\%$ ), although all of them exhibited clear and specular changes in O<sub>2</sub>Hb and HHb: a representative recording of this pattern is presented in figure 4.

### Hyperventilation

Muscle NIRS signals are all unresponsive to hyperventilation as well as O<sub>2</sub>Hb, HHb, and THI from the brain probe. A distinct response is only exhibited by TOI from the brain probe, in terms of a clear-cut and sustained decrease ( $-5.11 \pm 3.81\%$ ), significantly different ( $p < 0.01$ ) from the responses collected on the muscle ( $-1.03 \pm 2.70\%$ ) (figure 2, right).

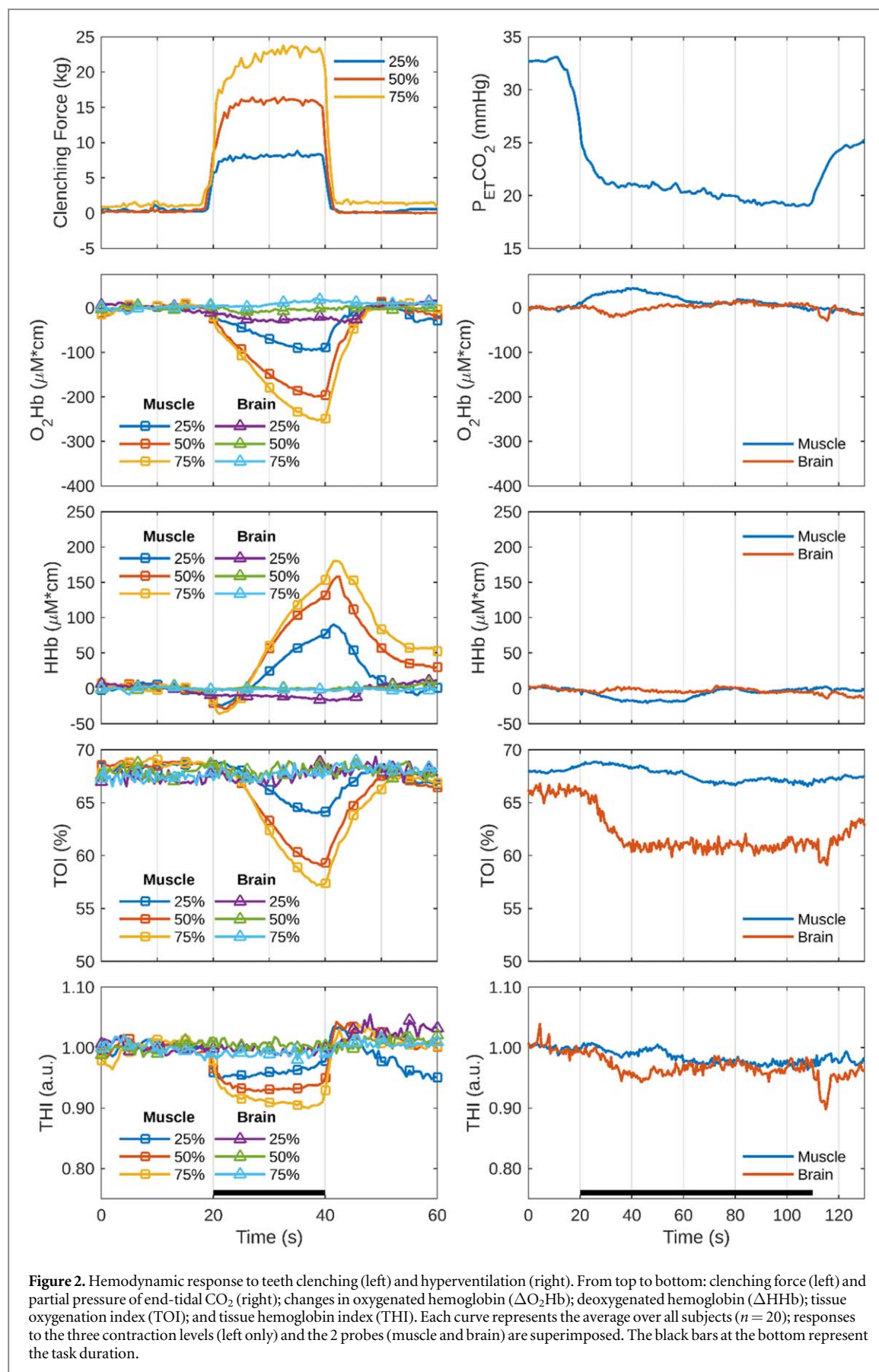
As shown in the box plot (figure 3, right), a TOI decrease was occasionally detected by the muscle probe: only in three subjects the absolute change was  $> 3\%$ .

## Discussion

In the present study the use of NIRS for hemodynamic monitoring of the temporalis muscle was tested during isometric muscle contractions (teeth clenching) and hyperventilation. Different levels of muscle contraction produced a marked and progressive decrease in tissue oxygenation (decrease in TOI and O<sub>2</sub>Hb, and increase in HHb) and blood volume (THI) in a force-level dependent way. In addition, NIRS variables were not affected by hyperventilation, which is known to provoke marked vasoconstriction and a decrease in oxygenation of cerebral tissue. Conversely, NIRS monitoring from the forehead correctly detected a consistent TOI decrease during hyperventilation and no changes during teeth clenching. These results demonstrate that NIRS monitoring can be used to reliably detect hemodynamic changes in the temporalis muscle, with no interference from changes in cerebral blood flow.

A number of studies investigating cerebral hemodynamics with functional NIRS evidenced the risk of getting artifacts and disturbances in NIRS signals from the temporalis muscle when optodes are placed on the temple region, as easily occurs when wearing functional NIRS headsets (Schecklmann *et al* 2017, Morais *et al* 2018, Nakajima *et al* 2020). To our knowledge, NIRS investigation of temporalis muscle was implemented only in two early studies, both from the same group (Kim *et al* 1999, Tsukiyama *et al* 1999). However, their observations were limited to the concentration changes of tHb, taking place during clenching and in the subsequent hyperemic phase. Unfortunately, no information was given about the adopted inter-optode distance, and the possible influence of cerebral hemodynamics on the putative muscle signals was not investigated.

The difficulty of discriminating between superficial and deep tissues is still a major limitation of the NIRS methodology. Vegetative reactions, emotional stimuli, and cognitive tasks may affect the superficial extracranial circulation and disturb the assessment of deeper cerebral hemodynamics (Canova *et al* 2011, Minati *et al* 2011,



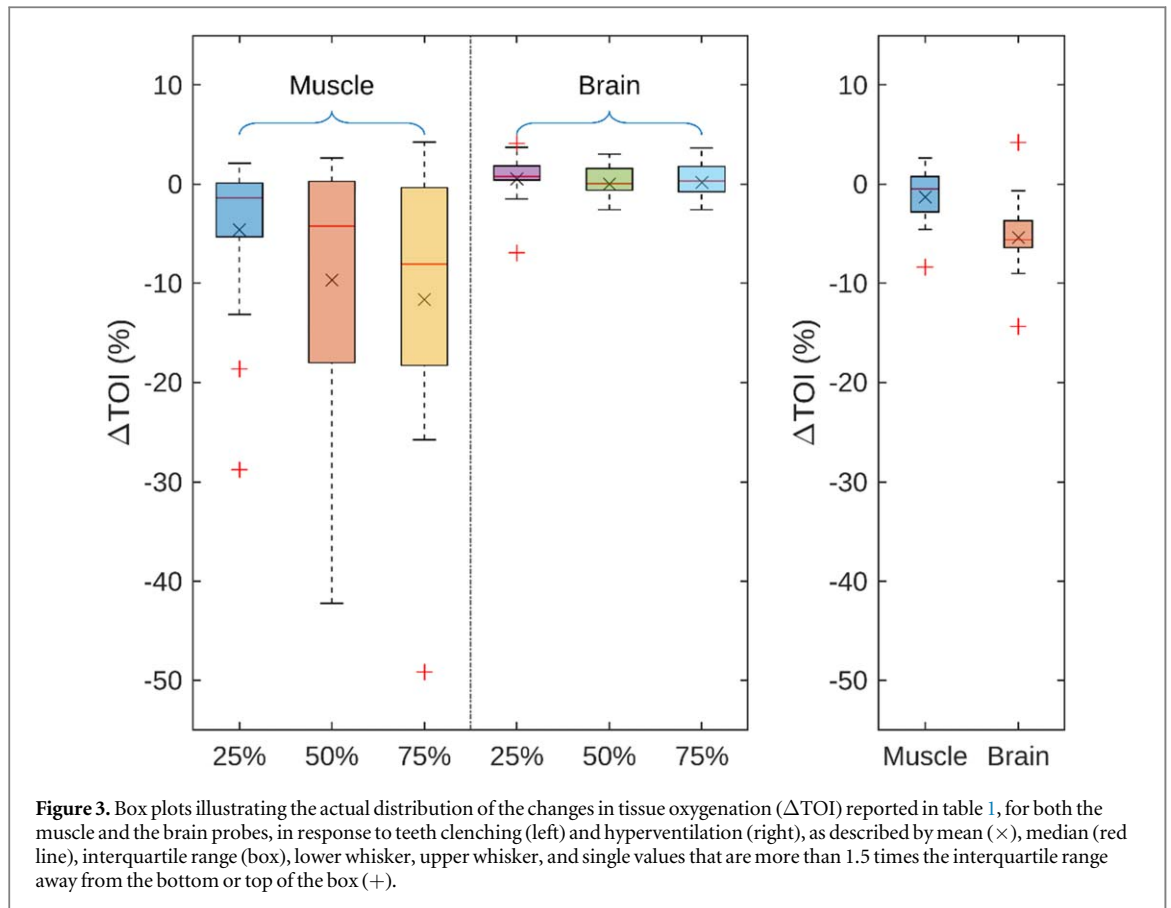
Kirilina *et al* 2013), just as thermoregulatory changes in the skin may disturb the assessment of hemodynamic changes in skeletal muscles (Messere and Roatta 2013, Grassi and Quaresima 2016). Different methodologies have been devised to limit or exclude the contribution from superficial tissues and focus the measurement in



**Table 1.** Changes exhibited by near-infrared spectroscopy variables in response to teeth clenching and hyperventilation (mean  $\pm$  standard deviation;  $n = 20$ ).

Parameter	Teeth clenching						Hyperventilation	
	Muscle			Brain			Muscle	Brain
	25% MVC	50% MVC	75% MVC	25% MVC	50% MVC	75% MVC		
$\Delta O_2Hb$ ( $\mu M^*cm$ )	$-92.43 \pm 96.71$	$-198.02 \pm 154.62$	$-250.96 \pm 136.90$	$-23.73 \pm 87.94$	$-1.73 \pm 18.75$	$18.46 \pm 33.29$	$4.32 \pm 48.64$	$6.36 \pm 61.04$
$\Delta HHb$ ( $\mu M^*cm$ )	$72.84 \pm 61.24$	$125.78 \pm 66.37$	$146.69 \pm 64.12$	$-14.74 \pm 52.95$	$-1.03 \pm 12.00$	$-1.46 \pm 14.65$	$-2.59 \pm 31.23$	$-4.98 \pm 24.89$
$\Delta TOI$ (%)	$-4.35 \pm 7.66$	$-9.40 \pm 12.28$	$-11.36 \pm 13.66$	$0.80 \pm 2.24$	$0.29 \pm 1.54$	$0.45 \pm 1.88$	$-1.03 \pm 2.70$	$-5.11 \pm 3.81$
$\Delta THI$ (a.u.)	$-0.03 \pm 0.08$	$-0.06 \pm 0.10$	$-0.09 \pm 0.13$	$-0.002 \pm 0.06$	$0.004 \pm 0.04$	$-0.01 \pm 0.04$	$-0.03 \pm 0.08$	$-0.03 \pm 0.07$

Note: MVC—maximum voluntary contraction.



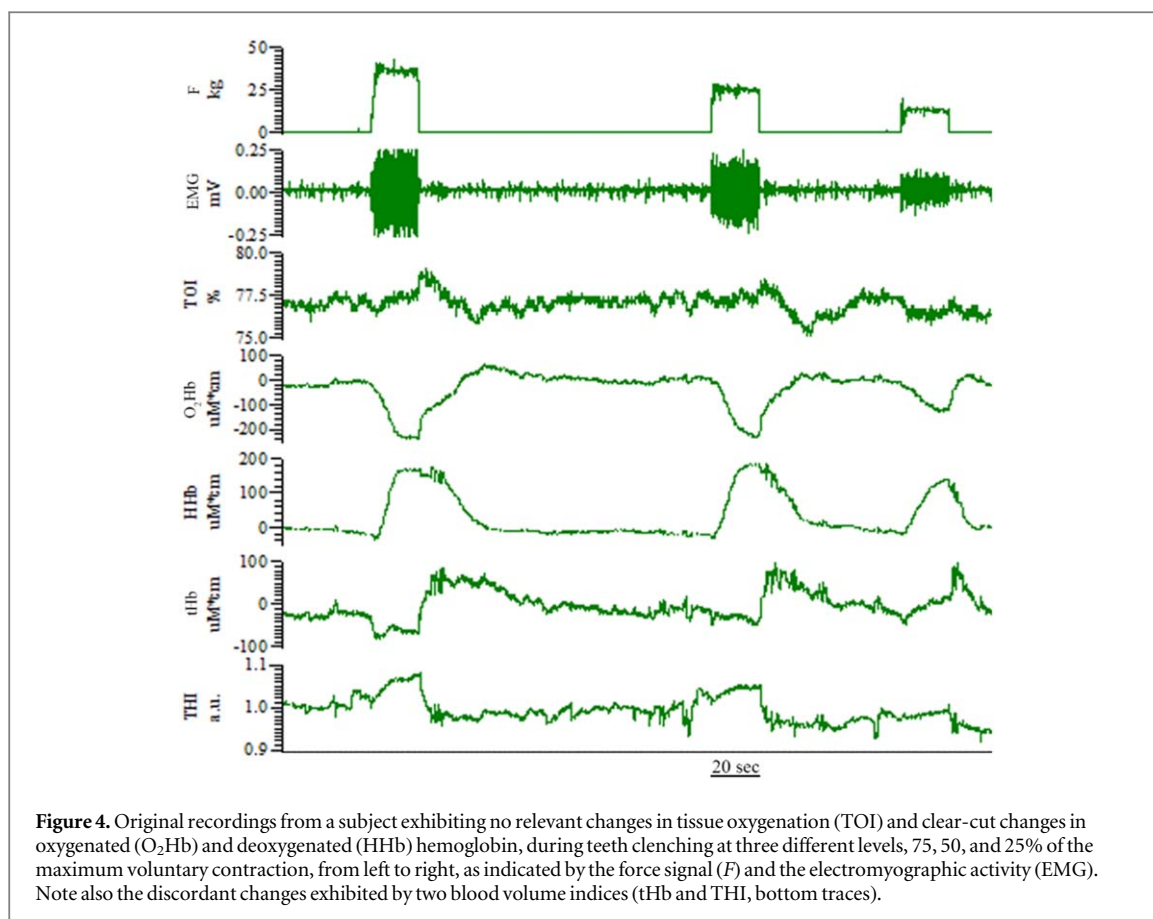
**Table 2.** Significance of main factors (probe location: muscle and brain; contraction level: 25, 50, and 75% of maximum voluntary contraction) during teeth clenching and muscle versus brain difference during hyperventilation ( $n = 20$ ).

Parameter	Teeth clenching			Hyperventilation Muscle/Brain
	Muscle/Brain	Contraction level	Interaction	
$O_2Hb$ ( $\mu M^*cm$ )	<0.001*	<0.001*	<0.001*	0.880
HHb ( $\mu M^*cm$ )	<0.001*	<0.001*	<0.001*	0.792
TOI (%)	0.003*	0.009*	0.005*	0.003*
THI (a.u.)	0.020*	0.047*	<0.001*	0.779

Note: (\*) statistical significance  $p = 0.05$ .

depth. In particular, several studies from our and other groups have pointed out that SRS effectively rejects contributions from superficial tissues allowing us to more specifically focus the measurement on the deeper brain (Quaresima *et al* 2000, Canova *et al* 2011) and muscle tissue (Messere and Roatta 2015, Messere *et al* 2018). For example, increased cerebral blood volume was erroneously detected by the classical B–L parameter tHb in contrast with the decrease detected by SRS variable THI in 33% of healthy subjects during hyperventilation and in 46% of subjects performing Valsalva maneuver (Canova *et al* 2011). Similar results were obtained when monitoring changes in skeletal muscles whereby increased blood flow in cutaneous tissues (Messere and Roatta 2013) and in superficial veins of the arm (Messere and Roatta 2015), by thermal stimuli produced increases in tHb but not THI. The data collected from the brain probe in the present study provide a further confirmation: during hyperventilation, only SRS parameter TOI was able to detect the decrease in cerebral oxygenation while the standard B–L parameters ( $O_2Hb$  and HHb) did not detect significant effects.

Investigation of the temporal muscle however presents a further challenge as the measurement needs to be focused on the intermediate muscle layer, i.e. requiring to prevent contributions from the brain, as well as from the skin. It could be objected that optical signals from the brain are too weak to disturb the signals reflected by the more superficial muscle. This may be true during the hyperemic response to muscle contraction, promoted not only by metabolic but also by mechanical stimuli on the musculo-vascular network (Clifford 2011) which can elicit a rapid dilatation even in response to short lasting (<1 s) contractions (Turturici *et al* 2012) resulting in



**Figure 4.** Original recordings from a subject exhibiting no relevant changes in tissue oxygenation (TOI) and clear-cut changes in oxygenated ( $\text{O}_2\text{Hb}$ ) and deoxygenated (HHb) hemoglobin, during teeth clenching at three different levels, 75, 50, and 25% of the maximum voluntary contraction, from left to right, as indicated by the force signal ( $F$ ) and the electromyographic activity (EMG). Note also the discordant changes exhibited by two blood volume indices (tHb and THI, bottom traces).

a marked increase in tissue oxygenation that may last more than 30 s (Messere *et al* 2018). Such responses were also observed in the temporalis muscle in response to brief teeth clenching and reported to ‘saturate’ NIRS signals and completely mask brain signals, i.e. producing large artifacts in functional NIRS recordings (Schecklmann *et al* 2017). However, in resting conditions perfusion in muscle may be 1/10 than in brain tissue, and the possibility that cerebral hemodynamic changes may affect the putative muscle signals needs to be prevented. This latter requirement can be obtained by reducing the inter-optode distance. Since the maximum depth of the NIRS sample volume is roughly equal to half of the inter-optode distance. Distances of 4 cm or greater were recommended for cerebral hemodynamics investigations (Quaresima *et al* 2000). Here, we maintained a 4 cm distance for the brain probe but adopted a shorter distance (3 cm) for the muscle probe. This choice was effective in making NIRS measurements on the temporalis muscle independent of cerebral hemodynamics. In fact, a strong stimulus like hyperventilation, which provokes a marked cerebral vasoconstriction and a marked drop in cerebral oxygenation ( $-5\%$  in the present study) did not generally affect the muscle measurement. At the same time, the muscle probe distinctly detected the typical hemodynamic changes of isometric muscle contractions, during teeth clenching. It can be observed in figure 2 (left) that the onset of contraction is associated with a sharp reduction of blood volume in the muscle (THI) which slowly recovers at a low contraction level (25% of maximum voluntary contraction), as previously observed (Kim *et al* 1999), but not at higher levels (50 and 75% of maximum voluntary contraction), which suggests that functional dilatory mechanisms are overcome by intramuscular pressures at high contraction levels.

It must be pointed out that in four subjects no evidence of contraction of the temporalis muscle could be detected from NIRS signals, in spite of clear electromyographic activation. Possible reasons behind this failure are the misplacement of NIRS probe due to an extended hairy region or a bad optical coupling between optodes and tissue, due to some hair interposed between them. Moreover, in about 1/3 of the subjects the responses were collected only from the B–L parameters  $\text{O}_2\text{Hb}$ , HHb, and tHb, not by SRS parameter TOI. Our interpretation is that the different indications result from the different sample volumes considered by two techniques; SRS excluding the superficial tissue layers, and B–L including both superficial and deep layers. Considering that the NIRS probe was generally located over the most anterior portion of the temporalis muscle, where it gets thinner, it is possible that, in these seven subjects, this muscle portion was too superficial to be adequately sampled by SRS methodology. This latter interpretation is also supported by the discordant indication provided by the blood volume indicators tHb (B–L) and THI (SRS), shown in figure 4: a pattern also encountered in a previous study (Canova *et al* 2011) and attributed to differences in sample volume, as already described above. On this basis, we

can conclude that specific monitoring of the temporalis muscle by NIRS is possible but should be carefully tested in individual subjects: upon sustained teeth clenching a specular increase/decrease pattern should be observed in HHb/O<sub>2</sub>Hb, possibly accompanied by a decrease in TOI, if available.

Muscles of the head present peculiar differences from limb muscles ranging from histology (Stål *et al* 1996), to function (Sciote *et al* 2003), to control of blood perfusion (Rashid and Roatta 2022). However, most functional and hemodynamic studies are carried out on the masseter muscle, while other masticatory and head muscles have been less investigated. The reliability of NIRS monitoring documented in the present study will hopefully promote basic and clinical investigations of perfusion and oxygenation in the temporalis muscle in physiological and pathological conditions.

While in the present study changes in blood flow were inferred from changes in tissue oxygenation, recent developments in near-infrared monitoring, by *diffuse correlation spectroscopy*, allow for direct assessment of blood flow changes in deep tissues (Shang *et al* 2017). This represents a promising methodology, which however has never been tested on masticatory muscles, as yet. However, this technique, being still based on near-infrared light scattering, potentially suffers from the same limitations of classical NIRS, such as sensitivity to movement artifacts and influence from cutaneous tissue layers (Bartlett *et al* 2021). For this reason, the present investigation is likely to be helpful for *diffuse correlation spectroscopy* applications in the temporalis muscle.

## Conclusion

By testing the response to teeth clenching and hyperventilation we were able to demonstrate the capacity of NIRS monitoring to focus the measurement of blood volume and tissue oxygenation on the temporalis muscle, with virtually no interference from the brain. Thanks to its non-invasiveness and ease of application, this technique will conveniently be adopted in new investigations on the temporalis muscle function, in health and disease.

## Acknowledgments

This study was supported by Ministero dell'Università e della Ricerca under 'Dipartimenti di Eccellenza ex L.232/2016' to Dipartimento di Neuroscienze 'Rita Levi Montalcini', Università degli Studi di Torino and A.R. was a recipient of Doctoral Fellowship funded by Agenzia Italiana per la Cooperazione allo Sviluppo (Partnership for Knowledge), Ministero degli Affari Esteri e della Cooperazione Internazionale, Italy. We are grateful to Dr Raffaele Pertusio for his technical assistance.

## Data availability statement

All data that support the findings of this study are included within the article. Data will be available from 5 March 2023.

## Authors' contributions

Both authors contributed equally to this manuscript.

## Conflict of interest

The authors declare no competing interests.

## ORCID iDs

Anas Rashid  <https://orcid.org/0000-0002-4644-4729>

Silvestro Roatta  <https://orcid.org/0000-0001-7370-2271>

## References

- Arbeille P, Yuan M, Bai Y, Jiang S, Gauquelin G, Aubry P, Wan Y, Custaud M A and Li Y 2011 Temporal artery flow response during the last minute of a head up tilt test, in relation with orthostatic intolerance after a 60 d head-down bedrest *PLoS One* **6** 1–5
- Bartlett M F, Akins J D, Oneglia A P, Brothers R M, Wilkes D and Nelson M D 2021 Impact of cutaneous blood flow on NIR-DCS measures of skeletal muscle blood flow index *J. Appl. Physiol.* **131** 914–26

- Canova D, Roatta S, Bosone D and Miceli G 2011 Inconsistent detection of changes in cerebral blood volume by near infrared spectroscopy in standard clinical tests *J. Appl. Physiol.* **110** 1646–55
- Chen W L *et al* 2020 Functional near-infrared spectroscopy and its clinical application in the field of neuroscience: advances and future directions *Front. Neurosci.* **14** 1–15
- Clifford P S 2011 Local control of blood flow *Adv. Physiol. Educ.* **35** 5–15
- Elazab E E B and Abdel-Hameed F A M 2006 The arterial supply of the temporalis muscle *Surg. Radiol. Anat.* **28** 241–7
- Exposto F G, Renner N, Bendixen K H and Svensson P 2021 Pain in the temple? headache, muscle pain or both: a retrospective analysis *Cephalalgia* **41** 1486–91
- Geers C, Nyssen-Behets C, Cosnard G and Lengelé B 2005 The deep belly of the temporalis muscle: an anatomical, histological and MRI study *Surg. Radiol. Anat.* **27** 184–91
- Grassi B and Quaresima V 2016 Near-infrared spectroscopy and skeletal muscle oxidative function *in vivo* in health and disease: a review from an exercise physiology perspective *J. Biomed. Opt.* **21** 0913131
- Jacobs B and Dussor G 2016 Neurovascular contributions to migraine: moving beyond vasodilation *Neuroscience* **338** 130–44
- Jensen K 1993 Extracranial blood flow, pain and tenderness in migraine. clinical and experimental studies *Acta Neurol. Scand. Suppl.* **147** 1–27
- Jensen K and Olesen J 1985 Temporal muscle blood flow in common migraine *Acta Neurol. Scand.* **72** 561–70
- Kim Y J, Kuboki T, Tsukiyama Y, Koyano K and Clark G T 1999 Haemodynamic changes in human masseter and temporalis muscles induced by different levels of isometric contraction *Arch. Oral Biol.* **44** 641–50
- Kirilina E, Yu N, Jelzow A, Wabnitz H, Jacobs A M and Tachtsidis I 2013 Identifying and quantifying main components of physiological noise in functional near infrared spectroscopy on the prefrontal cortex *Front. Hum. Neurosci.* **7** 1–17
- Langemark M, Jensen K and Olesen J 1990 Temporal muscle blood flow in chronic tension-type headache *Arch. Neurol.* **47** 654–8
- Lavigne G J, Khoury S, Abe S, Yamaguchi T and Raphael K 2008 Bruxism physiology and pathology: an overview for clinicians *J. Oral Rehabil.* **35** 476–94
- Maekawa K, Clark G T and Kuboki T 2002 Intramuscular hypoperfusion, adrenergic receptors, and chronic muscle pain *J. Pain* **3** 251–60
- Mason B N and Russo A F 2018 Vascular contributions to migraine: time to revisit? *Front. Cell. Neurosci.* **12** 1–10
- Messere A and Roatta S 2013 Influence of cutaneous and muscular circulation on spatially resolved versus standard Beer–Lambert near-infrared spectroscopy *Physiol. Rep.* **1** 1–10
- Messere A and Roatta S 2015 Local and remote thermoregulatory changes affect NIRS measurement in forearm muscles *Eur. J. Appl. Physiol.* **115** 2281–91
- Messere A, Tschakovskiy M, Seddone S, Lulli G, Franco W, Maffiolo D, Ferraresi C and Roatta S 2018 Hyper-oxygenation attenuates the rapid vasodilatory response to muscle contraction and compression *Front. Physiol.* **9** 1–12
- Minati L, Kress I U, Visani E, Medford N and Critchley H D 2011 Intra- and extra-cranial effects of transient blood pressure changes on brain near-infrared spectroscopy (NIRS) measurements *J. Neurosci. Methods* **197** 283–8
- Morais G A Z, Scholkmann F, Balardin J B, Furucho R A, Paula R C V, de, Biazoli C E and Sato J R 2018 Non-neuronal evoked and spontaneous hemodynamic changes in the anterior temporal region of the human head may lead to misinterpretations of functional near-infrared spectroscopy signals *Neurophotonics* **5** 1–10
- Nakajima K, Takeda T, Saito M, Konno M, Kawano Y, Suzuki Y, Nishino M, Matsuda Y, Ishigami K and Sakatani K 2020 effect of mastication muscle activity on prefrontal cortex NIRS measurement: a pilot study *Adv. Exp. Med. Biol.* **1232** 121–7
- Nakamura Y, Torisu T, Noguchi K and Fujii H 2005 Changes in masseter muscle blood flow during voluntary isometric contraction in humans *J. Oral Rehabil.* **32** 545–51
- Noumejni S R, Hoffmann C, Cornec D, Gestin S, Bressollette L and Jousse-Joulin S 2021 Temporal artery ultrasound to diagnose giant cell arteritis: a practical guide *Ultrasound Med. Biol.* **47** 201–13
- Petersen F B and Christensen L V 1973 Blood flow in human temporal muscle during tooth grinding and clenching as measured by <sup>133</sup>xenon clearance *Scand. J. Dent. Res.* **81** 272–275
- Quaresima V, Sacco S, Totaro R and Ferrari M 2000 Noninvasive measurement of cerebral hemoglobin oxygen saturation using two near infrared spectroscopy approaches *J. Biomed. Opt.* **5** 201–5
- Rashid A and Roatta S 2022 Differential control of blood flow in masseter and biceps brachii muscles during stress *Arch. Oral Biol.* **141** 1–10
- Rashid A, Santarcangelo E L and Roatta S 2022 Cerebral blood flow in healthy subjects with different hypnotizability scores *Brain Sci.* **12** 1–13 558
- Schecklmann M, Mann A, Langguth B, Ehli A C, Fallgatter A J and Haeussinger F B 2017 The temporal muscle of the head can cause artifacts in optical imaging studies with functional near-infrared spectroscopy *Front. Hum. Neurosci.* **11** 1–13
- Sciote J J, Horton M J, Rowleron A M and Link J 2003 Specialized cranial muscles: how different are they from limb and abdominal muscles? *Cells Tissues Organs* **174** 73–86
- Shah N, Melo L, Reid W D and Cioffi I 2019 Masseter deoxygenation in adults at risk for temporomandibular disorders *J. Dent. Res.* **98** 666–72
- Shang Y, Li T and Yu G 2017 Clinical applications of near-infrared diffuse correlation spectroscopy and tomography for tissue blood flow monitoring and imaging *Physiol. Meas.* **38** R1–26
- Stål P, Eriksson P O and Thornell L E 1996 Differences in capillary supply between human oro-facial, masticatory and limb muscles *J. Muscle Res. Cell Motil.* **17** 183–97
- Testa M, Geri T, Signori A and Roatta S 2015 Visual feedback of bilateral bite force to assess motor control of the mandible in isometric condition *Motor Control* **19** 312–24
- Testa M, Marco A D, Pertusio R, Roy P V, Cattrysse E and Roatta S 2016 A validation study of a new instrument for low cost bite force measurement *J. Electromyogr. Kinesiol.* **30** 243–8
- Testa M, Rolando M and Roatta S 2011 Control of jaw-clenching forces in dentate subjects *J. Orofac. Pain* **25** 250–60
- Tsukiyama Y, Kuboki T and Clark G T 1999 Cold pressor stimulation effect on hemodynamic changes following sustained isometric contraction in human jaw-closure muscles *J. Dent. Res.* **78** 1727–34
- Turturici M, Mohammed M and Roatta S 2012 Evidence that the contraction-induced rapid hyperemia in rabbit masseter muscle is based on a mechanosensitive mechanism, not shared by cutaneous vascular beds *J. Appl. Physiol.* **113** 524–31
- Veldhoen S, Klink T, Geiger J, Vaith P, Glaser C, Ness T, Duwendag D, Both M and Bley T A 2014 MRI displays involvement of the temporalis muscle and the deep temporal artery in patients with giant cell arteritis *Eur. Radiol.* **24** 2971–9
- Yap A U J and Chua A P 2016 Sleep bruxism: current knowledge and contemporary management *J. Conserv. Dent.* **19** 383–9
- Yu S K, Kim T H, Yang K Y, Bae C J and Kim H J 2021 Morphology of the temporalis muscle focusing on the tendinous attachment onto the coronoid process *Anat. Cell Biol.* **54** 308–14

# **Hemodynamic Changes in the Temporalis and Masseter Muscles During Stress in Healthy Humans**

Anas Rashid, Silvestro Roatta\*

Lab of Integrative Physiology, Department of Neuroscience “Rita Levi Montalcini”,  
University of Torino, Torino, Italy

## **Abstract**

Autonomic control of facial blood flow is an integral part of the social behavioral patterns. However, the specific control of blood flow in head muscles during stress is unknown. Aim of this study is to investigate the hemodynamic response of temporalis and masseter muscles in response to five different stressors. Sixteen healthy individuals were subjected to a randomized series of stressors, including cold pressor test, mental arithmetic test, apnea, isometric handgrip, and post-handgrip muscle ischemia, while in the sitting posture. Finger-pulse photoplethysmography was used to measure arterial blood pressure, heart rate, and cardiac output. Near-infrared spectroscopy was used to measure changes in tissue oxygenation and hemoglobin indices from the temporalis and masseter muscles. All stressors effectively and significantly increased arterial blood pressure. Tissue oxygenation index significantly increased in both investigated head muscles during mental arithmetic test (temporalis:  $4.22 \pm 3.52$  %; masseter:  $3.43 \pm 3.63$  %) and isometric handgrip (temporalis:  $3.45 \pm 3.09$  %; masseter:  $3.26 \pm 3.07$  %), suggesting increased muscle blood flow. Neither the masseter, nor the temporalis muscles evidenced a vasoconstrictive response to any of the stressors tested. In the different conditions, temporalis and masseter muscles exhibited similar hemodynamic patterns of response, which do not include the marked vasoconstriction generally observed in limb muscles. The peculiar sympathetic control of head muscles is possibly related to the involvement of these muscles in aggressive/defensive reactions and/or to their unfavorable position with regard to hydrostatic blood levels.

## **Keywords**

Blood flow, Oxygenation, Masseter, Temporalis, Muscle, Stress

## Introduction

Autonomic control of extracranial areas of the head is an integral and relevant component of social behavior, and includes control of pupil size, salivation, skin blood flow etc. [1] Regarding blood flow control, several systems including parasympathetic, sympathetic and trigeminal sensory systems are possibly involved, with a complex interplay of dilatory and constrictory actions [2,3]. While there is an agreement about the possible sympathetic dilatory action in facial skin, e.g., during flushing [4], whether a peculiar sympathetic control also concerns head muscles is unknown.

Interest in the control of muscle blood flow also comes from clinical studies. Altered masticatory muscle perfusion is implicated in numerous painful disorders afflicting head and orofacial regions [5,6], whereby inadequate delivery of oxygen and nutrients occurring during and after muscle contraction leads to muscle damage and functional impairment [7]. In this respect, the control of blood flow exerted by the sympathetic nervous system is of particular interest due to its general constrictory action oriented to limit blood flow, to both resting and working muscles [8,9] which has been implicated in pathophysiological mechanisms behind musculoskeletal disorders [10–12] and also in the orofacial area [13]. However, only few investigations have been carried out on the control of blood flow in masticatory muscles in physiological (e.g., acute stress exposure) [14,15] or pathological (e.g., chronic tension-type headache) [16] conditions.

The control of sympathetic outflow may be highly differentiated to different body regions and numerous reports described an increase rather than a decrease in blood flow or tissue oxygenation in the masseter muscle during experimental stress [7,14,17]. By the simultaneous recording of tissue oxygenation in the masseter and biceps brachii muscles [18], we recently confirmed these observations, during exposure to different sympathetic activation tests: significant tissue oxygenation decreased in the biceps and increased in the masseter muscle. The reason for a different hemodynamic response of the masseter muscle to stress is unclear, and it is also unknown whether this preferential dilatory rather than constrictory response is specific to the masseter muscle or is shared by other head muscles. In fact, we hypothesized that this feature could characterize head muscles in general, due to the unfavorable hydrostatic gradient that affects the head, compared to trunk and limb muscles, in humans in the erect posture.

Most studies of masticatory muscle perfusion have been confined to the masseter, a jaw-closing muscle, whereas other head muscles have been little considered for hemodynamic investigations. We recently validated the possibility of using near-infrared spectroscopy (NIRS) on the temporalis muscle. In particular, the possibility was excluded that interference from the deeper brain tissue could affect the measurement [19]. Thus, this present study aims to test the hypothesis that the dilatory response to acute stress observed in the masseter muscle is shared by the temporal muscle. NIRS monitoring will be simultaneously performed on temporal and masseter muscles but, differently from our previous study [18], the subjects will maintain the sitting rather than the supine position, in order to test the secondary hypothesis that the hemodynamic response to stress is independent of current head-heart

hydrostatic gradients. In fact, in our previous study, subjects were investigated in the supine position so that both the masseter and biceps muscles were positioned at heart level [18], and it is presently unknown whether these responses are affected by body posture.

## **Methods**

### **Subject and ethical approval**

Sixteen (8 males; age:  $25 \pm 4$  years; weight:  $69 \pm 15$  kg; height:  $173 \pm 10$  cm) healthy university students participated in this study. The investigation was carried out according to the Declaration of Helsinki and was approved by Comitato di Bioetica dell'Università degli Studi di Torino (Protocol # 60195). All subjects gave their written informed consent before participation.

### **Monitoring equipment and measurements**

Finger-pulse photoplethysmography (CNAP<sup>®</sup> Monitor, CNSystems Medizintechnik GmbH, Graz, Austria) was used to measure arterial blood pressure, heart rate, and cardiac output. Calibration of arterial blood pressure was periodically performed using a regular pneumatic cuff at the left arm.

A custom-made device based on film sensors (FlexiForce A201 Tekscan, Boston, MA, USA) was used to measure handgrip force [20] and visual feedback has been provided to each subject to maintain constant force during isometric handgrip.

Electromyographic signals (Quattro, OT Bioelettronica SRL, Torino, Italy; Gain 1200; Bandwidth 10 – 500 Hz) were recorded from right anterior temporal and right superficial masseter muscles by means of pairs of surface electrodes (FIAB SpA, Florence, Italy, inter-electrode distance 2.3 cm, inter-electrode axis parallel to the orientation of the muscle fibers, ground electrode stuck to the right ear), to detect possible involuntary muscle contraction throughout the experiment.

NIRS (NIRO-200NX, Hamamatsu Photonics, Hamamatsu, Japan) was used to measure changes in tissue oxygenation index (TOI, %) and tissue hemoglobin index (THI, a.u.). The device has two probes: one was placed over the left anterior temporal muscle [19] and the other over the left superficial masseter muscle [18].

### **Experimental procedures**

Experiments were conducted in a silent, light-attenuated, and temperature controlled (23 – 25 °C) room, with a subject sitting in a comfortable chair. All signals reached a stable condition, then a 10-min baseline was recorded, after which volunteers completed a sequence of five different tasks in a randomized order, described below, except post-handgrip muscle ischemia which immediately followed the isometric handgrip. All volunteers were periodically reminded to relax their head muscles, especially masticatory muscles.



**i. Cold pressor test**

The participant was asked to immerse and maintain for 1 min the right hand into a bucket filled with cold water (10 °C), and after the end of the task to rate the peak pain level experienced during the task using a visual analogue scale (from 0, no pain; to 10, worst imaginable pain).

**ii. Mental arithmetic test**

The participant was asked to progressively subtract the odd numbers (1, 3, 5 and so) from 1000 for 2 min while writing the outcome on the paper. One operator standing behind the subject monitored the outcome and compared it to a table reporting the correct answers, promptly asking the subject to repeat the calculation in case of error.

**iii. Apnea**

The participant was asked to hold their breath for 40 sec to maintain apnea.

**iv. Isometric handgrip**

The participant was asked to perform 50% of the maximum voluntary contraction with the right hand for 1 min using a previously calibrated handheld dynamometer [20]. To this end, they were provided with visual feedback from the computer monitor, which was continuously displaying the developed force and a horizontal cursor indicating the target force level, set at 50% of the maximum voluntary contraction.

**v. Post-handgrip muscle ischemia**

Ten seconds before the cessation of the isometric handgrip, a blood pressure cuff (Gima SpA, Milan, Italy), previously wrapped around the right arm, was inflated to 250 mmHg pressure and maintained at this level for 2 min to occlude arterial blood flow. The participant was later asked to rate the peak pain level experienced during the task, using a visual analogue scale.

## **Data analysis and statistics**

All signals were continuously digitally sampled (CED Micro 1401 acquisition board and Spike2 ver. 9.15, Cambridge Electronic Design, Cambridge, UK) at 100 Hz, and statistical analysis was performed using MATLAB<sup>®</sup> ver. R2023a (The MathWorks, Natick, MA, USA). The baseline values of all variables were obtained as the time average calculated over the 20-sec interval preceding the beginning of each task, while the task effect was assessed over the last 10-sec. The Kolmogorov-Smirnov test was used to assess the data's normal distribution. Student *t*-tests were used to assess the statistical significance of stress-induced changes in all variables. In addition, the difference between effects on temporal and masseter muscles is also investigated using Hochberg's test with Dunn/Sidak alpha correction for multiple comparisons. The results are presented as mean  $\pm$  standard deviation in the text and by box plots in the figures. Correlation of effects observed in temporal and masseter muscles was assessed by the Pearson's correlation coefficient, for the different tests. The significance level was set at  $p = 0.05$  for all analyses.

## **Results**

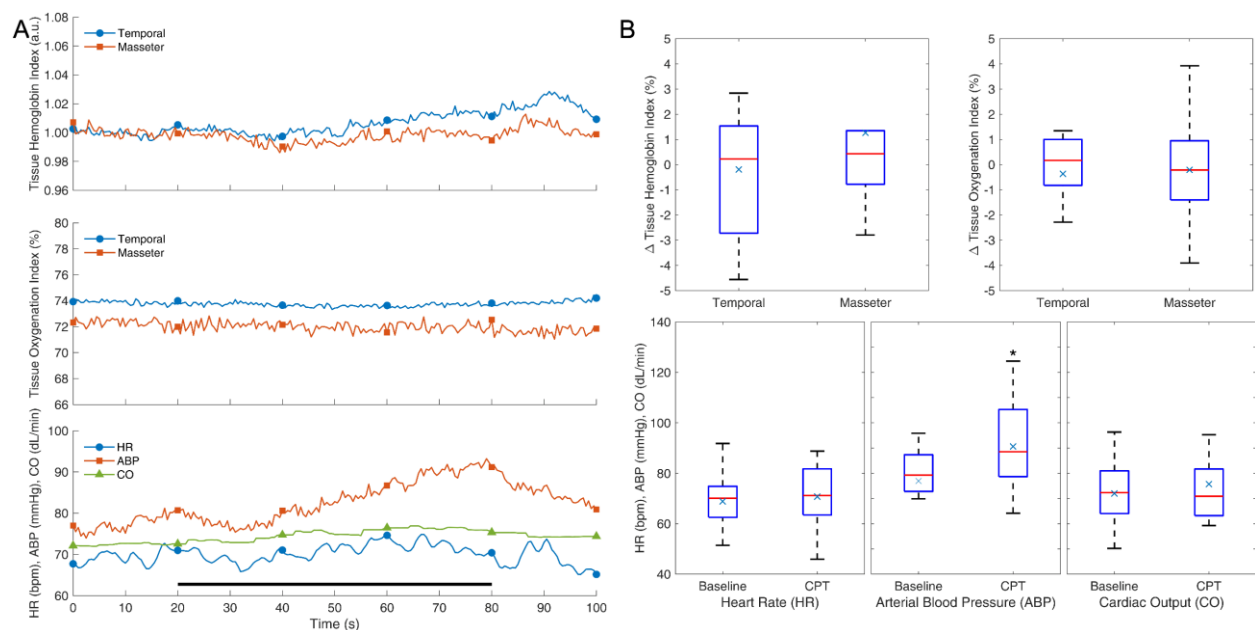
All subjects (excluding two from cold pressor test, one from isometric handgrip, and post-handgrip muscle ischemia) managed to maintain masticatory muscles relaxed both during

baseline intervals and stress tests so that no relevant sign of electromyography activation was detected. For the different tests, the time course of the response of NIRS and systemic variables is presented, along with the comparison of average effects in temporal and masseter muscles.

### i. Cold pressor test

Cold pressor test evoked a self-reported pain score of  $7.1 \pm 1.8$ . The hemodynamic response is reported by the average curves of Fig. 1A and the distribution of effects for the different variables is presented in Fig. 1B. The test significantly increased arterial blood pressure (from  $77.5 \pm 14.1$  to  $91.1 \pm 18.2$  mmHg,  $p < 0.05$ ) while producing a non-significant change in heart rate (from  $69.3 \pm 10.6$  to  $71.2 \pm 12.0$  bpm), cardiac output (from  $7.2 \pm 1.2$  to  $7.6 \pm 1.8$  dL/min) and TOI (temporal muscle: from  $72.3 \pm 5.0$  to  $72.0 \pm 5.2$  %; masseter muscle: from  $73.9 \pm 6.2$  to  $73.7 \pm 6.8$  %). The observed TOI changes in the two muscles were moderately correlated ( $r = 0.42$ ).

Finally, we investigated whether the observed vascular reaction ( $\Delta$ TOI) was correlated to the magnitude of the pressor response ( $\Delta$ ABP):  $r = 0.01$  for temporalis and  $r = 0.43$  for masseter muscle.

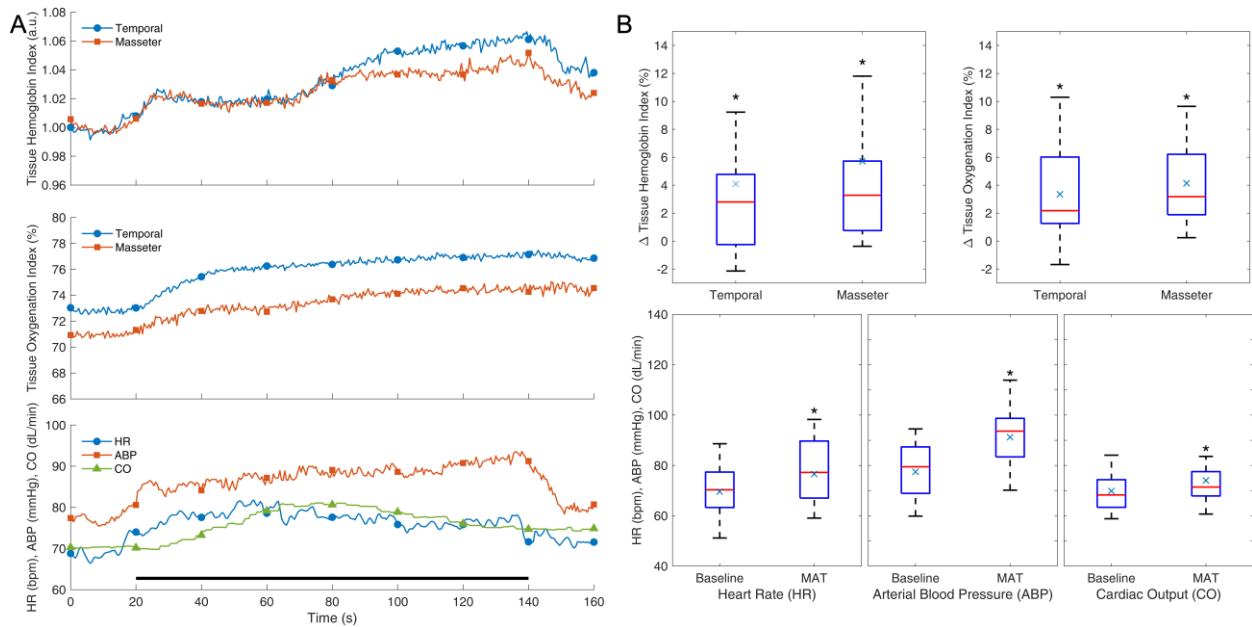


**Figure 1.** Response to cold pressor test (CPT). Average response curves (A) and distribution of effects (B) for different variables, as described by mean ( $\times$ ), median (red line), interquartile range (blue box), minimum (lower whisker), and maximum (upper whisker) values respectively. The black bar at the bottom indicates the duration of CPT. \*)  $p < 0.05$ ;  $n = 14$ .

### ii. Mental arithmetic test

The average response to the mental arithmetic test (Fig. 2A and B) also exhibited a significant increase in arterial blood pressure (from  $77.9 \pm 11.0$  to  $91.7 \pm 11.4$  mmHg,  $p < 0.05$ ), with significant changes also in heart rate (from  $70.0 \pm 10.1$  to  $77.0 \pm 12.2$  bpm,  $p < 0.05$ ) and cardiac output (from  $7.0 \pm 1.1$  to  $7.4 \pm 1.2$ ,  $p < 0.05$ ).

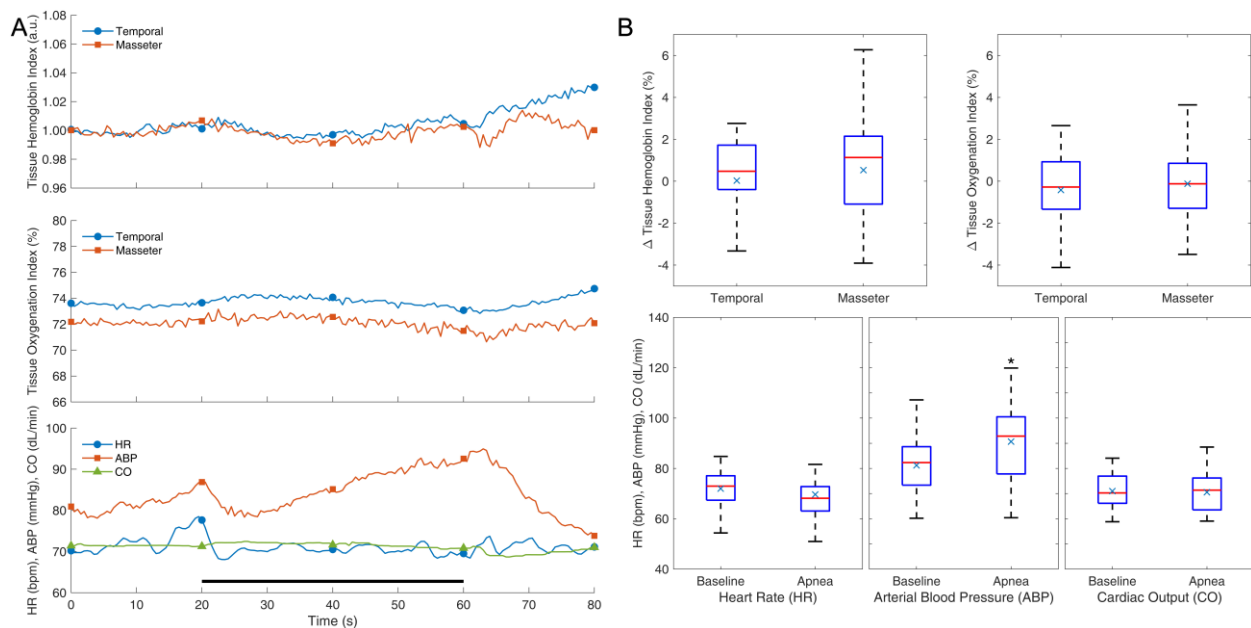
Tissue oxygenation and blood volume exhibited a significant increase in both temporal (TOI: from  $71.3 \pm 6.9$  to  $74.8 \pm 7.0$  %;  $\Delta$ THI  $0.04 \pm 0.06$  %,  $p < 0.05$ ) and masseter (TOI: from  $72.8 \pm 6.1$  to  $77.0 \pm 4.9$  %;  $\Delta$ THI:  $0.06 \pm 0.08$ ,  $p < 0.05$ ) muscles. The observed TOI changes in the two muscles exhibited strong correlation ( $r = 0.70$ ) but poor correlation with ABP changes ( $r < 0.23$ ).



**Figure 2.** Response to mental arithmetic test (MAT). Average response curves (A) and distribution of effects (B) for different variables. Notations as in Fig. 1. The black bar at the bottom indicates the duration of MAT. \*)  $p < 0.05$ ;  $n = 16$ .

### iii. Apnea

The response to apnea is reported by the average curves of Fig. 3A and the distribution of effects for the different variables is presented in Fig. 3B. The test significantly increased arterial blood pressure (from  $81.7 \pm 13.2$  to  $91.1 \pm 14.7$  mmHg,  $p < 0.05$ ) while producing a non-significant effect in heart rate (from  $72.4 \pm 9.7$  to  $70.1 \pm 12.3$  bpm), cardiac output (from  $7.14 \pm 0.7$  to  $7.10 \pm 0.8$  dL/min) and NIRS variables (temporal muscle TOI: from  $72.1 \pm 7.0$  to  $71.7 \pm 6.4$  %; masseter muscle TOI: from  $73.5 \pm 5.8$  to  $73.4 \pm 5.6$  %). The observed TOI changes in the two muscles exhibited strong correlation ( $r = 0.70$ ) and a moderate negative correlation with  $\Delta$ ABP:  $r = -0.48$  for temporalis and  $r = -0.34$  for masseter muscle.



**Figure 3.** Response to apnea. Average response curves (A) and distribution of effects (B) for different variables. Notations as in Fig. 1. The black bar at the bottom indicates the duration of apnea. \*)  $p < 0.05$ ;  $n = 16$ .

#### iv. Isometric handgrip and post-handgrip muscle ischemia

The response to isometric handgrip and post-handgrip muscle ischemia is presented by the average curves in Fig. 4A and the distribution of effects in Fig. 4B and C for the different variables.

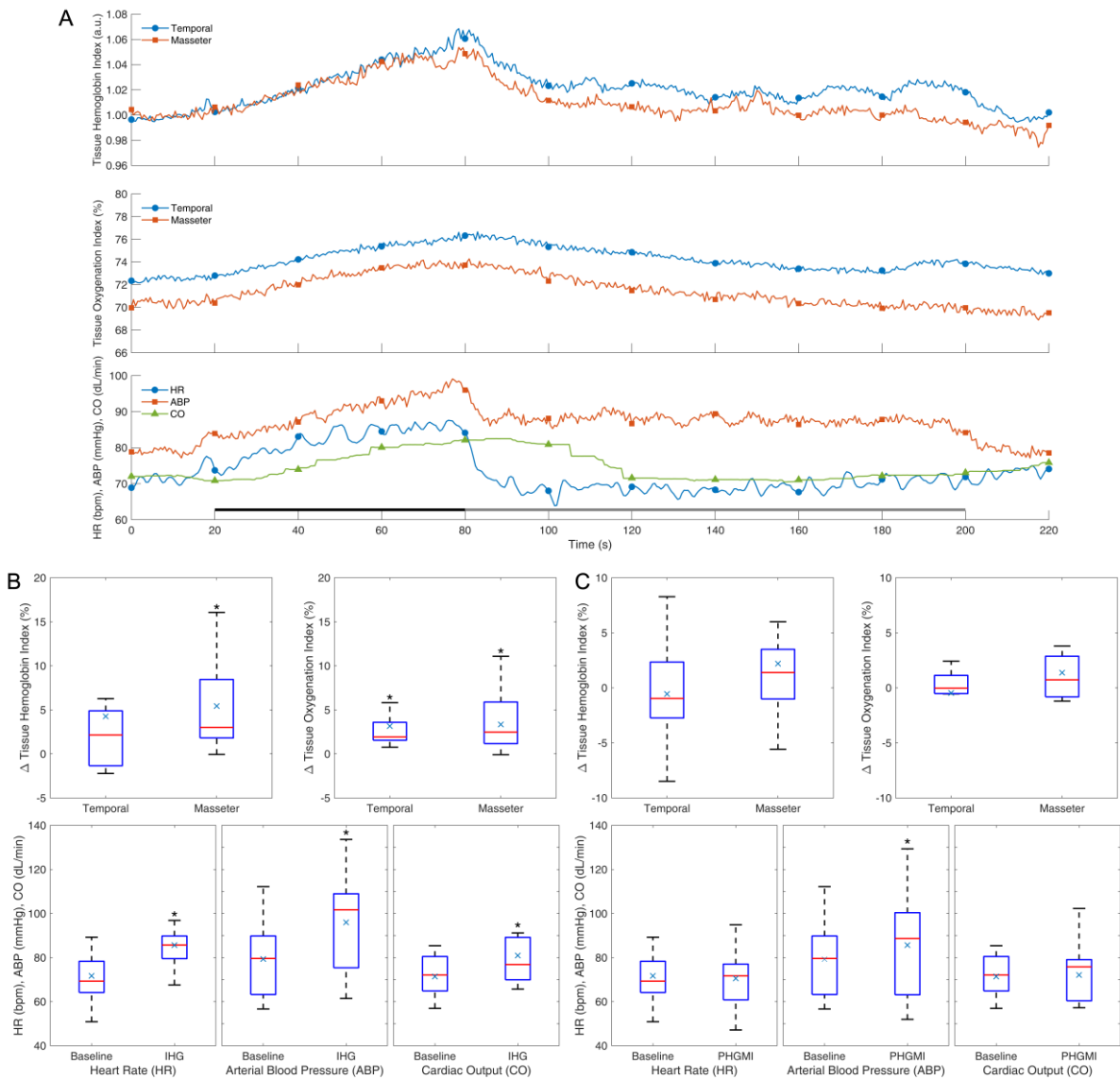
Isometric handgrip provoked a significant increase in arterial blood pressure (from  $79.8 \pm 18.0$  to  $96.4 \pm 21.8$  mmHg,  $p < 0.05$ ), heart rate (from  $72.1 \pm 11.1$  to  $86.1 \pm 11.5$  bpm,  $p < 0.05$ ) and cardiac output (from  $7.2 \pm 0.9$  to  $8.1 \pm 1.6$ ,  $p < 0.05$ ).

Tissue oxygenation increased in both temporal (from  $70.5 \pm 6.2$  to  $73.7 \pm 6.9$  %,  $p < 0.05$ ) and masseter (from  $72.5 \pm 6.1$  to  $76.0 \pm 5.6$  %,  $p < 0.05$ ) muscles, while THI increased only in masseter muscle ( $\Delta$ THI:  $0.06 \pm 0.05$  %,  $p < 0.05$ ). The observed TOI changes in the two muscles exhibited strong correlation ( $r = 0.78$ ), and poor correlation with  $\Delta$ ABP ( $r < 0.25$ ).

Compared to resting levels (before isometric handgrip), post-handgrip muscle ischemia exhibited a significant increase in arterial blood pressure (from  $79.8 \pm 18.0$  to  $86.1 \pm 22.4$  mmHg,  $p < 0.05$ ) while producing non-significant effects in heart rate (from  $72.1 \pm 11.1$  to  $71.0 \pm 13.0$  bpm) and cardiac output (from  $7.2 \pm 0.9$  to  $7.3 \pm 1.3$ ).

Also, near-infrared spectroscopy variables did not exhibit significant changes in temporal (TOI: from  $70.5 \pm 6.2$  to  $70.1 \pm 8.0$  %) and masseter (TOI: from  $72.5 \pm 6.1$  to  $74.0 \pm 6.8$  %) muscles. The observed TOI changes in the two muscles exhibited moderate correlation ( $r = 0.60$ ), and strong negative correlation with  $\Delta$ ABP ( $r < -0.7$ ).

Maximum pain score during post-handgrip muscle ischemia was:  $6.6 \pm 1.8$ .



**Figure 4.** Response to isometric handgrip (IHG) and post-handgrip muscle ischemia (PHGMI). Average response curves (A), distribution of effects of IHG (B), and PHGMI (C) for the different variables. Notations as in Fig. 1. The black and gray bars at the bottom indicate the duration of IHG and PHGMI, respectively. \*)  $p < 0.05$ ;  $n = 15$ .

## Discussion

The results described hemodynamic responses of temporalis and masseter muscles to different stressors, which effectively increased sympathetic activity, as indicated by the significant increase in arterial blood pressure in some cases accompanied by an increase in heart rate and cardiac output. In particular, tissue oxygenation significantly increased in both muscles during mental arithmetic test and isometric handgrip, accompanied by increased or unchanged blood volume which indicates increased muscle perfusion during these tests [18,21,22]. No significant changes were instead observed during cold pressor test, apnea, and post-handgrip muscle ischemia. However, none of the tested conditions provided evidence of

sympathetic-induced vasoconstriction. Both temporalis and masseter muscles consistently exhibited similar response patterns in all tested conditions.

It is well known that sympathetic activation may result in skin vasodilation in the facial area [23]. A number of NIRS studies also reported dilatory responses (increased oxygenation) in the masseter muscle in response to certain stress stimuli, e.g., cold pressor test [17], and mental calculation [24], although classical methodologies did not discriminate skin from muscle contribution [25]. This can be achieved by techniques such as spatially-resolved spectroscopy which effectively excludes contribution from the skin [26] and recently allowed us to prove that several types of stress result in specific dilatation of the masseter muscle, in contrast to limb muscles where marked vasoconstriction may take place [18,27].

The present results confirm this pattern. We are not emphasizing the dilatory responses observed during mental arithmetic test and isometric handgrip, as these are known to take place in limb muscles as well [18,28,29]. Unexpectedly, the significant TOI increase in response to cold pressor test and post-handgrip muscle ischemia previously observed for the masseter muscle [18] was no longer observed in the present study. While the absence of response to cold pressor test could be partly attributed to the milder stimulus intensity, in terms of water temperature (10 instead of 8 °C) and duration (1 instead of 2 min), the response to post-handgrip muscle ischemia has no apparent explanation except that the subject position was sitting instead of supine. Incidentally, both active and passive dilatory responses have found to be attenuated above as compared to below heart level [30–32]. It is possible that the unfavorable hydrostatic gradient affecting the head region or the increased sympathetic tone have attenuated the hyperemic response in the sitting position, compared to the supine. In fact, in human skeletal muscles, competing vascular actions are exerted by the dilatory action of circulating adrenaline and the constrictory action of the neurally released noradrenaline [33,34]. In this respect, it is interesting to observe that a poor positive correlation was observed between  $\Delta$ TOI and  $\Delta$ ABP in mental arithmetic test and isometric handgrip; while a strong negative correlation resulted in post-handgrip muscle ischemia. This observation fits with the concept of prevailing adrenaline secretion during mental arithmetic test and isometric handgrip [18,35,36] and prevailing noradrenaline constriction in post-handgrip muscle ischemia: the correlation is poor in the first case; whereby arterial blood pressure is largely mediated by the increase in cardiac output (significantly increased in these tests). On the contrary during post-handgrip muscle ischemia,  $\Delta$ ABP is mainly mediated by the increased vasoconstriction, being cardiac output unchanged or even decreased [18]. On this basis, it is plausible to speculate that the baroreflex-mediated increase in sympathetic vasoconstrictory tone, associated with the sitting position, has shifted the balance and attenuated the stress-related dilatory responses, compared to the supine position. Dedicated studies re-testing the responses to the same stressor in the same subjects in the two body postures may be designed to test this hypothesis.

Previous validation of NIRS measurement in the temporalis muscle evidenced that the placement of the NIRS probe could be critical in some subjects, probably due to the fact that the temporalis muscle becomes too thin and superficial under the hair-free area of the temple, in which case spatially-resolved spectroscopy measurements would not adequately sample

the muscle tissue, thus resulting in possible underestimation of the hemodynamic response. We cannot exclude that this could have happened also in the present study. In fact, we observed in a few subjects that changes in tissue oxygenation were considerably weaker than changes in oxygenated and deoxygenated hemoglobin.

Although simultaneous monitoring of a limb muscle was not performed in this study, a relevant outcome is that temporalis and masseter muscle exhibit consistently similar responses to the variety of employed stressors. In fact, this observation supports the hypothesis put forward in our previous study that muscle blood flow is differentially controlled in limb and head muscles. Previous studies investigating differences in blood flow control of lower and upper limb muscles evidenced stronger sympathetic constrictor effects in lower limbs [28,37], we speculate that the constrictory sympathetic action is modulated according to the hydrostatic gradients of the body with erect posture, i.e., the constrictory action is stronger where hydrostatic load and blood pressure are higher. Whether this effect is mediated by differences in sympathetic neural drive and/or differences in the density and distribution of adrenergic receptors subtypes remains to be investigated.

Therefore, head muscles appear to be similarly controlled by the autonomic nervous system under exposure to different types of stress and generally protected from stress-induced hypoperfusion. From a finalistic point of view, this could be meant to favor activity of jaw muscles, being frequently involved in aggressive/defensive behavior in different animal species. Protection from hypoperfusion may also be beneficial against the development of temporomandibular joint dysfunction [38–40]. It should however be noted that these considerations are based on average responses and that clear vasoconstrictive responses were occasionally observed in some subject, possibly depending on a different balance between beta- and alpha-adrenergic vascular control. Whether the susceptibility to temporomandibular joint disorders (such as myofascial orofacial pain and temporal headache) development depends on the individual hemodynamic responsiveness to stress needs to be ascertained.

### **Authors' Contributions**

Both authors contributed equally to this manuscript.

### **Acknowledgment**

A.R. was a recipient of a Doctoral Fellowship funded by Agenzia Italiana per la Cooperazione allo Sviluppo (Partnership for Knowledge), Ministero degli Affari Esteri e della Cooperazione Internazionale, Italy. We are grateful to Dr. Raffaele Pertusio for his technical assistance.

### **Data Availability Statement**

The data that support the findings are available from the corresponding author upon reasonable request.

## Conflict of Interest

The authors declare no competing interests.

## References

- [1] E.E. Benarroch, *Physiology and Pathophysiology of the Autonomic Nervous System, Continuum* (Minneapolis, Minn). 26 (2020) 12–24. <https://doi.org/10.1212/CON.0000000000000817>.
- [2] H. Izumi, Nervous Control of Blood Flow in the Orofacial Region, *Pharmacol. Ther.* 81 (1999) 141–161. [https://doi.org/10.1016/S0163-7258\(98\)00040-0](https://doi.org/10.1016/S0163-7258(98)00040-0).
- [3] H. Ishii, T. Niioka, H. Izumi, Parasympathetic Reflex Vasodilatation in the Masseter Muscle Compensates for Carotid Hypoperfusion During the Vagus-Mediated Depressor Response, *Brain Res.* 1370 (2011) 145–53. <https://doi.org/10.1016/j.brainres.2010.11.046>.
- [4] P.D. Drummond, J.W. Lance, Facial Flushing and Sweating Mediated by the Sympathetic Nervous System, *Brain.* 110 (1987) 793–803. <https://doi.org/10.1093/brain/110.3.793>.
- [5] D.A. Curtis, S.A. Gansky, O. Plesh, Deep and Superficial Masseter Muscle Blood Flow in Women, *J. Prosthodont.* 21 (2012) 472–477. <https://doi.org/10.1111/j.1532-849X.2012.00862.x>.
- [6] A. Dawson, B. Ghafouri, B. Gerdle, T. List, P. Svensson, M. Ernberg, Effects of Experimental Tooth Clenching on Pain and Intramuscular Release of 5-HT and Glutamate in Patients with Myofascial TMD, *Clin. J. Pain.* 31 (2015) 740–9. <https://doi.org/10.1097/AJP.0000000000000154>.
- [7] R.E. Delcanho, Y.J. Kim, G.T. Clark, Haemodynamic Changes Induced by Submaximal Isometric Contraction in Painful and Non-Painful Human Masseter Using Near-Infrared Spectroscopy, *Arch. Oral Biol.* 41 (1996) 585–596. [https://doi.org/10.1016/0003-9969\(96\)00009-X](https://doi.org/10.1016/0003-9969(96)00009-X).
- [8] G.D. Thomas, S.S. Segal, Neural Control of Muscle Blood Flow During Exercise, *J. Appl. Physiol.* 97 (2004) 731–738. <https://doi.org/10.1152/jappphysiol.00076.2004>.
- [9] S. Roatta, M. Mohammed, M. Passatore, Detecting Activation of the Sympatho-Adrenal Axis from Haemodynamic Recordings, in Conscious Rabbits Exposed to Acute Stress, *Acta Physiol.* 201 (2011) 323–37. <https://doi.org/10.1111/j.1748-1716.2010.02179.x>.
- [10] M. Koltzenburg, The Sympathetic Nervous System and Pain, in: D. A., B. JM. (Eds.), *Pharmacol. Pain (Handb. Exp. Pharmacol., Volume 130, Springer Verlag, Berlin, 1997: pp. 61–91*. [https://doi.org/10.1007/978-3-642-60777-6\\_4](https://doi.org/10.1007/978-3-642-60777-6_4).
- [11] W. Jänig, H.J. Häbler, Sympathetic Nervous System: Contribution to Chronic Pain, *Prog. Brain Res.* 129 (2000) 451–68. [https://doi.org/10.1016/s0079-6123\(00\)80003-5](https://doi.org/10.1016/s0079-6123(00)80003-5).
- [12] O. Hämmig, Work- and Stress-Related Musculoskeletal and Sleep Disorders Among Health Professionals: A Cross-Sectional Study in a Hospital Setting in Switzerland,



- BMC Musculoskelet. Disord. 21 (2020) 1–11. <https://doi.org/10.1186/s12891-020-03327-w>.
- [13] M. Melis, K. Zawawi, E. Al-Badawi, S.L. Lobo, N. Mehta, Complex Regional Pain Syndrome in the Head and Neck: A Review of the Literature, *J. Orofac. Pain.* 16 (2002) 93–104. <https://pubmed.ncbi.nlm.nih.gov/12043524/> (accessed May 3, 2023).
- [14] Y.J. Kim, T. Kuboki, Y. Tsukiyama, K. Koyano, G.T. Clark, Haemodynamic Changes in Human Masseter and Temporalis Muscles Induced by Different Levels of Isometric Contraction, *Arch. Oral Biol.* 44 (1999) 641–650. [https://doi.org/10.1016/S0003-9969\(99\)00059-X](https://doi.org/10.1016/S0003-9969(99)00059-X).
- [15] S. Ning, A. Taro, K. Masamitsu, T. Tomohiro, Y. Wataru, O. Noboru, S. Peter, Haemodynamic Reactions in Human Masseter Muscle During Different Types of Contractions, *Hokkaido J. Dent. Sci.* 36 (2016) 47–53. [https://eprints.lib.hokudai.ac.jp/journals/item.php?item=72245&handle=2115\\_60939&jname=318&vname=5683](https://eprints.lib.hokudai.ac.jp/journals/item.php?item=72245&handle=2115_60939&jname=318&vname=5683) (accessed December 6, 2022).
- [16] M. Langemark, K. Jensen, J. Olesen, Temporal Muscle Blood Flow in Chronic Tension-Type Headache, *Arch. Neurol.* 47 (1990) 654–658. <https://doi.org/10.1001/archneur.1990.00530060064020>.
- [17] K. Maekawa, T. Kuboki, G.T. Clark, M. Shinoda, A. Yamashita, Cold Pressor Stimulus Temperature and Resting Masseter Muscle Haemodynamics in Normal Humans, *Arch. Oral Biol.* 43 (1998) 849–859. [https://doi.org/10.1016/s0003-9969\(98\)00072-7](https://doi.org/10.1016/s0003-9969(98)00072-7).
- [18] A. Rashid, S. Roatta, Differential Control of Blood Flow in Masseter and Biceps Brachii Muscles During Stress, *Arch. Oral Biol.* 141 (2022) 1–10. <https://doi.org/10.1016/j.archoralbio.2022.105490>.
- [19] A. Rashid, S. Roatta, Hemodynamic Monitoring in the Human Temporalis Muscle Using Near-Infrared Spectroscopy, *Physiol. Meas.* 44 (2023) 1–10. <https://doi.org/10.1088/1361-6579/acd6d5>.
- [20] R. Pertusio, S. Roatta, 3D-Printed Encapsulation of Thin-Film Transducers for Reliable Force Measurement in Biomedical Applications, *Biomechanics.* 3 (2023) 115–123. <https://doi.org/10.3390/biomechanics3010011>.
- [21] R. Boushel, C.A. Piantadosi, Near-Infrared Spectroscopy for Monitoring Muscle Oxygenation, *Acta Physiol. Scand.* 168 (2000) 615–22. <https://doi.org/10.1046/j.1365-201x.2000.00713.x>.
- [22] P.J. Fadel, D.M. Keller, H. Watanabe, P.B. Raven, G.D. Thomas, Noninvasive Assessment of Sympathetic Vasoconstriction in Human and Rodent Skeletal Muscle Using Near-Infrared Spectroscopy and Doppler Ultrasound, *J. Appl. Physiol.* 96 (2004) 1323–1330. <https://doi.org/10.1152/japplphysiol.01041.2003>.
- [23] O. Vassend, S. Knardahl, Personality, Affective Response, and Facial Blood Flow During Brief Cognitive Tasks, *Int. J. Psychophysiol.* 55 (2005) 265–278. <https://doi.org/10.1016/j.ijpsycho.2004.08.005>.
- [24] O. Hidaka, M. Yanagi, K. Takada, Changes in Masseteric Hemodynamics Time-

- Related to Mental Stress, *J. Dent. Res.* 83 (2004) 185–190. <https://doi.org/10.1177/154405910408300220>.
- [25] B. Grassi, V. Quaresima, Near-Infrared Spectroscopy and Skeletal Muscle Oxidative Function In Vivo in Health and Disease: A Review from an Exercise Physiology Perspective, *J. Biomed. Opt.* 21 (2016) 091313–20. <https://doi.org/10.1117/1.JBO.21.9.091313>.
- [26] A. Messere, S. Roatta, Influence of Cutaneous and Muscular Circulation on Spatially Resolved Versus Standard Beer-Lambert Near-Infrared Spectroscopy, *Physiol. Rep.* 1 (2013) 1–10. <https://doi.org/10.1002/phy2.179>.
- [27] D.W. Wray, A.J. Donato, S.K. Nishiyama, R.S. Richardson, Acute Sympathetic Vasoconstriction at Rest and During Dynamic Exercise in Cyclists and Sedentary Humans, *J. Appl. Physiol.* 102 (2007) 704–712. <https://doi.org/10.1152/jappphysiol.00984.2006>.
- [28] N.J. Rusch, J.T. Shepherd, R.C. Webb, P.M. Vanhoutte, Different Behavior of the Resistance Vessels of the Human Calf and Forearm During Contralateral Isometric Exercise, Mental Stress, and Abnormal Respiratory Movements, *Circ. Res.* 48 (1981) 1118–30. <https://pubmed.ncbi.nlm.nih.gov/7226455/> (accessed October 18, 2021).
- [29] J.R. Carter, W.H. Cooke, C.A. Ray, Forearm Neurovascular Responses During Mental Stress and Vestibular Activation, *Am. J. Physiol. - Hear. Circ. Physiol.* 288 (2005) H904–7. <https://doi.org/10.1152/ajpheart.00569.2004>.
- [30] J.D. Trinity, J. McDaniel, M. Venturelli, A.S. Fjeldstad, S.J. Ives, M.A.H. Witman, Z. Barrett-O’Keefe, M. Amann, D. Walter Wray, R.S. Richardson, Impact of Body Position on Central and Peripheral Hemodynamic Contributions to Movement-Induced Hyperemia: Implications for Rehabilitative Medicine, *Am. J. Physiol. - Hear. Circ. Physiol.* 300 (2011) H1885–H1891. <https://doi.org/10.1152/ajpheart.00038.2011>.
- [31] J.L. Jasperse, J.K. Shoemaker, E.J. Gray, P.S. Clifford, Positional Differences in Reactive Hyperemia Provide Insight into Initial Phase of Exercise Hyperemia, *J. Appl. Physiol.* 119 (2015) 569–575. <https://doi.org/10.1152/jappphysiol.01253.2013>.
- [32] S. Seddone, A. Messere, S. Roatta, Vascular Reactivity of Cutaneous Circulation to Brief Compressive Stimuli, in the Human Forearm, *Eur. J. Appl. Physiol.* 120 (2020) 1041–1050. <https://doi.org/10.1007/s00421-020-04343-3>.
- [33] P. Montoya, S. Brody, K. Beck, R. Veit, H. Rau, Differential beta- and alpha-Adrenergic Activation During Psychological Stress, *Eur. J. Appl. Physiol. Occup. Physiol.* 75 (1997) 256–62. <https://doi.org/10.1007/s004210050157>.
- [34] Y. Terakawa, T. Ichinohe, Large-Dose Epinephrine Reduces Skeletal Muscle Blood Flow Under General Anesthesia in Rabbits, *Anesth. Prog.* 59 (2012) 118–122. <https://doi.org/10.2344/12-00006.1>.
- [35] A.D. Goldberg, L.C. Becker, R. Bonsall, J.D. Cohen, M.W. Ketterer, P.G. Kaufman, D.S. Krantz, K.C. Light, R.P. McMahan, T. Noreuil, C.J. Pepine, J. Raczynski, P.H. Stone, R.N. Dawn Strother, H. Taylor, D.S. Sheps, Ischemic, Hemodynamic, and Neurohormonal Responses to Mental and Exercise Stress: Experience from the Psychophysiological Investigations of Myocardial Ischemia study (PIMI), *Circulation*.

- 94 (1996) 2402–9. <https://doi.org/10.1161/01.cir.94.10.2402>.
- [36] M.J. Joyner, N.M. Dietz, Sympathetic Vasodilation in Human Muscle, *Acta Physiol. Scand.* 177 (2003) 329–36. <https://doi.org/10.1046/j.1365-201X.2003.01090.x>.
- [37] B. Eklund, L. Kaijser, Effect of Regional alpha- and beta-Adrenergic Blockade on Blood Flow in the Resting Forearm During Contralateral Isometric Handgrip, *J. Physiol.* 262 (1976) 39–50. <https://doi.org/10.1113/jphysiol.1976.sp011584>.
- [38] R.E. Delcanho, Masticatory Muscle Pain: A Review of Clinical Features, Research Findings and Possible Mechanisms, *Aust. Prosthodont. J.* 9 (1995) 49–59. <https://pubmed.ncbi.nlm.nih.gov/9063135/> (accessed April 2, 2023).
- [39] K. Maekawa, G.T. Clark, T. Kuboki, Intramuscular Hypoperfusion, Adrenergic Receptors, and Chronic Muscle Pain, *J. Pain.* 3 (2002) 251–60. <https://doi.org/10.1054/jpai.2002.125923>.
- [40] F.G. Exposto, N. Renner, K.H. Bendixen, P. Svensson, Pain in the Temple? Headache, Muscle Pain or Both: A Retrospective Analysis, *Cephalalgia.* 41 (2021) 1486–1491. <https://doi.org/10.1177/03331024211029234>.

## **DISCUSSION**

In the present thesis several investigations were carried out for the assessment of vascular reactivity to detect the peculiar characteristics and differences among individual organs and subject groups. Particularly, I focused on the cerebral and muscular control of blood flow in healthy humans. Here, the results are summarized and discussed separately for the two main topics.

### **A. Cerebrovascular Reactivity in Hypnotizable vs. Non-Hypnotizable Subjects**

First time, hypnotizability-related differences in the mechanisms controlling cerebral blood flow, cerebrovascular reactivity, and conductance during chemical (partial pressure of end-tidal carbon dioxide), mechanical (arterial blood pressure), cognitive and sensory stimulations were revealed in med-low and med-high hypnotizable healthy subjects [88,90,91].

The results showed that hypnotizability affected the correlations among the changes occurring during hyperventilation, rebreathing, mental computation, and trail making tasks with respect to basal conditions ( $\Delta$ ) in partial pressure of end-tidal carbon dioxide and arterial blood pressure with middle cerebral artery flow velocity [88]. During hyperventilation, med-lows exhibited a significant correlation between changes in middle cerebral artery flow velocity and changes in partial pressure of end-tidal carbon dioxide. While med-highs showed a significant correlation between changes in arterial blood pressure and changes in middle cerebral artery flow velocity [88]. The decrease in middle cerebral artery flow velocity observed during hyperventilation, despite scarce changes in arterial blood pressure, could be sustained by more sensitivity of their vessel muscle cells to blood pressure. The effect of nitric oxide on

precapillary sphincters and pericytes [115] may have contributed to the observed changes in middle cerebral artery flow velocity. These observations suggested that more frequent increases in systemic blood pressure are likely to occur in highs than in lows owing to their greater emotional intensity, empathy [106,116], and interoceptive sensitivity [117]. In addition, changes in synaptic glutamate due to tasks could induce increases in astrocyte calcium-mediated dilatory action independently from systemic blood pressure [118]. Since highs respond to cognitive tasks with larger glutamatergic cortical activity [86], they might be more prone than lows to undergo astrocyte-dependent nitric oxide release in everyday life.

During rebreathing, the lack of significant correlation between changes in middle cerebral artery flow velocity and changes in partial pressure of end-tidal carbon dioxide occurring in both groups may be due to the ceiling effect of carbon dioxide [88].

Moreover, cerebrovascular reactivity and conductance were also assessed and showed a significant correlation with changes in middle cerebral artery flow velocity only in med-lows during both hyperventilation and rebreathing. The findings support the view that hypnotizability is associated with the physiological correlates influencing everyday life independently from suggestions and induction of the hypnotic state [83,119].

Both mental computation and trail making tasks were differentially processed by med-lows and med-highs. Only med-highs exhibited evidence of functional hyperemia (increase in tissue oxygenation index, possibly accompanied by an increase in blood volume) and seem more responsive than med-lows to specific cognitive demands [90]. Again, this could be due to larger synaptic glutamate release, which increases the

astrocytes' calcium-mediated dilatory actions through the large release of nitric oxide [120,121].

During visual stimulation, blood flow velocity in the posterior cerebral artery increases in med-highs and med-lows, but these findings do not reveal hypnotizability-related differences between med-lows' and med-highs' stimulation-related hyperemia [91]. The low metabolic cost of tasks in highs was hypothesized owing to their mode of information processing which consists of poor local modulation of the electroencephalographic activity [108]. Moreover, the neurovascular coupling during cognitive tasks differs between med-lows and med-highs [90]. The unexpected absence of difference during visual stimulation can be related to the characteristics of the stimulus, although the low effect size of the comparisons between groups may have prevented the detection of significant hypnotizability-related differences [91].

To conclude, the above investigations help to understand the control of cerebral circulation in healthy subjects with different hypnotizability scores.

## **B. Vascular Reactivity to Stress in Masticatory and Limb Muscles**

For the first time, to our knowledge, the study focused on the differential control of blood flow in the head and limb muscles during stress. We hypothesized that autonomic vascular control could be differentiated to these body areas, also depending on the type of stress [78]. The results evidenced that: 1) all tests (cold-pressor, mental arithmetic, isometric handgrip, and post-handgrip muscle ischemia) effectively activated the sympathetic nervous system as revealed by significant increases in arterial blood pressure and/or heart rate, except apnea; 2) the masseter muscle tissue oxygenation index increased in all tests (although, non-significantly in apnea); 3) the biceps muscle tissue oxygenation index exhibited both increases (in isometric

handgrip) and marked decrease (in cold pressor test and post-handgrip muscle ischemia) depending on the stressor; and 5) tissue hemoglobin index changes were always concordant with tissue oxygenation index's, although generally less significant [78]. These observations support the hypothesis that sympathetic outflow to skeletal muscles of the head and limbs is differentially controlled in a stressor-dependent way [78].

After this publication, I was interested to extend the previous research using near-infrared spectroscopy on another head muscle i.e., temporalis. There was no specific methodology to study the temporalis muscle hemodynamics without the possible interference of cerebral hemodynamics. Therefore, the use of near-infrared spectroscopy for hemodynamic monitoring of the temporalis muscle was tested during isometric muscle contractions (teeth clenching) and hyperventilation. Different levels of muscle contraction produced a marked and progressive decrease in tissue oxygenation (decrease in tissue oxygenation index and oxygenated hemoglobin and increase in deoxygenated hemoglobin) and blood volume (tissue hemoglobin index) in a force-level dependent way. In addition, near-infrared spectroscopy variables were not affected by hyperventilation, which is known to provoke marked vasoconstriction and a decrease in oxygenation of cerebral tissue. Conversely, near-infrared spectroscopy monitoring from the forehead correctly detected a consistent tissue oxygenation index decrease during hyperventilation and no changes during teeth clenching. These results demonstrate that near-infrared spectroscopy monitoring can be used to reliably detect hemodynamic changes in the temporalis muscle, with no interference from changes in cerebral blood flow [122].

After demonstrating the reliability of near-infrared spectroscopy monitoring of the temporalis muscle, I could test the hemodynamic stress response in this muscle in

order to verify whether the pattern of response observed in the masseter muscle was shared by other head muscles. Therefore, the last study investigated the hemodynamic changes associated with the masseter and temporalis muscles during different stress conditions. The stressors (cold pressor, mental arithmetic, apnea, isometric handgrip, and post-handgrip muscle ischemia) effectively increased sympathetic activity, as indicated by the significant increase in arterial blood pressure. Moreover, temporal and masseter muscles exhibited a similar pattern of response in terms of near-infrared spectroscopy parameters (i.e., tissue oxygenation and hemoglobin indices), with no statistically significant differences. In particular, both muscles exhibited generally dilatory responses or the absence of vasoconstriction in all tested conditions, as indicated by increased tissue oxygenation and blood volume. Though, this present study is not aimed to unveil the physiological underlying mechanisms. The results on the masseter muscle are compatible with the ones previously reported [78] except for weaker effects during the cold pressor test, possibly due to warmer water (10 °C as compared to 8 °C). The results confirm the absence of vasoconstriction in both muscles, suggesting that this pattern of response is likely a unique characteristic of head muscles. It is worth mentioning that the absence of vasoconstriction is now observed in the erect position, while in the previous study, subjects were supine [78].

To conclude, the above investigations evidence a relevant difference in the neural control of muscle blood flow between head and limb muscles which adds to other known specificities of head muscle and may help to better understand the role of the sympathetic nervous system in the pathophysiology of stress-related musculoskeletal disorders.

### **C. Additional Research**

In addition to the above-discussed work, I contributed to **Papers VII to XIV** which are briefly summarized here. The research reported in **Paper VII** is related to the neural control of muscle



and was motivated by the fact that exercise augments hypoxia-induced ventilatory response in an exercise intensity-dependent manner [123]. A mutual influence of hypoxia-induced peripheral chemoreflex activation and exercise-induced muscle metaboreflex activation might mediate the augmentation phenomenon [124]. However, the nature of the integration of these reflexes remains unclear because some studies did not calculate the summed effect of reflex activation. These reflexes coactivation during isocapnic static handgrip exercise appeared to elicit a hyperadditive effect with regard to ventilation and an additive effect with regard to breathing-related sensations and emotions. These findings reveal the nature of the integration between two neural mechanisms that operate during small-muscle static exercise performed under hypoxia [125].

The research reported in **Paper VIII** is related to cerebral circulation and was motivated by the fact that impaired outflow of blood through the internal jugular veins can contribute to several neurodegenerative and neuroinflammatory disorders [126]. Currently, it is suspected that these neurological pathologies are associated with abnormal functioning of the astroglial-mediated interstitial fluid bulk flow (the so-called *glymphatic system*) [127]. The activation of the glymphatic system primarily depends on a temporary decrease of the cortical blood flow followed by a wave of inflow of the cerebrospinal fluid from the spinal canal to the cranial cavity [128]. Based on the results of flow simulations, *Simka et al.* suggested that strictures located at the level of the jugular foramen are probably more clinically relevant than pathological jugular valves [129]. Therefore, this *in silico* study is the continuation of previous work to understand the influence of stenoses located at the beginning of the internal jugular vein on the flow through this vein and the functioning of the jugular valve located downstream [130]. Simultaneously, I have the curiosity to contribute to the area of pharmaceutical sciences, particularly, analytical method development and validation, which involves the process of creating and testing new analytical techniques to accurately quantify active pharmaceutical

ingredients and drug products. Therefore, in accordance with Food and Drug Administration, and International Council for Harmonization guidelines [131–133], **Papers IX to XII** are oriented to develop and validate novel eco-friendly analytical separation methods based on capillary electrophoresis and high-performance liquid chromatography for simultaneous quantification of hypocholesterolemic (ezetimibe and simvastatin) [134], antihypertensive (hydrochlorothiazide and metoprolol tartrate), and antipsychotic (aripiprazole and risperidone) [135] drugs in pharmaceutical combined tablet dosage form. Further, **Papers XIII and XIV** are oriented to analyze the chemical constituents from plants (*Brachyotum naudinii* Triana and *Polypodium leucotomos*) [136] based on the above-mentioned analytical separation techniques.

## **PERSPECTIVE AND CONCLUDING REMARKS**

Relative to healthy controls, previous investigations pointed out that vascular reactivity declines with age and evidenced possible implications in the pathophysiology of vascular diseases such as hypertension and diabetes. Therefore, it is a valuable tool for assessing vascular health and a promising biomarker of hemodynamic impairment. Appropriate clinical vascular reactivity tests may facilitate early disease detection and thus contribute to the prevention and reduction of the associated risks. In addition, future research could target methodological consensus recommendations to facilitate more reliable and harmonized vascular reactivity measurement for use in clinical research and trials of new therapies.

The present doctoral thesis added new insights into the control of cerebral and muscular blood flow using two noninvasive hemodynamic imaging techniques (transcranial Doppler ultrasound and near-infrared spectroscopy) in healthy humans. These hemodynamic techniques proved effective to detect significant group differences. New techniques such as functional near-infrared spectroscopy, functional ultrasound, and functional magnetic resonance imaging may provide further insights, particularly for the investigation of cerebral hemodynamics due to increasing time and spatial resolution. Hopefully, the research reported in this thesis will serve to promote basic and clinical investigations on brain and muscle hemodynamics in physiological and pathological conditions.

## REFERENCES

- [1] Goodwill, A. G., Dick, G. M., Kiel, A. M., Tune, J. D., Regulation of Coronary Blood Flow. *Compr. Physiol.* 2017, 7, 321–382.
- [2] Secomb, T. W., Theoretical Models for Regulation of Blood Flow. *Microcirculation* 2008, 15, 765–775.
- [3] Sarelius, I., Pohl, U., Control of Muscle Blood Flow During Exercise: Local Factors and Integrative Mechanisms. *Acta Physiol.* 2010, 199, 349–365.
- [4] Bayliss, W. M., On the Local Reactions of the Arterial Wall to Changes of Internal Pressure. *J. Physiol.* 1902, 28, 220–231.
- [5] Mellander, S., Functional Aspects of Myogenic Vascular Control. *J. Hypertens. Suppl.* 1989, 7, S21-31.
- [6] Osol, G., Brekke, J. F., McElroy-Yaggy, K., Gokina, N. I., Myogenic Tone, Reactivity, and Forced Dilatation: A Three-Phase Model of *In Vitro* Arterial Myogenic Behavior. *Am. J. Physiol. Heart Circ. Physiol.* 2002, 283, H2260-7.
- [7] Schubert, R., Lidington, D., Bolz, S. S., The Emerging Role of Ca<sup>2+</sup> Sensitivity Regulation in Promoting Myogenic Vasoconstriction. *Cardiovasc. Res.* 2008, 77, 8–18.
- [8] Johnson, P. C., The Myogenic Response in the Microcirculation and Its Interaction with Other Control Systems. *J. Hypertens. Suppl.* 1989, 7, S33-40.
- [9] Welsh, D. G., Morielli, A. D., Nelson, M. T., Brayden, J. E., Transient Receptor Potential Channels Regulate Myogenic Tone of Resistance Arteries. *Circ. Res.* 2002, 90, 248–50.
- [10] Cipolla, M. J., in: Granger, D. N., Granger, J. (Eds.), Colloquium Series on Integrated Systems Physiology: From Molecule to Function to Disease. Morgan & Claypool

- Publishers LLC, California 2016, pp. 1–69.
- [11] Clark, K., Middelbeek, J., van Leeuwen, F. N., Interplay Between TRP Channels and the Cytoskeleton in Health and Disease. *Eur. J. Cell Biol.* 2008, 87, 631–40.
- [12] Korthuis, R. J., in: Granger, D. N., Granger, J. P. (Eds.), Colloquium Series on Integrated Systems Physiology: From Molecule to Function to Disease. Morgan & Claypool Publishers LLC, California 2011, p. 144.
- [13] Bagher, P., Segal, S. S., Regulation of Blood Flow in the Microcirculation: Role of Conducted Vasodilation. *Acta Physiol.* 2011, 202, 271–84.
- [14] Kjeldsen, K. P., Schmidt, T. A., Potassium Homeostasis and Pathophysiology of Hyperkalaemia. *Eur. Hear. J. Suppl.* 2019, 21, A2–A5.
- [15] Eckman, D. M., Nelson, M. T., Potassium Ions as Vasodilators: Role of Inward Rectifier Potassium Channels. *Circ. Res.* 2001, 88, 132–133.
- [16] Haddy, F. J., Vanhoutte, P. M., Feletou, M., Role of Potassium in Regulating Blood Flow and Blood Pressure. *Am. J. Physiol. - Regul. Integr. Comp. Physiol.* 2006, 290, R546–R552.
- [17] Shim, C. Y., Kim, S., Chadderdon, S., Wu, M., Qi, Y., Xie, A., Alkayed, N. J., Davidson, B. P., Lindner, J. R., Epoxyeicosatrienoic Acids Mediate Insulin-Mediated Augmentation in Skeletal Muscle Perfusion and Blood Volume. *Am. J. Physiol. - Endocrinol. Metab.* 2014, 307, E1097–E1104.
- [18] Sandoo, A., Zanten, J. J. C. . V. van, Metsios, G. S., Carroll, D., Kitas, G. D., The Endothelium and Its Role in Regulating Vascular Tone. *Open Cardiovasc. Med. J.* 2010, 4, 302.
- [19] Thengchaisri, N., Kuo, L., Hydrogen Peroxide Induces Endothelium-Dependent and -

- Independent Coronary Arteriolar Dilation: Role of Cyclooxygenase and Potassium Channels. *Am. J. Physiol. Heart Circ. Physiol.* 2003, 285, H2255–H2263.
- [20] Félétou, M., Vanhoutte, P. M., Endothelium-Derived Hyperpolarizing Factor: Where Are We Now? *Arterioscler. Thromb. Vasc. Biol.* 2006, 26, 1215–25.
- [21] Kitazono, T., Faraci, F. M., Taguchi, H., Heistad, D. D., Role of Potassium Channels in Cerebral Blood Vessels. *Stroke* 1995, 26, 1713–1723.
- [22] Wahl, M., Schilling, L., Regulation of Cerebral Blood Flow – A Brief Review. *Acta Neurochir. Suppl. (Wien)*. 1993, 59, 3–10.
- [23] Dawson, J. M., Hudlicka, O., Changes in the Microcirculation in Slow and Fast Skeletal Muscles with Long Term Limitations of Blood Supply. *Cardiovasc. Res.* 1990, 24, 390–395.
- [24] Bor-Seng-Shu, E., Kita, W. S., Figueiredo, E. G., Paiva, W. S., Fonoff, E. T., Teixeira, M. J., Panerai, R. B., Cerebral Hemodynamics: Concepts of Clinical Importance. *Arq. Neuropsiquiatr.* 2012, 70, 357–365.
- [25] Thomas, G. D., Neural Control of the Circulation. *Adv. Physiol. Educ.* 2011, 35, 28–32.
- [26] Fadel, P. J., Neural Control of the Circulation During Exercise in Health and Disease. *Front. Physiol.* 2013, 4, 1–2.
- [27] Wang, S. Y., Iida, H., Ohata, H., Iida, M., Watanabe, Y., Dohi, S., Vasoconstrictive versus Vasodilatory Effects of Alpha-2 Adrenergic Agonists on the Spinal Microcirculation. *Anesthesiology* 2000, 92, 1488–1489.
- [28] Dinunno, F. A., Joyner, M. J., Alpha-Adrenergic Control of Skeletal Muscle Circulation at Rest and During Exercise in Aging Humans. *Microcirculation* 2006, 13, 329–41.
- [29] Raven, P. B., Recent Advances in Baroreflex Control of Blood Pressure During Exercise

- in Humans: An Overview. *Med. Sci. Sports Exerc.* 2008, 40, 2033–2036.
- [30] Sofroniew, M. V., Vinters, H. V., Astrocytes: Biology and Pathology. *Acta Neuropathol.* 2010, 119, 7–35.
- [31] Macvicar, B. A., Newman, E. A., Astrocyte Regulation of Blood Flow in the Brain. *Cold Spring Harb. Perspect. Biol.* 2015, 7, 1–15.
- [32] Howarth, C., The Contribution of Astrocytes to the Regulation of Cerebral Blood Flow. *Front. Neurosci.* 2014, 8, 1–9.
- [33] Paulson, O. B., Newman, E. A., Does the Release of Potassium from Astrocyte Endfeet Regulate Cerebral Blood Flow? *Science.* 1987, 237, 896–898.
- [34] Ross, S. A., Domínguez, S., Nigam, N., Wakeling, J. M., The Energy of Muscle Contraction. III. Kinetic Energy During Cyclic Contractions. *Front. Physiol.* 2021, 12, 1–16.
- [35] Kirby, B. S., Carlson, R. E., Markwald, R. R., Voyles, W. F., Dinunno, F. A., Mechanical Influences on Skeletal Muscle Vascular Tone in Humans: Insight into Contraction-Induced Rapid Vasodilatation. *J. Physiol.* 2007, 583, 861–874.
- [36] Laughlin, M. H., Skeletal Muscle Blood Flow Capacity: Role of Muscle Pump in Exercise Hyperemia. *Am. J. Physiol.* 1987, 253, H993-1004.
- [37] Jasperse, J. L., Shoemaker, J. K., Gray, E. J., Clifford, P. S., Positional Differences in Reactive Hyperemia Provide Insight into Initial Phase of Exercise Hyperemia. *J. Appl. Physiol.* 2015, 119, 569–575.
- [38] Tschakovsky, M. E., Sheriff, D. D., Immediate Exercise Hyperemia: Contributions of the Muscle Pump vs. Rapid Vasodilation. *J. Appl. Physiol.* 2004, 97, 739–747.
- [39] Clifford, P. S., Kluess, H. A., Hamann, J. J., Buckwalter, J. B., Jasperse, J. L.,

- Mechanical Compression Elicits Vasodilatation in Rat Skeletal Muscle Feed Arteries. *J. Physiol.* 2006, 572, 561–567.
- [40] Turturici, M., Mohammed, M., Roatta, S., Evidence that the Contraction-Induced Rapid Hyperemia in Rabbit Masseter Muscle is Based on a Mechanosensitive Mechanism, Not Shared by Cutaneous Vascular Beds. *J. Appl. Physiol.* 2012, 113, 524–31.
- [41] Messere, A., Turturici, M., Millo, G., Roatta, S., Repetitive Muscle Compression Reduces Vascular Mechano-Sensitivity and the Hyperemic Response to Muscle Contraction. *J. Physiol. Pharmacol.* 2017, 68, 427–437.
- [42] Chen, Y. L., Wolin, M. S., Messina, E. J., Evidence for cGMP Mediation of Skeletal Muscle Arteriolar Dilation to Lactate. *J. Appl. Physiol.* 1996, 81, 349–54.
- [43] Moriyama, S., Ichinose, M., Dobashi, K., Matsutake, R., Sakamoto, M., Fujii, N., Nishiyasu, T., Hypercapnia Elicits Differential Vascular and Blood Flow Responses in the Cerebral Circulation and Active Skeletal Muscles in Exercising Humans. *Physiol. Rep.* 2022, 10, 1–12.
- [44] Rivers, R. J., Meininger, C. J., The Tissue Response to Hypoxia: How Therapeutic Carbon Dioxide Moves the Response toward Homeostasis and Away from Instability. *Int. J. Mol. Sci.* 2023, 24, 5181.
- [45] Ainslie, P. N., Duffin, J., Integration of Cerebrovascular CO<sub>2</sub> Reactivity and Chemoreflex Control of Breathing: Mechanisms of Regulation, Measurement, and Interpretation. *Am. J. Physiol. - Regul. Integr. Comp. Physiol.* 2009, 296, R1473–R1495.
- [46] Kety, S. S., Schmidt, C. F., The Effects of Altered Arterial Tensions of Carbon Dioxide and Oxygen on Cerebral Blood Flow and Cerebral Oxygen Consumption of Normal Young Men. *J. Clin. Invest.* 1948, 27, 484–92.
- [47] Reivich, M., Arterial PCO<sub>2</sub> and Cerebral Hemodynamics. *Am. J. Physiol.* 1964, 206, 25–



35.

- [48] Kontos, H. A., Raper, J. A., Patterson, J. L., Analysis of Vasoactivity of Local pH, PCO<sub>2</sub> and Bicarbonate on Pial Vessels. *Stroke* 1977, 8, 358–60.
- [49] Masamoto, K., Tanishita, K., Oxygen Transport in Brain Tissue. *J. Biomech. Eng.* 2009, 131, 1–6.
- [50] Taguchi, H., Heistad, D. D., Kitazono, T., Faraci, F. M., ATP-Sensitive K<sup>+</sup> Channels Mediate Dilatation of Cerebral Arterioles During Hypoxia. *Circ. Res.* 1994, 74, 1005–8.
- [51] Boero, J. A., Ascher, J., Arregui, A., Rovainen, C., Woolsey, T. A., Increased Brain Capillaries in Chronic Hypoxia. *J. Appl. Physiol.* 1999, 86, 1211–9.
- [52] Xu, K., LaManna, J. C., Chronic Hypoxia and the Cerebral Circulation. *J. Appl. Physiol.* 2006, 100, 725–30.
- [53] Johnston, A. J., Steiner, L. A., Gupta, A. K., Menon, D. K., Cerebral Oxygen Vasoreactivity and Cerebral Tissue Oxygen Reactivity. *Br. J. Anaesth.* 2003, 90, 774–86.
- [54] Faraci, F. M., Heistad, D. D., Regulation of Large Cerebral Arteries and Cerebral Microvascular Pressure. *Circ. Res.* 1990, 66, 8–17.
- [55] Nurkiewicz, T. R., Frisbee, J. C., Boegehold, M. A., in: McQueen, C. A. (Ed.), *Comprehensive Toxicology*. Elsevier, Amsterdam 2010, pp. 133–148.
- [56] Rudziński, W., Swiat, M., Tomaszewski, M., Krejza, J., Cerebral Hemodynamics and Investigations of Cerebral Blood Flow Regulation. *Nucl. Med. Rev.* 2007, 10, 29–42.
- [57] Pan, Y., Wan, W., Xiang, M., Guan, Y., Transcranial Doppler Ultrasonography as a Diagnostic Tool for Cerebrovascular Disorders. *Front. Hum. Neurosci.* 2022, 16, 1–11.
- [58] Naqvi, J., Yap, K. H., Ahmad, G., Ghosh, J., Transcranial Doppler Ultrasound: A Review of the Physical Principles and Major Applications in Critical Care. *Int. J. Vasc.*

- Med.* 2013, 2013, 1–13.
- [59] Benjamin, A., Zubajlo, R. E., Dhyani, M., Samir, A. E., Thomenius, K. E., Grajo, J. R., Anthony, B. W., A Novel Approach to the Quantification of the Longitudinal Speed of Sound and its Potential for Tissue Characterization (Part – I). *Ultrasound Med. Biol.* 2018, 44, 2739–2748.
- [60] Lovett, M. E., O’Brien, N. F., Transcranial Doppler Ultrasound, A Review for the Pediatric Intensivist. *Children* 2022, 9, 1–12.
- [61] D’Andrea, A., Conte, M., Scarafile, R., Riegler, L., Cocchia, R., Pezzullo, E., Cavallaro, M., Carbone, A., Natale, F., Russo, M. G., Gregorio, G., Calabrò, R., Transcranial Doppler Ultrasound: Physical Principles and Principal Applications in Neurocritical Care Unit. *J. Cardiovasc. Echogr.* 2016, 26, 28–41.
- [62] Brass, L. M., Pavlakis, S. G., Devivo, D., Piomelli, S., Mohr, J. P., Transcranial Doppler Measurements of the Middle Cerebral Artery: Effect of Hematocrit. *Stroke* 1988, 19, 1466–1469.
- [63] Purkayastha, S., Sorond, F., Transcranial Doppler Ultrasound: Technique and Application. *Semin. Neurol.* 2012, 32, 411–420.
- [64] Miller, K. B., Howery, A. J., Harvey, R. E., Eldridge, M. W., Barnes, J. N., Cerebrovascular Reactivity and Central Arterial Stiffness in Habitually Exercising Healthy Adults. *Front. Physiol.* 2018, 9, 1–9.
- [65] Clark, L. R., Nation, D. A., Wierenga, C. E., Bangen, K. J., Dev, S. I., Shin, D. D., Delano-Wood, L., Liu, T. T., Rissman, R. A., Bondi, M. W., Elevated Cerebrovascular Resistance Index is Associated with Cognitive Dysfunction in the Very-Old. *Alzheimers. Res. Ther.* 2015, 7, 1–9.
- [66] Yew, B., Nation, D. A., Initiative, for the A. D. N., Cerebrovascular Resistance: Effects

- on Cognitive Decline, Cortical Atrophy, and Progression to Dementia. *Brain* 2017, 140, 1987–2001.
- [67] Jöbsis, F. F., Noninvasive, Infrared Monitoring of Cerebral and Myocardial Oxygen Sufficiency and Circulatory Parameters. *Science*. 1977, 198, 1264–7.
- [68] Hamaoka, T., McCully, K. K., Niwayama, M., Chance, B., The Use of Muscle Near-Infrared Spectroscopy in Sport, Health and Medical Sciences: Recent Developments. *Philos. Trans. R. Soc. A Math. Phys. Eng. Sci.* 2011, 369, 4591–4604.
- [69] Grassi, B., Quaresima, V., Near-Infrared Spectroscopy and Skeletal Muscle Oxidative Function *In Vivo* in Health and Disease: A Review from an Exercise Physiology Perspective. *J. Biomed. Opt.* 2016, 21, 0913131–20.
- [70] Madsen, P. L., Secher, N. H., Near-Infrared Oximetry of the Brain. *Prog. Neurobiol.* 1999, 58, 541–560.
- [71] Arifler, D., Zhu, T., Madaan, S., Tachtsidis, I., Optimal Wavelength Combinations for Near-Infrared Spectroscopic Monitoring of Changes in Brain Tissue Hemoglobin and Cytochrome *c* Oxidase Concentrations. *Biomed. Opt. Express* 2015, 6, 933–947.
- [72] Bakker, A., Smith, B., Ainslie, P., Smith, K., in: Philip Ainslie (Ed.), Applied Aspects of Ultrasonography in Humans. IntechOpen, London 2012, p. 200.
- [73] Delpy, D. T., Cope, M., Quantification in Tissue Near-Infrared Spectroscopy. *Philos. Trans. R. Soc. B Biol. Sci.* 1997, 352, 649–659.
- [74] Messere, A., Roatta, S., Influence of Cutaneous and Muscular Circulation on Spatially Resolved versus Standard Beer-Lambert Near-Infrared Spectroscopy. *Physiol. Rep.* 2013, 1, 1–10.
- [75] Minati, L., Kress, I. U., Visani, E., Medford, N., Critchley, H. D., Intra- and Extra-

- Cranial Effects of Transient Blood Pressure Changes on Brain Near-Infrared Spectroscopy (NIRS) Measurements. *J. Neurosci. Methods* 2011, 197, 283–288.
- [76] Canova, D., Roatta, S., Bosone, D., Micieli, G., Inconsistent Detection of Changes in Cerebral Blood Volume by Near Infrared Spectroscopy in Standard Clinical Tests. *J. Appl. Physiol.* 2011, 110, 1646–1655.
- [77] Kirilina, E., Yu, N., Jelzow, A., Wabnitz, H., Jacobs, A. M., Tachtsidis, I., Identifying and Quantifying Main Components of Physiological Noise in Functional Near Infrared Spectroscopy on the Prefrontal Cortex. *Front. Hum. Neurosci.* 2013, 7, 1–17.
- [78] Rashid, A., Roatta, S., Differential Control of Blood Flow in Masseter and Biceps Brachii Muscles During Stress. *Arch. Oral Biol.* 2022, 141, 1–10.
- [79] Al-Rawi, P. G., Smielewski, P., Kirkpatrick, P. J., Evaluation of a Near-Infrared Spectrometer (NIRO 300) for the Detection of Intracranial Oxygenation Changes in the Adult Head. *Stroke* 2001, 32, 2492–2499.
- [80] Perrey, S., Non-Invasive NIR Spectroscopy of Human Brain Function During Exercise. *Methods* 2008, 45, 289–299.
- [81] Elkins, G. R., Barabasz, A. F., Council, J. R., Spiegel, D., Advancing Research and Practice: The Revised APA Division 30 Definition of Hypnosis. *Int. J. Clin. Exp. Hypn.* 2015, 63, 1–9.
- [82] Santarcangelo, E. L., Carli, G., Individual Traits and Pain Treatment: The Case of Hypnotizability. *Front. Neurosci.* 2021, 15, 1–6.
- [83] Santarcangelo, E. L., Scattina, E., Responding to Sensorimotor Suggestions: From Endothelial Nitric Oxide to the Functional Equivalence Between Imagery and Perception. *Int. J. Clin. Exp. Hypn.* 2019, 67, 394–407.

- [84] Landry, M., Lifshitz, M., Raz, A., Brain Correlates of Hypnosis: A Systematic Review and Meta-Analytic Exploration. *Neurosci. Biobehav. Rev.* 2017, 81, 75–98.
- [85] Picerni, E., Santarcangelo, E., Laricchiuta, D., Cutuli, D., Petrosini, L., Spalletta, G., Piras, F., Cerebellar Structural Variations in Subjects with Different Hypnotizability. *Cerebellum* 2019, 18, 109–118.
- [86] Acunzo, D. J., Oakley, D. A., Terhune, D. B., The Neurochemistry of Hypnotic Suggestion. *Am. J. Clin. Hypn.* 2021, 63, 355–371.
- [87] Acunzo, D. J., Terhune, D. B., A Critical Review of Standardized Measures of Hypnotic Suggestibility. *Int. J. Clin. Exp. Hypn.* 2021, 69, 50–71.
- [88] Rashid, A., Santarcangelo, E. L., Roatta, S., Cerebral Blood Flow in Healthy Subjects with Different Hypnotizability Scores. *Brain Sci.* 2022, 12, 1–13.
- [89] Weitzenhoffer, A. M., Hilgard, E. R., Stanford Hypnotic Susceptibility Scale, Forms A and B. *Consult. Psychol. Press* 1959.
- [90] Rashid, A., Santarcangelo, E. L., Roatta, S., Does Hypnotizability Affect Neurovascular Coupling During Cognitive Tasks? *Physiol. Behav.* 2022, 257, 1–5.
- [91] Rashid, A., Santarcangelo, E. L., Roatta, S., Cerebrovascular Reactivity During Visual Stimulation: Does Hypnotizability Matter? *Brain Res.* 2022, 1794, 1–4.
- [92] Kihlstrom, J. F., in: Spielberger, C. D. (Ed.), *Encyclopedia of Applied Psychology*. Elsevier Science Ltd. 2004, pp. 243–248.
- [93] Gans, C., Gaunt, A. S., Muscle Architecture in Relation to Function. *J. Biomech.* 1991, 24, 53–65.
- [94] McMillan, A. S., Hannam, A. G., Motor-Unit Territory in the Human Masseter Muscle. *Arch. Oral Biol.* 1991, 36, 435–41.

- [95] Korfage, J. A. M., Koolstra, J. H., Langenbach, G. E. J., Van Eijden, T. M. G. J., Fiber-Type Composition of the Human Jaw Muscles (Part 2) Role of Hybrid Fibers and Factors Responsible for Inter-Individual Variation. *J. Dent. Res.* 2005, 84, 784–93.
- [96] Stål, P., Eriksson, P. O., Thornell, L. E., Differences in Capillary Supply Between Human Oro-Facial, Masticatory and Limb Muscles. *J. Muscle Res. Cell Motil.* 1996, 17, 183–197.
- [97] Österlund, C., Thornell, L. E., Eriksson, P. O., Differences in Fibre Type Composition Between Human Masseter and Biceps Muscles in Young and Adults Reveal Unique Masseter Fibre Type Growth Pattern. *Anat. Rec.* 2011, 294, 1158–1169.
- [98] Van Eijden, T. M. G. J., Turkawski, S. J. J., Morphology and Physiology of Masticatory Muscle Motor Units. *Crit. Rev. Oral Biol. Med.* 2001, 12, 76–91.
- [99] Farago, E., Macisaac, D., Suk, M., Chan, A. D. C., A Review of Techniques for Surface Electromyography Signal Quality Analysis. *IEEE Rev. Biomed. Eng.* 2023, 16, 472–486.
- [100] Chowdhury, R. H., Reaz, M. B. I., Bin Mohd Ali, M. A., Bakar, A. A. A., Chellappan, K., Chang, T. G., Surface Electromyography Signal Processing and Classification Techniques. *Sensors* 2013, 13, 12431–12466.
- [101] McManus, L., De Vito, G., Lowery, M. M., Analysis and Biophysics of Surface EMG for Physiotherapists and Kinesiologists: Toward a Common Language with Rehabilitation Engineers. *Front. Neurol.* 2020, 11, 1–25.
- [102] Jambrik, Z., Santarcangelo, E. L., Ghelarducci, B., Picano, E., Sebastiani, L., Does Hypnotizability Modulate the Stress-Related Endothelial Dysfunction? *Brain Res. Bull.* 2004, 63, 213–216.
- [103] Jambrik, Z., Santarcangelo, E. L., Rudisch, T., Varga, A., Forster, T., Carli, G., Modulation of Pain-Induced Endothelial Dysfunction by Hypnotizability. *Pain* 2005,

116, 181–186.

- [104] Hoefl, F., Gabrieli, J. D. E., Whitfield-Gabrieli, S., Haas, B. W., Bammer, R., Menon, V., Spiegel, D., Functional Brain Basis of Hypnotizability. *Arch. Gen. Psychiatry* 2012, 69, 1064–1072.
- [105] Raz, A., Attention and Hypnosis: Neural Substrates and Genetic Associations of Two Converging Processes. *Int. J. Clin. Exp. Hypn.* 2005, 53, 237–58.
- [106] Facco, E., Testoni, I., Ronconi, L., Casiglia, E., Zanette, G., Spiegel, D., Psychological Features of Hypnotizability: A First Step Towards Its Empirical Definition. *Int. J. Clin. Exp. Hypn.* 2017, 65, 98–119.
- [107] Tellegen, A., Atkinson, G., Openness to Absorbing and Self-Altering Experiences (“Absorption”), A Trait related to Hypnotic Susceptibility. *J. Abnorm. Psychol.* 1974, 83, 268–77.
- [108] Ibáñez-Marcelo, E., Campioni, L., Phinyomark, A., Petri, G., Santarcangelo, E. L., Topology Highlights Mesoscopic Functional Equivalence Between Imagery and Perception: The Case of Hypnotizability. *Neuroimage* 2019, 200, 437–449.
- [109] Pacák, K., Palkovits, M., Stressor Specificity of Central Neuroendocrine Responses: Implications for Stress-Related Disorders. *Endocr. Rev.* 2001, 22, 502–48.
- [110] Roatta, S., Mohammed, M., Passatore, M., Detecting Activation of the Sympatho-Adrenal Axis from Haemodynamic Recordings, in Conscious Rabbits Exposed to Acute Stress. *Acta Physiol.* 2011, 201, 323–37.
- [111] Vissing, S. F., Differential Activation of Sympathetic Discharge to Skin and Skeletal Muscle in Humans. *Acta Physiol Scand Suppl.* 1997, 639, 1–32.
- [112] Eklund, B., Kaijser, L., Effect of Regional  $\alpha$ - and  $\beta$ -Adrenergic Blockade on Blood Flow

- in the Resting Forearm During Contralateral Isometric Handgrip. *J. Physiol.* 1976, 262, 39–50.
- [113] Rusch, N. J., Shepherd, J. T., Webb, R. C., Vanhoutte, P. M., Different Behavior of the Resistance Vessels of the Human Calf and Forearm During Contralateral Isometric Exercise, Mental Stress, and Abnormal Respiratory Movements. *Circ. Res.* 1981, 48, 1118-30.
- [114] Nakamura, Y., Torisu, T., Noguchi, K., Fujii, H., Changes in Masseter Muscle Blood Flow During Voluntary Isometric Contraction in Humans. *J. Oral Rehabil.* 2005, 32, 545–551.
- [115] Zambach, S. A., Cai, C., Helms, H. C. C., Hald, B. O., Dong, Y., Fordsmann, J. C., Nielsen, R. M., Hu, J., Lønstrup, M., Brodin, B., Lauritzen, M. J., Precapillary Sphincters and Pericytes at First-Order Capillaries as Key Regulators for Brain Capillary Perfusion. *Proc. Natl. Acad. Sci. U. S. A.* 2021, 118, 1–10.
- [116] Younger, J. W., Rossetti, G. C., Borckardt, J. J., Smith, A. R., Tasso, A. F., Nash, M. R., Hypnotizability and Somatic Complaints: A Gender-Specific Phenomenon. *Int. J. Clin. Exp. Hypn.* 2007, 55, 1–13.
- [117] Diolaiuti, F., Huber, A., Ciaramella, A., Santarcangelo, E. L., Sebastiani, L., Hypnotisability-Related Interoceptive Awareness and Inhibitory/Activating Emotional Traits. *Arch. Ital. Biol.* 2019, 157, 111–119.
- [118] Gordon, G. R. J., Howarth, C., MacVicar, B. A., Bidirectional Control of Blood Flow by Astrocytes: A Role for Tissue Oxygen and Other Metabolic Factors. *Adv. Exp. Med. Biol.* 2016, 903, 209–19.
- [119] Santarcangelo, E. L., Scattina, E., Complementing the Latest APA Definition of Hypnosis: Sensory-Motor and Vascular Peculiarities Involved in Hypnotizability. *Int. J.*



- Clin. Exp. Hypn.* 2016, 64, 318–330.
- [120] Nippert, A. R., Biesecker, K. R., Newman, E. A., Mechanisms Mediating Functional Hyperemia in the Brain. *Neuroscientist* 2018, 24, 73–83.
- [121] Poplawsky, A. J., Iordanova, B., Vazquez, A. L., Kim, S.-G., Fukuda, M., Postsynaptic Activity of Inhibitory Neurons Evokes Hemodynamic fMRI Responses. *Neuroimage* 2021, 225, 1–16.
- [122] Rashid, A., Roatta, S., Hemodynamic Monitoring in the Human Temporalis Muscle Using Near-Infrared Spectroscopy. *Physiol. Meas.* 2023, 44, 1–10.
- [123] Weil, J. V., Byrne-Quinn, E., Sodal, I. E., Kline, J. S., McCullough, R. E., Filley, G. F., Augmentation of Chemosensitivity During Mild Exercise in Normal Man. *J. Appl. Physiol.* 1972, 33, 813–9.
- [124] Fregosi, R. F., Seals, D. R., Hypoxic Potentiation of the Ventilatory Response to Dynamic Forearm Exercise. *J. Appl. Physiol.* 1993, 74, 2365–72.
- [125] Machado de Oliveira, D., Ribeiro Lopes, T., Silva Gomes, F., Rashid, A., Moreira Silva, B., Ventilatory Response to Peripheral Chemoreflex and Muscle Metaboreflex During Static Handgrip in Healthy Humans: Evidence of Hyperadditive Integration. *Exp. Physiol.* 2023, 108, 1–8.
- [126] Zivadinov, R., Chung, C. P., Potential Involvement of the Extracranial Venous System in Central Nervous System Disorders and Aging. *BMC Med.* 2013, 11, 1–23.
- [127] Plog, B. A., Nedergaard, M., The Glymphatic System in Central Nervous System Health and Disease: Past, Present, and Future. *Annu. Rev. Pathol.* 2018, 13, 379–394.
- [128] Fultz, N. E., Bonmassar, G., Setsompop, K., Stickgold, R. A., Rosen, B. R., Polimeni, J. R., Lewis, L. D., Coupled Electrophysiological, Hemodynamic, and Cerebrospinal Fluid

- Oscillations in Human Sleep. *Science*. 2019, 366, 628–631.
- [129] Simka, M., Latacz, P., Numerical Modeling of Blood Flow in the Internal Jugular Vein with the Use of Computational Fluid Mechanics Software. *Phlebology* 2021, 36, 541–548.
- [130] Rashid, A., Iqar, S. A., Rashid, A., Simka, M., Results of Numerical Modeling of Blood Flow in the Internal Jugular Vein Exhibiting Different Types of Strictures. *Diagnostics* 2022, 12, 1–14.
- [131] Validation of Analytical Procedures: Text and Methodology. European Medicines Agency, London 1995.
- [132] ICH Expert Working Group, International Conference on Harmonisation of Technical Requirements for Registration of Pharmaceuticals for Human Use: Pharmaceutical Development Q8(R2). 2009.
- [133] Center for Drug Evaluation and Research, Analytical Procedures and Methods Validation for Drugs and Biologics Guidance for Industry. U.S. Department of Health and Human Services, Food and Drug Administration, Silver Spring, Maryland 2015.
- [134] de Souza, A. M. C., Fajardo, F. A. G., Rashid, A., Tavares, M. F. M., Prado, M. S. A., Capillary Electrophoresis Method for Simultaneous Quantification of Hypocholesterolemic Drugs in Binary Mixture Formulation: Fast, Green, and Cost-Effective Alternative to HPLC. *Chromatographia* 2023, 86, 1–15.
- [135] Fajardo, F. A. G., Tavares, M. F. M., Rashid, A., Prado, M. S. A., Novel Eco-Friendly Stability Indicating Capillary Zone Electrophoresis Method for Determination of Aripiprazole in Tablet Dosage form: DoE Directed Optimization, Development and Method Validation. *J. Pharm. Sci.* 2022, 111, 3340–3351.
- [136] Cruz, R. Y. M. S., Arévalo, S. V., Rashid, A., Jara, M. R. A., Prado, M. S. A.,

Antioxidant and Photoprotective Potential of *Polypodium leucotomos*. *Explor. Med.*  
2022, 3, 607–616.

# APPENDIX

## SHORT COMMUNICATION

# Ventilatory response to peripheral chemoreflex and muscle metaboreflex during static handgrip in healthy humans: evidence of hyperadditive integration

Diogo Machado de Oliveira<sup>1</sup>  | Thiago Ribeiro Lopes<sup>1,2</sup> | Felipe Silva Gomes<sup>1</sup> |  
Anas Rashid<sup>3,4</sup>  | Bruno Moreira Silva<sup>1,4,5</sup> 

<sup>1</sup>Graduate Program in Translational Medicine, Federal University of São Paulo (Unifesp), São Paulo, SP, Brazil

<sup>2</sup>Paulista Association for the Development of Medicine (SPDM), São Paulo, SP, Brazil

<sup>3</sup>Department of Neuroscience 'Rita Levi Montalcini', University of Torino, Torino, Italy

<sup>4</sup>Graduate Program in Pulmonary Medicine, Unifesp, São Paulo, SP, Brazil

<sup>5</sup>Department of Physiology, Unifesp, São Paulo, SP, Brazil

## Correspondence

Bruno Moreira Silva, Botucatu street 862, Biomedical Sciences Building, 5th floor, São Paulo, SP, Brazil.

Email: [silva.bruno@unifesp.br](mailto:silva.bruno@unifesp.br)

## Funding information

The Coordination for the Improvement of Higher Education Personnel (CAPES) funded the study and supported D.M.O. A.R. was supported by a Doctoral Fellowship funded by Partnership for Knowledge (PFK) program of the Agenzia Italiana per la Cooperazione allo Sviluppo (AICS), Ministero degli Affari Esteri e della Cooperazione Internazionale (MAECI), Italy. B.M.S. received a scientific production award from the National Council for Scientific and Technological Development (CNPq; Process: 310110/2019-0).

Handling Editor: Ronan Berg

## Abstract

Exercise augments the hypoxia-induced ventilatory response in an exercise intensity-dependent manner. A mutual influence of hypoxia-induced peripheral chemoreflex activation and exercise-induced muscle metaboreflex activation might mediate the augmentation phenomenon. However, the nature of these reflexes' integration (i.e., hyperadditive, additive or hypoadditive) remains unclear, and the coactivation effect on breathing-related sensations and emotions has not been explored. Accordingly, we investigated the effect of peripheral chemoreflex and muscle metaboreflex coactivation on ventilatory variables and breathing-related sensations and emotions during exercise. Fourteen healthy adults performed 2-min isocapnic static handgrip, first with the non-dominant hand and immediately after with the dominant hand. During the dominant hand exercise, we (a) did not manipulate either reflex (control); (b) activated the peripheral chemoreflex by hypoxia; (c) activated the muscle metaboreflex in the non-dominant arm by post-exercise circulatory occlusion (PECO); or (d) coactivated both reflexes by simultaneous hypoxia and PECO use. Ventilation response to coactivation of reflexes (mean  $\pm$  SD,  $13 \pm 6$  l/min) was greater than the sum of responses to separated activations of reflexes (mean  $\pm$  SD,  $8 \pm 8$  l/min,  $P = 0.005$ ). Breathing-related sensory and emotional responses were similar between coactivation of reflexes and the sum of separate activations of reflexes. Thus, the peripheral chemoreflex and muscle metaboreflex integration during exercise appeared to be hyperadditive with regard to ventilation and additive with regard to breathing-related sensations and emotions in healthy adults.

## KEYWORDS

breathing, dyspnoea, isometric exercise, synergism

This is an open access article under the terms of the [Creative Commons Attribution](https://creativecommons.org/licenses/by/4.0/) License, which permits use, distribution and reproduction in any medium, provided the original work is properly cited.

© 2023 The Authors. *Experimental Physiology* published by John Wiley & Sons Ltd on behalf of The Physiological Society.

## 1 | INTRODUCTION

Exercise augments hypoxia-induced ventilatory response in an exercise intensity-dependent manner (Weil et al., 1972). A mutual influence of hypoxia-induced peripheral chemoreflex activation and exercise-induced muscle metaboreflex activation might mediate the augmentation phenomenon (Fregosi & Seals, 1993). However, the nature of the integration of these reflexes remains unclear because some studies did not calculate the summed effect of reflexes activation (Gujic et al., 2007; Houssiere et al., 2005). Additionally, when it was calculated, coactivation and summed effects paradoxically produced similar ventilatory responses (Edgell & Stickland, 2014), representing an additive integration that supports no interaction between the reflexes (Wilson & Teppema, 2016). Two methodological aspects might have blunted the coactivation ventilatory response in a previous study (Edgell & Stickland, 2014), likely explaining the lack of interaction between the reflexes. First, the muscle metaboreflex was activated via post-exercise circulatory occlusion (PECO) without contralateral limb exercise (Lam et al., 2019). Second, end-tidal carbon dioxide partial pressure (end-tidal  $P_{CO_2}$ ) was  $\sim 7$  mmHg lower during hypoxic PECO than during normoxic PECO (Algaith et al., 2019). Moreover, the coactivation effect on breathing-related sensations and emotions remains unexplored. Accordingly, we sought to test the hypothesis that peripheral chemoreflex and muscle metaboreflex coactivation during isocapnic exercise show hyperadditive integration, that is, they provoke greater ventilatory and breathing-related sensation and emotional responses when activated together than the sum of effects yielded by each reflex activation separately.

## 2 | METHODS

### 2.1 | Ethical approval

All individuals signed a written informed consent before participating in the study. The study was conducted following the latest version of the *Declaration of Helsinki*, approved by the Ethics Committee of the Federal University of São Paulo (process: 1051/2017), and registered in the publicly available Plataforma Brasil database (CAEE: 74619517.5.0000.5505; National Council of Health, Ministry of Health, Brazil).

### 2.2 | Participants

Seven men (age:  $24.4 \pm 3.6$  years, body mass:  $69.4 \pm 8.8$  kg, height:  $1.72 \pm 0.08$  m) and seven women (age:  $23.4 \pm 3.15$  years, body mass:  $61.4 \pm 9.5$  kg, height:  $1.66 \pm 0.06$  m) participated in the study. Nobody had previous exposure to acute or chronic hypoxia. Eligibility criteria were: age between 18 and 35 years, non-smoker, body mass index  $< 30$  kg/m<sup>2</sup>, no diagnosis of chronic diseases, and being sedentary (i.e., not engaged in regular physical activities) or engaged in regular physical activities at most three times a week.

### New Findings

- **What is the central question of this study?**

What is the effect of peripheral chemoreflex and muscle metaboreflex integration on ventilation regulation, and what is the effect of integration on breathing-related sensations and emotions?

- **What is the main finding and its importance?**

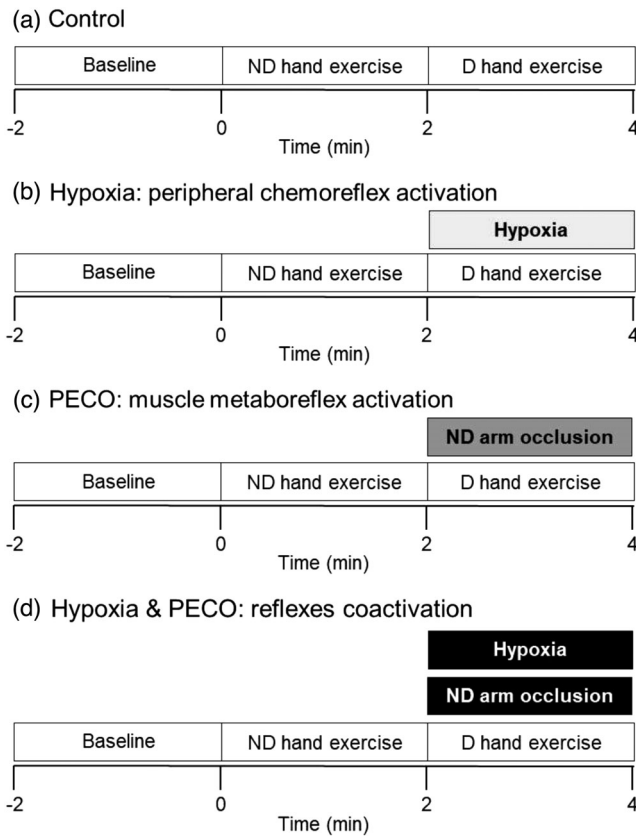
Peripheral chemoreflex and muscle metaboreflex coactivation during isocapnic static handgrip exercise appeared to elicit a hyperadditive effect with regard to ventilation and an additive effect with regard to breathing-related sensations and emotions. These findings reveal the nature of the integration between two neural mechanisms that operate during small-muscle static exercise performed under hypoxia.

### 2.3 | Experimental protocol

A first visit was used to familiarize the participants with the experimental procedures. Then, on two additional visits, we conducted experiments. The experimental visits occurred at the same period of the day, for a given participant, with an interval of at least 2 days and at most 7 days. Participants were instructed not to practice intense physical exercise for 48 h, not to ingest caffeine and alcohol for 24 h, and to ingest a light meal 2 h before the experiments. We sought to assess women during the beginning of the menstrual cycle, when oestrogen and progesterone levels are supposedly low, to increase the homogeneity of hormonal profiles. Ultimately, we managed to assess all women up to 8 days after the onset of menstruation.

### 2.4 | Experimental procedures

The participants were placed in the supine position on a large stretcher. The experiment had three 2-min consecutive phases (Figure 1): (a) baseline resting, (b) static handgrip exercise with the non-dominant hand, and (c) static handgrip exercise with the dominant hand. The experiment was repeated four times, varying the procedures during the dominant hand exercise. In this experimental phase, we (a) did not manipulate both reflexes (control); (b) activated the peripheral chemoreflex by hypoxia; (c) activated the muscle metaboreflex in the non-dominant arm by PECO; or (d) coactivated both reflexes by simultaneous hypoxia and PECO use. Two experiments were conducted per day, in random order, with at least a 30 min interval between them. Participants were blinded to the concentration of O<sub>2</sub> in the inspired air. Normoxia and hypoxia consisted of inhaling gas mixtures containing 21% O<sub>2</sub> with 90% N<sub>2</sub> and 10% O<sub>2</sub> with 90%



**FIGURE 1** Experimental protocol. Participants performed 2-min static handgrip under isocapnia, firstly with the non-dominant hand and immediately after with the dominant hand. During the dominant hand exercise, we (a) did not manipulate both reflexes (control); (b) activated the peripheral chemoreflex by hypoxia; (c) activated the muscle metaboreflex in the non-dominant arm by post-exercise circulatory occlusion (PECO); or (d) coactivated both reflexes by simultaneous hypoxia and PECO use. D, dominant; ND, non-dominant.

$N_2$ , respectively. Isocapnia was maintained throughout all experiments using a partial rebreathing set-up (Silva et al., 2018).

The target handgrip load definition took into account a physiological criterion rather than a fixed percentage of maximal voluntary contraction because interindividual differences in physiological responses (Lee et al., 2021) and exercise tolerance (Hunter et al., 2009) can occur for a fixed percentage level. The target load was identified for each hand in the familiarization visit. The load had to provoke a progressive increase in perceived effort, attaining a perceived effort between 5 and 8 a.u. on a 0–10 Borg scale at the end of 2 min of exercise. This range of perceived effort is compatible with an exercise intensity enough to provoke accumulation of intramuscular metabolites without being so hard to accomplish (Lopes et al., 2022; West et al., 1995), in an attempt to avoid apnoeas and breathing pattern irregularities. Surface electromyogram (EMG) was later used to verify the presence of exercise-induced metabolic stress, as the skeletal muscle's electrical activity increases during fatiguing static contractions (West et al., 1995). Muscle contraction metabolites were

arrested by manually inflating a cuff placed on the non-dominant arm to 220 mmHg before the end of the non-dominant hand exercise.

## 2.5 | Physiological measurements

An oro-nasal silicon mask was tightly adjusted to the participants' faces. Airflow,  $O_2$  partial pressure ( $P_{O_2}$ ) and  $CO_2$  partial pressure ( $P_{CO_2}$ ) were measured breath-by-breath (Quark CPET, Cosmed, Italy) by a bidirectional turbine, a paramagnetic sensor and a non-dispersive infrared sensor, respectively. Then, pulmonary ventilation, breathing frequency, tidal volume, and end-tidal  $P_{O_2}$  and  $P_{CO_2}$  were calculated. Pulse oxygen saturation was measured by an oximetry sensor placed on a toe of the right foot (Nonin Medical, Plymouth, MN, USA). The measured values were time-adjusted, considering a delay of 60 s between the monitoring in the foot and the oxyhaemoglobin desaturation in the central circulation during hypoxia exposure (Hamber et al., 1999). The electrical activity of the forearm flexor muscles was measured by two AgCl circular electrodes (MP43, MedPex, Republic of Korea) placed on the anteromedial surface of each forearm. A reference electrode was placed in the malleolus region of the right ankle. The raw EMG signal was sampled at 1 kHz, with a notch filter at 60 Hz (Dual Bioamp, ADInstruments, Bella Vista, NSW, Australia). The EMG signal was digitally filtered to a frequency bandwidth of 10–500 Hz (LabChart 3, ADInstruments). The root mean square (RMS) was calculated using 1-s EMG data surrounding the peak force during a maximal voluntary contraction and 20-s windows during the static handgrip exercise (LabChart 5, ADInstruments). Then, static handgrip exercise RMS data were converted into percentage values considering the maximal voluntary contraction RMS as 100% (West et al., 1995). Handgrip force was measured by a digital dynamometer (Grip Force Transducer, ADInstruments). The force tracing was projected on the ceiling, providing visual feedback to the participants.

## 2.6 | Sensory and emotional measurements

Once at baseline and every minute during exercise, one of the researchers asked the following questions: 'how intense is your sensation of breathing overall?' (Lewthwaite & Jensen, 2021) and 'how intense is your effort to perform the handgrip exercise?' (Lopes et al., 2022). The first question sought to assess the general intensity of breathing sensation unidimensionally, considering that the awareness of breathing intensity starts earlier and is more intense than other qualitative descriptors during exercise in healthy adults (Lewthwaite & Jensen, 2021). The second question assessed the perceived effort to squeeze the hand dynamometer (Lopes et al., 2022). The participants had to verbally answer these two questions considering Borg's 0–10 scale, which was placed in their eyesight. During the exercise, we asked just two questions so as not to distract the participant in performing the handgrip task and to minimize the influence of speaking on ventilation. After each experiment, the participants sat on a chair to answer the

Multidimensional Dyspnoea Profile (MDP) translated into Portuguese (Belo et al., 2019), considering their sensations and emotions at the end of the dominant hand exercise (i.e., focus period).

## 2.7 | Analysis of reflexes integration

Ventilatory data corresponding to the baseline period and the last 20 s of the first and second minutes of the non-dominant and dominant handgrip exercises were averaged. The last 20-s ventilatory and subjective data of the dominant handgrip exercise during hypoxia, PECO and hypoxia combined with PECO were subtracted from the corresponding control data to calculate the effect of each experimental manipulation. According to a previous proposition (Wilson & Teppema, 2016), a coactivation effect greater than the sum of effects yielded by each reflex activation separately was considered a hyperadditive integration. Similar coactivation and summed effects denoted an additive integration. A coactivation effect smaller than the summed effect was considered an hypoadditive integration.

## 2.8 | Statistical analyses

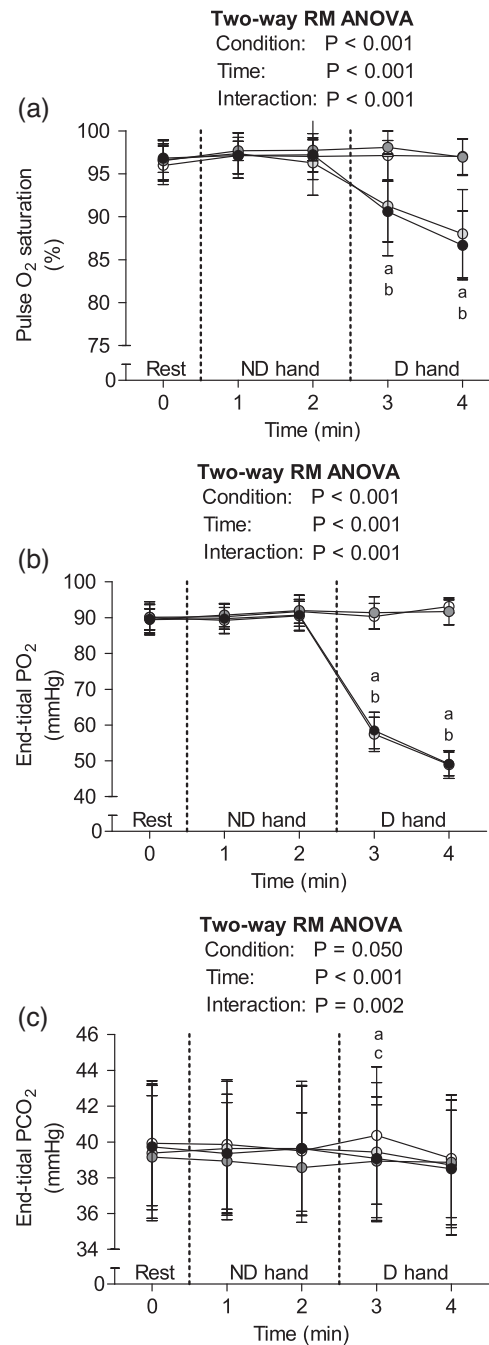
Data were analysed by either one-way or two-way repeated-measures analysis of variance (RM ANOVA), followed by the Tukey HSD *post hoc* test, if needed. All analyses were done in the software Statistica (version 12, StatSoft, Tulsa, OK, USA). Results are reported as the mean and standard deviation. Statistical significance was interpreted as  $P < 0.05$  in two-tailed analyses.

## 3 | RESULTS

The participants performed the handgrip exercise at  $32 \pm 6\%$  of the maximal voluntary contraction force with the non-dominant hand and  $32 \pm 5\%$  with the dominant hand. The forearm muscles' EMG and perceived effort increased during the non-dominant (EMG: 1st min:  $35 \pm 13$  vs. 2nd min:  $41\% \pm 14\%$ ,  $P = 0.001$ ; effort: 1st min:  $2.96 \pm 1.0$  vs. 2nd min:  $5.36 \pm 1.2$  a.u.,  $P < 0.001$ ) and the dominant (EMG: 1st min:  $34 \pm 9$  vs. 2nd min:  $41\% \pm 8\%$ ,  $P = 0.001$ ; effort: 1st min:  $3.97 \pm 1.0$  vs. 2nd min:  $6.24 \pm 1.3$  a.u.,  $P = 0.001$ ) handgrip exercise without differences among experiments (EMG:  $P = 0.140$ ; effort:  $P = 0.187$ ).

As expected, oxygen saturation and end-tidal  $P_{O_2}$  were lower in the hypoxia combined with PECO and in isolated hypoxia compared to the control during the dominant handgrip exercise (Figure 2a–c). In the first minute of the dominant handgrip exercise, end-tidal  $P_{CO_2}$  was lower in the hypoxia combined with PECO and in the isolated PECO experiments than in the control experiment. In the second minute of the dominant handgrip exercise, end-tidal  $P_{CO_2}$  was similar among all experiments.

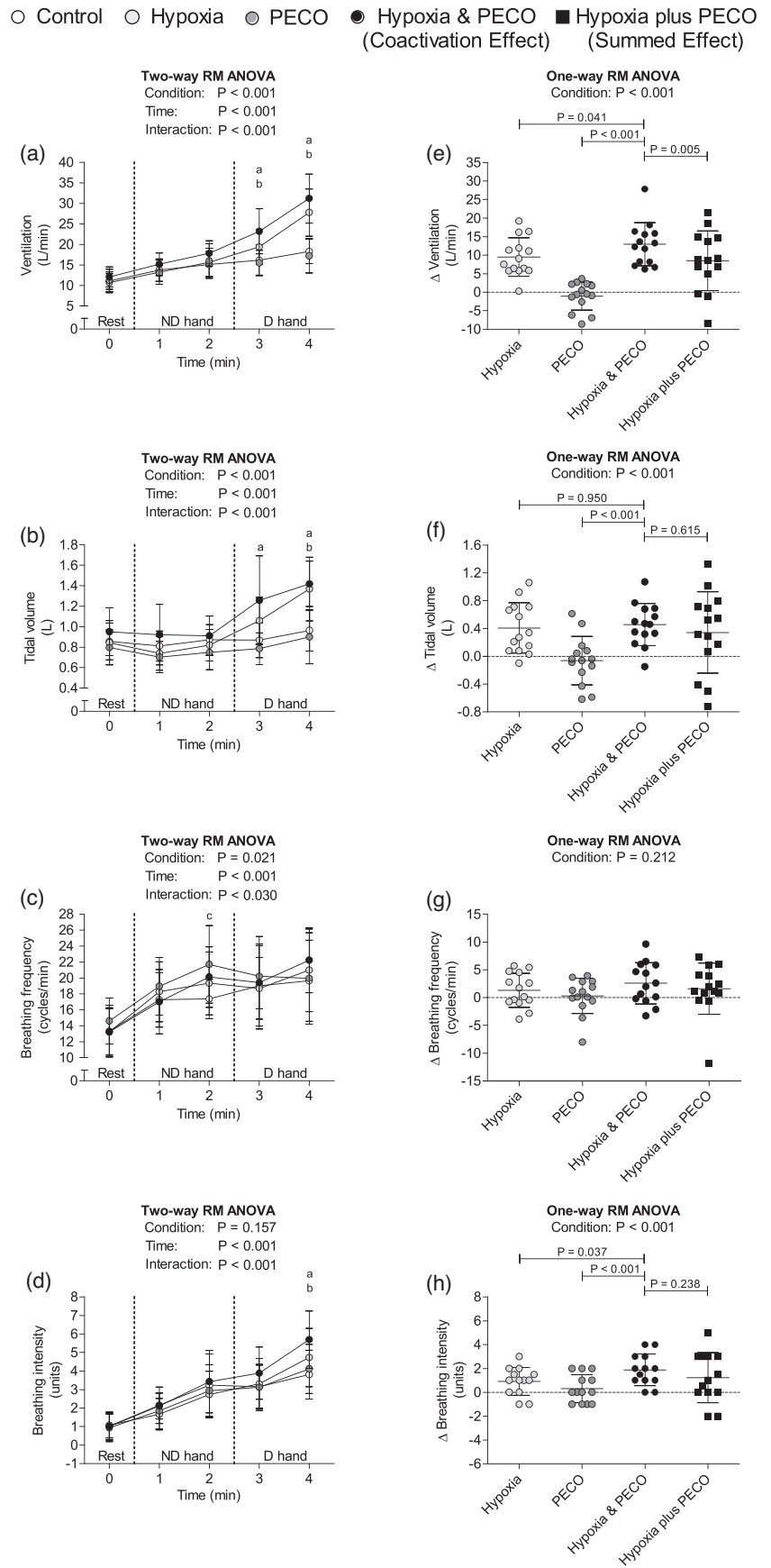
○ Control ○ Hypoxia ● PECO ● Hypoxia & PECO (Coactivation Effect)



**FIGURE 2** Time-adjusted oxyhaemoglobin saturation (a), end-tidal  $P_{O_2}$  (b), and end-tidal  $P_{CO_2}$  (c) at rest, 1st and 2nd min of non-dominant hand exercise (minutes 1 and 2 on the abscissa), and 1st and 2nd min of dominant hand exercise (minutes 3 and 4 on the abscissa). Data presented as the mean and standard deviation ( $n = 14$  for all variables) and analysed by two-way repeated-measures analysis of variance (RM ANOVA), followed by the Tukey *post hoc* test. (a)  $P < 0.05$  hypoxia and PECO versus control; (b)  $P < 0.05$  hypoxia versus control; (c)  $P < 0.05$  PECO versus control. D, dominant; ND, non-dominant; PECO, post-exercise circulatory occlusion.



**FIGURE 3** On the left, ventilation (a), tidal volume (b), breathing frequency (c), and breathing intensity (d) absolute values at rest, 1st and 2nd min of non-dominant hand exercise (minutes 1 and 2 in the abscissa axis), and 1st and 2nd min of dominant hand exercise (minutes 3 and 4 in the abscissa axis). On the right, ventilation (e), tidal volume (f), breathing frequency (g), and breathing intensity (h) change versus control. Data presented as the mean and standard deviation ( $n = 14$  for all variables) and analysed via two-way (a–d) or one-way (e–h) repeated measures analysis of variance (RM ANOVA), followed by the Tukey *post hoc* test. (a)  $P < 0.05$  hypoxia and PECO versus control; (b)  $P < 0.05$  hypoxia versus control; (c)  $P < 0.05$  PECO versus control. D, dominant; ND, non-dominant; PECO, post-exercise circulatory occlusion.



**TABLE 1** Multidimensional Dyspnoea Profile's sensory dimension, affective dimension 1 (dyspnoea) and 2 (other emotions) intensities

	Control	Hypoxia	PECO	Hypoxia and PECO	P	$\Delta$ Hypoxia	$\Delta$ PECO	$\Delta$ Hypoxia and PECO	$\Delta$ Hypoxia plus PECO	P
<b>Sensory dimension</b>										
My breathing requires muscle work or effort (a.u.)	2.07 ± 2.27	2.86 ± 2.07	2.00 ± 2.04	3.64 ± 2.27 <sup>a</sup>	0.001	0.79 ± 1.97	-0.07 ± 1.86	1.57 ± 1.87 <sup>b</sup>	0.71 ± 3.69	0.021
I am not getting enough air or I feel hunger for air (a.u.)	1.14 ± 2.21	1.57 ± 2.03	1.36 ± 2.10	2.64 ± 2.92	0.064	0.43 ± 2.65	0.21 ± 0.80	1.50 ± 2.62	0.64 ± 3.13	0.112
My chest and lungs feel tight or constricted (a.u.)	0.29 ± 0.47	0.57 ± 1.16	0.29 ± 0.47	0.50 ± 0.85	0.567	0.29 ± 0.99	0.00 ± 0.68	0.21 ± 0.80	0.29 ± 1.33	0.701
My breathing requires mental effort or concentration (a.u.)	3.00 ± 2.51	3.93 ± 2.73	3.50 ± 2.77	4.00 ± 2.48	0.049	0.93 ± 1.49	0.50 ± 1.95	1.00 ± 1.66	1.43 ± 3.27	0.175
I am breathing a lot (a.u.)	1.85 ± 2.35	2.36 ± 2.71	2.14 ± 2.91	3.14 ± 3.57	0.151	0.50 ± 2.59	0.29 ± 1.54	1.29 ± 1.68	0.79 ± 3.64	0.468
<b>Affective dimension 1</b>										
Dyspnoea (a.u.)	2.21 ± 0.47	3.50 ± 0.54	2.85 ± 0.57	4.21 ± 0.53 <sup>a</sup>	0.001	1.29 ± 1.33	0.64 ± 1.55	2.00 ± 1.66 <sup>b</sup>	1.93 ± 2.67 <sup>c</sup>	0.001
<b>Affective dimension 2</b>										
Depressed (a.u.)	0.07 ± 0.27	0.14 ± 0.53	0.07 ± 0.27	0.00 ± 0.00	-	0.07 ± 0.62	0.00 ± 0.39	-0.07 ± 0.27	0.07 ± 1.00	0.711
Anxious (a.u.)	2.00 ± 2.54	1.57 ± 0.94	1.36 ± 1.55	2.29 ± 2.33	0.598	-0.43 ± 2.53	-0.64 ± 3.56	0.29 ± 4.01	-1.07 ± 6.01	0.275
Frustrated (a.u.)	0.50 ± 1.87	0.21 ± 0.58	0.36 ± 0.93	0.14 ± 0.53	0.820	-0.29 ± 2.02	-0.14 ± 2.18	-0.36 ± 1.98	-0.43 ± 4.16	0.919
Angry (a.u.)	0.00 ± 0.00	0.14 ± 0.53	0.07 ± 0.27	0.00 ± 0.00	-	0.14 ± 0.53	0.07 ± 0.27	0.00 ± 0.00	0.21 ± 0.80	-
Afraid (a.u.)	0.43 ± 1.34	0.14 ± 0.36	0.07 ± 0.27	0.14 ± 0.36	0.527	-0.29 ± 1.14	-0.36 ± 1.39	0.00 ± 0.39	-0.64 ± 2.53	0.360

Data presented as means and standard deviation and compared among conditions with repeated measures ANOVA, followed by the Tukey *post hoc* test, when needed. *n* = 14. PECO, post-exercise circulatory occlusion.

<sup>a</sup>*P* < 0.05 hypoxia and PECO versus control.

<sup>b</sup>*P* < 0.05 hypoxia and PECO versus PPECO.

<sup>c</sup>*P* < 0.05 hypoxia plus PECO versus PECO.

During the dominant hand exercise, ventilation was higher in hypoxia combined with PECO and isolated hypoxia versus control (Figure 3a). In the first minute of this exercise, tidal volume was higher in hypoxia combined with PECO than in control (Figure 3b). Then, in the second minute, tidal volume was higher in hypoxia combined with PECO and in isolated hypoxia compared to control (Figure 3b). Breathing frequency was similar among experiments during the dominant hand exercise (Figure 3c). Breathing intensity was greater in hypoxia combined with PECO and in isolated hypoxia than in control in the second minute of the dominant hand exercise (Figure 3d).

Ventilation change was greater in hypoxia combined with PECO than in isolated hypoxia, isolated PECO and hypoxia plus PECO (i.e., hyperadditive integration; Figure 3e). Tidal volume change in hypoxia combined with PECO was greater than in isolated PECO, but similar to the changes in isolated hypoxia and hypoxia plus PECO (i.e., additive integration; Figure 3f). Breathing frequency changes were similar among experiments (i.e., additive integration; Figure 3g). Breathing intensity change was greater in hypoxia combined with PECO than in isolated hypoxia and in isolated PECO, but similar to the breathing intensity change in hypoxia plus PECO (i.e., additive integration; Figure 3h).

The intensity of respiratory muscle effort sensation was greater in hypoxia combined with PECO than in control (Table 1). The intensity of other breathing-related sensations was similar among conditions. Hypoxia combined with PECO and hypoxia plus PECO changes were similar for all sensations obtained with the MDP (i.e., additive integration). The intensity of dyspnoea was greater in hypoxia combined with PECO than in control. Hypoxia combined with PECO and hypoxia plus PECO changes were similar for all emotions obtained with the MDP (i.e., additive integration).

## 4 | DISCUSSION

The main result of the present study is that hypoxic air inhalation combined with metabolite arrest via PECO during exercise potentiated the ventilatory response versus isolated hypoxia and PECO exposure. As forearm EMG and perceived handgrip effort were similar between hypoxia and control during the dominant hand exercise, hypoxia likely increased ventilation via peripheral chemoreceptor activation (mainly the carotid chemoreceptors) rather than changing contracting muscle oxygenation and metabolism (Fregosi & Seals, 1993; Katayama et al., 2010). Furthermore, as both forearm EMG and perceived handgrip effort increased during exercise, exercise likely produced some metabolic stress resulting in metabolically sensitive muscle afferent activation during PECO (Bendahan et al., 1996; West et al., 1995). Therefore, the most likely explanation for the potentiated ventilatory response is an interaction between peripheral chemoreceptor and muscle metaboreceptor inputs.

Interestingly, PECO per se did not change ventilatory, sensory and emotional endpoints versus control. Perhaps, the dissimilar effect of PECO during normoxia and hypoxia is related to the amount of muscle metaboreceptors' afferent inputs. According to the study design, we

limited the exercise intensity to avoid breathing irregularities and apnoeas. Then, perhaps, the level of afferent inputs from muscle metaboreceptors was not enough to augment ventilatory, sensory and emotional responses in PECO versus the control condition. This hypothesis is supported by the data reported in the study that advanced the PECO use on one limb while the other is exercising (Lam et al., 2019), because exercise intensity influenced the ventilation response.

The hyperadditive interaction is coherent with evidence that exercise augments hypoxia-induced ventilatory responses in an exercise intensity-dependent manner (Weil et al., 1972). Moreover, it supports the hypothesis that the integration of the reflexes had been underestimated before (Edgell & Stickland, 2014), likely due to the use of PECO at rest (Lam et al., 2019) and the lack of CO<sub>2</sub> control (Alghaith et al., 2019). Our group previously reported that combined hypoxia-induced peripheral chemoreflex activation and passive limb-induced muscle mechanoreflex activation elicited a hyperadditive ventilatory response (Silva et al., 2018). Likewise, another group reported hypoxia-induced peripheral chemoreflex activation and overall exercise-induced muscle afferent activation elicited a hyperadditive ventilatory response (Wan et al., 2020). Therefore, present and past findings collectively support that both the mechanoreflex and the metaboreflex can potentiate the peripheral chemoreflex-induced ventilatory response. The potentiation can be mediated within the central nervous system (Davies & Lahiri, 1973) or at the peripheral chemoreceptors (O'Regan, 1981), requiring further investigation. The lack of hyperadditive responses concerning breathing-related sensations and emotions was unexpected and deserves investigation during whole-body dynamic exercise, which presumably has a greater effect on these endpoints than small muscle static exercise (Lewthwaite & Jensen, 2021).

## 5 | CONCLUSIONS

The peripheral chemoreflex and muscle metaboreflex integration appeared to be hyperadditive with regard to ventilation and additive with regard to breathing-related sensations and emotions during isocapnic small-muscle-mass static exercise.

## AUTHOR CONTRIBUTIONS

Diogo Machado de Oliveira, Thiago Ribeiro Lopes, Bruno Moreira Silva: conception or design of the work. Diogo Machado de Oliveira, Thiago Ribeiro Lopes, Felipe Silva Gomes, Anas Rashid, Bruno Moreira Silva: acquisition, analysis, or interpretation of data for the work. Diogo Machado de Oliveira, Thiago Ribeiro Lopes, Felipe Silva Gomes, Anas Rashid, Bruno Moreira Silva: drafting of the work or revising it critically for important intellectual content. All authors have read and approved the final version of this manuscript and agree to be accountable for all aspects of the work in ensuring that questions related to the accuracy or integrity of any part of the work are appropriately investigated and resolved. All persons designated as authors qualify for authorship, and all those who qualify for authorship are listed.

## ACKNOWLEDGEMENTS

The authors are grateful to Dr Gerhardus Hermanus Maria Schoorlemmer for assistance with the standardization of the experimental set-up.

## CONFLICT OF INTEREST

The authors have no conflict of interest to declare.

## DATA AVAILABILITY STATEMENT

Data are available on request from the authors.

## ORCID

Diogo Machado de Oliveira  <https://orcid.org/0000-0002-2967-5736>

Anas Rashid  <https://orcid.org/0000-0002-4644-4729>

Bruno Moreira Silva  <https://orcid.org/0000-0003-0473-3706>

## REFERENCES

- Alghaith, J. M., Balanos, G. M., Eves, F. F., & White, M. J. (2019). Sensitivity of the human ventilatory response to muscle metaboreflex activation during concurrent mild hypercapnia. *Experimental Physiology*, 104(3), 359–367.
- Belo, L. F., Rodrigues, A., Vicentin, A. P., Paes, T., de Castro, L. A., Hernandez, N. A., & Pitta, F. (2019). A breath of fresh air: Validity and reliability of a Portuguese version of the Multidimensional Dyspnea Profile for patients with COPD. *PLoS ONE*, 14(4), e0215544.
- Bendahan, D., Jammes, Y., Salvan, A. M., Badier, M., Confort-Gouny, S., Guillot, C., & Cozzone, P. J. (1996). Combined electromyography–31P-magnetic resonance spectroscopy study of human muscle fatigue during static contraction. *Muscle & Nerve*, 19(6), 715–721.
- Davies, R. O., & Lahiri, S. (1973). Absence of carotid chemoreceptor response during hypoxic exercise in the cat. *Respiration Physiology*, 18(1), 92–100.
- Edgell, H., & Stickland, M. K. (2014). Activation of the carotid chemoreflex secondary to muscle metaboreflex stimulation in men. *American Journal of Physiology. Regulatory, Integrative and Comparative Physiology*, 306(9), R693–R700.
- Fregosi, R. F., & Seals, D. R. (1993). Hypoxic potentiation of the ventilatory response to dynamic forearm exercise. *Journal of Applied Physiology*, 74(5), 2365–2372.
- Gujic, M., Laude, D., Houssière, A., Beloka, S., Argacha, J. F., Adamopoulos, D., Khaët, O., Elghozi, J. L., & van de Borne, P. (2007). Differential effects of metaboreceptor and chemoreceptor activation on sympathetic and cardiac baroreflex control following exercise in hypoxia in human. *The Journal of Physiology*, 585(1), 165–174.
- Hamber, E. A., Bailey, P. L., James, S. W., Wells, D. T., Lu, J. K., & Pace, N. L. (1999). Delays in the detection of hypoxemia due to site of pulse oximetry probe placement. *Journal of Clinical Anesthesia*, 11(2), 113–118.
- Houssiere, A., Najem, B., Ciarka, A., Velez-Roa, S., Naeije, R., & van de Borne, P. (2005). Chemoreflex and metaboreflex control during static hypoxic exercise. *American Journal of Physiology. Heart and Circulatory Physiology*, 288(4), H1724–H1729.
- Hunter, S. K., Griffith, E. E., Schlachter, K. M., & Kufahl, T. D. (2009). Sex differences in time to task failure and blood flow for an intermittent isometric fatiguing contraction. *Muscle & Nerve*, 39(1), 42–53.
- Katayama, K., Yoshitake, Y., Watanabe, K., Akima, H., & Ishida, K. (2010). Muscle deoxygenation during sustained and intermittent isometric exercise in hypoxia. *Medicine and Science in Sports and Exercise*, 42(7), 1269–1278.
- Lam, E., Greenhough, E., Nazari, P., White, M. J., & Bruce, R. M. (2019). Muscle metaboreflex activation increases ventilation and heart rate during dynamic exercise in humans. *Experimental Physiology*, 104(10), 1472–1481.
- Lee, J. B., Notay, K., Seed, J. D., Nardone, M., Omazic, L. J., & Millar, P. J. (2021). Sex differences in muscle metaboreflex activation after static handgrip exercise. *Medicine and Science in Sports and Exercise*, 53(12), 2596–2604.
- Lewthwaite, H., & Jensen, D. (2021). Multidimensional breathlessness assessment during cardiopulmonary exercise testing in healthy adults. *European Journal of Applied Physiology*, 121(2), 499–511.
- Lopes, T. R., Pereira, H. M., & Silva, B. M. (2022). Perceived exertion: Revisiting the history and updating the neurophysiology and the practical applications. *International Journal of Environmental Research and Public Health*, 19(21), 14439.
- O'Regan, R. G. (1981). Responses of carotid body chemosensory activity and blood flow to stimulation of sympathetic nerves in the cat. *The Journal of Physiology*, 315(1), 81–98.
- Silva, T. M., Aranda, L. C., Paula-Ribeiro, M., Oliveira, D. M., Medeiros, W. M., Vianna, L. C., Nery, L. E., & Silva, B. M. (2018). Hyperadditive ventilatory response arising from interaction between the carotid chemoreflex and the muscle mechanoreflex in healthy humans. *Journal of Applied Physiology*, 125(1), 215–225.
- Wan, H. Y., Weavil, J. C., Thurston, T. S., Georgescu, V. P., Bledsoe, A. D., Jessop, J. E., Buys, M. J., Richardson, R. S., & Amann, M. (2020). The muscle reflex and chemoreflex interaction: Ventilatory implications for the exercising human. *Journal of Applied Physiology*, 129(4), 691–700.
- Weil, J. V., Byrne-Quinn, E., Sodal, I. E., Kline, J. S., McCullough, R. E., & Filley, G. F. (1972). Augmentation of chemosensitivity during mild exercise in normal man. *Journal of Applied Physiology*, 33(6), 813–819.
- West, W., Hicks, A., Clements, L., & Dowling, J. (1995). The relationship between voluntary electromyogram, endurance time and intensity of effort in isometric handgrip exercise. *European Journal of Applied Physiology and Occupational Physiology*, 71(4), 301–305.
- Wilson, R. J., & Teppema, L. J. (2016). Integration of central and peripheral respiratory chemoreflexes. *Comprehensive Physiology*, 6(2), 1005–1041.

## SUPPORTING INFORMATION

Additional supporting information can be found online in the Supporting Information section at the end of this article.

**How to cite this article:** de Oliveira, D. M., Lopes, T. R., Gomes, F. S., Rashid, A., & Silva, B. M. (2023). Ventilatory response to peripheral chemoreflex and muscle metaboreflex during static handgrip in healthy humans: evidence of hyperadditive integration. *Experimental Physiology*, 1–8.  
<https://doi.org/10.1113/EP091094>

## Article

# Results of Numerical Modeling of Blood Flow in the Internal Jugular Vein Exhibiting Different Types of Strictures

Anas Rashid <sup>1,2</sup>, Syed Atif Iqar <sup>3</sup>, Aiman Rashid <sup>4</sup> and Marian Simka <sup>5,\*</sup><sup>1</sup> Department of Neuroscience “Rita Levi Montalcini”, University of Torino, 10125 Torino, Italy<sup>2</sup> Department of Electronics and Telecommunications, Polytechnic of Torino, 10129 Torino, Italy<sup>3</sup> Aston Institute of Photonic Technologies, College of Engineering and Physical Sciences, Aston University, Birmingham B4 7ET, UK<sup>4</sup> Department of Electrical and Electronic Engineering, University of Cagliari, 09123 Cagliari, Italy<sup>5</sup> Department of Anatomy, University of Opole, 45-052 Opole, Poland

\* Correspondence: msimka@uni.opole.pl

**Abstract:** The clinical relevance of nozzle-like strictures in upper parts of the internal jugular veins remains unclear. This study was aimed at understanding flow disturbances caused by such stenoses. Computational fluid dynamics software, COMSOL Multiphysics, was used. Two-dimensional computational domain involved stenosis at the beginning of modeled veins, and a flexible valve downstream. The material of the venous valve was considered to be hyperelastic. In the vein models with symmetric 2-leaflets valve without upstream stenosis or with minor 30% stenosis, the flow was undisturbed. In the case of major 60% and 75% upstream stenosis, centerline velocity was positioned asymmetrically, and areas of reverse flow and flow separation developed. In the 2-leaflet models with major stenosis, vortices evoking flow asymmetry were present for the entire course of the model, while the valve leaflets were distorted by asymmetric flow. Our computational fluid dynamics modeling suggests that an impaired outflow from the brain through the internal jugular veins is likely to be primarily caused by pathological strictures in their upper parts. In addition, the jugular valve pathology can be exacerbated by strictures located in the upper segments of these veins.

**Keywords:** computational fluid dynamics; flow separation; internal jugular vein; numerical modeling; fluid–structure interaction



**Citation:** Rashid, A.; Iqar, S.A.; Rashid, A.; Simka, M. Results of Numerical Modeling of Blood Flow in the Internal Jugular Vein Exhibiting Different Types of Strictures. *Diagnostics* **2022**, *12*, 2862. <https://doi.org/10.3390/diagnostics12112862>

Academic Editor: Paolo Zamboni

Received: 19 August 2022

Accepted: 16 November 2022

Published: 18 November 2022

**Publisher’s Note:** MDPI stays neutral with regard to jurisdictional claims in published maps and institutional affiliations.



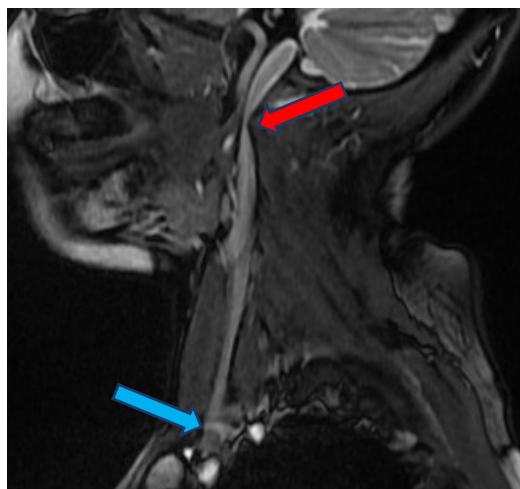
**Copyright:** © 2022 by the authors. Licensee MDPI, Basel, Switzerland. This article is an open access article distributed under the terms and conditions of the Creative Commons Attribution (CC BY) license (<https://creativecommons.org/licenses/by/4.0/>).

## 1. Introduction

The internal jugular vein (IJV) is a paired blood vessel which constitutes the primary outflow route of blood from the brain. A number of studies suggested that impaired outflow through these veins can contribute to several neurodegenerative and neuroinflammatory disorders, like multiple sclerosis, Parkinson’s disease, lateral amyotrophic sclerosis, and Ménière disease [1–5]. The IJV begins intracranially, leaves the cranial cavity through the jugular foramen (opening in the temporal bone), and continues downward through the neck to join the brachiocephalic vein located in the upper chest (Figure 1). Normally, there are no strictures of IJV at the level of the jugular foramen. Still, some individuals present with stenosis of IJV in this area, usually caused by abnormal bony processes [6–8]. The clinical relevance of these stenoses remains unclear. Previous research on flow disturbances in IJV mostly focused on the jugular valve, which is the valve situated at the caudal end of IJV, just above its connection with the brachiocephalic vein [9–12].

It is worth highlighting the potential clinical relevance of our in silico study. As mentioned earlier, abnormal outflow through IJVs can be found in many patients with neurodegenerative and neuroinflammatory disorders. Currently, it is suspected that these neurological pathologies are associated with abnormal functioning of the astroglial-mediated interstitial fluid bulk flow, the so-called glymphatic system [13]. The activation of the glymphatic system primarily depends on a temporary decrease of the cortical blood flow,

followed by a wave of inflow of the cerebrospinal fluid from the spinal canal to the cranial cavity [14]. Considering the Kellie–Monroe doctrine, proper interplay between the arterial and cerebrospinal flow requires an undisturbed venous outflow from the cranial cavity, and indeed an anomalous flow of the cerebrospinal fluid, as well as an imbalance between cerebral arterial and venous flow, has been demonstrated in multiple sclerosis patients [15–17]. About ten years ago, it was hoped that venous angioplasty for abnormal IJVs would be a much-awaited treatment for multiple sclerosis. However, a majority of randomized clinical trials on endovascular treatment for chronic cerebrospinal venous insufficiency in these patients did not reveal the clinical efficacy of endovascular procedures [18–23]. However, these treatments focused on the pathological jugular valves and primarily comprised balloon angioplasty and/or stenting for such aberrant valves. These approaches were not necessarily correct. Indeed, an expanded analysis of results of the BRAVE DREAMS (BRAIn VENous DRainage Exploited Against Multiple Sclerosis) trial revealed that only a subgroup of multiple sclerosis patients benefited from endovascular angioplasty at the level of jugular valve; it comprised patients presenting with horizontal endoluminal defects of the IJV and segmental stenosis with short endoluminal lesions of this vein [24].



**Figure 1.** The internal jugular vein with stricture in its upper part (red arrow), blue arrow points to the location of the jugular valve.

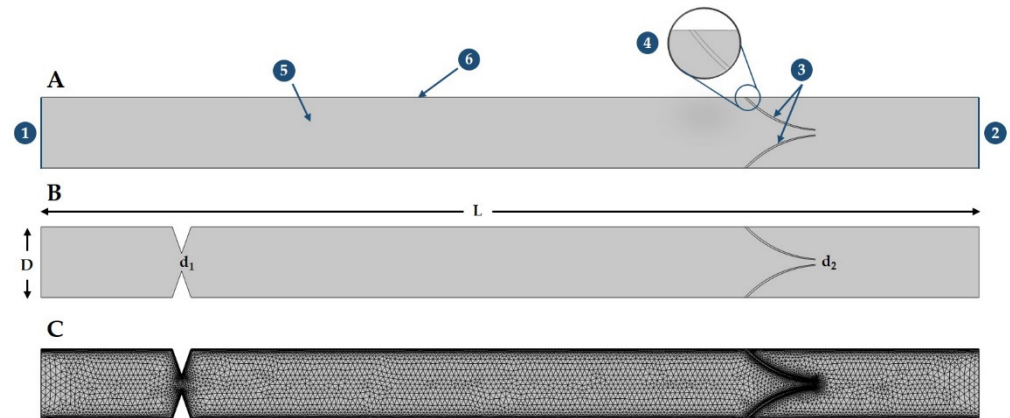
In our previous paper [25], based on the results of flow simulations, we suggested that strictures located at the level of the jugular foramen are probably more clinically relevant than the pathological jugular valves. These computer simulations suggested that strictures in the upper part of IJV are probably more clinically relevant. Importantly, there are some clinical reports on such entrapment of IJV by bony abnormalities in the upper part of this vein. It has also been demonstrated that correction of these strictures can decrease neurological symptoms [26–28].

This *in silico* study is the continuation of that research [25] and was aimed at understanding the influence of stenoses located at the beginning of IJV on the flow through this vein and the functioning of the jugular valve located downstream.

## 2. Materials and Methods

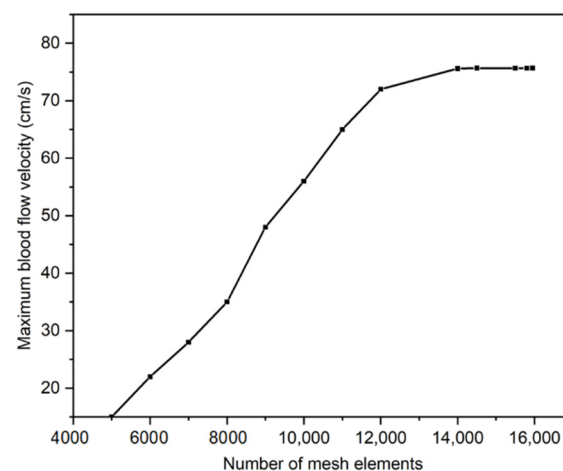
For the purpose of this study computational fluid dynamics (CFD) software, the COMSOL Multiphysics, version 5.1 (COMSOL Inc., Burlington, MA, USA), was used. For numerical simulation of the real-time blood flow in normal and abnormal IJVs, two-dimensional (2D) models of IJVs were built. The 2D computational domain, which was 200 mm long (L) and 15 mm wide (D) [29], involved stenosis at its beginning and a hyperelastic venous valve downstream (Figure 2). Figure 2A particularly shows the nomenclature of IJV 2D model, where the input and output of IJV are represented by 1 and 2, whereas the flexible

venous valve leaflets are denoted by 3 and 4. The fluid domain is represented by 5, whereas the walls of IJV are considered as a no-slip boundary shown by 6. A proximal stenosis ( $d_1$ ) and gap between valve leaflets ( $d_2$ ) are shown in Figure 2B. The geometry is discretized into free triangular components by considering all quality measures, which include optimal skewness, orthogonality, and aspect ratio (Figure 2C).



**Figure 2.** The scheme of the 2-dimensional model of the internal jugular vein and symmetrical 2-leaflets hyperelastic valve downstream; flow is from left to the right; this idealized model resembles real internal jugular vein with tandem stenosis from Figure 1. (A) without stenosis; (B) with 60% rigid stenosis at the beginning of this blood vessel ( $d_1$ ) and flexible valve ( $d_2$ ) downstream; and (C) free-triangular mesh with boundary layer.

The grid independency study was conducted for the maximum velocity in the domain at  $t = 3$  s. The study was conducted in a stepwise fashion, starting with a coarser mesh and then reducing the mesh element size until the maximum velocity of the blood in IJV became constant. Figure 3 shows the mesh independence study graph in which the mesh domain was optimized for 15,832 triangular elements.



**Figure 3.** Mesh independence study: maximum blood flow velocity against the number of mesh elements in the domain.

This model had a symmetric 2-leaflets valve. Models resembling veins with strictures in their upstream segments had a rapid contraction, which narrowed the lumen by 30%, 60%, or 75%. In total, four different 2D models of IJV were constructed: (A) vein without upstream stenosis; (B) vein with 30% upstream stenosis; (C) vein with 60% upstream stenosis; and (D) vein with 75% upstream stenosis (Figure 4).

Dirichlet boundary conditions (by specifying the values that a solution will take along the boundary of the domain like  $\mathbf{u} = U_{\text{inlet}}$  and  $p_{\text{outlet}} = 0$  Pa) were applied at

the inlet and outlet boundaries of the modeled blood vessels. The whole domain was discretized into a further two subdomains, blood (Domain 1) and venous valve (Domain 2). The turbulent flow modeling was coupled with solid mechanics module using the fluid–structure interaction approach, as the Reynold number ( $Re$ ) exceeds 2000 in all cases, where the constitutive relation for blood shear stress to shear strain was considered Newtonian. The nomenclature is described in Table 1.

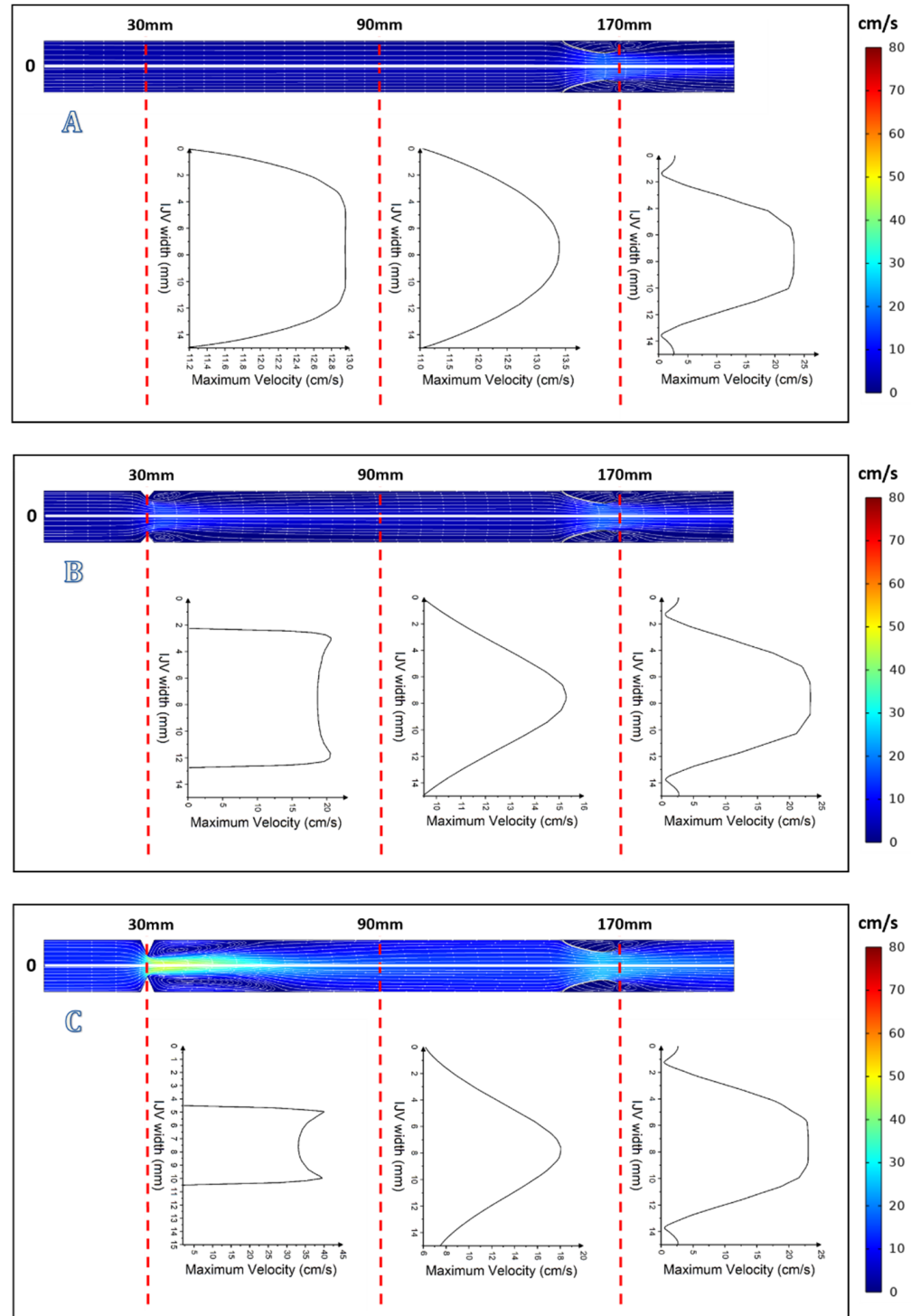
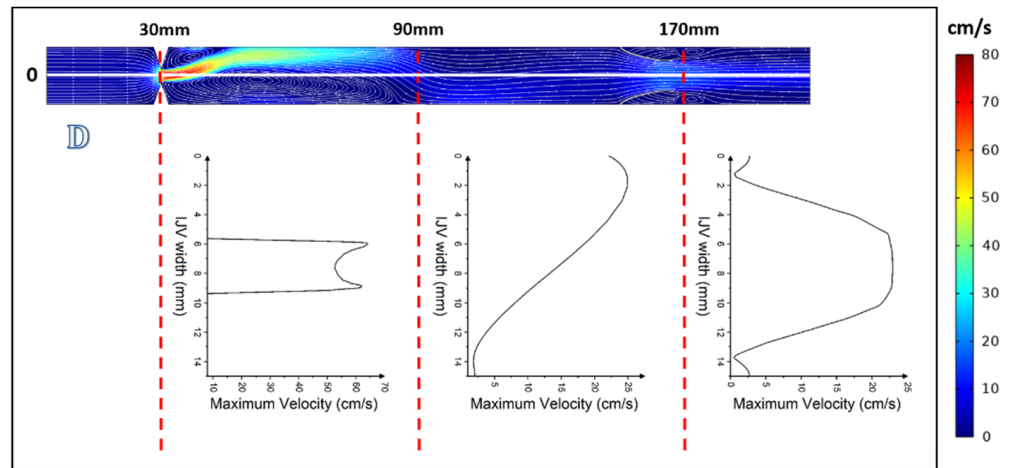


Figure 4. Cont.





**Figure 4.** Models of the internal jugular vein and symmetric 2-leaflets valve with velocity profiles at  $t = 0.25$  s: (A) without upstream stenosis; (B) with 30% upstream stenosis; (C) with 60% upstream stenosis; and (D) with 75% upstream stenosis.

**Table 1.** Nomenclature.

Quantity (Symbol)	Unit	Quantity (Symbol)	Unit
Density of blood ( $\rho$ )	$\text{kg m}^{-3}$	Partial derivative ( $\partial$ )	–
Time ( $t$ )	s	Fluid velocity ( $\mathbf{u}$ )	$\text{m s}^{-1}$
Fluid pressure ( $p$ )	Pa	Turbulent intensity ( $\mathbf{I}$ )	–
Dynamic viscosity ( $\mu$ )	Pa s	External forces ( $\mathbf{F}$ )	N
Turbulent kinetic energy ( $k$ )	J	Turbulent viscosity ( $\mu_T$ )	$\text{kg}^2 \text{s m}^{-3}$
Specific dissipation rate ( $\omega$ )	$\text{J kg}^{-1} \text{s}^{-1}$	Mean rotation-rate tensor ( $\Omega_{ij}$ )	–
Mean strain-rate tensor ( $S_{ij}$ )	–	Venous valve density ( $\rho_s$ )	$\text{kg m}^{-3}$
Displacement vector ( $\mathbf{u}_d$ )	m	Deformation gradient ( $\mathbf{F}$ )	–
Stress tensor ( $\mathbf{S}, \sigma$ )	$\text{N m}^{-2}$	Volume force ( $\mathbf{F}_V$ )	$\text{N m}^{-3}$
Elastic volume ratio ( $J_{el}$ )	–	Identity tensor ( $\mathbf{I}$ )	–
External stress tensor ( $\mathbf{S}_{ext}$ )	$\text{N m}^{-2}$	Strain energy density ( $W_s$ )	J
Lamé’s second parameter ( $\mu$ )	MPa	Lamé’s first parameter ( $\lambda$ )	MPa
Modulus of elasticity ( $E$ )	MPa	Poisson’s ratio ( $\nu$ )	–

The Reynolds Average Navier Stokes (RANS)  $k$ - $\omega$  numerical method was used to simulate the mean flow characteristics, as shown in Equations (1)–(4).

$$\rho \left[ \frac{\partial \mathbf{u}}{\partial t} + (\mathbf{u} \cdot \nabla) \mathbf{u} \right] = \nabla \cdot \left( -p \mathbf{I} + \mathbf{K} : \mu \left[ \nabla \mathbf{u} + (\nabla \mathbf{u})^T \right] \right) + \mathbf{F} \quad (1)$$

$$\rho \nabla \cdot \mathbf{u} = 0 \quad (2)$$

$$\rho \left[ \frac{\partial k}{\partial t} + (\mathbf{u} \cdot \nabla) k \right] = \nabla \cdot [(\mu + \mu_T \sigma^*) \nabla k] + P_k - \rho \beta_0^* \omega k \quad (3)$$

$$\rho \left[ \frac{\partial \omega}{\partial t} + (\mathbf{u} \cdot \nabla) \omega \right] = \nabla \cdot [(\mu + \mu_T \sigma) \nabla \omega] + \alpha \frac{\omega}{k} P_k - \rho \beta_0 \omega^2 \quad (4)$$

where,

$$\begin{aligned} \mathbf{K} &= (\mu + \mu_T) [\nabla \mathbf{u} + (\nabla \mathbf{u})^T]; \quad \mu_T = \rho \frac{k}{\omega} \\ P_k &= \mu_T \left[ \nabla \mathbf{u} : (\nabla \mathbf{u} + (\nabla \mathbf{u})^T) - \frac{2}{3} (\nabla \cdot \mathbf{u})^2 \right] - \frac{2}{3} \rho k \nabla \cdot \mathbf{u} \\ \alpha &= \frac{13}{25}; \quad \beta = \beta_0 f_\beta; \quad \beta^* = \beta_0^* f_\beta; \quad \sigma = \sigma^* = \frac{1}{2} \\ \beta_0 &= \frac{13}{125}; \quad f_\beta = \frac{1+70\chi_\omega}{1+80\chi_\omega}; \quad \chi_\omega = \left| \frac{\Omega_{ij}\Omega_{jk}S_{ki}}{(\beta_0^*\omega)^3} \right| \\ \beta_0^* &= \frac{9}{10}; \quad f_\beta = \begin{cases} 1 & \chi_k \leq 0 \\ \frac{1+680\chi_k^2}{1+400\chi_k^2} & \chi_k > 0 \end{cases} \quad \chi_k = \frac{1}{\omega^3} (\nabla k \cdot \nabla \omega) \\ \Omega_{ij} &= \frac{1}{2} \left( \frac{\partial \bar{u}_i}{\partial x_j} - \frac{\partial \bar{u}_j}{\partial x_i} \right); \quad S_{ij} = \frac{1}{2} \left( \frac{\partial \bar{u}_i}{\partial x_j} + \frac{\partial \bar{u}_j}{\partial x_i} \right) \end{aligned}$$

The incompressible flow without considering inertial terms (Stokes flow) was modeled. The material of the venous valve (Domain 2) was considered to be hyperelastic (a material whose constitutive model of stress–strain relationship derives from a strain energy density function rather than Hooke’s law). The neo-Hookean was used with compressible material features, and the mathematical model is given below in Equations (5) and (6).

$$\rho_s \frac{\partial^2 \mathbf{u}_d}{\partial t^2} = \nabla(\mathbf{FS})^T + \mathbf{F}_V \tag{5}$$

$$\sigma = J^{-1} \mathbf{FSF}^T \tag{6}$$

where,

$$\begin{aligned} \mathbf{F} &= \mathbf{I} + \nabla \mathbf{u}_d; \quad \mathbf{S} = \mathbf{S}_{ext} + \left( \frac{\partial W_s}{\partial \epsilon} \right) \\ W_s &= \frac{1}{2} \mu (\mathbf{I}_1 - 3) - \mu \ln(J_{el}) + \frac{1}{2} \lambda [\ln(J_{el})]^2; \quad \epsilon = \frac{1}{2} (\mathbf{F}^T \mathbf{F} - \mathbf{I}) \\ J &= \det(\mathbf{F}); \quad \mu = \frac{E}{2(1+\nu)}; \quad \lambda = \frac{E\nu}{(1+\nu)(1-2\nu)} \end{aligned}$$

Lamé’s parameters for hyperelastic are  $\mu = 1.0$  MPa and  $\lambda = 1.5$  MPa, considering modulus of elasticity  $E = 2.6$  MPa and Poisson’s ratio  $\nu = 0.3$  [30], whereas the properties of the fluid were set as follows: the density of fluid  $1055 \text{ kg m}^{-3}$  (density of blood at  $37^\circ\text{C}$  [31,32]) and the dynamic viscosity of fluid  $2.78 \times 10^{-3} \text{ Pa}\cdot\text{s}$  (viscosity of blood at  $37^\circ\text{C}$ ). The flow velocity was  $16 \pm 4 \text{ cm/s}$ , which is a typical IJV velocity in humans in the supine body position [33]. The density of the valve leaflets was set at  $1200 \text{ kg m}^{-3}$  [34]. To simulate fluctuations of flow velocity in the modeled vein in a living subject resulting from the pulsation of the adjacent carotid artery and respiratory movements, the sine function of velocity at the inlet (Boundary 1) of the model was applied (Figure 2A). This sine function plotted the period of fluid velocity against time, as shown in Equation (7). The initial velocity of the fluid was  $12 \text{ cm/s}$ , which increased up to  $16 \text{ cm/s}$  (mean velocity) at  $t = 1.5 \text{ s}$  and finally reached  $20 \text{ cm/s}$  (maximum velocity of blood) at  $t = 3 \text{ s}$ , whereas it dropped back to  $12 \text{ cm/s}$  at  $t = 6 \text{ s}$ .

$$U_{inlet} = \left[ 8 \sin\left(\frac{t}{6} \pi\right) + 12 \right] \text{ cm/s} \tag{7}$$

The static pressure boundary condition was used at the outlet (Boundary 2) of the modeled blood vessel as shown in Figure 2A, and the pressure value was set at  $p = 0 \text{ Pa}$ . For the venous valve, both ends were fixed at the external wall of the model using  $U_{solid} = 0 \text{ cm/s}$  condition, while the rest of the valve was allowed to move freely within the fluid regime. All simulations were continued until  $6 \text{ s}$  and the graphical representations of the flow were analyzed. All the computations were executed in the Intel-INSPIRON (Intel, Santa Clara, CA, USA) equipped with the Intel-R Core-TM i7-11 Gen processor and the Intel-R Iris-XR Plus graphic card, and it took around  $11 \text{ h}$  of computational time for one case.

### 3. Results

In the model of vein without upstream stenosis and a symmetric 2-leaflets valve, the flow was undisturbed (Figures 4A, 5A and 6A). Valve leaflets opened and closed symmetrically due to the vortices developing downstream of the valve [35]. A similar flow pattern was seen in the model with minor 30% stenosis and a normal 2-leaflets valve. In this model, there were vortices located downstream of the stenosis, but they did not significantly disturb the outflow, and neither did these vortices influence the functioning of valve leaflets (Figures 4B, 5B and 6B).

In the case of more severe upstream stenosis, with 60% and 75% narrowing of the lumen, by contrast to the above-discussed models in which the centerline velocity was positioned centrally, here the centerline velocity was positioned asymmetrically and the areas of reverse flow and flow separation developed (Figures 4C,D, 5C,D and 6C,D).

Importantly, in the models with significant upstream stenoses, vortices making the flow highly asymmetric were present at the entire course of the models, and not only just downstream of the stenosis, as in the model without significant upstream narrowing. These asymmetric flow pattern resulted in asymmetric bending of elastic valve leaflets (Figure 7).

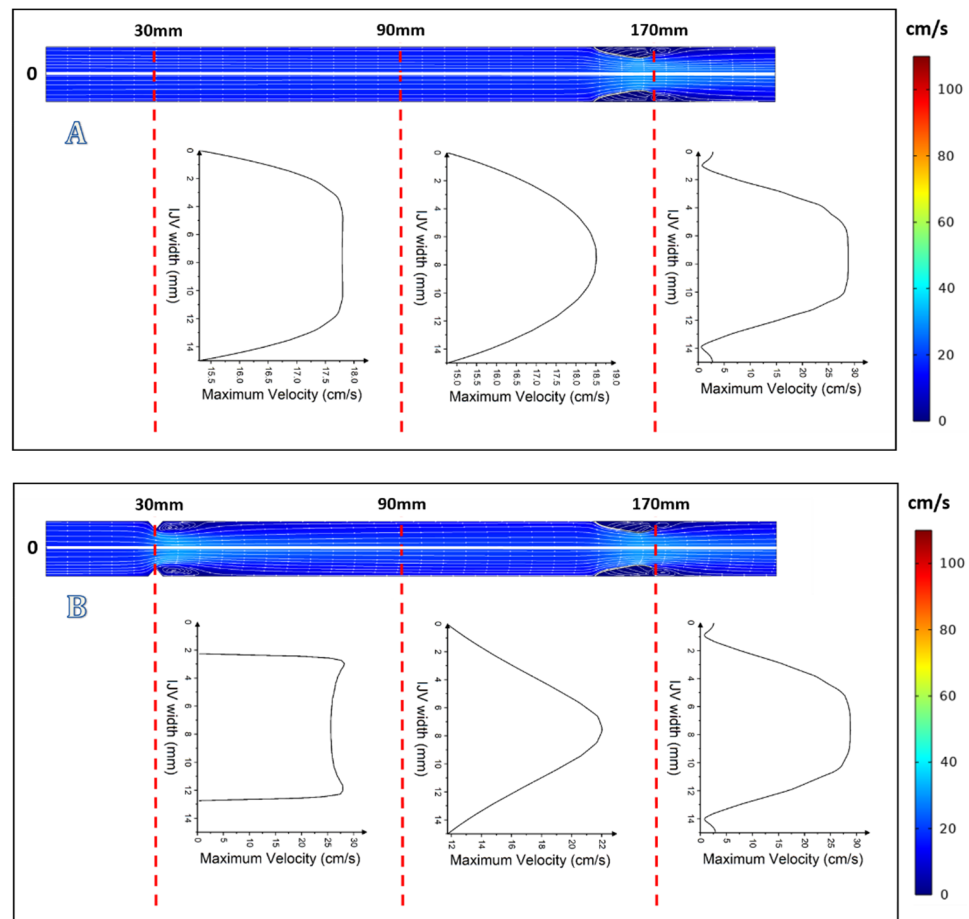
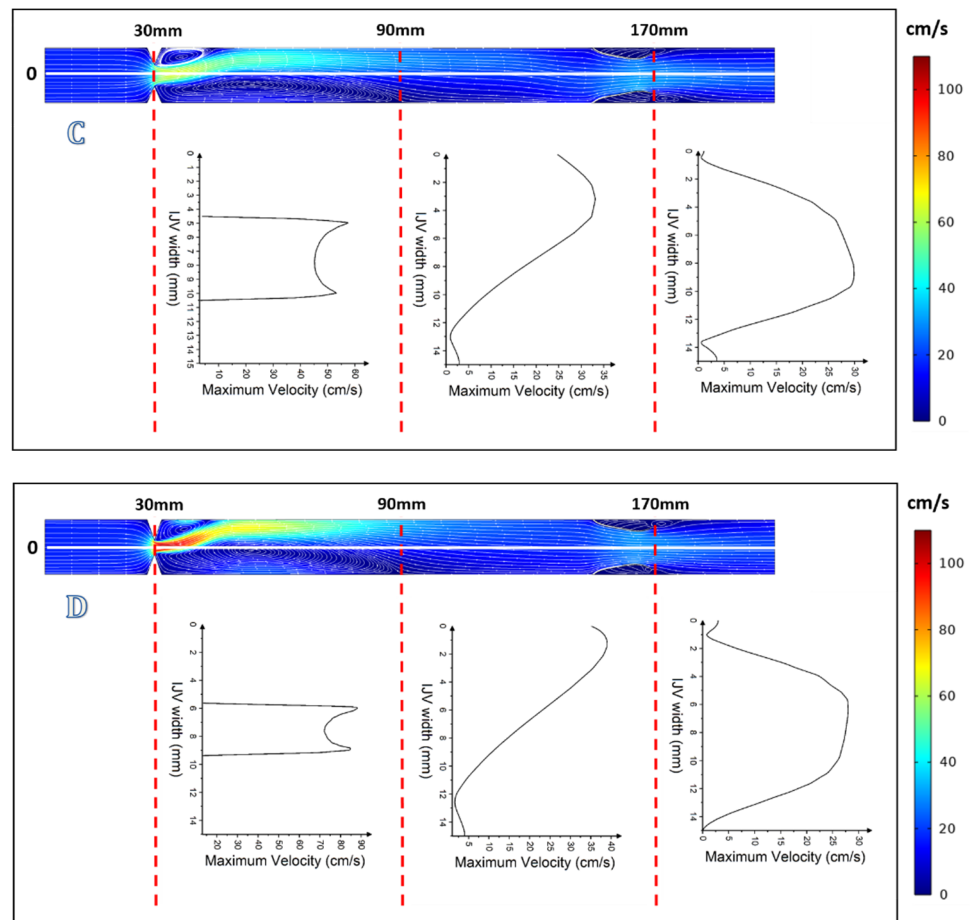
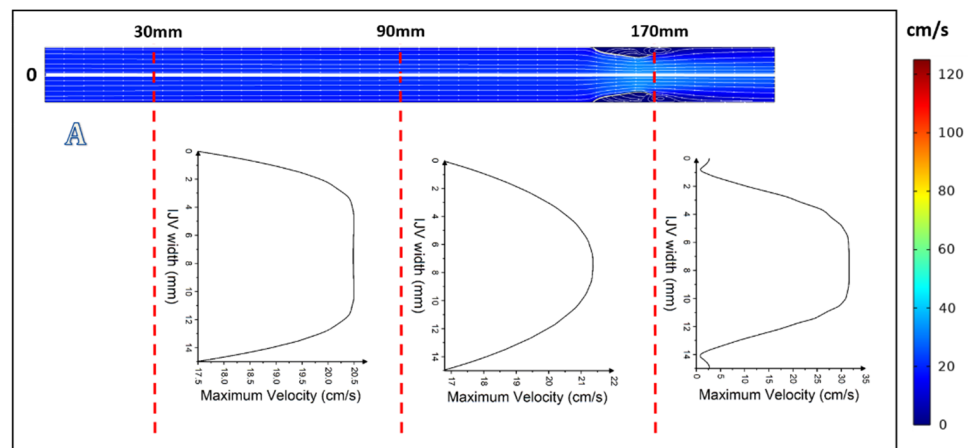


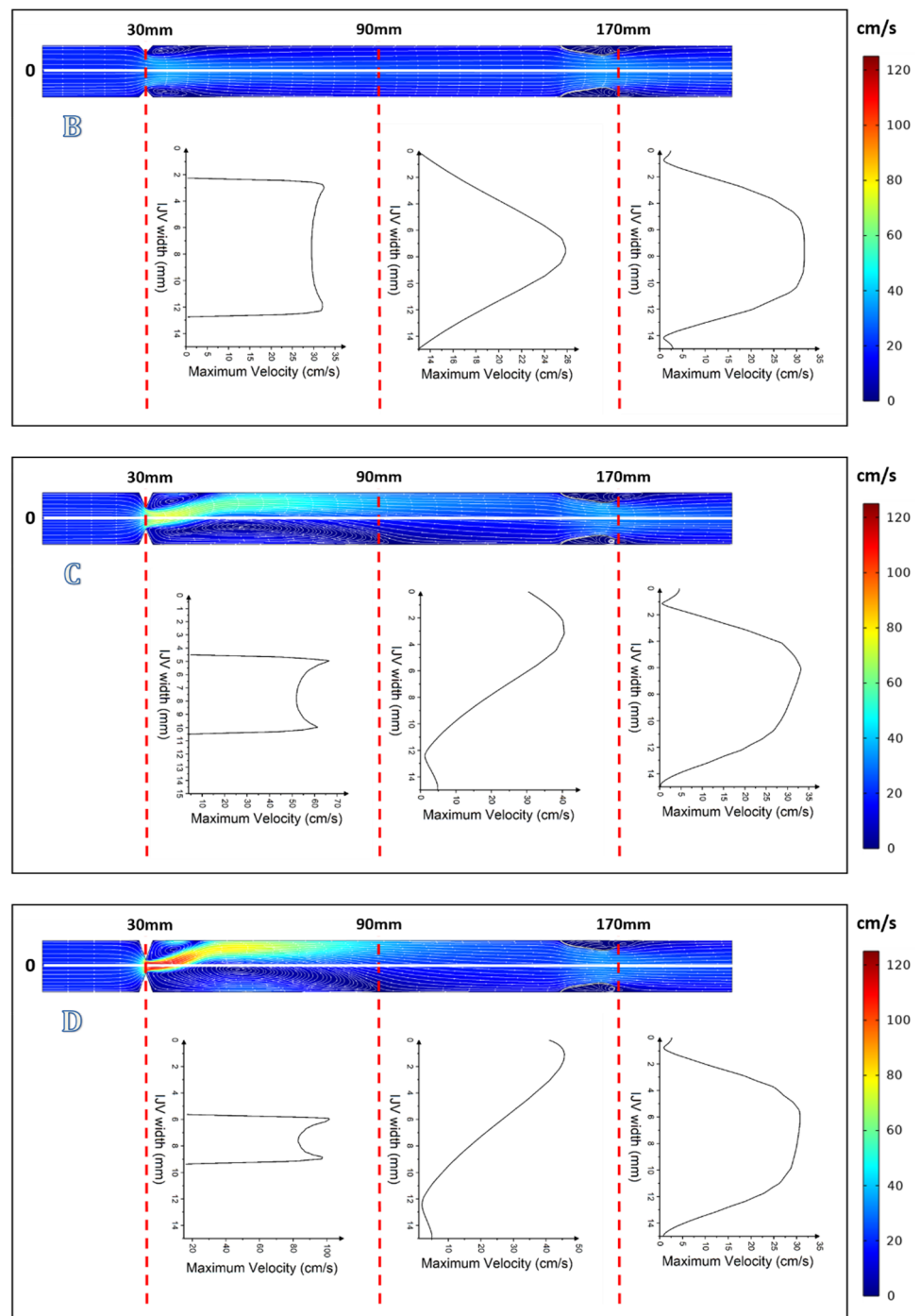
Figure 5. Cont.



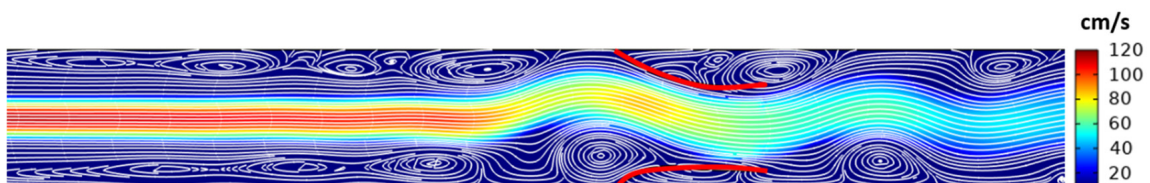
**Figure 5.** Graphical representation of flow with velocity profiles at  $t = 1.5$  s: (A) without upstream stenosis; (B) with 30% upstream stenosis; (C) with 60% upstream stenosis; and (D) with 75% upstream stenosis.



**Figure 6.** Cont.

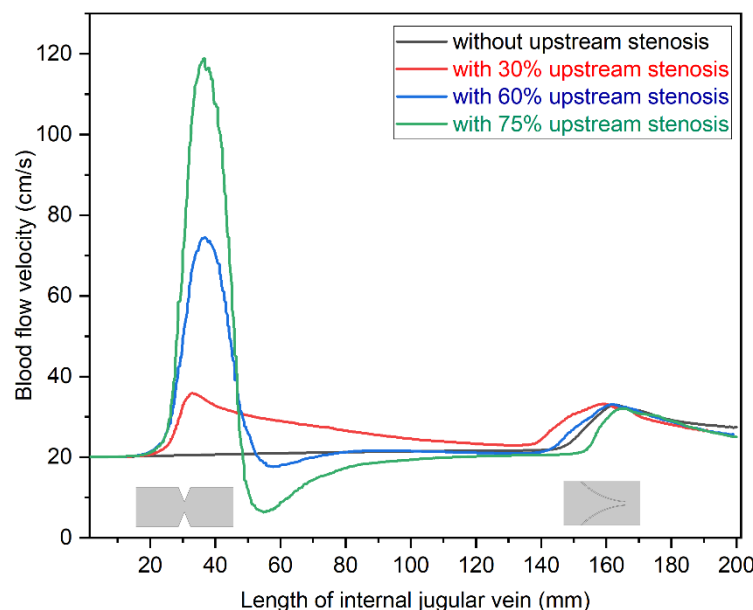


**Figure 6.** Graphical representation of flow with velocity profiles at  $t = 3$  s: (A) without upstream stenosis; (B) with 30% upstream stenosis; (C) with 60% upstream stenosis; and (D) with 75% upstream stenosis.



**Figure 7.** Asymmetric bending of valve leaflets (red) by vortices in the model D (with 75% upstream stenosis).

We also studied the relationship between the maximum velocities observed in the models of blood vessel depending on the degree of upstream stenosis. Graphical representation of the results is shown in Figure 8. The humps in flow velocity curve were observed at the stenosis and venous valve position as shown in this figure. The blood velocity increased significantly at stenosis for 60% and 75% cases, while there was only a minor increase of the velocity in the model with 30% stenosis. Interestingly, in two models with major stenosis (60% and 75%), velocity decreased just behind the stricture, which was not seen in the model with 30% stenosis. This phenomenon was probably related to flow separation in the cases with the major upstream stenoses.



**Figure 8.** Comparison of maximum velocity (20 cm/s) profiles against the length of the modeled internal jugular vein, recorded at  $t = 3$  s.

#### 4. Discussion

This study confirmed the results of our previous study [25], which was based on a different computational fluid mechanics (CFM) package. Similar to the findings of this research, we demonstrated that stenosis located at the beginning of the internal jugular vein can significantly affect the blood flow pattern. However, the most important finding is the phenomenon of valve leaflets distortion by asymmetric vortices evoked by nozzle-like strictures located upstream. To the best of our knowledge, this is the first *in silico* study on the investigation of the functioning of the jugular veins in the settings of IJV abnormal morphology. This was not possible to demonstrate on a previous CFM software, since the Flowsquare+ that was used in this study does not provide a possibility of building flexible structures.

These findings highlight the possible pathogenesis of abnormal jugular valves. Atypical structured jugular valves can be found in some healthy individuals, but these are primarily present in patients suffering from neuroinflammatory and neurodegenerative diseases [36–38]. Although some clinicians claimed a causative role for such aberrant jugular valves in neurological disorders, such an association has not been unequivocally proved [39]. The current consensus is that a majority of abnormal jugular valves represent congenital pathology, the so-called truncular malformations [40,41]. Still, research on such valves in multiple sclerosis patients suggested that their abnormality worsens with time [39]. Until now, the mechanism of such a progression has remained unclear. Our numerical simulation of blood flow in the IJV that exhibits significant stenosis in its upper segment offers a possible explanation: asymmetric vortices arising in the upper part of this vein, which are evoked by stenosis at the level of the jugular foramen (e.g., caused by an

elongated transverse process of the first vertebra), distort leaflets of the jugular valve. The pathological flow pattern around such distorted leaflets can theoretically alter the leaflets' physiology, leading to even more abnormal geometry. Indeed, jugular valves histopathological studies in multiple sclerosis patients revealed their abnormal ultrastructure, including defective endothelium and an inverted ratio between type I and type III collagen [42,43].

Our current work suggests that from a physical point of view there is an interplay between pathologies of IJV localized in the upper and lower part. To achieve a satisfactory clinical outcome in the patients, both types of lesions should be properly diagnosed and addressed. For example, stenosis at the beginning of the IJV would require resection of abnormal bony structures, while pathological jugular valves would require venous angioplasty. This can explain the low clinical efficacy of angioplasty procedures for the treatment of multiple sclerosis [23]. Of course, our findings should be confirmed by more precise investigations, including studies on real patients. Still, our report can provide a useful framework for future clinical surveys.

We acknowledge that there are limitations to our study. The findings of this research, albeit inspiring, should be ascertained using 3D CFD software. We utilized 2D models of the COMSOL Multiphysics software and considered the cylindrical plane to visualize the velocity profile in the modeled blood vessel. It should be mentioned that 2D simulations are widely used in the engineering sciences and are regarded to be within an order of magnitude of accuracy, as long as the problem is well-defined in the software and care is taken with regards to appropriate meshing and boundary conditions [44,45]. Still, there are known limitations of such a 2D approach. One of the solutions to this problem is the use of 2D-axisymmetric geometry, which limits these shortcomings, while very large computing resources and computing time, as in the case of 3D modeling, are not required [46,47]. This method should probably be used in future studies on the flow in the models of the IJV.

Additionally, morphology-based IJV models instead of simplified models would provide more detailed insight into the altered blood flow phenomena. Potentially, other properties of the IJV and surrounding tissues could contribute to abnormal outflow through this blood vessel. Besides, we studied one IJV blood flow, although in the living subjects blood flows out from the brain through two IJVs, as well as through the vertebral venous plexuses located on both sides of the spinal column. More precise and adequate modeling should consider these alternative outflow routes. It should be emphasized that a steady state was not achieved in our simulations due to the required computational expense. However, the computational results at 6 s provide a unique insight into the flow effects of strictures in the IJV. Finally, it should be mentioned that in this study the fluid was considered Newtonian. Blood is a non-Newtonian fluid. Since blood is shear-thinning fluid, slowing down its flow is associated with a higher flow resistance than that of a Newtonian fluid.

## 5. Conclusions

We demonstrated that our working hypothesis is credible and that impaired outflow from the brain through the internal jugular vein is likely to be primarily caused by pathological strictures in the upper part of these veins. In addition, jugular valve pathology can be exacerbated by flow disturbances evoked by strictures in the upper segments of these veins.

**Author Contributions:** Conceptualization, A.R. (Anas Rashid) and M.S.; methodology, S.A.I.; software, S.A.I.; validation, A.R. (Anas Rashid), A.R. (Aiman Rashid) and M.S.; formal analysis, A.R. (Anas Rashid), A.R. (Aiman Rashid) and S.A.I.; resources, A.R. (Anas Rashid); data curation, S.A.I.; writing—original draft preparation, A.R. (Anas Rashid) and M.S.; writing—review and editing, A.R. (Anas Rashid), S.A.I., A.R. (Aiman Rashid) and M.S.; visualization, A.R. (Anas Rashid), A.R. (Aiman Rashid) and S.A.I.; supervision, M.S.; project administration, M.S.; funding acquisition, A.R. (Anas Rashid). All authors have read and agreed to the published version of the manuscript.

**Funding:** Anas Rashid was supported by a Doctoral Fellowship funded by the Partnership for Knowledge (PFK) programme of the Agenzia Italiana per la Cooperazione allo Sviluppo (AICS), Ministero degli Affari Esteri e della Cooperazione Internazionale (MAECI), Italy.

**Institutional Review Board Statement:** Not applicable.

**Informed Consent Statement:** Not applicable.

**Data Availability Statement:** Metadata containing all graphic files depicting the flow in the modeled veins can be found in the repository: <https://reprod.icm.edu.pl/dataset.xhtml?persistentId=doi:10.18150/LFNDPV> (accessed on 21 June 2022). Preprint version of this paper is available in SSRN depository at: [https://papers.ssrn.com/sol3/papers.cfm?abstract\\_id=4143101](https://papers.ssrn.com/sol3/papers.cfm?abstract_id=4143101) (accessed on 22 June 2022).

**Conflicts of Interest:** The authors declare no conflict of interest.

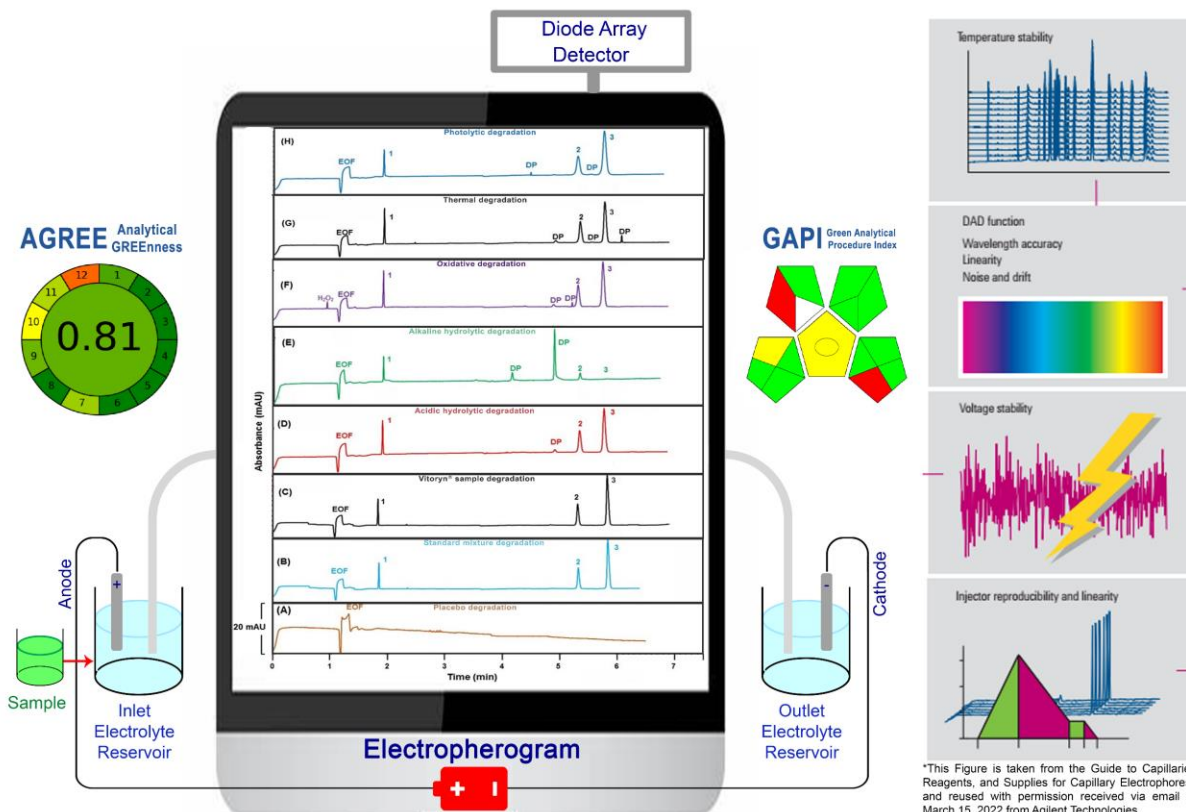
## References

- Zivadinov, R.; Chung, C.P. Potential Involvement of the Extracranial Venous System in Central Nervous System Disorders and Aging. *BMC Med.* **2013**, *11*, 260. [[CrossRef](#)] [[PubMed](#)]
- Beggs, C.; Chung, C.P.; Bergsland, N.; Wang, P.N.; Shepherd, S.; Cheng, C.Y.; Dwyer, M.G.; Hu, H.H.; Zivadinov, R. Jugular Venous Reflux and Brain Parenchyma Volumes in Elderly Patients with Mild Cognitive Impairment and Alzheimer's Disease. *BMC Neurol.* **2013**, *13*, 157. [[CrossRef](#)] [[PubMed](#)]
- Chung, C.P.; Beggs, C.; Wang, P.N.; Bergsland, N.; Shepherd, S.; Cheng, C.Y.; Ramasamy, D.P.; Dwyer, M.G.; Hu, H.H.; Wang, P.N. Jugular Venous Reflux and White Matter Abnormalities in Alzheimer's Disease: A Pilot Study. *J. Alzheimers Dis.* **2014**, *39*, 601–609. [[CrossRef](#)] [[PubMed](#)]
- Filipo, R.; Ciciarello, F.; Attanasio, G.; Mancini, P.; Covelli, E.; Agati, L.; Fedele, F.; Viccaro, M. Chronic Cerebrospinal Venous Insufficiency in Patients with Ménière's Disease. *Eur. Arch. Otorhinolaryngol.* **2015**, *272*, 77–82. [[CrossRef](#)] [[PubMed](#)]
- Alpini, D.C.; Bavera, P.M.; Hahn, A.; Mattei, V. Chronic Cerebrospinal Venous Insufficiency (CCSVI) in Meniere Disease. Case or Cause? *Sci. Med.* **2013**, *4*, 9–15.
- Li, M.; Sun, Y.; Chan, C.C.; Fan, C.; Ji, X.; Meng, R. Internal Jugular Vein Stenosis Associated with Elongated Styloid Process: Five Case Reports and Literature Review. *BMC Neurol.* **2019**, *19*, 112. [[CrossRef](#)]
- Feng, W.; Utriainen, D.; Trifan, G.; Elias, S.; Sethi, S.; Hewett, J.; Haacke, E.M. Characteristics of Flow through the Internal Jugular Veins at Cervical C2/C3 and C5/C6 Levels for Multiple Sclerosis Patients Using MR Phase Contrast Imaging. *Neurol. Res.* **2012**, *34*, 802–809. [[CrossRef](#)]
- Haacke, E.M.; Feng, W.; Utriainen, D.; Trifan, G.; Wu, Z.; Latif, Z.; Katkuri, Y.; Hewett, J.; Hubbard, D. Patients with Multiple Sclerosis with Structural Venous Abnormalities on MR Imaging Exhibit an Abnormal Flow Distribution of the Internal Jugular Veins. *J. Vasc. Interv. Radiol.* **2012**, *23*, 60–68. [[CrossRef](#)]
- Zivadinov, R.; Bastianello, S.; Dake, M.D.; Ferral, H.; Haacke, E.M.; Haskal, Z.J.; Hubbard, D.; Liasis, N.; Mandato, K.; Sclafani, S.; et al. Recommendations for Multimodal Noninvasive and Invasive Screening for Detection of Extracranial Venous Abnormalities Indicative of Chronic Cerebrospinal Venous Insufficiency: A Position Statement of the International Society for Neurovascular Disease. *J. Vasc. Interv. Radiol.* **2014**, *25*, 1785–1794. [[CrossRef](#)]
- Zhou, D.; Ding, J.Y.; Ya, J.Y.; Pan, L.Q.; Yan, F.; Yang, Q.; Ding, Y.C.; Ji, X.M.; Meng, R. Understanding jugular venous outflow disturbance. *CNS Neurosci. Ther.* **2018**, *24*, 473. [[CrossRef](#)]
- Veroux, P.; Giaquinta, A.; Perricone, D.; Lupo, L.; Gentile, F.; Virgilio, C.; Carbonaro, A.; De Pasquale, C.; Veroux, M. Internal Jugular Veins Out Flow in Patients with Multiple Sclerosis: A Catheter Venography Study. *J. Vasc. Interv. Radiol.* **2013**, *24*, 1790–1797. [[CrossRef](#)] [[PubMed](#)]
- Simka, M.; Latacz, P.; Ludyga, T.; Kazibudzki, M.; Świerad, M.; Janas, P.; Piegza, J. Prevalence of Extracranial Venous Abnormalities: Results from a Sample of 586 Multiple Sclerosis Patients. *Funct. Neurol.* **2011**, *26*, 197–203. [[PubMed](#)]
- Plog, B.A.; Nedergaard, M. The Glymphatic System in Central Nervous System Health and Disease: Past, Present, and Future. *Annu. Rev. Pathol.* **2018**, *13*, 379–394. [[CrossRef](#)] [[PubMed](#)]
- Fultz, N.E.; Bonmassar, G.; Setsompop, K.; Stickgold, R.A.; Rosen, B.R.; Polimeni, J.R.; Lewis, L.D. Coupled Electrophysiological, Hemodynamic, and Cerebrospinal Fluid Oscillations in Human Sleep. *Science* **2019**, *366*, 628–631. [[CrossRef](#)]
- Beggs, C.B.; Magnano, C.; Shepherd, S.J.; Marr, K.; Valnarov, V.; Hojnacki, D.; Bergsland, N.; Belov, P.; Grisafi, S.; Dwyer, M.G.; et al. Aqueductal Cerebrospinal Fluid Pulsatility in Healthy Individuals is Affected by Impaired Cerebral Venous Outflow. *J. Magn. Reson. Imaging* **2014**, *40*, 1215–1222. [[CrossRef](#)]
- Beggs, C.B.; Magnano, C.; Belov, P.; Krawiecki, J.; Ramasamy, D.P.; Hagemeyer, J.; Zivadinov, R. Internal Jugular Vein Cross-Sectional Area and Cerebrospinal Fluid Pulsatility in the Aqueduct of Sylvius: A Comparative Study between Healthy Subjects and Multiple Sclerosis Patients. *PLoS ONE* **2016**, *11*, e0153960. [[CrossRef](#)]
- Beggs, C.B.; Shepherd, S.J.; Cecconi, P.; Lagana, M.M. Predicting the Aqueductal Cerebrospinal Fluid Pulse: A Statistical Approach. *Appl. Sci.* **2019**, *9*, 2131. [[CrossRef](#)]



18. Zamboni, P.; Galeotti, R.; Menegatti, E.; Malagoni, A.M.; Gianesini, S.; Bartolomei, I.; Mascoli, F.; Salvi, F. A Prospective Open-Label Study of Endovascular Treatment of Chronic Cerebrospinal Venous Insufficiency. *J. Vasc. Surg.* **2009**, *50*, 1348–1358. [[CrossRef](#)]
19. Siddiqui, A.H.; Zivadinov, R.; Benedict, R.H.B.; Karmon, Y.; Yu, J.; Hartney, M.L.; Marr, K.L.; Valnarov, V.; Kennedy, C.L.; Ramanathan, M.; et al. Prospective Randomized Trial of Venous Angioplasty in MS (PREMiSe). *Neurology* **2014**, *83*, 441–449. [[CrossRef](#)]
20. Traboulsee, A.L.; Machan, L.; Girard, J.M.; Raymond, J.; Vosoughi, R.; Hardy, B.W.; Emond, F.; Gariepy, J.L.; Bone, J.N.; Siskin, G.; et al. Safety and Efficacy of Venoplasty in MS: A Randomized, Double-Blind, Sham-Controlled Phase II Trial. *Neurology* **2018**, *91*, e1660–e1668. [[CrossRef](#)]
21. Zamboni, P.; Tesio, L.; Galimberti, S.; Massacesi, L.; Salvi, F.; D’Alessandro, R.; Cenni, P.; Galeotti, R.; Papini, D.; D’Amico, R.; et al. Efficacy and Safety of Extracranial Vein Angioplasty in Multiple Sclerosis: A Randomized Clinical Trial. *JAMA Neurol.* **2018**, *75*, 35–43. [[CrossRef](#)] [[PubMed](#)]
22. Napoli, V.; Berchiolli, R.; Carboncini, M.C.; Sartucci, F.; Marconi, M.; Bocci, T.; Perrone, O.; Mannoni, N.; Congestri, C.; Benedetti, R.; et al. Percutaneous Venous Angioplasty in Patients with Multiple Sclerosis and Chronic Cerebrospinal Venous Insufficiency: A Randomized Wait List Control Study. *Ann. Vasc. Surg.* **2020**, *62*, 275–286. [[CrossRef](#)] [[PubMed](#)]
23. Simka, M. An Overview of Randomized Controlled Trials on Endovascular Treatment for Chronic Cerebrospinal Venous Insufficiency in Multiple Sclerosis Patients. *Phlebologie* **2021**, *50*, 76–80. [[CrossRef](#)]
24. Zamboni, P.; Galeotti, R.; Salvi, F.; Giaquinta, A.; Setacci, C.; Alborino, S.; Guzzardi, G.; Sclafani, S.J.; Maietti, E.; Veroux, P. Brave Dreams Research Group. Effects of Venous Angioplasty on Cerebral Lesions in Multiple Sclerosis: Expanded Analysis of the Brave Dreams Double-Blind, Sham-Controlled Randomized Trial. *J. Endovasc. Ther.* **2020**, *27*, 1526602819890110. [[CrossRef](#)] [[PubMed](#)]
25. Simka, M.; Latacz, P. Numerical Modeling of Blood Flow in the Internal Jugular Vein with the Use of Computational Fluid Mechanics Software. *Phlebologie* **2021**, *36*, 541–548. [[CrossRef](#)] [[PubMed](#)]
26. Ding, J.Y.; Zhou, D.; Pan, L.Q.; Ya, J.Y.; Liu, C.; Yan, F.; Fan, C.Q.; Ding, Y.C.; Ji, X.M.; Meng, R. Cervical Spondylotic Internal Jugular Venous Compression Syndrome. *CNS Neurosci. Ther.* **2020**, *26*, 47–54. [[CrossRef](#)] [[PubMed](#)]
27. Scerrati, A.; Norri, N.; Mongardi, L.; Dones, F.; Ricciardi, L.; Trevisi, G.; Menegatti, E.; Zamboni, P.; Cavallo, M.A.; De Bonis, P. Styloidogenic-cervical spondylotic internal jugular venous compression, a vascular disease related to several clinical neurological manifestations: Diagnosis and treatment—a comprehensive literature review. *Ann. Transl. Med.* **2021**, *9*, 718. [[CrossRef](#)]
28. De Bonis, P.; Menegatti, E.; Cavallo, M.A.; Sisini, F.; Trapella, G.; Scerrati, A.; Zamboni, P. JEDI (Jugular Entrapment, Dilated Ventricles, Intracranial Hypertension) Syndrome: A New Clinical Entity? A Case Report. *Acta Neurochir.* **2019**, *161*, 1367–1370. [[CrossRef](#)]
29. Jeon, J.C.; Choi, W.I.; Lee, J.H.; Lee, S.H. Anatomical Morphology Analysis of Internal Jugular Veins and Factors Affecting Internal Jugular Vein Size. *Medicina* **2020**, *56*, 135. [[CrossRef](#)]
30. Gataulin, Y.A.; Yukhnev, A.D.; Smirnov, S.I.; Rosukhovskiy, D.A. Numerical analysis of the leaflet elasticity effect on the flow in the model of a venous valve. *J. Phys. Conf. Ser.* **2019**, *1359*, 012010. [[CrossRef](#)]
31. Phillips, R.A.; Van Slyke, D.D.; Hamilton, P.B.; Dole, V.P.; Emerson, K., Jr.; Archibald, R.M. Measurement of specific gravities of whole blood and plasma by standard copper sulfate solutions. *J. Biol. Chem.* **1950**, *183*, 305–330. [[CrossRef](#)]
32. Trudnowski, R.J.; Rico, R.C. Specific Gravity of Blood and Plasma at 4 and 37 °C. *Clin. Chem.* **1974**, *20*, 615–616. [[CrossRef](#)]
33. Ciuti, G.; Righi, D.; Forzoni, L.; Fabbri, A.; Pignone, A.M. Differences Between Internal Jugular Vein and Vertebral Vein Flow Examined in Real Time with the Use of Multigate Ultrasound Color Doppler. *Am. J. Neuroradiol.* **2013**, *34*, 2000–2004. [[CrossRef](#)] [[PubMed](#)]
34. Tikhomolova, L.G.; Gataulin, Y.A.; Yukhnev, A.D.; Rosukhovskiy, D.A. Fluid–Structure Interaction Modelling of the Venous Valve with Elastic Leaflets. In *Proceedings of the Journal of Physics: Conference Series*; IOP Publishing: Bristol, UK, 2020; Volume 1697, pp. 1–6.
35. Lurie, F.; Kistner, R.L.; Eklof, B.; Kessler, D. Mechanism of Venous Valve Closure and Role of the Valve in Circulation: A New Concept. *J. Vasc. Surg.* **2003**, *38*, 955–961. [[CrossRef](#)]
36. Zivadinov, R.; Marr, K.; Cutter, G.; Ramanathan, M.; Benedict, R.H.B.; Kennedy, C.; Elfadil, M.; Yeh, A.E.; Reuther, J.; Brooks, C.; et al. Prevalence, Sensitivity, and Specificity of Chronic Cerebrospinal Venous Insufficiency in MS. *Neurology* **2011**, *77*, 138–144. [[CrossRef](#)]
37. Simka, M.; Hubbard, D.; Siddiqui, A.H.; Dake, M.D.; Sclafani, S.J.A.; Al-Omari, M.; Eisele, C.G.; Haskal, Z.J.; Ludyga, T.; Milošević, Z.V.; et al. Catheter Venography for the Assessment of Internal Jugular Veins and Azygous Vein: Position Statement by Expert Panel of the International Society for Neurovascular Disease. *Vasa* **2013**, *42*, 168–176. [[CrossRef](#)]
38. Mancini, M.; Lanzillo, R.; Liuzzi, R.; Di Donato, O.; Ragucci, M.; Monti, S.; Salvatore, E.; Morra, V.B.; Salvatore, M. Internal Jugular Vein Blood Flow in Multiple Sclerosis Patients and Matched Controls. *PLoS ONE* **2014**, *9*, e92730. [[CrossRef](#)]
39. Simka, M.; Ludyga, T.; Latacz, P.; Kazibudzki, M.; Majewski, E.; Zaniewski, M. Chronic Cerebrospinal Venous Insufficiency is Unlikely to be a Direct Trigger of Multiple Sclerosis. *Mult. Scler. Relat. Disord.* **2013**, *2*, 334–339. [[CrossRef](#)]
40. Simka, M.; Ludyga, T.; Kazibudzki, M.; Latacz, P.; Świerad, M. Multiple Sclerosis, An Unlikely Cause of Chronic Cerebrospinal Venous Insufficiency: Retrospective Analysis of Catheter Venography. *JRSM Short Rep.* **2012**, *3*, 1–6. [[CrossRef](#)]

41. Lee, B.B.; Baumgartner, I.; Berlien, P.; Bianchini, G.; Burrows, P.; Gloviczki, P.; Huang, Y.; Laredo, J.; Loose, D.A.; Markovic, J.; et al. Diagnosis and Treatment of Venous Malformations. Consensus Document of the International Union of Phlebology (IUP): Updated 2013. *Int. Angiol.* **2015**, *34*, 97–149.
42. Zamboni, P.; Tisato, V.; Menegatti, E.; Mascoli, F.; Giancesini, S.; Salvi, F.; Secchiero, P. Ultrastructure of Internal Jugular Vein Defective Valves. *Phlebology* **2015**, *30*, 644–647. [[CrossRef](#)] [[PubMed](#)]
43. Coen, M.; Menegatti, E.; Salvi, F.; Mascoli, F.; Zamboni, P.; Gabbiani, G.; Bochaton-Piallat, M.L. Altered Collagen Expression in Jugular Veins in Multiple Sclerosis. *Cardiovasc. Pathol.* **2013**, *22*, 33–38. [[CrossRef](#)] [[PubMed](#)]
44. Pérez, M.G.; Vakkilainen, E. A comparison of turbulence models and two and three dimensional meshes for unsteady CFD ash deposition tools. *Fuel* **2019**, *237*, 806–811. [[CrossRef](#)]
45. Abdi, R.; Krzaczek, M.; Tejchman, J. Comparative study of high-pressure fluid flow in densely packed granules using a 3D CFD model in a continuous medium and a simplified 2D DEM-CFD approach. *Granul. Matter* **2022**, *24*, 15. [[CrossRef](#)]
46. Trozzo, R.; Boedec, G.; Leonetti, M.; Jaeger, M. Axisymmetric boundary element method for vesicles in a capillary. *J. Comput. Phys.* **2015**, *289*, 62–82. [[CrossRef](#)]
47. Susan-Resiga, R.F.; Muntean, S.; Tănasă, C. Three-dimensional versus two-dimensional axisymmetric analysis for decelerated swirling flows. Conference on Modelling Fluid Flow (CMFF'09). In Proceedings of the 14th International Conference on Fluid Flow Technologies, Budapest, Hungary, 9–12 September 2009.



\*This Figure is taken from the Guide to Capillaries, Reagents, and Supplies for Capillary Electrophoresis and raised with permission received via email on March 15, 2022 from Agilent Technologies.

## GRAPHICAL ABSTRACT



# Capillary Electrophoresis Method for Simultaneous Quantification of Hypcholesterolemic Drugs in Binary Mixture Formulation: Fast, Green, and Cost-Effective Alternative to HPLC

Antonio Marcos Callejo de Souza<sup>1</sup> · Frank Alonso Gavilano Fajardo<sup>1</sup> · Anas Rashid<sup>2</sup> · Marina Franco Maggi Tavares<sup>3</sup> · María Segunda Aurora Prado<sup>1</sup>

Received: 29 December 2022 / Revised: 30 January 2023 / Accepted: 9 February 2023  
© The Author(s), under exclusive licence to Springer-Verlag GmbH Germany, part of Springer Nature 2023

## Abstract

A fast and sustainable environment-friendly micellar electrokinetic chromatography coupled with a diode array detector was investigated and validated in accordance with ICH requirements for the simultaneous quantification of ezetimibe and simvastatin in a tablet binary mixture formulation. Drugs' separation from their internal standard and degradation products was achieved using the optimized electrophoretic conditions: 50  $\mu\text{m}$  i.d.  $\times$  30 cm fused-silica capillary, background electrolyte composed of 20  $\text{mmol L}^{-1}$  sodium tetraborate buffer solution (pH 9, adjusted with *o*-phosphoric acid), 30  $\text{mmol L}^{-1}$  sodium dodecyl sulfate, 12% acetonitrile; with detection at 238 nm and voltage of +30 kV. Drugs were separated in less than 6 min. The method was linear with determination coefficients 0.9956 and 0.9920 for ezetimibe and simvastatin, respectively; and precise (intra-day 1.05% and 0.38%; inter-day 1.20% and 0.69%) for ezetimibe and simvastatin, respectively. Accuracy was tested through recovery and mean values ( $101.0 \pm 0.77\%$  for ezetimibe and  $100.4 \pm 0.35\%$  for simvastatin) were obtained. The proposed method is the first that determined ezetimibe and simvastatin in presence of their degradation products. This method can be successfully used in quality control laboratories as an alternative to HPLC technique for the simultaneous quantification of ezetimibe and simvastatin in their combined drug products and could also be used as a stability-indicating method. The proposed method greenness profile was confirmed using Green Analytical Procedure Index and Analytical GREENness tools with a final score of 11 and 0.81, respectively.

**Keywords** Hypercholesterolemia · Micellar electrokinetic chromatography · Ezetimibe · Simvastatin · Binary mixture formulation · Greenness evaluation

## Introduction

Cardiovascular disease appears to be the principal cause of death in the world involving hypercholesterolemia as a major risk factor [1]. It should be preferred to prescribe efficacious doses of statins to minimize low-density lipoprotein

as per international treatment guidelines on cardiovascular disease prevention [2]. Contrarily, 2nd or 3rd lipid-lowering drugs, i.e., fibrates, bile acid sequestrants, and ezetimibe are preferred over statin monotherapy for the management of high cardiovascular risk patients with hypercholesterolemia [3]. Since 2004, Food and Drug Administration approved ezetimibe/simvastatin combined tablet dosage form with ezetimibe fixed dose (10 mg) and simvastatin variable dose (10/20/40 mg) for both primary and secondary forms of hypercholesterolemia therapeutic management [4]. Last decade, the combination therapy of these drugs has been prescribed to maintain low-density lipoprotein in patients resistant to statin monotherapy or statin dose related side effects that showed successful clinical outcome [5].

Chemically, ezetimibe (Fig. 1A) named as (3*R*,4*S*)-1-(4-fluorophenyl)-3-[(3*R*)-3-(4-fluorophenyl)-3-hydroxypropyl]-4-(4-hydroxyphenyl)azetidin-2-one [6]

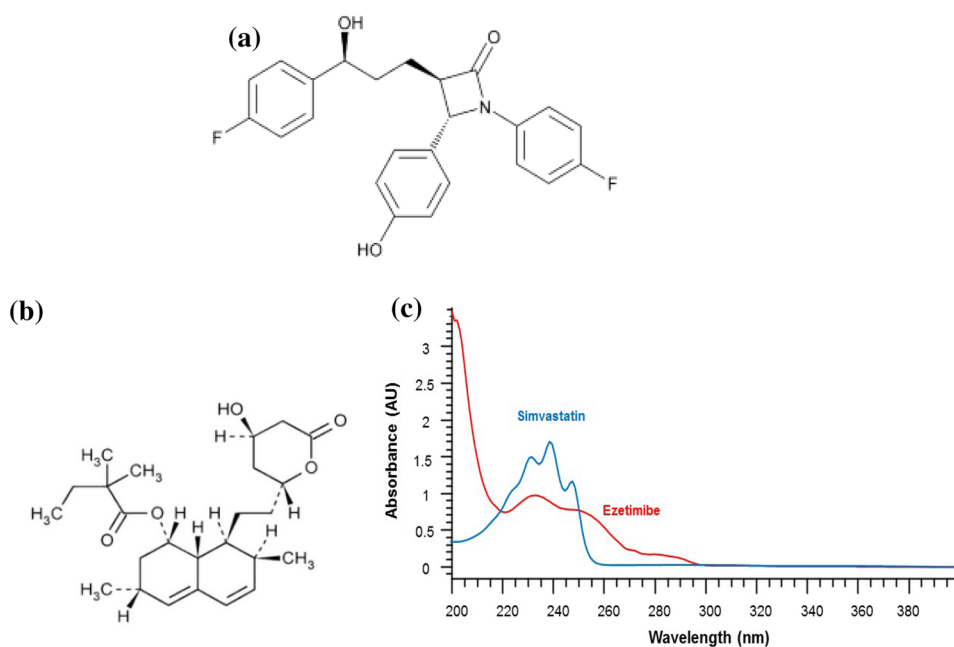
✉ María Segunda Aurora Prado  
msaprad06@usp.br

<sup>1</sup> Department of Pharmacy, School of Pharmaceutical Sciences, University of São Paulo, Av. Prof. Lineu Prestes 580, Block 13, Butantã, São Paulo 05508-000, Brazil

<sup>2</sup> Department of Neuroscience "Rita Levi Montalcini", School of Medicine and Surgery, University of Torino, Torino, Italy

<sup>3</sup> Department of Fundamental Chemistry, Institute of Chemistry, University of São Paulo, São Paulo, Brazil

**Fig. 1** Chemical structure of ezetimibe **A**, simvastatin **B**, and spectra overlap **C**



which inhibits cholesterol absorption and decreases excessive accumulation in blood vessels [7]. This distinct mechanism of action results in a synergistic cholesterol lowering effect when used together with statins that inhibits cholesterol synthesis in the liver [5].

Simvastatin (Fig. 1B) named as [(1*S*,3*R*,7*S*,8*S*,8*aR*)-8-[2-[(2*R*,4*R*)-4-hydroxy-6-oxooxan-2-yl]ethyl]-3,7-dimethyl-1,2,3,7,8,8*a*-hexahydronaphthalen-1-yl] 2,2-dimethylbutanoate [6] which inhibits 3-hydroxy-3-methylglutaryl-coenzyme A reductase for the treatment of hyperlipidemia.

The literature review reveals that ezetimibe and simvastatin were officially listed in the USP [6]. Furthermore, several analytical approaches have been recommended for the simultaneous determination of both drugs in combined pharmaceutical formulations and/or biological fluids by TLC [8], HPLC [8–12], UPLC [13], UPLC–MS/MS [14], UPLC–Q–TRAP/MS [1], LC–MS [15], LC–ESI–MS/MS [16], and HPLC–MS/MS [17]. Some of these methods require extensive instrumentation and time-consuming sample pretreatment methodologies, hence not ideal for routine use. The literature also reveals that the pharmaceutical drugs under investigation were simultaneously analyzed by UV spectrophotometric [18, 19] and capillary electrophoretic [20] methods.

The capillary electrophoresis is rapidly gaining importance as an alternative green analytical separation technique and used in several pharmaceutical and biopharmaceutical analysis [21]. It has various advantages over conventional chromatographic methods such as short analysis time, low reagent consumption, without organic solvents, small sample volume, long-lasting capillary columns, high separation

efficiency (millions of theoretical plates), and faster sample development [22], consequently diminishing the impact on environment [23].

At the present, only one capillary electrophoresis method has been described for simultaneous determination of ezetimibe and simvastatin in tablets, and the analytes were determined in a long time, i.e., approximately 10 min [20], this might be due to longer capillary column. Therefore, in this work, we proposed a validated micellar electrokinetic chromatography method, mode of capillary electrophoresis, for the simple and fast simultaneous determination of ezetimibe and simvastatin in binary mixtures under optimized analytical conditions. Moreover, the stability-indicating potential of the proposed method was first time investigated under stress degradation conditions (thermal, oxidative, photolytic, alkaline and acidic hydrolysis) for both ezetimibe and simvastatin, while highlighting the use of green background electrolyte. The proposed method greenness was also determined by using Green Analytical Procedure Index and Analytical GREENness approaches.

## Materials and Methods

### Chemicals, Reagents and Samples

The active pharmaceutical ingredients ezetimibe and simvastatin with purities of 100.0% and 99.8%, respectively, were donated by Merck Sharp & Dohme (Sao Paulo, Brazil), internal standard losartan potassium was obtained from Sigma-Aldrich (Sao Paulo, Brazil), and Vyturin® (Merck Sharp & Dohme, Sao Paulo, Brazil) tablet (ezetimibe 10 mg

and simvastatin 20 mg) were procured from community pharmacy. Analytical grade methanol, hydrogen peroxide, hydrochloric acid, acetonitrile was brought from Merck (Sao Paulo, Brazil); while *o*-phosphoric acid, sodium dodecyl sulfate, sodium tetraborate-10-hydrate, dibasic sodium phosphate, and sodium hydroxide were procured from Sigma-Aldrich (Sao Paulo, Brazil). Deionized water was obtained from Milli-Q<sup>®</sup> (Millipore Corp., Bedford, MA, USA) ultrapure purification system.

### Instrument

P/ACE<sup>™</sup> MDQ (Beckman Coulter, Inc., Fullerton, CA, USA) capillary electrophoresis system equipped with diode array detector and 32 Karat<sup>™</sup> software (ver. 8.0) was employed for data acquisition.

### Condition of Electrophoretic Separation

50  $\mu\text{m}$  internal diameter  $\times$  42 cm total (30 cm effective) length uncoated fused-silica capillary (Polymicro Technologies, Phoenix, AZ, USA) was used by adjusting temperature (30 °C) and voltage (+30 kV) with detection at 238 nm to perform the electrophoretic separation. The samples were injected by applying pressure of 0.3 psi for 3 s (1 psi = 6894.76 Pa) at cathodic side.

### Background Electrolyte Preparation

Aqueous stock solutions (100 mmol L<sup>-1</sup>) of sodium tetraborate buffer (pH 9, adjusted with *o*-phosphoric acid) and sodium dodecyl sulfate were separately prepared. The pH was measured using Gehaka<sup>®</sup> Mettler Toledo pH meter (Sao Paulo, Brazil). The optimized background electrolyte (30 mmol L<sup>-1</sup> sodium dodecyl sulfate, 20 mmol L<sup>-1</sup> sodium tetraborate buffer solution pH 9 and 12% acetonitrile) was prepared by transferring sodium tetraborate (5 mL) and sodium dodecyl sulfate (7.5 mL) stock solutions into a 25 mL volumetric flask, deionized water (8 mL), pH 9 adjusted with *o*-phosphoric acid solution, then acetonitrile (3 mL) was added, and deionized water was used to complete the volume. This mixture was sonicated for 10 min and filtered through a 0.45  $\mu\text{m}$  polyvinylidene fluoride filter before injected on the capillary electrophoresis instrument.

### Capillary Conditioning

Before using, new capillary was conditioned with NaOH 1 mol L<sup>-1</sup> for 30 min, followed by deionized water for 20 min and finally with background electrolyte for 30 min. At the beginning of each working day, the capillary was rinsed with NaOH 1 mol L<sup>-1</sup> for 15 min, deionized water for 10 min and then 20 min with background electrolyte.

Between runs, the capillary was washed with NaOH 1 mol L<sup>-1</sup> (1 min) and with the running buffer (1.5 min) to ensure reproducibility of the assay. Finally, at the end of the day, the capillary was flushed with NaOH 1 mol L<sup>-1</sup> for 10 min and water for 10 min.

### Preparation of Stock Standard and Test-Mixture Solutions

Internal standard, ezetimibe and simvastatin stock standard solutions (1000  $\mu\text{g mL}^{-1}$ ) were separately prepared in diluent methanol–water (25:75, v/v) by weighing 10 mg of each one into three 10 mL amber volumetric flasks. The solutions were sonicated for 3 min to aid dissolution then filtered through 0.45  $\mu\text{m}$  polyvinylidene fluoride filters and finally stored at 4 °C. The solutions were found stable for up to 15 days.

For the test-mixture, aliquots from each stock standard solution were transferred into a 2 mL amber volumetric flask and diluted to volume with diluent. The final concentrations were 100  $\mu\text{g mL}^{-1}$  for ezetimibe and internal standard, while 200  $\mu\text{g mL}^{-1}$  for simvastatin. The test-mixture was sonicated for 3 min, filtered in a 0.45  $\mu\text{m}$  polyvinylidene fluoride filter and injected on the capillary electrophoresis instrument.

### Pharmaceutical and Placebo Stock and Working Preparation

Twenty tablets of Vitoryn<sup>®</sup> containing 10/20 mg of ezetimibe/simvastatin were weighed and finely powdered. An amount of powder corresponding to 10 mg of ezetimibe and 20 mg of simvastatin was transferred into 10 mL amber volumetric flask and added 5 mL of methanol, the mixture was sonicated for 15 min to aid dissolution with occasional shaking, and diluted to volume with the same solvent. The solution was filtered through a 0.45  $\mu\text{m}$  polyvinylidene fluoride filter. The obtained concentration was 1000  $\mu\text{g mL}^{-1}$  for ezetimibe and 2000  $\mu\text{g mL}^{-1}$  for simvastatin.

Placebo matrix was prepared according to the following formula: microcrystalline cellulose (46.8%), lactose monohydrate (45%), magnesium stearate (2%), propyl galate (0.1%), citric acid (1%), sodium croscarmellose (3%), hydroxypropyl methylcellulose (2%) and butylhydroxyanisole (0.1%).

An aliquot of 200  $\mu\text{L}$  from sample stock solution was volumetrically transferred into a 2 mL amber volumetric flask, and 200  $\mu\text{L}$  of internal standard stock solution was added and the volume was completed with diluent to prepare the working sample solution. The final concentrations

were  $100 \mu\text{g mL}^{-1}$  for ezetimibe and internal standard, while  $200 \mu\text{g mL}^{-1}$  for simvastatin. The solution was filtered in a  $0.45 \mu\text{m}$  polyvinylidene fluoride filter before being injected.

## Method Validation

### System Suitability

The system suitability test was carried out to ensure the system resolution and reproducibility. The test was performed by injecting six replicates of working mix standard solutions of simvastatin ( $200 \mu\text{g mL}^{-1}$ ), ezetimibe and internal standard ( $100 \mu\text{g mL}^{-1}$ ). The assessed parameters were theoretical plates (N), peak area, migration time, resolution (Rs) and tailing factor.

### Specificity/Selectivity

The specificity of proposed method for the determination of ezetimibe and simvastatin was assessed by injecting the Vitoryn<sup>®</sup> sample, placebo, standard solutions and diluent into the capillary electrophoresis system.

Selectivity and forced degradation stability indicating studies for ezetimibe and simvastatin were applied under hydrolytic (alkaline and acidic), photolytic, thermolytic and oxidative stress conditions according to ICH Q1A(R2) requirements [24]. Ezetimibe and simvastatin standards solutions, Vitoryn<sup>®</sup> sample solution and placebo were submitted for each forced degradation condition.

The peak purity for both drugs in the obtained electropherograms was evaluated with diode array detector. The interference from tablet excipients was performed by subjecting the placebo to the same stress conditions as Vitoryn<sup>®</sup> samples.

### Alkaline and Acidic Hydrolysis

The concentration of  $1 \text{ mg mL}^{-1}$  for ezetimibe and  $2 \text{ mg mL}^{-1}$  for simvastatin of Vitoryn<sup>®</sup> sample was carried out for alkaline (0.1 N NaOH) and acidic (0.1 N HCl) hydrolysis. The solutions were placed at room temperature and under light protection for 7 days.

Thereafter,  $200 \mu\text{L}$  of each solution was transferred volumetrically to  $2 \text{ mL}$  amber volumetric flask, internal standard stock solution ( $200 \mu\text{L}$ ) and diluent ( $1.6 \text{ mL}$ ) were added, obtaining final concentrations of  $100 \mu\text{g mL}^{-1}$  of ezetimibe and internal standard, while  $200 \mu\text{g mL}^{-1}$  of simvastatin. The solutions were sonicated for 5 min then, filtered in a  $0.45 \mu\text{m}$  polyvinylidene fluoride filter before being used. The same procedure was made with placebo tablets.

## Thermal and Photolytic Degradation

$500 \text{ mg}$  of powder from Vitoryn<sup>®</sup> sample was transferred separately to two Petri plates, one of these was placed in a hot oven at  $60 \text{ }^\circ\text{C}$  (thermal degradation) and the other one, was exposed to direct sunlight (photolytic degradation). After 7 days, an appropriate amount of each powder equivalent to  $10 \text{ mg}$  of ezetimibe and  $20 \text{ mg}$  of simvastatin was transferred into two  $10 \text{ mL}$  amber volumetric flasks. The contents were diluted with  $5 \text{ mL}$  of methanol and sonicated for  $15 \text{ min}$ . The volume was completed with the same diluent. The mixtures were submitted at the same condition as in *section alkaline and acidic hydrolysis (second paragraph)*.

### Oxidative Degradation

Appropriate amount of Vitoryn<sup>®</sup> sample powder equivalent to  $10 \text{ mg}$  of ezetimibe and  $20 \text{ mg}$  of simvastatin were transferred into a  $10 \text{ mL}$  amber volumetric flask. The content was diluted with  $5 \text{ mL}$  of methanol, and  $2.5 \text{ mL}$  of 3% hydrogen peroxide. The mixture was sonicated for  $15 \text{ min}$  and submitted at the same condition as in *section alkaline and acidic hydrolysis (second paragraph)*.

### Linearity and Range

Linearity was verified by preparing five concentrations by diluting adequate amounts of internal standard, ezetimibe, and simvastatin stock standard solutions in diluent. The concentration ranges from  $80$  to  $120 \mu\text{g mL}^{-1}$  for ezetimibe,  $160$  to  $240 \mu\text{g mL}^{-1}$  for simvastatin, and fixed concentration of internal standard ( $100 \mu\text{g mL}^{-1}$ ) were obtained. Three analytical curves for ezetimibe and simvastatin were constructed by plotting the peak area ratio (ezetimibe or simvastatin peak area/internal standard peak area) against ezetimibe or simvastatin concentrations, respectively. Electropherograms were recorded for the solutions injected in triplicate. The method of least squares regression and analysis of variance were used to determine method linearity ( $p = 0.05$ ). The data homoscedasticity and linearity were analyzed through an *F* test.

### Detection and Quantification Limits

The limit of detection and quantification for ezetimibe and simvastatin were measured using the following equations according to ICH guidelines:

$$\text{Limit of detection} = 3.3(\sigma / \alpha), \quad (1)$$

$$\text{Limit of quantification} = 10(\sigma / \alpha), \quad (2)$$

where  $\sigma$  is the standard deviation of the intercept of the mean of three analytical curves, determined by a linear regression model and  $\alpha$  is the slope of the corresponding analytical curve [25].

### Accuracy

Accuracy was determined in terms of percent recovery. Placebo matrix was spiked with ezetimibe and simvastatin standard solutions at three different concentration levels 80, 100 and 120  $\mu\text{g mL}^{-1}$  for ezetimibe and 160, 200 and 240  $\mu\text{g mL}^{-1}$  for simvastatin, equivalent to 80, 100 and 120% of the analytical concentrations, respectively. Each determination was performed in triplicate to obtain the mean and relative standard deviation percentage.

### Precision

Method precision was evaluated by repeatability (intra-day) and intermediate (inter-day) analysis. Six determinations from sample solution, on the same day by a single analyst, were performed to study the repeatability. Intermediate precision was evaluated in the same way as repeatability but by different analyst in a different day. Sample Vytorin<sup>®</sup> (ezetimibe 10 mg and simvastatin 20 mg) solution with constant concentration of internal standard (100  $\mu\text{g mL}^{-1}$ ) were used. The results were expressed in terms of relative standard deviation percentage for ezetimibe and simvastatin content in the tablets.

### Robustness

The robustness was performed by evaluating slight deliberate changes of the optimal analytical conditions such as hydrodynamic injection time (0.1 s and 0.5 s, optimal 0.3 s) and % of organic modifier (10% and 14% acetonitrile, optimal 12%). The responses were evaluated in terms of system suitability i.e., tailing factor, resolution, and efficiency (theoretical plates).

## Results and Discussion

For quality control laboratories, it is very important to develop separation methods for simultaneous quantitation of drugs in combined dosage forms that do not demand pretreatment. Capillary electrophoresis is an alternative technique for this purpose. It offers wide applications [22] and several benefits such as fast analysis, good resolution, low sample consumption, high efficiency and get over several disadvantages of HPLC technique [26]. It is also considered an eco-friendly analytical technique since it uses very small volumes of organic solvents or sometimes does not use them,

preventing or reducing the generation of hazardous waste. In addition, it uses long lasting and versatile capillary columns, the same capillary can be used to analyze from small ions to macromolecules. This feature also makes it an economical technique [23].

### Method Development and Optimization

Different trials were carried out to optimize the simultaneous separation of ezetimibe and simvastatin within a short analytical time with good resolution. The electrolyte pH adjustment is very important to keep the electroosmotic flow and the migration velocities of weak electrolyte components constant. Thus, a stable and reproducible migration behavior of the analytes can be achieved. The effective mobility of cationic and anionic analytes is strongly dependent on their  $pK_a$  value related to background electrolyte pH. However, it is worth mentioning that even for substances without effective mobility, it can move through the capillary due to electroosmotic flow, which in turn, is also dependent on background electrolyte pH [27]. In the separation of neutral substances, the pH adjustment has little influence on selectivity; however, a pH value must be selected for the system in which the surfactant micelles are ionized in such a way to allow their migration at a different rate than electroosmotic flow [28].

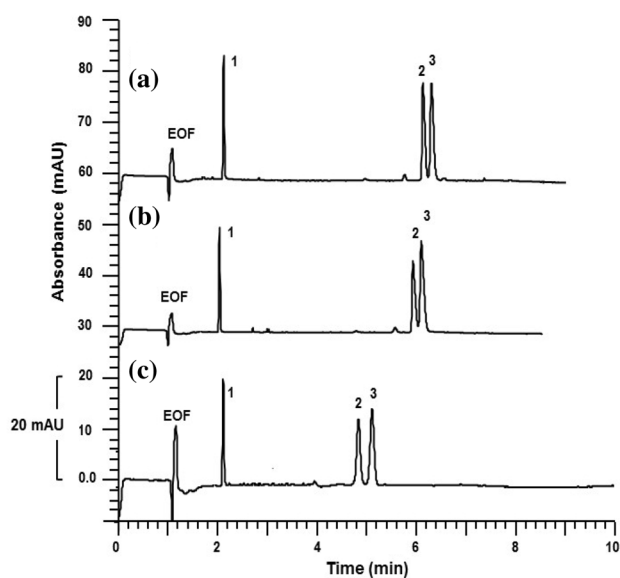
As ezetimibe and simvastatin drugs are water insoluble, this problem can be overcome by using micelles as additives [29]. Solutes interact with a migrating micellar phase and this mechanism allows separation of neutral and charged species [22]. Additives act as a pseudo-stationary phase for the separation of closely compounds and other unresolved compounds in capillary zone electrophoresis [30].

Then micellar electrokinetic chromatography method was performed by addition of sodium dodecyl sulfate surfactant above its critical micellar concentration. This provides a chromatographic partition between pseudo-stationary phase (micelles), formed when the surfactants are above their critical micellar concentration, and the aqueous background electrolyte. To obtain a good separation, effects of pH, buffer concentration, sodium dodecyl sulfate concentration, organic modifier, applied voltage, injection time and detection wavelength were studied.

### Effect of pH Value

The effect of pH was performed from 7 to 9 since  $pK_a$  values of ezetimibe and simvastatin were between 9.75 and 14.91 [31, 32]. For optimum resolution between analytes, the background electrolyte pH should be in the range of the corresponding  $pK$  values of the analytes [22]. The initial sodium tetraborate buffer concentration was set at 20  $\text{mmol L}^{-1}$  as background electrolyte, containing 30  $\text{mmol L}^{-1}$  sodium dodecyl sulfate, the buffer pHs were modified by



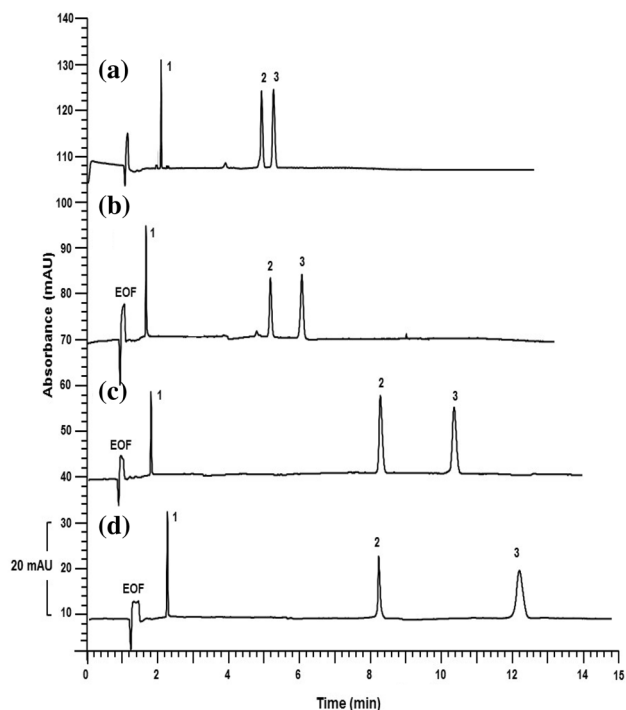


**Fig. 2** Electropherograms of the effect of pH. **A** pH 7, **B** pH 8, and **C** pH 9 of sodium tetraborate buffer background electrolyte on the separation of standard mixture of ezetimibe, simvastatin and internal standard ( $100 \mu\text{g mL}^{-1}$ ). Electrophoretic conditions: uncoated fused-silica capillary with  $50 \mu\text{m i.d.} \times 42 \text{ cm}$  total ( $30 \text{ cm}$  effective) length; electrolyte:  $20 \text{ mmol L}^{-1}$  sodium tetraborate buffer solution, and  $30 \text{ mmol L}^{-1}$  sodium dodecyl sulfate; hydrodynamic injection:  $0.3 \text{ psi}/3 \text{ s}$ ; applied voltage:  $+30 \text{ kV}$ ; temperature:  $30 \text{ }^\circ\text{C}$ ; UV detection at  $238 \text{ nm}$ . Peaks: (1) losartan potassium (internal standard), (2) ezetimibe, (3) simvastatin, and (EOF) electroosmotic flow

using *o*-phosphoric acid and NaOH solutions. As sodium tetraborate buffer pH increased, the electroosmotic flow was also increased which resulted in shorter migration time (pH 9), but the analytes could not be well separated (Fig. 2C). To obtain complete separation, organic modifier was added to the background electrolyte (Fig. 3B). Here, pH was set at 9 under constant conditions, temperature  $30 \text{ }^\circ\text{C}$ , injection time  $0.3 \text{ psi}/3 \text{ s}$  and voltage  $+30 \text{ kV}$ .

### Effect of Organic Modifier

In micellar electrokinetic chromatography, the presence of water-miscible organic solvents such as methanol, 2-propanol and acetonitrile usually improve resolution and/or variation in the selectivity. They reduce capacity factor of highly hydrophobic solutes to within or near the ideal range because of altering the retention mechanism by changing the polarity of the aqueous phase, electrolyte viscosity and zeta potential. The organic solvents contribute to reduce the electroosmotic velocity and expand the migration time window and increase resolution [33]. However, these solvents in high concentrations cannot be used as they can breakdown micellar structure. Generally, the maximum content of the organic solvent that can be used is 20% or so [30]. The influence of acetonitrile and methanol in background electrolyte



**Fig. 3** Electropherograms of the effect of sodium dodecyl sulfate concentration. **A**  $20 \text{ mmol L}^{-1}$ , **B**  $30 \text{ mmol L}^{-1}$ , **C**  $40 \text{ mmol L}^{-1}$ , and **D**  $50 \text{ mmol L}^{-1}$  on the separation of standard mixture of simvastatin ( $200 \mu\text{g mL}^{-1}$ ), ezetimibe and internal standard ( $100 \mu\text{g mL}^{-1}$ ). Electrophoretic conditions: uncoated fused-silica capillary with  $50 \mu\text{m i.d.} \times 42 \text{ cm}$  total ( $30 \text{ cm}$  effective) length; electrolyte:  $20 \text{ mmol L}^{-1}$  sodium tetraborate buffer solution (pH 9),  $\times \text{ mmol L}^{-1}$  sodium dodecyl sulfate and 12% acetonitrile; hydrodynamic injection:  $0.3 \text{ psi}/3 \text{ s}$ ; applied voltage:  $+30 \text{ kV}$ ; temperature:  $30 \text{ }^\circ\text{C}$ ; UV detection at  $238 \text{ nm}$ . Peaks: (1) losartan potassium (internal standard), (2) ezetimibe, (3) simvastatin, and (EOF) electroosmotic flow

was performed in concentration range 5 to 15% (v/v). The results showed a decrease of electroosmotic flow mobility giving longer analysis time when used 15% of solvent, especially when methanol was used, since methanol is more viscous than acetonitrile. Therefore, acetonitrile was chosen for further analysis. Ezetimibe and simvastatin were nearly co-eluted in a low amount of acetonitrile  $\leq 8\%$ . The separation between the analytes under study was getting increased with the increase in the further levels of acetonitrile. Hence, 12% (v/v) acetonitrile was chosen as the optimum concentration for the complete separation of ezetimibe and simvastatin (Fig. 3B), under constant conditions of pH 9, temperature  $30 \text{ }^\circ\text{C}$ , injection time  $0.3 \text{ psi}/3 \text{ s}$  and voltage  $+30 \text{ kV}$ .

### Effect of Surfactant Concentration

Sodium dodecyl sulfate is the most used surfactant in micellar electrokinetic chromatography. Surfactants are added to background electrolyte in concentrations above their critical micellar concentration to form micelles. Analytes distribute

according to their hydrophobicity in and outside of the micelles and they are separated by their different affinity to the micelles [30].

In the present work, the effect of surfactant concentration on the migration times of ezetimibe and simvastatin was studied. Sodium dodecyl sulfate concentration was evaluated in the range of 20 to 50 mmol L<sup>-1</sup>. The obtained results shown that sodium dodecyl sulfate concentration had high effect in the mobility of the two analytes. The higher sodium dodecyl sulfate concentration the higher migration time. Hence, 30 mmol L<sup>-1</sup> sodium dodecyl sulfate was chosen for this study because it gave sharp peaks, short analysis time (approximately 5.8 min) (Fig. 3) compared with Yardimci and Özaltın work [20], they determined the analytes in approximately 10 min.

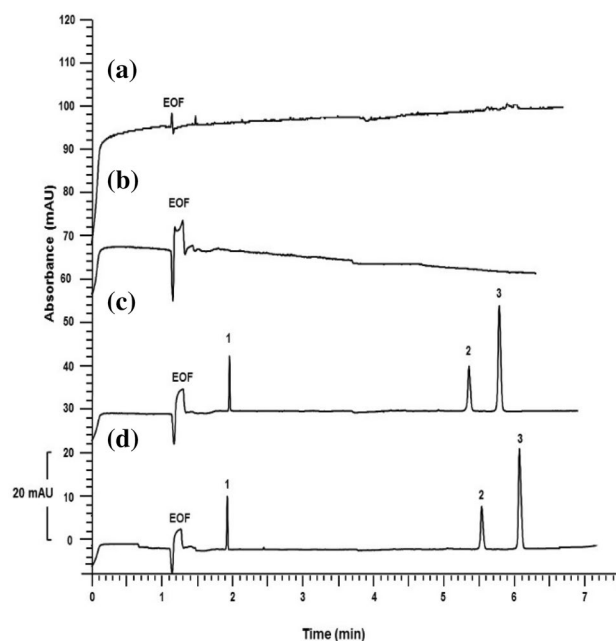
### Effect of Borate Buffer Concentration

The influence of borate buffer concentration on the separation of ezetimibe and simvastatin was analyzed with concentration 20, 30 and 40 mmol L<sup>-1</sup> at pH 9. It was observed that migration time increased with increasing borate concentration. The higher buffer concentration the higher background electrolyte viscosity and the lower electroosmotic flow mobility. Furthermore, the current increased ( $\approx 82 \mu\text{A}$ ) with increasing borate concentration, above 30 mmol L<sup>-1</sup>. No change of the retention order was observed. Therefore, 20 mmol L<sup>-1</sup> borate buffer was chosen for its good symmetric peaks and analysis time (Fig. 4C).

### Effect of Applied Voltage, Injection Time and Capillary Temperature

Regarding the applied voltage, values from 20 to 30 kV were tested using the optimized background electrolyte. The results showed that by increasing voltage, migration times decreased, it is owing to increase in electroosmotic flow, since the magnitude of electroosmotic flow is directly proportional to the strength of the electric field [33]. Hence, a voltage of 30 kV was chosen which producing best peak shape with short migration time of the analytes.

Another instrumental parameter evaluated was the injection time. The volume injected depends essentially on the injection time and it affects area, width, and height of the peaks. In this way, tests were carried out with times of 1, 3 and 5 s with hydrodynamic injection at 0.3 psi. It was observed that above 3 s there was a widening at baseline peaks, causing their distortion and deformation. Good peak shapes for ezetimibe and simvastatin (Fig. 4C) were observed with 3 s injection time. Therefore, this injection time was used for further experiments.



**Fig. 4** Electropherograms at the finally optimized micellar electrokinetic chromatography method. **A** background electrolyte, **B** Vitoryn® placebo sample, **C** standard mixture of 100 µg mL<sup>-1</sup> ezetimibe, 200 µg mL<sup>-1</sup> simvastatin and 100 µg mL<sup>-1</sup> internal standard, **D** Vitoryn® sample (100 µg mL<sup>-1</sup> ezetimibe and 200 µg mL<sup>-1</sup> simvastatin) and 100 µg mL<sup>-1</sup> internal standard. Electrophoretic conditions are the same as in Fig. 3 with 30 mmol L<sup>-1</sup> sodium dodecyl sulfate. Peaks: (1) losartan potassium (internal standard), (2) ezetimibe, (3) simvastatin, and (EOF) electroosmotic flow

Capillary temperature was also investigated in the range from 25 to 40 °C. Best results were observed at 30 °C in terms of current generated in the capillary, resolution and run time. Increasing the temperature above 30 °C resulted in shorter run time but poor resolution and high current. Therefore, temperature of 30 °C was selected for further analysis.

### Selection of Detection Wavelength

Using diode array detector, absorption spectra of ezetimibe and simvastatin showed maximum absorbance at 238 nm. Figure 1C shows an overlap of ezetimibe and simvastatin spectra. In addition, samples of the tablet matrix do not showed interference at this wavelength (Fig. 4D). Thus, we thereafter used a 238 nm detection wavelength for all experiments.

### Internal Standard

Internal standard improves the quantitative performance of capillary electrophoresis methods in terms of linearity, precision, and recovery data. It eliminates error introduced by variability in voltage, injection volume or electroosmotic

flow [34]. Some substances such as clozapine, promethazine and losartan potassium were tested as internal standard candidates. Losartan potassium ( $100 \mu\text{g mL}^{-1}$ ) was the most suitable due to good absorbance in the method wavelength. Complete separation of internal standard, ezetimibe and simvastatin were obtained with migration times of 2.0, 5.4 and 5.8 min, respectively (Fig. 4).

### Optimized Electrolyte Composition

The best results were obtained by using the electrolyte composed of  $20 \text{ mmol L}^{-1}$  sodium tetraborate buffer solution (pH 9, adjusted with *o*-phosphoric acid),  $30 \text{ mmol L}^{-1}$  sodium dodecyl sulfate, and 12% acetonitrile. The quantitative determination of the analytes was performed at +30 kV and  $30^\circ\text{C}$ . Under these conditions, ezetimibe and simvastatin were separated below 6 min (Fig. 4).

### Method Validation

The validation of an analytical method ensures credibility during routine use, being sometimes referred to as a process which provides documented evidence that the method is suitable for its purpose. The proposed method was fully validated as per ICH guidelines [25].

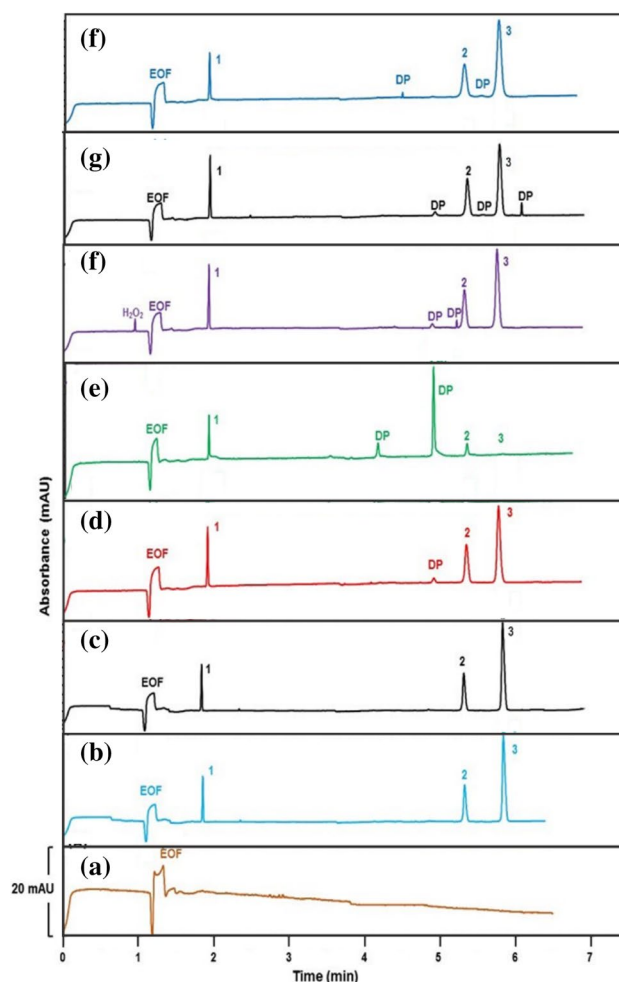
### System Suitability

The obtained results of six replicate injections showed that the parameters tested were within the acceptable range. Ezetimibe and simvastatin were well separated at 5.4 and 5.8 min, respectively, expressing excellent resolution (mean resolution 7). The tailing factor for both ezetimibe and simvastatin peaks never exceeded 1.5 indicating good peak symmetry (acceptance limit is  $<2$ ). The theoretical plates were always  $>10,000$  in all electropherograms which ensured good efficiency throughout the developed separation process [25]. The proposed method offers high sensitivity, and both drugs can be detected accurately. The analytes were well separated from the degradation products. Results are presented in Table 1.

**Table 1** System suitability results

Parameter	Ezetimibe $\pm$ RSD% <sup>a</sup>	Simvastatin $\pm$ RSD% <sup>a</sup>
Migration time (min)	$5.40 \pm 0.7$	$5.80 \pm 0.9$
Peak area (mAU)	$14,556 \pm 4.8$	$33,996 \pm 4.1$
Theoretical plates (N)	$12,507 \pm 13.4$	$101,066 \pm 10.5$
Tailing factor	$1.1 \pm 0.2$	$1.2 \pm 0.3$
Resolution (Rs)	7.0	

<sup>a</sup>Mean of six replicates



**Fig. 5** Electropherograms of forced degradation study. **A** placebo, **B** standard mixture of  $100 \mu\text{g mL}^{-1}$  ezetimibe,  $200 \mu\text{g mL}^{-1}$  simvastatin and  $100 \mu\text{g mL}^{-1}$  internal standard, **C** Vitoryn<sup>®</sup> sample ( $100 \mu\text{g mL}^{-1}$  ezetimibe and  $200 \mu\text{g mL}^{-1}$  simvastatin, **D** acidic hydrolysis ( $0.1 \text{ mol L}^{-1}$  HCl); **E** alkaline hydrolysis ( $0.1 \text{ mol L}^{-1}$  NaOH), **F** oxidative conditions (3% hydrogen peroxide), **G** thermal conditions ( $60^\circ\text{C}$ ), and **H** photolytic conditions (visible light) for 7 days for all above conditions. Electrophoretic conditions are the same as in Fig. 2 except pH 9. Peaks: (1) losartan potassium (internal standard), (2) ezetimibe, (3) simvastatin, and (EOF) electroosmotic flow

### Specificity/Selectivity and Forced Degradation Stability Indicating Capability

The electropherograms of background electrolyte, standards (ezetimibe and simvastatin), placebo and Vitoryn<sup>®</sup> sample were compared to evaluate the specificity of the proposed method. The specificity was demonstrated by the absence of interference among ezetimibe, simvastatin and excipients from Vitoryn<sup>®</sup> samples (Fig. 4).

Selectivity and stability indicating capability of the analytical method was performed through forced degradation study. Peak purity was assessed using diode array detector.

The analysis was carried out to ensure that the proposed method was able to separate ezetimibe and simvastatin from the degradation products generated during the forced degradation study. The samples were subjected to stress conditions by acidic and alkaline hydrolysis, oxidative, thermal (60 °C) and photolytic degradation for 7 days. It was observed that sample was sensitive to acidic hydrolysis, with the formation of one degradation product in 5.1 min (Fig. 5D). In alkaline hydrolysis, it was observed degradation of ezetimibe and almost total degradation of simvastatin, showing two degradation products at 4.3 and 5.1 min (Fig. 5E). In oxidative condition, it was observed the formation of two degradation products at 5.1 and 5.3 min (Fig. 5F). Under heating test, it was observed the formation of three degradation products at 5.1, 5.7 and 6.2 min (Fig. 5G). Under photolytic stress, there were observed two degradation products at 4.5 and 5.7 min (Fig. 5H). In all cases, ezetimibe, simvastatin and internal standard peaks showed purity factor greater than 99%. In addition, resolution between the analyte peaks and the possible degradation product was greater than 1.5, which shows acceptable degree of method specificity.

## Linearity and Range

The data obtained from plotting the peak area ratios (ezetimibe or simvastatin/internal standard) versus drug concentrations confirmed the method linearity in the concentration range between 80 and 120  $\mu\text{g mL}^{-1}$  for ezetimibe; while 160 and 240  $\mu\text{g mL}^{-1}$  for simvastatin. The correlation equations obtained for the linear model were  $y=0.0373x-1.1003$  and  $y=0.0417x-1.7465$  with determination coefficient of 0.9956 and 0.9920 for ezetimibe and simvastatin, respectively. Analysis of variance at 95% was performed to verify the good fitting of the micellar electrokinetic chromatography method, to evaluate its linearity and the validity of linear regression. From the obtained data (Table 2) we can see there was significant regression since calculated  $F$  was greater than critical  $F$ .

Therefore, analysis of variance showed that the adjustment of the linear model is appropriate for the two curves constructed, since the  $p$  values found were lower than  $F_{\text{critical}}$  values, indicating that the variances of the response in  $Y$  are independent of the concentration levels in  $X$ . The adjustment to the linear model was verified by normal and random distribution of the residuals (Fig. 6A and 6B), thus showing that there is no dependency between the values. Therefore, the homoscedasticity assumption is satisfied indicating a good fit for the linear model.

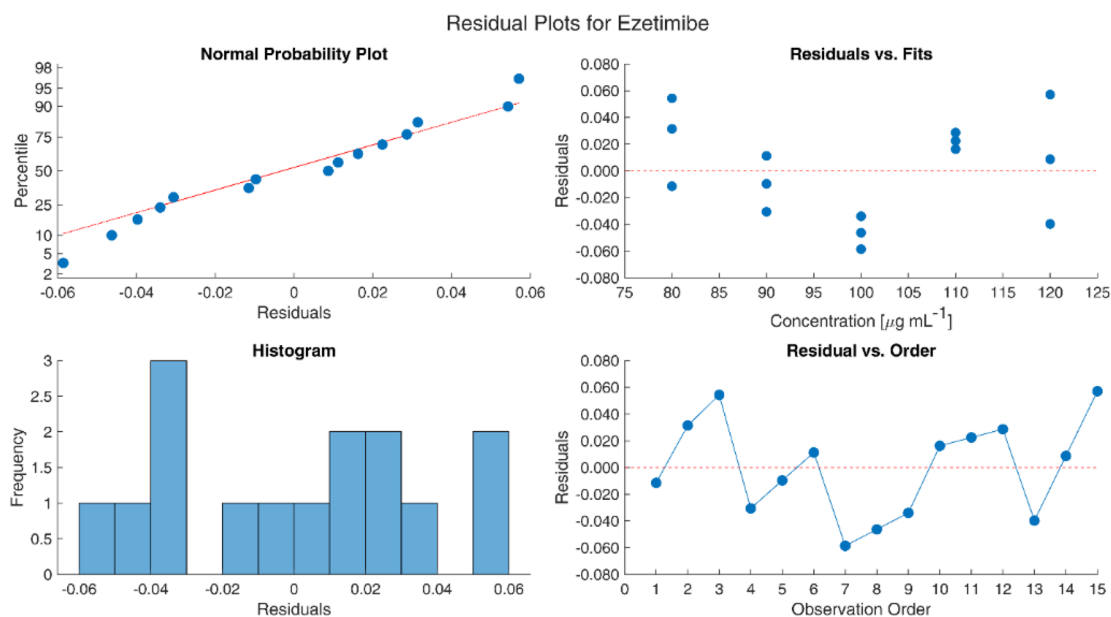
**Table 2** Linearity, detection, and quantification limits

Parameter	Analyte							
	Ezetimibe	Simvastatin						
Range (%)	80–120	80–120						
Concentration range <sup>a</sup> ( $\mu\text{g mL}^{-1}$ )	80–120	160–240						
Intercept ( $b$ )	−1.1003	−1.7465						
Slope ( $a$ )	0.0373	0.0417						
Determination coefficient ( $R^2$ )	0.9956	0.9920						
Intercept standard deviation ( $S_b$ )	0.0694	0.2101						
Slope standard deviation ( $S_a$ )	0.0006	0.0010						
Probability ( $p$ )	$7.04 \times 10^{-10}$	$1.47 \times 10^{-6}$						
Significance ( $F$ )	$1.05 \times 10^{-16}$	$5.23 \times 10^{-15}$						
Detection limit ( $\mu\text{g mL}^{-1}$ )	6.14	16.63						
Quantification limit ( $\mu\text{g mL}^{-1}$ )	18.63	50.40						
Ezetimibe and simvastatin analysis of variance (analytical curve)								
	DF EZT	SVT	SS EZT	SVT	MS EZT	SVT	$F_{\text{cal}}$ EZT	SVT
Regression	1	1	4.169581	20.857873	4.169581	20.857873	2938.07	1605.96
Residual	13	13	0.018449	0.168841	0.001419	0.012987		
Total	14	14	4.188030	21.02671				

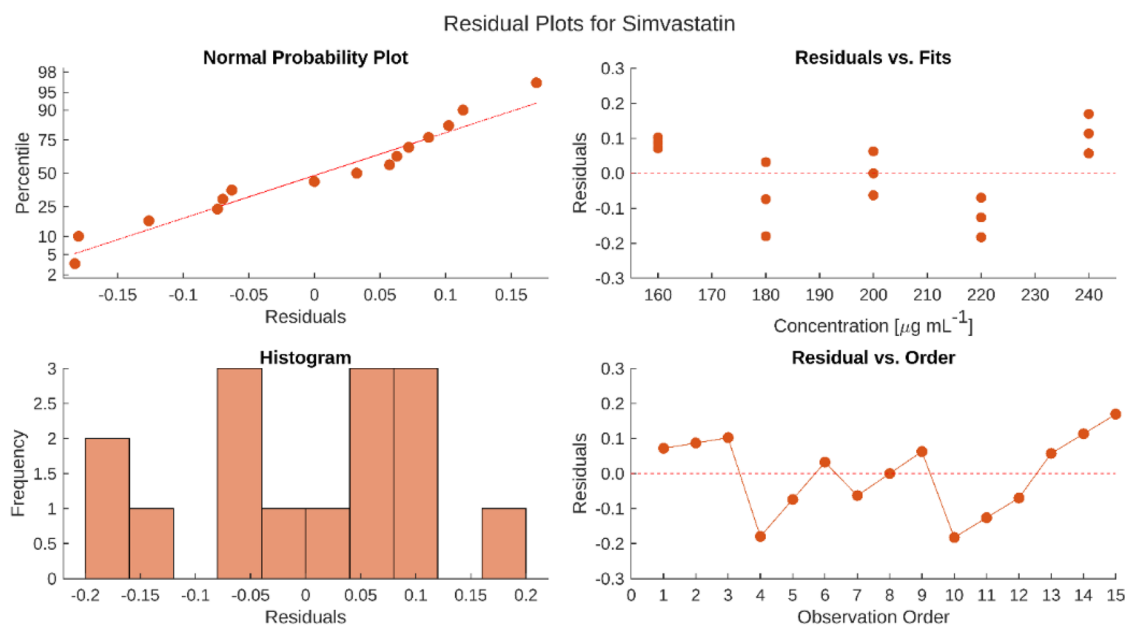
<sup>a</sup>Five data points, triplicate at each concentration level

$F_{\text{critical}}$ : 2.48,  $\alpha=0.05$

DF degrees of freedom, SS sum of squares, MS mean squares, EZT ezetimibe, SVT simvastatin



(a) Residual plots for ezetimibe for linear regression model.



(b) Residual plots for simvastatin for linear regression model.

Fig. 6 A Residual plots for ezetimibe for linear regression model. B Residual plots for simvastatin for linear regression model

### Limits of Detection and Quantification

Limits of detection and quantification was obtained by using the equations specified in section detection and quantification limits, demonstrate that the method is sensitive and viable to be applied for the determination

of ezetimibe and simvastatin in combined dosage forms (Table 2).

### Accuracy

The proposed analytical method accuracy was evaluated by determining the mean percent recoveries of ezetimibe

**Table 3** Recovery results for ezetimibe and simvastatin

Analyte	Theoretical (claimed) concentration ( $\mu\text{g mL}^{-1}$ )	Concentration found ( $\mu\text{g mL}^{-1}$ )	Recovery <sup>a</sup> (%)	Mean recovery <sup>b</sup> (%)
Ezetimibe	80	80.1	100.1 $\pm$ 1.6	101.0 $\pm$ 0.77
	100	101.6	101.6 $\pm$ 0.3	
	120	121.4	101.2 $\pm$ 1.2	
				RSD% 0.76
Simvastatin	160	160.6	100.4 $\pm$ 1.6	100.4 $\pm$ 0.35
	200	200.2	100.1 $\pm$ 1.5	
	240	241.9	100.8 $\pm$ 1.1	
				RSD% 0.35

<sup>a</sup>Mean of three replicates  $\pm$  SD<sup>b</sup>Mean of all recovery levels  $\pm$  SD ( $n=9$ )

and simvastatin standards added to the placebo matrix using three replicate determinations at three different levels (80, 100 and 120% of the working concentration). The obtained mean recoveries were 101.0% for ezetimibe and 100.4% for simvastatin with RSD% < 1, demonstrating the method accuracy (Table 3). Recovery values in the range of  $100 \pm 2\%$  of the target value are considered acceptable [35].

### Precision

The repeatability and intermediate method precision (intra- and inter-day, respectively) were assessed. The repeatability ( $n=6$ ) was evaluated as the RSD% of six independent samples, performed in the same day and by the same analyst. The intra-day mean assay was  $9.95 \pm 0.10$  mg/tablet (RSD% 1.05) for ezetimibe and  $19.68 \pm 0.08$  mg/tablet (RSD% 0.38) for simvastatin. The intermediate precision was assessed by the analyses of other six independent samples by a different analyst, which showed mean assay of  $10.07 \pm 0.12$  mg/tablet (RSD% 1.20) for ezetimibe and  $19.77 \pm 0.14$  mg/tablet (RSD% 0.69) for simvastatin. Both repeatability and intermediate precision levels showed low RSD% values (< 2) which confirmed the good method precision. These results also indicated that the mean of the assay  $10.01 \pm 0.12$  mg/tablet (RSD% 1.24) for ezetimibe and  $19.73 \pm 0.11$  mg/tablet (RSD% 0.58) for simvastatin was in good agreement with the label claim for Vitorin<sup>®</sup> tablets. The RSD% was < 2, demonstrating that the precision of the analytical method is satisfactory (Table 4).

### Robustness

The proposed method robustness test showed deliberate changes in the injection time and in the proportion of the organic solvent that can interfere in the instrumental responses. It was observed broad peaks at baseline for both

**Table 4** Precision analysis for the quantification of ezetimibe and simvastatin

Analyte	Labeled value	Intra-day Found		Inter-day ( $n=12$ )	
		I. Analyst	II. Analyst		
Ezetimibe	10	9.9	9.9		
	10	10.1	10.2		
	10	10.0	10.1		
	10	9.8	10.2		
	10	9.9	10.0		
	10	10.0	10.0		
	Mean	9.95	10.07	10.01	
	SD	0.10	0.12	0.12	
	RSD%	1.05	1.20	1.24	
Simvastatin	20	19.7	20.0		
	20	19.7	19.8		
	20	19.6	19.6		
	20	19.7	19.7		
	20	19.8	19.7		
	20	19.6	19.8		
		Mean	19.68	19.77	19.73
		SD	0.08	0.14	0.11
	RSD%	0.38	0.69	0.58	

SD standard deviation, RSD% relative standard deviation percent

analytes when injection time decreased (symmetry > 2), on the other hand, when the injection time increased no broad peaks was observed (symmetry < 2). Contrarily, decreasing the proportion of organic solvent makes the asymmetry factor better as compared to increased organic solvent. While increasing the theoretical plates makes the injection time and proportion of organic solvent decreased, on the other hand, when the injection time and proportion of organic solvent increased then the theoretical plates decreased. Resolution was unaffected with deliberate change in injection time and proportion of organic solvent (Table 5).

**Table 5** Robustness analysis for the quantification of ezetimibe and simvastatin

Condition	Ezetimibe			Simvastatin	
	Injection time (s)	Tailing factor*	N*	Rs*	Tailing factor*
0.1	2.6	303,936	8	2.6	215,398
0.3	1.1	222,227	7	1.7	105,749
0.5	0.9	129,372	7	1.3	54,074
Acetonitrile (%)					
10	1.2	176,390	13	1.2	56,821
12	1.1	222,227	7	1.7	105,749
14	2.1	142,235	7	1.3	55,378

\*Mean of three determinations

N Efficiency (theoretical plates)

## Stability of Solutions

The stability of sample solutions even as standards working solutions in the diluting solvent (methanol and ultrapure water) was checked, no changes were detected within 8 h at room temperature. On the other hand, the standard stock solutions were stored in refrigerator at 4 °C, they were stable for at least two weeks. Peaks areas and migration time of the drugs seemingly remained unchanged (RSD% < 2). No significant degradation was observed during that period.

## Application of the Proposed Method to the Commercial Pharmaceutical Preparation

Ezetimibe and simvastatin analysis in their combined tablets (Vitoryn<sup>®</sup>) was performed using the developed and validated micellar electrokinetic chromatography method. The assay of ezetimibe and simvastatin in commercial pharmaceutical formulation indicated a mean value of  $10.10 \pm 0.77$  mg/tablet (101.0%, RSD% 0.76) for ezetimibe and  $10.04 \pm 0.35$  mg/tablet (100.4%, RSD% 0.35) for simvastatin. There was good agreement between the obtained results and the label claim for ezetimibe and simvastatin tablets (Table 3). The results were satisfactory, and they are within tolerance limits (95 to 105% label claim) [6].

## Greenness Assessment of the Proposed Method

Green Analytical Procedure Index [36] and Analytical GREENness [37] were employed in this study to evaluate the method greenness.

According to Green Analytical Procedure Index, three different colored (green, yellow and red) pictograms (five-pentagram) allowed us to determine the method greenness in which green color is considered to be more eco-friendly as compared to other two colors (yellow and red). The result showed that 10 regions are shaded green, 2 yellow, 2 red and 1 white indicating the proposed method greenness (Table 6A). A numerical estimation was also made

with HPLC [10] which revealed that 4 regions are green, 4 yellow, 6 red and 1 white making the reported method less green as compared to the proposed micellar electrokinetic chromatography method.

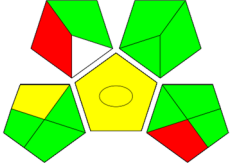
Analytical GREENness found to be comprehensive, convenient, reliable and straightforward evaluation approach which gathers both quantitative and qualitative aspects of comparison. According to this approach, each of the 12 parameters has a score from 0.0 to 1.0 which is indicated by a specific pictogram color ranging from red (0.0) to dark green (1.0). In this work, the final score was 0.81 indicating the greenness of the proposed micellar electrokinetic chromatography method (Table 6B). A numerical estimation was also made with HPLC [10] which revealed less green (0.67) as compared to the proposed method.

Therefore, both are highly recommended approaches that produces an easily interpretable and informative results for the greenness assessment [36, 37].

## Conclusion

A fast, sustainable and green micellar electrokinetic chromatography method has been investigated for the simultaneous quantification of ezetimibe and simvastatin. The method was fully optimized and validated as per ICH guideline and was successfully applied for the analysis of ezetimibe/simvastatin in binary mixture tablet dosage form and in the presence of their degradation products after submitted to different forced degradation conditions (oxidative, thermal, photolytic, alkaline and acidic hydrolysis). The proposed method was the first to be considered stability indicating since it enabled the determination of the active pharmaceutical ingredients without any interference under different forced degradation conditions. To our knowledge, there is no work with this intend, on the other hand there is only one research in which ezetimibe and simvastatin were determined simultaneously using

**Table 6** Greenness assessment

Parameter	Response
<b>(A) Green analytical procedure index</b>	
<i>Sample Preparation</i>	
(1) Collection	In-line
(2) Preservation	None
(3) Transport	None
(4) Storage	Under normal conditions
(5) Method type	Simple procedures
(6) Extraction scale	Not applicable
(7) Reagents/solvents used	Non-green reagents/solvents
(8) Additional treatments	None
<i>Solvents/reagents</i>	
(9) Amount	< 10 mL (< 10 g)
(10) Health hazard	Slightly irritant and toxic; National Fire Protection Association (NFPA) score 1
(11) Safety hazard	Highest NFPA stability/flammability score 1
<i>Instrumentation</i>	
(12) Energy	< 0.1 kWh/sample
(13) Occupational hazard	Hermetic sealing of analytical procedure
(14) Waste	< 1 mL (< 1 g)
(15) Waste treatment	No treatment
<i>Method type</i>	
Type of analysis	Qualitative and quantitative
<b>(B) Analytical GREENness</b>	
(1) Sample treatment	In-field sampling and direct analysis
(2) Sample amount	0.025 g
(3) Device positioning	In-line
(4) Sample preparation stages	3 or fewer
(5) Miniaturization and automation	Miniaturized and automatic
(6) Derivatization	None
(7) Waste	1 mL
(8) Analysis throughput	7 analytes; 70/h
(9) Energy Consumption	0.4 kWh
(10) Reagents and source	Some reagents are bio-based
(11) Toxic solvent/reagent amount	0.3 mL
(12) Operator's safety	Toxic to aquatic life, highly flammable, explosive, corrosive
Green analytical procedure index and analytical GREENness evaluation result	 

capillary electrophoresis in 10 min. In this work, we determined the analytes in less than 6 min. The proposed micellar electrokinetic chromatography method has several advantages like specific, accurate and cost-effective. Therefore, it can be successfully applied in quality control laboratories for determining ezetimibe and simvastatin in

their combined binary mixture. Furthermore, the method consumes less solvent with high separation efficiency. Green Analytical Procedure Index and Analytical GREENness metrics were used to demonstrate the greenness of the proposed method.



**Acknowledgements** The authors wish to thank Fundação de Amparo à Pesquisa do Estado de São Paulo (FAPESP), São Paulo, Brazil (Process 2012/50595-8) for financial support, Coordenação de Aperfeiçoamento de Pessoal de Nível Superior (CAPES), Brazil (Process 88882.377651/2019-01) for FAGF scholarship.

**Author Contributions** AMCS and FAGF: investigation, methodology, formal analysis, data curation, software, writing—original draft. MFMT: conceptualization, visualization, and resources. AR and MSAP: conceptualization, validation, resources, writing—review and editing, supervision, and project administration.

**Data Availability** The data that support the findings of this study is available from the corresponding author upon reasonable request.

## Declarations

**Competing interests** The authors declare no competing interests.

**Conflict of interest** All contributing authors declare no conflict of interest.

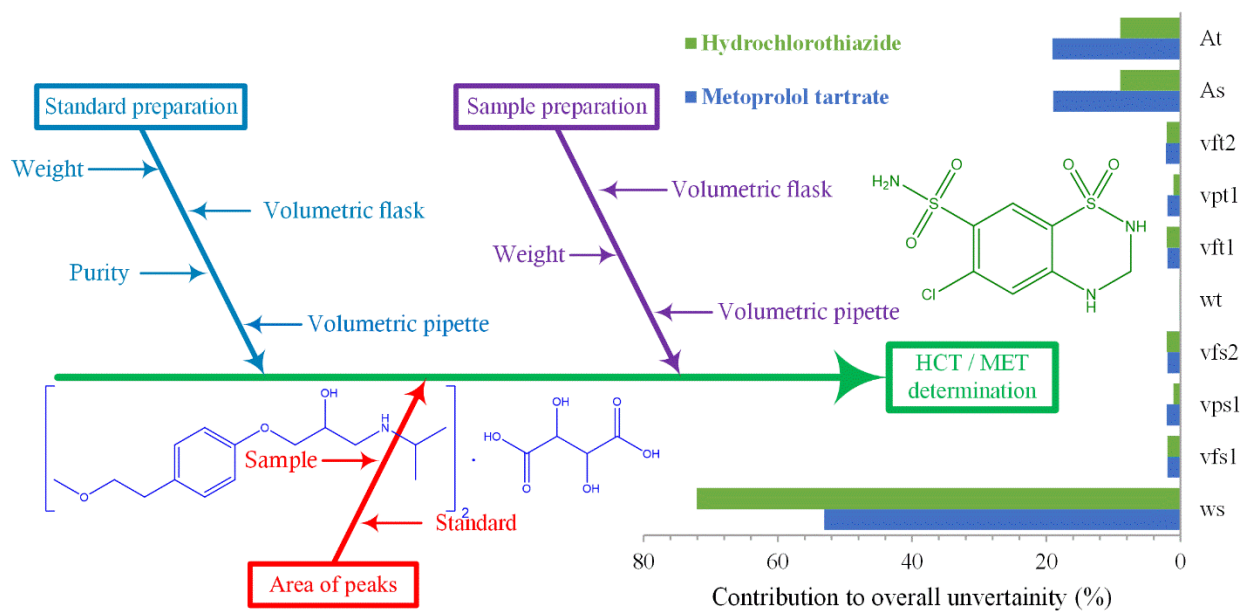
## References

- Du Q, Zhang Y, Wang J, Liu B (2021) Simultaneous determination and quantitation of hypolipidemic drugs in fingerprints by UPLC-Q-TRAP/MS. *J Chromatogr B Anal Technol Biomed Life Sci* 1175:1–9. <https://doi.org/10.1016/j.jchromb.2020.122496>
- Davies JT, Delfino SF, Feinberg CE et al (2016) Current and emerging uses of statins in clinical therapeutics: a review. *Lipid Insights* 9:13–29. <https://doi.org/10.4137/LPI.S37450>
- Schiele F, Farnier M, Krempf M et al (2018) A consensus statement on lipid management after acute coronary syndrome. *Eur Hear J Acute Cardiovasc Care* 7:532–543. <https://doi.org/10.1177/2048872616679791>
- Bove M, Fogacci F, Cicero AFG (2017) Pharmacokinetic drug evaluation of ezetimibe + simvastatin for the treatment of hypercholesterolemia. *Expert Opin Drug Metab Toxicol* 13:1099–1104. <https://doi.org/10.1080/17425255.2017.1381085>
- Kei AA, Filippatos TD, Elisaf MS (2016) The safety of ezetimibe and simvastatin combination for the treatment of hypercholesterolemia. *Expert Opin Drug Saf* 15:559–569. <https://doi.org/10.1517/14740338.2016.1157164>
- United States Pharmacopeial Convention (2021) United States Pharmacopoeia-National Formulary (USP–NF). United States Pharmacopeial Convention, Rockville
- Jeu LA, Cheng JWM (2003) Pharmacology and therapeutics of ezetimibe (SCH 58235), a cholesterol-absorption inhibitor. *Clin Ther* 25:2352–2387. [https://doi.org/10.1016/s0149-2918\(03\)80281-3](https://doi.org/10.1016/s0149-2918(03)80281-3)
- Shrestha B, Stephenrathinaraj B, Sharan Patel S et al (2010) Simultaneous HPTLC estimation of simvastatin and ezetimibe in tablet dosage form. *E-J Chem* 7:1206–1211
- Al-Hashimi NN, Shahin RO, Al-Hashimi AN et al (2019) Cetyl-Alcohol-Reinforced Hollow Fiber Solid/Liquid-Phase Microextraction and HPLC-DAD Analysis of Ezetimibe and Simvastatin in Human Plasma and Urine. *Biomed Chromatogr* 33:1–8. <https://doi.org/10.1002/bmc.4410>
- Desai PR, Mehta PJ, Ojha SK, Chokshi AB (2018) Simultaneous quantification of related substances of ezetimibe and simvastatin in combined dosage form using a novel stability-indicating liquid chromatographic method. *Acta Chromatogr* 30:85–94. <https://doi.org/10.1556/1326.2017.00273>
- Fahad AMM, Rasheed AS, Ali HH (2022) Separation and determination of simvastatin on ZIC-HILIC stationary phases by hydrophilic interaction chromatography in pharmaceutical material products. *Mater Today Proc* 49:2817–2821. <https://doi.org/10.1016/j.matpr.2021.09.535>
- Kurbanoglu S, Esim O, Ozkan CK et al (2019) Development and validation of RP-LC method for the simultaneous determination of simvastatin and ezetimibe in fixed-dose combination tablets and in rabbit serum. *Chromatographia* 82:279–285. <https://doi.org/10.1007/s10337-018-3642-x>
- Devu S, Gupta A, Srinivas KS et al (2012) Development and validation of stability indicating RP-UPLC method for simultaneous determination in fixed dose combination of ezetimibe and simvastatin. *Chromatogr Sep Tech* 3:1–7. <https://doi.org/10.4172/2157-7064.1000131>
- Wang D, Qin F, Chen L et al (2008) Determination of simvastatin in human plasma using ultra-performance liquid chromatography-tandem mass spectrometry. *Chinese J Chromatogr* 26:327–330
- Elawady T, Ibrahim F, Belal F (2021) Simultaneous determination of ezetimibe, atorvastatin and simvastatin using quadrupole LC-MS: application to combined tablets and plasma after SPE. *Acta Chromatogr* 33:245–252. <https://doi.org/10.1556/1326.2020.00752>
- Karanam SR, Katakam P, Chandu BR et al (2014) Simultaneous determination of ezetimibe and simvastatin in rat plasma by stable-isotope dilution LC-ESI-MS/MS and its application to a pharmacokinetic study. *J Pharm Anal* 4:286–294. <https://doi.org/10.1016/j.jpha.2013.08.002>
- Huang L, Shou L, Hu L, Zhou M (2019) Simultaneous determination of 45 addition chemical drugs in hyperglycemic, hyperlipidemic and hypertensive people's health foods by HPLC-MS/MS. *Chinese J Pharm Anal* 39:484–495
- Magdy N, Ayad MF (2015) Two smart spectrophotometric methods for the simultaneous estimation of simvastatin and ezetimibe in combined dosage form. *Spectrochim Acta Part A Mol Biomol Spectrosc* 137:685–691. <https://doi.org/10.1016/j.saa.2014.08.042>
- de Souza FH, Todeschini V, Sangoi MD (2018) Chemometric-assisted spectrophotometric method for the simultaneous quantitative determination of ezetimibe and simvastatin in their combined dosage forms. *J AOAC Int* 101:1015–1020. <https://doi.org/10.5740/jaoacint.17-0124>
- Yardimci C, Özaltın N (2010) Simultaneous determination of ezetimibe and simvastatin in pharmaceutical preparations by MEKC. *J Chromatogr Sci* 48:95–99. <https://doi.org/10.1093/chromsci/48.2.95>
- Marina ML, Ríos Castro A, Valcárcel Cases M (2005) Analysis and detection by capillary electrophoresis. *Comprehensive analytical chemistry*, 1st edn. Elsevier, Amsterdam, pp 1–30
- Karger BL (1998) Capillary Electrophoresis: Overview and Perspective. In: Khaledi MG (ed) *High performance capillary electrophoresis: theory, techniques, and applications*, 1st edn. John Wiley & Sons Ltd, New York, pp 3–23
- Ranasinghe M, Quirino JP (2021) Can we replace liquid chromatography with the greener capillary electrophoresis? *Curr Opin Green Sustain Chem* 31:1–8. <https://doi.org/10.1016/j.cogsc.2021.100515>
- ICH Expert Working Group (2003) International Conference on Harmonisation of Technical Requirements for Registration of Pharmaceuticals for Human Use: Stability Testing of New Drug Substances and Products Q1A(R2)
- European Medicines Agency (1995) International Conference on Harmonisation of Technical Requirements for Registration of Pharmaceuticals for Human Use: Validation of Analytical Procedures (Text and Methodology) Q2(R1)

26. Ragab MAA, Abdel-Hay MH, Ahmed HM, Mohyeldin SM (2019) Application of Capillary Zone Electrophoresis Coupled with a Diode Array Detector (CZE-DAD) for Simultaneous Analysis of Ibuprofen and Phenylephrine. *J AOAC Int* 102:473–479. <https://doi.org/10.5740/jaoacint.18-0134>
27. Beckers JL, Boček P (2003) The preparation of background electrolytes in capillary zone electrophoresis: golden rules and pitfalls. *Electrophoresis* 24:518–535. <https://doi.org/10.1002/elps.200390060>
28. Gomes TVD (2012) Desenvolvimento e Validação Intralaboratorial do Método por Cromatografia Eletrocínética Capilar Micelar para Determinação de Vitamina K1 e k3 em chá Verde e em Suplemento Farmacêuticos. Pontifícia Universidade Católica do Rio de Janeiro
29. Voeten RLC, Ventouri IK, Haselberg R, Somsen GW (2018) Capillary electrophoresis: trends and recent advances. *Anal Chem* 90:1464–1481. <https://doi.org/10.1021/acs.analchem.8b00015>
30. Terabe S, Otsuka K, Ichikawa K et al (1984) Electrokinetic separations with micellar solutions and open-tubular capillaries. *Anal Chem* 56:111–113. <https://doi.org/10.1021/ac00265a031>
31. (2022) Simvastatin: Uses, Interactions, Mechanism of Action. In: DrugBank Online. <https://go.drugbank.com/drugs/DB00641>. Accessed 11 Aug 2022
32. (2022) Ezetimibe: Uses, Interactions, Mechanism of Action. In: DrugBank Online. <https://go.drugbank.com/drugs/DB00973>. Accessed 11 Aug 2022
33. Otsuka K, Terabe S (1998) Micellar Electrokinetic Chromatography. *Mol Biotechnol* 9:253–271. <https://doi.org/10.1007/BF02915799>
34. Altria KD (2002) Improved Performance in Capillary Electrophoresis Using Internal Standards. *LC-GC Eur* 1–5
35. Shabir GA (2003) Validation of high-performance liquid chromatography methods for pharmaceutical analysis: understanding the differences and similarities between validation requirements of the US food and drug administration, the US pharmacopeia and the international Conf. *J Chromatogr A* 987:57–66. [https://doi.org/10.1016/s0021-9673\(02\)01536-4](https://doi.org/10.1016/s0021-9673(02)01536-4)
36. Plotka-Wasyłka J (2018) A new tool for the evaluation of the analytical procedure: green analytical procedure index. *Talanta* 181:204–209. <https://doi.org/10.1016/j.talanta.2018.01.013>
37. Pena-Pereira F, Wojnowski W, Tobiszewski M (2020) AGREE-analytical greenness metric approach and software. *Anal Chem* 92:10076–10082. <https://doi.org/10.1021/acs.analchem.0c01887>

**Publisher's Note** Springer Nature remains neutral with regard to jurisdictional claims in published maps and institutional affiliations.

Springer Nature or its licensor (e.g. a society or other partner) holds exclusive rights to this article under a publishing agreement with the author(s) or other rightsholder(s); author self-archiving of the accepted manuscript version of this article is solely governed by the terms of such publishing agreement and applicable law.



## GRAPHICAL ABSTRACT

## **Validation, Measurement Uncertainty Estimation and Green Evaluation of UHPLC for Simultaneous Determination of Antihypertensive Drugs in Binary Tablet**

Claudia Vilela de Oliveira <sup>1</sup>, Adriano Peron <sup>2</sup>, Anas Rashid <sup>3</sup>, Frank Alonso Gavilano Fajardo <sup>1</sup>, Felipe Rebello Lourenço <sup>1</sup>, Marina Franco Maggi Tavares <sup>4</sup>, María Segunda Aurora Prado <sup>1\*</sup>

<sup>1</sup> Department of Pharmacy, School of Pharmaceutical Sciences, University of São Paulo, São Paulo, Brazil

<sup>2</sup> AB Sciex Comércio de Instrumentos Laboratoriais Ltda, São Paulo, Brazil

<sup>3</sup> Department of Neuroscience “Rita Levi Montalcini”, School of Medicine and Surgery, University of Torino, Torino, Italy

<sup>4</sup> Department of Fundamental Chemistry, Institute of Chemistry, University of São Paulo, São Paulo, Brazil

### **ABSTRACT**

A novel green ultra-high performance liquid chromatography method was validated and estimated the measurement uncertainty for simultaneous determination of metoprolol tartrate (MET) and hydrochlorothiazide (HCT) in binary tablet. Method was performed using a Zorbax<sup>®</sup> SB-C18 column with isocratic elution (flow rate 0.9 mL min<sup>-1</sup>) and maintained with 25 °C column temperature. The acetonitrile:water:triethylamine (17:83:0.2 v/v) was used as a mobile phase. Both analytes were separated in approximately 1 min. Analytical curves were linear with R<sup>2</sup> of 0.9991 and 0.9903 for MET and HCT, respectively. Detection limits were 2.42 and 1.05 µg mL<sup>-1</sup> for MET and HCT, respectively and quantitation limits were 7.34 µg mL<sup>-1</sup> for MET and 3.19 µg mL<sup>-1</sup> for HCT. The intra- and inter-day precision measurements RSD% were 0.39, 0.61 and 0.72, 1.2 % for MET and HCT respectively. Method accuracy by recovery tests was between 100 ± 2 %. Measurement uncertainties obtained using Eurachem procedure were 100.1 ± 2.8 % and 100.3 ± 2.4 % for MET and HCT, respectively. UHPLC method was accurate, precise, linear, specific/selective and did not interfere with the tablet excipients and their degradation products. Hence, the proposed method is more eco-friendly compared with three reported methods and can be effectively implemented for analytical quality control in the pharmaceutical industries.

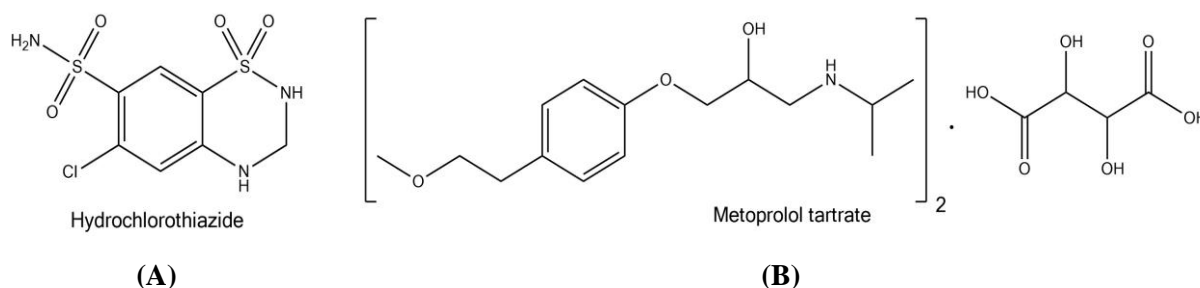
### **KEYWORDS**

UHPLC; Antihypertensive Drugs; Measurement Uncertainty; Greenness

## 1. INTRODUCTION

Among cardiovascular diseases, hypertension is one of the most serious medical conditions characterized by an increase in systolic blood pressure higher than 130 mmHg [1] with an estimated 1.28 billion people worldwide [2]. The challenge of diagnosing and treating hypertension is immense because most hypertensive patients are asymptomatic and the symptoms are usually associated with vital organs such as brain, heart, and kidney [3]. However, all organs suffer from the consequences of high-pressure levels, as all vessels can be reached [4].

WHO and Eighth Joint National Committee recommend thiazide diuretics as the first-line therapy for primary hypertensive condition due to their showed effectiveness and reduced cost [5]. Among the most commonly prescribed drugs include hydrochlorothiazide, chlorthalidone, indapamide, and metolazone [6]. Hydrochlorothiazide is chemically 2*H*-1,2,4-benzothiadiazine-7-sulfonamide, 6-chloro-3,4-dihydro-1,1-dioxide (**Fig. 1A**), and among the pioneer diuretics [7] prescribed in combination with other anti-hypertensive drugs, such as metoprolol tartrate (cardioselective beta-adrenergic antagonist) in hypertrophic cardiomyopathy, myocardial infarction, vascular headache, and migraine which proved to be more effective than any other drug used by itself [8]. Metoprolol tartrate is chemically 1,1-dioxide 1-[4-(2-methoxyethyl)phenoxy]-3-[(1-methylethyl)amino]-2-propanol, 2*R*,3*R*-dihydroxybutanedioate (**Fig. 1B**).



**Fig. 1.** Chemical structure of hydrochlorothiazide and metoprolol tartrate.

Several methods are available to determine the metoprolol tartrate and hydrochlorothiazide including supercritical fluid chromatography [9], liquid chromatography-mass spectrometry [10–16], gas chromatography-mass spectrometry [17], ultra performance liquid chromatography-mass spectrometry [18], high performance liquid chromatography (HPLC) [19–23], ultra performance liquid chromatography [24,25], voltammetry [26], spectrophotometry [27], and potentiometry [28]. The literature reveals few HPLC methods to determine simultaneously both active pharmaceutical ingredients in tablets, but longer retention time, high amount of carbon-based solvents in the mobile phase, and buffer solution have been used [20,21,23]. *Garg et al.* [20] identified the analytes in 8 min using high quantity of methanol (95%), while *Rawool et al.* [21] determined the analytes in 11 min using methanol and phosphate buffer (40:60) as mobile phase. Though, the latter did not provide sufficient information for system suitability. Another author separates the metoprolol tartrate, hydrochlorothiazide, and relevant impurities in 13 min using acetonitrile and sodium phosphate buffer as mobile phase in gradient elution mode [23].

HPLC is a well-established separation technique that has been used in several areas, including chemistry, forensics, toxicology, clinical and environmental analysis, to solve many analytical problems. Recently many improvements have been incorporated into this technique, including the development of new stationary phases and chromatographic support [29]. Ultra-high performance liquid chromatography (UHPLC) technique is an example of them that was developed with the introduction of porous particles in the stationary phase with less than 2  $\mu\text{m}$  diameter, in response to the ongoing search for a faster and more efficient analysis [30]. This method is based on the same HPLC separation principle but uses chromatography columns from 5 to 10 cm in length, and internal diameters from 1 to 2.1 mm, filled with small size ( $\leq 2 \mu\text{m}$ ) particles [31]. A higher mobile phase linear velocity increases the resolution and detectability while reducing the time analysis which ultimately leads to a significant increase in the chromatographic pressure. As a result, appropriate equipment, capable of operating at high pressure up to 1,000 bar ( $\sim 15,000$  psi) is used to achieve maximum chromatographic performance [32].

Green analytical chemistry, an offshoot of green chemistry, is defined as the exploitation of methodologies and techniques aiming to minimize the generation of hazardous chemical waste by selecting green reagents and solvents as well as by choosing energy-efficient instruments to the extent i.e., technically and economically feasible. To address and cover all the twelve principles of green chemistry [33,34], two highly recommended approaches i.e., Analytical GREENness and Green Analytical Procedure Index were employed for comprehensive evaluation of the proposed method greenness.

Laboratories need to estimate measurement uncertainty for their quantitative methods to comply with ISO/IEC 17025 requirements. Measurement uncertainty is a component of uncertainty in all the individual steps of an analytical procedure [35]. Generally, a measurement result is only an approximation or estimation of the measured value and thus only complete when accompanied by a declaration of uncertainty of this estimate [36,37].

According to the authors' knowledge, there is no validation, measurement uncertainty estimation, and greenness evaluation of UHPLC method reported for the simultaneous quantitation of hydrochlorothiazide and metoprolol tartrate in tablets. Therefore, the present research describes a fast, simple, validated, and optimized UHPLC method for the simultaneous quantitation of hydrochlorothiazide and metoprolol tartrate in binary tablets. Both drugs were determined in less than 1 min using less quantity of organic solvent and without buffer solution as compared to the reported HPLC methods [20,21,23]. Moreover, measurement uncertainty calculation which is based on validation of the analytical procedure is described. Additionally, a comprehensive greenness assessment using two different green analytical chemistry metrics (Analytical GREENness and Green Analytical Procedure Index) was performed for the proposed method and compared with previously reported HPLC methods.

## 2. MATERIALS AND METHODS

### 2.1. Chemical, reagent and sample

Metoprolol tartrate (98%) and hydrochlorothiazide (98%) were provided by Sigma-Aldrich (Sao Paulo, Brazil) and Foundation for Popular Medicine (Sao Paulo, Brazil), respectively. Selopress<sup>®</sup> coated tablets (hydrochlorothiazide 12.5 mg and metoprolol tartrate 100 mg) and placebo (monohydrate lactose, silicon dioxide, microcrystalline cellulose, magnesium stearate, povidone, and sodium starch glycolate) were purchased from AstraZeneca (Sao Paulo, Brazil). Acetonitrile and methanol HPLC grade were obtained from J. T. Baker (Sao Paulo, Brazil). Hydrogen peroxide, sodium hydroxide, *o*-phosphoric acid, hydrochloric acid, and triethylamine were obtained from Merck<sup>®</sup> (Sao Paulo, Brazil). The purified water was obtained using Milli-Q<sup>®</sup> system.

### 2.2. Instrumentation and conditions

An Agilent 1200 UHPLC system, equipped with a degasser, an autosampler, a quaternary pump and a photodiode array detector was used for drug analyses. A Zorbax<sup>®</sup> SB-C18 (50 mm x 2.1 mm i.d., 1.8  $\mu$ m particle size) chromatographic column was used. The acetonitrile:water:triethylamine (17:83:0.2 v/v), pH 3.0 adjusted with *o*-phosphoric acid was used as mobile phase. The flow rate was 0.9 mL min<sup>-1</sup>. An absorbance wavelength of 225 nm was selected, the column temperature was maintained at 25 °C, and the sample injection volume was 0.2  $\mu$ L.

### 2.3. Standard stock solutions' preparation

10 mg of metoprolol tartrate was accurately weighed and transferred into a 10 mL amber volumetric flask, 5 mL of methanol was added, and the mixture was stirred until completely dissolved. Milli-Q<sup>®</sup> purified water was used to complete the volume and the sonication was performed for 5 min. Metoprolol tartrate final concentration was 1000  $\mu$ g mL<sup>-1</sup>. The same procedure was used to prepare hydrochlorothiazide standard stock solution with final concentration of 1000  $\mu$ g mL<sup>-1</sup>.

### 2.4. Test-mixture standard preparation

Aliquots from hydrochlorothiazide and metoprolol tartrate stock standard solutions were transferred into amber volumetric flask (10 mL), methanol (5 mL) was added, and Milli-Q<sup>®</sup> purified water was used to complete the volume. Final concentrations were 12.5  $\mu$ g mL<sup>-1</sup> and 100  $\mu$ g mL<sup>-1</sup> for hydrochlorothiazide and metoprolol tartrate, respectively. The sonication of test mixture was done for 3 min, the solution was filtered with 0.45  $\mu$ m filter, and injected into UHPLC instrument.

### 2.5. Sample stock and working solutions' preparation

The tablets (twenty) were weighed and crushed to obtain a fine powder. Three quantities of powder were

accurately weighed and then transferred into three amber volumetric flasks (100 mL). After methanol (50 mL) was added, the flasks were shaken manually for a few minutes and then the volume was adjusted to the mark with Milli-Q<sup>®</sup> water; further, the flasks were sonicated for 10 min. Final concentrations of hydrochlorothiazide (100, 125 and 150  $\mu\text{g mL}^{-1}$ ) and metoprolol tartrate (800, 1000 and 1200  $\mu\text{g mL}^{-1}$ ) were obtained.

To prepare desired working sample solutions, aliquots from sample stock solutions were transferred into amber volumetric flasks (10 mL), methanol (5 mL) was added and finally, the volume was completed with Milli-Q<sup>®</sup> water. The solutions were sonicated for 5 min, filtered in a 0.45  $\mu\text{m}$  filter, and injected into UHPLC instrument.

## 2.6. Method validation

The method validation was performed according to the guidelines of United States Pharmacopeia [38] and International Conference on Harmonization [39].

### 2.6.1. Specificity/selectivity

Method specificity was evaluated by confirming the separation of metoprolol tartrate and hydrochlorothiazide peaks from tablet excipients. Method selectivity was assessed by forced degradation conditions (photolytic, oxidative, neutral, alkaline, and acidic hydrolysis). Neutral, acidic, and alkaline degradations were carried out in ultrapure water, 0.1 M HCl and 0.1 M NaOH, respectively. After degradation, last two were neutralized. 3%  $\text{H}_2\text{O}_2$  solution was used for oxidative stress and photodegradation was performed by exposing the samples in a photostability UV light chamber for 60 h at 254 nm. Metoprolol tartrate (1000  $\mu\text{g mL}^{-1}$ ) and hydrochlorothiazide (125  $\mu\text{g mL}^{-1}$ ) sample solutions were prepared and refluxed for 2 and 24 h at 80 °C except photolytic condition. Aliquots were taken and transferred to 10 mL amber volumetric flasks and diluted with Milli-Q<sup>®</sup> water to obtain final concentrations of 12.5  $\mu\text{g mL}^{-1}$  and 100.0  $\mu\text{g mL}^{-1}$  for hydrochlorothiazide and metoprolol tartrate, respectively and filtered before being injected. Peak purities were performed for selectivity assessment by using photodiode array detector.

### 2.6.2. Linearity

Aliquots of hydrochlorothiazide and metoprolol tartrate stock standard solutions were transferred to five amber volumetric flasks (10 mL) and ultrapure water was used to complete the final volume. Linearity was evaluated in triplicate at five concentration levels for metoprolol tartrate (80.0, 90.0, 100.0, 110.0 and 120.0  $\mu\text{g mL}^{-1}$ ) and hydrochlorothiazide (10.0, 11.25, 12.5, 13.75 and 15.0  $\mu\text{g mL}^{-1}$ ). Analytical curves (three) were constructed by plotting metoprolol tartrate and hydrochlorothiazide concentrations against their peak areas. Least-square method was used to calculate the regression lines. Method's linearity ( $p$  value = 0.05) was determined by using the analysis of variance.



### 2.6.3. Detection and quantitation limits

According to the International Conference on Harmonization Q2 (R1) guideline [39], detection and quantitation limits were calculated based on response standard deviation and analytical curve slope ( $n = 3$ ).

### 2.6.4. Precision

Method precision (repeatability and intermediate precision) was studied. Repeatability was performed by the determination of ten independent samples in the median concentration (100%) of the analytical curve. Samples ( $12.5 \mu\text{g mL}^{-1}$  for hydrochlorothiazide and  $100.0 \mu\text{g mL}^{-1}$  for metoprolol tartrate) were prepared and analyzed on the same day under the same experimental conditions. Intermediate precision was analyzed at three different concentration levels ( $10.0$ ,  $12.5$  and  $15.0 \mu\text{g mL}^{-1}$  for hydrochlorothiazide and  $80.0$ ,  $100.0$  and  $120.0 \mu\text{g mL}^{-1}$  for metoprolol tartrate) in triplicate over three consecutive days. All results were calculated by average percent relative standard deviation.

### 2.6.5. Accuracy

Accuracy was determined as the percent recovery of standard added at known concentration to the sample. Recovery based on three concentration levels (80, 100 and 120 % of the label claim) was assessed. Known quantities of hydrochlorothiazide ( $5.0$ ,  $6.25$  and  $7.5 \mu\text{g mL}^{-1}$ ) and metoprolol tartrate ( $40.0$ ,  $50.0$  and  $60.0 \mu\text{g mL}^{-1}$ ) standard solutions were added to commercial sample solutions. Accuracy was determined in triplicate.

### 2.7. Measurement uncertainty evaluation and risk assessment

Measurement uncertainty estimations were performed according to Eurachem/Citac guides, both using bottom-up and top-down approaches [36,37]. Combined uncertainties associated with the quantification of metoprolol tartrate and hydrochlorothiazide were obtained from individual uncertainties components through weighing and diluting (volumetric flasks and pipettes) associated with standard and sample solution preparations, as well as repeatability from peak areas obtained from chromatograms. The general uncertainty propagation law equation is presented below:

$$u_y = \sqrt{\sum_i^n \left( u_{x_i}^2 \left( \frac{\partial y}{\partial x_i} \right)^2 \right) + \sum_i^n \sum_j^n \left( u_{x_i} u_{x_j} \left( \frac{\partial y}{\partial x_i} \right) \left( \frac{\partial y}{\partial x_j} \right) r_{ij} \right)} \quad (\text{Eq. 1})$$

where  $y$  and  $u_y$  are measured value and respective combined standard uncertainty,  $u_{x_i}$  and  $u_{x_j}$  are the uncertainty values of  $x_i$  and  $x_j$  inputs, and  $r_{ij}$  is the correlation between the  $x_i$  and  $x_j$  input values.

Alternatively, measurement uncertainties associated with the quantification of metoprolol tartrate and hydrochlorothiazide were estimated based on the results obtained from in-house validation. In this case, the

measurement uncertainties are associated with accuracy and precision used to calculate combined and expanded uncertainties [40]. The general model equation used to evaluate in-house validation uncertainty data is presented below:

$$u_y = \sqrt{(1 - R)^2 + s_p^2} \quad (\text{Eq. 2})$$

where  $u_y$  – combined standard uncertainty,  $R$  – mean recovery value (accuracy), and  $s_p$  – standard deviation of the intermediate precision.

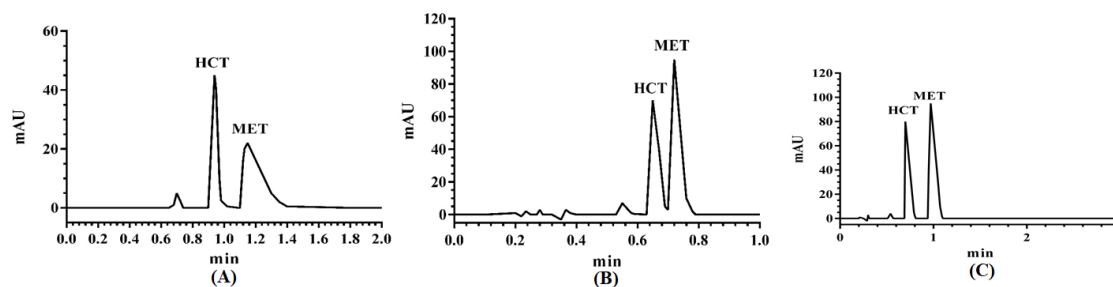
The false risk conformity decisions due to measurement uncertainties was estimated using a frequentist probability approach. Consumers' (probability to accept a lot that should be rejected) and producers' (probability to reject a lot that should be accepted) by Monte Carlo method. This method was applied using MS-Excel spreadsheet with 50,000 simulations. Monte Carlo method was employed using MS-Excel formula “=NORM.INV(RAN(), y,  $u_y$ )”, where  $y$  and  $u_y$  are the measured values (e.g. metoprolol tartrate or hydrochlorothiazide assay value) and respective combined standard uncertainty. The consumers' and producers' risk values were calculated as  $N_{OUT}/(N_{OUT} + N_{IN})$  and  $N_{IN}/(N_{OUT} + N_{IN})$ , where  $N_{IN}$  and  $N_{OUT}$  are the number of simulated values within and out of the specification limits (note:  $N_{IN} + N_{OUT} = 50,000$ ). The MS-Excel spreadsheet used to calculate the consumers' and producers' risk values is available as *supplementary material (Risk Assessment.xlsx)*.

### 3. RESULTS AND DISCUSSION

#### 3.1. Method development and optimization

The preliminary chromatographic method for simultaneous determination of hydrochlorothiazide and metoprolol tartrate was developed using Zorbax<sup>®</sup> SB-C18 column (50 mm x 2.1 mm i.d., 1.8  $\mu$ m particle size), a mixture of acetonitrile:water (20:80 v/v), pH 3.0 adjusted with *o*-phosphoric acid was used as mobile phase. The flow rate was 0.9 mL min<sup>-1</sup>, the column temperature was set at 25 °C, and the detection wavelength was fixed at 225 nm.

**Fig. 2A** shows the separation of analytes, however, the peaks are deformed and presenting enlargement at baseline. The metoprolol tartrate asymmetry is due to the interaction of amine functionality with the residual silanols of the stationary phase. To improve peak symmetry, 0.2% triethylamine was added to the mobile phase which will cover residual silanols, hence avoiding enlargement and resolution was a little bit compromised (**Fig. 2B**).



**Fig. 2.** Chromatogram of metoprolol tartrate (MET) and hydrochlorothiazide (HCT). Conditions: Zorbax® SB-C18 column (50 mm x 2.1 mm i.d., 1.8 µm particle size), pH 3.0 adjusted with *o*-phosphoric acid, column temperature 25 °C, flow rate 0.9 mL min<sup>-1</sup>, and detection at 225 nm. Mobile phase: (A) acetonitrile:water (20:80 v/v); (B) acetonitrile:water:triethylamine (20:80:0.2 v/v); and (C) acetonitrile:water:triethylamine (17:83:0.2 v/v).

To optimize the proposed method, Central Composite Design with Doehlert was used to adjust quadratic models [41,42]. The tested models are expressed in **Table 1**, while their statistical significance assessed by analysis of variance was expressed in **Table 2**.

**Table 1** Central Composite Design for hydrochlorothiazide (Y1) and metoprolol tartrate (Y2) resolutions as function of pH (X1) and acetonitrile (% ACN) proportion (X2).

X1 (pH)	X2 (% ACN)	Resolution	
		Y1 (HCT)	Y2 (MET)
2.3	17	4.82	7.14
2.5	12	1.6	14.19
2.5	22	0	1.6
3.0	10	0	20.9
3.0	17	4.85	6.68
3.0	24	0.86	1.08
3.5	12	0	16.32
3.5	22	1.42	0.92
3.7	17	4.75	7.6

**Table 2** Analysis of variance results for hydrochlorothiazide (Y1) and metoprolol tartrate (Y2) resolutions as function of pH (X1) and acetonitrile proportion (X2).

Source	Y1				Y2			
	Coef	DF	SS	<i>p</i> value	Coef	DF	SS	<i>p</i> value
Regression		2	16.0811	0.078		4	411.549	0.000
R <sup>2</sup>	0.57				0.995			
Constant	-18.40				36.64			
Linear		1	0.1324	0.806		2	392.817	0.000

X1					5.31	1	0.554	0.350
X2	2.528	1	0.1324	0.806	-3.129	1	392.263	0.000
Quadratic		1	15.9487	0.030		1	16.758	0.004
X1								
X2	-	1	15.9487	0.030	0.0754	1	16.758	0.004
	0.0736							
Interaction						1	1.974	0.117
X1 * X2					-0.281	1	1.974	0.117
Error		6	12.0012			4	1.981	
Total		8	28.0823			8	413.529	

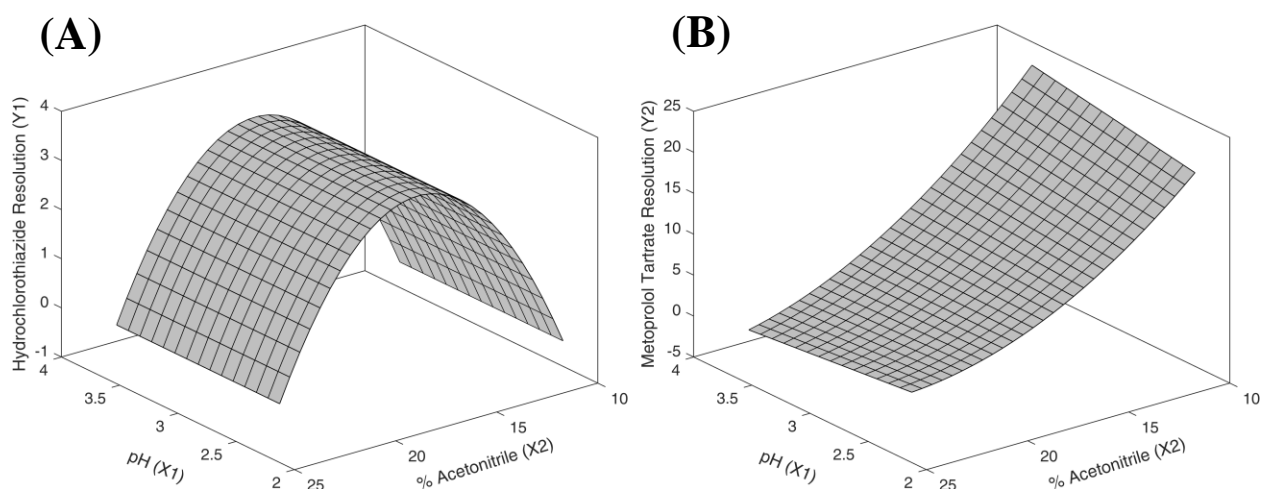
$R^2$  = Determination coefficient; Coef = coefficient; DF = degrees of freedom; SS = sum of squares

The regression equations and determination coefficients for hydrochlorothiazide (Y1) and metoprolol tartrate (Y2) resolutions as function of pH (X1) and acetonitrile proportion (X2) are expressed in equations (Eq. 3 and 4), respectively.

$$Y1 = -18.40 + 2.528*X2 - 0.0736*X2^2 \quad (\text{Eq. 3})$$

$$Y2 = 36.64 + 5.31*X1 - 3.129*X2 + 0.0754*X2^2 - 0.281*X1*X2 \quad (\text{Eq. 4})$$

**Fig. 3A** represents 3D response surface plot for hydrochlorothiazide (Y1) resolution and **Fig. 3B** for metoprolol tartrate (Y2) resolution as function of pH (X1) and acetonitrile proportion (X2). Hydrochlorothiazide resolution ( $R_{s(\text{hydrochlorothiazide degradation product} - \text{hydrochlorothiazide})}$ ) and metoprolol tartrate resolution ( $R_{s(\text{hydrochlorothiazide} - \text{metoprolol tartrate})}$ ) suffer more interference with variation in acetonitrile concentration and there was almost no change with pH variation.



**Fig. 3.** Response surface. (A) hydrochlorothiazide (Y1) and (B) metoprolol tartrate (Y2) resolutions as function of pH (X1) and acetonitrile proportion (X2).

The resolution was maximized, when 17% of acetonitrile and pH 3 were used. Under these conditions,

resolutions of 4.85 for hydrochlorothiazide degradation product – hydrochlorothiazide and 6.68 for hydrochlorothiazide – metoprolol tartrate were obtained.

The proposed UHPLC method for determining both drugs simultaneously was validated using the following conditions: Zorbax<sup>®</sup> SB-C18 column (50 mm x 2.1 mm i.d., 1.8 µm particle size), and acetonitrile:water:triethylamine (17:83:0.2 v/v) pH 3.0 adjusted with *o*-phosphoric acid. The injection volume was 0.2 µL, the column temperature was set at 25 °C, and the eluent was monitored by the detection wavelength of 225 nm.

**Fig. 2C** shows metoprolol tartrate and hydrochlorothiazide chromatogram obtained at optimized chromatographic conditions.

### 3.2. Method validation

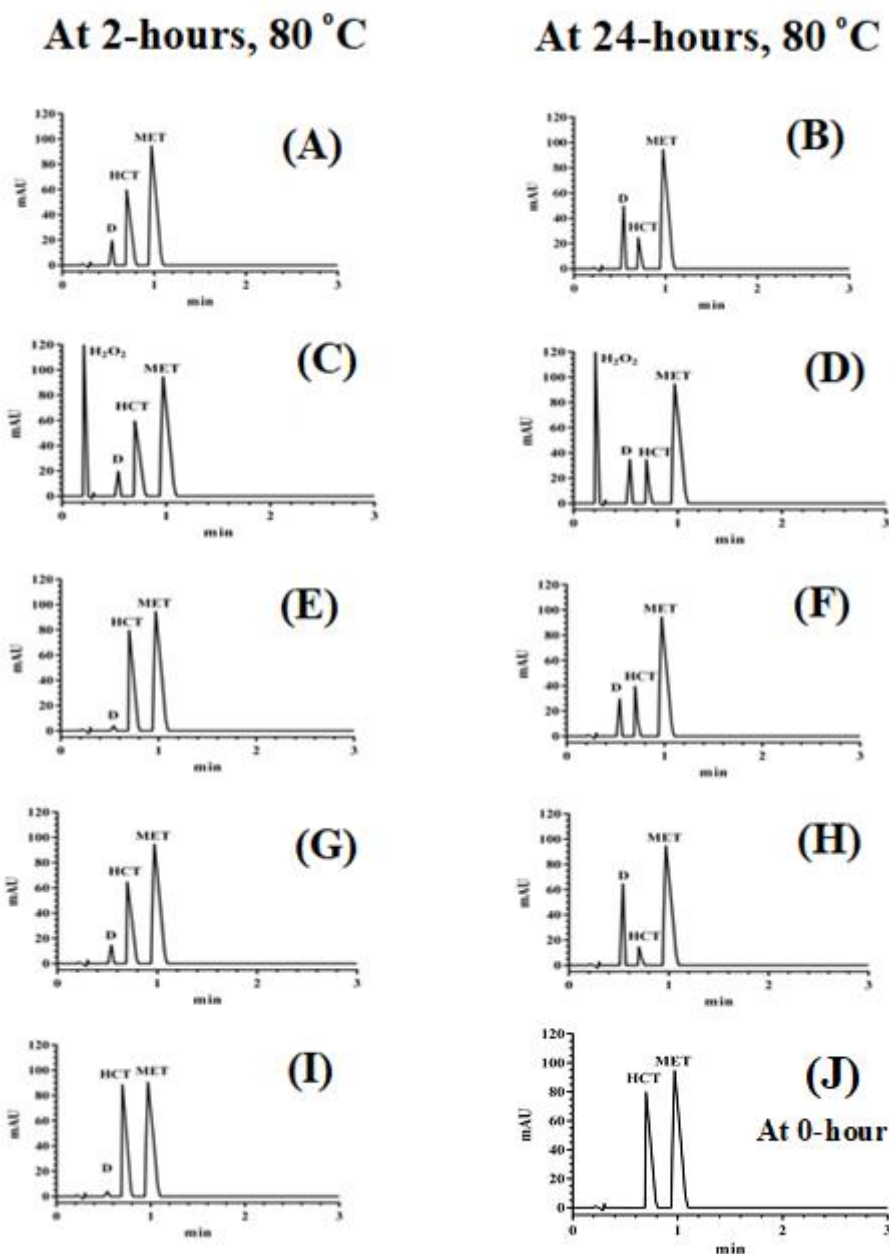
The assessed parameters were specificity/selectivity, precision, linearity, accuracy, detection and quantification limits [38,39]. Robustness was assessed by Central Composite Design response from method development and optimization.

#### 3.2.1. System suitability

In chromatographic methods, system suitability assessment is very important to confirm the acceptable performance of the instrument used for analytical measurements [43]. This process generates the production of accurate and replicable data which can be submitted with confidence to regulatory agencies. Typically, the system suitability parameters include tailing factor, resolution, retention time, and number of theoretical plates [44].

#### 3.2.2. Specificity/Selectivity

Method specificity was evaluated through a solution containing a mixture of tablet excipients. No interferences were detected at retention times of metoprolol tartrate and hydrochlorothiazide in the sample solution. Peak purities higher than 99.8% were obtained for metoprolol tartrate and hydrochlorothiazide by using photodiode array detector, which shows the excipients did not coelute with main peaks (Fig. 4J). Thereby, the presented method is applicable for the determination of both active pharmaceutical ingredients.



**Fig. 4.** Chromatograms of metoprolol tartrate (MET) and hydrochlorothiazide (HCT) after forced degradation conditions at 2 h – 80 °C and 24 h – 80 °C. (A) and (B) neutral hydrolysis; (C) and (D) oxidative; (E) and (F) basic hydrolysis; (G) and (H) acidic hydrolysis; (I) photolytic and (J) 0-hour without stress. Conditions: Zorbax<sup>®</sup> SB-C18 column (50.0 mm x 2.1 mm i.d., 1.8 µm particle size); mobile phase: acetonitrile:water:triethylamine (17:83:0.2 v/v) pH 3.0 adjusted with *o*-phosphoric acid, sample injection 2.0 µL, flow rate 0.9 mL min<sup>-1</sup>, column temperature 25 °C, and UV detection at 225 nm. D = degradation product.

Method selectivity was assessed by performing metoprolol tartrate and hydrochlorothiazide under forced degradation conditions (photolytic, oxidative, neutral, basic, and acidic hydrolysis) to demonstrate whether their degradation products either interfere or not for the determination of hydrochlorothiazide and

metoprolol tartrate. One hydrochlorothiazide degradation product was observed after 2 and 24 h for oxidative and neutral hydrolysis (0.56 min), acidic and basic hydrolysis (0.55 min), while no degradation product was observed with metoprolol tartrate (**Fig. 4**). Peak purities were performed and purity factor higher than 999 (metoprolol tartrate 999.95 and hydrochlorothiazide 999.96) were obtained by using photodiode array detector. There was no interference from the obtained degradation products with the quantification of analytes under study.

### 3.2.3. Linearity

Metoprolol tartrate (concentration range: 80.0 to 120.0  $\mu\text{g mL}^{-1}$ ) and hydrochlorothiazide (concentration range: 10.0 to 15.0  $\mu\text{g mL}^{-1}$ ) were used to construct the analytical curves. Good linearities with determination coefficients  $> 0.99$  for both active pharmaceutical ingredients were obtained. To check the method good fitting, an analysis of variance was performed and there was significant regression,  $F_{\text{calculated}} = 152.85 > F_{\text{critical}} = 2.48$  for hydrochlorothiazide and  $F_{\text{calculated}} = 1934.34 > F_{\text{critical}} = 2.48$  for metoprolol tartrate,  $\alpha = 0.05$ . It demonstrates that linear model is suitable for the curves, since critical  $F$  values were higher than found  $p$  values, indicating  $Y$  (response variances) is independent of  $X$  (concentration levels). Moreover,  $F$  values observed from the regression analysis were greater than critical  $F$ . Therefore, **Table 3** shows the existence of a linear relationship between  $X$  and  $Y$  variables.

**Table 3** System suitability, linearity, limits of detection and quantitation, precision and accuracy of the proposed method.

Analytical feature	Metoprolol tartrate	Hydrochlorothiazide
Retention time (min) <sup>a</sup>	0.96 $\pm$ 0.01	0.70 $\pm$ 0.01
Column efficiency (N) <sup>a</sup>	1716 $\pm$ 4.23	1777 $\pm$ 4.92
Tailing factor <sup>a</sup>	1.36 $\pm$ 0.03	1.32 $\pm$ 0.03
Resolution (Rs) <sup>a</sup>	4.03 $\pm$ 0.05	
Determination coefficient (R <sup>2</sup> )	0.9991	0.9903
Concentration range ( $\mu\text{g mL}^{-1}$ ) <sup>b</sup>	80.0 – 120.0	10.0 – 15.0
Intercept	2.893	-13.794
Slope (S)	2.187	10.381
Critical	2.48	2.48
P	0.6147	0.2840
Detection limit ( $\mu\text{g mL}^{-1}$ )	2.42	1.05
Quantitation limit ( $\mu\text{g mL}^{-1}$ )	7.34	3.19
Intra-day precision (% RSD) <sup>c</sup>	1.20 $\pm$ 2.70	0.72 $\pm$ 0.87
Inter-day precision (% RSD) <sup>d</sup>	0.62 $\pm$ 0.30	0.39 $\pm$ 0.22
Accuracy (% Recovery) (Mean $\pm$ SD) <sup>e</sup>	101.13 $\pm$ 0.64	100.60 $\pm$ 0.26

a: Mean  $\pm$  SD of six determinations.

b: Five concentrations, each concentration level in triplicate.

c: Mean  $\pm$  SD of ten determinations.

d: Mean  $\pm$  SD of nine determinations.

e: Average of nine determinations.

% RSD = percent relative standard deviation.

#### 3.2.4. Detection and quantitation limits

Following formula is used to calculate the detection and quantitation limits.

$$\text{Detection limit} = 3.3 \sigma/S \text{ and Quantitation limit} = 10 \sigma/S$$

where  $\sigma$  – standard deviation of y-intercepts of regression lines,  $S$  – slope estimated from analytical curves of metoprolol tartrate and hydrochlorothiazide. Detection and quantitation limits for metoprolol tartrate were  $2.42 \mu\text{g mL}^{-1}$  and  $7.34 \mu\text{g mL}^{-1}$  and for hydrochlorothiazide were  $1.05 \mu\text{g mL}^{-1}$  and  $3.19 \mu\text{g mL}^{-1}$ , respectively.

#### 3.2.5. Precision

The intra-day (repeatability) and inter-day (intermediate) precisions were calculated as percent relative standard deviation for sample solutions containing metoprolol tartrate and hydrochlorothiazide to prove its applicability. The intra-day precision was estimated to be  $0.72 \pm 0.87$  and  $1.20 \pm 2.70$  % for hydrochlorothiazide and metoprolol tartrate, respectively; and the inter-day precision was estimated to be  $0.39 \pm 0.22$  % for hydrochlorothiazide and  $0.62 \pm 0.30$  % for metoprolol tartrate. The results confirmed that the proposed method was highly precise [45] (**Table 3**).

#### 3.2.6. Accuracy

Recovery tests were carried out at three concentration levels (low, middle, and high) from the analytical curve to obtain the method accuracy. Recovery was obtained by spiking known quantities of hydrochlorothiazide and metoprolol tartrate standards to known sample quantities in triplicate. The average percentage recoveries for hydrochlorothiazide and metoprolol tartrate demonstrated that the presented method was highly accurate [45] (**Table 3**).

#### 3.3. Uncertainty measurement

To indicate the test reliability, the measurement uncertainties were estimated according to Eurachem/Citac guidelines [46]. The uncertainty estimation results of any test depend on the knowledge of critical points of the analytical procedure, it is essential to know the factors that can influence the final result. To avoid the double uncertainty contribution, which could lead to overestimation of the combined uncertainty, the diagram of cause and effect was constructed, also known as Ishikawa or Fishbone diagram (*graphical*



*abstract*).

Standard uncertainties of metoprolol tartrate and hydrochlorothiazide were estimated based on the validation method, experimental studies, certificate information, and calibration results (**Table 4**).

**Table 4** Quantification of uncertainties and conversion to standard deviation of the uncertainty of each component which is used to estimate the combined uncertainties associated with the quantification of metoprolol tartrate (MET) and hydrochlorothiazide (HCT) in pharmaceutical binary tablet.

Uncertainties sources	Standard uncertainty ( $x$ )	Relative standard uncertainty ( $u_x$ )
Preparation of standard solution		
Weight of MET RS ( $ws$ )	10.0 mg	0.1 mg
Weight of HCT RS ( $ws$ )	10.0 mg	0.1 mL
Volumetric flask ( $vfs1$ )	10.000 mL	0.017 mL
Volumetric pipette ( $vps1$ )	1.0000 mL	0.0017 mL
Volumetric flask ( $vfs2$ )	10.00 mL	0.017 mL
Preparation of sample solution		
Weight of sample ( $wt$ )	345.0 mg	0.1 mg
Volumetric flask ( $vft1$ )	100.00 mL	0.17 mL
Volumetric pipette ( $vpt1$ )	1.0000 mL	0.0017 mL
Volumetric flask ( $vft2$ )	10.000 mL	0.017 mL
Repeatability of peak area		
Area of MET in Standard ( $As$ )	221.73	1.33
Area of MET in Sample ( $At$ )	221.86	1.33
Area of HCT in Standard ( $As$ )	120.83	0.43
Area of HCT in Sample ( $At$ )	121.20	0.44
Expanded final uncertainty		
Quantification of MET (%)	100.1%	2.8%*
Quantification of HCT (%)	100.3%	2.4%*

RS = Reference Standard.

\*Expanded uncertainty using a coverage factor  $k = 2.0$  with 95% confidence level.

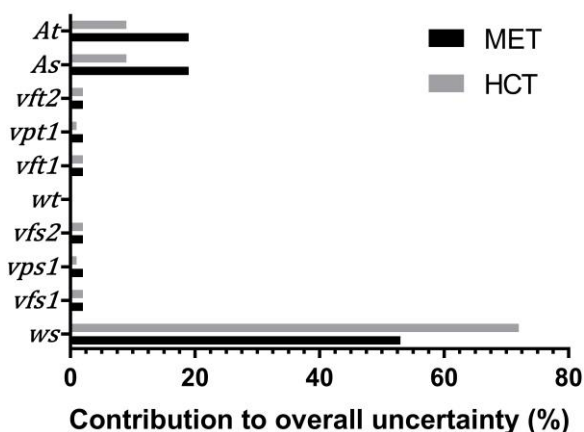
For each source of uncertainty, variables of entry were determined, and uncertainties associated with each source were quantified. Correlations between variables were assumed to be negligible. Combined and expanded uncertainties were calculated using the following equation (**Eq. 5**).

$$u_{C\%} = C\% \sqrt{\left(\frac{u_{ws}}{ws}\right)^2 + \left(\frac{u_{vfs1}}{vfs1}\right)^2 + \left(\frac{u_{vps1}}{vps1}\right)^2 + \left(\frac{u_{vfs2}}{vfs2}\right)^2 + \left(\frac{u_{wt}}{wt}\right)^2 + \left(\frac{u_{vft1}}{vft1}\right)^2 + \left(\frac{u_{vpt1}}{vpt1}\right)^2 + \left(\frac{u_{vft2}}{vft2}\right)^2 + \left(\frac{u_{As}}{As}\right)^2 + \left(\frac{u_{At}}{At}\right)^2} \quad (\text{Eq. 5})$$

where  $ws$  and  $u_{ws}$  are weight of reference standard and its respective uncertainty,  $vfs1$  and  $u_{vfs1}$  are

volume of volumetric flask used to prepare standard stock solution and its respective uncertainty,  $vps1$  and  $u_{vps1}$  are volume of volumetric pipette used to prepare standard diluted solution and its respective uncertainty,  $vfs2$  and  $u_{vfs2}$  are volume of volumetric flask used to prepare standard diluted solution and its respective uncertainty,  $wt$  and  $u_{wt}$  are weight of test sample and its respective uncertainty,  $vft1$  and  $u_{vft1}$  are volume of volumetric flask used to prepare test stock solution and its respective uncertainty,  $vpt1$  and  $u_{vpt1}$  are volume of volumetric pipette used to prepare test diluted solution and its respective uncertainty,  $vft2$  and  $u_{vft2}$  are volume of volumetric flask used to prepare test diluted solution and its respective uncertainty,  $As$  and  $u_{As}$  are peak area obtained for reference standard diluted solution and its respective uncertainty, and  $At$  and  $u_{At}$  are peak area obtained for test diluted solution and its respective uncertainty.

The main uncertainties identified for the test were associated with the weight of metoprolol tartrate and hydrochlorothiazide reference standards, contributing to 53 and 72 % of overall uncertainties. It can be explained due to the small amount of reference standards used. Moreover, the variability of peak areas for metoprolol tartrate and hydrochlorothiazide in sample and standard solutions contributed with 9 and 19 % of overall uncertainty, respectively. A contribution summary of each component is shown in **Fig. 5A**.



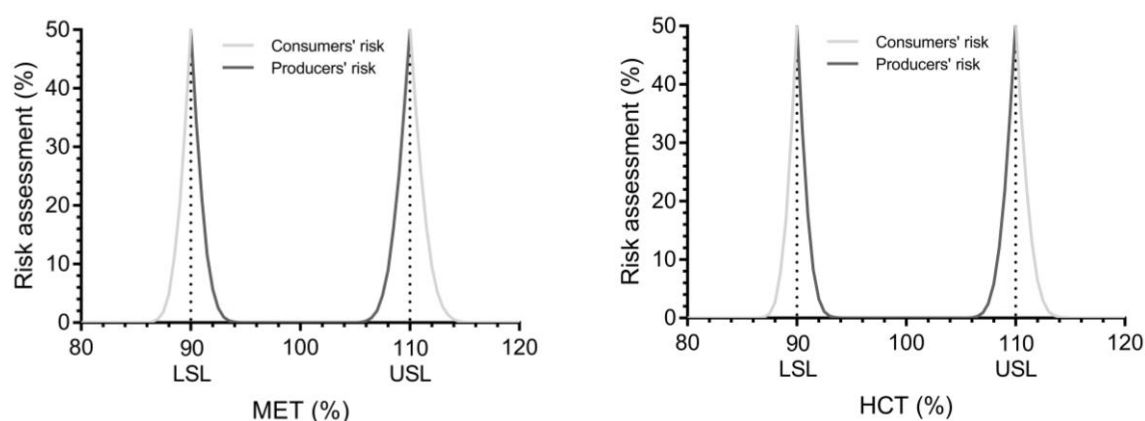
**Fig. 5A.** Contribution of each source of uncertainty to the overall uncertainty associated with the quantification of metoprolol tartrate (MET) and hydrochlorothiazide (HCT) by ultra-high performance liquid chromatography.  $ws$  = weight of MET reference standard;  $ws$  = weight of HCT reference standard;  $vfs1$  = volumetric flask;  $vps1$  = volumetric pipette;  $vfs2$  = volumetric flask;  $wt$  = weight of sample;  $vft1$  = volumetric flask;  $vpt1$  = volumetric pipette;  $vft2$  = volumetric flask;  $As$  = area of MET in standard;  $At$  = area of MET in sample;  $As$  = area of HCT in standard; and  $At$  = area of HCT in sample.

The metoprolol tartrate and hydrochlorothiazide content results and their uncertainty measurement obtained using Eurachem procedure were  $100.1 \pm 2.8$  % and  $100.3 \pm 2.4$  %, respectively. These results were closely to ones found with Monte Carlo simulation ( $100.1 \pm 2.74$  % for hydrochlorothiazide and  $100.3 \pm 2.37$  % for metoprolol tartrate) and using in-house validation data ( $100.0 \pm 2.99$  % for hydrochlorothiazide

and  $100.3 \pm 2.58\%$  for metoprolol tartrate). Measurement uncertainty values obtained from validation data were calculated using the accuracy and precision results at  $12.5 \mu\text{g mL}^{-1}$  and  $100 \mu\text{g mL}^{-1}$  for hydrochlorothiazide and metoprolol tartrate, respectively. 50,000 assay results were simulated and calculated by random raw data using Monte Carlo method.

It is worth to be mentioned that the uncertainty value for metoprolol tartrate ( $U_{MET} = 2.8\%$ ) was found to be higher than the target uncertainty value ( $U^t = 2.5\%$ ). On the contrary, the measurement uncertainty value obtained for hydrochlorothiazide ( $U_{HCT} = 2.4\%$ ) was lower than the target uncertainty ( $U^t = 2.5\%$ ). The uncertainty associated with weight of the reference standard may be improved in order to obtain an uncertainty value for hydrochlorothiazide below the target uncertainty value.

Measurement uncertainty information should be taken into account to reduce false risk of conformity/non-conformity decisions. Thus, considering the measurement uncertainties values obtained for metoprolol tartrate and hydrochlorothiazide, the false risk conformity decisions were estimated using Monte Carlo simulations. Consumers' and producers' particular risks as a function of metoprolol tartrate and hydrochlorothiazide quantification are presented in **Fig. 5B**.



**Fig. 5B.** Consumers' and producers' risks due to measurement uncertainties estimated as a function of metoprolol tartrate (MET) and hydrochlorothiazide (HCT) quantifications. LSL = Lower Specification Limit; USL = Upper Specification Limit.

Alternatively, guard bands may be used to define acceptance (or rejection) region which ensures a reduced risk of false acceptance (or rejection). Generally, by multiplying the uncertainty value ( $u$ ) by an adequate coverage factor ( $k$ , usually 1.64 for a 5% risk of false decision), it is possible to obtain the guard band ( $g$ ). In order to provide a lower risk of false acceptance (consumer's risk), the guard band ( $g$ ) is subtracted and added to the upper and lower specification limits, respectively. Considering measurement uncertainty values obtained for metoprolol tartrate and hydrochlorothiazide and specification interval from 90 to 110 %, the acceptance limits are from 92 to 108 % and from 92.3 to 107.7 % for metoprolol tartrate and hydrochlorothiazide, respectively. On the other hand, the guard band ( $g$ ) is added and subtracted to the upper and lower specification limits to provide a lower risk of false rejection (producer's risk). Thus, the

lower and upper rejection limits will be 88% and 102% for metoprolol tartrate and 87.7% and 102.3% for hydrochlorothiazide, respectively.



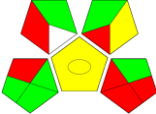

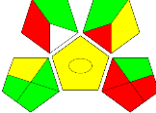



### 3.4. Application of the proposed method

Both active pharmaceutical ingredients (hydrochlorothiazide and metoprolol tartrate) were analyzed using the validated UHPLC method in binary Selopress<sup>®</sup> coated tablets. The assay of hydrochlorothiazide and metoprolol tartrate in the pharmaceutical formulation indicated a mean value of  $12.94 \pm 0.53$  mg/tab (103.52%, %RSD = 0.53) and  $99.94 \pm 0.08$  mg/tab (99.94%, %RSD = 0.08), respectively that found to be in good compliance with label claim amount 90 – 110 % [38].

### 3.5. Evaluation of proposed method greenness and comparison with three reported methods

Based on green analytical chemistry approaches (Analytical GREENness and Green Analytical Procedure Index), the developed UHPLC method were evaluated. Green Analytical Procedure Index shows green, yellow, or red colors which represent the low, medium, or high environmental concerns. Results showed that 6 regions are shaded green, 5 yellow, 3 red, and 1 white indicating the proposed method was more greener compared to three reported high-performance liquid chromatographic methods (**Table 5**).

**Table 5** Evaluation of proposed method and comparison with literature

Method	Mobile phase	Run time (min)	Flow rate (mL min <sup>-1</sup> )	Waste (mL/run)	Green Analytical Procedure Index	Analytical GREENness
UHPLC Proposed Method	acetonitrile:water:triethylamine (17:83:0.2 v/v)	3	0.9	2.7	 (6 Green, 5 Yellow, 3 Red)	 0.79
HPLC [20]	methanol:water (95:5 v/v)	13	1.2	15.6	 (6 Green, 2 Yellow, 6 Red)	 0.59
HPLC [21]	phosphate buffer:methanol (60:40 v/v)	14	1	14	 (6 Green, 3 Yellow, 5 Red)	 0.69
HPLC [23]	A) sodium phosphate buffer 34mM; B) acetonitrile at a gradient elution: 15% B; 15%-90% B; 90%-15% B; 15% B	13	1	13	 (4 Green, 4 Yellow, 6 Red)	 0.7

Analytical GREENness also reveals the greenness profile by specific pictogram color ranging from red to dark green with a score from 0.0 to 1.0. The proposed UHPLC method was more eco-friendly with a final score of 0.79 as compared to three reported HPLC methods (**Table 5**). Therefore, both are highly recommended and widely used approaches that produce an informative and easily interpretable result for the assessment of greenness.

#### **4. CONCLUDING REMARKS**

A fast, linear, precise, accurate, and robust UHPLC method was developed, optimized and validated by using Central Composite Design for simultaneous quantitation of hydrochlorothiazide and metoprolol tartrate in pharmaceutical binary tablet and in presence of their degradation products. No interference was detected at retention times of both active pharmaceutical ingredients from matrix sample. The forced degradation conditions (photolytic, oxidative, neutral, acidic, and alkaline hydrolysis) were also performed. No metoprolol tartrate degradation product was observed, while one hydrochlorothiazide degradation product was observed when the sample was submitted to photolytic, oxidative, neutral, acidic and alkaline hydrolysis.

The novelty of the described UHPLC method is the validation and measurement uncertainty estimation. The producer's and consumer's risks were estimated for compliance assessment using uncertainty measurement and Monte Carlo simulations to obtain a reliable analytical procedure. Moreover, the proposed method greenness is also evaluated and compared with the published HPLC methods. Therefore, the proposed method can be effectively implemented for analytical quality control in the pharmaceutical industries.

#### **ACKNOWLEDGMENTS**

The authors would like to thank Agilent Technologies Brazil Ltda. for instrumental support, Fundação de Amparo à Pesquisa do Estado de São Paulo, Brazil for financial support (2012/50595-8), and Coordenação de Aperfeiçoamento de Pessoal de Nível Superior, Brazil for FAGF scholarship (88882.377651/2019-01).

#### **CONFLICTS OF INTEREST**

The authors declare that they have no known competing financial interests or personal relationships that could have appeared to influence the reported work.

#### **DATA AVAILABILITY STATEMENT**

The data that support the findings of this study is available from the corresponding author upon reasonable request.

#### **ORCID**

*Claudia Vilela de Oliveira* <https://orcid.org/0000-0003-4200-2533>

*Adriano Peron* <https://orcid.org/0000-0002-7111-3171>

*Anas Rashid* <https://orcid.org/0000-0002-4644-4729>

Frank Alonso Gavilano Fajardo <https://orcid.org/0000-0002-6018-1697>

Felipe Rebello Lourenço <https://orcid.org/0000-0002-2630-151X>

Marina Franco Maggi Tavares <https://orcid.org/0000-0002-7395-3502>

María Segunda Aurora Prado <https://orcid.org/0000-0002-9956-9410>

## REFERENCES

- [1] Y. Ostchega, C.D. Fryar, T. Nwankwo, D.T. Nguyen, Hypertension Prevalence Among Adults Aged 18 and Over: United States, 2017-2018, *Natl. Cent. Heal. Stat. Data Br.* 364 (2020) 1–8. <https://pubmed.ncbi.nlm.nih.gov/32487290/> (accessed August 14, 2022).
- [2] WHO, Hypertension, World Heal. Organ. (2022). <https://www.who.int/news-room/fact-sheets/detail/hypertension> (accessed August 14, 2022).
- [3] G.A. Mensah, J.B. Croft, W.H. Giles, The Heart, Kidney, and Brain as Target Organs in Hypertension, *Cardiol. Clin.* 20 (2002) 225–247. [https://doi.org/10.1016/S0733-8651\(02\)00004-8](https://doi.org/10.1016/S0733-8651(02)00004-8).
- [4] S. Oparil, M.C. Acelajado, G.L. Bakris, D.R. Berlowitz, R. Cífková, A.F. Dominiczak, G. Grassi, J. Jordan, N.R. Poulter, A. Rodgers, P.K. Whelton, Hypertension, *Nat. Rev. Dis. Prim.* 2018 41. 4 (2018) 1–21. <https://doi.org/10.1038/nrdp.2018.14>.
- [5] C. Armstrong, JNC8 Guidelines for the Management of Hypertension in Adults, *Am. Fam. Physician.* 90 (2014) 503–504. [www.aafp.org/afpAmericanFamilyPhysician503](http://www.aafp.org/afpAmericanFamilyPhysician503) (accessed July 13, 2021).
- [6] D.H. Ellison, Clinical Pharmacology in Diuretic Use, *Clin. J. Am. Soc. Nephrol.* 14 (2019) 1248–1257. <https://doi.org/10.2215/CJN.09630818>.
- [7] F.H. Messerli, S. Bangalore, Half a Century of Hydrochlorothiazide: Facts, Fads, Fiction, and Follies, *Am. J. Med.* 124 (2011) 896–899. <https://doi.org/10.1016/j.amjmed.2011.05.009>.
- [8] A.S. Go, J. Yang, J.H. Gurwitz, J. Hsu, K. Lane, R. Platt, Comparative Effectiveness of beta-Adrenergic Antagonists (Atenolol, Metoprolol Tartrate, Carvedilol) on the Risk of Rehospitalization in Adults with Heart Failure, *Am. J. Cardiol.* 100 (2007) 690–696. <https://doi.org/10.1016/j.amjcard.2007.03.084>.
- [9] P.A. Pandya, P.A. Shah, P.S. Shrivastav, Application of Supercritical Fluid Chromatography for Separation and Quantitation of 15 Co-Formulated Binary Anti-Hypertensive Medications Using a Single Elution Protocol, *Biomed. Chromatogr.* 35 (2021) e5035. <https://doi.org/10.1002/bmc.5035>.
- [10] F. Gao, M. Zhang, X. Cui, Z. Wang, Y. Sun, J. Gu, Simultaneous Quantitation of Hydrochlorothiazide and Metoprolol in Human Plasma by Liquid Chromatography-Tandem Mass Spectrometry., *J. Pharm. Biomed. Anal.* 52 (2009) 149–154. <https://doi.org/10.1016/j.jpba.2009.12.012>.
- [11] R.M. Borkar, B. Raju, R. Srinivas, P. Patel, S.K. Shetty, Identification and Characterization of

- Stressed Degradation Products of Metoprolol Using LC/Q-TOF-ESI-MS/MS and MS(n) Experiments, *Biomed. Chromatogr.* 26 (2012) 720–736. <https://doi.org/10.1002/bmc.1721>.
- [12] A.A. Mahajan, A.K. Thaker, K. Mohanraj, LC, LC-MS/MS Studies for the Identification and Characterization of Degradation Products of Hydrochlorothiazide and Establishment of Mechanistic Approach towards Degradation, *J. Braz. Chem. Soc.* 23 (2012) 445–452. <https://doi.org/10.1590/S0103-50532012000300010>.
- [13] M. Thevis, O. Krug, H. Geyer, F. Wenzel, J. Bux, L. Stahl, W. Hollmann, A. Thom, W. Schänzer, Monitoring Drug Residues in Donor Blood/Plasma Samples Using LC-(MS)/MS: A Pilot Study, *Drug Test. Anal.* 5 (2013) 380–3. <https://doi.org/10.1002/dta.1457>.
- [14] Ş.C. Mahu, M. Hăncianu, L. Agoroaei, I.C. Grigoriu, A.M. Strugaru, E. Butnaru, Fixed Dose Combinations with Selective beta-Blockers: Quantitative Determination in Biological Fluids, *Rev. Med. Chir. Soc. Med. Nat. Iasi.* 119 (2015) 585–91. <https://pubmed.ncbi.nlm.nih.gov/26204671/> (accessed April 18, 2022).
- [15] J.O. Johannsen, H. Reuter, F. Hoffmann, C. Blaich, M.H.J. Wiesen, T. Streichert, C. Müller, Reliable and Easy-to-Use LC-MS/MS-Method for Simultaneous Determination of the Antihypertensives Metoprolol, Amlodipine, Canrenone and Hydrochlorothiazide in Patients with Therapy-Refractory Arterial Hypertension, *J. Pharm. Biomed. Anal.* 164 (2019) 373–381. <https://doi.org/10.1016/j.jpba.2018.11.002>.
- [16] J. Wei, W. Ma, G. Yao, Q. Jia, X. Cheng, H. Ouyang, Y. Chang, X. Chen, J. He, A High Throughput HPLC-MS/MS Method for Antihypertensive Drugs Determination in Plasma and Its Application on Pharmacokinetic Interaction Study with Shuxuetong Injection in Rats, *Biomed Res. Int.* 2019 (2019) 1–10. <https://doi.org/10.1155/2019/7537618>.
- [17] C. Brunelli, C. Bicchi, A. Di Stilo, A. Salomone, M. Vincenti, High-Speed Gas Chromatography in Doping Control: Fast-GC and Fast-GC/MS Determination of beta-Adrenoceptor Ligands and Diuretics, *J. Sep. Sci.* 29 (2006) 2765–71. <https://doi.org/10.1002/jssc.200500387>.
- [18] A. Thomas, H. Geyer, W. Schänzer, C. Crone, M. Kellmann, T. Moehring, M. Thevis, Sensitive Determination of Prohibited Drugs in Dried Blood Spots (DBS) for Doping Controls by Means of a Benchtop Quadrupole/Orbitrap Mass Spectrometer, *Anal. Bioanal. Chem.* 403 (2012) 1279–89. <https://doi.org/10.1007/s00216-011-5655-2>.
- [19] D.L. Hertzog, J.F. McCafferty, X. Fang, R.J. Tyrrell, R.A. Reed, Development and Validation of a Stability-Indicating HPLC Method for the Simultaneous Determination of Losartan Potassium, Hydrochlorothiazide, and Their Degradation Products, *J. Pharm. Biomed. Anal.* 30 (2002) 747–760. [https://doi.org/10.1016/S0731-7085\(02\)00385-0](https://doi.org/10.1016/S0731-7085(02)00385-0).
- [20] G. Garg, S. Saraf, S. Saraf, Spectrophotometric and Column High-Performance Liquid Chromatographic Methods for Simultaneous Estimation of Metoprolol Tartrate and Hydrochlorothiazide in Tablets, *J. AOAC Int.* 91 (2008) 1045–50. <https://pubmed.ncbi.nlm.nih.gov/18980117/> (accessed April 18, 2022).

- [21] N.D. Rawool, A. Venkatchalam, Analytical Method for the Simultaneous Estimation of Hydrochlorothiazide and Metoprolol Tartrate Using RP HPLC, *Indian J. Pharm. Sci.* 73 (2011) 219–223. <https://doi.org/10.4103/0250-474x.91565>.
- [22] R.A. Shaalan, T.S. Belal, Gradient HPLC-DAD Determination of the Antihypertensive Mixture of Amlodipine Besylate, Valsartan, and Hydrochlorothiazide in Combined Pharmaceutical Tablets, *J. Liq. Chromatogr. Relat. Technol.* 35 (2012) 215–230. <https://doi.org/10.1080/10826076.2011.597071>.
- [23] Q. Xu, Advancing USP Compendial Methods for Fixed Dose Combinations: A Case Study of Metoprolol Tartrate and Hydrochlorothiazide Tablets, *J. Pharm. Anal.* 9 (2019) 77–82. <https://doi.org/10.1016/j.jpha.2018.12.003>.
- [24] D.D. Rao, N. V. Satyanarayana, S.S. Sait, Y.R. Reddy, K. Mukkanti, Simultaneous Determination of Losartan Potassium, Atenolol and Hydrochlorothiazide in Pharmaceutical Preparations by Stability-Indicating UPLC, *Chromatographia.* 3–4 (2009) 647–651. <https://doi.org/10.1365/S10337-009-1221-X>.
- [25] S. Nalwade, V.R. Reddy, D.D. Rao, I.K. Rao, Rapid Simultaneous Determination of Telmisartan, Amlodipine Besylate and Hydrochlorothiazide in a Combined Poly Pill Dosage Form by Stability-Indicating Ultra Performance Liquid Chromatography, *Sci. Pharm.* 79 (2011) 69–84. <https://doi.org/10.3797/scipharm.1006-10>.
- [26] C.A.R. Salamanca-Neto, A.P.P. Eisele, V.G. Resta, J. Scremin, E.R. Sartori, Differential Pulse Voltammetric Method for the Individual and Simultaneous Determination of Antihypertensive Drug Metoprolol and Its Association with Hydrochlorothiazide in Pharmaceutical Dosage Forms, *Sensors Actuators B.* 230 (2016) 630–638. <https://doi.org/10.1016/j.snb.2016.02.071>.
- [27] M. Stolarczyk, R. Ekiert, J. Krzek, W. Rzeszutko, Determination of Metoprolol and Hydrochlorothiazide by Derivative Spectrophotometric Method in Pharmaceutical Preparations, *Acta Pol. Pharm. – Drug Res.* 63 (2006) 169–173.
- [28] N.K. Ramadan, H.M. Mohamed, A.A. Mostafa, Miniaturized Membrane Sensors for Potentiometric Determination of Metoprolol Tartrate and Hydrochlorothiazide, *Acta Chim. Slov.* 59 (2012) 344–52. <https://pubmed.ncbi.nlm.nih.gov/24061251/> (accessed April 18, 2022).
- [29] F.T. Mattrey, A.A. Makarov, E.L. Regalado, F. Bernardoni, M. Figus, M.B. Hicks, J. Zheng, L. Wang, W. Schafer, V. Antonucci, S.E. Hamilton, K. Zawatzky, C.J. Welch, Current Challenges and Future Prospects in Chromatographic Method Development for Pharmaceutical Research, *TrAC Trends Anal. Chem.* 95 (2017) 36–46. <https://doi.org/10.1016/j.trac.2017.07.021>.
- [30] L. Nováková, P. Svoboda, J. Pavlík, Ultra-High Performance Liquid Chromatography, in: S. Fanali, P.R. Haddad, C.F. Poole, M.-L. Riekkola (Eds.), *Liq. Chromatogr. Fundam. Instrum.*, 2nd ed., Elsevier, 2017: pp. 719–769. <https://doi.org/10.1016/B978-0-12-805393-5.00029-4>.
- [31] L. Maldaner, I.C.S.F. Jardim, The State of the Art of Ultra Performance Liquid Chromatography, *Quim. Nova.* 32 (2009) 214–222. <https://doi.org/10.1590/S0100-40422009000100036>.



- [32] T.H. Walter, R.W. Andrews, Recent Innovations in UHPLC Columns and Instrumentation, *TrAC Trends Anal. Chem.* 63 (2014) 14–20. <https://doi.org/10.1016/j.trac.2014.07.016>.
- [33] J. Płotka-Wasyłka, A New Tool for the Evaluation of the Analytical Procedure: Green Analytical Procedure Index, *Talanta*. 181 (2018) 204–209. <https://doi.org/10.1016/j.talanta.2018.01.013>.
- [34] F. Pena-Pereira, W. Wojnowski, M. Tobiszewski, AGREE – Analytical GREEnness Metric Approach and Software, *Anal. Chem.* 92 (2020) 10076–10082. <https://doi.org/10.1021/acs.analchem.0c01887>.
- [35] P. Konieczka, J. Namieśnik, Estimating Uncertainty in Analytical Procedures Based on Chromatographic Techniques, *J. Chromatogr. A.* 1217 (2010) 882–891. <https://doi.org/10.1016/j.chroma.2009.03.078>.
- [36] B.N. Taylor, Guidelines for Evaluating and Expressing the Uncertainty of NIST Measurement Results, Gaithersburg, MD, 1994. <https://doi.org/10.6028/NIST.tn.1297>.
- [37] G.N.W. Leung, E.N.M. Ho, W.H. Kwok, D.K.K. Leung, F.P.W. Tang, T.S.M. Wan, A.S.Y. Wong, C.H.F. Wong, J.K.Y. Wong, N.H. Yu, A Bottom-Up Approach in Estimating the Measurement Uncertainty and Other Important Considerations for Quantitative Analyses in Drug Testing for Horses, *J. Chromatogr. A.* 1163 (2007) 237–246. <https://doi.org/10.1016/j.chroma.2007.06.035>.
- [38] United States Pharmacopeial Convention, United States Pharmacopoeia – National Formulary (USP – NF), United States Pharmacopeial Convention, Rockville, MD, 2021.
- [39] Validation of Analytical Procedures: Text and Methodology, European Medicines Agency, London, 1995. [https://database.ich.org/sites/default/files/Q2%28R1%29\\_Guideline.pdf](https://database.ich.org/sites/default/files/Q2%28R1%29_Guideline.pdf) (accessed July 14, 2021).
- [40] IAEA, Measurement Uncertainty: A Practical Guide for Secondary Standards Dosimetry Laboratories, Dosimetry & Medical Radiation Physics Section International Atomic Energy Agency, Vienna, 2008.
- [41] S.L.C. Ferreira, W.N.L. Dos Santos, C.M. Quintella, B.B. Neto, J.M. Bosque-Sendra, Doehlert Matrix: A Chemometric Tool for Analytical Chemistry—Review, *Talanta*. 63 (2004) 1061–1067. <https://doi.org/10.1016/j.talanta.2004.01.015>.
- [42] R.F. Teófilo, M.M.C. Ferreira, Chemometrics II: Spreadsheets for Experimental Design Calculations, A Tutorial, *Quim. Nova*. 29 (2006) 338–350. <https://doi.org/10.1590/S0100-40422006000200026>.
- [43] C. Hartmann, J. Smeyers-Verbeke, D.L. Massart, R.D. McDowall, Validation of Bioanalytical Chromatographic Methods, *J. Pharm. Biomed. Anal.* 17 (1998) 193–218. [https://doi.org/10.1016/s0731-7085\(97\)00198-2](https://doi.org/10.1016/s0731-7085(97)00198-2).
- [44] Center for Drug Evaluation and Research, Reviewer Guidance: Validation of Chromatographic Methods, 1994.
- [45] L. Huber, Validation of Analytical Methods: Review and Strategy, *LC GC Mag. Liq. Gas Chromatogr.* 1 (1997) 1–17. [www.labcompliance.com](http://www.labcompliance.com) (accessed February 5, 2023).

- [46] S. Ellison, A. Williams, EURACHEM/CITAC Guide Quantifying Uncertainty in Analytical Measurement, 3rd ed., EURACHEM, 2012.



Contents lists available at ScienceDirect

Journal of Pharmaceutical Sciences

journal homepage: [www.jpharmsci.org](http://www.jpharmsci.org)

Pharmaceutics, Drug Delivery and Pharmaceutical Technology

## Novel Eco-Friendly Stability Indicating Capillary Zone Electrophoresis Method for Determination of Aripiprazole in Tablet Dosage form: DoE Directed Optimization, Development and Method Validation

Frank Alonso Gavilano Fajardo<sup>a</sup>, Marina Franco Maggi Tavares<sup>b</sup>, Anas Rashid<sup>c</sup>,  
María Segunda Aurora Prado<sup>a,\*</sup>

<sup>a</sup> Department of Pharmacy, School of Pharmaceutical Sciences, University of São Paulo, São Paulo, Brazil

<sup>b</sup> Department of Fundamental Chemistry, Institute of Chemistry, University of São Paulo, São Paulo, Brazil

<sup>c</sup> Department of Neuroscience "Rita Levi Montalcini", School of Medicine and Surgery, University of Torino, Torino, Italy

## ARTICLE INFO

## Article history:

Received 23 June 2022

Revised 18 August 2022

Accepted 19 August 2022

Available online xxx

## Keywords:

Aripiprazole

Design of experiments

Stability indicating method

Capillary zone electrophoresis

## ABSTRACT

In this work, a novel environment-friendly stability indicating capillary zone electrophoresis (CZE) method has been developed and validated for assaying the aripiprazole (ARP) in tablet dosage form. The separation of ARP from its degradation products and internal standard was achieved using a fused silica capillary column (30.2 cm x 75  $\mu\text{m}$  ID), a background electrolyte containing 6 mmol L<sup>-1</sup> ammonium formate buffer (pH 3) with 5% methanol under a potential of 15 kV and detection at 214 nm. The stability indicating ability of the method was investigated by analyzing ARP after being subjected to acidic, alkaline, thermal, photolytic, and oxidative stress conditions, according to ICH guidelines. Design of experiments was used during forced degradation and method optimization. Oxidation was the main degradation pathway among those evaluated. The drug was separated from its oxidative degradation products in less than 4 min. CZE method was linear between 60 – 140  $\mu\text{g mL}^{-1}$ ,  $R^2 = 0.9980$ , precise (intra-day 0.88% and inter-day 1.30%). The average recovery was  $100.93 \pm 0.77\%$ . This is the first method in the literature for quantification of ARP in the presence of its related degradation products with high separation efficiency, low operation cost and minimum solvent consumption. This method could be helpful in the routine quality control analysis in the pharmaceutical industries with least harmful effect on the environment. CZE is considered an eco-friendly alternative of conventionally HPLC methods.

© 2022 Published by Elsevier Inc. on behalf of American Pharmacists Association.

## Introduction

Stability study is mandatory for the pharmaceutical industry to ensure the quality of the drug products. Both Food and Drug Administration<sup>1</sup> and International Conference on Harmonization (ICH) Q1A (R2)<sup>2</sup> guidelines state the requirement of stability testing to better understand the drug substance quality along with changes in drug product under the influence of forced degradation. This should be carried out using stability indicating methods that can resolve and accurately quantify the drug substances as well as the degradation products. In order to assess the stability conditions of a given drug, it is essential that these methodologies be fully validated;<sup>3</sup> although

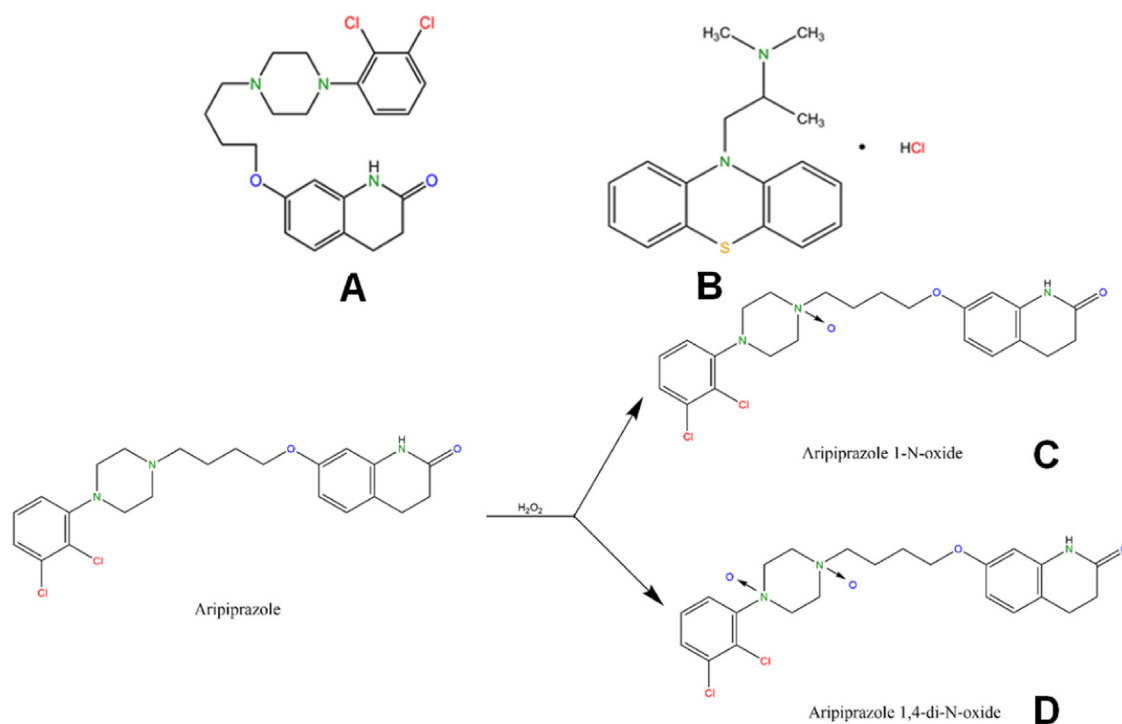
the regulatory guidelines only define the concept of stress testing, but they do not provide detailed procedural information.<sup>4</sup> A new approach in this field is to evaluate the interdependence of forced degradation parameters by applying the Design of Experiments (DoE) concept.<sup>5</sup> DoE is an established tool for the development of analytical methods.<sup>6,7</sup> It has been used to successfully develop stability indicating and impurity profiling methods which include the separation of various components.<sup>8</sup> Similarly, DoE can also be applied for the analytical method optimization.<sup>9</sup>

Aripiprazole (ARP, Fig. 1A) is a third-generation atypical antipsychotic approved for the treatment of schizophrenia, bipolar disorder, depression, and autism spectrum disorders.<sup>10</sup> It acts as a partial dopamine D2, partial serotonin 5-HT1A receptor agonist and 5-HT2A receptor antagonist.<sup>11–13</sup>

The literature reveals several methods for the determination of ARP and/or its active metabolite dehydroaripiprazole in the presence or absence of degradation products after forced degradation tests

\* Corresponding author at: Department of Pharmacy, School of Pharmaceutical Sciences, University of São Paulo, Av. Prof. Lineu Prestes 580, Block 13, Butantã, 05508-000, São Paulo, Brazil.

E-mail address: [msaprad06@usp.br](mailto:msaprad06@usp.br) (M.S.A. Prado).



**Figure 1.** Chemical structure of aripiprazole (A), promethazine (B) and oxidation of aripiprazole: (C) aripiprazole-1-N-oxide (D) aripiprazole 1,4-di-N-oxide

(stability indicating methods) in both pharmaceutical dosage form and biological fluids by means of gas chromatography with mass spectrometry,<sup>14</sup> high-performance liquid chromatography (HPLC) with ultraviolet and diode array detection,<sup>15–24</sup> or mass spectrometry detection.<sup>25–30</sup> Some of them make use of time-consuming sample pre-treatment methodologies or require expensive instrumentation. Other papers reported the spectrophotometric method,<sup>31–33</sup> voltametric method<sup>34,35</sup> and capillary electrophoresis (CE) method<sup>36–38</sup> for the analysis of ARP in biological fluids.

Capillary electrophoresis, family of electric field-driven microscale separation modes, is the fastest expanding separation technique in pharmaceutical analysis as it presents itself as an alternative technique compared to HPLC.<sup>39,40</sup> The analysis of drugs and impurities is often challenging and requires powerful separation techniques. Capillary electrophoresis can be used for this purpose due to its high separation efficiency and high throughput automation.<sup>39–42</sup> Besides that, CE is considered as an alternative green ecofriendly separation technique, because it uses a small sample volume along with small amount of reagents and a minimum or no organic solvents, thus reducing the environmental impact by reducing the generation of organic waste.<sup>43</sup>

Few CE methods for the analysis of ARP and its metabolites are reported. ARP and its active metabolite (dehydroaripiprazole) were determined by capillary zone electrophoresis in plasma with sample pretreatment by liquid–liquid extraction and the analytes were determined in 12 min.<sup>37</sup> Musenga et al.<sup>36</sup> developed a CE method for the analysis of ARP from plasma of schizophrenic patients, good linear response and precision assays were obtained. However, problems with migration time repeatability, inadequate peak shape and matrix effect (spikes and higher background noise) were observed. Another research showed the use of CE method to quantify ARP and dehydroaripiprazole in psychiatric patient's blood samples using 80 mmol L<sup>-1</sup> 2-3% dimethylsulfoxide-phosphate as a buffer at pH 3.0 but with a very long runtime of 30 min.<sup>38</sup>

To the best of our knowledge, no stability indicating capillary zone electrophoresis (CZE) method for the determination of ARP in the

presence of its degradation products and in pharmaceutical dosage forms has been published or described in the literature. This fact indicates there is need to develop a fast, simple, and accurate stability indicating CZE method to determine ARP. This is the novelty of this work added to the use of an eco-friendly BGE taking into consideration operator's health and environmental safety.

The method was validated for its intended purpose. ARP was subjected to various stress conditions (e.g., hydrolysis (acid, alkaline), oxidation, thermal, and photolysis) according to the ICH Q1A(R2) guideline. The study of forced degradation and optimization of CZE conditions for the separation of ARP and its oxidative degradation products (ODPs) was performed by applying the concept of DoE.

## Materials and Methods

### Chemicals, Reagents, and Samples

ARP standard was kindly donated by Apsen Farmacêutica (Sao Paulo, Brazil). Promethazine hydrochloride (used as internal standard – IS) (Fig. 1B) was purchased from Sigma Aldrich (Sao Paulo, Brazil). Aristab® (Aché Laboratórios, Sao Paulo, Brazil), tablets containing 10 mg of ARP were obtained from a local pharmacy. Hydrochloric acid, sodium hydroxide, hydrogen peroxide, HPLC grade acetonitrile, HPLC grade methanol were purchased from Merck (Sao Paulo, Brazil). Ammonium formate and formic acid were obtained from Sigma Aldrich (Sao Paulo, Brazil). Ultrapure water was obtained from a Milli-Q water purification system (Milli-Q Gradient System, Millipore Corp., Bedford, MA, USA) and was used for all analyses.

### Instrumentation

CE measurements were carried out on P/ACE MDQ (Beckman Coulter, Fullerton, CA, USA) and Agilent 7100 (Agilent Technologies, Inc., Santa Clara, CA, USA) capillary electrophoresis instruments. Both instruments were equipped with a diode array detector (DAD). Instrument control, data collection and evaluation were performed

with Karat® v. 8.0 and OpenLab ChemStation® software for P/ACE MDQ and Agilent 7100 capillary electrophoresis instruments, respectively. Analytical runs were carried out on an uncoated fused silica capillary with 30.2 cm total length and 75  $\mu\text{m}$  i.d. (Polymicro Technologies, Phoenix, AZ, USA). The pH values of the running buffer solutions were adjusted using a Mettler Toledo pH meter model PG1800 (Gehaka, Sao Paulo, Brazil). Photolytic degradation was carried out using a photostability chamber (Model 424-CF, Ethik, SP, Brazil). Furthermore, the ultrasound T14 model (Thornton, Sao Paulo, Brazil) and Mettler analytical balance model AB204 (Mettler Toledo, Sao Paulo, Brazil) were used.

### Preparation of Solutions

#### Diluent

The diluent used for working solutions was a mixture of acetonitrile, methanol and 6  $\text{mmol L}^{-1}$  ammonium formate solution in the proportion 35:15:50, adjusted to pH 3.0 with formic acid.

#### Standards and Samples Stock and Working Solutions

ARP stock standard solution was prepared by weighing 25 mg of ARP standard into a 25 mL amber volumetric flask followed by dilution with acetonitrile (final concentration 1000  $\mu\text{g mL}^{-1}$ ). Promethazine (IS) stock solution was prepared by dissolving 50 mg of promethazine standard into a 25 mL amber volumetric flask with purified water (final concentration 2000  $\mu\text{g mL}^{-1}$ ).

To prepare the stock sample solution, twenty tablets of Aristab® containing 10 mg of ARP were accurately weighed and powdered using a sterile mortar and pestle to obtain a fine powder. An appropriate amount of powder equivalent to 10 mg of ARP was transferred into a 10 mL amber volumetric flask. The content was diluted with 6 mL of diluent, the mixture was sonicated for 10 min and then diluted to volume with the same diluent, obtaining a final concentration of 1000  $\mu\text{g mL}^{-1}$  of ARP.

The standard and sample working solutions were prepared by mixing 800  $\mu\text{L}$  of IS stock solution (2000  $\mu\text{g mL}^{-1}$ ) and 1000  $\mu\text{L}$  of ARP stock standard or sample solutions (1000  $\mu\text{g mL}^{-1}$ ) and then diluting with diluent into 10 mL amber volumetric flask. The final concentration of ARP in both standard and sample working solutions was 100  $\mu\text{g mL}^{-1}$  and the final concentration of the IS was 160  $\mu\text{g mL}^{-1}$ .

All standard and sample solutions were filtered through a 0.45  $\mu\text{m}$  polytetrafluoroethylene (PTFE) membrane filter (Millex-GN, Millipore Corp., Bedford, MA, USA) and stored in a refrigerator. Sample solutions demonstrated to be stable at least for 60 days at 4 °C. Before using, they were kept out of the refrigerator until they reached room temperature.

#### Background Electrolyte

A stock ammonium formate solution (100  $\text{mmol L}^{-1}$ ) was prepared, and then appropriate running electrolyte solutions were obtained from this stock solution. The optimized BGE was composed of ammonium formate 6  $\text{mmol L}^{-1}$  at pH 3.0, adjusted with formic acid, and 5% of methanol, which was prepared by mixing 6 mL of the stock solution with 80 mL ultrapure water, followed by pH adjustment to 3.0 with formic acid before the addition of 5 mL of methanol. This solution was then transferred to a 100 mL volumetric flask and the volume was completed with ultrapure water. BGE solutions were filtered through a 0.45  $\mu\text{m}$  polyvinylidene difluoride (PVDF) membrane filter (Millipore Corp., Bedford, MA, USA) before analysis.

#### CE Conditions

The system was thermostated at 25 °C. The conditioning of a new capillary was comprised of flushing NaOH 1.0  $\text{mol L}^{-1}$  for 30 min,

ultrapure water for 20 min, and then BGE for 30 min. On every working day, before running the first sample, the capillary was flushed with NaOH 0.1  $\text{mol L}^{-1}$  for 20 min, followed by ultrapure water for 20 min and then BGE for another 20 min. Between each run, the capillary was flushed with NaOH 0.1  $\text{mol L}^{-1}$  for 1 min, followed by ultrapure water for 1 min, and finally with BGE for 2 min. Injections were performed in hydrodynamic mode at 0.4 psi for 5 s. The applied voltage for separation was 15 kV (positive polarity) with a BGE consisted of 6  $\text{mmol L}^{-1}$  ammonium formate, adjusted to pH 3.0 with formic acid, and 5% of methanol. Signals were detected at 214 nm.

#### Forced Degradation Study

Forced degradation studies were carried out under hydrolytic (acidic and alkaline), oxidative, photolytic, and thermal conditions as per ICH Q1A(R2) recommendations<sup>2</sup> by submitting ARP standard and sample solutions of Aristab® for each forced degradation condition. Acidic and alkaline hydrolysis were conducted in 0.1  $\text{mol L}^{-1}$  of HCl and NaOH, respectively at concentration of 1  $\text{mg mL}^{-1}$  ARP. The solutions remained at room temperature for 7 days and under light protection. After that, the solutions were neutralized.

Oxidative degradation was conducted in 3%  $\text{H}_2\text{O}_2$ , the samples were left at room temperature for 7 days and protected from the light. Separated sample of acidic, alkaline and oxidative solutions, as above mentioned, were also exposed at 60 °C for 2 h.

Photolytic degradation was performed in a photostability chamber by exposing the drug in solid state for 50 and 120 h. A period of 50 h was the minimum time to reach the light dosage of UVA (at least 200-watt hours per square meter) and visible light (at least 1.2 million lux hours) according to the ICH guidelines.<sup>44</sup> Thermal degradations were carried out in a stove at 105 °C for 2 and 7 days.

After degradations, aliquot of IS stock solution was added to all degraded solutions, then diluted with diluent to the final concentration of 100  $\mu\text{g mL}^{-1}$  of ARP and 160  $\mu\text{g mL}^{-1}$  of IS, as described in Section 2.3.2.

#### Preliminary Study of Application of DoE During Oxidative Forced Degradation

The solution where degradation had occurred was used for further development method. CZE conditions for the separation of ARP and its degradation products were investigated by varying the applied voltage (10 – 25 kV), capillary temperature (20 – 30 °C), hydrodynamic injection time (3 – 6 s), types and pH of BGE (ammonium formate/formic acid and ammonium acetate/acetic acid buffers (pH 2.2 – 3.5), BGE concentrations (5 – 25  $\text{mmol L}^{-1}$ ) and the use of an organic modifier (methanol) as component of the BGE.

Full factorial design ( $2^3$ ) was used to optimize oxidative forced degradation condition. The factors analyzed were BGE pH and concentration, and methanol (organic modifier). A set of preliminary studies was performed to establish the low and high levels of each factor. MATLAB® v. R2022a (The MathWorks, Natick, MA, USA) program was used to obtain optimum BGE conditions.

#### Oxidative Degradation Optimization Study by DoE

Factors affecting ARP oxidation (hydrogen peroxide concentration, temperature, and time) were studied and optimized by a  $2^3$  full factorial design to degrade the drug by 10%. Therefore, 1  $\text{mg mL}^{-1}$  of ARP was mixed with  $X_1$  %  $\text{H}_2\text{O}_2$  and heated for  $X_2$  h at  $X_3$  °C. Two levels were chosen for each variable. The high level (+1) for  $X_1$ ,  $X_2$  and  $X_3$  was 20%, 5 h and 60 °C, respectively, whereas the low level (-1) for  $X_1$ ,  $X_2$  and  $X_3$  was 10%, 2 h and 40 °C, respectively. Since three variables were considered at two levels, a  $2^3$  full factorial design was conducted to set up eight experiments. Using Minitab® v. 20.3 (Minitab

LLC., State College, PA, USA), a Pareto chart was evaluated to find the critical factors. Therefore, contour plot graphics and the software prediction tool were used to characterize the variables  $X_1$ ,  $X_2$  and  $X_3$ . Finally, experiments were performed using calculated theoretical values of  $X_1$ ,  $X_2$  and  $X_3$  to confirm whether the experimental % degradation matched the calculated one.

#### System Suitability

To ensure repeatability, system performance, and separation quality throughout the assay development, the system suitability test was carried out by injecting six replicates of ARP ( $100 \mu\text{g mL}^{-1}$ ) and promethazine ( $160 \mu\text{g mL}^{-1}$ ) used as IS. The evaluated parameters were plate number, tailing factor, peak area ratio, ARP migration time, and resolution between ARP and IS.

#### Method Validation

##### Selectivity/Specificity

The selectivity of the method was examined by subjecting the ARP standard and Aristab<sup>®</sup> samples to different stress conditions as described in Section 2.5. The peak purity of ARP was assessed with the help of DAD. Potential interference from tablet additives was assessed by subjecting the placebo to the same degradation conditions as ARP samples. The placebo was prepared according to the qualitative formula of Aristab<sup>®</sup> (lactose monohydrate, maize starch, microcrystalline cellulose, hydroxypropyl cellulose, magnesium stearate and red iron oxide). The quantity of each excipient was calculated taking into consideration the concentration percentage described in handbooks of pharmaceutical excipients.<sup>45</sup> The specificity of the proposed method has been established by injecting the diluent, placebo matrix solution, standard solution, and pharmaceutical product (Aristab<sup>®</sup>) into the CE system.

##### Linearity, Detection Limit (DL) and Quantitation Limit (QL)

To determine the linearity of the CZE method, three analytical curves containing five concentrations of ARP standard solutions in the range of  $60 \mu\text{g mL}^{-1}$  to  $140 \mu\text{g mL}^{-1}$ , and a fixed concentration of IS ( $160 \mu\text{g mL}^{-1}$ ), were constructed. The analytical curves were obtained by plotting peak area ratios (ARP peak area/IS peak area) against ARP concentrations. The least square regression method and analysis of variance (ANOVA) were used to determine the method's linearity ( $p$ -value = 0.05).

The values for DL and QL were calculated according to the following equations:  $DL = 3.3 (\sigma/\alpha)$  and  $QL = 10 (\sigma/\alpha)$ , where  $\sigma$  is the standard deviation of the y-axis intercept and  $\alpha$  corresponds to the mean slope.<sup>46</sup> The values were expressed as concentration ( $\mu\text{g mL}^{-1}$ ).

##### Accuracy

Accuracy of the proposed method was confirmed by spiking, which consisted of spiking the placebo of the pharmaceutical product (Aristab<sup>®</sup>) with ARP standard separately at three different levels 80, 100 and 120% of the nominal concentration (80, 100 and  $120 \mu\text{g mL}^{-1}$ , respectively). Triplicate determinations of each level have been recorded.

##### Precision

Repeatability and intermediate precision analysis were conducted to evaluate the method precision. Repeatability was tested by assaying six independent sample solutions, prepared as mentioned in Section 2.3 using the P/ACE MDQ capillary electrophoresis instrument. Intermediate precision was evaluated on an Agilent 7100 electrophoresis instrument by analyzing another set of six sample solutions, which were prepared by a different analyst on a different day. Standard solution of ARP ( $100 \mu\text{g mL}^{-1}$ ) and constant IS solution ( $160 \mu\text{g}$

$\text{mL}^{-1}$ ) were used for the precision experiments. Precision was expressed by the relative standard deviation percentage (RSD%) for ARP content in the tablets.

##### Robustness

The most important parameters that influence the analytical performance of this method were evaluated in the method optimization as described in Section 2.3. However, other parameters that are likely to be changed during analysis and consequently affect the method performance were also studied. Slight changes of the optimal applied voltage ( $\pm 2 \text{ kV}$ ), capillary temperature ( $\pm 1 \text{ }^\circ\text{C}$ ) and hydrodynamic injection time ( $\pm 1 \text{ s}$ ) were evaluated. Peak area ratios of ARP/IS were then compared for each altered condition with the reference optimal condition.

## Results and Discussion

### Method Development

#### General Settings

Capillary electrophoresis technique has emerged as a powerful analytical tool for rapid separation of analytes and overcomes many of the drawbacks of HPLC.<sup>47</sup> CE is considered an environment-friendly alternative separation technique, and it has several advantages such as the use of small volume of buffer solutions (approximately 10 to 100 nL per injection) compared to the HPLC method which uses between 10 to 20  $\mu\text{L}$  per injection, rather than hazardous solvents and hence prevents organic waste generation and harmful interferences. The silica fused capillary is long lasting due to resistance to chemical attack, malleability and mechanical resistance, these characteristics make it an economical method.<sup>43</sup>

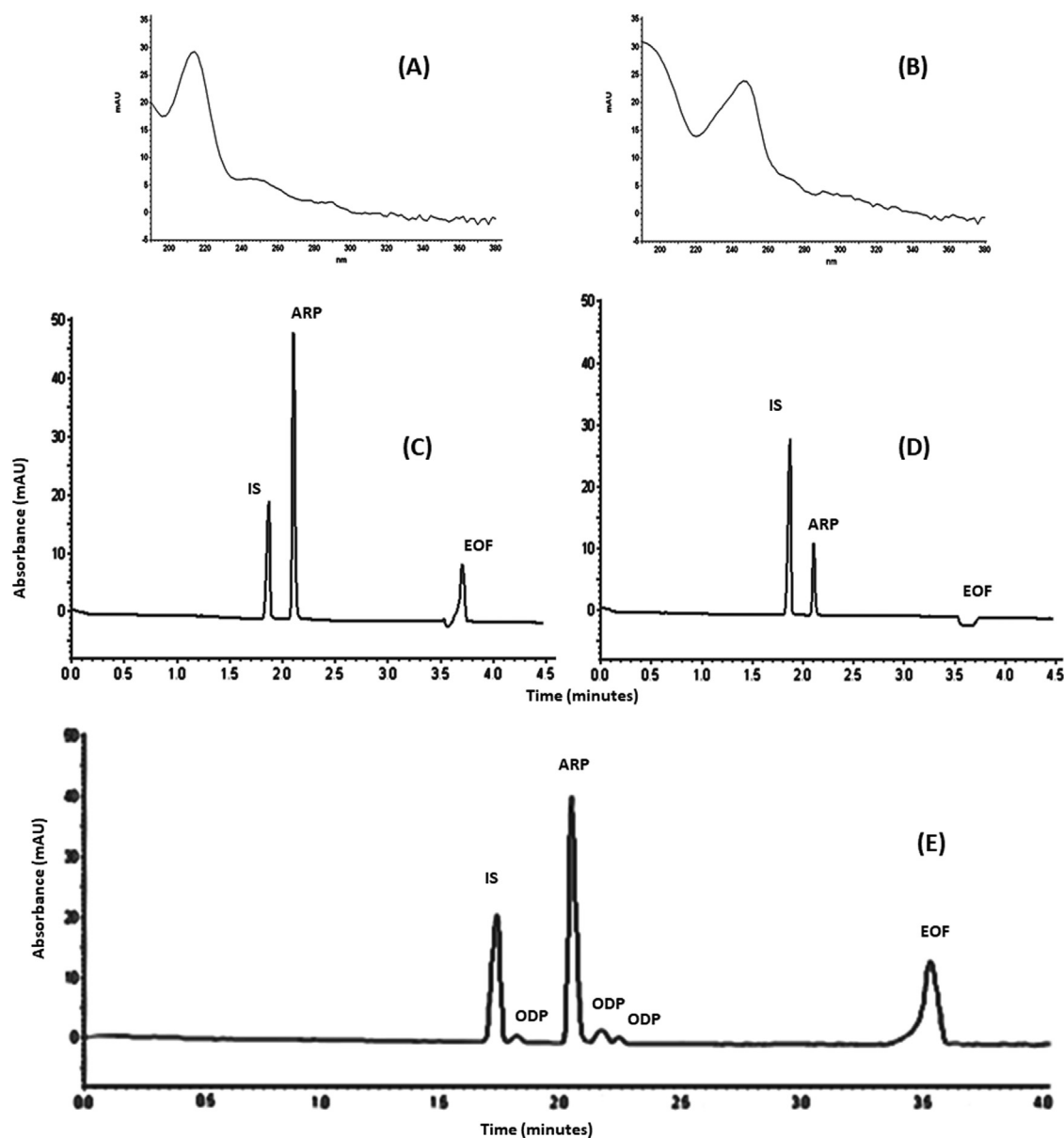
Different parameters were studied and optimized to develop a CZE method, mode of CE, for the separation of ARP from its degradation products after submitted to stress testing with acceptable resolution and short analysis time.

The main function of BGE is to provide the transport of electric current for the separation of the analytes. The BGE should primarily provide an appropriate migration of the analytes in a reasonable time with no peak broadening and migration interferences.<sup>48</sup> Thereby, the most important parameters that affect the CZE method were investigated to find the most suitable system and BGE for the determination and separation of ARP and its degradation products taking into consideration acceptable resolution and short analysis run time.

Aripiprazole is a weak base with  $pK_a$  of 7.46, which corresponds to the protonation equilibrium of the tertiary amine groups (piperidinic group);<sup>49,50</sup> therefore, at pH lower than  $pK_a$ , the analyte is fully protonated and thus positively charged. This characteristic makes CZE a suitable technique for ARP determination, considering that the analyte will migrate electrophoretically towards the cathode under the influence of an electric field.

To maintain the ARP positively charged, an acidic BGE was used during method development. Ammonium formate at  $10 \text{ mmol L}^{-1}$  concentration buffered at pH 3.0 with formic acid gave good results regarding peak symmetry, which proves that the buffer co-ion has similar mobility to the analyte and therefore this buffer system was further investigated. A constant applied voltage of 15 kV, hydrodynamic injection of 0.4 psi for 5 s, and temperature at  $25 \text{ }^\circ\text{C}$  were initially established for the experiments. The migration time of ARP was 2.1 min (Fig. 2).

A variable to consider during method development is the detection wavelength. The UV spectrum of ARP standard solution exhibits two maxima absorptions at 214 and 254 nm (Figs. 2A and 2B, respectively). In order to assure maximum sensitivity and accuracy of the method, 214 nm was selected. Figure 2C confirms that the analysis of ARP in pH 3.0 at 214 renders a much higher signal-to-noise ratio



**Figure 2.** Method development for ARP: Selection of wavelength. UV absorption spectrum of ARP standard solution at 214 nm (A) and at 254 nm (B). Electropherograms of the ARP standard solution ( $100 \mu\text{g mL}^{-1}$ ) and IS ( $160 \mu\text{g mL}^{-1}$ ) at 214 nm (C) and at 254 nm (D). ARP degraded with 10%  $\text{H}_2\text{O}_2$  for 2 h at  $60^\circ\text{C}$  (ARP  $100 \mu\text{g mL}^{-1}$  and IS  $160 \mu\text{g mL}^{-1}$ ) (E). Conditions: uncoated silica-fused capillary (30.2 cm total length  $\times$   $75 \mu\text{m}$  i.d.; electrolyte:  $10 \text{ mmol L}^{-1}$  ammonium formate/formic acid, pH 3.0; hydrodynamic injection:  $0.4 \text{ psi/5 s}$ ; applied voltage:  $+15 \text{ kV}$ ; temperature:  $25^\circ\text{C}$ . Peaks: Promethazine (IS), Aripiprazole (ARP), Electroosmotic Flow (EOF).

than at 254 nm (Fig. 2D). In addition, samples of Aristab<sup>®</sup> tablet matrix did not show interference at this wavelength (Fig. 6A). Therefore, the wavelength of 214 nm was used in all experiments.

Another concern regarding method development was the selection of IS to improve precision. Several compounds such as risperidone, levomepromazine, chlorpromazine and promethazine were tested as IS candidates. Promethazine ( $160 \mu\text{g mL}^{-1}$ ) was the most suitable due to acceptable resolution with ARP and good absorbance in the wavelength of the method. Complete separation of IS and ARP was obtained with migration times of 1.85 min and 2.15 min, respectively (Fig. 2C).

After ARP was submitted to hydrolytic (acid and alkaline), thermal, oxidative, and photolytic conditions, no degradation products were detected after hydrolytic, thermal, and photolytic conditions. However, after oxidative ( $\text{H}_2\text{O}_2$ ) stress, three peaks of ARP degradants were observed (ODPs) (Fig. 2E). Therefore, the sample degraded in

$\text{H}_2\text{O}_2$  was employed for further development and method optimization by DoE.

From preliminary tests, when used a voltage of 15 kV, the resolution and peak shape of the ODPs were compromised. The greater the voltage, the shorter the migration time of ARP and DPs, but resolution decreases. Through method development, the most critical separation was observed between two degradation products in the  $\text{H}_2\text{O}_2$ -degraded sample in the time range of 2.0 – 2.5 min (Fig. 2E). Therefore, to improve the resolution of this critical pair, a voltage of 12 kV was established for further development.

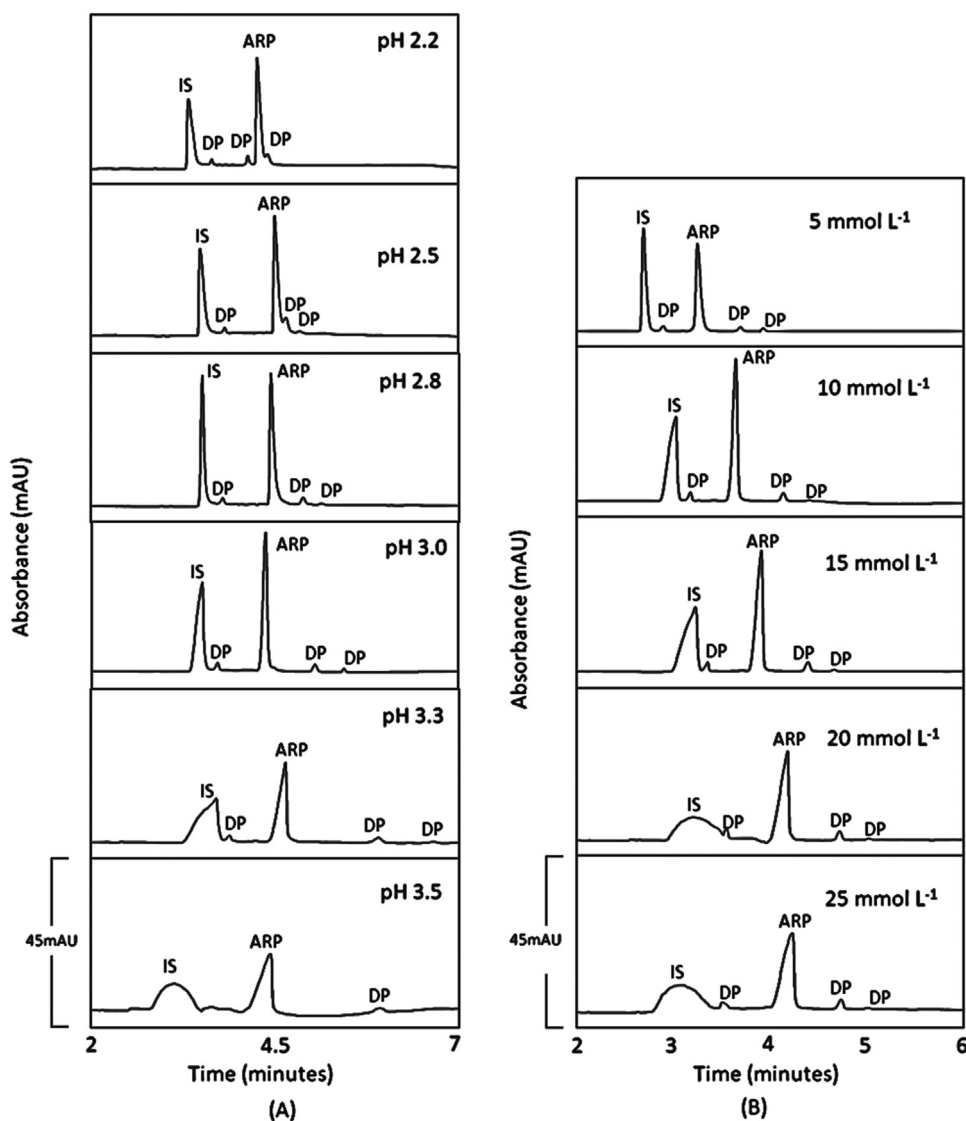
The first step was to choose a suitable type and pH of the BGE. For further potential use of the method with mass spectrometry, two volatile electrolyte systems were evaluated: ammonium formate/formic acid and ammonium acetate/acetic acid as buffer solutions, which present adequate buffering capacity around pH 3.0. Both buffer

solutions were evaluated at pH range from 2.2 to 3.5, and buffer concentrations from 5 to 25 mmol L<sup>-1</sup>. When ammonium acetate/acetic acid buffer was used at concentrations and pHs above mentioned, wide peaks of ARP and high current were observed. It is known that the higher the salt concentration, the higher the viscosity and the higher the current.

When ammonium formate/formic acid buffer in the pH range from 2.2 to 3.0 (Fig. 3A) and concentration range from 5 to 10 mmol L<sup>-1</sup> (Fig. 3B) was used, improvement of the ARP peak shape, ODPs and IS, as well as low current values (approximately 40  $\mu$ A) were observed. However, broader peaks of ARP and IS were observed when the pH varied from 3.3 to 3.5 (Fig. 3A), probably due to the lower solubility of ARP as the pH increases. In addition, it was observed that resolution between ARP and their ODPs was compromised from pH 2.2 to 2.5 (Fig. 3A). To improve the resolution between ARP and ODPs, it was considered the use of methanol as a BGE organic modifier. Tests using methanol concentrations higher than 5% showed a tendency to form wide peaks, as well as an increase in migration time (Fig. not shown).

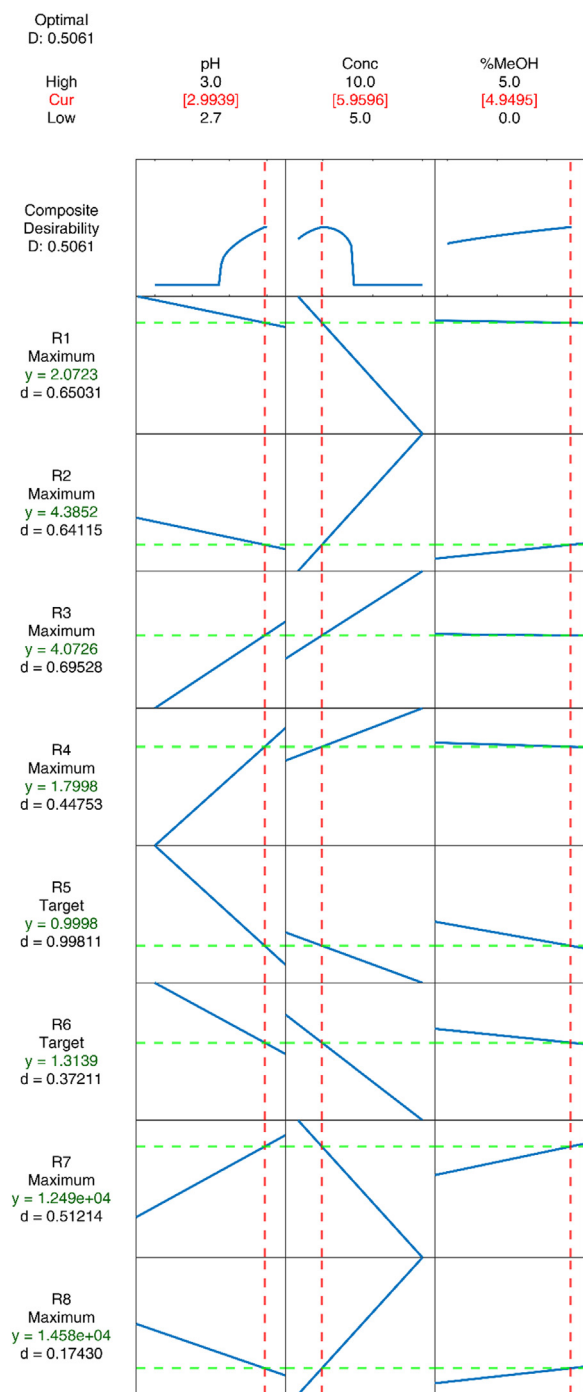
#### Method Optimization by DoE

During the preliminary experiments in the method development for oxidative degradation, three factors were found to affect greatly the CZE method performance, they are BGE pH ( $X_1$ ), BGE concentration ( $X_2$ ) and methanol used as organic modifier ( $X_3$ ). Therefore, a full factorial design ( $2^3$ ) was carried out for the optimization of electrophoretic conditions. The levels were chosen based on the preliminary tests described in Section 3.1.1. The high levels (+1) for  $X_1$ ,  $X_2$  and  $X_3$  were 3.0, 10 mmol L<sup>-1</sup> and 5%, respectively, and the low levels (-1) for  $X_1$ ,  $X_2$  and  $X_3$  were 2.7, 5 mmol L<sup>-1</sup> and 0%, respectively. Eight experiments were performed in duplicate and subjected to evaluation. Eight response factors were selected: resolutions between IS and ODP1 (R1), ARP and ODP1 (R2), ARP and ODP2 (R3), and between ODP2 and ODP3 (R4); tailing factors of IS (R5) and ARP (R6) peaks; plate number calculated for the IS (R7) and ARP (R8) peaks. Optimum BGE conditions were obtained by using the MATLAB® v. R2022a fit linear regression model, in which it was set to obtain maximum resolution values for R1, R2, R3, and R4, and a minimum value of 1.5. For tailing factor responses (R5 and R6), it was set to obtain 1.0 value,



**Figure 3.** Electropherograms of effect of pH values (2.2 to 3.5) (A) and ammonium formate/formic acid concentration (5 to 25 mmol L<sup>-1</sup>) (B) on the peak shape and resolution of IS, ARP and oxidative degradation products. Sample: ARP degraded with 10% H<sub>2</sub>O<sub>2</sub> for 2 h at 60 °C (ARP 100  $\mu$ g mL<sup>-1</sup> and IS 160  $\mu$ g mL<sup>-1</sup>). Conditions: uncoated silica-fused capillary (30.2 cm total length x 75  $\mu$ m i.d.); electrolyte: 10 mmol L<sup>-1</sup> ammonium formate/formic acid; hydrodynamic injection: 0.4 psi/5 s; applied voltage: +12 kV; temperature: 25 °C; detection at 214 nm. Peaks: Promethazine (IS), Aripiprazole (ARP), Degradation Product (DP).





**Figure 4.** Response optimizer showing the optimum capillary zone electrophoresis conditions.

between the range of 0.9 to 1.6, while for the plate number (R7 and R8), it was set to obtain the maximum possible values. The optimum BGE conditions are shown in Fig. 4 (6 mmol L<sup>-1</sup> ammonium formate/formic acid buffer, pH 3.0 and 5% methanol).

The average of three determinations using the predicted conditions from Minitab® v. 20.3 showed resolutions above 2.0 (R1 = 2.2, R2 = 5.7, R3 = 5.5, R4 = 2.6), tailing factor near 1 (R5 = 1.05, R6 = 1.35) and theoretical plates above 10000 (R7 = 18643, R8 = 24823).

The effect of voltage was also studied in the range of 10 to 25 kV, and 15 kV was chosen as the optimum voltage due to short run time (less than 4 min) and a low current obtained (23 μA) with no impact of the CZE method performance. Therefore, optimized conditions

were: BGE composed of 6 mmol L<sup>-1</sup> ammonium formate buffered at pH 3.0 with formic acid and 5% of methanol; +15 kV applied voltage; hydrodynamic injection (0.4 psi for 5 s), detection wavelength at 214 nm and temperature at 25 °C.

#### Optimization of Oxidative Degradation Conditions by DoE

From forced degradation results, the oxidative stress with 3% H<sub>2</sub>O<sub>2</sub> for 2 h at 60 °C resulted in a 4.6% reduction in the ARP content (Table 2).

The experimental design and all oxidative degradation experiments performed by the factorial design are summarized in Table 3. When the obtained results from oxidative degradation were subjected to multiple regression, the following equation was obtained:

$$Y = -5.97 + 0.320 X_1 + 0.1526 X_2 - 2.02 X_3 - 0.00348 X_1 X_2 - 0.2530 X_1 X_3 + 0.0728 X_2 X_3 + 0.00580 X_1 X_2 X_3$$

From the plot of the effect of factors' interactions on % oxidative degradation using multiple regression (Fig. 5), we can observe that temperature (X<sub>3</sub>) was the most significant factor compared to the time of exposure (X<sub>2</sub>) and H<sub>2</sub>O<sub>2</sub> concentration (X<sub>1</sub>). Results showed that all interactions between the factors were also significant. Optimum conditions for 10% ARP degradation under oxidative degradation, indicated by the Minitab® v. 20.3 optimizer tool, suggested the use of 10% H<sub>2</sub>O<sub>2</sub> and heating at 50 °C for 3 h (Fig. 6D). These conditions were adopted, and 11% ARP degradation was obtained. As ARP is susceptible to oxidation in the piperazine group, the oxidative test gave rise to aripiprazole-1-N-oxide (Fig. 1C) and gave rise to aripiprazole 1,4-di-N-oxide (Fig. 1D).<sup>51</sup> The predominant species could be aripiprazole-1-N-oxide, because the aliphatic amines (the -NH<sub>2</sub> group is attached to an alkyl group which is an electron donating group and the lone pair of electrons on nitrogen are readily available) are more reactive as compared to the aromatic amines (the -NH<sub>2</sub> group is attached to a -C<sub>6</sub>H<sub>5</sub> group, which is an electron withdrawing group. So, the availability of a lone pair of electrons on N is decreased).

#### Method Validation

##### System Suitability

To ensure the system was working correctly during all analyses, a system suitability test was performed. The results for six replicates showed that the parameters tested (migration time, resolution, tailing factor, and plate numbers) were within the acceptable range.<sup>46</sup> ARP and IS peaks were baseline resolved, with average migration time of 3.06 min and 2.54 min, respectively; good resolution was obtained (R<sub>s</sub> > 5.0) between the peaks; the tailing factor for both ARP and IS peaks never exceeded 1.4 indicating good peak symmetry (acceptance limit is < 2). Average plate numbers were always > 10000. The proposed CZE method presented high sensitivity and ARP can be detected accurately. Results are presented in Table 1.

##### Specificity/Selectivity and Forced Degradation Study

The specificity of the proposed CZE method was demonstrated by the absence of interference among ARP and excipients in the pharmaceutical product (Aristab®).

To establish the stability indicating capacity of the method, forced degradation studies were performed. For acidic, alkaline, oxidative, photolytic, and thermal studies, the drug was first degraded by taking intermediate stressor strength, temperature and time points. Results are shown in Fig. 6 and summary of the conditions and quantitative results are presented in Table 2. Results were calculated using a control in each degradation condition and expressed as % residual content for ARP.

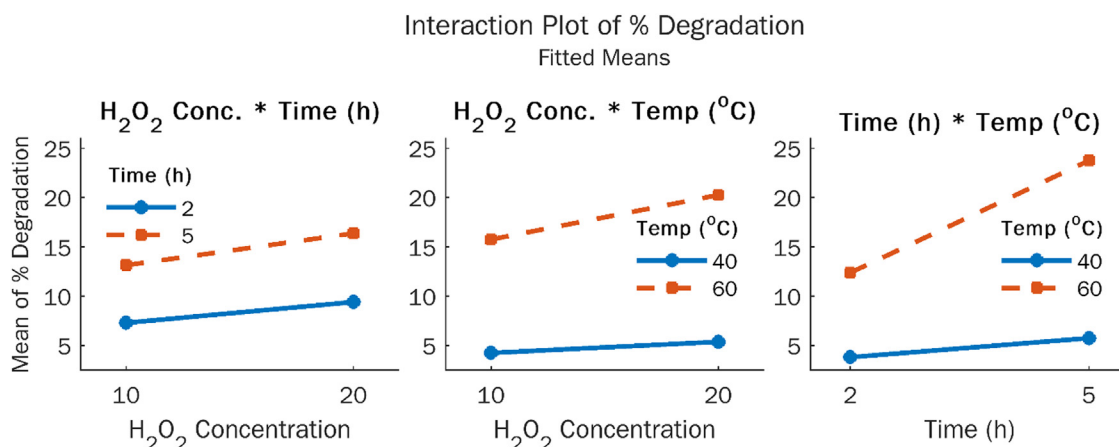


Figure 5. Interaction plot of the effect of factors' interactions on % oxidative degradation.

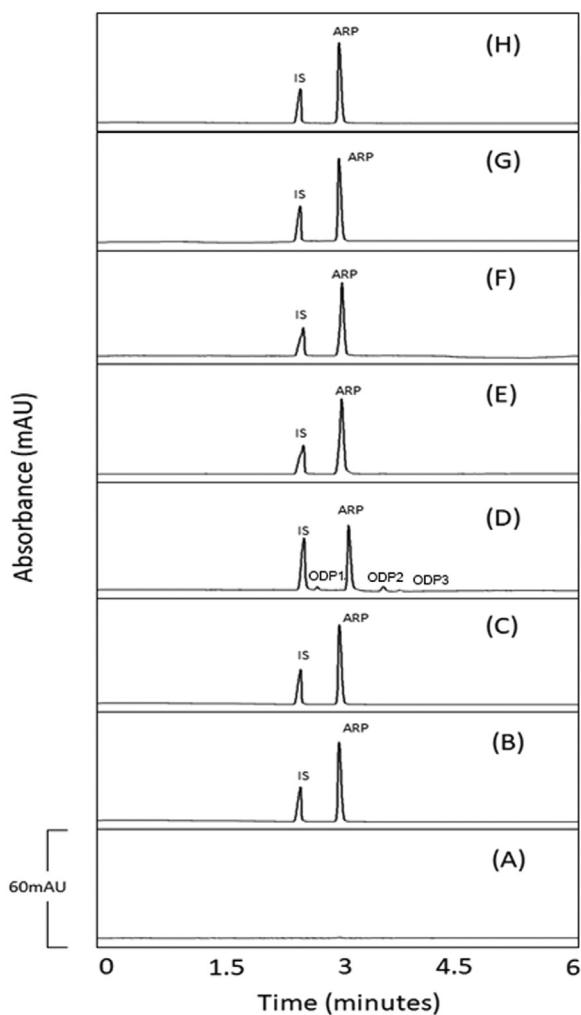


Figure 6. Electropherograms at the final capillary zone electrophoresis optimized conditions. (A) Placebo sample of Aristab®; (B) Standard solution of ARP (100 μg mL<sup>-1</sup>) and IS (160 μg mL<sup>-1</sup>) (without stress); (C) Sample of Aristab® (without stress); (D) Aristab® sample under oxidative conditions (10% H<sub>2</sub>O<sub>2</sub> at 50 °C for 3 h); (E) Aristab® sample under acidic hydrolysis (0.1 mol L<sup>-1</sup> HCl at 60 °C for 2 h); (F) Aristab® sample under alkaline hydrolysis (0.1 mol L<sup>-1</sup> NaOH at 60 °C for 2 h); (G) Aristab® sample under thermal conditions (105 °C for 48 h) and (H) Aristab® sample under photolytic conditions (UVA/visible light for 50 h). Conditions: uncoated silica-fused (30.2 cm total length x 75 μm i.d.); electrolyte: 6 mmol L<sup>-1</sup> ammonium formate/formic acid pH 3.0 with 5% of methanol; hydrodynamic injection: 0.4 psi/5 s; applied voltage: +15 kV; temperature: 25 °C; detection at 214 nm. Peaks: Promethazine (IS), Aripiprazole (ARP), Oxidative Degradation Product (ODP) 1, 2 and 3.

The CZE results of these intermediate conditions, expressed in the terms of percentage of total degradation, were used to select the parameter levels of forced degradation for full factorial design.

DoE was only applied to oxidative condition. Whereas acidic, alkaline, photolytic, and thermal conditions were excluded because the sample exposed to these stress conditions and under the optimum BGE did not show any degradation peaks (Figs. 6E, 6F, 6G and 6H, respectively).

The oxidative stress in 3% H<sub>2</sub>O<sub>2</sub> for 7 days at room temperature and 2 h at 60 °C resulted in a 15% and 4.6% reduction in the ARP content, respectively (Table 2). Three peaks, after oxidative degradation condition, were observed at 2.75 min (ODP1), 3.57 min (ODP2) and 3.77 min (ODP3) (Fig. 6D). The analyte peak had a purity higher than 99%, which suggested that there was no co-migration, and the method was specific. The peak purity was verified by DAD. Moreover, Aristab® tablet matrix samples, in all degradation conditions, did not show any peak that might interfere or co-migrate with ARP (Fig. 6A).

Table 1  
System suitability results (acceptance limits RSD% < 2).

	MT		Tailing factor		N		PAR	Rs
	IS	ARP	IS	ARP	IS	ARP		
Mean <sup>a</sup>	2.544	3.060	0.817	1.321	11616	21618	1.583	5.466
Standard deviation	0.023	0.025	0.010	0.015	141.807	183.069	0.014	0.040
RSD%	1.018	0.828	1.213	1.101	1.221	0.847	0.906	0.733

MT: Migration Time, N: Efficiency (number of plates), PAR: Peak Area Ratio, Rs: Resolution, IS: Internal Standard, ARP: Aripiprazole.

<sup>a</sup> Mean of six replicates.

Table 2  
Stress conditions used for forced degradation test and drug residual content under each condition.

Degradation type	Stressor	Exposition time with temperature	ARP residual content (%) ± SD <sup>a</sup>
Acid	0.1 mol L <sup>-1</sup> HCl	7 days, room temp.	98.50 ± 0.47
		2 h, 60 °C	99.31 ± 0.30
Alkaline	0.1 mol L <sup>-1</sup> NaOH	7 days, room temp.	98.56 ± 0.28
		2 h, 60 °C	99.29 ± 0.31
Oxidative	3% H <sub>2</sub> O <sub>2</sub>	7 days, room temp.	84.95 ± 0.26
		2 h, 60 °C	95.45 ± 0.62
Thermal	105 °C	2 days	99.21 ± 0.23
		7 days	99.37 ± 0.26
Photolytic	UVA/visible light	50 h	99.62 ± 0.25
		120 h	99.49 ± 0.19

ARP: Aripiprazole.

<sup>a</sup> n = 2 for each condition.

**Table 3**  
Experimental matrix of  $2^3$  factorial design for oxidative degradation.

Exp. Number	Level of factor in experiment			% Degradation <sup>a</sup>
	X <sub>1</sub>	X <sub>2</sub>	X <sub>3</sub>	
1	-1	-1	-1	3.31
2	+1	-1	-1	4.70
3	-1	+1	-1	5.37
4	+1	+1	-1	6.13
5	-1	-1	+1	10.90
6	+1	-1	+1	13.91
7	-1	+1	+1	20.81
8	+1	+1	+1	26.67

<sup>a</sup>  $n = 2$  for each condition.

**Table 4**  
Method validation regarding linearity and detection and quantitation limits by capillary zone electrophoresis method.

Parameter	ARP
Concentration range ( $\mu\text{g mL}^{-1}$ )	60–140
Intercept ( $b$ )	-0.4562
Slope ( $a$ )	0.0161
Determination coefficient ( $R^2$ )	0.9983
Standard deviation of intercept ( $S_b$ )	0.0191
Standard deviation of slope ( $S_a$ )	0.0001
Significance $F$	$2.14 \times 10^{-19}$
Detection Limit ( $\mu\text{g mL}^{-1}$ )	3.92
Quantitation Limit ( $\mu\text{g mL}^{-1}$ )	11.89

#### Analysis of Variance in the analytical curve of ARP

	DF	SS	MS	$F_{cal}$
Regression	1	3.12692698	3.12692698	7643.54
Residual	13	0.00531822	0.00040909	
Total	14	3.13224520		

DF: Degrees of Freedom, SS: Sum of Squares, MS: Mean Squares, ARP: Aripiprazole.  $F_{critical}$ ,  $\alpha = 0.05 = 4.67$ .

#### Linearity, Detection, and Quantitation Limits

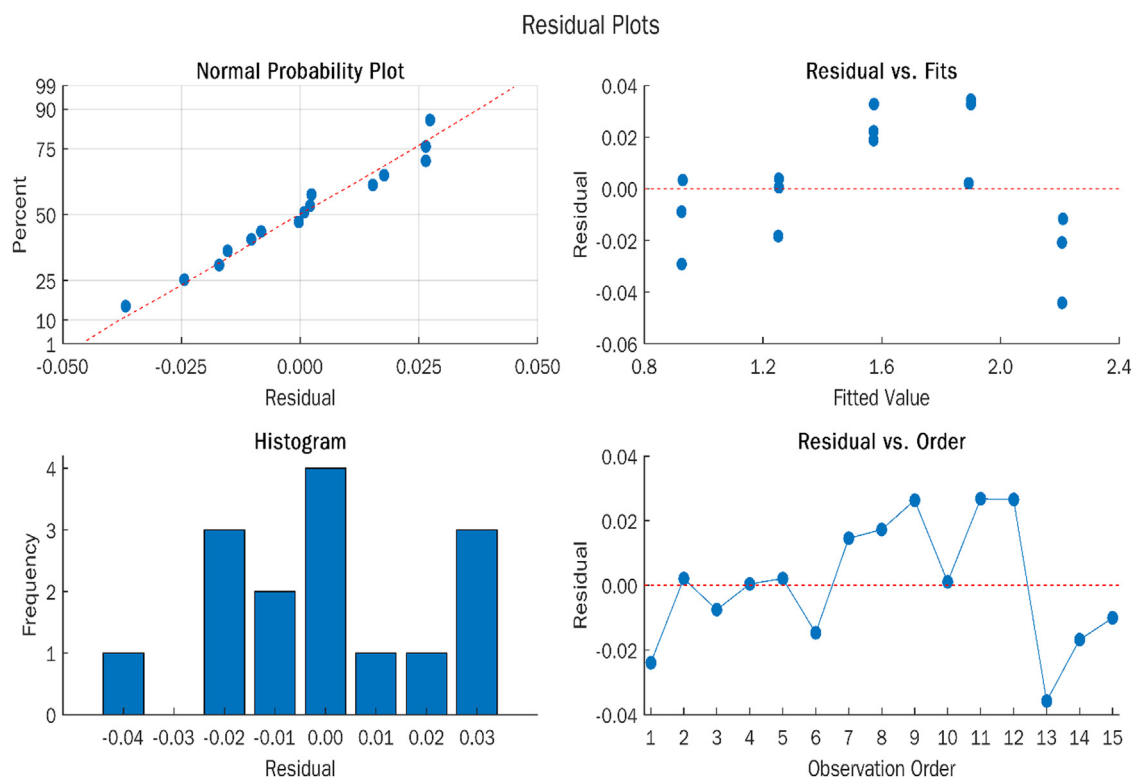
Data obtained from plotting peak area ratios between ARP and IS versus drug concentrations, in the range of 60 to 140  $\mu\text{g mL}^{-1}$ , confirmed the linearity of the CZE proposed method, an adequate coefficient of determination ( $R^2 = 0.9983$ ) was obtained (Table 4). To verify the good fitting of the method, ANOVA was performed at 95% significance level. The ANOVA allowed to evaluate the method linearity and the validity of the linear regression. The value obtained for the  $F_{calculated}$  was higher than  $F_{critical}$  ( $F_{calculated} = 7643.54 > F_{critical} = 4.67$ ,  $\alpha = 0.05$ ) which indicate significant difference between the values obtained from the analytical curves that shows good linear relationship between peak areas and drug's concentrations.

The residual plot graphic shows that residuals are normally and randomly distributed, besides, residuals are independent of each other (Fig. 7). Therefore, the homoscedasticity assumption is satisfied indicating a good fit for the linear model.

The detection and quantitation limits were calculated using the regression parameters, slope, and standard deviation of the intercept. Small values of DL and QL are showed in Table 4 indicating good sensitivity of the proposed CZE method.

#### Accuracy

The accuracy of the proposed CZE method was evaluated by determining the percentage recovery of ARP standard added to the placebo in triplicate experiments at three different levels (80, 100 and 120%). The closeness of the found values compared to the theoretical concentrations at different levels proved the trueness/accuracy of the proposed method. According to the acceptable recovery range from 98 to 102% suggested by the Association of Official Analytical Chemists (AOAC) guideline,<sup>52</sup> the results were excellent with an average recovery of  $100.93 \pm 0.77\%$  (Table 5).



**Figure 7.** Residual plots graph for the linear regression model.

**Table 5**  
Recovery and precision data for determination of ARP by the proposed capillary zone electrophoresis method.

Recovery				
Theoretical concentration ( $\mu\text{g mL}^{-1}$ )	Concentration found <sup>a</sup> ( $\mu\text{g mL}^{-1}$ )	Recovery (% $\pm$ SD) <sup>a</sup>	RSD%	Mean Recovery (% $\pm$ SD) <sup>b</sup>
80	80.93	101.17 $\pm$ 0.43	0.42	100.93 $\pm$ 0.77
100	101.03	101.03 $\pm$ 0.43	0.42	
120	120.72	100.60 $\pm$ 1.10	1.09	
Precision				
Concentration ( $\mu\text{g mL}^{-1}$ )	Intra-day			
	Mean recovery <sup>c</sup> ( $\mu\text{g mL}^{-1}$ )	SD	RSD%	
100	99.29	0.09	0.88	
100	Inter-day			
	Mean recovery <sup>d</sup> ( $\mu\text{g mL}^{-1}$ )	SD	RSD%	
	99.49	0.13	1.29	

SD: Standard Deviation, RSD: Relative Standard Deviation.

<sup>a</sup> Mean of three replicates.

<sup>b</sup> Mean of all recovery levels ( $n = 9$ ).

<sup>c</sup> Mean of six determinations and one analyst.

<sup>d</sup> Mean of twelve determinations and two analysts.

**Table 6**  
Robustness results for drug quantification (acceptance limit RSD% < 2).

Condition	Peak area ratio (ARP/IS)	
	Mean <sup>a</sup>	RSD%
Applied voltage (kV)		
13	1.5490	1.36
15	1.5738	1.18
17	1.5541	1.34
Capillary temperature ( $^{\circ}\text{C}$ )		
24	1.5841	0.26
25	1.5883	0.16
26	1.5745	1.01
Injection time (s)		
4	1.5756	1.53
5	1.5636	0.83
6	1.5471	0.97

ARP: Aripiprazole, IS: Internal Standard, RSD: Relative Standard Deviation kV: kiloVolt.

<sup>a</sup> Average of three determinations.

#### Precision

The precision was evaluated in terms of repeatability (intra-day) and intermediate precision (inter-day). The RSD% for intra- and inter-day precision were 0.88 and 1.29, respectively. Both repeatability and intermediate precision results showed low RSD% values (< 2%), confirming that the proposed CZE method is precise. Results are presented in Table 5.

#### Robustness

No significant effects were observed upon applying small deliberately changes in the electrophoretic conditions (applied voltage, capillary temperature, or hydrodynamic injection time). The results are shown in Table 6, the RSDs% in all cases were less than 2%, which ensures the robustness of the proposed CZE method.

#### Application

The developed CZE method was applied for the analysis of ARP in its pharmaceutical preparation (Aristab<sup>®</sup> tablets). The assay of ARP in commercial formulations indicated a mean value of  $9.95 \pm 0.13$  mg/tab (99.5%, RSD% = 1.3), which is in good agreement with the label claim for ARP tablets (Table 5). The results were found to be satisfactory, and they are within tolerance limits (95 – 105% label claim).<sup>3</sup> Therefore, the results successfully demonstrated that the proposed CZE method was suitable for the determination of aripiprazole in tablets.

## Conclusion

A new environmentally friendly stability indicating capillary zone electrophoretic method for the determination of ARP in pharmaceutical formulations was developed and validated. In this study, ARP was subjected to stress studies in accordance with the ICH guidelines. Acidic and alkaline hydrolysis, photolytic and thermal conditions did not promote any ARP degradation that could be visualized by the proposed method. The drug underwent extensive degradation under oxidative stress. DoE optimization approach-based development method was capable to determine ARP in the presence of its degradation products, after oxidative stress. To date, this is the first stability indicating CZE method concerning the quantification of ARP in the presence of its degradation products. The proposed method achieves satisfactory separation of ARP from the degradation products. Statistical analysis of the results showed that the method was linear, precise, accurate and robust. The precision and accuracy indicated the high method quality; the robustness results indicated the wide method applicability. No interference from any components of pharmaceutical dosage form or degradation products was observed. The CZE method is simple, easily implemented and possibly has many advantages over conventional chromatographic methods, including reduction in the use of organic solvents, small sample volume, and increased efficiency and resolution. For example, we utilized 5% of methanol (approximately 6.25 mL) for the analysis of ARP in 5 min of total run time compared to HPLC method (approximately 250 mL) at the same condition in one week. Therefore, this new method leads to a feasible, cost-effective, and rapid method that can be successfully applied for routine quality control analysis of ARP in pharmaceutical preparations in the presence of its degradation products.

## Conflicts of Interest

All contributing authors declare no conflicts of interest.

## Declaration of Interests

The authors declare that they have no known competing financial interests or personal relationships that could have appeared to influence the work reported in this paper.

The authors declare the following financial interests/personal relationships which may be considered as potential competing interests:

María Segunda Aurora Prado reports financial support was provided by Fundação de Amparo à Pesquisa do Estado de São Paulo (FAPESP), Brazil. Frank Alonso Gavilano Fajardo reports financial support was provided by Coordenação de Aperfeiçoamento de Pessoal de Nível Superior (CAPES), Brazil.

## Acknowledgments

The authors wish to thank the Coordenação de Aperfeiçoamento de Pessoal de Nível Superior (CAPES), Brazil (Process 88882.377651/2019-01) for FAGF scholarship, the Fundação de Amparo à Pesquisa do Estado de São Paulo (FAPESP), Brazil (Process 2012/50595-8) for financial support, while Aspen Farmacêutica and Aché Laboratórios do Brasil for providing drug substance and drug product. The authors would also like to thank to Agilent Technologies for instrumental support.

## References

- Center for Drug Evaluation and Research. *Analytical Procedures and Methods Validation for Drugs and Biologics Guidance for Industry*. U.S. Department of Health and Human Services, Food and Drug Administration; 2015.
- ICH Expert Working Group. *International Conference on Harmonisation of Technical Requirements for Registration of Pharmaceuticals for Human Use: Stability Testing of New Drug Substances and Products Q1A(R2)*. 2003.
- United States Pharmacopoeial Convention. *United States Pharmacopoeia – National Formulary (USP – NF)*. United States Pharmacopoeial Convention; 2021.
- Bakshi M, Singh S. Development of validated stability-indicating assay methods: critical review. *J Pharm Biomed Anal*. 2002;28(6):1011–1040. [https://doi.org/10.1016/s0731-7085\(02\)00047-x](https://doi.org/10.1016/s0731-7085(02)00047-x).
- ICH Expert Working Group. *International Conference on Harmonisation of Technical Requirements for Registration of Pharmaceuticals for Human Use: Pharmaceutical Development Q8(R2)*. 2009.
- Skrdl PJ, Wang T, Antonucci V, et al. Use of A QUALITY-BY-DESIGN APPROACH TO JUSTIFY REMOVAL OF the HPLC weight % assay from routine api stability testing protocols. *J Pharm Biomed Anal*. 2009;50(5):794–796. <https://doi.org/10.1016/j.jpba.2009.06.027>.
- Peraman R, Bhadraya K, Padmanabha Reddy Y. Analytical quality by design: a tool for regulatory flexibility and robust analytics. *Int J Anal Chem*. 2015;1–9. <https://doi.org/10.1155/2015/868727>. Published online.
- Orlandini S, Pinzauti S, Furlanetto S. Application of quality by design to the development of analytical separation methods. *Anal Bioanal Chem*. 2013;405(2–3):443–450. <https://doi.org/10.1007/s00216-012-6302-2>.
- Lundstedt T, Seifert E, Abramo L, et al. Experimental design and optimization. *Chemom Intell Lab Syst*. 1998;42(1–2):3–40. [https://doi.org/10.1016/S0169-7439\(98\)00065-3](https://doi.org/10.1016/S0169-7439(98)00065-3).
- Prommer E. Aripiprazole. *Am J Hosp Palliat Care*. 2017;34(2):180–185. <https://doi.org/10.1177/1049909115612800>.
- Naber D, Lambert M. Aripiprazole: a new atypical antipsychotic with a different pharmacological mechanism. *Prog Neuropsychopharmacol Biol Psychiatry*. 2004;28(8):1213–1219. <https://doi.org/10.1016/j.pnpb.2004.06.020>.
- DeLeon A, Patel NC, Crismon ML. Aripiprazole: a comprehensive review of its pharmacology, clinical efficacy, and tolerability. *Clin Ther*. 2004;26(5):649–666. [https://doi.org/10.1016/s0149-2918\(04\)90066-5](https://doi.org/10.1016/s0149-2918(04)90066-5).
- Harrison TS, Perry CM. Aripiprazole: a review of its use in schizophrenia and schizoaffective disorder. *Drugs*. 2004;64(15):1715–1736. <https://doi.org/10.2165/00003495-200464150-00010>.
- Huang HC, Liu CH, Lan TH, et al. Detection and quantification of aripiprazole and its metabolite, dehydroaripiprazole, by gas chromatography-mass spectrometry in blood samples of psychiatric patients. *J Chromatogr B*. 2007;856(1–2):57–61. <https://doi.org/10.1016/j.jchromb.2007.05.026>.
- Dedania Z, Dedania RR, Sheth N, Gajra B, Patel JB. Development and validation of a stability-indicating high performance liquid chromatography assay for aripiprazole in bulk drug substance. *Asian J Pharm Biol Res*. 2011;1(2):123–128.
- Djordjević Filjović N, Pavlović A, Nikolić K, Agbaba D. Validation of an HPLC method for determination of aripiprazole and its impurities in pharmaceuticals. *Acta Chromatogr*. 2014;26(1):13–28. <https://doi.org/10.1556/ACHrom.26.2014.1.15>.
- Kalaichelvi R, Thangabalan B, Srinivasa Rao D. Validated RP-HPLC method for analysis of aripiprazole in a formulation. *J Chem*. 2010;7(3):827–832. <https://doi.org/10.1155/2010/935279>.
- Mondal P, Shobha Rani S. A new stability indicating validated method for the determination of aripiprazole in bulk and tablet dosage form using RP-HPLC. *Int J Pharm Pharm Sci*. 2013;5(5):1–6.
- Narayana M, Chandrasekhar K. A validated specific stability-indicating RP-HPLC method for aripiprazole and its related substances. *J Chem Pharm Res*. 2012;4(9):4426–4435.
- Nerkar P, Gide P, Chitnis A, Mahajan H, Gattani S. Development of stability indicating reverse phase HPLC method for aripiprazole from solid dosage form. *Int J Pharm Sci Nanotechnol*. 2009;2(2):572–581. <https://doi.org/10.37285/ijpsn.2009.2.2.12>.
- Pai NR, Dubhashi DS. Development of stability indicating, validated HPLC method for quantitative determination of aripiprazole and its impurities. *Der Pharm Lett*. 2010;2(4):1–10.
- Rmandić M, Malenović A. Chaotropic chromatography method development for the determination of aripiprazole and its impurities following analytical quality by design principles. *J Sep Sci*. 2020;43(16):3242–3250. <https://doi.org/10.1002/jssc.201900985>.
- Soponar F, Sandru M, David V. Quantitative evaluation of aripiprazole and its five related chemical impurities from pharmaceuticals using a HPLC-DAD method. *Rev Roum Chim*. 2014;59(11–12):1037–1046.
- Srinivas KSV, Buchireddy R, Madhusudhan G, Mukkanti K, Srinivasulu P. Stress degradation studies on aripiprazole and development of a validated stability indicating LC method. *Chromatographia*. 2008;68(7–8):635–640. <https://doi.org/10.1365/S10337-008-0739-7>.
- Kubo M, Mizooka Y, Hirao Y, Osumi T. Development and validation of an LC-MS/MS method for the quantitative determination of aripiprazole and its main metabolite, OPC-14857, in human plasma. *J Chromatogr B*. 2005;822(1–2):294–299. <https://doi.org/10.1016/j.jchromb.2005.06.023>.
- Patel DP, Sharma P, Sanyal M, Shrivastav PS. SPE-UPLC-MS/MS method for sensitive and rapid determination of aripiprazole in human plasma to support a bioequivalence study. *J Chromatogr B*. 2013;925:20–25. <https://doi.org/10.1016/j.jchromb.2013.02.022>.
- Krishna MVNM, Rao SV, Venugopal NVS. Identification of degradation impurities in aripiprazole oral solution using LC–MS and development of validated stability indicating method for assay and content of two preservatives by RP-HPLC. *J Liq Chromatogr Relat Technol*. 2017;40(14):741–750. <https://doi.org/10.1080/10826076.2017.1357572>.
- Reddy G, Reddy GVR, Kumar AP, Reddy BV, Gauttam HD. Identification of degradation products in aripiprazole tablets by LC-QToF mass spectrometry. *Eur J Chem*. 2010;1(1):20–27. <https://doi.org/10.5155/eurjchem.1.1.20-27.11>.
- Wojnicz A, Belmonte C, Koller D, et al. Effective phospholipids removing microelution-solid phase extraction LC-MS/MS method for simultaneous plasma quantification of aripiprazole and dehydroaripiprazole: application to human pharmacokinetic studies. *J Pharm Biomed Anal*. 2018;151:116–125. <https://doi.org/10.1016/j.jpba.2017.12.049>.
- Cao Y, Zhao F, Chen J, et al. A simple and rapid LC-MS/MS method for the simultaneous determination of eight antipsychotics in human serum, and its application to therapeutic drug monitoring. *J Chromatogr B*. 2020;1147:122–129. <https://doi.org/10.1016/j.jchromb.2020.122129>.
- Kalaichelvi R, Thangabalan B, Rao DS, Jayachandran E. UV Spectrophotometric determination of aripiprazole in bulk and pharmaceutical formulation. *J Chem*. 2009;6(S1):S87–S90. <https://doi.org/10.1155/2009/542919>.
- Jain R, Kashaw SK, Jain R, Mishra P, Kohli D V. Visible spectrophotometric method for the determination of aripiprazole in tablets. *Indian J Pharm Sci*. 2011;73(1):74–76. <https://doi.org/10.4103/0250-474X.89760>.
- Sandeep K, Induri M, Sudhakar M. Validated spectrophotometric quantification of aripiprazole in pharmaceutical formulations by using multivariate technique. *Adv Pharm Bull*. 2013;3(2):469–472. <https://doi.org/10.5681/apb.2013.078>.
- Aşangil D, Hüdaî Taşdemir I, Kılç E. Adsorptive stripping voltammetric methods for determination of aripiprazole. *J Pharm Anal*. 2012;2(3):193–199. <https://doi.org/10.1016/j.jpba.2012.01.009>.
- Merli D, Dondi D, Ravelli D, Tacchini D, Profumo A. Electrochemistry and analytical determination of aripiprazole and octoclothepein at glassy carbon electrode. *J Electroanal Chem*. 2013;711:1–7. <https://doi.org/10.1016/j.jelechem.2013.09.036>.
- Musenga A, Saracino MA, Spinelli D, et al. Analysis of the recent antipsychotic aripiprazole in human plasma by capillary electrophoresis and high-performance liquid chromatography with diode array detection. *Anal Chim Acta*. 2008;612(2):204–211. <https://doi.org/10.1016/j.aca.2008.02.046>.
- Hwang PL, Wei SY, Yeh HH, Ko JY, Chang CC, Chen SH. Simultaneous determination of aripiprazole and its active metabolite, dehydroaripiprazole, in plasma by capillary electrophoresis combining on-column field-amplified sample injection and application in schizophrenia. *Electrophoresis*. 2010;31(16):2778–2786. <https://doi.org/10.1002/elps.201000237>.
- Tsai CJ, Yu YH, Chiu HJ, et al. The quantitative detection of aripiprazole and its main metabolite by using capillary-electrophoresis. *J Chinese Med Assoc*. 2011;74(6):267–271. <https://doi.org/10.1016/j.jcma.2011.04.006>.
- Rochet J-C. *Pharmaceutical analysis: a textbook for pharmacy students and pharmaceutical chemists*. Am J Pharm Educ. 2006;70(2):1–4.
- Altria KD. *Capillary Electrophoresis Guidebook: Principles, Operation, and Applications (Methods in Molecular Biology)*. Humana Press Inc.; 1996. Vol 52.
- Klampf CW. Recent advances in the application of capillary electrophoresis with mass spectrometric detection. *Electrophoresis*. 2006;27(1):3–34. <https://doi.org/10.1002/elps.200500523>.
- Kumar R, Guttman A, Rathore AS. Applications of capillary electrophoresis for biopharmaceutical product characterization. *Electrophoresis*. 2022;43(1–2):143–166. <https://doi.org/10.1002/elps.202100182>.
- Ranasinghe M, Quirino JP. Can we replace liquid chromatography with the greener capillary electrophoresis? *Curr Opin Green Sustain Chem*. 2021;31: 100515. <https://doi.org/10.1016/j.cogsc.2021.100515>.
- European Medicines Agency. *International Conference on Harmonisation: Photostability Testing of New Active Substances and Medicinal Products Q1B*. 1998.

45. Sheskey PJ, Hancock BC, Moss GP, Goldfarb DJ. *Handbook of Pharmaceutical Excipients*. 9th ed. The Pharmaceutical Press; 2020.
46. European Medicines Agency. International Conference on Harmonisation of Technical Requirements for Registration of Pharmaceuticals for Human Use: Validation of Analytical Procedures (Text and Methodology) Q2(R1).; 1995.
47. Aurora-Prado MS, Silva CA, Tavares MFM, Altria KD. Determination of folic acid in tablets by microemulsion electrokinetic chromatography. *J Chromatogr A*. 2004;1051(1-2):291–296. <https://doi.org/10.1016/j.chroma.2004.08.042>.
48. Beckers JL, Boček P. The preparation of background electrolytes in capillary zone electrophoresis: golden rules and pitfalls. *Electrophoresis*. 2003;24(3):518–535. <https://doi.org/10.1002/elps.200390060>.
49. Chemicalize. Chemicalize - Instant Cheminformatics Solutions (Calculations and Predictions). Chemaxon. 2022. Accessed April 15, 2022; <https://chemicalize.com/welcome/chemical-calculations-and-predictions>.
50. PubChem. Aripiprazole. 2022. Accessed April 15, 2022; <https://pubchem.ncbi.nlm.nih.gov/compound/Aripiprazole>.
51. Satyanarayana B, Sumalatha Y, Kumar SS, Venkatraman S, Reddy GM, Reddy PP. Synthesis and characterization of N-oxides and metabolites of antipsychotic drug, aripiprazole. *Heterocycl Commun*. 2005;11(6):485–490. <https://doi.org/10.1515/HC.2005.11.6.485>.
52. Horwitz W. 17th ed. *Official Methods of Analysis*. 1. The Association of Official Analytical Chemists (AOAC) International; 2000.

## Development and Validation of an Analytical Method for Determination of Risperidone in Tablet Formulation

Victor Barnabe de Pontes <sup>a</sup>, Anas Rashid <sup>b</sup>, María Segunda Aurora Prado <sup>a,\*</sup>

<sup>a</sup>Department of Pharmacy, School of Pharmaceutical Sciences, University of São Paulo, São Paulo, Brazil

<sup>b</sup>School of Medicine and Surgery, University of Torino, Torino, Italy

### Abstract

**Objective:** The study aims to develop and validate an analytical method for the quantitative determination of risperidone in pharmaceutical formulations (tablets) by applying the high-performance liquid chromatography (HPLC) technique.

**Materials and methods:** The analysis was performed using an HPLC. The methodology was developed on the selected technique based on the physicochemical properties of the molecule and the method was optimized with literature recommended data. The statistical analysis was applied to validate the following parameters including specificity, linearity, range or interval, precision, accuracy and robustness; which was carried out according to the internationally accepted guidelines.

**Results:** The risperidone concentration was 30  $\mu\text{g mL}^{-1}$  using the mobile phase as a diluent, consisting of pH 3.0 buffer with 0.5% triethylamine:methanol (55:45), the flow rate was 1.5  $\text{mL min}^{-1}$ , oven temperature of 25 °C, injection of 30  $\mu\text{L}$ , UV detection at 235 nm wavelength and Chromolit Performance RP-18e chromatographic column (100 mm x 4.6 mm), with run time set at 6 minutes. The validation of the methodology proved that the method is specific for risperidone, with no interfering peaks being detected in the retention time; linear with a coefficient of determination  $R^2$  greater than 0.99; with the recovery for each of the solutions between 98.0% and 102.0%; accurate with the relative standard deviation (RSD) of the results between the 6 solutions equivalent to 100%, less than 2.0% and robust, due to the RSD of the contents between the three samples, for each of the flow conditions, temperature and proportion of mobile phase, present a value below 5%. The concentration range defined for the method was 80% to 120% because the acceptance criteria for linearity, accuracy and precision were met in this range.

Conclusion: This method was properly validated, meeting the requirements for the product, being safe and consistent for the intended purpose, and can be used for routine batch control and stability, as it follows all the requirements established by current legislation mentioned in the methods section.

**Keywords**

Antipsychotic, Risperidone, HPLC, Tablets



## Introduction

Risperidone (RSP) is a second-generation atypical antipsychotic agent of the benzisoxazole group used for the treatment of schizophrenia and the acute manic phase of bipolar disorder [1]. After oral administration, RSP is completely absorbed from the gastrointestinal tract and undergoes hydroxylation to yield paliperidone (9-hydroxyrisperidone), an active metabolite that has a pharmacologic profile and potency similar to RSP [2]. The primary action of risperidone is to decrease dopaminergic and serotonergic pathway activity in the brain, therefore decreasing symptoms of schizophrenia and mood disorders. It has a high binding affinity for serotonergic 5-HT<sub>2A</sub> receptors when compared to dopaminergic D<sub>2</sub> receptors in the brain [3,4].

Schizophrenia is a chronic psychiatric disorder with a heterogeneous genetic and neurobiological background and a significant negative impact on patient(s) quality of life, associated with high costs resulting from long-term treatments and special demands on health services, family attendants and caregivers [5]. Considering the prevalence of schizophrenia, around 1% of the population is at risk (15-45 years) [6]. It is assumed that there are at least one million schizophrenic patients within Brazil, and of these, approximately 300,000 are refractory [7].

The warning issued by ANVISA highlighted an increased risk of ischemic stroke in elderly patients who use this medication [8–10]. Also, there are documented reports of its relationship with Pisa syndrome due to high doses of risperidone [11–13]. To date, all analytical methods described in the literature for the determination of risperidone in biological fluids involve HPLC [14–21], gas chromatography [22], capillary electrophoresis [23], hyphenated techniques and liquid chromatography-mass spectrometry [24–28]. Some of these techniques require solid-phase extraction to prepare the sample which makes it difficult to use them for daily analyses, so simple and more optimized methods are needed for routine analyses.

To achieve this objective, analytical methods must be carefully developed and validated, as it ensures that the analysis performed provide reliable results depending on the method or procedure used. This work will be aimed at the development and validation of the method for the quantification of risperidone in pharmaceutical formulations (tablet) using the HPLC technique according to the criteria established by the official bodies: United States Pharmacopoeia [29], International Conference on Harmonization [30] and ANVISA

concerning reproducibility, specificity, linearity, range, detection limit, quantification limit, precision, accuracy, and robustness. Hence, this method can be used in Quality Control Laboratories for content analysis, content uniformity in activities involving batch release for commercialization as well as stability studies. Hence in the present work, we developed a simple, precise, accurate, selective and robust liquid chromatographic method for the determination of risperidone in a pharmaceutical dosage form as an alternative.

## **Materials and methods**

### **Instrumentation**

The experimental analyses were carried out by using Shimadzu<sup>®</sup> HPLC system (Shimadzu Corporation, Kyoto, Japan). The equipment was composed of Workstation Class-VP ver. 6.14 software (SCL-10Avp system controller); automatic injector (SIL-10ADvp); solvent pumping system (LC-10ADvp); online degassing system (DGU-14A); temperature control oven (CTO-10AC); and UV/Vis photodiode array detector (SPD-M10Avp).

### **Chromatographic conditions**

The separation was performed on a Chromolith<sup>®</sup> Performance RP-18 endcapped (100 mm x 4.6 mm i.d., 2 µm particle size) (Merck, Sao Paulo, Brazil).

### **Reagents, chemicals and sample**

The active pharmaceutical ingredient risperidone was donated by local pharmaceutical industry (Sao Paulo, Brazil). Film-coated tablet Risperidone 2 mg was procured from local community pharmacy (Sao Paulo, Brazil). Analytical grade methanol, triethylamine, and *o*-phosphoric acid were purchased from (Merck, Sao Paulo, Brazil), while deionized water was obtained from Milli-Q<sup>®</sup> ultrapure purification system (Millipore Corp., Bedford, MA, USA).

Placebo was composed of croscarmellose sodium (1.5%), silicon dioxide (1.0%), monohydrate lactose (55%), magnesium stearate (1.0%), hypromellose (5.5%), microcrystalline cellulose (34.5%), titanium dioxide (0.17%), macrogol (1.3%), Food, Drugs and Cosmetics Yellow No. 6 aluminum lake (0.03%). All the excipients were also donated by local pharmaceutical industry (Sao Paulo, Brazil).

This technique was chosen due to the solubility of risperidone in moderately polar solvents and the detection by ultraviolet (UV) light beam based on the fact that risperidone has conjugated double bonds and, therefore, absorbance in the UV region (Figure 1(a)). The stationary phase was chosen to retain the active pharmaceutical ingredient in the column and have an affinity for it, reproducing a method with a capacity factor greater than or equal to 0.5. The column initially used was a Synergi Hydro C18 80-Å 100mm x 4.6mm 4µm, which in addition to having octadecyl chains also has polar groups (Figure 1(b)), which contributes to the retention of risperidone, which also has a non-polar structure with some polar groups (Figure 1(a)).

The choice of using a buffer with a determined pH was based on the fact that it provides greater stability to the method with minimal variations in retention time, as the buffer guarantees a stable conformation to the molecule (either ionic or molecular form). The pKa of risperidone is 8.63 [31] which demonstrates its basic character, with a defined pH of 3.0 guaranteeing the molecule in its ionic form. The initial proportion of buffer was 45% and methanol 55% with isocratic elution, and an initial working flow of 0.8 mL min<sup>-1</sup> in an attempt to provide greater interaction between the molecule and the stationary phase. The oven temperature was 25 °C, thus opting for not being a preponderant factor for the retention of the molecule. The wavelength was adjusted at 235 nm because it presents a considerably good absorption region with an adequate signal amplitude to reduce response variations.

Water is always the first-choice solvent due to its very low elution power compared to the mobile phase for reverse-phase techniques. Due to the low solubility of risperidone in water, the extraction solvent initially chosen was the mobile phase itself. The risperidone concentration was 30 µg mL<sup>-1</sup> for both the standard and the sample. Calibration of the system for quantification of risperidone was by external calibration and performance indices were extracted at each step of the development to assess the improvement of the method.

#### *Stability of analytical solutions*

The sample solution prepared at intermediate precision was used. This solution was kept in the lab at room temperature and injected again after 24 h of preparation.

#### *Specificity*

The sample and placebo were subjected to forced degradation conditions including temperature, light, humidity, oxidation, acidic and basic hydrolysis.

Also to assess whether any degradation compound interfered in the quantification of the compound of interest. Interference in the chromatogram was evaluated through visual analysis and content results in each degradation condition, as well as the appearance of possible degradation products from the sample and the interferences of these degradation peaks with the peak of interest.

The sample solution was subjected to conditions of forced degradation for 24 h and then prepared according to the analytical method. Solutions with a placebo subjected to the same conditions as the samples were also prepared to assess the interference of any peaks (from the placebo) with the peak of interest. In parallel, it was prepared from the linearity test placebo contaminated with a standard to assess its recovery under normal conditions.

#### *Preparation of stock standard and working solutions*

The risperidone stock standard solution was prepared in mobile phase (name) to obtain the concentration of  $300 \mu\text{g mL}^{-1}$ . To prepare working solution, 1 mL of stock standard solution was transferred into 10 mL amber volumetric flask and the volume was completed with the same solvent. The solution was sonicated for 3 mins and filtered (name) before being used. The risperidone final concentration of  $30 \mu\text{g mL}^{-1}$  was obtained.

#### *Preparation of stock sample solution*

##### *Placebo stock solution*

1524.20 mg of the placebo was weighed in a 100 mL volumetric flask. About 25 mL of mobile phase was added and dissolved in ultrasound for 15 min. The volume was made up with the mobile phase and then homogenized.

##### *Dilution*

An automatic micropipette was used to transfer each aliquot of the risperidone stock solution to a 50 mL amber volumetric flask as shown in Table 2. Three solutions of each concentration were prepared. The volume of each volumetric flask was made up of a mobile phase and the solutions were filtered with a Millex HV  $0.45 \mu\text{m}$  filter (Millipore).

##### *Linearity*

Solutions of five concentrations corresponding to 80%, 90%, 100%, 110% and 120% of the theoretical active concentrations were prepared, with three solutions of each concentration. Each solution was injected, in ascending order of the active concentrations. The result obtained in this step was used to check the accuracy and range of this method.

#### *Accuracy*

Accuracy was established within the range of the analytical procedure and expresses the distance between an obtained value and the theoretical value, i.e., the recovery of a method, its systematic error or trend was evaluated, which corresponds to the difference between the added value and the obtained value, analyzing solutions prepared from the already mentioned concentration of the sample. The results of the 80%, 100% and 120% concentration solutions analyzed in the linearity step were used to verify the accuracy of the analysis method.

#### *Range*

It was demonstrated that the analysis method has an appropriate precision, accuracy and linearity in the range of 80% to 120% (inclusive) of the active sample concentration.

#### *Robustness*

The ability of the method to remain unaffected by small variations was evaluated, thus obtaining an indication of its reliability during its normal use. Robustness testing is used to identify critical method parameters. This involves making deliberate variations on the method parameters and investigating the effect of the result. In this case, we changed the parameters by  $\pm 5\%$  to what was defined in the development and we verified if the result variation was greater than 5%, which could be considered critical for the robustness of the method. It was verified whether there was variation in the results by changing the oven temperature by  $\pm 1.25^\circ\text{C}$ ; flow by  $\pm 5\%$ ; in addition, the percentage of methanol in the mobile phase by  $\pm 5\%$ .

#### *Repeatability*

Repeatability evaluated whether the operating conditions of the system remain adequate under the reading of different replicates. Experimentally, it was obtained through the consecutive injection of six samples at the level of 100% of the target concentration. The evaluation of the mean values and RSD were analyzed. Six different samples from the same batch were prepared

and analyzed with a concentration equivalent to 100% of the established range for this analytical method. The result was expressed in RSD and used in the intermediate precision test.

### *Intermediate Precision*

Two analysts analyzed the same sample from the same batch, six times for content, using the same equipment on different days. Each analyst prepared their sample and mobile phase solutions. Each analyst prepared six sample solutions for the Intermediate precision study. The analyzes performed in the repeatability test were used for the intermediate precision test, reproducing the standard deviation between the means of the results of each one.

## **Results and discussion**

### *a) System 1*

In the initial working condition, risperidone eluted in 3.55 min (Figure 2(a)), which represented a previous definition of the chromatographic conditions, and then we proceed with the method optimization step. The peak of interest presented with a large base width and posterior tail, this can occur when there is a strong interaction of the substance with the stationary phase and that sometimes is not necessary for its retention in an adequate time. The tail factor presented was 2.254, out of the recommended literature, which advises it to be 0.9 – 1.5 [32]. The triethylamine plays an important role in minimizing the tail of the peak, as to interact with the silanol groups of the column hampers dispersion of the sample.

### *b) System 2*

There was an increase in the proportion of methanol to 45% and in the flow to 1.5 mL min<sup>-1</sup>, it was expected a reduction in the retention time, but what happened was an increase to 1.919 min, in addition there was an increase in the buffer, the triethylamine concentration was increased to 0.5%, which provided better peak symmetry (Figure 2(d)). From the observed data, we can see that the substance has greater affinity for the buffer than for methanol, because by increasing the proportion of methanol to 45%, we decreased the proportion of buffer to 55%, which increased the elution time of risperidone, even with increased flow. The tail factor was 1.492(<1.5), theoretical plates >2000 and K' of 2.392.

### *c) System 3*

The methanol ratio was reduced to 45%, so the peak elution was expected to be delayed and its width increased (Figure 3(a)), then the oven temperature was increased to verify the effect on improving column efficiency. The configuration was not acceptable, as the performance parameters worsened, tail factor is 2.118, theoretical plates < 2000.

*d) System 4*

There was a reduction in flow to 0.9 mL min<sup>-1</sup>, with improvement in symmetry and an increase in retention time to 2.991 min (Figure 3(b)). This configuration provided an improvement in peak symmetry with a tail factor of 1.838, but still according to the literature recommendations [32], and theoretical plates of 2193.

*e) System 5*

The column was replaced by a normal C18, without polar groups, in this case a Chromolith® Performance RP – 18e (Figure 1(c)), with a reduction in the proportion of methanol to 50% and an increase in flow to 1.0 mL min<sup>-1</sup>. We promptly obtained an improvement in peak symmetry with a reduction in the tail and base width, with a tail factor of 1.865 and also contributing to the increase in amplitude (Figure 3(c)), this is due to the absence of the polar interaction that existed with the previous column.

*f) System 6*

In this test, the furnace temperature returned to 25°C, as no improvement was observed with its increase, the proportion of methanol was reduced to 30% and the flow rate increased to 1.2 mL min<sup>-1</sup>. The retention time was very close to the dead volume of the column, presenting a K' (capacity factor) of 0.916 (Figure 3(d)). In addition to the impracticality of the retention time, symmetry worsened and theoretical plates worsened, with a value of 642, lower than recommended in the literature ( $\geq 2000$ ) [32].

At this stage of development, the chromatographic conditions and methodology were defined, as all performance parameters were met, signal amplitude and retention time were adequate, and the running time could be set at 6 minutes. From this moment on, work continued on the validation of the method. Below are the results of each of the steps of the validation of the risperidone content analysis method by HPLC (finished product).

*Analytical curve and system adequacy*

The generated calibration curve and the reproducibility of the system were verified during the execution of the analysis in each of the validation steps. For all steps, the acceptance criteria were met and mentioned in Table 3.

#### *Determination of post time*

The sample solution was injected into the chromatograph and the flow was maintained for 60 min. The retention time was around 2 minutes for the risperidone peak. As after the elution of the risperidone peak, the elution of other peaks that could interfere with subsequent injections is not observed, it was established with a run time of 6 minutes, which was sufficient time for the elution of all peaks that could interfere with subsequent elution and for the signal to return to baseline.

#### *Stability of analytical solutions*

The stability study of the solutions aims to determine whether the compound of interest remains stable in the sample solution at room temperature under the lab's analysis conditions for a period of 24 hours. The Sample 1 solution was prepared in the intermediate precision analysis step 1. Table 4 presents the results obtained for the stability of the analytical solutions:

#### *Specificity*

This method is specific for the determination of Risperidone at the determined wavelength (235 nm), free from the interference of signals from other substances present in solvents used for the preparation of standard and sample solutions, was verified. In addition, when analyzing the sample under conditions of acid, basic, oxidative, light, humidity and temperature stress for 24 hours, it was possible to visually verify, through the chromatograms below (Figure 2 (b-c)), that there was no formation of degradation products that co-eluted with risperidone, showing that the method is specific for the determination of risperidone even under stress conditions. Table 5 shows the results obtained for specificity.

Additionally, a non-stressed placebo sample was injected, and no peak from the placebo that co-elutes with the retention time of risperidone was observed (Figure 2(e)). In addition, standard-contaminated placebo samples were prepared and injected into the accuracy test. Recovery within the range of 98-102% led us to conclude that placebo does not interfere with the quantification of risperidone.



### *Linearity*

Linearity aims to verify the proportionality between the concentration of the active substance and its response within a given range. Three solutions of each concentration corresponding to 80%, 90%, 100%, 110% and 120% were prepared. Table 6 and Figure 1(c) present the results obtained for Linearity. It can be stated that the method is linear for quantification of risperidone, with a coefficient of determination of 0.9995, which is within the acceptance criteria (Table 7).

### *Accuracy*

Accuracy assesses the method's recovery i.e. the systematic error or trend, which corresponds to the difference between the added value and the obtained value, by analyzing prepared solutions of known concentration. The results of the 80%, 100% and 120% concentration solutions analyzed in the linearity step were used to verify the accuracy of the analysis method. Table 8 shows the results obtained in accuracy. The recovery for each of the solutions must be between 98.0% to 102.0%, therefore the method is validated for the accuracy parameter.

### *Range*

It was demonstrated that the test method has an appropriate level of precision, accuracy and linearity in the range of 80% to 120% (inclusive) of the concentration of the active in the solution, thus the acceptance criteria for linearity, accuracy and precision were met.

### *Robustness*

To verify the robustness, the following analytical parameters were evaluated: a) oven temperature change by  $\pm 1.25^{\circ}\text{C}$ ; b) flow change by  $\pm 5\%$ ; and c) change in methanol proportion by  $\pm 2.25\%$ . Table 9 presents the results obtained in the method robustness. It can be considered that this method is robust for the conditions evaluated, as the relative standard deviation between the three injections were less than 5%.

### *Repeatability*

The repetitive conditions of the analysis were evaluated, involving the activities of preparing the solutions by the same analyst and equipment, with the same sequence of injections. To verify the accuracy, the relative standard deviation between the 6 solutions were evaluated

(Table 10). The RSD obtained for the active at the 6 concentrations met the acceptance criteria ( $\leq 2\%$ ), proving the precision of the analytical method [33].

### *Intermediate Precision*

Structural variations intrinsic to the preparation procedure and their influence on the final result of the analytical process were analyzed. Two analysts analyzed the same sample from the same batch six times for grade, using the same equipment. Each analyst prepared their standard solutions and their sample solutions, in addition to the mobile phase. Analyst 1 was considered the one who performed all other validation steps and Analyst 2 was another analyst. Before analyst 2 performed the analysis, training was given by analyst 1, who highlighted the critical points of the method. Below are the results obtained for Precision – Intermediate Analysts 1 and 2 (Table 10).

The RSD for 12 analyzed samples was less than 2% and the absolute percentage difference between the means of the results of each analyst was also less than 2%. Hence, this shows the method reproducibility. This method is simple as compared to other methods, for example, which require the addition of reagents and more sample preparation steps [34,35]. In addition, UV detection system used is very common, accessible and low cost, others use more costly as well as complex detection methods [36]. Faster, more sensitive and affordable methods such as voltammetry and spectrophotometry have been developed and cited in papers [37,38], but techniques like the first is not always usual and familiar in rebladed laboratories and the pharmaceutical industry, and the second is not very specific as HPLC.

There are currently developed methods employing thin layer chromatography technique followed by detection and quantification by densitometry [39,40], these in turn, can constitute a great advantage over HPLC, as the chromatographic interface made of silica is much lower cost compared to packed HPLC columns. During the literature search, methodologies were observed using the HPLC technique with the use of an internal standard in the system calibration [41]. Internal calibration is generally used to correct possible losses in the system by correcting the area of the substance of interest according to the loss, but the successful validation performed in this work consolidated the external calibration for quantification, thus eliminating the need for use of internal standards.

### **Conclusion**

After performing the tests and verifying the obtained results, it can be concluded that the method was properly validated, but some observations must be made. This method provides excellent applicability in laboratory routine, but it is important to know, in the routine, how long it is possible to postpone sample injections, in the "Stability of Analytical Solutions" test, it was proven that the samples do not have stability within 24 hours, therefore, more tests must be done in order to define the time that the samples remain with their concentration unchanged, being able to evaluate the result in times 6, 8, 10, 12, 16 hours after preparation.

The defined running time makes it possible to quickly obtain the result, which makes it practical and usual in the routine analysis at pharmaceutical industries. However, it can be concluded that the validated method is consistent and meets the requirements for the product and is acceptable for routine batch control and drug stability studies for registration.

## References

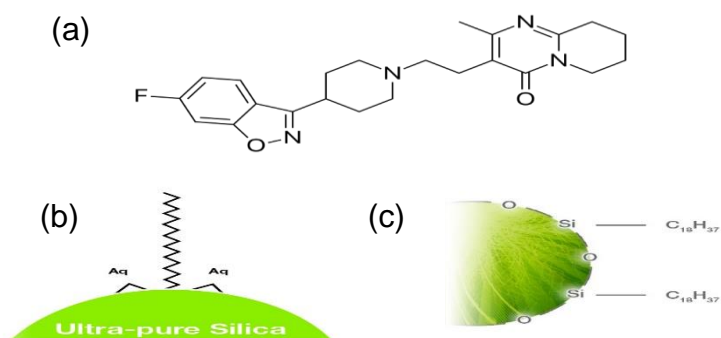
- [1] Mauri, M. C., Paletta, S., Maffini, M., Colasanti, A., Dragogna, F., Pace, C. Di, Altamura, A. C., Clinical Pharmacology of Atypical Antipsychotics: An Update. *EXCLI J.* 2014, 13, 1163–1191.
- [2] Belotto, K. C. R., Raposo, N. R. B., Ferreira, A. S., Gattaz, W. F., Relative Bioavailability of Two Oral Formulations of Risperidone 2 mg: A Single-Dose, Randomized-Sequence, Open-Label, Two-Period Crossover Comparison in Healthy Brazilian Volunteers. *Clin. Ther.* 2010, 32, 2106–15.
- [3] Schotte, A., Janssen, P. F., Megens, A. A., Leysen, J. E., Occupancy of Central Neurotransmitter Receptors by Risperidone, Clozapine and Haloperidol, Measured Ex Vivo by Quantitative Autoradiography. *Brain Res.* 1993, 631, 191–202.
- [4] Sumiyoshi, T., Kido, H., Sakamoto, H., Urasaki, K., Suzuki, K., Yamaguchi, N., Mori, H., Shiba, K., Yokogawa, K., In Vivo Dopamine-D2 and Serotonin-5-HT<sub>2</sub> Receptor Binding Study of Risperidone and Haloperidol. *Pharmacol. Biochem. Behav.* 1994, 47, 553–7.
- [5] Lindner, L. M., Marasciulo, A. C., Farias, M. R., Grohs, G. E. M., Economic Evaluation of Antipsychotic Drugs for Schizophrenia Treatment within the Brazilian Healthcare System. *Rev. Saude Publica* 2009, 43, 62–69.
- [6] Kahn, R. S., Sommer, I. E., Murray, R. M., Meyer-Lindenberg, A., Weinberger, D. R., Cannon, T. D., O'Donovan, M., Correll, C. U., Kane, J. M., Os, J. van, Insel, T. R., Schizophrenia. *Nat. Rev. Dis. Prim.* 2015, 1, 1–23.

- [7] Elkis, H., Clozapine, Refractory Schizophrenia and Evidence. *Brazilian J. Psychiatry* 2001, 23, 59–60.
- [8] Elkis, H., Louzã, M. R., New Antipsychotics for the Treatment of Schizophrenia. *Arch. Clin. Psychiatry (São Paulo)* 2007, 34, 193–97.
- [9] Balbino, E. E., Dias, M. F., Pharmacovigilance: A Step Towards the Rational Use of Medicinal Plants and Herbal Medicines. *Brazilian J. Pharmacogn.* 2010, 20, 992–1000.
- [10] Shin, J.-Y., Choi, N.-K., Jung, S.-Y., Lee, J., Kwon, J. S., Park, B.-J., Risk of Ischemic Stroke with the Use of Risperidone, Quetiapine and Olanzapine in Elderly Patients: A Population-Based, Case-Crossover Study. *J. Psychopharmacol.* 2013, 27, 638–44.
- [11] Cordeiro, Q., Zung, S., Vallada, H., Pisa Syndrome Induced by Rapid Increase and High Dosage of Risperidone. *Arq. Neuropsiquiatr.* 2008, 66, 896–7.
- [12] Iuppa, C. A., Diefenderfer, L. A., Risperidone-Induced Pisa Syndrome in MS: Resolution with Lurasidone and Recurrence with Chlorpromazine. *Ann. Pharmacother.* 2013, 47, 1223–8.
- [13] Güneş, S., Ekinçi, Ö., Direk, M. Ç., Yıldırım, V., Okuyaz, Ç., Toros, F., Risperidone Induced Pisa Syndrome in a Male Adolescent. *Clin. Psychopharmacol. Neurosci.* 2016, 14, 104–6.
- [14] El-Sherif, Z. A., El-Zeany, B., El-Houssini, O. M., High Performance Liquid Chromatographic and Thin Layer Densitometric Methods for the Determination of Risperidone in the Presence of Its Degradation Products in Bulk Powder and in Tablets. *J. Pharm. Biomed. Anal.* 2005, 36, 975–81.
- [15] Karabas, I., Orkoula, M. G., Kontoyannis, C. G., Analysis and Stability of Polymorphs in Tablets: The Case of Risperidone. *Talanta* 2007, 71, 1382–6.
- [16] Locatelli, I., Mrhar, A., Grabnar, I., Simultaneous Determination of Risperidone and 9-Hydroxyrisperidone Enantiomers in Human Blood Plasma by Liquid Chromatography with Electrochemical Detection. *J. Pharm. Biomed. Anal.* 2009, 50, 905–10.
- [17] Torres V, P., Sepulveda C, M. J., Von Plessing R, C., Pharmacokinetic Study of Risperidone: Application of a HPLC Method with Solid Phase Extraction. *J. Chil. Chem. Soc.* 2011, 56, 606–9.
- [18] Mandrioli, R., Micolini, L., Lateana, D., Boncompagni, G., Raggi, M. A., Analysis of Risperidone and 9-Hydroxyrisperidone in Human Plasma, Urine and Saliva by MEPS-LC-UV. *J. Chromatogr. B Anal. Technol. Biomedical Life Sci.* 2011, 879, 167–73.
- [19] Jones, T., Breda, K. Van, Charles, B., Dean, A. J., McDermott, B. M., Norris, R., Determination of Risperidone and 9-Hydroxyrisperidone Using HPLC, in Plasma of

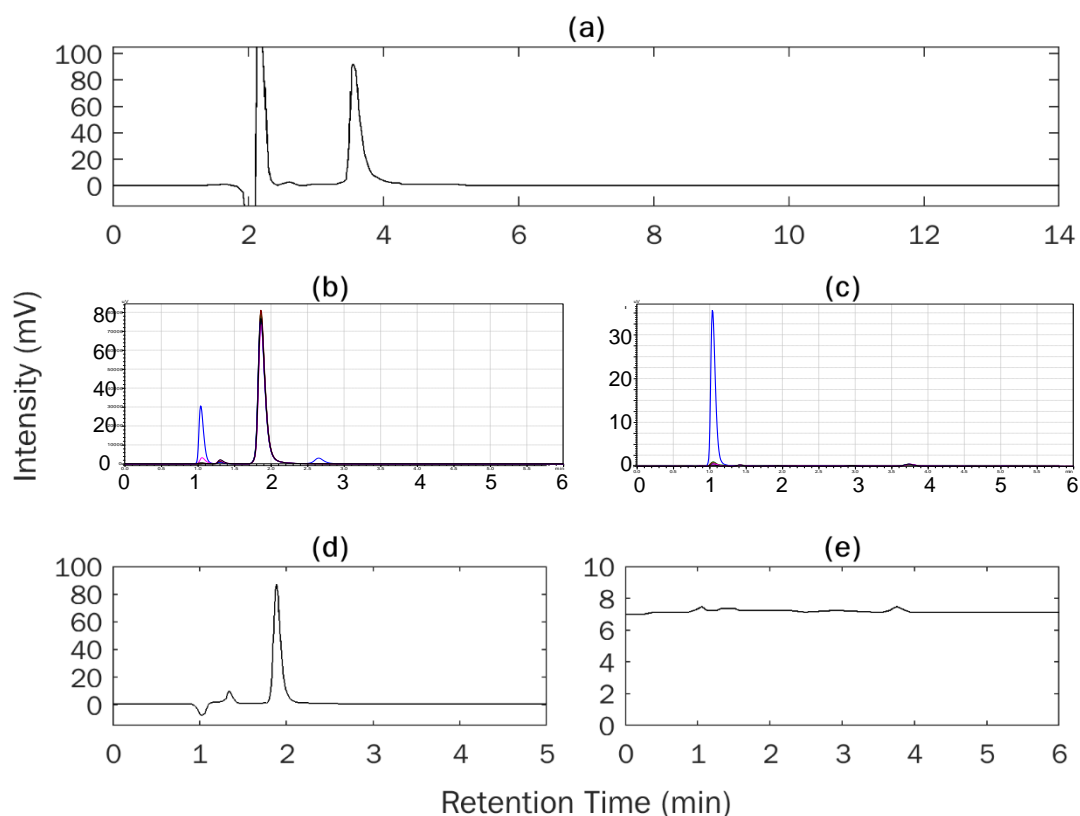
- Children and Adolescents with Emotional and Behavioural Disorders. *Biomed. Chromatogr.* 2009, 23, 929–34.
- [20] Mercolini, L., Grillo, M., Bartoletti, C., Boncompagni, G., Raggi, M. A., Simultaneous Analysis of Classical Neuroleptics, Atypical Antipsychotics and Their Metabolites in Human Plasma. *Anal. Bioanal. Chem.* 2007, 388, 235–43.
- [21] Raggi, M. A., Bugamelli, F., Sabbioni, C., Saracino, M. A., Petio, C., HPLC-DAD Determination of Plasma Levels of the Antipsychotic Risperidone and Its Main Metabolite for Toxicological Purposes. *J. Sep. Sci.* 2005, 28, 245–50.
- [22] Maurer, H. H., Kraemer, T., Kratzsch, C., Peters, F. T., Weber, A. A., Negative Ion Chemical Ionization Gas Chromatography-Mass Spectrometry and Atmospheric Pressure Chemical Ionization Liquid Chromatography-Mass Spectrometry of Low-Dosed and/or Polar Drugs in Plasma. *Ther. Drug Monit.* 2002, 24, 117–24.
- [23] Danel, C., Barthélémy, C., Azarzar, D., Robert, H., Bonte, J.-P., Odou, P., Vaccher, C., Analytical and Semipreparative Enantioseparation of 9-Hydroxyrisperidone, the Main Metabolite of Risperidone, Using High-Performance Liquid Chromatography and Capillary Electrophoresis. Validation and Determination of Enantiomeric Purity. *J. Chromatogr. A* 2007, 1163, 228–36.
- [24] Orkoula, M. G., Kontoyannis, C. G., Non-Destructive Quantitative Analysis of Risperidone in Film-Coated Tablets. *J. Pharm. Biomed. Anal.* 2008, 47, 631–5.
- [25] Schneider, S., Sibille, E., Yegles, M., Neels, H., Wennig, R., Mühe, A., Time Resolved Analysis of Risperidone and 9-Hydroxy-Risperidone in Hair Using LC/MS-MS. *J. Chromatogr. B Anal. Technol. Biomedical Life Sci.* 2009, 877, 2589–92.
- [26] Tanaka, Y., Ohkawa, T., Yasui, H., Development of a Novel High-Throughput Analytical Methodology, Multiple Injection Method, for Quantitative Analysis in Drug Metabolism and Pharmacokinetic Studies Using Liquid Chromatography with Tandem Mass Spectrometry. *Biol. Pharm. Bull.* 2011, 34, 1187–93.
- [27] Cai, H.-L., Zhu, R.-H., Li, H.-D., Zhang, J., Li, L.-F., MultiSimplex Optimization of Chromatographic Separation and Dansyl Derivatization Conditions in the Ultra Performance Liquid Chromatography-Tandem Mass Spectrometry Analysis of Risperidone, 9-Hydroxyrisperidone, Monoamine and Amino Acid Neurotransmitters. *J. Chromatogr. B Anal. Technol. Biomedical Life Sci.* 2011, 879, 1993–9.
- [28] Meulder, M. De, Remmerie, B. M. M., Vries, R. de, Sips, L. L. A., Boom, S., Hooijschuur, E. W. J., Merbel, N. C. van de, Timmerman, P. M. M. B. L., Validated LC-MS/MS Methods for the Determination of Risperidone and the Enantiomers of 9-

- Hydroxyrisperidone in Human Plasma and Urine. *J. Chromatogr. B Anal. Technol. Biomedical Life Sci.* 2008, 870, 8–16.
- [29] United States Pharmacopeial Convention, United States Pharmacopoeia – National Formulary (USP – NF). United States Pharmacopeial Convention, Rockville, MD 2021.
- [30] Validation of Analytical Procedures: Text and Methodology. European Medicines Agency, London 1995.
- [31] Wan, H., Rehgren, M., Giordanetto, F., Bergström, F., Tunek, A., High-Throughput Screening of Drug-Brain Tissue Binding and In Silico Prediction for Assessment of Central Nervous System Drug Delivery. *J. Med. Chem.* 2007, 50, 4606–15.
- [32] Harris, D. C., Lucy, C. A., Quantitative Chemical Analysis. W.H. Freeman and Company Ltd, New York 2020.
- [33] Wielgos, T., Turner, P., Havel, K., Validation of Analytical Capillary Electrophoresis Methods for Use in a Regulated Environment. *J. Capillary Electrophor.* 1997, 4, 273–8.
- [34] Narayana, B., Veena, K., A New and Simple Method for the Spectrophotometry Determination of Risperidone. *Oxid. Commun.* 2011, 34, 660–6.
- [35] Dubey, S. K., Singhvi, G., Tyagi, A., Agarwal, H., Krishna, K. V., Spectrophotometric Determination of pKa and Log P of Risperidone. *J. Appl. Pharm. Sci.* 2017, 7, 155–8.
- [36] Josefsson, M., Roman, M., Skogh, E., Dahl, M.-L., Liquid Chromatography/Tandem Mass Spectrometry Method for Determination of Olanzapine and N-Desmethylolanzapine in Human Serum and Cerebrospinal Fluid. *J. Pharm. Biomed. Anal.* 2010, 53, 576–82.
- [37] Taşdemir, I. H., Çakirer, O., Electrochemical and Spectrophotometric Methods to Assay of Risperidone an Antipsychotic Drug in Pharmaceutical and Biological Samples. *Asian J. Chem.* 2010, 22, 6353–60.
- [38] Tasdemir, I. H., Çakirer, O., Erk, N., Kiliç, E., Square-Wave Cathodic Adsorptive Stripping Voltammetry of Risperidone. *Collect. Czechoslov. Chem. Commun.* 2011, 76, 159–176.
- [39] Maślanka, A., Krzek, J., Patrzalek, A., Determination of Risperidone in Tablets in the Presence of Its Degradation Products and Placebo-Derived Constituents. *Acta Pol. Pharm.* 2009, 66, 461–70.
- [40] Patel, S. K., Patel, N. J., TLC Determination of Amitriptyline HCl, Trifluoperazine HCl, Risperidone and Alprazolam in Pharmaceutical Products. *Chromatographia* 2008, 69, 393–396.

- [41] Baldania, S. L., Bhatt, K. K., Mehta, R. S., Shah, D. A., RP-HPLC Estimation of Risperidone in Tablet Dosage Forms. *Indian J. Pharm. Sci.* 2008, 70, 494–497.



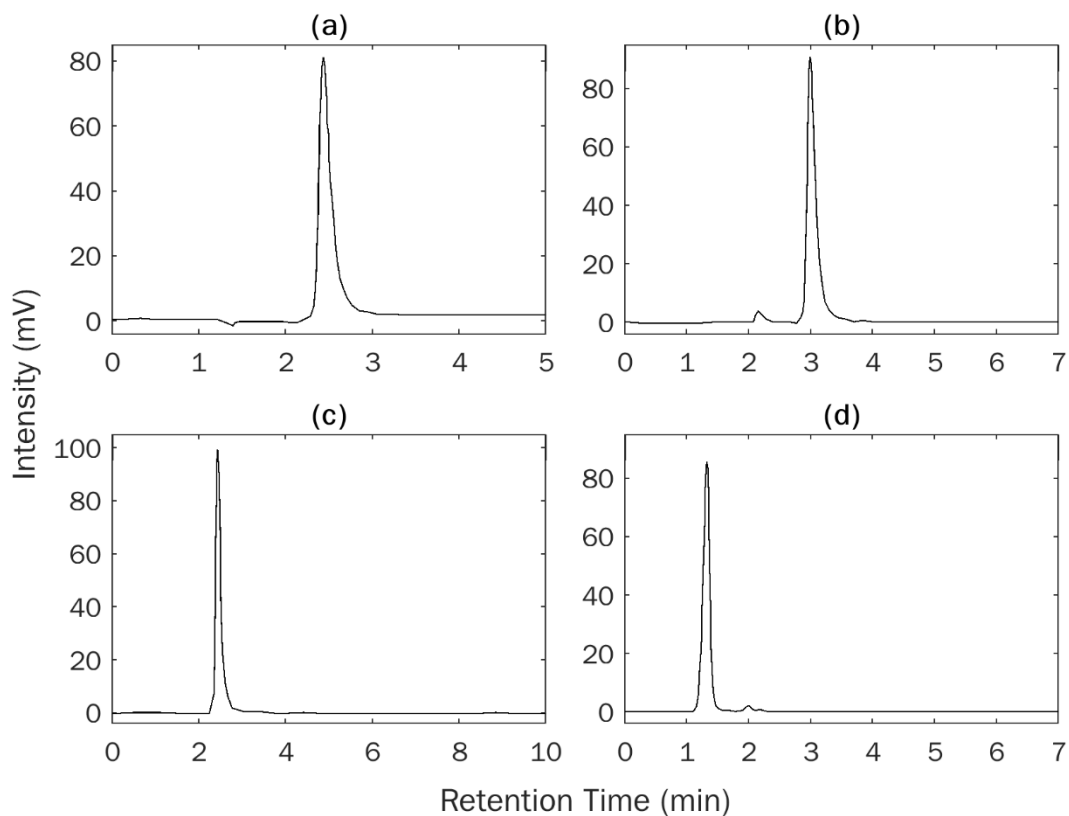
**Figure 1:** (a) Risperidone chemical structure. (b) Synergi Hydro C18 column stationary phase: C18 phase capped with polar groups that provide extreme hydrophobicity and strong polar selectivity, as well as good stability in aqueous mobile phases. Indicated for separations of weakly hydrophobic compounds. (c) Stationary phase of Chromolith® Performance RP – 18e column, surface schematic of monolithic silica particle with 18 carbon chains.



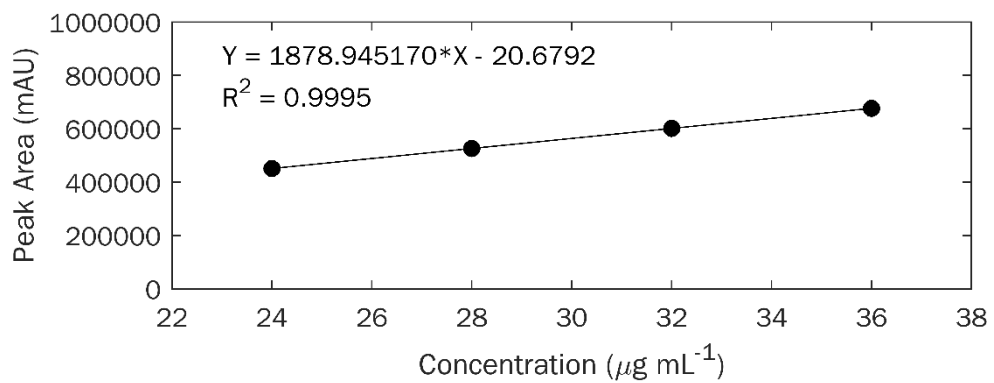
**Figure 2.** (a) Chromatogram for system 1. Conditions: mobile phase 55% methanol/45% water, containing 0.2% triethylamine and pH 3.0 adjusted with orthophosphoric acid; Synergi Hydro C18 column (100 mm x 4.6 mm, 4  $\mu$ m); flow 0.8 mL min<sup>-1</sup>; (b) sample under stress conditions (c) placebo under stress conditions (d) system 2 (e) non-stressed placebo.



Conditions: mobile phase 45% methanol:55% water, containing 0.5% triethylamine and pH 3.0 adjusted with orthophosphoric acid; Chromolith® Performance RP – 18e column (100 mm x 4.6 mm); 1.5 mL min<sup>-1</sup> flow; risperidone concentration 30.00 µg mL<sup>-1</sup> in mobile phase as diluent; detection at 235 nm and column temperature 25°C.



**Figure 3.** Chromatogram. (a) system 3 (b) system 4. Conditions: mobile phase 45% methanol:55% water (c) system 5. Conditions mobile phase: 50% methanol:50% water (d) system 6. Conditions mobile phase: 30% methanol:70% water; containing 0.2% triethylamine and pH 3.0 adjusted with orthophosphoric acid; Chromolith® Performance RP-18e column (100 mm x 4.6 mm); flow rate (a-c) 1.0 mL min<sup>-1</sup> (b) 0.9 mL min<sup>-1</sup> (d) 1.2 mL min<sup>-1</sup>; risperidone concentration 30.00 µg mL<sup>-1</sup> in mobile phase as diluent; detection at 235 nm and column temperature (a-b) 31°C and (c-d) 25°C.



**Figure 4.** Analytical curve for risperidone. Concentration range 24.13 – 36.20 µg mL<sup>-1</sup>.

Table 1: Degradation conditions for specificity.

Degradation Condition	Matrix/Condition
Temperature	60°C
Acidic	0.1M HCl
Basic	0.1M NaOH
Oxidation	3% H <sub>2</sub> O <sub>2</sub>
Moisture	75% RH ±5%
Light	UV-B fluorescent

Table 2: Preparation table for Linearity and Accuracy.

Linearity/Accuracy (%)	Standard stock solution volume (mL)		Flask volume for dilution (mL)	Risperidone concentration (mg mL <sup>-1</sup> )
	Risperidone	Placebo		
<i>Linearity</i>				
80%	4.0	8.0	50.00	0.024
90%	4.5	9.0	50.00	0.027
100%	5.0	10.0	50.00	0.030
110%	5.5	11.0	50.00	0.033
120%	6.0	12.0	50.00	0.036
<i>Accuracy</i>				
80%	4.0	8.0	50.00	0.024
100%	5.0	10.0	50.00	0.030
120%	6.0	12.0	50.00	0.036

Table 3. Acceptance criteria.

Validation Parameter	Acceptance Criteria	Results obtained
Analytical curve and system adequacy	The RSD of peak areas of risperidone in the five injections of standard solution 1 should be ≤ 2.0%.	All criteria were met for all stages of validation.
	Recovery from standard solution 2 injection should be between 98.0% and 102.0%.	
	The recovery of the injection of standard solution 1 at the end must be between 98.0% and 102.0%.	
	The tail factor for the risperidone peak should be a maximum of 1.50. Column efficiency, determined by the risperidone peak, must be a minimum of 2000 theoretical plates.	
		Tail Factor: 1.49 Theoretical Plates: 2062

Table 4. Stability of analytical solutions.

Time	Initial	After 24 hours
Anhydrous content (%)	1,917	2.109
Recovery	N/A	110.0%

Table 5. Results obtained for specificity.

<b>Solutions*</b>	<b>Composition</b>	<b>Retention Time (RT)</b>	<b>Content (mg/comp)</b>
<i>Solution 1</i>	HCl Sample – 24 hours	1,857	1.86
	Recovery	-	93%
<i>Solution 2</i>	NaOH Sample – 24 hours	1,859	1.80
	Recovery	-	90%
<i>Solution 3</i>	H <sub>2</sub> O <sub>2</sub> Sample – 0 hour	1,854	1.81
	Recovery	-	90.5%
<i>Solution 4</i>	Sample 60°C	1,857	1.89
	Recovery	-	94.5%
<i>Solution 5</i>	Light Sample	1,857	1.98
	Recovery	-	99%
<i>Solution 6</i>	Moisture Sample	1,855	1.93
	Recovery	-	96.5%

\*Content of Normal Sample – Theoretical is 2.00 mg/comp.

Table 6. Results obtained in linearity.

<b>Linearity (%)</b>	<b>Power plug Test (mL)</b>	<b>Risperidone Concentration (<math>\mu\text{g mL}^{-1}</math>)</b>		<b>Areas</b>	<b>Average Areas</b>
		<b>Theoretical</b>	<b>Experimental</b>		
80	4.0	24.13	23.84	436264	435242
			23.78	434975	
			23.75	434488	
90	4,5	27.15	26.26	480500	487269
			26.77	489791	
			26.86	491515	
100	5.0	30.17	29.86	546340	544263
			29.80	545142	
			29.59	541308	
110	5.5	33.18	33.01	603897	603773
			33.01	603918	
			33.00	603505	
120	6.0	36.20	36.03	659190	660427
			36.14	661177	
			36.12	660914	

Table 7. Acceptance criteria and Statistical results obtained from the analytical curve of risperidone.

Validation Parameter	Acceptance Criteria	Results obtained
Linearity	The correlation coefficient "r" must be greater than or equal to 0.99.	$R^2 = 0.9995$
	Visually, the graphics are presented like a straight line.	Yes
	The slope and the intersection with the Y axis must also be reported.	Angular Coefficient (a): 18789451.70 Y Intercept (b): - 20679.2

Table 8. Results obtained in accuracy.

Accuracy (%)	Power Plug Test (mL)	Risperidone Concentration ( $\mu\text{g mL}^{-1}$ )		Areas	Recovery (%)	Recovery Average (%)	RSD (%)
		Theoretical	Experimental				
80	4.0	24.13	23.84	436264	98.80%	98.60%	0.2
			23.78	434975	98.50%		
			23.75	434488	98.40%		
100	5.0	30.17	29.86	546340	99.00%	98.60%	0.5
			29.80	545142	98.80%		
			29.60	541308	98.10%		
120	6.0	36.20	36.33	659190	99.50%	99.70%	0.2
			36.14	661177	99.80%		
			36.12	660914	99.80%		

Table 9. Method robustness.

Condition	Content
<i>Change in oven temperature by <math>\pm 1.25^\circ\text{C}</math> (<math>\pm 5\%</math>)</i>	
Oven temperature at $-1.25^\circ\text{C}$ ( $23.75^\circ\text{C}$ )	2.12
Original oven temperature ( $25^\circ\text{C}$ )	2.12
Oven temperature at $+1.25^\circ\text{C}$ ( $26.25^\circ\text{C}$ )	2.13
RSD	0.19%
<i>Change in mobile phase flow by <math>\pm 0.075 \text{ mL min}^{-1}</math> (<math>\pm 5\%</math>)</i>	
Mobile Phase Flow in minus $0.1 \text{ mL min}^{-1}$ ( $0.9 \text{ mL min}^{-1}$ )	2.14
Original Mobile Phase Flow ( $1.0 \text{ mL min}^{-1}$ )	2.11
Mobile Phase Flow in plus $0.1 \text{ mL min}^{-1}$ ( $1.1 \text{ mL min}^{-1}$ )	1.99
RSD	3.66%
<i>Change in the proportion of methanol by <math>\pm 2.25\%</math> (<math>\pm 5\%</math>)</i>	
Proportion of Methanol at 2.25% ( $42.75\%$ )	2.08
Proportion of original Methanol ( $45\%$ )	2.10
Proportion of Methanol by 2.25% ( $47.25\%$ )	2.13
RSD	1.16%

Table 10. Method accuracy and results obtained at intermediate precision.

<b>Precision</b>	<b>Weight (mg)</b>	<b>Risperidone area</b>	<b>Risperidone content (mg/comp.)</b>	<b>Average (%)</b>	<b>RSD (%)</b>	<b>Absolute Difference (%)</b>
<i>Method accuracy</i>						
Sample 1	306.8	524299	1.93			
Sample 2	306.7	528156	1.90			
Sample 3	308.1	521097	1.89	1.91	0.93	N.A
Sample 4	308.3	518817	1.89			
Sample 5	307.8	519474	1.92			
Sample 6	307.6	526975	1.93			
<i>Intermediate precision</i>						
Sample 1	306.8	524299	1.93			
Sample 2	306.7	528156	1.90			
Sample 3	308.1	521097	1.89			
Sample 4	308.3	518817	1.89			
Sample 5	307.8	519474	1.92			
Sample 6	307.6	526975	1.93	1.92	1.11	1.05
Sample 7	309.6	534908	1.94			
Sample 8	309.7	528882	1.92			
Sample 9	308.4	528313	1.92			
Sample 10	308.5	520936	1.89			
Sample 11	308.0	535276	1.95			
Sample 12	308.1	532855	1.94			

***Brachyotum naudinii* Triana Flower Chemical Screening by UHPLC-MS/MS, Preliminary Toxicity and *In Vitro* Antioxidant Potential**

Marco Rolando Aronés Jara <sup>1,\*</sup>, Edgar Cárdenas Landeo <sup>1</sup>, Kirianova Godoy Bautista <sup>1</sup>, Elyen Almendra Ortiz Pérez <sup>1</sup>, Juan Clímaco Paniagua Segovia <sup>1</sup>, Hugo Roberto Luna Molero <sup>1</sup>, Stephanny Massiel Barbarán Vilcatoma <sup>1</sup>, Mónica Gómez Quispe <sup>1</sup>, Jesús Javier Paniagua Segovia <sup>2</sup>, Anas Rashid <sup>3</sup>, María Segunda Aurora Prado <sup>4,\*</sup>

<sup>1</sup> Professional School of Pharmacy and Biochemistry, Faculty of Health Sciences, National University of San Cristóbal of Huamanga, Ayacucho 05003, Peru

<sup>2</sup> Professional School of Engineering in Food Industries, Faculty of Chemical Engineering and Metallurgy, National University of San Cristóbal of Huamanga, Ayacucho 05003, Peru

<sup>3</sup> School of Medicine and Surgery, University of Torino, Torino 10125, Italy

<sup>4</sup> Department of Pharmacy, School of Pharmaceutical Sciences, University of São Paulo, São Paulo 05508-000, Brazil

\* Correspondence: marco.arones@unsch.edu.pe (M.R.A.J.); msaprad06@usp.br (M.S.A.P)

## ABSTRACT

The chemical compounds of *Brachyotum naudinii* Triana flowers were analyzed by using UHPLC-MS/MS. Anthocyanin dry extract from flowers was obtained by accelerated solvent extraction using 70° ethanol acidified with citric acid at pH 3.18 and drying was carried out by spray drying. Preliminary toxicity of anthocyanin dry extract was evaluated on *Artemia salina* Leach and antioxidant capacity was measured by DPPH• and ABTS<sup>•+</sup> radical scavenging methods, while FRAP iron complex was used to measure the reducing capacity. Results showed that flowers are composed of 39% tannins, 21% flavonol glycosides, 14% organic acids, 11% anthocyanins (new compounds), 7% coumaric acid derivatives, 4% polar lipids, and 4% disaccharides. Anthocyanin dry extract exhibited moderate toxicity against *Artemia salina* ( $LC_{50} = 106.9 \pm 9.9 \mu\text{g mL}^{-1}$ ) and showed inhibitory effects on DPPH• and ABTS<sup>•+</sup> radical and reducing capacity of FRAP iron complex, although statistically different than Trolox ( $p < 0.05$ ). *Brachyotum naudinii* flowers are a source of phenolic and new anthocyanin compounds, and anthocyanin dry extract has antioxidant potential.

## KEYWORDS

*Brachyotum naudinii* Triana; endemic species of rocky outcrops; UHPLC-MS/MS; new bioactive compounds.



## 1. INTRODUCTION

*Brachyotum naudinii* Triana is a species that belongs to the Melastomataceae family and grows in various regions of South America. Its purple and violet flowers are very showy [1,2] which apart from attracting pollinators, are a potential source for obtaining natural dyes [3]. This native species grows in the high Andean areas and has a high population density in the beds of rocky outcrops of Bosque de Piedras de Huaraca located at 3627 meters above sea level in Ayacucho region (Peru).

Melastomataceae is the seventh-largest family of flowering plants. Among the main chemical constituents present in these flowers are terpenoids, simple phenolics, quinones, lignans, glycosides, wide range of tannins or polyphenols, mainly oligomers of hydrolysable tannins with molecular weights up to 4600 Da, some flavonoids and acylated anthocyanins [4].

The anthocyanins isolated from the flowers of Melastomataceae family species correspond to pelargonidin, cyanidin, peonidin, delphinidin, and malvidin glycosides [4]. In addition, the presence of malvidin derivatives has been reported in the flowers of the following species: *Melastoma malabathricum*, *Tibouchina semidecandra*, *Tibouchina granulosa*, and *Tibouchina urvilleana* [4].

Anthocyanins are secondary metabolites biosynthesized by plants as a defense and adaptation mechanism against ultraviolet radiation, therefore they have significant antioxidant, photoprotective, and coloring properties which make them suitable for cosmetic, coloring, and food industries to replace currently used synthetic compounds. Likewise, they can also be used as an alternative to potentially carcinogenic synthetic dyes [2].

The malvidin anthocyanin pigment gives violet-blue color to flowers, leaves, and aerial plant parts. Few human studies have been found with this molecule as compared to other anthocyanins. These studies demonstrated that malvidin has powerful antioxidant and photoprotective activities, and prevents the formation of some cancers, such as pancreatic, colon, and breast cancer [5,6].

Despite the fact that *B. naudinii* is a species with a high population density and its flowers are probably an important source of phenolic and anthocyanin compounds, no ethnobotanical or

biochemical studies have been reported. Chemical studies carried out on the Melastomataceae family support the hypothesis that *B. naudinii* flowers could contain antioxidant and photoprotective potential like malvidin.

The evaluation of antioxidant activity by using colored stable free radicals, such as 2,2-diphenyl-1-picrylhydrazyl (DPPH), 2,2'-azino-bis-(3-ethylbenzothiazoline-6-sulfonic acid) (ABTS), or ferric complex 2,4,6-tripyridyl-s-triazine (TPTZ), makes possible the preliminary classification of different plant species according to their antioxidant potential [7]. This activity is correlated proportionally with the content of phenolic compounds [7].

The bioassay against *Artemia salina* Leach allows cytotoxicity level evaluation of natural products [8,9], and guides the subsequent evaluation of biological activities taking into account the possible human health risk [10,11]. Besides, this bioassay can help to investigate the highly toxic extracts with potential use in the manufacturing of pest repellents and related products, especially in agribusiness [12,13].

Taking into account these considerations, the present study aimed to evaluate the chemical composition of *B. naudinii* flowers by using ultra-high performance liquid chromatography-tandem mass spectrometry (UHPLC-MS/MS). It also aimed to evaluate preliminary toxicity against *Artemia salina* and *in vitro* antioxidant potential of anthocyanin dry extract.

## 2. MATERIALS AND METHODS

### 2.1. Collection of botanical material and taxonomical identification

*B. naudinii* Triana flowers were collected in April from the rocky outcrops of Bosque de Piedras de Huaraca, located in the community of Huaraca in the populated center of Anchacchuasi (District Vinchos), Huamanga, Ayacucho, Peru. The geographical coordinates are 13°18'58.9" (South Latitude), 74°26'55.8" (West Longitude), and an altitude of 3627 meters above sea level.

The taxonomical identification was carried out in Herbarium CPUN "Isidoro Sánchez Vega", Universidad Nacional de Cajamarca (UNC), Cajamarca, Peru with deposit number 24656.

### 2.2. Phytochemical screening by UHPLC-MS/MS of *B. naudinii* flowers

First, the flowers were dried by lyophilizer (Labotec, South Africa) operated at  $-42\text{ }^{\circ}\text{C}$  and  $0.013\text{ mbar}$  for 72 h, then crushed in a porcelain mortar and stored in aluminum containers with hermetic closure.

The chemical identification of flower components was carried out by using Dionex UltiMate™ 3000 UHPLC system coupled to Q Exactive™ Plus Hybrid Quadrupole-Orbitrap™ Mass Spectrometer (Thermo Fisher Scientific GmbH, Germany) equipped with a heated electrospray probe. Separations were carried out on a Luna Omega C18 ( $150\text{ mm} \times 2.1\text{ mm}$ ,  $1.6\text{ }\mu\text{m}$ ) column (Phenomenex, USA). The chromatographic conditions were: mobile phase A: water – 0.1% formic acid, and B: acetonitrile – 0.1% formic acid; gradient elution: 90% A and 10% B (0 min), 90% A and 10% B (1 min), 100% B (16 min), 100% B (18 min), 90% A and 10% B (20 min); flow rate:  $0.3\text{ mL min}^{-1}$ ; injection volume:  $3\text{ }\mu\text{L}$  and column temperature:  $40\text{ }^{\circ}\text{C}$ . The mass spectrometry range was  $120 - 1500\text{ m/z}$  using microscan 1 (resolution 70,000; automatic gain control target:  $1 \times 10^6$  and max ion time 100 ms) and microscan 2 (resolution 17,500; automatic gain control target:  $2 \times 10^5$  and max ion time 50 ms). The electrospray ionization (negative/positive); voltage 2.5 / 3.0; capillary temperature  $280\text{ }^{\circ}\text{C}$ ; carrier gas  $\text{N}_2$  (shroud flow 40 and makeup flow 10); gas heating temperature  $400\text{ }^{\circ}\text{C}$ ; S-lens radiofrequency level 100 and Normalized Collision Energy 20, 40 and 60 were selected.

For the analysis, 50 mg lyophilized flowers were weighed and transferred into a 10 mL volumetric flask then the methanol-water solution (9:1) was added to complete the volume. The mixture was placed in an ultrasonic bath for 10 min. Then, pH 2 was adjusted with 50  $\mu\text{L}$  of concentrated acetic acid. This mixture was filtered through a  $0.25\text{ }\mu\text{m}$  polyvinylidene fluoride disc filter and injected into UHPLC instrument.

### 2.3. Obtaining anthocyanin dry extract from *B. naudinii* flowers

5 g freeze-dried flowers were weighed and mixed with 2.5 g diatomaceous earth. The mixture was conditioned in a 66 mL stainless steel extraction cell (equipped with a 27 mm cellulose filter) using Dionex™ ASE™ 150 Accelerated Solvent Extractor (Thermo Fisher Scientific, USA). The proposed method extraction conditions were: temperature  $80\text{ }^{\circ}\text{C}$ ; static time 5 min; rinse volume 60%; purge time 120 sec; and three static cycles. The extraction was performed with  $70^{\circ}$  ethanol acidified with citric acid at pH 3.18 [14,15]. The extract was concentrated using

a R-3000® rotary evaporator (BÜCHI Labortechnik AG, Switzerland) at 50 °C, which was dried by spray drying using Mini Spray Dryer B-290 (BÜCHI Labortechnik AG, Switzerland) at 120 °C inlet temperature, 5% pump and 100% suction [16]. The anthocyanin dry extract was stored in a desiccator at room temperature.

#### 2.4. Total phenolic content of anthocyanin dry extract from *B. naudinii* flowers

The extract's total phenolic content was quantified using Folin–Ciocâlteu reagent (1M; 99.5%; Merck KGaA; Germany) [17]. A dry extract solution was prepared at a concentration of 320 µg mL<sup>-1</sup> in 70° ethanol. 100 µL of this solution was measured and 500 µL of Folin–Ciocâlteu reagent (1:10) and 400 µL of 7.5% Na<sub>2</sub>CO<sub>3</sub> were added. After 30 min, the absorbance at 765 nm was performed using a GENESYS™ 150 UV-Vis spectrophotometer (Thermo Fisher Scientific, USA). Total phenolic content was calculated from the gallic acid standard curve ( $y = 0.010x + 0.013$ ;  $R^2 = 0.996$ ) and expressed in milligrams of gallic acid equivalent per gram of dry extract (mg GAE/g).

#### 2.5. Total anthocyanin content of anthocyanin dry extract from *B. naudinii* flowers

Total anthocyanin content was quantified by pH-differential method [18]. Anthocyanin dry extract was dissolved in 70° ethanol to obtain 10 mg mL<sup>-1</sup> solution. Further, two concentrations of 1 mg mL<sup>-1</sup> were prepared in pH 1.0 and 4.5 buffer solutions in triplicate. The absorbance at 520 and 720 nm was performed using respective buffer solutions as blank. Total anthocyanin content (mg/100g) was calculated, according to the following equation:

$$\text{Total anthocyanin content (mg/100g)} = [(A^* \times MW/\epsilon \times l) \times (DF) \times (V_{s(\text{mL})}/W_{s(\text{g})})] \times 100$$

where, A\*: absorbance difference between two wavelengths; MW: molecular weight for cyanidin-3-glycoside (449.2 g mol<sup>-1</sup>);  $\epsilon$ : molar extinction coefficient for cyanidin-3-glycoside (26,900 L mol<sup>-1</sup> cm<sup>-1</sup>); DF: dilution factor; l: path length (1 cm); Vs: sample volume; Ws: sample weight.

#### 2.6. Preliminary toxicity bioassay of anthocyanin dry extract from *B. naudinii* flowers

The preliminary toxicity of anthocyanin dry extract was evaluated against crustacean *Artemia salina* larvae. 50 mg *Artemia salina* cysts were placed in an Erlenmeyer flask with 350 mL of

seawater (3.8 g / 100 mL) and incubated for 24 h at room temperature (20 – 25 °C). with artificial light and slow bubbling oxygen supply [19,20].

10,000 µg mL<sup>-1</sup> dry extract solution was prepared by weighing 20 mg of anthocyanin dry extract and dissolved in 0.5 mL of dimethyl sulfoxide and 1.5 mL of distilled water. From this solution, aliquots of 500, 250, 50, and 5 µL were transferred into four vials by diluting with seawater to 5 mL and the final concentrations of 1000, 500, 100, and 10 µg mL<sup>-1</sup> were obtained. Then 10 *Artemia salina* nauplii were transferred into each vial (in triplicate) and one yeast suspension drop (3 mg dry yeast / 5 mL seawater) was added as food. After 24 h, the survivor number of each dilution was counted and LC<sub>50</sub> was calculated using Probits method [19,20].

## 2.7. Antioxidant capacity assay of anthocyanin dry extract from *B. naudinii* flowers

### 2.7.1. Determination of antioxidant capacity by 2,2-diphenyl-1-picrylhydrazyl free radical (DPPH<sup>•</sup>) scavenging method

DPPH<sup>•</sup> assay was performed as described by *Sousa et al.* [17] using DPPH reagent (95%; Alfa Aesar, Germany). Extract dilutions at concentrations from 25 to 250 µg mL<sup>-1</sup> in 70° ethanol were prepared from 500 µg mL<sup>-1</sup> solution. Aliquots of 300 µL of each solution were taken and 2.7 mL of DPPH solution (40 µg mL<sup>-1</sup>) was added. After 30 min, the absorbance at 515 nm was measured by calibrating the spectrophotometer with the blank (300 µL water and 2.7 mL DPPH). The percentages of DPPH<sup>•</sup> remaining (%DPPH<sub>REM</sub>) were calculated from the calibration curve of DPPH<sup>•</sup> prepared with concentrations from 1 to 40 µg mL<sup>-1</sup> ( $y = 0.028x - 0.014$ ;  $R^2 = 0.9987$ ), according to the following equation:

$$\%DPPH_{REM} = [DPPH_C / DPPH_{C_0}] \times 100$$

where, DPPH<sub>C</sub>: DPPH<sup>•</sup> concentration (µg mL<sup>-1</sup>) after the reaction with the extract and Trolox; DPPH<sub>C0</sub>: DPPH initial concentration (µg mL<sup>-1</sup>).

EC<sub>50</sub>, the amount of antioxidant necessary to decrease the initial concentration of DPPH<sup>•</sup> by 50%, was determined using the OriginPro version 8, from an exponential curve ( $y = -y_0 + A \cdot e^{R_0 \cdot x}$ ) obtained from the values of the remaining DPPH<sup>•</sup> percentage as a function of extract concentration and was compared to 6-hydroxy-2,5,7,8-tetramethyl-chroman-2-carboxylic acid (Trolox 97%; Sigma-Aldrich Chemicals, Russia).

The antioxidant activity percentage was calculated by the following equation:

$$\text{Antioxidant activity (\%)} = [(A_c - (A_m - A_b)) / (A_c)] \times 100$$

where,  $A_c$ : control absorbance;  $A_m$ : extract and/or Trolox absorbance and  $A_b$ : blank absorbance. Extract and Trolox antioxidant activities were compared at the concentration of  $100 \mu\text{g mL}^{-1}$ .

### 2.7.2. Determination of antioxidant capacity by 2,2'-azinobis(3-ethylbenzothiazoline-6-sulfonic acid) radical cation (ABTS<sup>•+</sup>) method

ABTS<sup>•+</sup> assay was performed as described by *Rivas-Morales et al.* [7] using ABTS reagent (98%; Alfa Aesar, USA). Extract dilutions at concentration from 25 to  $250 \mu\text{g mL}^{-1}$  in 96° ethanol were prepared from  $500 \mu\text{g mL}^{-1}$  solution. Aliquots of  $20 \mu\text{L}$  of each dilution were taken then  $980 \mu\text{L}$  of ABTS<sup>•+</sup> radical solution were added, left to stand for 7 min and absorbance at 734 nm was measured, calibrating the spectrophotometer with the blank ( $20 \mu\text{L}$  water,  $980 \mu\text{L}$  ABTS<sup>•+</sup> radical solution).

The antioxidant activity percentage was calculated by the following equation:

$$\text{Antioxidant activity (\%)} = [(A_c - (A_m - A_b)) / (A_c)] \times 100$$

where,  $A_c$ : control absorbance;  $A_m$ : extract and/or Trolox absorbance, and  $A_b$ : blank absorbance. Extract and Trolox antioxidant activities were compared at the concentration of  $100 \mu\text{g mL}^{-1}$ .

EC<sub>50</sub> was determined using OriginPro version 8, from a straight-line equation ( $y = bx + a$ ), obtained from antioxidant activity (%) values as a function of extract concentration ( $\mu\text{g mL}^{-1}$ ) and compared with Trolox EC<sub>50</sub>.

### 2.7.3. Determination of antioxidant capacity by ferric reducing antioxidant power (FRAP) method

FRAP assay was performed as described by *Rivas-Morales et al.* [7] using FRAP reagent ( $\geq 99.0\%$ ; Sigma-Aldrich Chemie GmbH, Switzerland). Extract dilutions at concentration from 25 to  $250 \mu\text{g mL}^{-1}$  in 96° ethanol were prepared from  $500 \mu\text{g mL}^{-1}$  solution. Aliquots of  $20 \mu\text{L}$  of

each dilution were taken then 980  $\mu\text{L}$  of FRAP reagent was added and left to stand for 30 min and the absorbance was measured at 593 nm, calibrating the spectrophotometer with the blank (20  $\mu\text{L}$  water, 980  $\mu\text{L}$  FRAP reagent).

The antioxidant activity percentage was calculated by the following equation:

$$\text{Antioxidant activity (\%)} = \left[ \frac{(A_c - (A_m - A_b))}{(A_c)} \right] \times 100$$

where,  $A_c$ : control absorbance;  $A_m$ : extract and/or Trolox absorbance, and  $A_b$ : blank absorbance. Extract and Trolox antioxidant activities were compared at the concentration of 100  $\mu\text{g mL}^{-1}$ .

$\text{EC}_{50}$  was determined using the OriginPro version 8, from an exponential curve ( $y = -y_0 + A \cdot e^{R_0 \cdot x}$ ), obtained from antioxidant activity (%) values as a function of extract concentration ( $\mu\text{g mL}^{-1}$ ) and compared with Trolox  $\text{EC}_{50}$ .

## 2.8. Statistical analysis

The averages of total phenolic content, total anthocyanin content, antioxidant activity,  $\text{EC}_{50}$  and  $\text{LC}_{50}$  correspond to the average of three repetitions. Previously, Shapiro-Wilk normality and Levene homoscedasticity tests were performed. The comparison of means was evaluated using Student's  $t$  test for independent samples, analysis of variance and Tukey's multiple comparisons with 95% confidence interval. The analysis was carried out using the Statistical Package for Social Sciences (SPSS) version 28.0 (SPSS Inc., USA).

## 3. RESULTS

### 3.1. *B. naudinii* flowers chemical profile

The positive and negative modes were used to obtain the ion masses and also each ion fractionation profile (**Figure S1**). The metabolite identification was performed by comparing the retention times and the spectral profiles of each mass detected.

Twenty-eight compounds were identified from *B. naudinii* flowers, including phenolic compounds such as nilotin M2, remurin B, galloyl pedunculagin, casuarinin, and pedunculagin.

In addition, three new anthocyanin compounds were identified which confirms *B. naudinii* flowers pigment correspond to anthocyanin (**Table 1**).

The three new compounds 20, 21 and 23 have important MS-ESI-signals which confirm the abundance of these anthocyanins in *B. naudinii* flowers. The preliminary analysis indicates that it could be malvidin derivatives, and their chemical formulas are presented in **Table 1**.

### 3.2. Content of total phenolic compounds and total anthocyanins in anthocyanin dry extract from *B. naudinii* flowers

The anthocyanin dry extract from *B. naudinii* flowers has a moderate total phenolic content, which was calculated from a gallic acid calibration curve ( $y = 0.010x + 0.013$ ; determination coefficient ( $R^2$ ) of 0.996). The anthocyanin content in the dry extract was also moderate (**Table 2**).

### 3.3. Preliminary toxicity bioanalysis of anthocyanin dry extract from *B. naudinii* flowers with *Artemia salina*

There was no evidence of mortality while evaluating the bioassay of *Artemia salina* control, and it confirms that the diluent was appropriate. The median lethal concentration ( $LC_{50}$ ) value of anthocyanin dry extract was calculated by adjusting a logarithmic curve to the number of dead nauplii according to the Probits method [12,13] and the value corresponds to three repetitions and its standard error confirms the measurement precision (**Table 3**).

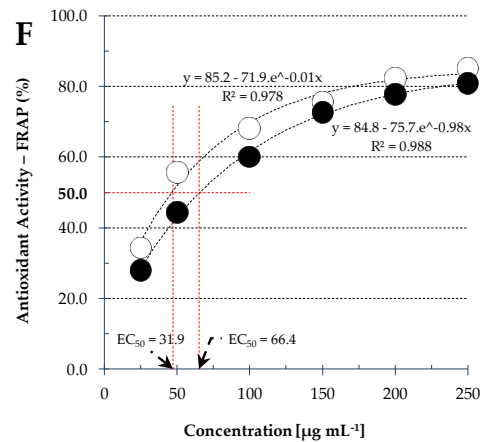
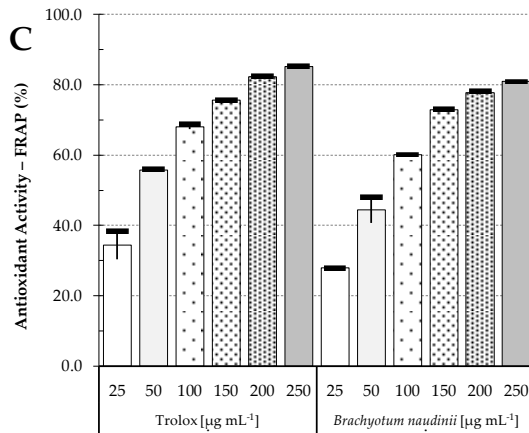
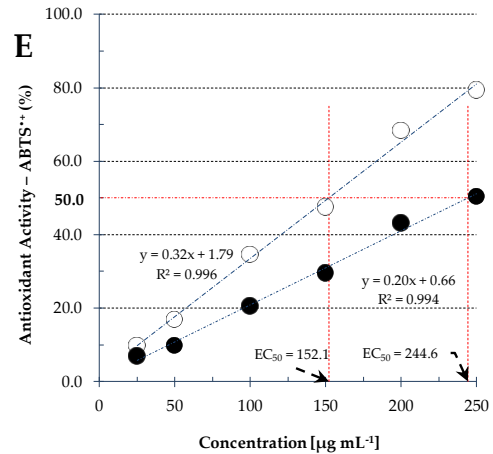
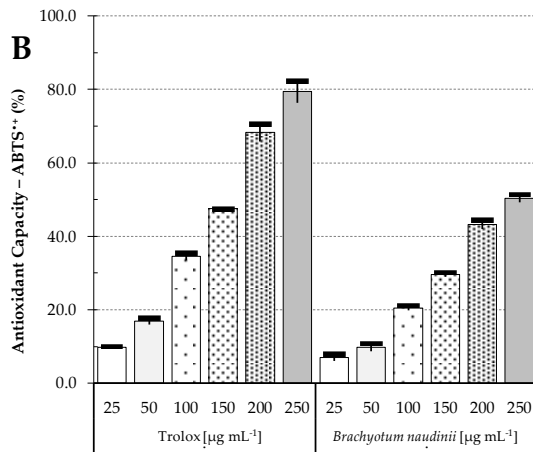
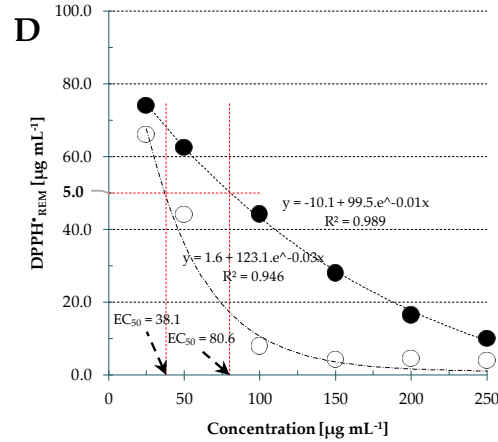
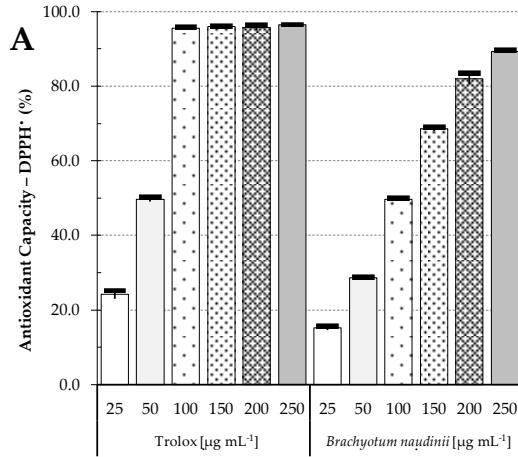
### 3.4. Antioxidant activity of anthocyanin dry extract from *B. naudinii* flowers

The antioxidant activity of anthocyanin dry extract from *B. naudinii* flowers was evaluated using DPPH<sup>•</sup>, ABTS<sup>•+</sup>, and FRAP methods (**Table 2**) and the percentages of antioxidant activity were statistically compared with Trolox at a concentration of 100  $\mu\text{g mL}^{-1}$  ( $p < 0.05$ , Student's  $t$  test for independent samples). The percentage of antioxidant activity was statistically different than Trolox ( $p < 0.05$ ), evaluated with three methods.

The antioxidant activity was also expressed as median effective concentration ( $EC_{50}$ ), whose values are the result of the antioxidant activity evaluation at various extract concentrations which show better antioxidant potential (**Figure 1 and Table S1**). The  $EC_{50}$  value evaluated by DPPH,



ABTS and FRAP methods was compared with Trolox EC<sub>50</sub> ( $p < 0.05$ , Student's  $t$  test for independent samples). In all three methods, EC<sub>50</sub> was statistically higher than Trolox ( $p < 0.05$ ), and it should be noted that the lower EC<sub>50</sub>, the greater the antioxidant activity.



**Figure 1.** Antioxidant activity of anthocyanin dry extract from *B. naudinii* flowers compared to Trolox as a function of concentration. Antioxidant activity expressed as percentage and median effective concentration ( $EC_{50}$ ). The broken red lines correspond to the interpolation for  $EC_{50}$  calculation.

The dry extract of anthocyanins from *B. naudinii* flowers' antioxidant activity was also evaluated at concentrations from 25 to 250  $\mu\text{g mL}^{-1}$  and compared with Trolox by DPPH $\cdot$ , ABTS $^{+\cdot}$ , and FRAP methods (**Figure 1**).

Using DPPH $\cdot$  method, the extract and Trolox antioxidant activity as a function of concentration fits an exponential curve ( $y = -y_0 + A \cdot e^{R_0 \cdot x}$ ), with  $R^2$  of 0.989 and 0.946, respectively (**Figure 1D**), and  $EC_{50}$  was calculated that found statistically different ( $p < 0.05$ ; Student's  $t$  test for independent samples). The extract antioxidant activity at 250  $\mu\text{g mL}^{-1}$  was statistically similar to Trolox at concentrations of 100, 150, 200 and 250  $\mu\text{g mL}^{-1}$  ( $p > 0.05$ ; Tukey's multiple comparison test) (**Figure 1A**). Trolox at the concentration  $\geq 100 \mu\text{g mL}^{-1}$  showed  $> 95\%$  antioxidant activity, hence 100  $\mu\text{g mL}^{-1}$  was the most appropriate concentration to compare with the extract (**Figure 1A and Table S1**). Therefore, it can be concluded that Trolox has approximately 2.5 times more antioxidant potential than the extract.

Using ABTS $^{+\cdot}$  method, the extract and Trolox antioxidant activity as a function of concentration is adjusted to a straight-line equation ( $y = b \cdot x + a$ ), with  $R^2$  of 0.994 and 0.966, respectively (**Figure 1E**). The extract and Trolox  $EC_{50}$  values were statistically different ( $p < 0.05$ ; Student's  $t$  test for independent samples). The extract antioxidant activity percentage at concentrations from 25 to 250  $\mu\text{g mL}^{-1}$  was statistically lower than Trolox ( $p < 0.05$ ; Tukey's multiple comparison test) (**Figure 1B**).

Using FRAP method, the extract and Trolox antioxidant activity as a function of concentration fit an exponential curve ( $y = y_0 + A \cdot e^{R_0 \cdot x}$ ), with  $R^2$  of 0.988 and 0.978, respectively (**Figure 1F**). The extract and Trolox  $EC_{50}$  values were statistically different ( $p < 0.05$ ; Student's  $t$  test for independent samples). The extract antioxidant activities at 150, 200 and 250  $\mu\text{g mL}^{-1}$  were statistically similar to Trolox ( $p < 0.05$ ; Tukey's multiple comparison test). Therefore, it can be concluded that Trolox has approximately 2.1 times more antioxidant potential than the extract.

#### 4. DISCUSSION

According to the analysis, *B. naudinii* Triana flowers are composed of 39% tannins, 21% flavonol glycosides, 14% organic acids, 11% anthocyanins, 7% coumaric acid derivatives, 4% polar lipids, and 4% disaccharides. In genus *Brachyotum*, the presence of phenolic compounds, flavonoids, and anthocyanins with antioxidant and photoprotective activities has been reported as well as triterpenes, corosolic acid and ursolic acid with activity against Plasmodium [21]. Melastomataceae family biosynthesizes a wide variety of phenolic compounds, flavonoids, anthocyanins, tannins, and triterpenes, with antioxidant, antimicrobial, and antitumor activities [3,4]. The phenols nilotin and remurin were identified from *Tamarix nilotica* leaves [22], while galloyl pedunculagin was identified from *Terminalia calamansanai* leaves. Casuarinin was identified from *Terminalia catappa* Linn bark, *Terminalia chebula* Retz fruit, and *Terminalia arjuna* Linn bark; while pedunculagin was identified from *Terminalia chebula* Retz. fruit [23].

Identification of anthocyanins by mass spectrometry is generally performed in positive mode since these molecules are easily protonatable at acidic pH [24,25], however, it is difficult to distinguish anthocyanins from flavonol glycosides in complex plant matrices using the positive ionization mode, as both have similar molecular ions and fragmentation patterns [26]. In contrast, negative mode anthocyanins describe a characteristic ionization and fragmentation pattern [24,25]. Therefore, both positive and negative modes were used. The characteristic fragment ion of aglycone cyanidin is 287 in positive mode [24,27]. This fragment ion in positive mode has been detected in three compounds (20, 21 and 23) that could not be identified by the spectral database. For this reason, these three compounds were considered to be anthocyanin and must be subsequently confirmed by nuclear magnetic resonance spectroscopy analysis. This hypothesis is also supported by anthocyanin detection in previous phytochemical screening tests carried out by this group and the presence of these molecules in the genus *Brachyotum* and the family Melastomataceae reported by other authors [3,4]. However, the preliminary analysis indicates that they could be malvidin derivatives, which should be isolated and analyzed using a spectroscopic technique in order to determine the correct structures. In this regard, the presence of malvidin glycosides has been identified in the flowers of different species of the Melastomataceae family. For example, malvidin-3-O-glucoside and malvidin-3,5-diglucoside have been identified from *Tibouchina grandiflora* flowers [3]. This reinforces the hypothesis that *B. naudinii* flowers contain malvidin derivatives. Likewise, malvidin is a natural antioxidant

present in plants that are used as a food supplement and as an active ingredient in anti-aging and anti-wrinkle creams [5,6].

In negative mode, the fragment ion 285 has been detected in Kaempferol-3-O-rhamnoside (Table 1), a flavonol glycoside, which is in accordance with *Sun et al.* [24] and *Mansour et al.* [25] works.

Plants constitute an inexhaustible reservoir of bioactive molecules with enormous structural variability and biological activity. The exquisite specialization of biosynthetic machinery of plants has been improved million years ago to develop the molecular mechanisms necessary for the synthesis of active metabolites that are used as chemical defense weapons against predators and in response to abiotic environmental stress in which they live to adapt and survive.

Plants have reached such a degree of sophistication that each part has its own metabolite fingerprint. Phenolic compounds, flavonoids, and anthocyanins are synthesized as a defense mechanism against predators and abiotic stress generated by drought, salinity, pH changes, and ultraviolet radiation [28,29]. The metabolite profile of *B. naudinii* flowers obtained by tandem mass spectrometry reveals the presence of important molecules with antioxidant and photoprotective activities such as phenolic compounds, flavonoids, and anthocyanins [4] and the adaptation of this species to climate with high radiation, support the hypothesis that this species biosynthesizes these compounds as a defense mechanism against UV radiation.

One of the metabolites detected by tandem mass spectrometry has been shikimic acid, a key molecule for the biosynthesis of phenolic compounds. Similarly, the presence of phenolic compounds such as  $\beta$ -glucogallin, a polyphenolic antioxidant precursor of ellagitannin biosynthesis [30] with a protective effect on lens epithelial cells in ocular cataracts [31], the antiglaucoma effect [32], aldose reductase inhibition, anti-inflammatory and protection of tissue damage in neuropathy and diabetic retinopathy [33].

Another important metabolite with biological activity is pedunculagin, a phenolic compound with significant anti-inflammatory activity in the treatment of acne vulgaris, hyperkeratosis (via  $5\alpha$  reductase inhibition) [34], and capacity to regenerate keratinocytes, and therefore useful both in the prevention and treatment of cellular aging [35].

Casuarinin, a phenolic compound with anti-inflammatory activity, capable of inhibiting TNF- $\alpha$  [36], and antiviral activity against herpes simplex [37], has also been detected.

The performed analysis also reports the acyl spermidines presence, this metabolite has been detected in *Sambucus nigra* inflorescences by using mass spectrometry [38], which is consistent with our analysis, since plant flowers were used. Using electrospray mass spectrometry, another metabolite lysophosphatidylcholine (polar lipid) was detected in *B. naudinii* leaves [39].

LC<sub>50</sub> of anthocyanin dry extract from *B. naudinii* flowers was less than 1000  $\mu\text{g mL}^{-1}$ , therefore considered as an active substance [19]. According to the toxicity classification, *B. naudinii* flower extract is considered moderately toxic (100 to 500  $\mu\text{g mL}^{-1}$ ) [4]. The *Artemia salina* bioassay can be used routinely in phytochemical research, since it is a broad-spectrum assay that allows analyzing the presence of pesticides, mycotoxins, anesthetics, and morphine-type compounds, among others [4]. The LC<sub>50</sub> value does not show physiological or biological activities, though it is an indicator of toxicity at the cellular level that guides the search for new bioactive natural products [4]. The results indicate that anthocyanin dry extract from *B. naudinii* flowers is biologically active, therefore it is recommended to continue biodirected studies.

To determine the antioxidant potential of anthocyanin dry extract from *B. naudinii* flowers, EC<sub>50</sub> ( $80.6 \pm 0.9 \mu\text{g mL}^{-1}$ ; DPPH $\cdot$ ) was calculated and compared to Trolox ( $38.1 \pm 0.2 \mu\text{g mL}^{-1}$ ; DPPH $\cdot$ ) using an equal concentration of both anthocyanin dry extract and Trolox. Although it is true that the antioxidant activity of anthocyanin dry extract is statistically different from Trolox ( $p < 0.05$ ), it is necessary to indicate that Trolox is a chemically pure substance and has been tested at the same concentration. In this regard, a study on total phenols and antioxidant activity by using DPPH $\cdot$  from five medicinal plants reported the following EC<sub>50</sub> values of  $27.6 \pm 0.8$ ,  $44.5 \pm 1.1$ ,  $78.5 \pm 5.0$ ,  $42.23 \pm 1.7$ ,  $42.2 \pm 1.7$ ,  $50.2 \pm 0.8$  and  $111.1 \pm 12.4 \mu\text{g mL}^{-1}$  for *Terminalia brasiliensis* (peel and leaves), *Cenostigma macrophyllum* (leaves), *Terminalia fagifolia* (leaves), *Qualea grandiflora* (leaves) and *Copernicia prunifera* (roots), respectively [17]. Comparing EC<sub>50</sub> of anthocyanin dry extract from *B. naudinii* flowers ( $80.6 \pm 0.9 \mu\text{g mL}^{-1}$ ), we can observe that it has moderate antioxidant activity, which could increase with an optimization process. This comparison is pertinent since the method used to evaluate the antioxidant activity of *B. naudinii* was the same as mentioned above.

The antioxidant activity has been demonstrated using *in vitro* methods i.e., the uptake capacity tests against stable non-biological radicals (DPPH<sup>•</sup> and ABTS<sup>•+</sup>) and the total reduction capacity test (FRAP). Although, these methods have limitations, such as extrapolating the results to biological models and the presence of interferents, allowing us to demonstrate the antioxidant potential and rank the plant species. The obtained results showed that *B. naudinii* flowers are a potential source of antioxidants. It is suggested to evaluate the antioxidant activity in *in vitro* enzymatic models and *in vivo* assays. Likewise, it is recommended to evaluate the antioxidant activity in different fractions, such as hexane, ethyl acetate, and methanol.

There is no evidence of ethnopharmacological use of *B. naudinii* flowers; however, the presence of phenolic compounds, moderate toxic activity, important anthocyanin content with antioxidant potential, and the background of other species, highly recommend continuing the biochemical studies. The wide range of metabolites found in *B. naudinii* flowers makes it a species with potential application in the pharmaceutical, biochemical, cosmetic, dye, and biotechnological industries.

## **5. CONCLUDING REMARKS**

In the present study, 28 compounds were detected in *Brachyotum naudinii* Triana flowers, including tannins and flavonoid glycosides being the most abundant. In addition, three unidentified compounds that could correspond to anthocyanins were detected. Preliminary toxicity results indicated that anthocyanin dry extract is moderately toxic. Furthermore, this species demonstrated antioxidant activity by inhibiting the radical DPPH<sup>•</sup> and ABTS<sup>•+</sup> as well as reducing the iron complex FRAP. The flowers contain phenolic compounds with *in vitro* antioxidant potential and are a source of new anthocyanin compounds. Further work will help to characterize the novel anthocyanin compounds by using nuclear magnetic resonance spectroscopy.

## **FUNDING**

This project was financed within the framework of Concurso de Proyecto de Investigación Científica y Tecnológica para Docentes, with resources from Fondo de Desarrollo Socioeconómico de Camisea (FOCAM), Perú (R. 2013-UNSCH-CU).

## CONFLICTS OF INTEREST

The authors declare no conflict of interest.

## DATA AVAILABILITY STATEMENT

The data that support results and findings of this study is available from the corresponding authors upon request.

## INSTITUTIONAL REVIEW BOARD STATEMENT

This study was approved by Universidad Nacional de San Cristóbal de Huamanga, Ayacucho, Perú (391-2014-UNSCH-COG-R).

## REFERENCES

- [1] Bussmann, R. W., Malca-García, G., Glenn, A., Sharon, D., Chait, G., Díaz, D., Pourmand, K., Jonat, B., Somogy, S., Guardado, G., Aguirre, C., Chan, R., Meyer, K., Kuhlman, A., Townesmith, A., Effio-Carbajal, J., Frías-Fernandez, F., Benito, M., Minimum Inhibitory Concentrations of Medicinal Plants Used in Northern Peru as Antibacterial Remedies. *J. Ethnopharmacol.* 2010, 132, 101–8.
- [2] Harborne, J. B., Grayer, R. J., The Flavonoids Advances in Research Since 1986. Routledge, London 2017, pp. 589–618.
- [3] Serna, D. M. O., Martínez, J. H. I., Phenolics and Polyphenolics from Melastomataceae Species. *Molecules* 2015, 20, 17818–17847.
- [4] Ibáñez-Calero, S. L., Afonso, K. E. L., Tapia, E. L. Y., Lizarazu, J., Espinoza, R. Z., Gironda, T. S., A Screening for Natural Colorants in the Zongo Valley with Probable Antioxidant and/or Photo-Protector Activities. *Investig. Desarro.* 2016, 1, 5–24.
- [5] Bub, A., Watzl, B., Heeb, D., Rechkemmer, G., Briviba, K., Malvidin-3-Glucoside Bioavailability in Humans after Ingestion of Red Wine, Dealcoholized Red Wine and Red Grape Juice. *Eur. J. Nutr.* 2001, 40, 113–20.
- [6] Hyun, J. W., Chung, H. S., Cyanidin and Malvidin from *Oryza sativa* cv. Heugjinjubyeo

- Mediate Cytotoxicity against Human Monocytic Leukemia Cells by Arrest of G<sub>2</sub>/M Phase and Induction of Apoptosis. *J. Agric. Food Chem.* 2004, 52, 2213–7.
- [7] Rivas-Morales, C., Oranday-Cárdenas, M. A., Verde-Star, M. J., Investigación en Plantas de Importancia Médica. OmniaScience, Barcelona 2016.
- [8] Betim, F. C. M., de Oliveira, C. F., de Souza, A. M., Szabo, E. M., Zanin, S. M. W., Miguel, O. G., Miguel, M. D., Dias, J. de F. G., *Ocotea nutans* (Nees) Mez (Lauraceae): Chemical Composition, Antioxidant Capacity and Biological Properties of Essential Oil. *Brazilian J. Pharm. Sci.* 2019, 55, 1–10.
- [9] Farias, A. L. F., Rodrigues, A. B. L., Martins, R. L., Rabelo, É. de M., Farias, C. W. F., de Almeida, S. S. M. da S., Chemical Characterization, Antioxidant, Cytotoxic and Microbiological Activities of the Essential Oil of Leaf of *Tithonia diversifolia* (Hemsl) A. Gray (Asteraceae). *Pharmaceuticals* 2019, 12, 1–14.
- [10] Mesquita, K. D. S. M., Feitosa, B. de S., Cruz, J. N., Ferreira, O. O., Franco, C. de J. P., Cascaes, M. M., Oliveira, M. S. de, Andrade, E. H. de A., Chemical Composition and Preliminary Toxicity Evaluation of the Essential Oil from *Peperomia circinnata* Link var. *circinnata*. (Piperaceae) in *Artemia salina* Leach. *Molecules* 2021, 26, 1–21.
- [11] Nadeem, H. R., Akhtar, S., Sestili, P., Ismail, T., Neugart, S., Qamar, M., Esatbeyoglu, T., Toxicity, Antioxidant Activity, and Phytochemicals of Basil (*Ocimum basilicum* L.) Leaves Cultivated in Southern Punjab, Pakistan. *Foods* 2022, 11, 1–13.
- [12] Lee, M. Y., Essential Oils as Repellents against Arthropods. *Biomed Res. Int.* 2018, 2018, 1–9.
- [13] Cossolin, J. F. S., Pereira, M. J. B., Martínez, L. C., Turchen, L. M., Fiaz, M., Bozdoğan, H., Serrão, J. E., Cytotoxicity of *Piper aduncum* (Piperaceae) Essential Oil in Brown Stink Bug *Euschistus heros* (Heteroptera: Pentatomidae). *Ecotoxicology* 2019, 28, 763–770.
- [14] Sarker, S. D., Latif, Z., Gray, A. I., Methods in Biotechnology. Humana Press, New Jersey 2005, pp. 1–529.
- [15] Barros, F., Dykes, L., Awika, J. M., Rooney, L. W., Accelerated Solvent Extraction of



- Phenolic Compounds from *Sorghum brans*. *J. Cereal Sci.* 2013, 58, 305–312.
- [16] Kanojia, G., ten Have, R., Brugmans, D., Soema, P. C., Frijlink, H. W., Amorij, J. P., Kersten, G., The Effect of Formulation on Spray Dried Sabin Inactivated Polio Vaccine. *Eur. J. Pharm. Biopharm.* 2018, 129, 21–29.
- [17] Sousa, C. M. D. M., Silva, H. R. E., Vieira, G. M., Ayres, M. C. C., Da Costa, C. L. S., Araújo, D. S., Cavalcante, L. C. D., Barros, E. D. S., Araújo, P. B. D. M., Brandão, M. S., Chaves, M. H., Total Phenolics and Antioxidant Activity of Five Medicinal Plants. *Quim. Nova* 2007, 30, 351–355.
- [18] Jimenez, C. D. C., Flores, C. S., Tian, J. H. Q., Schwartz, S. J., Giusti, M., Caracterización de las Antocianinas de los Frutos. *Rev. Univ.* 2021, 140, 13–26.
- [19] Sánchez, L., Neira, A., Bioensayo General de Letalidad en *Artemia salina*, a las Fracciones del Extracto Etanólico de *Psidium guajava*. L y *Psidium guineense*. Sw. *Cult. Científica* 2005, 3, 40–5.
- [20] Mayorga, P., Pérez, K. R., Cruz, S. M., Cáceres, A., Comparison of Bioassays Using the Anostracan crustaceans *Artemia salina* and *Thamnocephalus platyurus* for Plant Extract Toxicity Screening. *Rev. Bras. Farmacogn.* 2010, 20, 897–903.
- [21] Ibañez-Calero, S. L., Jullian, V., Maurel, S., Chavez de Michel, L. R., Bravo, J. A., Gimenez, A., Sauvain, M., Application of Ferriprotoporphyrin Biocrystallization Inhibition Test to Find Antiplasmodial Compounds in the Flora of the “Zongo Valley.” *Rev. Boliv. Química* 2012, 29, 71–79.
- [22] Orabi, M. A. A., Taniguchi, S., Sakagami, H., Yoshimura, M., Yoshida, T., Hatano, T., Hydrolyzable Tannins of Tamaricaceous Plants. V. Structures of Monomeric-Trimeric Tannins and Cytotoxicity of Macrocyclic-Type Tannins Isolated from *Tamarix nilotica*<sup>1</sup>. *J. Nat. Prod.* 2013, 76, 947–56.
- [23] Chang, Z., Zhang, Q., Liang, W., Zhou, K., Jian, P., She, G., Zhang, L., A Comprehensive Review of the Structure Elucidation of Tannins from *Terminalia* Linn. *Evidence-Based Complement. Altern. Med.* 2019, 2019, 1–26.

- [24] Sun, J., Lin, L. Z., Chen, P., Study of the Mass Spectrometric Behaviors of Anthocyanins in Negative Ionization Mode and Its Applications for Characterization of Anthocyanins and Non-Anthocyanin Polyphenols. *Rapid Commun. Mass Spectrom.* 2012, 26, 1123–1133.
- [25] Mansour, K. A., Moustafa, S. F., Abdelkhalik, S. M., High-Resolution UPLC-MS Profiling of Anthocyanins and Flavonols of Red Cabbage (*Brassica oleracea* L. var. *capitata* f. *rubra* DC.) Cultivated in Egypt and Evaluation of Their Biological Activity. *Molecules* 2021, 26, 1–10.
- [26] Janna, O., Khairul, A., Maziah, M., Mohd, Y., Flower Pigment Analysis of *Melastoma malabathricum*. *African J. Biotechnol.* 2016, 5, 170–174.
- [27] Solarte, N., Cejudo-Bastante, M. J., Hurtado, N., Heredia, F. J., First Accurate Profiling of Antioxidant Anthocyanins and Flavonols of *Tibouchina urvilleana* and *Tibouchina mollis* Edible Flowers Aided by Fractionation with Amberlite XAD-7. *Int. J. Food Sci. Technol.* 2022, 57, 2416–2423.
- [28] Berland, H., Albert, N. W., Stavland, A., Jordheim, M., McGhie, T. K., Zhou, Y., Zhang, H., Deroles, S. C., Schwinn, K. E., Jordan, B. R., Davies, K. M., Andersen, Ø. M., Auronidins are a Previously Unreported Class of Flavonoid Pigments that Challenges when Anthocyanin Biosynthesis Evolved in Plants. *Proc. Natl. Acad. Sci. U. S. A.* 2019, 116, 20232–20239.
- [29] Kiani, R., Arzani, A., Mirmohammady Maibody, S. A. M., Polyphenols, Flavonoids, and Antioxidant Activity Involved in Salt Tolerance in Wheat, *Aegilops cylindrica* and their Amphidiploids. *Front. Plant Sci.* 2021, 12, 1–13.
- [30] Schulenburg, K., Feller, A., Hoffmann, T., Schecker, J. H., Martens, S., Schwab, W., Formation of  $\beta$ -Glucogallin, the Precursor of Ellagic Acid in Strawberry and Raspberry. *J. Exp. Bot.* 2016, 67, 2299–308.
- [31] Ma, Y., Liu, F., Xu, Y., Protective Effect of  $\beta$ -Glucogallin on Damaged Cataract against Methylglyoxal Induced Oxidative Stress in Cultured Lens Epithelial Cells. *Med. Sci. Monit.* 2019, 25, 9310–9318.

- [32] Cao, T., Wang, J., Wu, Y., Wang, L., Zhang, H., Antiglaucoma Potential of  $\beta$ -Glucogallin is Mediated by Modulating Mitochondrial Responses in Experimentally Induced Glaucoma. *Neuroimmunomodulation* 2021, 27, 142–151.
- [33] Li, L., Chang, K. C., Zhou, Y., Shieh, B., Ponder, J., Abraham, A. D., Ali, H., Snow, A., Petrash, J. M., Labarbera, D. V., Design of an Amide N-Glycoside Derivative of  $\beta$ -Glucogallin: A Stable, Potent, and Specific Inhibitor of Aldose Reductase. *J. Med. Chem.* 2014, 57, 71–77.
- [34] Kim, M., Yin, J., Hwang, I. H., Park, D. H., Lee, E. K., Kim, M. J., Lee, M. W., Anti-Acne Vulgaris Effects of Pedunculagin from the Leaves of *Quercus mongolica* by Anti-Inflammatory Activity and 5 $\alpha$ -Reductase Inhibition. *Molecules* 2020, 25, 1–8.
- [35] Kim, H. H., Kim, D. H., Oh, M. H., Park, K. J., Heo, J. H., Lee, M. W., Inhibition of Matrix Metalloproteinase-1 and Type-I Procollagen Expression by Phenolic Compounds Isolated from the Leaves of *Quercus mongolica* in Ultraviolet-Irradiated Human Fibroblast Cells. *Arch. Pharm. Res.* 2015, 38, 11–17.
- [36] Kwon, D. J., Bae, Y. S., Ju, S. M., Goh, A. R., Choi, S. Y., Park, J., Casuarinin Suppresses TNF- $\alpha$ -Induced ICAM-1 Expression via Blockade of NF- $\kappa$ B Activation in HaCaT Cells. *Biochem. Biophys. Res. Commun.* 2011, 409, 780–5.
- [37] Cheng, H. Y., Lin, C. C., Lin, T. C., Antiherpes Simplex Virus Type 2 Activity of Casuarinin from the Bark of *Terminalia arjuna* Linn. *Antiviral Res.* 2002, 55, 447–455.
- [38] Kite, G. C., Larsson, S., Veitch, N. C., Porter, E. A., Ding, N., Simmonds, M. S. J., Acyl Spermidines in Inflorescence Extracts of Elder (*Sambucus nigra* L., Adoxaceae) and Elderflower Drinks. *J. Agric. Food Chem.* 2013, 61, 3501–3508.
- [39] Maatta, S., Scheu, B., Roth, M. R., Tamura, P., Li, M., Williams, T. D., Wang, X., Welti, R., Levels of *Arabidopsis thaliana* Leaf Phosphatidic Acids, Phosphatidylserines, and Most Trienoate-Containing Polar Lipid Molecular Species Increase During the Dark Period of the Diurnal Cycle. *Front. Plant Sci.* 2012, 3, 1–12.

**Table 1.** Determination of *B. naudinii* lyophilized flowers chemical compounds by UHPLC-MS/MS.

N°	T <sub>R</sub> (min)	MS-ESI-	MS <sup>2</sup>	MS-ESI+	MS <sup>2</sup>	Nominal mass	Molecular formula	Structure
1	1.97	341.1090	179,0556 161,0449 119,0341	365,1053 [M+Na]	203,0526 185,0421	342	C <sub>12</sub> H <sub>22</sub> O <sub>11</sub>	Disaccharide
2	2.01	195.0555	177.0399 159.0292 129.0185 99.0078 87.0077 75.0077			196	C <sub>6</sub> H <sub>12</sub> O <sub>7</sub>	Gluconic acid
3	2.15	173.0449	155.0343 137.0237 111.0442 93.0336 83.0492 73.0285			174	C <sub>7</sub> H <sub>10</sub> O <sub>5</sub>	Shikimic acid
4	2.17	133.0135	115.0028 89.0234 72.9921 71.0128			134	C <sub>4</sub> H <sub>6</sub> O <sub>5</sub>	Malic acid
5	2.80	191.0193	173.0086 129.0185 111.0079 87.0078 85.0285 57.0335			192	C <sub>6</sub> H <sub>8</sub> O <sub>7</sub>	Citric acid
6	2.80	481.0626	421.0410 300.9991 275.0198 257.0091 229.0140 203.0345 201.0191			482	C <sub>20</sub> H <sub>18</sub> O <sub>14</sub>	1,3-hexahydroxy-phenol glucose
7	2.81	331.0673	169.0137 151.0030 123.0079			332	C <sub>13</sub> H <sub>16</sub> O <sub>10</sub>	$\beta$ -Glucogallin

			101.0234					
			89.0234					
			71.0128					
8	4.36	783.0695	481.0627	802.1090	303.0132	784	C <sub>34</sub> H <sub>24</sub> O <sub>22</sub>	Pedunculagin (isomer 1)
			300.9992	[M+NH <sub>4</sub> <sup>+</sup> ]	277.0341			
			275.0199		259.0236			
			257.0097		231.0289			
			229.0138		215.0338			
			203.0346		187.0387			
			201.0191		109.0287			
			185.0240					
9	4.69	783.0693	481.0627	802.1091	303.0132	784	C <sub>34</sub> H <sub>24</sub> O <sub>22</sub>	Pedunculagin (isomer 2)
			300.9989	[M+NH <sub>4</sub> <sup>+</sup> ]	277.0341			
			275.0197		259.0235			
			257.0090		231.0286			
			229.0140		215.0337			
			203.0344		187.0388			
			201.0188		109.0287			
			185.0241					
10	6.96	483.0783	331.0669			484	C <sub>20</sub> H <sub>20</sub> O <sub>14</sub>	1,6-digaloyl-glucoside
			313.0568					
			271.0460					
			211.0245					
			169.0136					
			125.0235					
11	8.04	935.0802	917.0690			936	C <sub>41</sub> H <sub>28</sub> O <sub>26</sub>	Galloyl pedunculagin
			873.0795					
			855.0668					
			573.0529					
			571.0733					
			383.0405					
			349.0356					
			315.0147					
12	8.59	953.0900	935.0795	972.1304	635.0869	954	C <sub>41</sub> H <sub>30</sub> O <sub>27</sub>	Remurin B
			651.0723	[M+NH <sub>4</sub> <sup>+</sup> ]	617.0766			
			633.0723		303.0132			
			300.9990		277.0341			
			275.0198		259.0235			
			257.0090		231.0287			
			229.0140		153.0182			

			203.0346					
			201.0188					
13	8.73	953.0800	917.0682			936	C <sub>41</sub> H <sub>28</sub> O <sub>26</sub>	Casuarinine (isomer 1)
			783.0685					
			659.0525					
			633.0735					
			571.0736					
			329.0301					
			300.9994					
			299.0197					
14	9.18	967.1064	935.0790	986.1461	617.0774	968	C <sub>42</sub> H <sub>32</sub> O <sub>27</sub>	Nilotinin M2
			633.0723	[M+H <sub>4</sub> <sup>+</sup> ]	335.0397			
			300.9990		303.0132			
			275.0197		277.0339			
			257.0091		259.0235			
			229.0142		231.0287			
			203.0345		153.0181			
15	9.50	635.0896	465.0674			636	C <sub>27</sub> H <sub>24</sub> O <sub>18</sub>	1,3,6-tri- <i>O</i> -galloylglucose
			313.0566					
			211.0244					
			193.0133					
			169.0136					
			151.0028					
			125.0235					
16	10.22	479.0830	316.0226	481.0974	319.0446	480	C <sub>21</sub> H <sub>20</sub> O <sub>13</sub>	Myricetin 3- <i>O</i> -hexoside
			287.0198		273.0388			
			271.0249		245.0443			
			259.0249		217.0498			
			214.0269		167.0340			
			178.9981		153.0184			
			151.0029					
17	10.30	935.0801	917.0689			936	C <sub>41</sub> H <sub>28</sub> O <sub>26</sub>	Casuarinine (isomer 2)
			783.0703					
			633.0737					
			450.9941					
			329.0301					
			300.9991					
			283.9965					
			275.0199					
			257.0092					

			229.0141					
18	10.71	463.0884	316.0225			464	C <sub>21</sub> H <sub>20</sub> O <sub>12</sub>	Myricitrin
			300.0276					
			287.0198					
			271.0248					
			259.0248					
			242.0220					
			178.9980					
			151.0030					
19	10.76	477.0674	301.0351	479.0916	303.0796	478	C <sub>22</sub> H <sub>18</sub> O <sub>13</sub>	Quercetin 3- <i>O</i> -glucuronide
			283.0254		285.0405			
			255.0301		257.0450			
			245.0457		229.0491			
			227.0250		153.0180			
			178.9980		113.0233			
			151.0030		85.0288			
			121.0287					
20	10.83	787.2094	665.1670	771.2130	639.1700	787	C <sub>37</sub> H <sub>34</sub> O <sub>19</sub> <sup>+</sup>	Unknown anthocyanin (new compound)
			501.1039	[M-H <sub>2</sub> O+H] <sup>+</sup>	463.1227			
			479.1196		331.0810			
			347.0773		315.0494			
			329.0666		299.0546			
			314.0434		287.0547			
			261.0770		270.0517			
			193.0137		242.0571			
			165.0187					
			149.0237					
			137.0236					
21	11.0	829.2201	637.1564	813.2230	639.1701	861	C <sub>39</sub> H <sub>42</sub> O <sub>20</sub> <sup>+</sup>	Unknown anthocyanin (new compound)
			521.1302	[M-H <sub>2</sub> O+H] <sup>+</sup>	505.1329			
			501.1040		331.0810			
			347.0773		315.0495			
			329.0668		287.0547			
			314.0432		270.0518			
			299.0198		242.0571			
			193.0138					
			165.0187					
			149.0237					
			137.0236					
			123.0079					

22	11.29	447.0935	300.0276 271.0248 255.0298 243.0293 227.0346 178.9982 151.0029			448	C <sub>21</sub> H <sub>20</sub> O <sub>11</sub>	Quercetin-3- <i>O</i> -rhamnoside
23	11.31	859.2302	667.1663 521.1302 347.0771 329.0668 314.0434 299.0199 193.0138 165.0187 149.0237	843.2331 [M-H <sub>2</sub> O+H] <sup>+</sup>	669.1804 505.1294 331.0810 315.0496	861	C <sub>40</sub> H <sub>45</sub> O <sub>21</sub> <sup>+</sup>	Unknown anthocyanin (new compound)
24	11.70	625.1206	479.0830 463.0880 316.0225 300.0273 287.0201 271.0248 259.0245 242.0225 214.0272 178.9982			626	C <sub>30</sub> H <sub>26</sub> O <sub>15</sub>	Myricetina 3'- <i>O</i> -(6''- <i>p</i> - coumaroyl) glucoside
25	11.79	431.0897	285.0402 255.0298 227.0347 211.0399 185.0604 163.0031 107.0124			432	C <sub>21</sub> H <sub>20</sub> O <sub>10</sub>	Kaempferol-3- <i>O</i> -rhamnoside
26	12.39	598.2566	478.1990 462.2036 452.2205 342.1459 332.1617 316.1664 145.0287	600.2702	454.2332 436.2228 308.1964 292.2015 275.1748 204.1019 163.0388	599	C <sub>34</sub> H <sub>37</sub> N <sub>3</sub> O <sub>7</sub>	<i>N</i> -caffeoyl- <i>N,N</i> -di- <i>p</i> - coumaroylspermidine



			135.0443		147.0440			
			119.0493		119.0492			
27	13.00	582.2617	462.2039	584.2751	438.2383	583	C <sub>34</sub> H <sub>37</sub> N <sub>3</sub> O <sub>6</sub>	Tricoumaroyl spermidine
			342.1462		420.2275			
			316.1670		292.2016			
			299.1405		275.1749			
28	17.73	564.3314	504.3102			519	C <sub>26</sub> H <sub>50</sub> NO <sub>7</sub> P	Lysophosphatidylcholine (18:2)
		[M+FA-H]	279.2332					
			224.0694					
			78.9850					

\* The values of MS-ESI- and MS-ESI+ correspond to the adducts [M-H]- and [M+H]+, respectively. In the case of another adduct, it will be indicated within the same box. FA: Formic acid.

**Table 2.** Total phenolic compounds and total anthocyanins content in the dry extract of anthocyanins from *B. naudinii* flowers

Sample	TPC (mg GAE/g)	TAC (mg CYG/g)
Anthocyanin dry extract	194.8 ± 4.07	1148.6 ± 59.9

GAE/g: milligrams of gallic acid equivalent per gram of dry extract; mg **CYG/g**: milligrams of cyanidin 3-O-glucoside equivalent per gram of dry extract. TPC: total phenolic content and TAC: total anthocyanin content.






**Table 3.** Preliminary toxicity of anthocyanin dry extract from *B. naudinii* flowers

Concentration (µg mL <sup>-1</sup> )	Mortality (%)	LC <sub>50</sub> (µg mL <sup>-1</sup> )	Goodness of Fit Test	Classification [14]
1000	100.0			
500	100.0			
100	20.0	106.9 ± 9.9*	0.025	Moderately toxic
10	10.0			

\* Values are expressed as mean and standard deviation (n = 3). LC<sub>50</sub>: lethal concentration.



## Antioxidant and photoprotective potential of *Polypodium leucotomos*

Rosy Yesela Mancilla Santa Cruz<sup>1,2</sup> , Sharon Velásquez Arévalo<sup>3</sup> , Anas Rashid<sup>1,4</sup> , Marco Rolando Aronés Jara<sup>2</sup> , María Segunda Aurora Prado<sup>1\*</sup> 

<sup>1</sup>Department of Pharmacy, School of Pharmaceutical Sciences, University of São Paulo, São Paulo 05508-000, Brazil

<sup>2</sup>Professional School of Pharmacy and Biochemistry, Faculty of Health Sciences, National University of San Cristóbal of Huamanga, Ayacucho 05001, Peru

<sup>3</sup>Department of Pharmacotechnics, Faculty of Pharmacy and Biochemistry, National University of Trujillo, Trujillo 13011, Peru

<sup>4</sup>School of Medicine and Surgery, University of Torino, Torino 10125, Italy

**\*Correspondence:** María Segunda Aurora Prado, Department of Pharmacy, School of Pharmaceutical Sciences, University of São Paulo, Av. Prof. Lineu Prestes 580, Block 13, Butanta, São Paulo 05508-000, Brazil. [msaprad06@usp.br](mailto:msaprad06@usp.br)

**Academic Editor:** Md Noushad Javed, K.R. Mangalam University, India

**Received:** September 9, 2022 **Accepted:** November 14, 2022 **Published:** December 29, 2022

**Cite this article:** Cruz RYMS, Arévalo SV, Rashid A, Jara MRA, Prado MSA. Antioxidant and photoprotective potential of *Polypodium leucotomos*. Explor Med. 2022;3:607–16. <https://doi.org/10.37349/emed.2022.00117>

### Abstract

In recent years, *Polypodium leucotomos* has emerged with a great interest for having medicinal and therapeutic potential. It is producing very promising results due to the presence of antioxidant and photoprotective properties. Electronic libraries and databases, including Scopus, PubMed, Google Scholar, Science Direct, and Web of Science were searched to identify relevant studies; 79 publications contributed to this review regarding *Polypodium leucotomos* botanical aspects, chemical composition, antioxidant and photoprotective activity. It is used in complementary and alternative therapies with various pharmaceutical dosage forms (systemic or topical). Thanks to the composition of phytochemical constituents present in the leaves and rhizomes which confer antioxidant and photoprotective activity that has clinical therapeutic potential to be used as systemic and topical sunscreen of natural origin for the prevention of different types of skin diseases caused by harmful ultraviolet A and ultraviolet B radiations. However, more studies are needed in the future to test the ability and enhance the capacity of sunscreen and sunblock in cosmetic formulations. To conclude, it is recommended to carry out scientific studies based on different analytical methods to evaluate the phytoconstituents potential and to develop stable pharmaceutical formulations according to the skin phototype.

### Keywords

*Polypodium leucotomos*, antioxidant, photoprotective

### Introduction

*Polypodium leucotomos*—a tropical fern belonging to the genus *Polypodium* and to the family Polypodiaceae—originated from South and Central America [1, 2] which was traditionally used due to its anti-tumor and anti-inflammatory properties [3]. In 1788, this species was first introduced in Europe after the botanical

© The Author(s) 2022. This is an Open Access article licensed under a Creative Commons Attribution 4.0 International License (<https://creativecommons.org/licenses/by/4.0/>), which permits unrestricted use, sharing, adaptation, distribution and reproduction in any medium or format, for any purpose, even commercially, as long as you give appropriate credit to the original author(s) and the source, provide a link to the Creative Commons license, and indicate if changes were made.



expedition in Peru and Chile by Hipólito Ruiz López (botanist) funded by the Spanish Crown and later spread to other areas [4]. It has been shown to contain saponins [1] and phenolic compounds: vinyl acid, chlorogenic acid, ferulic acid, caffeic acid, and coumaric acid [5–7] extracted from rhizomes [1, 8] and leaves [9, 10]. It is beneficial for specific dermatological pathologies [11] such as skin tumors [3, 12, 13], rash [14], erythema and pigmentation [12, 13, 15], melanoma [16], photodermatitis [13, 17, 18], vitiligo [19, 20], melasma, psoriasis, and atopic dermatitis [2, 21, 22]. It particularly reduces the skin deterioration induced by exposed ultraviolet (UV) rays [11, 23, 24] to minimize photoaging [25], therefore, it gained considerable interest in cosmetic and dermatological research. Further, the research demonstrated the positive effects in tonsillitis [26], trichomoniasis [4], infectious diseases [27], acute colitis [28], scalp keratosis [29, 30], polymorphic light eruption [14, 31] as well as immunomodulation of lymphocytes and cytokines [32] and it was also used as a dietary supplement [33].

The *Polypodium leucotomos* pharmaceutical preparations are available as oral capsule (act as a systemic antioxidizing agent), topical gel, cream, spray and compact makeup powder to protect the skin from sunlight (or invisible UV rays) exposure [2]. Besides, it is one of the global public health problems. Overexposure to solar radiation has a significant impact on skin health [34] such as sunburn, photoaging, photodermatitis, photosensitivity, immunosuppression and photocarcinogenesis [35, 36]; the latter being of great concern due to the increase in cases [37, 38]. Therefore, it is highly beneficial due to its chemoprotective, immunomodulatory, anti-inflammatory and antioxidant properties. In addition, it is attributed for the inhibition of photoisomerization as well as apoptosis that leads directly to DNA damage, and it also prevents immunosuppression [7, 25, 39, 40] which were proven in *in vitro* and *in vivo* studies, involving human, cell and animal studies [22, 41].

It is necessary to highlight that the harmful biological effects of UV radiation will depend on the energy that it diffuses [42]; while UVA, UVB and UVC spectral ranges of solar radiation comprise from 100 to 400 nm. Among them, UVA and UVB radiations are of great biological importance as they are concerned with mild to chronic skin damage and compromise the skin integrity [43]. Hence, the skin is the primary organ that eventually receives the most exposure [44], as there is a direct relationship between skin and UV radiation and this relationship generates reactive oxygen species that alter the structure and function of the skin [45]. For this reason, the dermatological studies carried out on *Polypodium leucotomos* have demonstrated its potential antioxidant activity [5, 10] due to the presence of phenolic compounds. Since, they have the ability to bind with free radicals, which are agents that prevent or delay oxidation by inhibiting the initiation of oxidative reactions and thus producing beneficial effects on human health [46, 47].

Free radicals are highly reactive unstable species and when reacting with UV rays, they can even lead to cell death [48] which implies they are responsible for photoaging, immunosuppression, phototoxicity, photoallergic and photocarcinogenesis [9, 47, 49, 50]. To avoid these damages, strategies are sought out such as photoprotection with natural antioxidants to limit them thus preventing erythema, inflammation, wrinkles, photoaging and skin cancer [51].

The area of cosmetic science has emerged in the last three decades to maintain cutaneous homeostasis and to neutralize the free radicals induced by damaging UV rays. The researchers are trying their best to formulate the skin preparation without causing toxicity or unwanted effects [52]. Some traditional sunscreen contains inorganic compounds such as titanium dioxide and zinc oxide [33] that dissociate UVA and UVB rays. Perhaps they are often visible as an undesirable opaque layer on the skin, though these are metallic particles that are considered highly toxic for the skin [53].

Therefore, researchers have been studying the compounds present in the *Polypodium leucotomos* which is considered as a UV protector. In recent years, there is a very high demand for its oral formulation as antioxidant capsules [41]. It should be important to highlight that the *Polypodium leucotomos* extract has been patented with the name Fernblock® XP [54].

The aim of this review is to gather the information from published studies to evaluate the antioxidant and photoprotective properties. The databases of Scopus, PubMed, Google Scholar, Science Direct and Web of Science were searched and an exhaustive review was carried out with publications from the year 2010

to 2022. A total of 117 reviews and research articles were collected, 79 contributing to this review with a topic of interest to carry out this work. In English, the following search words were used and mentioned here: “*Polypodium leucotomos*”; and other word combinations were also made like “*Polypodium leucotomos*” with “antioxidant”, “photoprotective”, “cancer”, “anti-inflammatory”, “photoaging”, “UV radiation”, “phenolic compounds”, “reactive oxygen species”, “skin” and “Fernblock”. After thorough evaluation, a discussion was held to highlight its antioxidant and photoprotective properties.

## Taxonomy

The taxonomic classification is shown in [Table 1](#).

**Table 1.** Taxonomic classification of *Polypodium leucotomos*

Kingdom	Plantae
Class	Equisetopsida
Order	Polypodiales
Suborder	Polypodiineae
Family	Polypodiaceae
Genus	<i>Polypodium</i>
Species	<i>leucotomos</i>

## Distribution

The geographical distribution ranges from Central America to South America, mainly in Bolivia, Brazil, Mexico and Peru [10, 26]. Besides, it cultivates in humid environment, and it grows on developed tree trunks. Its adaptation and vegetation reach the height of 1,200 to 2,200 meters above sea level [8].

## Phytochemical constituents

The phytochemical constituents are presented in [Table 2](#) and the chemical structures are shown in [Figure 1](#).

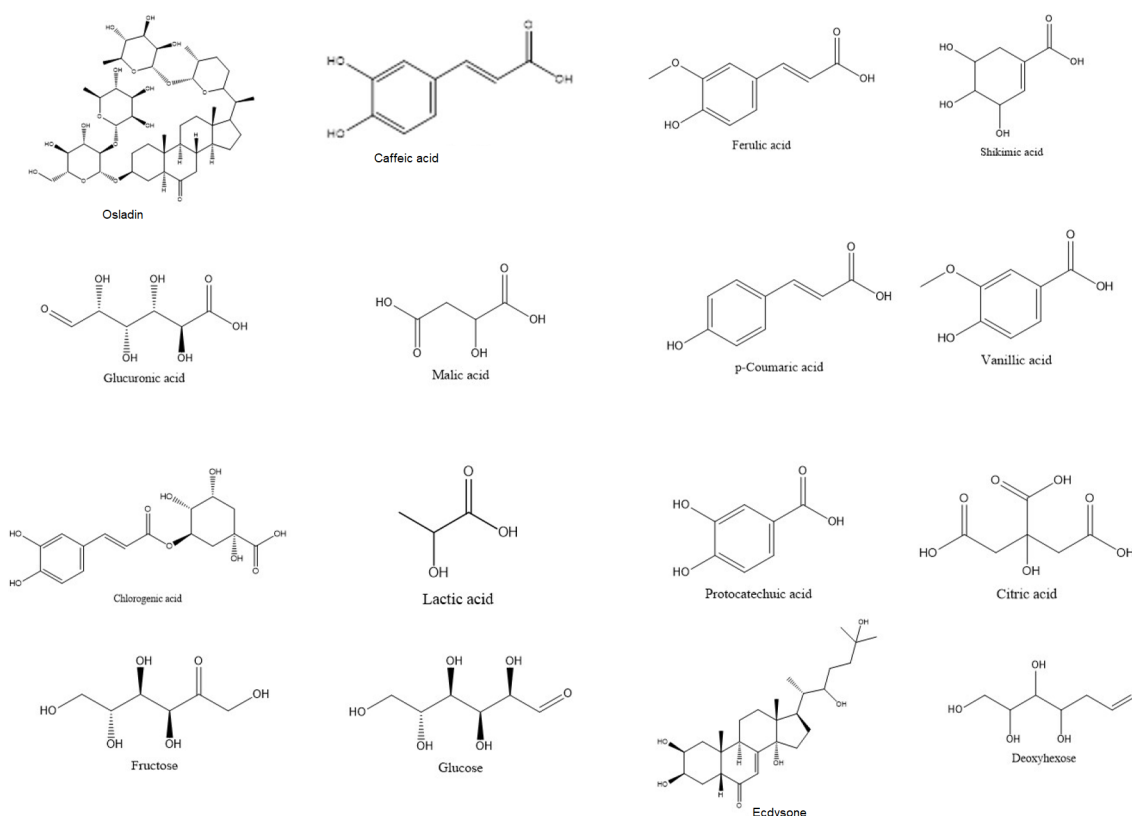
**Table 2.** Phytochemical constituents

Phytochemical constituents	Chemical compound	Plant part	Refs.
Saponins	Osladin, calagualine	Rhizome	[8, 55]
Phenolic compounds	Caffeic acid: 3,4-dihydroxycinnamic acid, Ferulic acid: 3-methoxy-4-hydroxycinnamic acid	Leaves	[56]
Biological acid molecules	Shikimic acid, glucuronic acid, malic acid, coumaric acid: 4-hydroxycinnamic acid, vanillic acid: 3-methoxy-4-hydroxybenzoic acid, chlorogenic acid: 3-caffeoylquinic acid, lactic acid, protocatechuic acid: 3,4-dihydroxybenzoic acid, citric acid	Rhizome and leaves	[56]
Monosaccharides	Fructose, glucose	Rhizome and leaves	[56]
Steroids	Ecdysone	Rhizome	[8]
Others	Oleoresin, deoxyhexose, potassium nitrate	Rhizome	[8]

## Antioxidant activity

Antioxidants are substances that can neutralize the actions of oxidants that cause free radicals, thus endogenous cellular antioxidants are released into the bloodstream that is subsequently trapped by free radicals, which maintains oxidant-antioxidant homeostasis [57]. The free radical is an atom that has an unpaired (free) electron; this characteristic makes them very reactive to capture an electron from molecules to become stable, thus reaching their electrochemical stability. Usually, the free radical tends to initiate a chain reaction and lead to the destruction and damage to cell membranes and tissues. In our body, this action occurs continuously and we need antioxidants to control this process [48, 58]. It will not be beneficial for health when our body has to tolerate excess free radicals that are produced by endogenous and exogenous

oxidant species such as solar radiation [57, 59, 60]. The latter is considered as the major source of free radical production that causes inflammation, acceleration of cellular aging, and initiation of skin cancer [61].



**Figure 1.** Chemical structure

The phytochemical extracts were demonstrated to have antioxidant activity and photoprotective properties [6]. However, if we compare the activities between the rhizomes and the leaves, the leaves showed high activity due to the presence of phenols, tannins and flavonoids [8, 13, 62], which was determined using oxygen radical scavenging methods such as ferric reducing antioxidant power (FRAP), 2,2-azino-bis-3-ethylbenzothiazoline-6-sulfonic acid (ABTS), and oxygen radical absorbance capacity (ORAC) [3, 11, 63]. Of note, health benefits of polyphenols using human skin cells demonstrated to be good skin photo protectors and photocarcinogenesis inhibitors, therefore, widely incorporated in medicinal and cosmetic products [64, 65].

Reactive oxygen species (superoxide anion, hydroxyl radical, hydrogen peroxide, and singlet oxygen) are important oxidizing agents that have been considered to be involved in skin aging and various diseases such as cerebrovascular, Parkinson's, multiple sclerosis, heart, cancer, and others [57, 66, 67]. This plant demonstrated its antioxidant effect by eliminating reactive species [6, 68] while inactivating the oxidative stress response that is a precursor of inflammation, aging, androgenic alopecia and skin cancer [68]. Further, it is not limited to reactive oxygen species, but it also prevents the synthesis of nitric oxide that participates in cell damage [69].

## Photoprotective activity

The skin is highly sensitive to UV rays which cause sunburn, photoaging, immunosuppression and photocarcinogenesis. It has caught the attention of researchers to develop alternatives in photoprotection that may have a filtering system for UVA and UVB radiations [35]. We are familiar that our body undergoes series of preventive mechanisms to counteract short- and long-term solar damage, but they are not enough due to the increase in intensity and duration of solar radiation exposure, whether due to the environmental pollution or ozone layer thinning that is subsequently responsible for skin cancer which considered a global health problem [70, 71].

In this scenario, the most affected people are those that have fair skin and even more if they live in the regions closest to the earth equator that has a higher solar irradiance [72]. The use of sunscreen and sunblock is one of the protective measures. Hence, the efficient development of skin products should be with high protection factors that are less irritating, with lower amounts of synthetic agents and above all easy accessibility in the market [73]. The skin products should not cause adverse reactions such as dermatitis or causing skin sensitivity and thinning. The adverse reaction usually happens when we use sunscreens in a very concentrated way that have phototoxic effects and thus a high risk for consumers [74]. To resolve this problem, the researchers are trying to introduce phytocosmetics from natural compounds that have proven scientific quality, safety and efficacy established during different studies [75].

This has been proven to successfully inhibit skin damage induced by UVA and UVB rays by reducing DNA mutations, inhibiting inflammation, improving the immune response and ultimately decreasing the photo-induced erythema. Recently, *in vitro* and *in vivo* studies that include animal models and human clinical trials proved that phytotherapeutic treatments are of great interest and hence beneficial for humans [38, 40, 76].

## Polypodium preparation

The Polypodium preparations are mentioned in Table 3.

**Table 3.** Polypodium preparation

Polypodium preparation	Result of interest	Photoprotective activity (assays)	Radiation type	Route and dose	Refs.
Capsule	Significant reduction of cutaneous reaction and symptoms/photoprotection treatment in idiopathic photodermatitis	<i>In vivo</i> —human	UVA/UVB	Oral Used dose: 480 mg/day	[18]
Capsule	Decreased erythema/increased minimal erythema dose (MED)	<i>In vivo</i> —human	UVB	Oral Used dose: 120–1,080 mg/day	[16, 40, 77]
Hydrophilic extract	Prevention and delay of typical lesions (eruptions) caused by UVR	<i>In vivo</i> —human	UVA/UVB	Oral Used dose: 720, 960, 1,200 mg/day	[14]
Extract	Inhibition of elastase activity/stimulation of cell expression/strengthening cell matrix/prevention in photoaging	<i>In vitro</i> —enzymes and substrate	UVA/UVB	Enzyme (starting concentration of 1 µg/µL) with its substrate 0.5 mM	[78]
Extract	Negative photobiological effects/reduction of UVB rays	<i>In vivo</i> —human	UVB	Oral Used dose: 480 mg/day	[7]
Hydrophilic extract (Fernblock)	Cell damage prevention/increased expression of matrix metalloproteinase-1 and cathepsin K/slowing expression of fibrillin 1, 2 and elastin	<i>In vitro</i> —cell cultures (human dermal fibroblasts)	Infrared A and visible light	Incubation	[11]
Extract	Decrease in darkening, cyclooxygenase-2 (marker of cell damage)	<i>In vivo</i> —human	Visible light	Oral Used dose: 480 mg/day	[79]
Extract (Fernblock)	Protective activity against oxidative stress and aging	<i>In vitro</i> —non-tumorigenic human keratinocyte cells	UVB	Incubation	[68]

## Conclusions

Different studies have demonstrated that this plant extract possesses anti-inflammatory, antioxidant, photoprotective and immunomodulatory activities making this species a powerful agent against solar induced aging and skin cancer. The capsule dosage form is very popular, widely accessible, and viable for all people around the globe. Hence, its antioxidant activity greatly facilitates its usage and thus preventing the skin damage caused by harmful UV radiation.

After an exhaustive review, no studies have been found for this plant based on its phytochemical performance, whether taken from leaves or rhizomes. It is recommended to carry out these studies for better evaluation of this plant. Likewise, it is worth mentioning that no scientific study carried out to determine the antioxidant capacity by 2,2-diphenyl-1-picryl-hydrazyl-hydrate (DPPH) free radical electron-transfer method, while stability studies are required for different pharmaceutical formulations as there is no widely approved dose according to the skin phototype. Hence, nowadays it is necessary to carry out these studies on damaging UVC rays to make better formulations with other active ingredients to produce synergy in the photoprotective and antioxidant capacity.

## Abbreviations

UV: ultraviolet

## Declarations

### Author contributions

RYMSC and SVA: Investigation, Methodology, Formal analysis, Visualization, Writing—original draft. MRAJ: Supervision. AR and MSAP: Conceptualization, Methodology, Formal analysis, Writing—review & editing, Project administration, Supervision.

### Conflicts of interest

The authors declare that they have no conflicts of interest.

### Ethical approval

Not applicable.

### Consent to participate

Not applicable.

### Consent to publication

Not applicable.

### Availability of data and materials

Not applicable.

### Funding

Not applicable.

### Copyright

© The Author(s) 2022.

## References

1. Horvath A, Alvarado F, Szöcs J, de Alvarado ZN, Padilla G. Metabolic effects of calagualine, an antitumoral saponine of *Polypodium leucotomos*. *Nature*. 1967;214:1256–8.
2. Choudhry SZ, Bhatia N, Ceilley R, Hougeir F, Lieberman R, Hamzavi I, et al. Role of oral *Polypodium leucotomose* extract in dermatologic diseases: a review of the literature. *J Drugs Dermatol*. 2014;13:148–53.
3. Efectos del extracto de *Polypodium leucotomos* sobre la tumorogénesis inducida por la radiación ultravioleta [Internet]. Theses and Dissertations Online; [cited 2022 Sep 9]. Available from: <http://hdl.handle.net/10803/8754>
4. Nogal-Ruiz JJ, Gómez-Barrío A, Escario JA, Martínez-Fernández AR. Effect of Anapsos in a murine model of experimental trichomoniasis. *Parasite*. 2003;10:303–8.

5. Garcia F, Pivel JP, Guerrero A, Brieva A, Martinez-Alcazar MP, Caamano-Somoza M, et al. Phenolic components and antioxidant activity of Fernblock, an aqueous extract of the aerial parts of the fern *Polypodium leucotomos*. *Methods Find Exp Clin Pharmacol*. 2006;28:157–60.
6. Gombau L, García F, Lahoz A, Fabre M, Roda-Navarro P, Majano P, et al. *Polypodium leucotomos* extract: antioxidant activity and disposition. *Toxicol Vitr*. 2006;20:464–71.
7. Kohli I, Shafi R, Isedeh P, Griffith JL, Al-Jamal MS, Silpa-Archa N, et al. The impact of oral *Polypodium leucotomos* extract on ultraviolet B response: a human clinical study. *J Am Acad Dermatol*. 2017;77:33–41.e1.
8. Saorin DCM, inventor. Transformação de *Polypodium leucotomos* extrato seco das raízes no fotoprotetor oral sob forma de cápsulas. Portuguese patent PI 0904487-6 A2. 2011 Jan 4.
9. Bhatia N. *Polypodium leucotomos*: a potential new photoprotective agent. *Am J Clin Dermatol*. 2015;16:73–9.
10. Parrado C, Mascaraque M, Gilaberte Y, Juarranz A, Gonzalez S. Fernblock (*Polypodium leucotomos* extract): molecular mechanisms and pleiotropic effects in light-related skin conditions, photoaging and skin cancers, a review. *Int J Mol Sci*. 2016;17:1026.
11. Zamarrón A, Lorrio S, González S, Juarranz Á. Fernblock prevents dermal cell damage induced by visible and infrared A radiation. *Int J Mol Sci*. 2018;19:2250.
12. Schalka S, Vitale-Villarejo MA, Agelune CM, Bombarda PCP. Benefícios do uso de um composto contendo extrato de *Polypodium leucotomos* na redução da pigmentação e do eritema decorrentes da radiação ultravioleta. *Surg Cosmet Dermatol*. 2014;6:344–8. Portuguese.
13. Schalka S, Steiner D, Ravelli FN, Steiner T, Terena AC, Marçon CR, et al.; Brazilian Society of Dermatology. Brazilian consensus on photoprotection. *An Bras Dermatol*. 2014;89:1–74.
14. Tanew A, Radakovic S, Gonzalez S, Venturini M, Calzavara-Pinton P. Oral administration of a hydrophilic extract of *Polypodium leucotomos* for the prevention of polymorphic light eruption. *J Am Acad Dermatol*. 2012;66:58–62.
15. Charoo NA. Hyperpigmentation: looking beyond hydroquinone. *J Cosmet Dermatol*. 2022;21:4133–45.
16. Aguilera P, Carrera C, Puig-Butille JA, Badenas C, Lecha M, González S, et al. Benefits of oral *Polypodium leucotomos* extract in MM high-risk patients. *J Eur Acad Dermatol Venereol*. 2013;27:1095–100.
17. Caccialanza M, Percivalle S, Piccinno R, Brambilla R. Photoprotective activity of oral *Polypodium leucotomos* extract in 25 patients with idiopathic photodermatoses. *Photodermatol Photoimmunol Photomed*. 2007;23:46–7.
18. Caccialanza M, Recalcati S, Piccinno R. Oral *Polypodium leucotomos* extract photoprotective activity in 57 patients with idiopathic photodermatoses. *G Ital Dermatol Venereol*. 2011;146:85–7.
19. Middelkamp-Hup MA, Bos JD, Rius-Diaz F, Gonzalez S, Westerhof W. Treatment of vitiligo vulgaris with narrow-band UVB and oral *Polypodium leucotomos* extract: a randomized double-blind placebo-controlled study. *J Eur Acad Dermatol Venereol*. 2007;21:942–50.
20. Searle T, Al-Niaimi F, Ali FR. *Polypodium leucotomos* as an adjunct to the treatment of vitiligo. *J Am Acad Dermatol*. 2022;86:e65.
21. Szczurko O, Boon HS. A systematic review of natural health product treatment for vitiligo. *BMC Dermatol*. 2008;8:2.
22. Berman B, Ellis C, Elmets C. *Polypodium leucotomos*--an overview of basic investigative findings. *J Drugs Dermatol*. 2016;15:224–8.
23. Gonzalez S, Gilaberte Y, Philips N. Mechanistic insights in the use of a *Polypodium leucotomos* extract as an oral and topical photoprotective agent. *Photochem Photobiol Sci*. 2010;9:559–63.



24. Torricelli P, Fini M, Fanti PA, Dika E, Milani M. Protective effects of *Polypodium leucotomos* extract against UVB-induced damage in a model of reconstructed human epidermis. *Photodermatol Photoimmunol Photomed*. 2017;33:156–63.
25. Parrado C, Gilaberte Y, Philips N, Juarranz A, Gonzalez S. Chapter 34 - Fern extract, oxidative stress, and skin cancer. In: Preedy VR, Patel VB, editors. *Cancer (second edition): oxidative stress and dietary antioxidants*. San Diego: Academic Press; 2021. pp. 387–98.
26. Sánchez-Rodríguez C, Peraza Cruces KR, Rodrigáñez Riesco L, García-Vela JA, Sanz-Fernández R. Immunomodulatory effect of *Polypodium leucotomos* (Anapsos) in child palatine tonsil model. *Int J Pediatr Otorhinolaryngol*. 2018;107:56–61.
27. Solivellas BM, Martín TC. *Polypodium leucotomos* extract use to prevent and reduce the risk of infectious diseases in high performance athletes. *Infect Drug Resist*. 2012;5:149–53.
28. Gálvez J, Sánchez de Medina F, Romero J, Zarzuelo A. Effect of *Polypodium leucotomos* on acute, chronic and reactivated trinitrobenzene sulphonic acid colitis in rats. *Inflammopharmacology*. 2000;8:89–105.
29. Auriemma M, Di Nicola M, Gonzalez S, Piaserico S, Capo A, Amerio P. *Polypodium leucotomos* supplementation in the treatment of scalp actinic keratosis: could it improve the efficacy of photodynamic therapy? *Dermatol Surg*. 2015;41:898–902.
30. Piaserico S, Mazzetto R, Sartor E, Bortoletti C. Combination-based strategies for the treatment of actinic keratoses with photodynamic therapy: an evidence-based review. *Pharmaceutics*. 2022;14:1726.
31. Stump M, Dhinsa H, Powers J, Stone M. Attenuation of actinic prurigo eruptions with *Polypodium leucotomos* supplementation. *Pediatr Dermatol*. 2022;39:145–6.
32. Sempere-Ortells JM, Campos A, Velasco I, Marco F, Ramirez-Bosca A, Diaz J, et al. Anapsos (*Polypodium leucotomos*) modulates lymphoid cells and the expression of adhesion molecules. *Pharmacol Res*. 2002;46:185–90.
33. Thompson KG, Kim N. Dietary supplements in dermatology: a review of the evidence for zinc, biotin, vitamin D, nicotinamide, and polypodium. *J Am Acad Dermatol*. 2021;84:1042–50.
34. Dedios M, Ninell J. Niveles de radiación ultravioleta, fenotipos e infraestructura de protección solar en instituciones educativas de Piura, Perú. *Rev Colomb Enfermería*. 2017;15:40–9. Spanish.
35. Garnacho Saucedo GM, Salido Vallejo R, Moreno Giménez JC. Efectos de la radiación solar y actualización en fotoprotección. *An Pediatr (Engl Ed)*. 2020;92:377.e1–9. Spanish.
36. Subhadarshani S, Athar M, Elmets CA. Photocarcinogenesis. *Curr Derm Rep*. 2020;9:189–99.
37. García-Malinis AJ, Gracia-Cazaña T, Zazo M, Aguilera J, Rivas-Ruiz F, de Troya Martín M, et al. Hábitos y conocimientos sobre fotoprotección y factores de riesgo para quemadura solar en corredores de maratones de montaña. *Actas Dermo-Sifiliogr*. 2021;112:159–66. Spanish.
38. Gracia-Cazaña T, González S, Parrado C, Juarranz Á, Gilaberte Y. La influencia del exposoma en el cáncer de piel. *Actas Dermo-Sifiliogr*. 2020;111:460–70. Spanish.
39. Palomino OM. Current knowledge in *Polypodium leucotomos* effect on skin protection. *Arch Dermatol Res*. 2015;307:199–209.
40. Parrado C, Nicolas J, Juarranz A, Gonzalez S. The role of the aqueous extract *Polypodium leucotomos* in photoprotection. *Photochem Photobiol Sci*. 2020;19:831–43.
41. Nestor MS, Berman B, Swenson N. Safety and efficacy of oral *Polypodium leucotomos* extract in healthy adult subjects. *J Clin Aesthet Dermatol*. 2015;8:19–23.
42. Narayanan DL, Saladi RN, Fox JL. Ultraviolet radiation and skin cancer. *Int J Dermatol*. 2010;49:978–86.
43. Corrêa Mde P. Solar ultraviolet radiation: properties, characteristics and amounts observed in Brazil and South America. *An Bras Dermatol*. 2015;90:297–313.
44. Bharath AK, Turner RJ. Impact of climate change on skin cancer. *J R Soc Med*. 2009;102:215–8.

45. Bosch R, Philips N, Suárez-Pérez JA, Juarraz A, Devmurari A, Chalensouk-Khaosaat J, et al. Mechanisms of photoaging and cutaneous photocarcinogenesis, and photoprotective strategies with phytochemicals. *Antioxidants (Basel)*. 2015;4:248–68.
46. Scalbert A, Johnson IT, Saltmarsh M. Polyphenols: antioxidants and beyond. *Am J Clin Nutr*. 2005;81:215S–7S.
47. Khatoun M, Islam E, Islam R, Rahman AA, Alam AH, Khondkar P, et al. Estimation of total phenol and *in vitro* antioxidant activity of *Albizia procera* leaves. *BMC Res Notes*. 2013;6:121.
48. San-Miguel A, Martín-Gil FJ. Importancia de las especies reactivas al oxígeno (radicales libres) y los antioxidantes en clínica. *Gac Med Bilbao*. 2009;106:106–13. Spanish.
49. Esteva E. Fotoprotección. *Offarm*. 2005;24:64–72. Spanish.
50. Seto Y, Ohtake H, Sato H, Onoue S. Phototoxic risk assessment of dermally-applied chemicals with structural variety based on photoreactivity and skin deposition. *Regul Toxicol Pharmacol*. 2020;113:104619.
51. Taylor JH, Rosen CF. Correction to: systemic photoprotection. *Curr Derm Rep*. 2020;9:362.
52. Dunaway S, Odin R, Zhou L, Ji L, Zhang Y, Kadekaro AL. Natural antioxidants: multiple mechanisms to protect skin from solar radiation. *Front Pharmacol*. 2018;9:392.
53. Smijs TG, Pavel S. Titanium dioxide and zinc oxide nanoparticles in sunscreens: focus on their safety and effectiveness. *Nanotechnol Sci Appl*. 2011;4:95–112.
54. Serini S, Guarino R, Ottens Vasconcelos R, Celleno L, Calviello G. The combination of sulfuraphane and Fernblock® XP improves individual beneficial effects in normal and neoplastic human skin cell lines. *Nutrients*. 2020;12:1608.
55. González S, Pathak MA. Inhibition of ultraviolet-induced formation of reactive oxygen species, lipid peroxidation, erythema and skin photosensitization by *Polypodium leucotomos*. *Photodermatol Photoimmunol Photomed*. 1996;12:45–56.
56. Gonzalez S, Gilaberte Y, Philips N, Juarraz A. Fernblock, a nutraceutical with photoprotective properties and potential preventive agent for skin photoaging and photoinduced skin cancers. *Int J Mol Sci*. 2011;12:8466–75.
57. Herrera MC, León SV, Tolentino RG, Francisca MV, Vázquez CCR. Antioxidantes: perspectiva actual para la salud humana. *Marcela Rev chil nutr*. 2015;42:2. Spanish.
58. Avello M, Suwalsky M. Radicales libres, antioxidantes naturales y mecanismos de protección. *Atenea*. 2006:161–72. Spanish.
59. Salido FP, Fernández JJR. Influencia de los radicales libres en el envejecimiento celular. *Offarm*. 2002;21:96–100. Spanish.
60. Addor FAS. Antioxidants in dermatology. *An Bras Dermatol*. 2017;92:356–62.
61. Silva SAME, Michniak-Kohn B, Leonardi GR. An overview about oxidation in clinical practice of skin aging. *An Bras Dermatol*. 2017;92:367–74.
62. González S, Lucena SR, Delgado P, Juarraz A. Comparison of several hydrophilic extracts of *Polypodium leucotomos* reveals different antioxidant moieties and photoprotective effects *in vitro*. *J Med Plants Res*. 2018;12:336–45.
63. Capote R, Alonso-Lebrero JL, García F, Brieva A, Pivel JP, González S. *Polypodium leucotomos* extract inhibits trans-urocanic acid photoisomerization and photodecomposition. *J Photochem Photobiol B*. 2006;82:173–9.
64. Nichols JA, Katiyar SK. Skin photoprotection by natural polyphenols: anti-inflammatory, antioxidant and DNA repair mechanisms. *Arch Dermatol Res*. 2010;302:71–83.
65. Afaq F, Katiyar SK. Polyphenols: skin photoprotection and inhibition of photocarcinogenesis. *Mini Rev Med Chem*. 2011;11:1200–15.

66. García LAEZ. El envejecimiento y el estrés oxidativo. *Rev Cubana Invest Bioméd.* 2002;21:3. Spanish.
67. Vaquero-Raya EC, Molero-Richard X. Especies reactivas de oxígeno en las enfermedades inflamatorias del páncreas: ¿una posible diana terapéutica? *Gastroenterol Hepatol.* 2005;28:473–84. Spanish.
68. Delgado-Wicke P, Rodríguez-Luna A, Ikeyama Y, Honma Y, Kume T, Gutierrez M, et al. Fernblock® upregulates NRF2 antioxidant pathway and protects keratinocytes from PM<sub>2.5</sub>-induced xenotoxic stress. *Oxid Med Cell Longev.* 2020;2020:2908108.
69. El-Haj N, Goldstein N. Sun protection in a pill: the photoprotective properties of *Polypodium leucotomos* extract. *Int J Dermatol.* 2015;54:362–6.
70. Bosqueta LG. Los peligros de la radiación solar. Fotoprotección. *Offarm.* 2001;20:75–84. Spanish.
71. Marcos FV. La Contaminación ambiental como factor determinante de la salud. *Rev Esp Salud Publica.* 2005;79:117–27. Spanish.
72. Sanmartín Jimenez O. The rising incidence of melanoma and nonmelanoma skin cancer obliges us to persevere with primary and secondary prevention campaigns. *Actas Dermo-Sifiliográficas.* 2017;108:324.
73. Ramos MFS, Santos EP, Dellamora-Ortiz GM. Avaliação da atividade antisolar e estudos preliminares de fotodegradação da propolis. *Rev Fitos.* 2010;5:3. Portuguese.
74. Nascimento LF, Santos EP, Aguiar AP. Fotoprotetores orgânicos: pesquisa, inovação e a importância da síntese orgânica. *Rev Virtual Quim.* 2014;6:190–223. Portuguese.
75. Vieira CBS, Orlanda JFF. Atividade antioxidante e fotoprotetora do extrato etanólico de *Ocimum gratissimum* L. (alfavaca, Lamiaceae). *Rev Cubana Plant Med.* 2018;23:3. Portuguese.
76. Korman AM, Reynolds KA, Nabhan F, Konda B, Shah MH, Kaffenberger BH. Vandetanib-induced phototoxic drug eruption treated with *Polypodium leucotomos* extract: a case report and review of the literature. *J Clin Aesthet Dermatol.* 2019;12:35–8.
77. Emanuele E, Bertona M, Biagi M. Comparative effects of a fixed *Polypodium leucotomos*/Pomegranate combination versus *Polypodium leucotomos* alone on skin biophysical parameters. *Neuro Endocrinol Lett.* 2017;38:38–42.
78. Philips N, Gonzalez S. Beneficial regulation of elastase activity and expression of tissue inhibitors of matrixmetalloproteinases, fibrillin, transforming growth factor- $\beta$ , and heat shock proteins by *P. leucotomos* in nonirradiated or ultraviolet-radiated epidermal keratinocytes. *ISRN Oxidative Med.* 2013;2013:257463.
79. Mohammad TF, Kohli I, Nicholson CL, Treyger G, Chaowattanapanit S, Nahhas AF, et al. Oral *Polypodium leucotomos* extract and its impact on visible light-induced pigmentation in human subjects. *J Drugs Dermatol.* 2019;18:1198–203.